Alma Mater Studiorum – Università di Bologna

DOTTORATO DI RICERCA IN

CHIMICA

Ciclo XXXII

Settore Concorsuale: 03/C1

Settore Scientifico Disciplinare: CHIM/06

PEPTIDOMIMETIC LIGANDS FOR TUNING INTEGRIN-MEDIATED SIGNALLING: RATIONAL DESIGN, SYNTHESIS AND THERANOSTIC APPLICATIONS

Presentata da: Michele Anselmi

Coordinatore Dottorato   Supervisore

Prof.ssa Domenica Tonelli   Prof. Luca Gentilucci

                                                 Co-Supervisore

                                                 Prof. Dr. Norbert Sewald

Esame finale anno 2020

Table of contents

List of abbreviations

2D, 3D = two-, three-dimensional

Ac$_2$O: acetic anhydride

AMBER = assisted model building with energy refinement

AMPUMP: 1-(4-(aminomethyl)phenyl)-3-(*o*-methylphenyl)urea

BBB: blood brain barrier

Bn: benzyl

Boc: *tert*-butyloxycarbonyl protecting group

Boc$_2$O: Di-*tert*-butyl dicarbonate

Bzl: benzoyl

Cbz: benzyloxycarbonyl protecting group

CPP: cyclo pentapeptide

Cy: cyclohexane

DCC: *N,N′*-Dicyclohexylcarbodiimide

DCM: dichloromethane

DIC: *N,N′*-Diisopropylcarbodiimide

DIPEA: *N,N*-Diisopropylethylamine

DMAP: 4-(Dimethylamino)pyridine

DMF: dimethylformamide

DMSO: dimethyl sulfoxide

ECM: extracellular matrix

EDC·HCl: *N*-(3-Dimethylaminopropyl)-*N′*-ethylcarbodiimide hydrochloride

EEDQ: *N*-Ethoxycarbonyl-2-ethoxy-1,2-dihydroquinoline

EGF: epidermal growth factor

ELISA: Enzyme-linked Immunosorbent Assay

ESI-MS: Electro Spray Ionization Mass analysis

Et$_2$O: diethylether

EtOAc: ethyl acetate

Fmoc: 9-fluorenylmethoxycarbonyl protecting group

Fmoc-Dap(Boc)-OH: N_α-Fmoc-N_β-Boc-2,3-diaminopropionic acid

gCOSY: gradient COrrelation SpectroscopY

HATU: 1-[Bis(dimethylamino)methylene]-1*H*-1,2,3-triazolo[4,5-*b*]pyridinium 3-oxid hexafluorophosphate

HBTU: *N,N,N′,N′*-Tetramethyl-*O*-(1H-benzotriazol-1-yl)uranium hexafluorophosphate

HIPF: Hexafluoroisopropanol

HOAt: 1-Hydroxy-7-azabenzotriazole

HOBt: 1-Hydroxybenzotriazole hydrate

HPLC: High Performance Liquid Chromatography

Ig: immunoglobulin

IL: Interleukin

MD: molecular dynamics

MPUPA: *o*-methylphenylureaphenylacetyl

MW: microwave

MW: molecular weight

NMM: *N*-methyl morpholine

NMR: Nuclear Magnetic Resonance

OBn: benzyl ether or ester

O*t*Bu: tert-butyl ether or ester

OVA: ovalbumin

Pd/C: palladium on activated carbon

PE: petroleum ether

PIFA: (Bis(trifluoroacetoxy)iodo)benzene

ppm: parts per million

PSI: plexin-semaphorin-integrin

QSAR: Quantitative Structure-Activity Relationship

ROESY: Rotating-frame nuclear Overhauser effect correlation spectroscopy

RP-HPLC: Reverse-Phase High Performance Liquid Chromatography

RT: room temperature

TBTU: *O*-(Benzotriazol-1-yl)-*N,N,N′,N′*-tetramethyluronium tetrafluoroborate

TEA: triethylamine

TFA: trifluoroacetic acid

THF: tetrahydrofuran

TIS: triisopropylsilane

TLC: Thin Layer Chromatography

TsCl: toluene-4-sulfonylchloride or tosyl chloride

VT-NMR: variable temperature-nuclear magnetic resonance

Amino acid*	One-letter code	Three-letter code
Alanine	A	Ala
Arginine	R	Arg
Asparagine	N	Asn
Aspartic acid	D	Asp
Cysteine	C	Cys
Glutamine	Q	Gln
Glutamic acid	E	Glu
Glycine	G	Gly
Histidine	H	His
Isoleucine	I	Ile
Leucine	L	Leu
Lysine	K	Lys
Methionine	M	Met
Phenylalanine	F	Phe
Proline	P	Pro
Serine	S	Ser
Threonine	T	Thr
Tryptophan	W	Trp
Tyrosine	Y	Tyr
Valine	V	Val

* D-amino acids are described by D-Xaa in the three-letter code and/or with the small letter in the one-letter code.

1. INTRODUCTION

1.1. Integrin receptors

Integrins are a major class of cell-surface adhesion receptors in all metazoans and are involved in fundamental adhesive events including cell-cell, cell-ECM and cell-pathogens interactions. The name "integrin" was given to denote their key role in maintaining the integrity of the cytoskeleton-ECM linkage.[1] Integrins are type-I heterodimeric transmembrane glycoproteins composed by a non-covalent association of two different subunits, α- and β-.[2, 3] In mammals 18 α- and 8 β-subunits are combined to form 24 different dimers (Figure 1), each of which exhibits different tissue-expression and binding affinity towards specific ligands (Table 1). Integrins are widely expressed and every nucleated cell is characterized by specific integrin cell-surface exposure. According to the α-subunits ligand-binding specificity they can be divided into four different main groups: laminin-binding integrins (α_3, α_6 and α_7), collagen-binding integrins (α_1, α_2, α_{10}, and α_{11}), leukocyte integrins (α_4, α_L, α_M, α_X, and α_D), and RGD recognizing integrins (α_V, α_5, α_8 and α_{IIb}).[4]
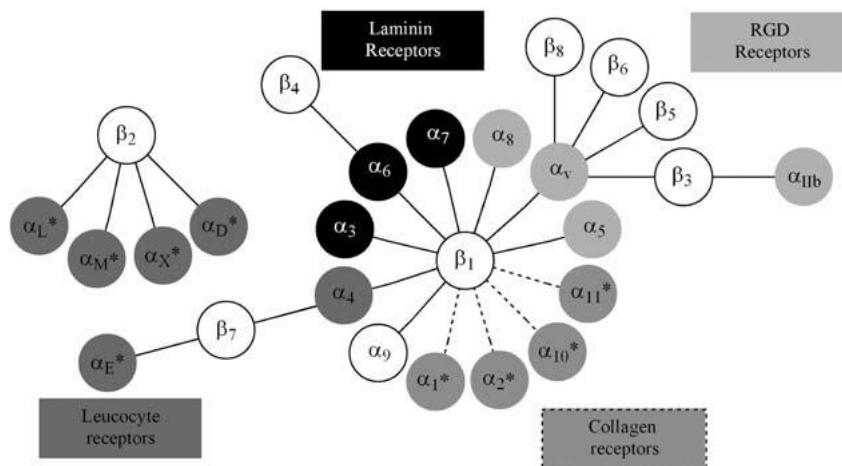
Figure 1. Integrin classification according to α- and β-subunit combinations, and their specific ligands: RGD, laminin, collagen, and leucocytes. Asterisks (*) indicate α-subunits containing I-domain.

By dynamic adhesive interactions with the surrounding cells and extracellular matrix, integrins communicate information about the chemical identity and physical state of their ligands or environment inside the cells. The activation of these intracellular signalling pathways is responsible for the control of cell shape, migration, growth, survival, and cell-type-specific gene expression.[2] Therefore, integrin-mediated adhesion and signaling events are important in

normal physiological processes including immune response, tissue morphogenesis, wound healing, hemostasis, cell survival and cell differentiation. On the other hand, dysregulation of these processes results in pathological diseases from autoimmune and inflammatory diseases to thrombotic vascular disorder to angiogenesis of cancer and its metastasis.[5] In line with this evidence, integrin receptors have generated widespread interest as targets in the field of drug discovery for therapy, diagnosis and drug delivery approaches.

| Integrin	Synonym	Ligands	Binding Motifs	Distribution in Cells	Physiology Pathology	Inhibitors
αIIbβ3	GpIIb/IIIa, CD41/CD61	FN, VN, FG, vWF, CD40L, prothrombin, TSP	RGD	Platelets	Thrombosis	Abciximab, eptifabitide, tirofiban
αvβ3	VNR, CD51/CD61	FN, VN, LM, FG, Fibrin, TSP, TN-C, vWF, CO, OP, MMP-2, Del-1, BSP, FGF-2, Thrombin, CCN1	RGD	Endothelial cells, some tumor cells (e.g., glioblastomas, melanomas, ovarian, breast and prostate cancers), platelets, monocytes, osteoclasts, fibroblasts	Angiogenesis (tumor, ischemic tissues), bone diseases	Vitaxin, abegrin, etitumumab, cilengitide, L000845704
αvβ5	CD51/CD19	VN, Del-1, CCN1	RGD	Endothelial cells, some tumor cells, fibroblast	Angiogenesis	Etitumumab
α4β1	VLA-4, CD49d/CD29	VCAM-1, FN, OP	LDV, LDT IDS	Leukocytes	Allergy, inflammation, autoimmune diseases	Natalizumab, firategrast, valategrast
α4β7	LPAM-1, CD49d/ITGB7	VCAM-1, FN, MadCAM-1	LDV	Lymphocytes	Inflammation, autoimmune diseases, IBD	Natalizumab
α5β1	FNR, VLA-5, GPIc-IIa, ECMR-VI, CD49e/CD29	FN, fibrin	RGD, PHSRN	Endothelial cells, platelets, lymphocytes	Angiogenesis (tumor, retinal), age-related macular degeneration	Volociximab, ATN-161
αDβ2	CD11d/CD18	ICAM-3, VCAM	VCAM-1	leucocytes	Auto-immune inflammation	
αLβ2	LFA-1, CD11a/CD18	ICAM-1, ICAM-2, ICAM-3	Glu-34 of ICAM-1	Leucocytes	Immune reaction, inflammation, psoriasis	Efalizumab, BIRT2584
αMβ2	Mac-1, CR3, CD11b/CD18	ICAM-1, VCAM, FG, iC3b	Acid residue in domain 3 of ICAM-1	Leucocytes, monocytes, macrophages	Immune reaction, inflammation	
αXβ2	P150, CD11c/CD18	FG, iC3b		Leucocytes	Immune reaction, inflammation	

Table 1. Integrins tissue distribution, endogenous ligands and minimal binding motifs, related pathologies (image source: Arosio *et. al.*).[6]

1.2. Integrin structure

The α and β subunits are composed by several domains interconnected via flexible linkers. Each subunit is formed by a relatively large extracellular domain of ~ 1000 and ~ 700 residues respectively, a single transmembrane domain, and a short cytoplasmic tail (except β4).[3] The extracellular domains are responsible for the ligand binding and therefore determine ligand specificity of the respective heterodimers.[7, 8] Electron microscopy (EM) and X-ray crystal structure studies of several integrins (*e.g.*, αIIbβ3, αvβ3, αXβ2) have demonstrated that the overall shape of integrin ectodomain consists of a large "head" onto two long "legs" with flexible "knees" (Figure 2).[9-14]
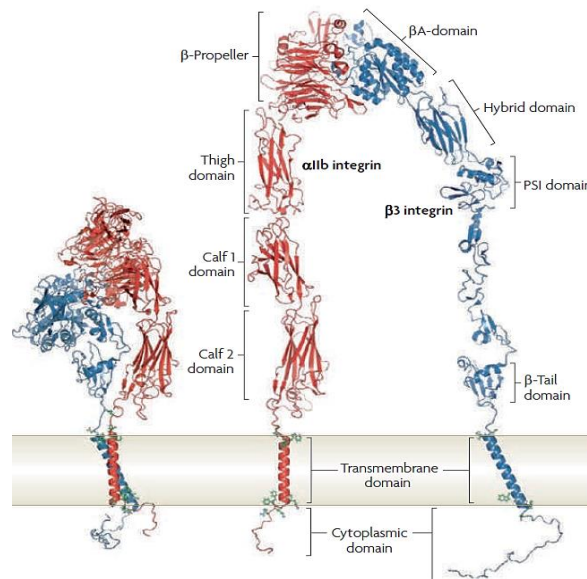
Figure 2. Integrin structure (image source: Shattil *et. al.*)[15]

1.2.1. The α subunit

The α subunit is composed by four distinct extracellular domains: a seven-bladed β-propeller, a thigh, calf-1 and calf-2 domains (Figure 3a) which form together the "leg" structure that supports the integrin "head" (β-propeller).[7, 14] The last three or four blades of the β-propeller contain domains that bind Ca^{2+} on the lower side of the blades facing away from the ligand-binding surface. Ca^{2+}-binding to these sites has been shown to affect the ligand binding.[16] Nine of the 18 integrin α chains include an additional domain of ~200 amino acids termed αI-domain, inserted between the blades 2 and 3 of the β-propeller.[17] Therefore, integrins are grouped into two classes: αI-containing and αI-lacking domain (Figure 3).

The αI domain has six-stranded β-sheets surrounded by seven α-helices generating a Rossman-like fold and, it has been found in the $β_2$ integrin subgroup, in the collagen-binding integrins belonging to the $β_1$ subfamily ($α_1$, $α_2$, $α_{10}$, $α_{11}$), and in the $α_E β_7$ heterodimer.[4] In αI-containing integrins the α head is composed of β-propeller domain and αI-domain, while in αI-less integrins a single β-propeller forms α head (Figure 3c and 2d). αI-domain is the ligand binding domain in αI-containing integrins, whereas the βI-domain forms a major ligand binding pocket in αI-less integrins (Figure 3c and 2d).[18-20]

Ligand binding occurs in the so-called metal-ion-dependent adhesion site (MIDAS) motif through coordination of Mg^{2+} ion by Asp, Glu sidechains or carboxylic acid of the ligands in

extrinsic or intrinsic way (Figure 3c and 2d).[21] The thigh and calf domains have similar Ig-like β-strand folds made by 140~160 residues.[11]
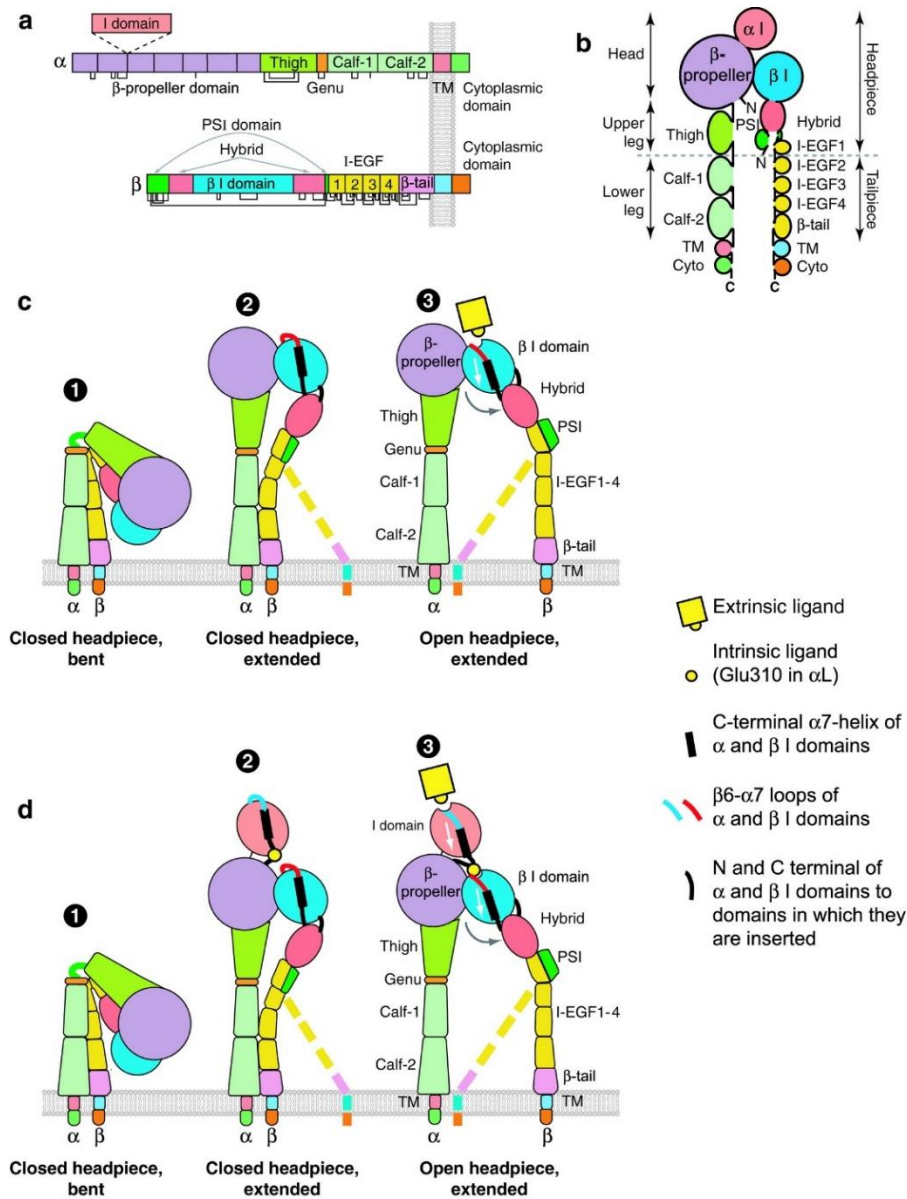
Figure 3. Integrin structure and conformational rearrangements. (*a*) Organization of domains within the primary structures. Dashed lines denote α subunits containing I domain. Cysteines and disulfides are shown as lines below the stick figures. (*b*) Schematic α and β subunit domains from the N- to C- terminus. (*c-d*) Conformational rearrangement of domains during activation of αI-less integrins (*c*) or αI-containing integrins (*d*). The β subunit lower legs are flexible and are therefore shown in what may be the predominant (solid representation) and less predominant (dashed lines) orientations (image source: Luo *et. al.*).[22]

Moreover, two connecting regions are important for the integrin flexibility: the first is the linker between the β-propeller and the thigh; the second is the "genu" or "knee" at the bend between the thigh and the calf-1 domain. The "genu" in the α-subunit is located close to the

similar bend in the β subunit, thereby allowing extension by a hinging at the knees (Figure 3). The αI domain is connected to the β-propeller domain by a flexible linker while the other four α-leg domains have relatively rigid structures.[7]

1.2.2. The β subunit

The β subunit of integrins contains eight extracellular domains with flexible and complex interconnections: a βI-domain, a hybrid, a plexin-semaphorin-integrin (PSI), four cysteine-rich epidermal growth factor (EGF) repeats and a β-tail domain (Figure 3a,b).[7, 14] βI-domain is structurally homologous to the αI-domain sharing the same overall fold and, it is inserted into the hybrid domain to forms the β head of all integrin β subunits.

Three sites are present on the top face of βI-domain: 1) the first site, known as MIDAS, is directly involved in the ligand binding in αI-less integrins and indirectly in the αI-containing integrin via coordination of Mg^{2+} ion by the Asp/Glu residue or carboxylic acid of the ligands; 2) the second site is adjacent to MIDAS, therefore, termed AdMIDAS (Adjacent-to-MIDAS), is a negative regulatory site responsible for integrin inhibition (high concentration of Ca^{2+}) or activation (high concentration of Mn^{2+}).[23] 3) The third is a Ca^{2+}-binding site termed SyMBS (synergistic metal ion-binding site) which has a positive synergic effect on ligand binding.[13, 23, 24] The PSI domain of β_3 integrin subgroup is divided into two portions connected by a long-range disulfide bond between Cys13-435.[18, 25] Even the four EGF domains are linked by several Cys disulfide bond (Figure 3a).[13, 25] In general, the β-leg seems to be more flexible than the α-leg, especially between EGF-1 and EGF-2 domain and, at the PSI/hybrid and hybrid/ I-EGF1 junctions (Figure 3c and 3d) as evidenced by crystal structures studies.[7, 18]

1.3. Role of divalent cations in integrin function

Several structural studies (crystallography, EM and NMR) have demonstrated that integrins exist in three conformational states: 1) bent conformation with closed headpiece, 2) extended conformation with closed headpiece and, 3) extended conformation with open headpiece corresponding to a low- (inactive), intermediate- (active), and high-affinity states (active with ligand bound), respectively (Figure 3c and 3d).[10-12, 26] The balance between these states is regulated by both local and global conformational rearrangements.[27] It is assumed that integrin activation occurs by a switchblade-like opening of the headpiece-tailpiece interface which moves the integrin ligand-binding headpiece away from the cell membrane.[22, 28]

Normally, integrins are in the equilibrium among these conformational states that can be shifted by internal or external stimuli, such as talin and kindlin proteins or extracellular metal ions.[27, 29] However, the concept that the extended-open integrin conformation corresponds to the conformation with high affinity remains controversial since it has been demonstrated that RGD ligand can bind the bent conformation of integrin $\alpha_v\beta_3$ and activate "inside-out" signalling without promoting integrin extension and headpiece opening.[30, 31]

Divalent cations are essential for integrin functions since they stabilize the structure in an active state modulating the ligand binding, in a positive or a negative way.[14, 32, 33] Removal of divalent cations using, for example, EDTA completely inhibits integrin-ligand binding. Physiologically, most integrins in the presence of a millimolar concentration of Ca^{2+} and Mg^{2+} appear to be in the resting state. Ca^{2+} ion has generally an inhibitory effect on integrin ligand binding, but its removal and the contemporary presence of Mg^{2+} have shown to promote the ligand binding. However, other studies have revealed a synergistic activation of the integrins in the presence of a micromolar concentration of Ca^{2+} with a suboptimal concentration of Mg^{2+}. Differently, Mn^{2+} ion can shift integrins into the active state with high affinity conformations even in the presence of a millimolar concentration of Ca^{2+}.[34]

1.3.1.   The αI-domain

The MIDAS site on the top face of the αI-domain physiologically binds Mg^{2+} which in turn is coordinated by five side chains from three different loops. The first, β1-α1 loop contains three coordinating residues in sequence, Asp-Xaa-Ser-Xaa-Ser (DXSXS), characteristic of the cation-binding site (Figure 4B and C). The second, α3-α4 loop and, the third β4-α5 loop, donate the other two coordinating residues by Thr and Asp, respectively (Figure 4B and C).[22] Structural studies of αI-domains in the presence/absence of ligand and with mutations that stabilize distinct affinity states, have provided a mechanistic understanding of conformational regulation during both priming and ligand binding.

The αI-domain has been crystallized in three conformations: closed, intermediate, and open.[21, 35] These conformations demonstrate distinct positioning of the α7-helix of β6-α7 loop along αI-domain of MIDAS metal ion coordination. In both, closed and open α_MI domain, the MIDAS metal ion shares the primary coordinating residues with Ser142, Ser144 and, the secondary coordinating residue with Asp140 of the β1-α1 loop (Figure 4B and C). In the closed conformation, Thr209 of the α3-α4 loop and Asp242 of the β4-α5 loop form indirect and direct

bonds to MIDAS metal ion, respectively; while three water molecules complete the coordination sphere (Figure 4B).[32] In the open structure, the metal ion moves of ~2.3 Å resulting in a slight change in its coordination: Thr209 now coordinates the MIDAS metal ion directly, whereas Asp242 is in the secondary coordination sphere (Figure 4A-C). Moreover, a Glu residue, contributed by the ligand, replaces one water molecule at the sixth metal ion coordination site (Figure 4C).[14]

Local changes in coordination at the MIDAS are associated with backbone movements of β1-α1 and β4-α5 loops which induces downward displacement of β6-α7 loop resulting in 7Å rearrangement of C-terminal α7-helix (Figure 4A). The axial displacement of the α7-helix represents a critical connection for the diffusion of conformational signals from the MIDAS of αI-domain to other integrin domains and vice versa.[12, 14] This is sufficient to priming the αI-domain into higher-affinity open states.[12, 22, 32]
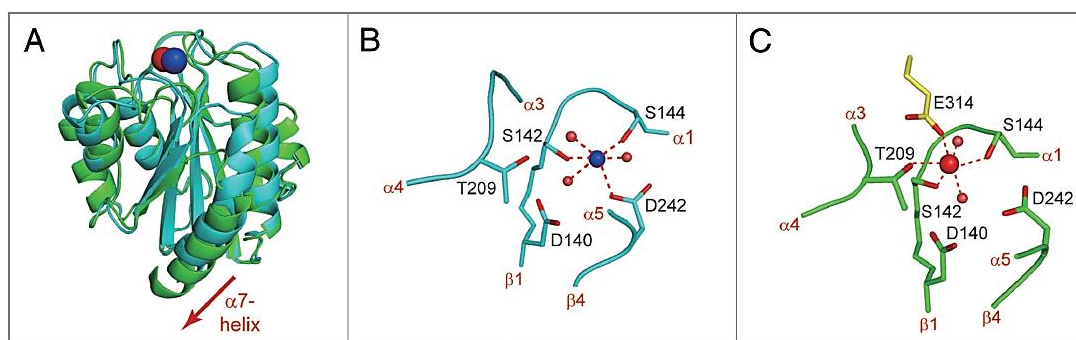
Figure 4. Structural rearrangements of αMI-domain within MIDAS. (A) Superposition of integrin αMI-domains in low-affinity (pdb1JLM, cyan) and high-affinity (pdb1IDO, green) conformations. Blue and red spheres denote the MIDAS metal ions in low- and high-affinity conformations, respectively. (B) αMI-domains MIDAS from closed (pdb1JLM) to (C) open (pdb1IDO). Metal ion coordination is shown in red dashed lines. Glu314 coordinates the Mg^{2+} into MIDAS and is shown in yellow. Blue and red spheres are Mn^{2+} and Mg^{2+}, respectively, and small red spheres are coordinating water-molecule oxygens (image adapted from Zhang *et. al.*).[14]

1.3.2. The βI-domain

As αI-domain, the βI-domain ligand binding site assumes a similar Rossmann-like fold with a central six-stranded β-sheet surrounded by eight helices. Unlike αI-domain has only one MIDAS site, the βI-domain contains three metal ion-binding sites linearly interconnected that are the heart of the ligand binding site in the β-subunits. The MIDAS site is located at the centre and it is flanked by the synergistic metal ion-binding site (SyMBS) and adjacent to MIDAS site (AdMIDAS) (Figure 5D-G).[11-14, 23] Electron density measurement revealed the presence of

Mg^{2+} ion at the MIDAS site and Ca^{2+} ion within the two flanking sites. In the transition from low- to high-affinity state, the C-terminal α7-helix of the βI-domain undergoes a similar downward movement of αI-domain which allosterically increases the ligand binding affinity. In addition, it is also coupled with the swing-out movement of the hybrid domain correlated to βI-domain.[27, 36]

➢ *βI-domain MIDAS*

Similarly to αI, the MIDAS βI-domain displays the conservative motif, Asp-Xaa-Ser-Xaa-Ser (DXSXS), crucial for coordinating the metal ion and consequently for ligand binding.[11] Geometrically, the $β_3$ MIDAS consists of the side chains of Asp119, Ser121, Ser123, Glu220 and Asp251 (Figure 5E-F). Mutations on this site completely remove ligand binding confirming their key role in the coordination of the metal ion which in turn is crucial for ligand binding in αI-containing and αI-less integrins.[12, 18] Crystal structures of $β_3$ integrins have revealed that during ligand binding the Asp carboxyl side chain of the RGD sequence, coordinates the Mg^{2+} within MIDAS in β subunit. The transition of βI-domain from low- to high-affinity state shows the movement of the β1-α1 loop with the consequent displacement of Asp251 to coordinate Ca^{2+} at the AdMIDAS that makes the MIDAS more electrophilic toward the acidic ligand residue (Figure 5E-F).[12, 13]

➢ *βI-domain AdMIDAS*

Located adjacent to MIDAS, the AdMIDAS represent a regulatory site responsible of integrin inhibition or activation, depending on which types of the divalent cation are bound: Ca^{2+} ion inhibits integrin activation while Mn^{2+} ion promotes activation. These two metal ions compete for the binding at this site. In the bent conformation, the not optimal orientation of the binding site prevents the binding of endo- or exogenous ligands. However, integrins in the bent conformation can bind ligands, as previously shown by soaking an RGD ligand-mimetic peptide into preformed crystals.[22] In the unliganded low-affinity conformation of $β_3$ integrin, the AdMIDAS Ca^{2+} coordinates the carbonyl oxygen of Met335 in β6-α7 loop (Figure 5E).[13] Consequently, the downward movement of βI-domain α7-helix is blocked and the integrins are stabilized in the low-affinity-closed conformation. By contrast, in the high-affinity liganded-open $β_3$ I-domain, the Met335 coordination breakage is followed by the downward displacement of α7-helix of β1-α1 loop with formation of a new coordination between the AdMIDAS ion and the carboxyl side-chain of the Asp251 (Figure 5F).[12] Loss of the Met335

carbonyl coordination and enhancement of affinity for ligand is favoured by substitution of Ca^{2+} with Mn^{2+} ion.[37] However, mutagenesis studies on $\alpha_4\beta_7$ and $\alpha_L\beta_2$ integrins that mediate both rolling and firm cell-adhesion, revealed that removal of metal ion occupancy at the AdMIDAS site induced integrin activation.[24, 38, 39] Whereas for $\alpha_5\beta_1$, $\alpha_2\beta_1$ and $\alpha_{IIb}\beta_3$ integrins that mediate only firm cell adhesion upon activation, AdMIDAS mutations decreased ligand binding.[20, 40] This can be explained by the presence in β_2 and β_7 of an Asp residue close to Asp242 residue instead of an Ala residue in β_1 and β_3 integrins. The additional Asp (Asp243) in β_2 coordinates the neighbouring MIDAS in the low-affinity state making it more negative than that of β_3 and β_1 (Figure 5G).[9] During integrin activation, the movement of Asp243 in β_2 to the AdMIDAS along with the frontal Asp242, will reduce the negativity of MIDAS and lead to higher affinity for ligands. AdMIDAS mutations suppress the allosteric conformational changes and the outside-in signalling of integrins.[40] Thus, AdMIDAS plays a key role in the transmission of the integrin conformational changes from βI-domain to the hybrid domain through the interaction of Met335 (in β_3) of the $\beta6$-$\alpha7$ loop.[14]

➢ *βI-domain SyMBS*

SyMBS is a Ca^{2+}-binding site with a positive regulatory effect for integrin-ligand binding. Mutations at this site cancel ligand binding in $\alpha_2\beta_1$, $\alpha_5\beta_1$, $\alpha_{IIb}\beta_3$, $\alpha_L\beta_2$ integrins and, promotes the shifting from high- to low-affinity state of $\alpha_4\beta_7$ integrin, thus, demonstrate that integrin activation is dependent on the occupancy of metal ion at SyMBS.[14, 41] In addition, further cation-π interaction with a conserved aromatic residue (Tyr or Phe) at the specificity-determining loop (SDL) (Figure 5E-G) contributes to stabilize the SyMBS metal ion coordination and, maintain a suitable SDL conformation. Removal of this interaction involves a dramatic reduction of $\alpha_4\beta_7$-MAdCAM-1 affinity binding.[42] As mentioned above, low concentration of Ca^{2+} together with a suboptimal concentration of Mg^{2+} have a synergistic effect in helping ligand binding since, Ca^{2+} at SyMBS may facilitate the specific orientation of the shared Glu carboxylic side chain in $\beta3$ subunit, which in turn stabilizes MIDAS Mg^{2+} occupancy (Figure 5F).[13]
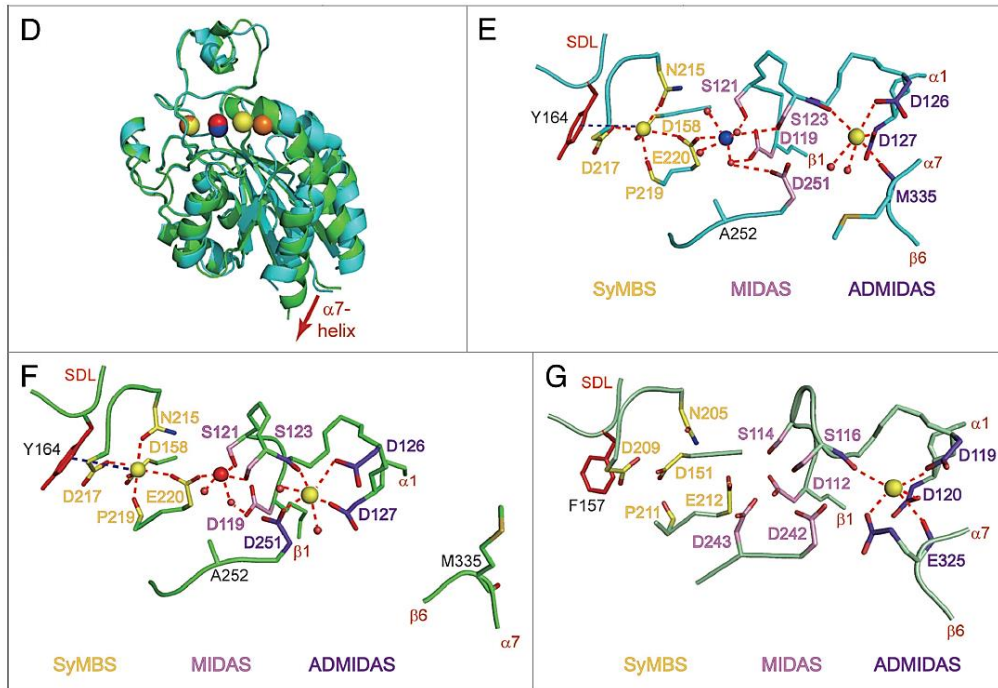
Figure 5. (D) Superposition of βI-domain of integrin $\alpha_{IIb}\beta_3$ in low-affinity (pdb3FCS, cyan) and high-affinity (pdb3FCU, green) conformations. Blue and red spheres denote Mg^{2+} in low- and high-affinity MIDAS, respectively. Orange and yellow spheres denote Ca^{2+} in low- and high-affinity βI-domains, respectively. (E) Structure of low affinity (pdb3FCS) and (F) high-affinity (pdb3FCU) β3 metal ion-binding sites. (G) Structure of metal ion-binding sites in low-affinity β2 (pdb3K6S) (image adapted from Zhang *et. al.*).[14]

1.4. Integrin signalling

Most integrins are present on the cell surface in an inactive conformation with low affinity for their endogenous ligands. However, they undergo rapid activation upon various stimuli.[15, 29] Integrins are unique bidirectional signalling receptors that connect extra- with intracellular environment. In "outside-in" signalling, ligand binding activates intracellular signalling pathways. [43, 44] On the other hand, in "inside-out" signalling, signals received from the inside activate intracellular signalling pathways that affect the integrin cytoplasmatic domains and make the ectodomain capable of ligand binding.[27] Upon "outside-in" or "inside-out" signalling activation, integrins regulate important functions including cell adhesion, migration, growth, and differentiation.[22, 45] The ability of integrins to bind and associate with various components of the ECM or soluble ligands largely depends on the structural conformations of the two subunits and, distinct conformations are crucial for regulating both "inside-out" and "outside-in" cell signalling.[31, 46]

1.4.1. "Inside-out" signalling

As already mentioned, many structural studies suggested the presence at least of two major conformational states of the α- and β-extracellular domain corresponding to a bent (closed) and an extended (open) form.[11] Integrins are inactive when the extracellular domain is folded as V-shape with the ligand-binding headpiece facing the membrane and the cytoplasmic tails are closely juxtaposed by charge-charge interaction (Figure 6); while they become active and highly adhesive toward its ligand when the extracellular domain is extended and the tails are separate.[22, 26, 47] The bent conformation is stabilized by interactions between the transmembrane domains (TMD) of the α- and the β-subunit. TMDs have usually about 20 hydrophobic amino acids and it is proceeded by a positively charged residue, Arg or Lys. The membrane-proximal region of most integrin α subunits contains a Gly-Phe-Phe-Lys-Arg (GFFKR) motif that is highly conserved among the species, while the integrin β subunits contain more hydrophobic residues than the α subunits.
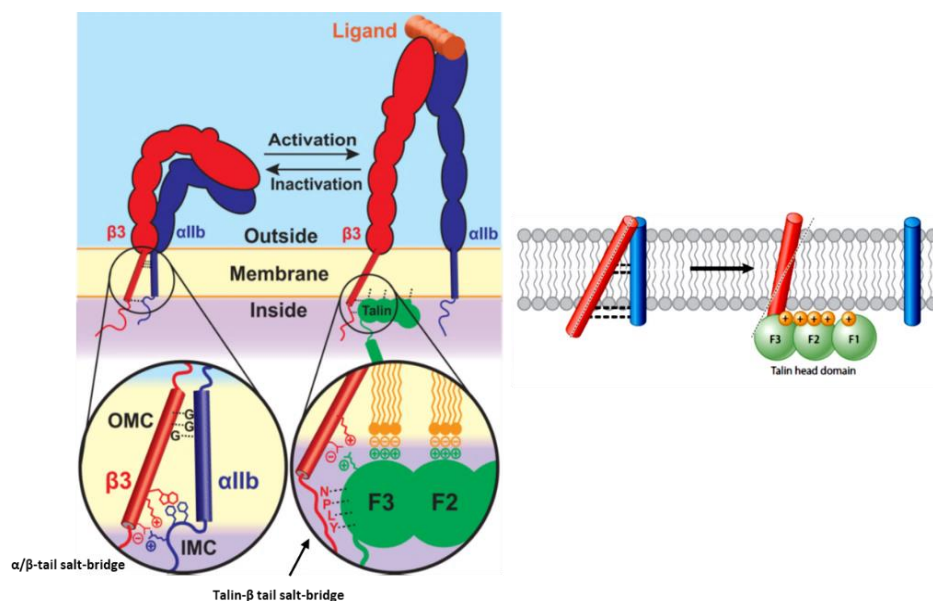
Figure 6. "Inside-out" integrin signalling. Talin binding to the β cytoplasmic tail is followed by talin-membrane lipid interaction, through the basic residues (yellow spheres), leading to changes of the tilt angle. F1, F2, and F3 (green) are subdomains of the FERM (band 4.1, ezrin, radixin, and moesin) domain contained in the talin head domain (image source: Iwamoto *et. al.*).[48]

The connection between the TMDs is mediated by two clasp-like binding interfaces: the outer membrane clasp (OMC) made by glycine packing interactions between both α- and β-TMDs and, the inner membrane clasp (IMC) which results from stacking of hydrophobic residues at the cytoplasmic end induced by GFFKR motif, enabling the formation of an

α_{IIb}(D723)/β_3(R995) salt bridge (Figure 6).[48, 49] Both OMC and IMC permits an interaction that stabilizes the low-affinity state of the integrin and, breakage of these clasps is crucial for integrin activation. The breakup can be mediated either by intracellular signals ("inside-out" activation) or extracellular ligand binding ("outside-in" activation) that stabilizes the active conformation (Figure 6).[50]

> **Talin: an essential mediator of integrin activation**

Talin is a 270 kDa cytoplasmic protein, composed by 50 kDa N-terminal head domain and 220 kDa C-terminal rod domain.[51] The talin head domain contains a FERM domain, (band 4.1, Ezrin, Radixin, and Moesin homology domain) further divided into F1, F2, F3 and non-homologous F0 subdomains (Figure 7).[52] The F3 subdomain contains a PTB (phospho-tyrosine binding) domain that binds to the conserved membrane-proximal NPxY motif of the β cytoplasmic tail.[53, 54] It has been proposed that the binding of talin is controlled by phosphorylation of the NPxY tyrosine residue and thereby acts as a regulatory switch.[55] Indeed, binding of talin F3 domain to β-tails promotes breaking of the inhibitory salt bridge between the α- and β-tail of TMDs and, consequently a new salt bridge between F3 and a Lys residue of the β-tail is formed (Figure 6 and 7).[56, 57]

This reorients the TMD β-subunits and disengages the inhibitory clasps leading to conformational changes in the integrin extracellular domains with increases of ligand binding affinity (Figure 7).[48, 50] Therefore, when talin is bound to β integrins it works mainly as a structural adaptor that interacts with the actin cytoskeleton. The talin rod domain contains multiple binding sites for actin, vinculin and an autoinhibitory binding site. Indeed, talin generally exists in an autoinhibited head-tail conformation that can be rapidly released by calpain-mediated proteolysis or by binding of phosphatidylinositol (4,5)-bisphosphate to initiate signalling integrin activation (Figure 7).[58]

> **Kindlins: critical regulators of integrin activation**

Kindlin is another FERM domain-containing protein important for integrin activation. In mammals there are three types of kindlin proteins: kindlin-1, kindlin-2, and kindlin-3.[54] Kindlins are highly conserved in animals and, defects or mutations on these family members can cause serious diseases. Unlike talin strongly binds to the membrane proximal region of the

β-tail, kindlin F3 domain interacts with the membrane distal NxxY motif.[59] Although the detailed mechanisms of integrin activation remain uncertain, it is clear that kindlins cooperate with talin during integrin activation and, a direct interaction of kindlin with the β-integrin tail is required, but apparently not sufficient, for integrin activation. They are mainly responsible for integrin clustering rather than directly promoting conformational integrin activation (Figure 7 and 8).[50, 57, 60]
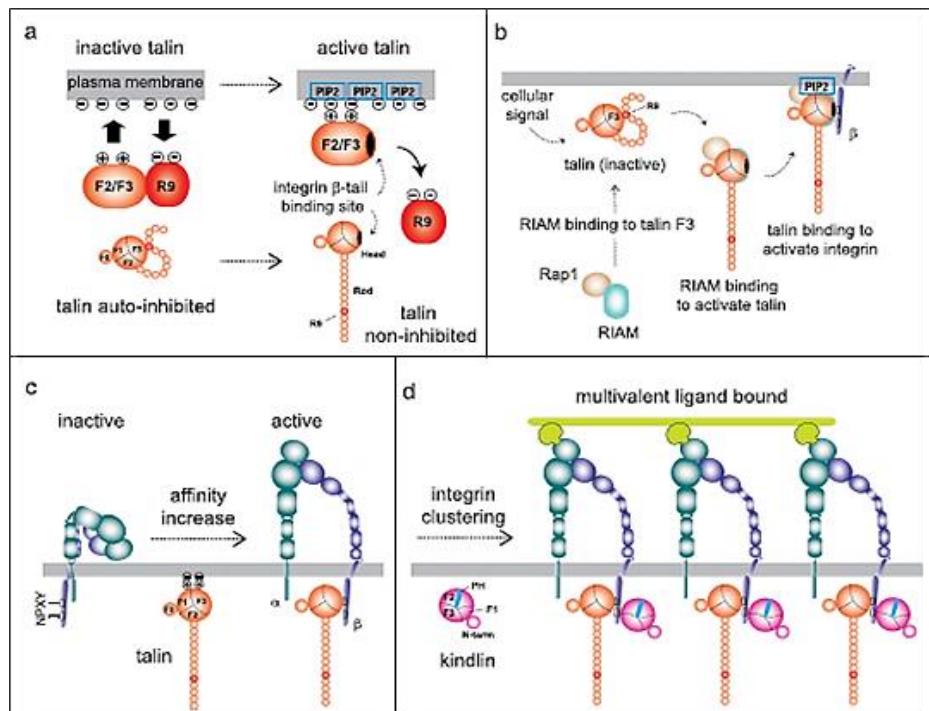
Figure 7. Integrin activator talin and co-activator kindlin. (a) The auto-inhibition of talin is release either by phosphorylation or partial proteolysis. (b) Recruitment of talin to integrin is mediated by binding Rap1-RIAM complex. (c) Binding of talin to the integrin triggers the dissociation of the α/β integrin cytoplasmic domains, thereby inducing active extended conformation. (d) Kindlin acts as a co-activator to stabilize integrin-mediated cell adhesion that involves multivalent ligand binding (image source: Park *et. al.*).[61]

> ➤ **Inhibitors of talin-integrin interactions**

In addition to integrin activators, there are also inhibitory proteins such as filamin, integrin cytoplasmic-domain-associated protein 1 (ICAP-1) etc., that compete with talin for integrin β cytoplasmic tail binding, therefore, they presumably inhibit integrin activation in this way.[62] Filamin is one of the best characterized which shares an overlapping binding region with talin for the integrin β-tail, thus, the competition for the same binding site can promote inactivation by displacement of the talin. Moreover, filamin competes also with kindlin for the same integrin

β-tail binding.[63] Another well-characterized integrin inhibitor is ICAP-1 which binds kindlin-binding NPxY motif in the membrane-distal of β$_1$ integrins through its PTB-domain but inhibits also the binding of talin to the integrin tail.[64] Integrin-talin interactions may also be inhibited by overexpression of other proteins like SHARPIN (SHANK-associated RH domain-interacting protein) although the detailed mechanism is still unknown.[65, 66]
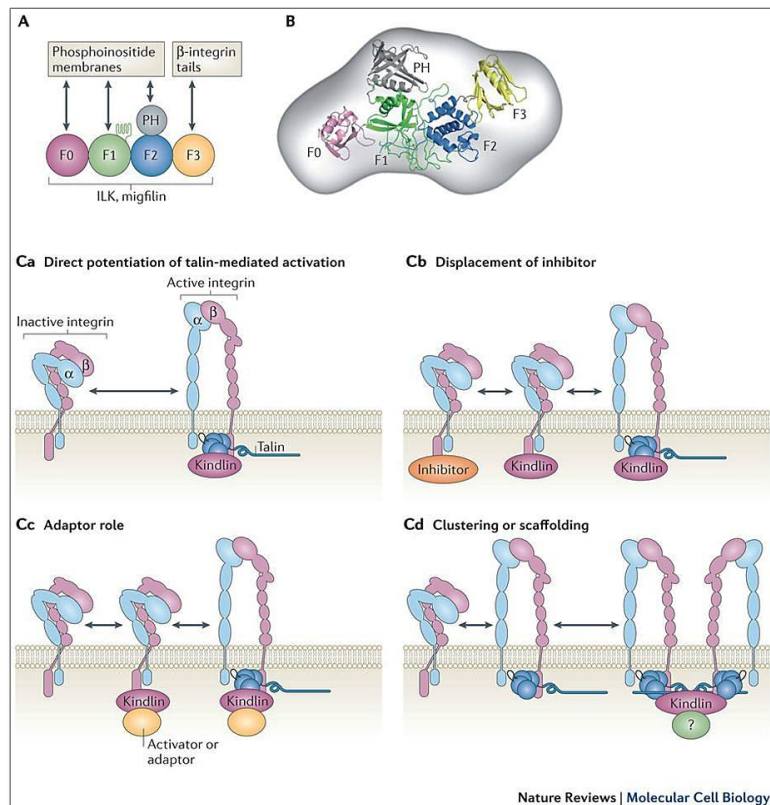
Figure 8. Kindlin integrin coactivator. (A) Schematic representation of kindlin domain organization and interaction binding partners. (B) Kindlin orientation structure based on X-ray and NMR studies. (C) Hypothetical models for cooperation between talin and kindlin during integrin activation. Kindlin directly potentiates talin-mediated integrin activation (Ca) by binding both the β-integrin tail and the membrane optimizing the exposure of the talin-binding site. Kindlin binding displaces inhibitors, facilitating talin binding and activation (Cb). Recruitment of other activating or adaptor proteins that cooperate with talin to activate integrins (Cc). Direct or indirect (via another kindlin-binding protein; indicated by the question mark) clustering induced by kindlin results in enhancement of talin-mediated integrin avidity (Cd) (image source: Calderwood *et. al.*).[50]

1.4.2. "Outside-in" signalling

Physiologically, integrins are in bent conformation and only a fraction adopts an extended conformation with high affinity for their ligands. The stabilization of the high-affinity state occurs after inside-out activation and increases the ligand-binding valency or avidity

(clustering) to the ECM. Through tight attachment to the cytoskeleton, the integrin clusters not only provide stable connections between cells and ECM but also transfer extracellular information within the cytoplasm that culminate in the recruitment of effectors to the cytoplasmatic tails. Extracellular ligand-bound integrins induce dramatic changes in the organization of the cytoskeleton which activate a variety of complexes intracellular pathways, termed focal adhesions, that regulate the cell fate.[43, 67] Both, lateral association (clustering) of integrin heterodimers and conformational changes of the receptors are required for conveying outside-in signals.[9, 22, 68] Although many elements of the outside-in signalling network have been identified, it is still unclear how the clustering of integrins and the binding of ECM proteins triggers the signalling activation.
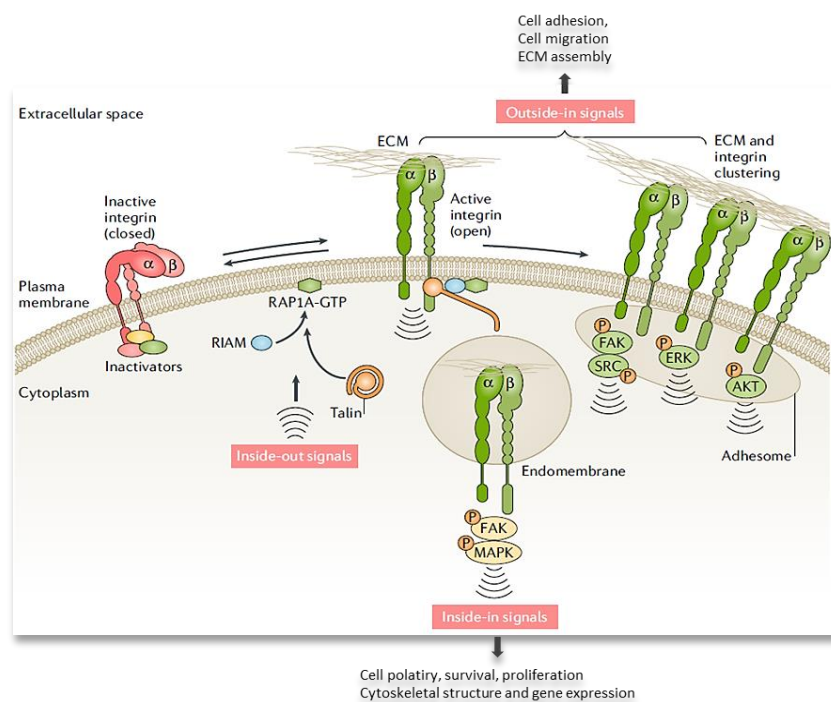
Figure 9. "Inside-out" and "outside-in" integrin signalling (image source: Hamidi *et. al.*).[69]

The discovery that cell adhesion and integrin clustering activate the tyrosine phosphorylation via focal adhesion kinase (FAK) activation was a key step for understanding the function of integrins.[70] Indeed, the FAK recruitment to the integrin cytoplasmic tail constitutes the early event in outside-in signalling.[71] FAK is a tyrosine-kinase protein important for adhesion, Rho-family GTPase activation, cell migration and cross-talk between growth-factor signalling and integrins.[44, 72] It is composed by an N-terminal FERM domain, a central catalytic domain, a proline-rich domain and a C-terminal focal-adhesion-targeting domain (FAT) that binds to

paxillin[73] and talin.[74] At resting state, FAK is inhibited by self-interaction of the FERM domain with its catalytic domain that blocks the accessibility of the substrate.[75] Schaller *et. al.* have demonstrated that the interaction between FAK-FERM-domain and integrin β-tail causes the shift of the FERM domain from its catalytic domain allowing the suppression of its autoinhibition.[76] This prompts FAK activation by autophosphorylation of Try397 residue and concomitant Src activation, which in turn, further phosphorylates FAK by promoting its kinase activity and interaction with other proteins. The Src tyrosine-kinase proteins (SFKs) control cell spreading.[77] They can bind directly to the β-integrin tails contributing to the reinforcement of the initial integrin-mediated adhesions by activating downstream kinases and adaptors.[67, 78] SFKs also bind to phosphorylate FAK and FAK-binding proteins. Integrin adhesion also activates, among other pathways, the RAS–MAPK and PI3K–AKT signalling nodes. In addition, responds to "inside-out" signals, whereby stimulation of small GTPase RAP1A activity on the plasma membrane triggers recruitment of RAP1-GTP-interacting adaptor molecule (RIAM) to activate talin. The latter binds to the integrin β-tail triggering an extended open receptor conformation and recruitment of additional integrin-activating proteins such as kindlins, paxillin and vinculin and thereby spreading the activation signals (Figure 9).[15] Meanwhile, integrin activation is counterbalanced by inactivating proteins such as ICAP-1, filamin and SHARPIN which, directly or indirectly, limit the ability of talin to bind and activate "inside-out" signal.[62, 66]

1.5. Role of integrins in cancer progression

As previously mentioned, integrins are bidirectional signalling receptors that respond to external signals ("outside-in" signalling) and in parallel, transduce internal signals to the matrix ("inside-out" signalling), thus playing a crucial role in cell-cell and ECM communication.[2] The involvement in both, physiological (e.g. cell migration, proliferation, survival, and apoptosis) and pathological processes (e.g. tumor invasion, metastasis), identified this family of adhesion receptors as validated drug targets, thereby opening the way for the development of specific integrin sub-type antagonists.

During the past decades has been widely demonstrated that integrins are involved in every stage of tumorigenesis and cancer progression including cancer initiation and proliferation, local invasion and intravasation into vasculature, survival of circulating tumour cells, extravasation into the secondary site and metastatic colonization of the new tissue, ECM

remodelling, angiogenesis, tumor growth and apoptosis resistance (Figure 10).[69] Among these, the $\alpha_v\beta_3$ $\alpha_v\beta_5$ and $\alpha_5\beta_1$ integrin subtypes represent a well-established tumor-associated receptors intensively studied in oncology field. To date, most efforts have been devoted to the development of small molecules targeting the $\alpha_v\beta_3$, $\alpha_v\beta_5$, $\alpha_5\beta_1$ integrins implicated in cancer, albeit no integrin-based anticancer drugs have been approved yet.
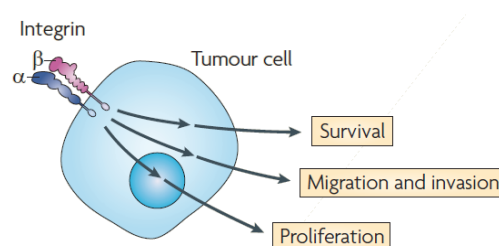
Figure 10. Integrins and their different functions in cancer cells (image source: Desgrosellier *et. al.*)[79]

Integrin $\alpha_v\beta_3$ interacts with several tyrosine kinase receptors (RTKs), including the receptors for epidermal growth factor (EGF), platelet-derived growth factor (PDGF), insulin and vascular endothelial growth factor (VEGF) establishing a complex "cross-talk" networks that control the behaviour of the endothelial cells, thus, making $\alpha_v\beta_3$ integrin a principal marker of angiogenesis.[79, 80] Angiogenesis is the process of formation of new blood vessels from pre-existing ones for the transport of vital nutrients and oxygen which are fundamental not only for physiological processes (*e.g.,* fetal development, ovulation, wound healing, growth, tissue remodelling) but also for survival and growth of tumor masses.[81]

Moreover, $\alpha_v\beta_3$ is capable to recruit and activate specific extracellular proteases (*i.e.,* MMP2 and plasmin) that promote the ECM degradation and remodelling, key processes for tumor invasion and metastasis.[82] As a matter of fact, $\alpha_v\beta_3$ integrin has been found widely overexpressed on the blood vessel of a variety of solid tumors and in the majority of cancer cells (*e.g.,* melanoma, breast cancer, glioblastoma, pancreatic tumor, cervical and prostate carcinoma) but not on healthy tissues. For this reason, $\alpha_v\beta_3$ has long been considered and investigated as a pharmacological target for antitumor applications.[79, 83]

1.5.1. RGD integrin ligands

In 1984 Ruoslahti and coworkers discovered the tripeptide sequence Arg-Gly-Asp (RGD, Figure 11) as minimal recognition motif of many natural ligands (fibrinogen, fibronectin, vitronectin, plasminogen, laminin, MMP-2, etc.) that bind the $\alpha_V\beta_3$ integrin receptor, essential in cell adhesion.[84]
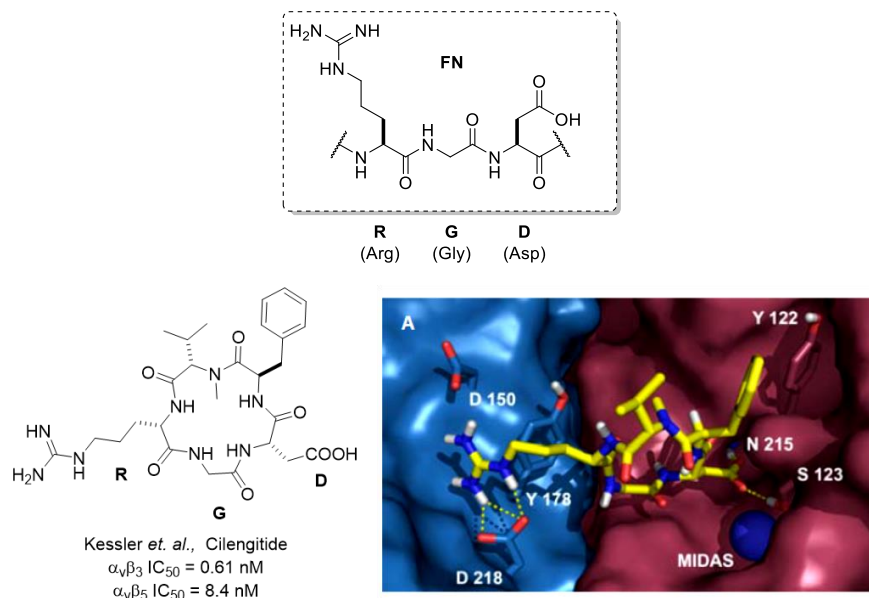
Figure 11: RGD sequence and molecular structure of the potent Cilengitide, *c*[RGDf-*N*(Me)V]. Crystal structure of integrin $\alpha_V\beta_3$ in complex with Cilengitide (PDB ID: 1L5G).[12] Image adapted from[85].

However, the comprehension of the interactions between the RGD and $\alpha_V\beta_3$ was possible only in 2002, when Xiong and coworkers [12] reported the crystal structure of the extracellular segment of the $\alpha_V\beta_3$ integrin receptor cocrystallized with the integrin binder Cilengitide (Figure 11). This cyclic RGD pentapeptide was developed by Kessler *et al*. [86] and represents an important milestone in this field. Cilengitide showed a highly potent antagonistic activity and selectivity towards integrins $\alpha_V\beta_3$ and $\alpha_V\beta_5$ (Figure 11), therefore, it was clinically tested for the treatment of glioblastoma and other tumor forms. Unfortunately, its use as anticancer agent was discontinued in Phase III clinical trials due to atypical "pro-angiogenic" behaviour at low concentrations (acts as an agonist), while at high concentration suppresses the angiogenesis (acts as an antagonist).[87] The crystal structure provided the structural rationale of its high affinity, in particular, it showed an extended conformation of the RGD sequence in the binding pocket with a 9Å distance between the Cβ atoms of the Arg and Asp residues: this folding

allows the Arg side chain to interact with two anionic aspartic acid residues (Asp218 and Asp150) in the α-subunit, whereas the Asp binds to Asn and Ser residues and to a divalent metal cation in MIDAS region of the β-subunit.[88] The Gly residue at the interface between both subunits presents weak hydrophobic interactions with the carbonyl group of Arg216, same than the aromatic group of the ligand with Tyr122 (Figure 11).[12, 88] All these integrin-ligand interactions suggested the structural requirements that were considered as a starting point for the development of synthetic $\alpha_V\beta_3$ integrin ligands with high affinity.

Over the last decades, following these key structural requirements, the research has been focused on the development of RGD-bearing peptide/peptidomimetic and semi-peptidic ligands of $\alpha_V\beta_3$ integrin.[89] Many synthetic strategies have been applied to improve the biological and pharmacokinetic properties (*e.g.*, affinity, selectivity, metabolic stability, optimal biodistribution) of the RGD native sequence, including the introduction of unnatural amino acids flanking the RGD sequence, cyclization,[90] variation of stereochemical configuration of the constituent amino acids [91] and N-methylation [92] that allowed to identify a large number of linear and cyclic RGD-bearing compounds.

In this context cyclic compound, in which the RGD motif is properly constrained by macrocyclization, are viewed as useful templates for the discovery of lead compounds. The introduction of rigid turn-inducing motif, usually mimetic of natural amino acids or constrained scaffolds (heterocycles), generate appropriate folding in the templates that favour the matching within the integrin pocket, thereby increases the receptor affinity. To date, several RGD-based cyclic peptides with high affinity and selectivity have been reported in the literature over the years and some examples are shown in Figure 12.

Despite the expectations, the $\alpha_V\beta_3/\alpha_V\beta_5$ integrin binders originally designed as antiangiogenic agents to be directly used for cancer treatment have generally had unsuccessful results in clinical trials and most of them are still under clinical evaluation. However, the ability of these compounds to selectively recognize tumor-overexpressed integrins has attracted great interest in tumor therapy. In this regard, RGD-based integrin ligands have been widely investigated for the development of drug delivery systems to selectively target the tumor cells[93] overexpressing the $\alpha_V\beta_3$ receptor and release the cytotoxic agents specifically within the cell after internalization *via* receptor-mediated endocytosis,[94-96] but also to selectively deliver liposomes,[97] nanoparticles,[98] and for imaging application.[99, 100] (An extended review about RGD conjugates used in drug delivery and theranostics can be found in references).[6, 93, 94, 101, 102]
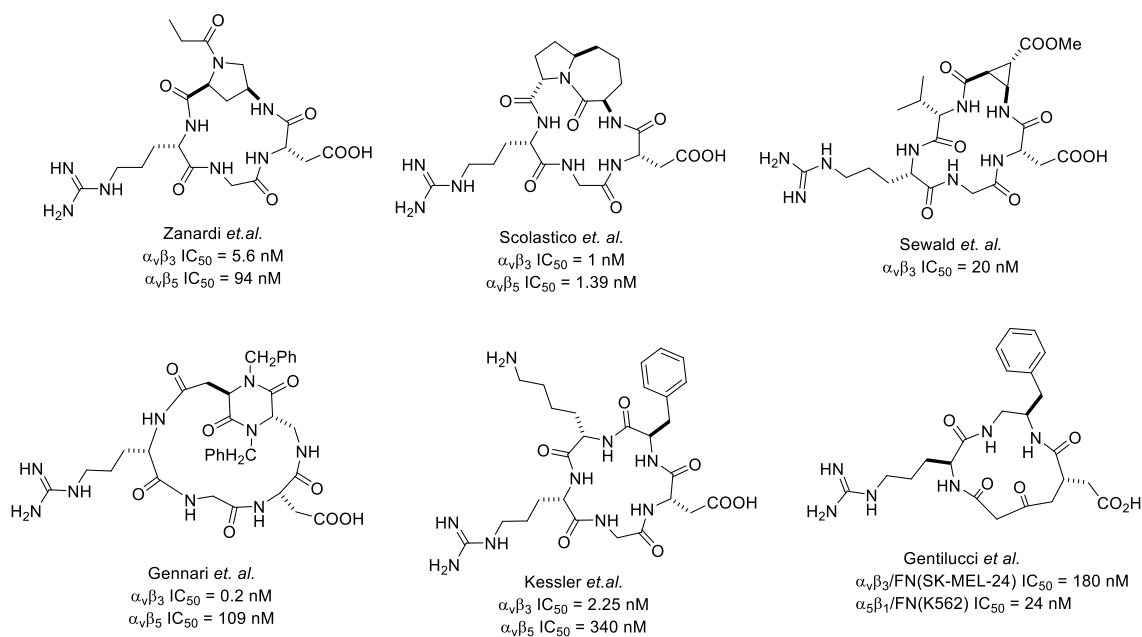
Figure 12. Examples of integrin ligands and relative integrin affinity expressed as IC_{50} value.[103, 104]

1.6.   Role of integrins in inflammatory responses

Inflammation is a reaction of the immune system against injury, infection, or antigenic stimulation occurred in the host and, it is characterized by local accumulation of blood leukocytes, plasma protein and fluids at the extravascular site of the trauma.[105] If the initiating events are not resolved and the condition becomes chronic, there can be sustained extravasation of lymphocytes that can exacerbate the inflammatory condition, which in turn will continue to recruit more inflammatory cells resulting in unwanted tissue destruction.[106] Correct homing of leukocytes at the sites of infection/tissue damaged is a fundamental prerequisite for the development of a normal immune response. These processes engage a well-regulated series of events that normally involves cytokines, chemokines and cell adhesion molecules (CAMs), therefore, it is easily assumed that deregulation of these fine-regulated physiological events is at the base of the development of many chronic inflammatory diseases including asthma, multiple sclerosis (MS), rheumatoid arthritis (RA), inflammatory bowel disease (IBD), Crohn's disease (CD), ulcerative colitis (UC), allergic conjunctivitis and psoriasis.

Integrin adhesion receptors, specifically the α_4- and β_2- integrin subtypes, play an essential role in leukocyte trafficking and each phase of the immunosurveillance, since, they are constitutively expressed on most leukocyte cell types including B- and T-lymphocytes,

eosinophils, monocytes, mast cells and basophils, but not on neutrophils.[107] The natural ligands of integrin $\alpha_4\beta_1$ (VLA-4, very late activating antigen-4 or CD49d) include the vascular cell adhesion molecule-1 (VCAM-1) expressed on cytokine-stimulated endothelial cells,[108, 109] the fibronectin (FN) expressed on the ECM,[110-112] and the junctional adhesion molecule-2 (JAM-2) expressed at cell-cell junctions on endothelial cells.[113] VLA-4 binds the ligands VCAM-1 and FN through the minimal tripeptide sequence Ile-Asp-Ser (IDS)[114] and Leu-Asp-Val (LDV),[110] respectively (Figure 14). Moreover, VLA-4 can also bind by the same minimal epitopes of VCAM-1, the mucosal addressin cell adhesion molecule-1 ligand (MAdCAM-1)[115] mainly expressed on the gut, although the interaction is significantly weaker.[116] Indeed, MAdCAM-1 is the primary ligand of the $\alpha_4\beta_7$ heterodimer which is recognized by the tripeptide sequence Leu-Asp-Thr (LDT, Figure 14). This ligand is involved in the homing of lymphocytes to the gastrointestinal tract, thereby is correlated to inflammatory pathologies of this body district.[117] Both α_4 integrins ($\alpha_4\beta_1$ and $\alpha_4\beta_7$) interact with the alternatively spliced connecting segment-1 (CS-1) domain of the plasma FN.[112] On the endothelial surface there are also expressed immunoglobulin super family (IgSF) ligands, namely the intercellular adhesion molecules (ICAM-1 to -5) which specifically bind to β_2 integrins, $\alpha_L\beta_2$ (LFA-1) and $\alpha_M\beta_2$ (Mac-1).[105, 118]

1.6.1. Leukocytes recruitment: "tethering and rolling"

During an inflammatory response, the recruitment and extravasation of the leukocytes into inflamed tissue occurs in a well-defined cascade of events that include tethering, rolling, firm adhesion, and transmigration. During these steps, different integrins on different leukocyte cell-types undergo "inside-out" and "outside-in" activation (Figure 13).[107]

➢ *Tethering and rolling*

Normally, leukocytes circulate in the bloodstream as non-adherent cells with integrins in a low-affinity state to avoid undesired adhesion that could lead to pathological conditions. During an immune response, leukocytes are attracted by inflammatory chemokines secreted by the damaged tissue.[119, 120] At an early stage, the leukocyte rolling along the blood vessel wall is regulated by low-affinity interactions mediated by E- and P-selectin receptors present on the endothelial surface.[121] Stimulated by these interactions and by proinflammatory chemokines, integrins undergo a shift from an intermediate- to an high-affinity conformation via "inside-

out" signalling that leads to the general reduction of the leukocyte's velocity in the bloodstream (Figure 13).[38]

➢ *Firm adhesion*

During the rolling, the inflammatory signals presented by the endothelial cells at the sites of inflammation prompt the arrest of lymphocytes. Binding of chemokines to leukocyte's GPCRs promotes the switch of its VLA-4 to an extended high-affinity conformation. Thus, activated VLA-4 adhere more strongly to their counter-ligand resulting in a firm attachment and arrest of rolling cells on the endothelial surface.[122] The leukocyte arrest occurs in correspondence of the high density of cell adhesion molecules, VCAM-1 and ICAM-1 (Figure 13), whereby are overexpressed in response to the local release of inflammatory cytokines, chemokines, tumor necrosis factor alpha (TNFa) and interleukin-1 (IL-1) from the adjacent endothelial cells. Integrin "clustering" at the leukocyte/endothelial interface is stimulated by lateral movement of integrins along the cell surface in direction of the site of endothelial ligand presentation. The resulting increases in avidity may be crucial to trigger outside-in signalling and promote post-adhesion strengthening.
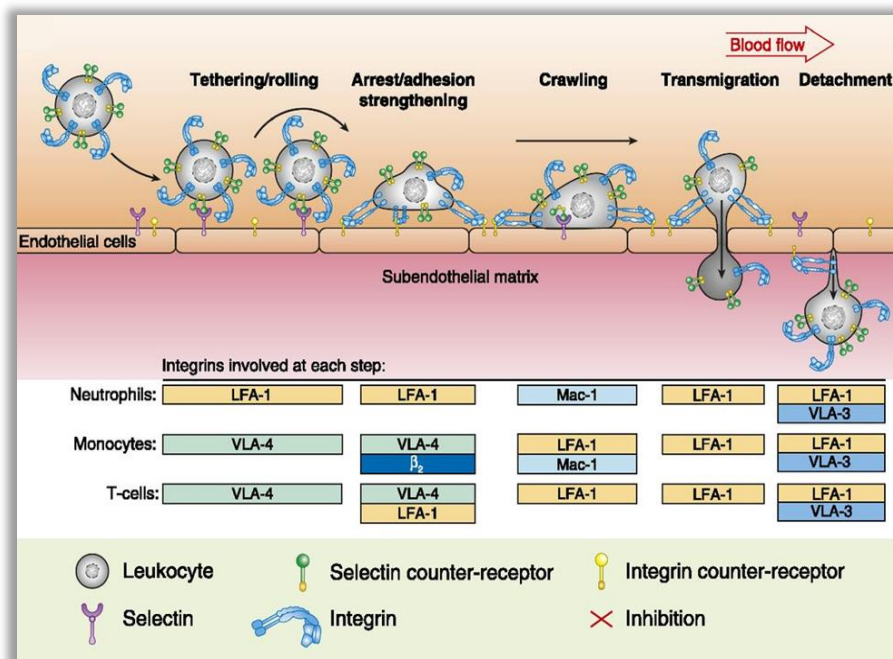
Figure 13. Role of integrin VLA-4 in leukocyte recruitment and trafficking: tethering and rolling mechanism (image adapted from Herter *et. al.*)[107]

> *Transmigration and detachment*

The tight binding of integrin to ligands ICAM-1 and VCAM-1, induces a rapid cytoskeletal rearrangement on the bound leukocytes and subsequent migration within the inflamed site through the endothelial tight junctions (diapedesis). Activated endothelium forms ring-like membrane structures enriched with ICAM-1 and VCAM-1 that are maintained for the duration of transmigration (Figure 13).[123] The transmigration process requires a dynamic balance of cellular adhesiveness that is achieved not only by integrin activation but also by well-regulated integrin deactivation.[61, 124, 125] In this scenario, if the infection or inflammation is not resolved there can be exaggerated extravasation of lymphocytes capable to worsen the pathological condition resulting in systemic tissue damage that finally leads to the development of chronic inflammation. This harmful process is at the basis of many inflammatory diseases. Noteworthy, the overexpression of the ligands ICAM-1 and VCAM-1 on the endothelial surface at the site of inflammation represents a clear marker for many chronic inflammatory autoimmune diseases such as RA, MS, CD and IBD, and contribute directly to their development. Furthermore, it has been demonstrated a pivotal role of $\alpha_4\beta_1$ integrin in tumor angiogenesis associated with chronic inflammation, because it is also involved in the recruitment of multipotent bone marrow stem cells, suggesting that this condition may promote the positive angiogenetic switch in tumors. Consequently, integrin $\alpha_4\beta_1$ can be also considered a marker of the metastatic risk.[126]

In light of this, $\alpha_4\beta_1$ and $\alpha_4\beta_7$ integrin antagonists, capable to inhibit the adhesion of leukocytes to their ligands, represent a new approach for the treatment of tumors and autoimmune diseases. To this purpose, several $\alpha_4\beta_1$ and $\alpha_4\beta_7$ antagonists including monoclonal antibodies (mAbs), peptidic and non-peptidic small-molecules have been developed.[79, 106, 127-129] However, integrin agonists could also have benefits in the blockade of the leukocyte's extravasation, since the stronger upstream adhesion should prevent the normal cell migration processes within the inflamed tissue, therefore opening novel opportunities for therapeutics.[130, 131]

Due to their high target selectivity, mAbs have gained great success in therapeutic application and to date, represent the most investigated approaches in literature. Currently, two mAbs have reached market approval: Natalizumab, a $\alpha_4\beta_1$ and $\alpha_4\beta_7$ integrins antagonist, approved for the treatment of MS and UC [132] although cases of progressive multifocal encephalopathy (PML) as a fatal adverse effect have been observed;[133] Vedolizumab, a $\alpha_4\beta_7$ antagonist approved for the treatment UC and CD.[134] On the other hand, significant drawbacks,

such as long circulation time and poor diffusion in the tissues, high manufacturing costs and the immunogenicity have prompted many researchers to find valuable alternatives. A large number of peptides and organic small-molecules have been reported in literature, even though they are under clinical investigation, hence, still far from marketing approval.

Small molecules that selectively bind to $\alpha_4\beta_1$ or $\alpha_4\beta_7$ integrins have been designed on the basis of the tripeptide recognition epitopes LDV, IDS and LDT, found in the respective binding sites of the ECM ligands FN, VCAM-1 and MAdCAM (Figure 14). These sequences share a highly conserved aspartic acid residue in the central position, as well as the RGD motif previously mentioned (Figure 11) that is essential to coordinate the MIDAS metal ion (Mg^{2+}, Mn^{2+}) in the β-subunit. Certainly, these sequences have represented the starting point for the design of small-molecule antagonists.[106, 127, 135]
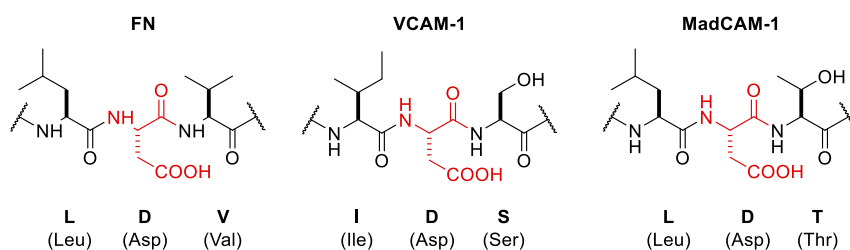
Figure 14. The LDV, IDS and LDT peptide sequences

Despite the crystal structures of ligand-receptor complex is still lacking, deduction based on homology models, [125, 136] MD, QSAR studies on small library of LDV mimicking ligands [137] and docking studies, [138, 139] have suggested that a hypothetical $\alpha_4\beta_1$ ligand should have, as general structural features, a carboxyl moiety mimicking the Asp side chain, essential to coordinate the metal cation in the β-subunit, well-spaced from a hydrophobic group mimicking the Leu side chain of the LDV sequence targeting the opposite α subunit.

Based on these considerations, in the late 1990s, Adams *et al.* identified a potent and highly selective inhibitor of $\alpha_4\beta_1$ by introducing a simple hydrophobic "cap" 4-[*N*'-(2-methylphenyl)ureido]phenylacetyl (MPUPA) at the *N*-terminus of the LDV sequence.[140] This compound, later termed **BIO1211** (MPUPA-LDVP, Figure 15), was the most powerful of a small library of oligopeptide analogues and thereby, has been taken into account as a prototype for the design of several $\alpha_4\beta_1$ antagonists. However, despite its efficacy in the animal model, considerable drawbacks such as instability to hydrolases and poor pharmacokinetic profile, due

essentially to the hydrolytic cleavage of the terminal dipeptide moiety and its rapid clearance *in vivo* have limited its application.[141]
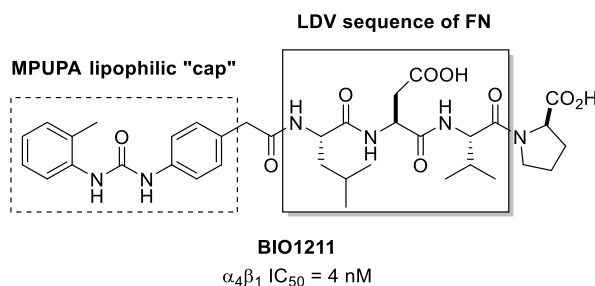
Figure 15. Structure of the BIO1211 $\alpha_4\beta_1$ integrin antagonist.

The identification of alternative non-peptidic structures, in place of the LDV sequence, is viewed as a reasonable approach for developing novel classes of therapeutic agents with improved pharmacokinetic properties and high potency. A great variety of small peptidic and non-peptidic ligands interfering with the VCAM-1/VLA-4 interactions have been extensively described in the literature. [142] Linear and cyclic peptide derivatives are predominantly based on the LDV-binding motif, whereas privileged scaffolds for small-molecule antagonists are phenylureido-LDV-peptidomimetics (relatively selective for $\alpha_4\beta_1$) and acylphenylalanine derivatives (biselective for $\alpha_4\beta_1$ and $\alpha_4\beta_7$).[143] Some examples of $\alpha_4\beta_1$ integrin lead compounds are shown in Figure 16. Vanderslice *et. al.,* reported that the simple introduction of oxymethylene bond and protection of the carboxylic terminal as methyl ester, in the structure of the nanomolar antagonist TBC3486 (**II**) converted it into a micromolar $\alpha_4\beta_1$ agonist THI0019 (**I**, Figure 16) that proved to increase rolling, spreading, adhesion, and migration of $\alpha_4\beta_1$-dependent cells *in vitro*.[131] By linking fluoro-prolinol derivatives to halogen or alkyl-substituted aromatic PUPA fragment, the Daiichi Sankyo Ltd. researchers discovered a nanomolar $\alpha_4\beta_1$ antagonist with improved oral bioavailability (**III**; Figure 16).[144] Lately, Setoguchi *et. al.* have explored the modification of the PUPA fragment with other lipophilic groups developing highly potent $\alpha_4\beta_1$ antagonist (**IV**, Figure 16).[145] Selected members of this library are currently in clinical development.[143] Aventis Pharmaceuticals developed HMR1031 (**V**), a PUPA-containing ligand that reached the phase II clinical trials, but the suspect risk of teratogenicity decreased the interest in this compound.[146] Anyway, a similar molecule was lately reported to prevent the development of arthritis in Lyme disease infection (**VI**, Figure 16).[147]

An important family of small molecule ligands possesses an N-acylated para-substituted phenylalanine core.[106, 148] Among them, proline-phenylalanine derivatives showed excellent activity but lacks satisfactory bioavailability because of its peptidic nature.[149] Therefore, many efforts have been directed to improving the pharmacokinetic profile and oral availability. Dichloro-substituted benzamides on biphenylalanine scaffolds were ascribed as lead structure for the development of selective and potent $\alpha_4\beta_1$ derivatives. The most advanced small-molecule drug candidate is the orally bioavailable AJM-300 (**VIII**, Figure 16) that possesses a phenyl-pirimidindione instead of biphenyl fragment and displayed nanomolar IC_{50} against $\alpha_4\beta_1$. This compound is currently in clinical Phase III for the treatment of IBD, UC, and CD.[150] Firategrast[151] developed by Tanabe and GSK, belongs to the same class of compounds it reached phase II trials for MS, and currently, is studied as a facilitator in the "in utero" hematopoietic cell transplantation (IUHCT) in a pioneering approach for critical fetal diseases treatment (**VII**, Figure 16).
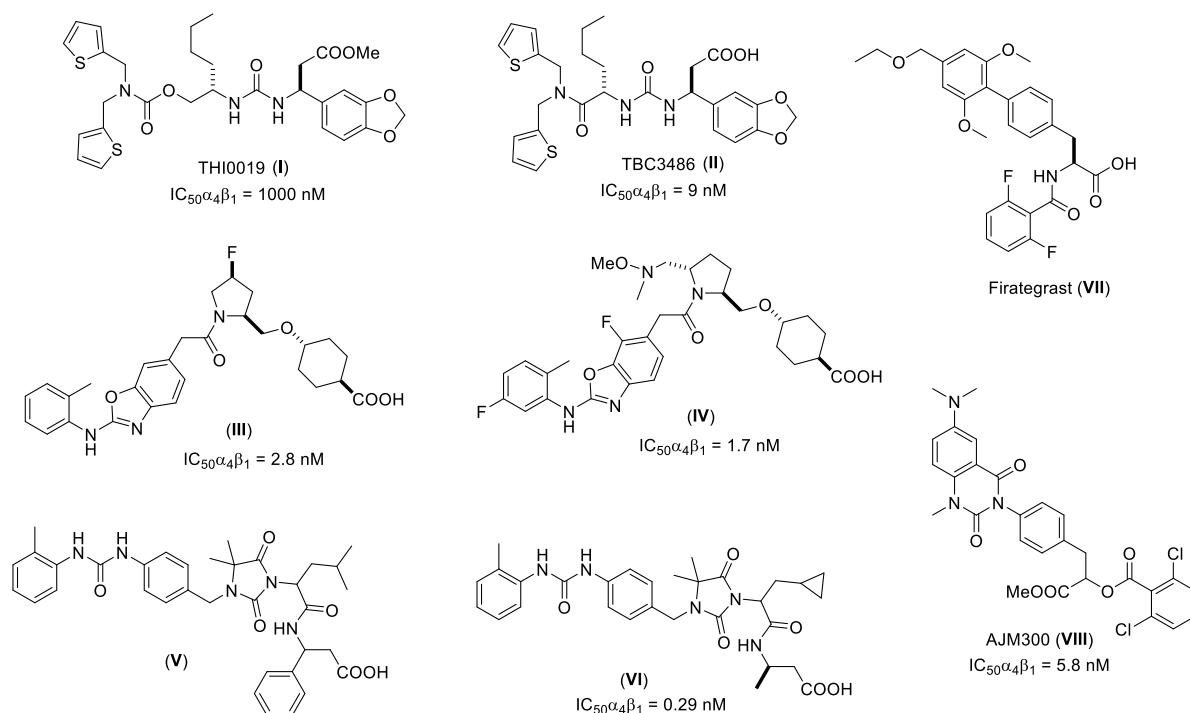
**Figure 16.** Selected examples of $\alpha_4\beta_1$ integrin ligand lead compounds in clinical trials.

1.7. Peptidomimetic approaches in medicinal chemistry

Most biological and physiological functions are mediated by peptides and proteins and their interactions with the respective counter receptors, therefore, it is not surprising that, to date,

synthetic peptides may constitute potential drugs against a variety of diseases.[152] However, rarely, native peptides can be utilized as such as drugs. In many cases, the structural and chemical properties need to be modified and improved, but without affecting the biological activity. Indeed, the overall efficacy of the native peptides is typically limited by an *in vivo* instability towards the protease hydrolysis, a lack of bioavailability, due to inability to cross the biological barriers (i.e., gut mucosa, BBB) and, a rapid liver and/or kidneys clearance.[153, 154] One way to improve stability, solubility and bioavailability of peptides is represented by the peptidomimetic approach.[152, 155] This strategy consists of replacing portions of biologically active peptides with non-peptidic structural elements, that still retain the essential pharmacophore binding groups and the 3D topology, and thereby, are capable to mimic the agonist or antagonist behaviour of the natural parent peptide.[153, 154] This biologically active peptide-surrogates are defined peptidomimetics and, over the years, have inspired great interest in the field of organic synthesis.

Normally, in peptidomimetic compounds, different and suitable modifications based on SAR studies are commonly introduced in the minimal bioactive sequence of the native peptides. These modifications generally include the insertion of D-amino acids or unusual amino acids instead of the natural L-residues, N- and Cα-alkylation, cyclization, glycosylation, deamination, C-terminus amidation, etc.[153, 154, 156] For instance, the replacement of L-amino acid with its D-configured equivalent is a simple and common strategy to improve the peptide stability since enzymes do not recognize and hydrolyse unnatural amino acids. In addition, this modification can promote and stabilize different conformations of the peptide backbone.[157] Yet, the backbone can be modified by substitution of the cleavable peptide bond with an isosteric or isoelectronic surrogate that resembles the transition state of its hydrolysis.[158] Examples of the most used isosters are the azapeptides, reduced amides, retro-inverso peptides, peptoids, sulphonamide/thioamide peptides/peptoids etc. (Figure 17). The peptoids, reported by Zuckermann *et al.*[159] are peptidomimetics in which the side chain of an amino acid is "shifted" to the α-amino group, leading to enzymatically stable N-alkylated peptides, as well as the N-methylated analogues.[92] In azapeptides, the Cα- of the backbone is substituted by an isoelectronic nitrogen atom, while the side chains remain unchanged (Figure 17).[160] In retro-inverso peptides the normal amino acid sequence is reversed, namely from C- to N-terminus, and the natural L-amino acids are generally substituted by D-amino acids to help maintain the similar side chain topology.[161, 162] Peptidomimetics containing an isoster of one or more

peptide bonds (e.g. a reduced amide CH$_2$-NH or a C=C) are often referred to as pseudopeptides (Figure 17).[153]
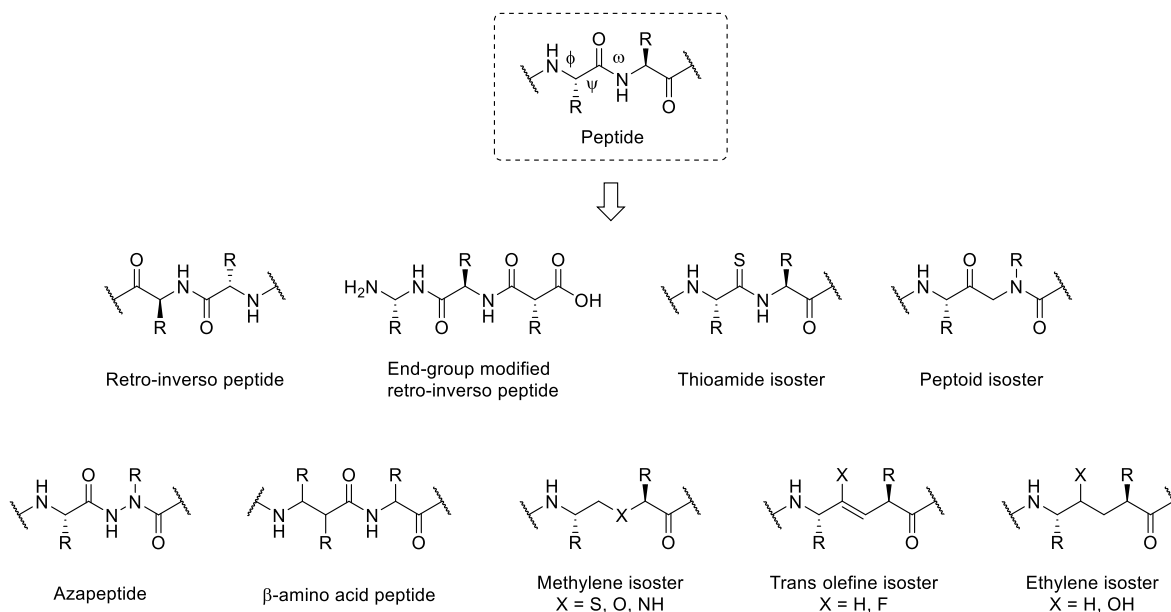
Figure 17. Examples of peptide bond isosters.

Other important and widely investigated modifications include the incorporation of unnatural amino acids such as β-, γ-, or δ-amino acids, N-alkylated amino acids, α- or β-substituted α-amino acids, residues with modified side chains, dehydroamino acids proline analogues, etc. (Figure 18). Generally, these residues exert a "local" conformational bias in the immediate proximity of their position. For instance, the presence of an additional C-C bond in β-amino acid residues should result in greater backbone flexibility, however several researcher, including Seebach *et al.*,[163, 164] Gellman *et al.*,[165] and others,[166] reported that β-oligomers composed by β^2- and β^3-amino acids building blocks or α- and β-amino acids (hybrid α/β-peptides) are folded into well-defined secondary structures (helices, β-sheet, hairpin turn). These amino acid features have been used to design peptidomimetics with therapeutic potential such as hormones, MHC-binding beta-peptides, opioid peptides, somatostatin or amphipathic β-peptide inhibitors of membrane-bound proteins.[163]

Unfortunately, linear native peptides are highly flexible and exist, in aqueous solution, in numerous conformations (dynamic equilibrium). This aspect contributes to reducing its target affinity and/or selectivity. Structural restrictions and more rigid peptides can be obtained by cyclization of the linear backbone.[167-169]
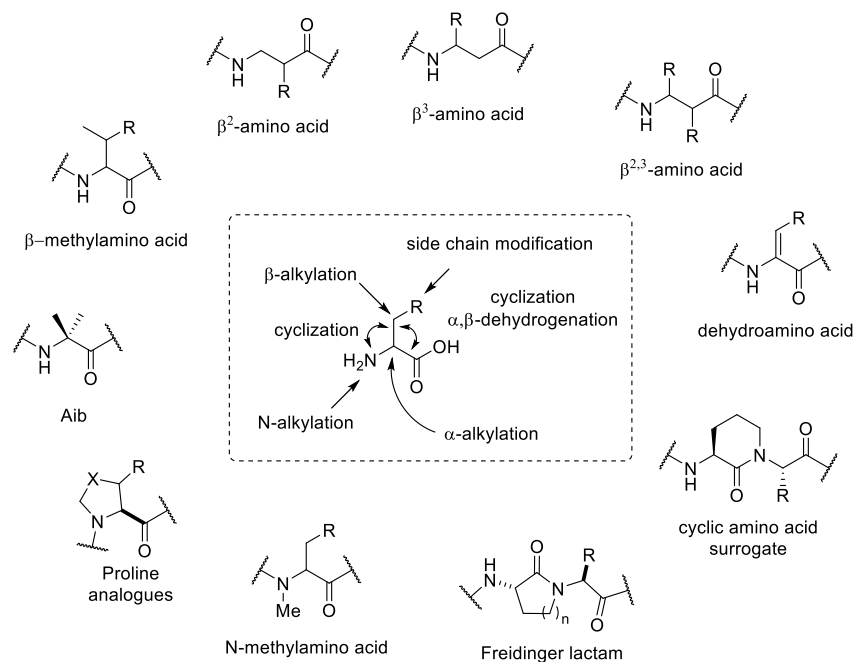
Figure 18. Examples of the modified amino acid residues (constrained and not).

Cyclization is one of the best-explored strategies to reduce the conformational freedom[170] and promote the biologically active conformation of a linear peptide since allows the pharmacophoric sidechains in a well-defined orientation in the target space. This approach was first proposed by Kessler who termed it "spatial screening" and is based on the rational design of conformationally distinct cyclic peptides to explore the 3D arrangement of the pharmacophoric groups.[104, 171, 172] The application of this concept led to the discovery of the integrin antagonist, Cilengitide (c[RGDf*N*(Me)V]), a cyclic pentapeptide containing the RGD sequence (Figure 11). This peptide shows a βII'/γ-turn conformation with D-Phe arranged in the *i*+1 position of the βII'-turn, while on the other side of the cycle the RGD motif forms a tight γ-turn with Gly in the central position. They studied the effect on the conformation and the biological activity caused by a single D-amino acid substitution: it was shown that D-amino acid forces the adoption of a βII'-turn at different sites of the peptide (Figure 19).[85] Therefore, βII'-turn conformation was recognized as a fundamental feature for selective binding to the $\alpha_v\beta_3$ integrin over other RGD-binding integrins.

For these reasons, small cyclic peptides have emerged as useful templates in drug design. In addition, cyclic variants display higher *in vivo* stability to exo- and endoproteases. [154, 169]
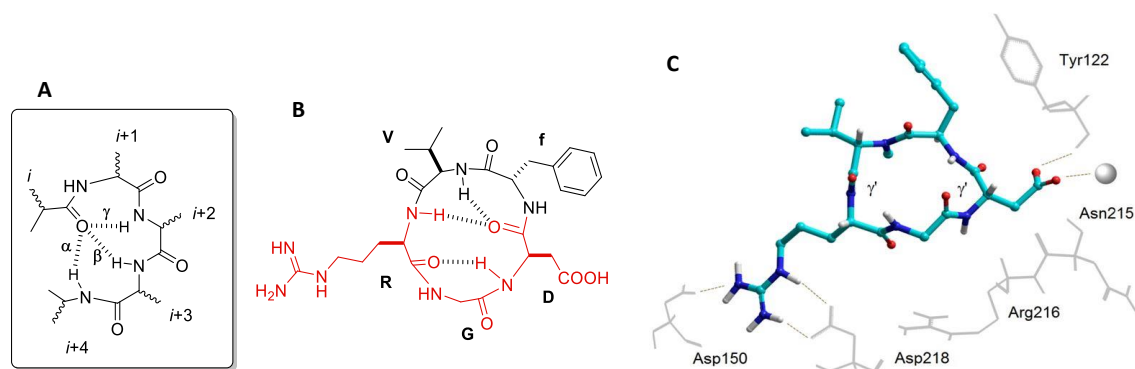
Figure 19. A) Simple illustration of α-, β-, and γ-turns; B) Chemical structure of the cyclic pentapeptides *c*(RGDfV). The RGD sequence is shown as red. Dashed lines represent essential hydrogen bonds required to stabilize the βII'-turn and γ-turn. C) Cilengitide-integrin $\alpha_v\beta_3$ interaction (PDB ID: 1L5G); the sphere represents Mn^{+2} ion (image source: De Marco *et. al.*).[128]

Similarly, when a single β-amino acid is incorporated into a cyclic tetra- or pentapeptide, this preferably occupies the central position of a modified γ-turn conformation that is extended by one CH_2 group and hence, called a pseudo-γ-turn (Ψγ). The conformational bias of the β-amino acid residue employed even overrides the strong preference of a D-amino acid residue, commonly found in the *i*+1 position of βII'-turns.[173] Thus, the β-amino acids act as γ-turn mimetics and stabilizes the overall secondary structure. These findings could provide a new expedient for the design of cyclic peptides with control of conformation.

Depending on its functional groups, linear peptides typically assembled on inert and insoluble polymer as solid support, can be cyclized in four different ways: head-to-tail (C-terminus to N-terminus), head-to-side chain, side chain-to-tail or side-chain-to-side-chain (Figure 20). Apart the use of (di)sulfide, amide, and other obvious bridges other examples of efficient macrocyclization methods include copper catalysed azide–alkyne cycloadditions,[174] ring-closing metathesis,[175] multicomponent macrocyclization strategies etc.[176]
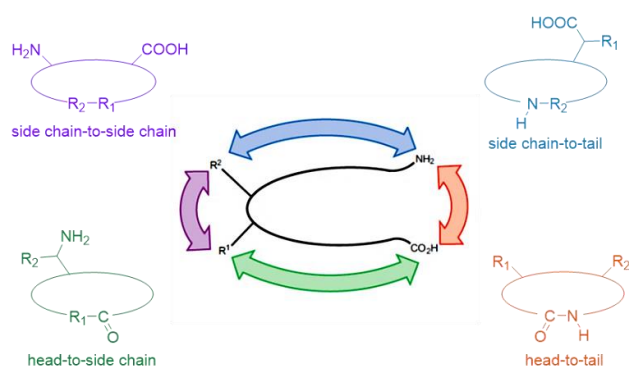
Figure 20. The four possible ways a peptide can be constrained in a macrocycle (image adapted from White *et. al.*).[167]

In last decades, the drug discovery field of peptides and peptidomimetics has reported an exponential growth and a large number of peptides entered the clinical studies as potential therapeutic agents, covering a wide range of therapeutic areas, from cancer to cardiovascular diseases and to antimicrobial or metabolic disorder (Figure 21). These results prove that the peptidomimetic approach represents a well-established strategy for developing novel and effective non-toxic therapeutic agents.
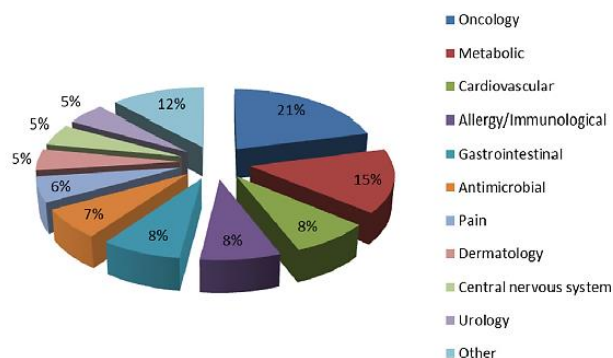
Figure 21. Therapeutic categories of peptide candidates in the commercial pipeline (image source: Tsomaia).[177]

The favourable features of peptides and mimetics such as high specificity, selectivity, small dimensions, ease of modification and high biocompatibility make them promising candidates in a variety of growing fields including targeted drug delivery systems (oncology and imaging), nanotechnology field and diagnostic/biomedical application for the development of new biomaterials, biodevices, biosensors, and bioelectronics.

2. AIM OF THE THESIS

In light of the above introduction, it is evident the essential role of integrin receptors for the regulation of many physiological and pathological processes. The involvement in a wide range of diseases including cancer, infection, thrombosis, inflammation and autoimmune disorders, has revealed their substantial potential as validate drug targets. However, so far few integrin inhibitors have reached marketing approval.[129] To this purpose, extensive efforts have been devoted to the development of small-molecule ligands as integrin antagonists and, recently, agonist ligands have been taken into account as promising therapeutics.

Our research group contributed to this field with the development of potential drug candidates for the treatment of α_4- and α_v-integrin-related diseases. Keeping in mind the fundamental structural features for the integrin binding, the phenylureido-LDV privileged scaffold of BIO1211 (Figure 15), taken as a reference compound, was properly modified by introducing a rigid five-membered ring as amide bond isosters. In agreement with the peptidomimetic principles, conformationally restraints and more stable/bioavailable derivatives have been synthesized (Figure 22).

Recently, 5-aminomethyloxazolidine-2,4-dione (Amo) dipeptide scaffold, obtained from intramolecular cyclization of isoserine (*iso*Ser) or other α-hydroxy-β-amino acid residues was successfully introduced as a central core into peptidomimetics. The α/β hybrid Amo scaffold can be considered a β^2-homo analogue of the well-known Freidinger lactam. This retro sequence (**IX**, Figure 22) displayed nanomolar IC_{50} antagonism in cell adhesion assays with $\alpha_4\beta_1$ integrin-expressing Jurkat E6.1 cells and its natural ligand VCAM-1.[178] Tolomelli *et al.* developed a small library of compounds containing rigid 3,4-dehydro-β-proline ring as a central core which was introduced through an original RCM (ring-closing metathesis) cyclization of diallylamino derivatives.[179] These compounds showed an excellent affinity to $\alpha_4\beta_1$ integrin based on the stereochemistry of the heterocyclic core; the (*R*)-configured (**X** and **XI**, Figure 22) was the most powerful, thus suggesting a specific disposition of the lipophilic chain for the two enantiomers.[180] On the other hand, following the peptidomimetic retro-strategy, Gentilucci *et. al.* introduced a β^2-proline ring as central core in a PUPA-derivative for exerting a markedly overall rigidity. Compound **XII** (Figure 22), containing the Asp residue acylated with a benzyl moiety at the *N*-terminus, showed nanomolar IC_{50} in inhibition cell adhesion assays.[181]
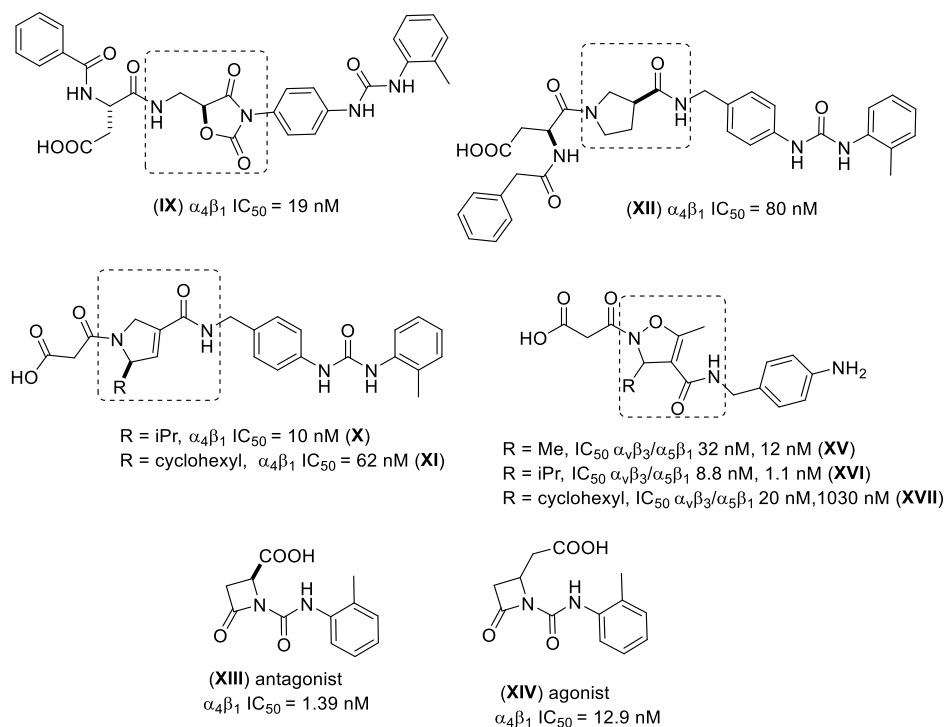
Figure 22. Relevant PUPA-based structure containing a constrained central core.

Introduction of suitable decorations on four-membered β-lactam scaffolds afforded effective α4β1 integrin agonists and antagonists, suggesting that small modifications in ligand structure could induce a dramatic effect on their agonist/antagonist behaviour [182] presumably due to the receptor stabilization in active or inactive conformations (**XIII** and **XIV**, Figure 22) as observed by Vanderslice and co-workers. Yet, rigid derivative containing isoxazolines as central scaffolds showed interesting nanomolar IC$_{50}$ activity, toward α$_V$β$_3$ and α$_5$β$_1$, acting in this case as RGD mimetics. In particular, compound **XVI** with R = *i*Pr exhibited the highest activity against both α$_V$β$_3$ and α$_5$β$_1$ receptors with IC$_{50}$ of 8.8 nM and 1.1 nM, respectively (Figure 22).[183] These results confirmed the importance of the constrained central cores in conferring and stabilizing the overall structure in a well-defined conformation and, prompted us to investigate other backbone modification to improve activity and stability.

The aim of the present work is focused on the synthesis and biological evaluation of novel hybrid α/β-peptidomimetic ligands for integrin α4β1 to potentially treat chronic inflammatory autoimmune diseases. Moving from our previous results and, applying the peptidomimetic strategy, we designed a small library of linear (Chapter 3 and 4) and cyclic peptidomimetics (Chapter 5) based on the phenylureido-LDV scaffolds, aimed at improving activity, stability and explore the chemical space of the α4β1 integrin binding pocket since the structure has not

yet been crystallized. In this regard docking experiments on the rigid cyclopeptides will be presented. This study allowed to identify a nanomolar $\alpha_4\beta_1$ lead antagonist which was fully characterized *in vitro* and *in vivo* for the treatment of ocular allergic conjunctivitis.

In order to explore new methods for monitoring the course of the inflammatory processes, we designed a nanostructured device functionalized with peptidomimetics capable to detect specific integrin-expressing cells as inflammatory disease biomarkers (Chapter 6). Therefore, peptides with suited linker were anchored onto a specific surface coated with dye-loaded Zeolite L-crystal nanoparticles, to reproduce the high density of multi-valency binding normally present in the proximity of the sites of inflammation. In perspective, these systems may represent prototypes for rapid and non-invasive diagnosis of inflammatory or other diseases, from one drop of blood or other fluids easily obtainable from the patients.

During the period spent in the laboratory of Prof. Norbert Sewald at the University of Bielefeld in Germany, a project based on the development of a drug delivery systems for cancer therapy was implemented (Chapter 7). In the last decades, this approach has attracted great interest as a promising alternative to overcome the selectivity drawbacks of the traditional chemotherapeutic agents. More selectivity at tumor site could be achieved by the conjugation of highly cytotoxic payload, in our study the picomolar Cryptophycin, through a suitable protease-cleavable linker to specific ligand capable of binding to the tumor-overexpressed receptors, while sparing the healthy tissues. Since integrin $\alpha_v\beta_3$ is overexpressed on the neovasculature in a variety of solid tumor, but not on healthy cells, the RGD-peptides have been extensively exploited as a tumor-targeting ligand. In this study, new RGD-Cryptophycin conjugates were synthesized and evaluated in biochemical assays including stability, cleavage experiments and integrin binding to assess their structural properties.

As final goal, in attempt to make peptide synthesis, that generally uses large excess of reagents and solvents, more sustainable and greener, we successfully developed a new alternative way for a solvent-free peptide bonds formation using the mechanochemistry approach (Chapter 8). Moreover, these reactions have also been performed under ultra-mild minimal solvent-grinding conditions, using organic-green solvents and common, inexpensive laboratory equipment. Standard amino acids and coupling agents were employed in the presence of nanocrystalline hydroxyapatite as a reusable, bio-compatible inorganic basic and "green" catalyst.

3. HYBRID α/β-PEPTIDOMIMETICS: A RATIONAL APPROACH FOR THE DEVELOPMENT OF $\alpha_4\beta_1$ INTEGRIN ANTAGONISTS

The work described in this Chapter was recently published:

– Dattoli S. D., Baiula M., De Marco R., Bedini A., Anselmi M., Gentilucci L.* and Spampinato S.* DS-70, a novel and potent α_4 integrin antagonist, is an effective treatment for experimental allergic conjunctivitis in guinea pigs. *British Journal of Pharmacology* **2018,** 175 (20), 3891-3910. DOI: 10.1111/bph.14458.

3.1. Introduction

Allergic conjunctivitis is a type-1 hypersensitivity reaction related to the generation of IgE antibodies in response to certain external allergens.[184] In allergic conjunctivitis the early phase reaction (humoral immunity) is promoted by the release of pro-inflammatory cytokines and chemokines and, is generally characterized by ocular itching, hyperaemia, swelling of the surrounding eyelids, chemosis and tearing. This is followed, after 6-12 h, by a late phase sustained by the production of cytokines and chemokines, that involves the recruitment and conjunctival infiltration of eosinophils and other immune cells (cell-mediated immunity).[185] The latter event requires the interaction between leukocyte surface-adhesion receptors, such as integrins and selectins, and adhesion molecules expressed on the conjunctival endothelium, namely ICAM-1[186] and VCAM-1.[187] Increased levels of cell adhesion molecules on the microvasculature and factors that regulate these molecules may perpetuate the inflammation in allergic conjunctivitis.[188] Integrin receptors, specifically the $\alpha_4\beta_1$ and $\alpha_4\beta_7$ subtypes, are directly involved in this phenomenon since they are widely expressed on most leukocytes, and contribute to their activation and migration during inflammatory reactions.[187] Studies using monoclonal antibodies have confirmed that α_4-integrin contributes to eosinophil recruitment and infiltration in inflamed conjunctiva and then, to the development of its pathogenesis.[189] The blockade of α_4 integrin may represent a useful therapeutic strategy to treat allergic eye diseases, given that current therapies only alleviate the clinical symptoms (glucocorticoids, antihistamines and mast cell-stabilizing agents). Drugs are frequently administered topically in the conjunctival fornix to treat this pathology,[184] thus low MW α_4 antagonists are suitable for administration via this route and may representing a safer alternative.

In this context, inspired by our recent results on the development of $\alpha_4\beta_1$ integrin ligands for treating inflammatory diseases,[178, 181] we rationally designed a simplified hybrid α/β-

peptidomimetic through the molecular assembly of distinct pharmacophore moieties identified in the BIO1211 structure and in the bioactive LDV sequence of the ECM ligands aimed to obtain low MW α_4 antagonists. The (D)-β^2-proline (equal to S- absolute stereochemistry) moiety was introduced as a central core in order to confer conformational rigidity, due to the reduced allowed rotations, and enzymatic stability. The latter is flanked by the MPUPA α_4-targeting moiety at the N-terminus, and a simple Gly residue at the C-terminus, that coordinates the MIDAS β1-subunit. These pharmacophoric groups are spaced by 14-15 C-C bonds that seem to be the optimal distance for the integrin binding. Similar to BIO1211 prototype, **DS70** showed a straight sequence (Figure 23). Moving from our previous studies on retro-peptide sequences (**IV**, Figure 22) that showed higher efficacy against $\alpha_4\beta_1$ integrins compared to the corresponding straight sequences, the partially retro-inverso analogue **DS23** was also synthesized.[178, 181] Differently, the (D)-β^2-proline core was connected at the C-terminus to the amino variant of MPUPA, namely the AMPUMP [1-(4-(aminomethyl)phenyl)-3-(*o*-methyl)urea], that acts as an α_4-targeting fragment, while at the N-terminus the malonic moiety, equivalent to Gly residue, is placed to coordinate the MIDAS β1-subunit (Figure 23).
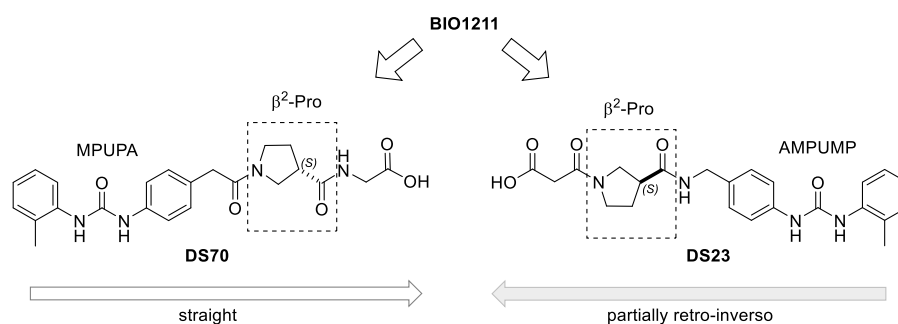
Figure 23. Design of DS70 and DS23: straight and partially retro-inverso hybrid α/β-peptidomimetics structure.

The potential efficacy of these two compounds was determined by *in vitro* and *in vivo* experiments. The most potent DS70 was pharmacologically characterized using a scintillation proximity assay to measure its affinity for $\alpha_4\beta_1$ integrin and its effect on cell adhesion mediated by different integrins. The effects of DS70 on VCAM-1-mediated degranulation of a human mast cell line and eosinophilic cell line expressing $\alpha_4\beta_1$ and, on VCAM-1-mediated phosphorylation of ERK 1/2 in Jurkat E6.1 cell were also investigated. Finally, *in vivo* studies in ovalbumin-sensitized (OVA) guinea pigs showed that DS70 reduces in a dose-dependent

manner the clinical symptoms of allergic conjunctivitis, conjunctival α4 integrin expression and conjunctival levels of chemokines and cytokines.

3.2. Results and Discussion

3.2.1. Peptide synthesis

The linear peptides BIO1211, synthesized as a reference compound, and **DS70**, were assembled manually by Solid-Phase Peptide Synthesis (SPPS) on a Wang resin preloaded with Fmoc-Gly using Fmoc-protected amino acids and microwave irradiation conditions. The removal of the Fmoc groups was performed by treatment with piperidine in DMF under microwave irradiation for 2 min. Coupling between each residue was carried out using the activating agents DCC and HOBt in DCM/DMF (4:1, *v/v*) under microwave irradiation for 10 min.
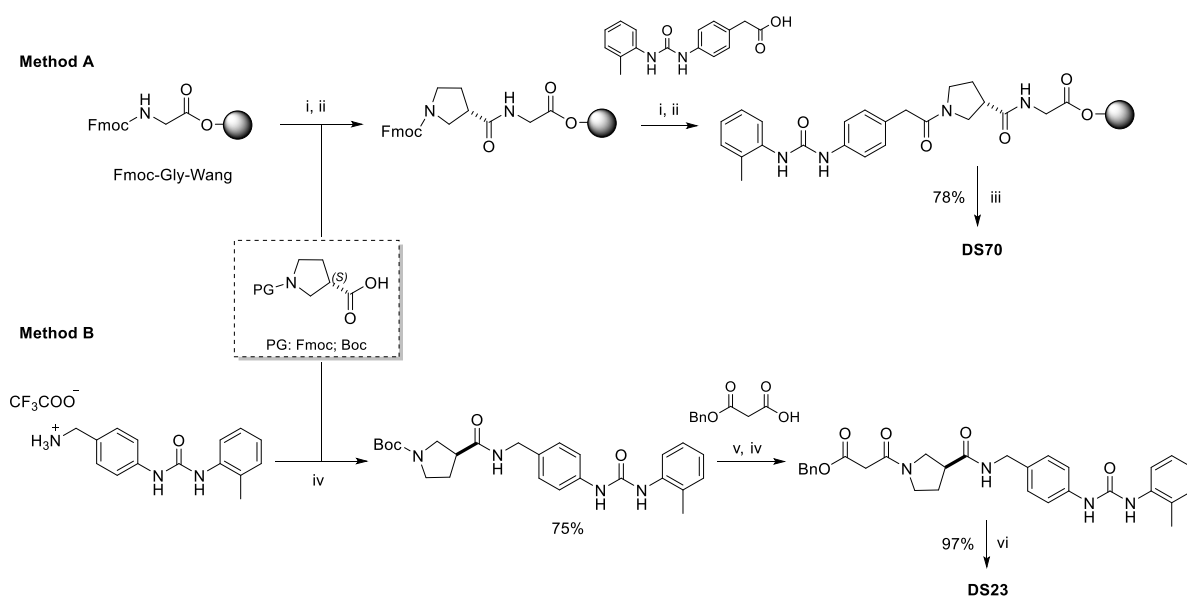
Scheme 1. Synthetic scheme for DS70 and DS23. *Reagent and conditions.* **Method A**: i) 20% piperidine, DMF, MW, 2 min (x2); ii) Fmoc-(D)-β^{2}Pro-OH, DCC, HOBt, DCM/DMF, MW, 10 min; same repeated for MPUPA; iii) TFA/H$_2$O/TIS/PhOH (90:5:5), RT, 2 h. *Reagent and conditions.* **Method B**: iv) Boc-(D)-β^{2}Pro-OH, HBTU, HOBt, DIPEA, DCM/DMF, MW, 10 min; same repeated for *mono*-benzyl malonic acid; v) 25% TFA/DCM, RT, 1 h; vi) H$_2$, Pd/C, EtOH, RT, 4 h.

Peptide cleavage was accomplished by treatment the peptidyl-resin with TFA in the presence of scavengers. The crude products were simply precipitated from ice-cold Et$_2$O and collected in almost quantitative yield by centrifuge. On the other hand, the partially retro-inverso

sequence **DS23** was prepared in solution. AMPUMP was coupled with Boc-protected β^2-Pro in 4:1 (*v/v*) solution of DCM/DMF under microwave irradiation with the aid of HOBt/HBTU/DIPEA. Boc-deprotection of the resulting dipeptide was carried out in 25% TFA/DCM and was followed by coupling with 3-(benzyloxy)-3-oxopropanoic acid under the same conditions previously described. The resulting benzyl ester was deprotected by catalytic hydrogenation giving **DS23** in good yield. For all peptides, the purity was assessed by RP-HPLC (96-98% purity) while the chemical identity was determined by ESI-MS, 1D and 2D NMR spectroscopy.

3.2.2.   Biological evaluation

Pharmacological characterization of **DS70** and **DS23** was performed by the research group of Prof. Dr. M. S. Spampinato (department of Pharmacology, University of Bologna). *In vitro* experiments were carried out using the scintillation proximity assay (SPA) to measure their affinity to the $\alpha_4\beta_1$ integrin and their effects on the $\alpha_4\beta_1$-mediated cell adhesion. In contrast with our previous results where the retro-sequence showed higher affinity to $\alpha_4\beta_1$ integrin, here to our surprise, the straight peptide **DS70** showed to be more effective than **DS23** as an antagonist of $\alpha_4\beta_1$ integrin and, therefore, we focused our research efforts on this compound. Complete biological characterization was performed including *in vivo* experiments on guinea pig model of allergic conjunctivitis.

➢ **Integrin binding affinity: SPA and cell adhesion assays**

The binding affinity of the novel hybrid α/β-peptidomimetics was measured using SPA assay and was compared to that of the reference compound BIO1211. As reported in Table 2, BIO1211 and DS70 proved to be the most effective compounds with a nanomolar IC_{50} inhibition of [^{125}I]-FN binding. Moreover, these compounds showed to inhibit the cell adhesion of $\alpha_4\beta_1$ integrin-expressing Jurkat E6.1 cells to VCAM-1 or FN ligands with a nanomolar activity (Table 2).

Further cell adhesion assays were performed only on DS70 employing several integrin-expressing cells. Similar IC_{50} values were observed with $\alpha_4\beta_1$ integrin-expressing HMC 1.1 and EoL-1 cell line in the presence of VCAM-1 and FN (Table 3).

Table 2. SPA binding to bead-associated $\alpha_4\beta_1$ integrin and inhibition of Jurkat E6.1 cell adhesion of the reference compound BIO1211, DS70 and DS23 to VCAM-1 (2 μg·mL^{-1}) and FN (10 μg·mL^{-1}).

Compound	SPA IC$_{50}$ (nM)^b	Cell adhesion Jurkat/ VCAM-1 IC$_{50}$ (nM)	Cell adhesion Jurkat/ FN IC$_{50}$ (nM)
BIO1211	8.80 ± 3.4 (0.08–46.7)^c	4.60 ± 3.0 (0.05–25.1)	5.50 ± 4.0 (0.09–37.6)
DS-70	8.3 ± 3.2 (0.1–37.2)	5.04 ± 0.51 (0.05–37.3)	4.3 ± 1.7 (0.04–23.4)
DS-23	47.7 ± 4.1 (4.6–161.4)	40.3 ± 7.1 (3.4–127.6)	51 ± 5.0 (4.8–192.4)

^{a}Results were generated by measuring, in a cell-free SPA, the inhibition of [^{125}I]-FN binding by the assayed compounds on Jurkat E6.1 cell lysates in the presence of 10 increasing concentrations of each compound (10^{-12}–10^{-3} M) and a fixed amount of radioligand (100 000 counts per minute).
^{b}Six independent experiments were run in quadruplicate.
Data are expressed as means ± SD (with ^{c}95% confidence limits).

As shown in Table 3, DS70 did not inhibit the adhesion of cell lines not expressing the $\alpha_4\beta_1$ receptor. However, approximately 8 folds less potent inhibition activity was observed upon RPMI 8866 cells expressing the $\alpha_4\beta_7$ integrin subtype compared to its natural ligand MAdCAM-1. Therefore, it is reasonable to assume that DS70 may be considered a dual antagonist of $\alpha_4\beta_1/\alpha_4\beta_7$ integrin receptors.

Table 3. Effect of DS70 upon different integrin-mediated human adhesion cells.

| Cell/integrin expressed	Adhesion molecule	IC$_{50}$ (nM)^b
HMC-1/$\alpha_4\beta_1$	VCAM-1	8.4 ± 1.9 (0.1–32.4)^c
EoL-1/$\alpha_4\beta_1$	VCAM-1	9.7 ± 3.2 (1.2–38.6)
RPMI8860/$\alpha_4\beta_7$	MAdCAM-1	70 ± 6.5 (6.9–260.8)
Jurkat/$\alpha_L\beta_2$	ICAM-1	>5000
HL60/$\alpha_M\beta_2$	Fibrinogen	>5000
K562/$\alpha_5\beta_1$	FN	>5000
SK-MEL-24/$\alpha_V\beta_3$	FN	>5000
MCF7/$\alpha_V\beta_5$	Fibrinogen	>5000
HT-29/$\alpha_V\beta_6$	FN	>5000
HEL/$\alpha_{IIb}\beta_3$	Fibrinogen	>5000
D283/$\alpha_9\beta_1$	FN	>5000

^{a}In a cell-based assay, the adhesion of a cell line preferentially expressing a specific integrin heterodimer to an immobilized adhesion molecule was measured.
^{b}Six independent experiments were run in quadruplicate.
Data are expressed as means ± SD (with ^{c}95% confidence limits).

➢ *In vitro* **enzymic stability of DS70**

The stability of DS70 in mouse serum at 37 °C was compared to that of BIO1211. As shown in Figure 24, DS70 was more stable showing just a 21% of degradation rate after 8 h, while the half-life of BIO1211 was approximately of 0.27 h. These data support the hypothesis that the presence of the β-amino acid scaffold markedly increases the enzymatic stability of the peptidomimetic.
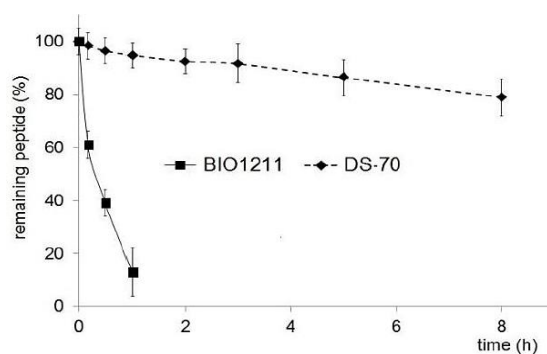

Figure 24. Degradation of BIO1211 and DS70 in mouse serum. Samples were analysed by RP-HPLC ESI-MS at 0, 0.15, 0.5, 1.0, 2.0, 4.0, 6.0 and 8.0 h Values are presented as mean ± SD (n = 5).

> **VCAM-1-mediated ERK 1/2 phosphorylation signalling**

Intracellular signalling generated by the interaction of the ECM components with integrin $\alpha_4\beta_1$ involves second messengers, such as ERK 1/2, that contribute to α_4 integrin-mediated cell functions.[190] The addition of DS70 alone to Jurkat E6.1 cells did not cause any significant increase in ERK 1/2 phosphorylation compared to vehicle-treated cells (data not shown). A significant increase in ERK 1/2 phosphorylation was detected 60 min after Jurkat E6.1 cells were exposed to VCAM-1-coated plates (2 $\mu g \cdot mL^{-1}$). Pre-incubation with DS70 (10^{-10}-10^{-4} M) for 60 min produced a concentration-dependent decrease in VCAM-1-mediated ERK 1/2 phosphorylation (Figure 25 A-B). DS70 was also effective in reducing, in a concentration-related manner, ERK 1/2 phosphorylation induced by VCAM-1 in HMC 1.1 and EoL-1 cells (Figure 25 D-E and F-G).

> **DS70 binding to $\alpha_4\beta_1$ integrin modulates HUTS-21 epitope exposure in Jurkat E6.1 cells**

Integrins exist in three major conformations: an inactive or bent conformation, an intermediate-activity conformation and a high-activity open conformation. Conformational changes in integrin subunits may be monitored using conformation-specific antibodies that recognize a specific epitope that is exposed only in a defined structural conformation.[191] We used the PE-conjugated (PhycoErythrin) HUTS-21 mAb to determine whether the binding of DS70 to $\alpha_4\beta_1$ integrin alters its conformation. This mAb recognizes a ligand-induced binding site epitope that is masked in the inactive integrin but is exposed upon agonist binding or partial integrin activation. The epitope recognized by HUTS-21 has been mapped to the hybrid domain of β_1 integrin.[191] This mAb was added to Jurkat E6.1 cells in the presence of VCAM-1 (2 $\mu g \cdot mL^{-1}$), and fluorescence was assayed using flow cytometry.
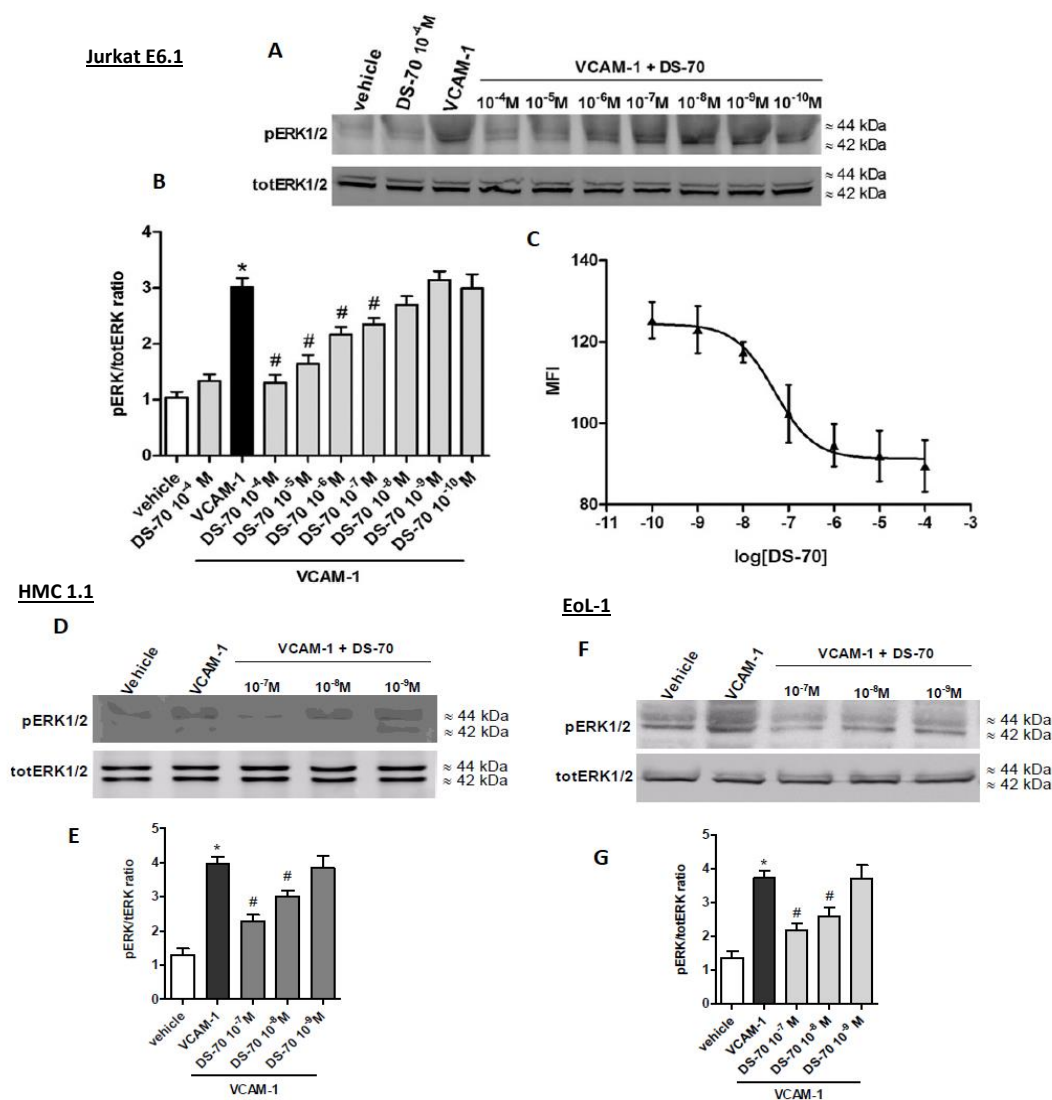
Figure 25. Effects of DS70 on ERK1/2 phosphorylation mediated by VCAM-1 in (A-B) Jurkat E6.1, (D-E) HMC1.1 and (F-G) EoL-1 cells. (A, D, F) Representative Western blots for each cell lines: control cells plated on VCAM-1 had a much stronger signal for pERK1/2 than vehicle-treated cells. DS70 reduces VCAM-1-induced pERK1/2, whereas, at a higher concentration (10^{-4} M), it was not able to modify pERK1/2 in the absence of this adhesion molecule. (B) (E) (G) Semiquantitative densitometry analysis of the bands from five independent experiments (mean ± SD); the amount of pERK1/2 is normalized to that of total ERK1/2. *P < 0.05, significantly different from vehicle; #P < 0.05, significantly different from VCAM-1. (C) Mean fluorescence intensity (MFI) due to the anti-β_1 integrin mAb PE-conjugated HUTS-21 plotted against different concentrations of DS70 added to Jurkat E6.1 cells in the presence of VCAM-1 (5 μg·mL^{-1}) was measured. Each point represents the mean ± SD of five independent experiments carried out in triplicate. VCAM-1 administered alone was able to promote epitope exposure and a significant increase of MFI over vehicle-treated cells exposed to PE-conjugated HUTS-21 alone (MFI values were 130 ± 3 vs. 80 ± 4; n = 5. P < 0.05, significantly different from VCAM-1 alone. Non-specific binding of an isotype control PE-conjugated mAb added to Jurkat E6.1 cells produced an MFI of 38 ± 4 (n = 5) that was subtracted from all samples.

As expected, HUTS-21 binds to β_1 integrin and exhibits increased Jurkat cell-associated fluorescence compared to the cells expose to an isotype control mAb. The binding of $\alpha_4\beta_1$ integrin to its endogenous ligand VCAM-1 induces a conformational rearrangement in the β_1 subunit that exposes the HUTS-21 epitope and increases antibody binding. As shown in Figure 25 C, DS70 (10^{-10}-10^{-4} M) concentration-dependently reduced the exposure of the HUTS-21 epitope as it decreased mAb binding in the presence of VCAM-1 with an IC_{50} of $4.33 \cdot 10^{-8}$ M. DS70 alone (10^{-10}-10^{-4} M) did not result in any significant exposure of the mAb epitope registered as an increase of fluorescence (data not shown). Thus, DS70 seems to act as an $\alpha_4\beta_1$ integrin antagonist, as it favours the inactive and/or intermediate-activity conformations of this integrin.

➢ DS70 inhibits VCAM-1-mediated mast cell and eosinophil degranulation

Since integrins α_4 are expressed on mast cells, they contribute to the acute degranulation of this leukocytes during inflammatory/allergic reactions. Consistent with this latter observation, VCAM-1 (2 $\mu g \cdot mL^{-1}$) caused significant degranulation of the human mast cell line HMC1.1, as assayed by measuring the release of β-hexosaminidase into the cell supernatant. This effect was prevented by exposing the cells to a mAb that binds to the $\alpha_4\beta_1$ integrin expressed on the cell surface. Pre-treatment with DS70 (10^{-10}-10^{-4} M) for 60 min prior to VCAM-1 administration, caused a concentration-dependent inhibition of VCAM-1-induced mast cell degranulation (Figure 26A). Moreover, VCAM-1 or IL-5 promotes a significant EoL-1 degranulation which was assayed by measuring the release of eosinophil peroxidase in cell culture medium. IL-5-induced release of eosinophil peroxidase was significantly increased following a 4 h incubation in VCAM-1-coated wells; this effect was blocked by a mAb that binds to α_4 integrin. DS70 prevents in a concentration-related manner (10^{-10}-10^{-4} M), the IL-5-induced release of eosinophil peroxidase from cells maintained in VCAM-1-coated wells whereas, DS70 was not effective when added to control cells (Figure 26B).
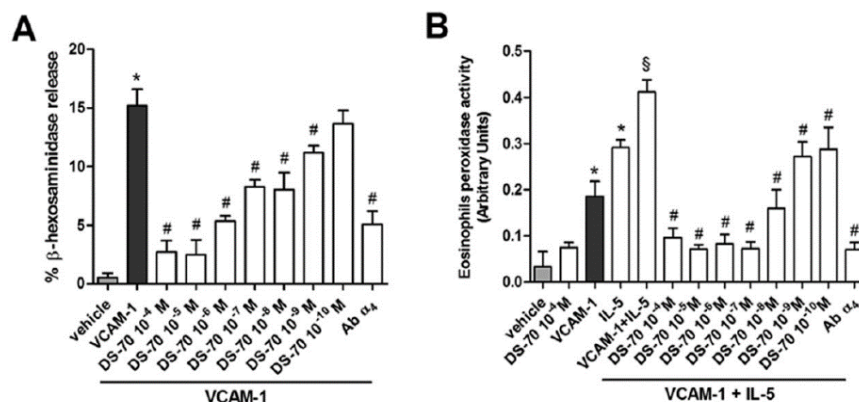
Figure 26. DS70 antagonizes HMC1.1 cell degranulation (A) and eosinophil peroxidase release from the eosinophils EoL-1 cells (B). (A) In HMC1.1 cell seeded on VCAM-1 (2 μg·mL^{-1})-coated plates, a pronounced increase of β-hexosaminidase release is observed. DS-70 decreases in concentration-dependent manner β-hexosaminidase release. VCAM-1-induced β-hexosaminidase release is significantly prevented in cells treated with a monoclonal antibody anti-α$_4$. Degranulation is expressed as percentage of β-hexosaminidase released over total content measured in cells lysed with Triton X-100. (B) VCAM-1 (5 μg·mL^{-1}) exposure promotes a significant increase of eosinophil peroxidase release from EoL-1 cells and elevates IL-5 (50 ng·mL^{-1})-induced release of this enzyme. DS70 added to the cells prior to exposure to VCAM-1 and IL-5, significantly reduces eosinophil peroxidase release. Even here, eosinophil peroxidase release caused by VCAM-1 + IL-5 is significantly prevented by pre-treatment with a monoclonal antibody anti-α$_4$. Data are expressed as the mean ± SD of five experiments carried out in triplicate. *$P < 0.05$, significantly different from vehicle; #$P < 0.05$, significantly different from VCAM-1 (panel A) or VCAM-1 + IL-5 (panel B); §$P < 0.05$, significantly different from IL-5.

> ➢ **Cell apoptosis and necrosis evaluation**

We analysed the capacity of DS70 to induce apoptosis and necrosis in the three cell lines used in this study: Jurkat E6.1, HMC 1.1 and EoL-1. Cells were treated with DS70 (10^{-10}-10^{-4} M) for 6 h, and cell apoptosis and/or necrosis were assessed by flow cytometry; we measured annexin V-PE fluorescence using 7-AAD-induced (7-aminoactinomycin D) apoptotic cells as a positive control. As shown in Figure 27, DS70 did not cause any significant apoptotic cell death in the three cell lines investigated. Compared with the control, the number of live cells did not decrease, and the percentages of early apoptotic cells, late apoptotic/secondary necrotic or damaged cells did not change in the presence of DS70.
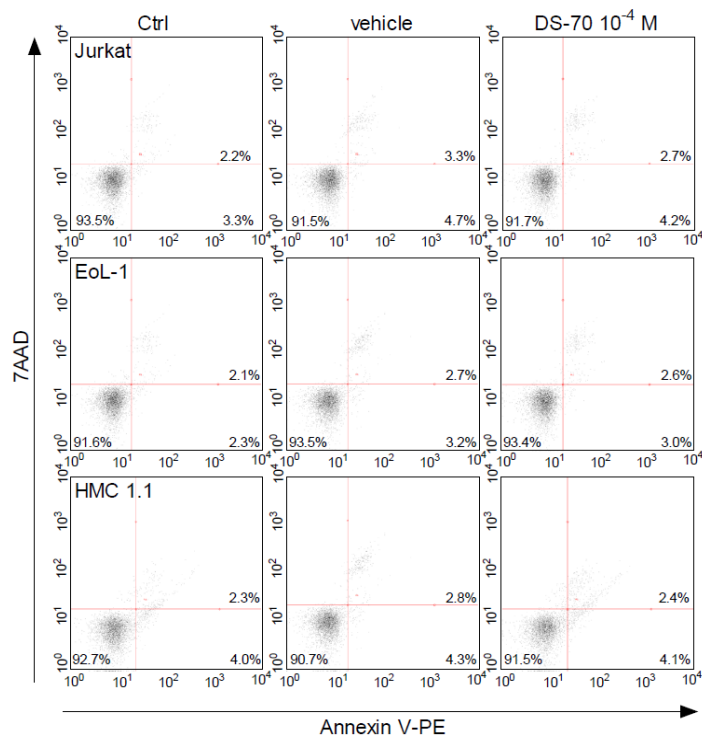
Figure 27. Density plots showing the percentage distribution of Jurkat E6.1, HMC 1.1 and EoL-1 control and vehicle or DS70 (10^{-4} M, 6 h) treated cells. Non-apoptotic cells (Annexin V and 7-AAD negative) represent 90-95% of the total cell population after treatment. Quadrants: (top left) damaged cells, (top right) late apoptotic/secondary necrotic cells, (lower left) live cells, (lower right) early apoptotic cells. These figures are from a representative experiment carried out at least five times in triplicate.

➢ *In vivo* **experiments on guinea pig animal model of allergic conjunctivitis**

Guinea pigs were actively immunized via intraperitoneal injection administration (i.p.) of ovalbumin (OVA) and challenged with OVA instilled into the conjunctival sac 21 days later. One hour after challenge, during the early phase reaction, clinical observations revealed typical early phase symptoms of allergic conjunctivitis, such as tearing and discharge conjunctival redness and chemosis. The mean clinical score reached the maximum 2 h after allergen challenge and thereafter showed a progressive decrease. At 24 h after challenge, the conjunctiva did not present any relevant clinical symptom.[184] The administration of DS70 eye drops (0.01, 0.05 and 0.1%, w/v) in the conjunctival sac of both eyes (30 μL per eye) of OVA-sensitized guinea pigs 30 and 10 min before topical ovalbumin challenge reduced inflammatory signs observed in the early and late phases of conjunctival allergy in a dose-dependent manner. The 0.1% dose was the most effective. The topical administration of DS70 eye drops (0.1%;

administered twice 20 min apart) in control guinea pigs sensitized with saline did not cause any significant sign of discomfort or any conjunctival inflammatory symptoms (Figure 28).
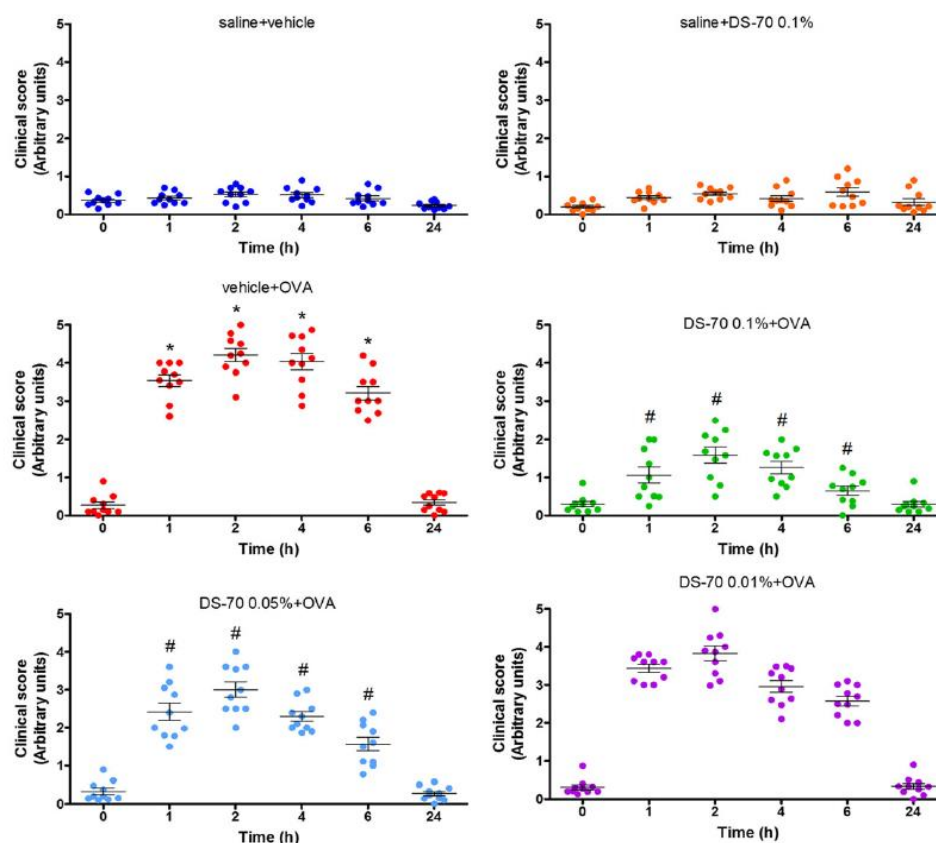
Figure 28. Guinea pigs sensitized and challenged with OVA and treated with the vehicle used to dissolve DS70 (vehicle + OVA) responded with an increase in clinical score index. Administration of DS70 significantly counteracts, in a dose-related manner, pathological signs and improves eye appearance. Data are presented as scatter plot and refer to the mean ± SD (five animals per group were included, and both eyes were evaluated; $n = 10$). *$P < 0.05$, significantly different from saline + vehicle; #$P < 0.05$, significantly different from vehicle + OVA.

A selective and sensitive LM-MS/MS method was developed for the analysis of DS70 and the internal standard levocabastine hydrochloride in the guinea pig conjunctiva. Both the analyte and the internal standard had similar molecular weight and clogP values. Adopting this procedure, DS70 administered to the conjunctival fornix (30 μL of 0.1 g·100 mL^{-1}) twice, 30 min apart, was detected in the conjunctiva 1 h after the first treatment (7780 ± 1000 ng·g^{-1} wet tissue). Interestingly, conjunctival DS70 was also detected at lower levels, 6 h after the first treatment (3450 ± 800 ng·g^{-1} wet tissue). The effects of DS70 on allergic ocular conjunctivitis were compared to those induced by a reference drug dexamethasone (Figure 29). Dexamethasone eye drops (0.1%, w/v) administered to a separate group of guinea pigs

sensitized and challenged with OVA as described above produced a reduction of allergic conjunctivitis, superimposable on the effect elicited by DS70 (0.1%) (Figure 29).
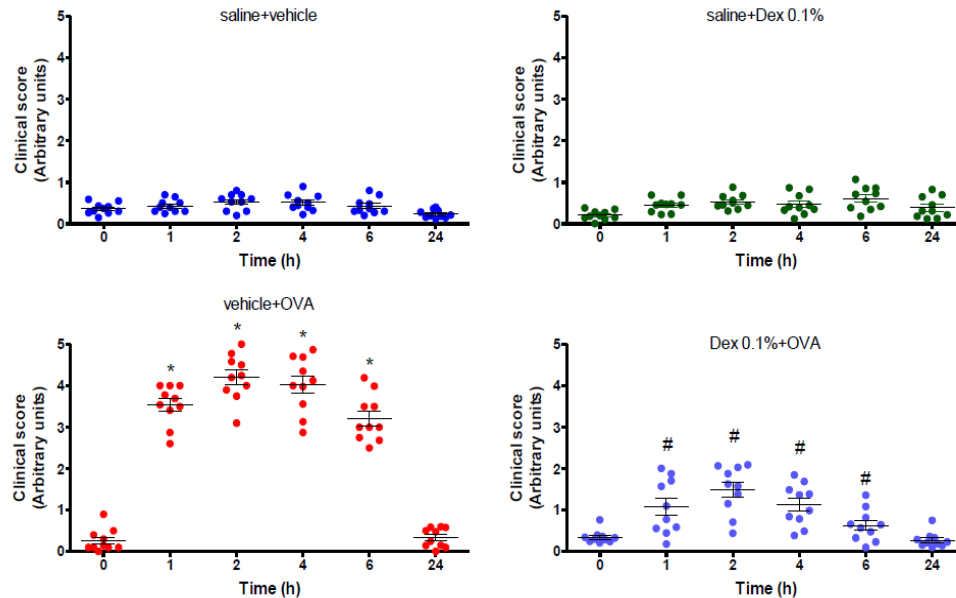
Figure 29. Effects of dexamethasone (Dex) on conjunctival symptoms induced by OVA in guinea pigs. Administration of Dex significantly counteracts pathological signs and improves eye appearance. In control guinea pigs sensitized with saline and treated with the vehicle (saline + vehicle) or Dex (saline + Dex 0.1%) no signs of allergic conjunctivitis were observed. Data are presented as scatter plot and refer to the mean ± SD (5 animals per group were included and both eyes were evaluated; $n = 10$). *$P < 0.05$ significantly different from saline + vehicle; #$P < 0.05$ significantly different from vehicle + OVA.

These data are in agreement with previous work.[192] Guinea pigs were killed 24 h later, and tissues were analysed histologically. Numerous mast cells infiltrating the lamina propria and stroma of the conjunctiva were observed, and most had degranulated in guinea pigs sensitized and challenged with OVA. It was possible to recognize both metachromatic and degranulated mast cells with May–Grünwald–Giemsa staining (Figure 30A).

In contrast to vehicle-treated guinea pigs, DS70 caused a dose-dependent reduction in the number of infiltrating degranulated mast cells, and the majority were granulated mast cells (Figures 31A and 30A). Similarly, eosinophil infiltration and eosinophil peroxidase activity, which are used as an index of the conjunctival infiltration of eosinophils,[193] were increased in specimens of tarsal conjunctiva obtained from guinea pigs killed 24 h after antigen sensitization and challenge, whereas a notable, dose-dependent reduction in both parameters was observed in DS70-treated guinea pigs (Figure 31B-C).
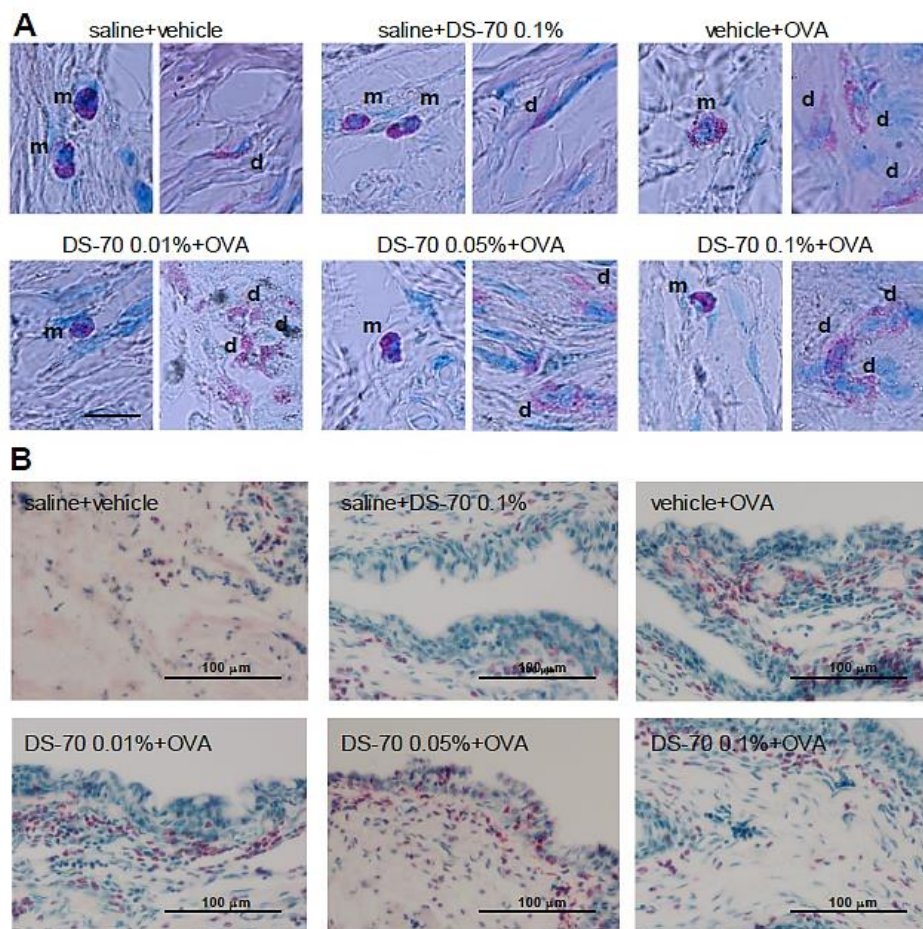
Figure 30. (A) Histologic analysis of OVA-mediated conjunctival mast cell degranulation. Photomicrographs of tarsal conjunctiva stained with May-Grünwald-Giemsa. Both metachromatic (m) and degranulated (d) mast cells are shown. Black bar = 25 μm. (B) Substantial eosinophil infiltration (Luna's staining) is observed in OVA-treated guinea pigs (vehicle + OVA) in comparison to animals sensitized with saline and treated with the vehicle used to dissolve DS70 (saline + vehicle) and to animals sensitized with saline and treated with DS70 alone (saline + DS70 0.1%) (5 animals per group were included and both eyes were evaluated; $n = 10$). Scale bar = 100 μm.

Exposure of OVA-sensitized guinea pigs to the topical challenge of OVA instilled into the conjunctival sac induced a significant increase in α_4 integrin levels in sections of tarsal conjunctiva after 24 h, as measured by immunohistochemistry. This increase may be a consequence of the elevated infiltration of leukocytes, such as eosinophils expressing this integrin in the conjunctiva, including mast cells.
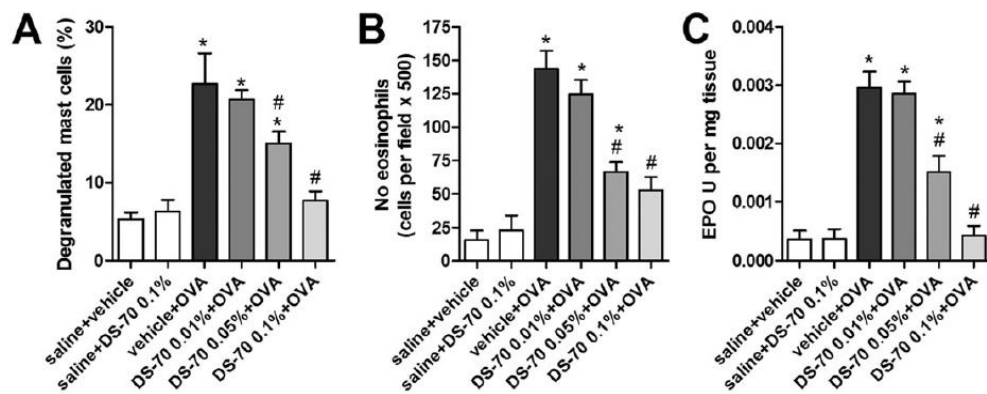
Figure 31. DS70 prevents, in a dose-dependent manner, conjunctival infiltration and degranulation of mast cells and eosinophils. (A) The number of degranulated mast cells was evaluated in photographs taken of 10 random fields of 10 different conjunctival sections (see photomicrographs in Figure 30A) and reported as percentage of degranulated mast cells (calculated with the following formula: DMC/MC × 100). (B) Effects of DS70 eye drops on conjunctival eosinophil infiltration 24 h after topical challenge with ovalbumin. Substantial eosinophil infiltration was observed in guinea pigs sensitized and topically challenged with OVA. In OVA-sensitized guinea pigs, treated with DS70 eye drops and challenged with OVA, there was a lower, dose-related, eosinophil infiltration than in conjunctiva of guinea pigs treated with OVA alone. The number of eosinophils was determined in photographs taken of 10 random fields of 10 different sections (see Figure 30B). (C) Effects of DS70 eye drops on conjunctival eosinophil peroxidase levels 24 h after topical challenge with OVA. Data refer to the mean ± SD (five animals per group were included, and both eyes were evaluated; $n = 10$). *$P < 0.05$, significantly different from saline + vehicle; #$P < 0.05$, significantly different from vehicle + OVA.
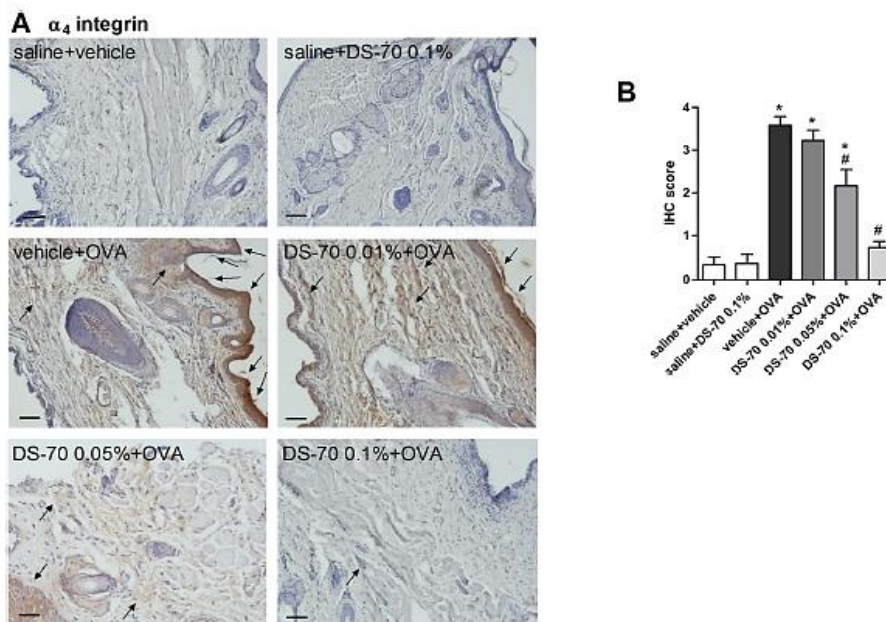
Figure 32. Topical treatment with DS70 in guinea pigs sensitized and challenged with OVA reduces conjunctival levels of α_4 integrin. (A) Photomicrographs of the conjunctiva 24 h after topical challenge with OVA and pretreatment with DS70 (0.01, 0.05 and 0.1%). Black arrows in panel A indicate hot spots of expression. (B) IHC score was assigned as reported in the Methods. Guinea pigs sensitized with saline and treated with the vehicle used to dissolve DS70 (saline + vehicle) showed basal levels of expression, as animals sensitized with saline and treated with DS70 alone (saline + DS70 0.1%). In guinea pigs sensitized and challenged with ovalbumin and treated with the vehicle used to dissolve DS70 (vehicle + OVA), IHC score is markedly increased, and DS70 at the

50

concentration 0.1% maximized the reduction that can be seen already observed at 0.05%. Data are presented as the mean ± SD (five animals per group were included, and both eyes were evaluated: $n = 10$). Black bars = 50 μm. *$P < 0.05$, significantly different from saline + vehicle; #$P < 0.05$, significantly different from vehicle + OVA.

Interestingly, DS70 significantly reduced α_4 integrin expression in conjunctival specimens obtained from treated guinea pigs in a dose-dependent manner (Figure 32). Immunofluorescence analysis carried out on sections obtained from tarsal conjunctiva specimens of guinea pigs sensitized and challenged with OVA showed double staining for tryptase, as marker of mast cells and α_4 integrin.[194] Moreover, the double staining of MBP (major basic protein), a marker of eosinophils,[195] and α_4 integrin showed the presence of both proteins in specimens of tarsal conjunctiva (Figure 33). Numerous cells positive for double staining were observed, confirming that α_4 integrin is expressed on both mast cells and eosinophils localized in conjunctival specimens (Figure 33).
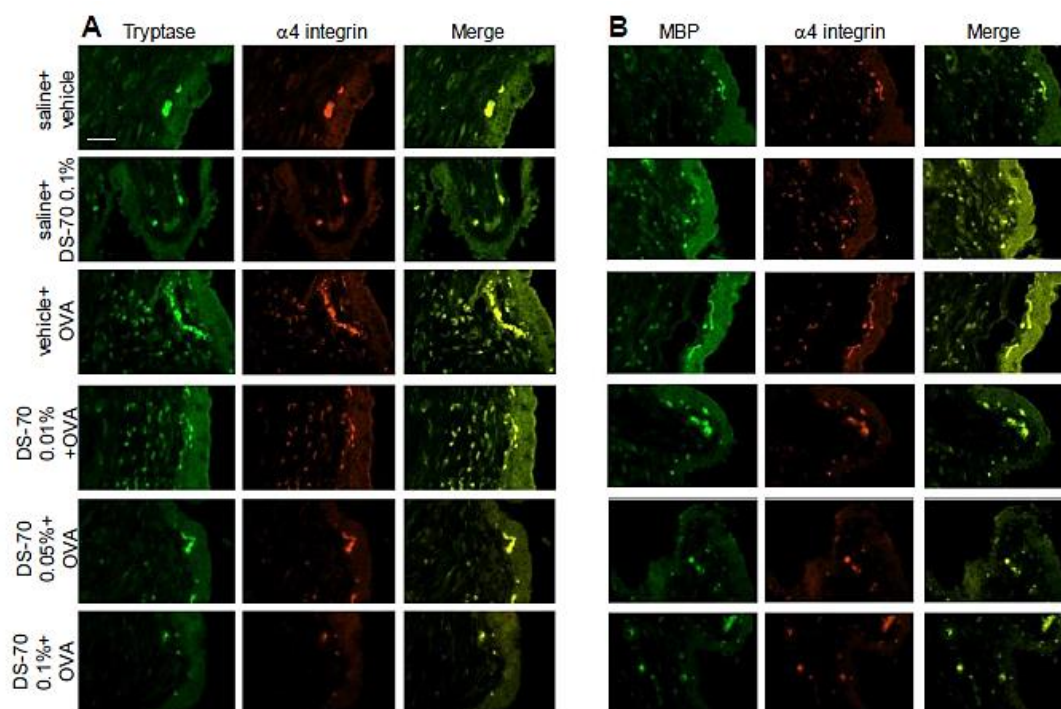
Figure 33. Co-localization of mast cell tryptase or MBP (major basic protein), markers for mast cells and eosinophils respectively, with α_4 integrin in conjunctival sections of guinea pigs sensitized and challenged with OVA and treated with DS70. (A) Mast cell tryptase and α_4 integrin colocalize on mast cells in conjunctival sections of guinea pig. Double immunofluorescence staining images for tryptase (*green*) and α4 integrin (*red*) are shown. (B) MBP and α_4 integrin colocalize on eosinophils in conjunctival sections of guinea pig. Double immunofluorescence staining images for MBP (*green*) and α_4 integrin (*red*) are shown (5 animals per group were included and both eyes were evaluated: $n = 10$). Scale bar = 50 μm.

➢ **Conjunctival levels of chemokine and cytokine mRNAs and protein content of CCL5 and CCL11 in OVA-treated guinea pigs**

Ovalbumin challenge in actively immunized guinea pigs, induced a significant elevation of the levels of mRNAs for IL-8, IL-1β, CCL5 and CCL11, and of protein levels of CCL5 and CCL11, in tarsal conjunctival specimens after 24 h. Pre-treatment with DS70 prior to ovalbumin challenge effectively and dose-dependently reduce the conjunctival levels of the cytokine and chemokine mRNAs (Figure 34) as well as CCL5 and CCL11 protein levels (Figure 35).
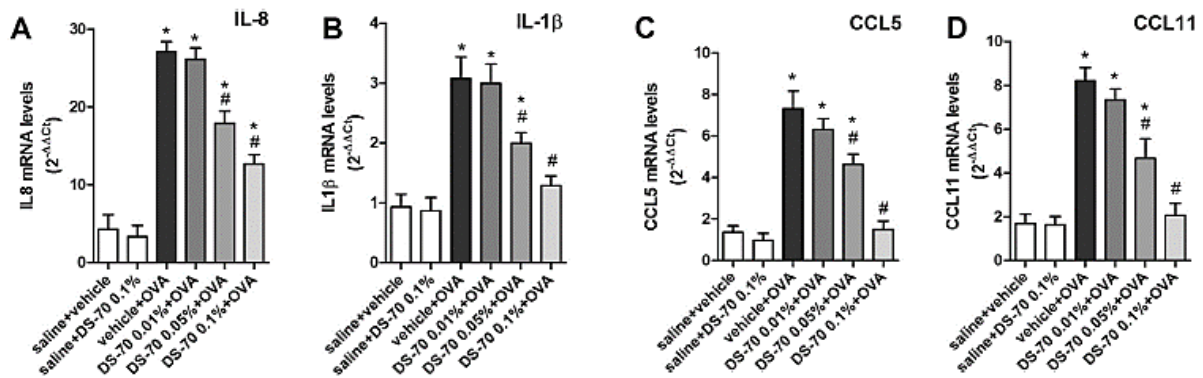
Figure 34. DS-70 eye drops (0.1% suspension) induced a significant down-regulation of IL-8, IL-1β, CCL5 and CCL11 transcripts in conjunctiva. Relative fold changes in mRNA levels were calculated using the $\Delta\Delta C_t$ method as described in the Methods. Ovalbumin challenged animals (vehicle + OVA) behave as positive control; DS70 0.05% and DS70 0.1% reduce this increase. Values are the mean ± SD (5 animals per group were included, and both eyes were evaluated; $n = 10$). *P < 0.05, significantly different from saline + vehicle; #P < 0.05, significantly different from vehicle + OVA.
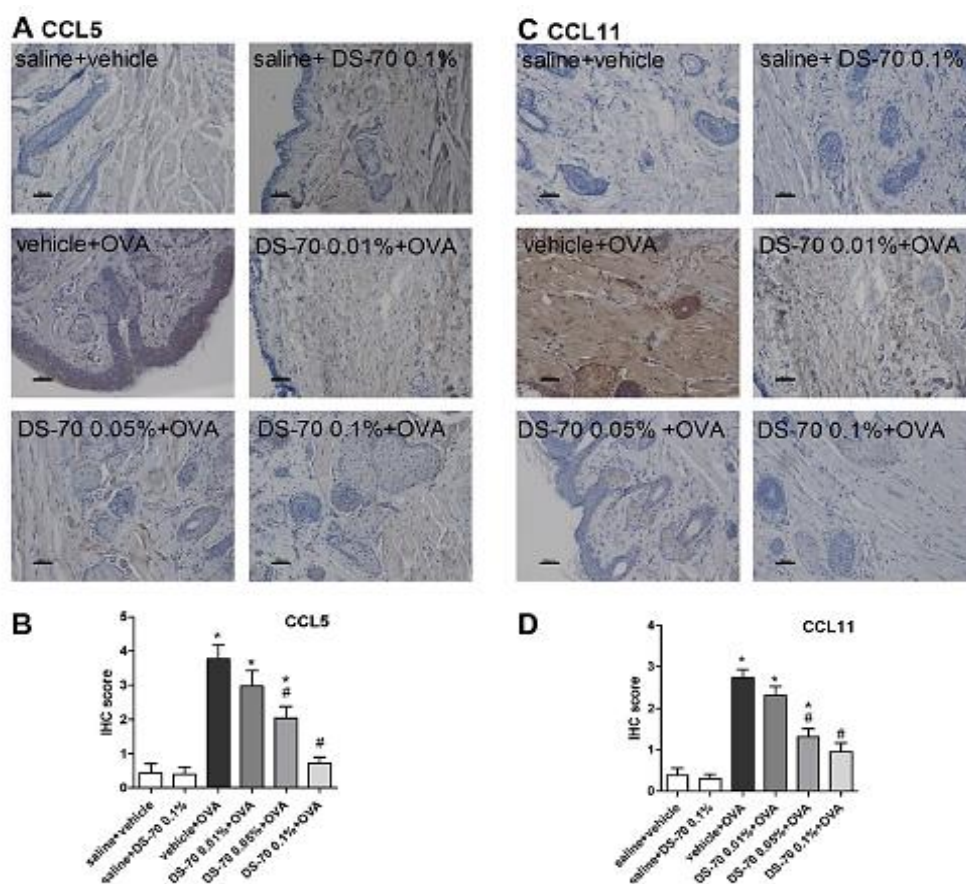
Figure 35. DS70 reduces CCL5 and CCL11 conjunctival expression. Conjunctival sections were examined by IHC for the expression of chemokines and the IHC scores calculated. (A-C) Representative photographs stained with specific primary antibodies are shown. (B-D) IHC scores assigned. Tissue sections from guinea pigs treated with saline (saline + vehicle) and DS70 alone (saline + DS70, 0.1%) were used as a negative control. Scale bar = 50 μm. Data are presented as mean $\pm$ SD (5 animals per group were included, and both eyes were evaluated; n = 10). *$P < 0.05$, significantly different from saline + vehicle; #$P < 0.05$, significantly different from vehicle + OVA.

3.3. Conclusion

In summary, two novel hybrid α/β-peptidomimetics were designed as $\alpha_4\beta_1$ integrin antagonist for the treatment of allergic conjunctivitis. On the basis of the fundamental requirements to interact with $\alpha_4\beta_1$ integrin receptor, a β^2-Pro residue was selected as a central core for the synthesis of a straight and a partially retro-inverso peptidomimetic, containing on one side, a diphenylurea moiety (MPUPA and AMPUMP, respectively), and on the other side, a free carboxylic acid group (Gly and malonyl, respectively). The compounds were successfully synthesized, and they showed a remarkable chemical and enzymatic stability in mouse serum (only 20% was degraded after 8 h) compared to BIO1211 reference compound. Complete pharmacological characterization was carried out only on DS70 (straight sequence), since

differently from our previous studies, it resulted more active than the analogue DS23 (partially retro inverso). DS70 binds to integrin $\alpha_4\beta_1$ with nanomolar affinity preventing the adhesion of α_4 integrin-expressing cells, antagonizes the VCAM-1-mediated degranulation of mast cells and eosinophils, and the ERK1/2 phosphorylation. DS70 shows to reduce in a dose-dependent manner the clinical symptoms of allergic conjunctivitis, the conjunctival α_4 integrin expression and the conjunctival levels of chemokines and cytokines in OVA-sensitized guinea pigs. To the best of our knowledge, this report is the first to describe a low MW compound that acts as an effective antagonist of α_4 integrin, after direct topical administration in the conjunctival fornix in an appropriate animal model of allergic conjunctivitis.

3.4. Experimental section

General methods for peptidomimetics synthesis

Standard chemicals and the protected amino acids were obtained from commercial sources and used without any purification. The purity of intermediates and final products were analysed by reverse-phase (RP)-HPLC, performed on Agilent 1100 series apparatus, equipped with a RP column Phenomenex (Torrance, CA, USA) No 00D-4439-Y0 Gemini 3 μm C_{18} 110 Å, LC column 100 × 3.0 mm; diode-array detection was set at 210 nm. Mobile phase description: gradient from 0.1% formic acid (0.1 mL·100 mL^{-1}) in H_2O/acetonitrile (9:1) up to formic acid (0.1 mL·100 mL^{-1}) in H_2O/acetonitrile (2:8) in 20 min, flow rate = 1.0 mL·min^{-1}. Semipreparative RP-HPLC utilized an Agilent 1100 series apparatus (Agilent, Technologies, Waldbronn, Germany), equipped with a RP column ZORBAX No 977150-102 Eclipse XDB C_{18} PrepHT cartridge 21.2 × 150 mm, 7 μm (Agilent Technologies). Mobile phase description: gradient from trifluoroacetic acid (TFA; 0.1 g·100 mL^{-1}) in H_2O/acetonitrile (8:2) to TFA (0.1 mL·100 mL^{-1}) in acetonitrile (100%) in 10 min, flow rate = 12 mL·min^{-1}. Electrospray ionization MS analysis was performed on a HP mass spectrometer MSD 1100 detector (Agilent Technologies) with single quadrupole. The procedures under microwave irradiation utilized the microwave oven Micro-SYNTH microwave labstation (Milestone Inc., Shelton, CT, USA) and temperature was controlled by using a built-in advanced fibre optic automatic control. ^{1}H-NMR analysis was performed on an apparatus Varian Gemini 400 MHz (Agilent Technologies); peptide samples were dissolved in DMSOd_6 to the final concentration of 0.01 M and analysed in 5 mm tubes at room temperature. Solvent suppression of residual moisture required the

standard 'PRESAT' solvent pre-saturation procedure; chemical shifts (δ) are expressed as ppm. DMSO was used as an internal standard, by setting δ H = 2.50 ppm. The following abbreviations are used: s, singlet; d, doublet; t, triplet; dd, double doublet and m, multiplet. The assignment of all resonances was based on two-dimensional gradient selected correlation spectroscopy experiments. **Refer to Dattoli *et. al.* for general biological methods.**[196]

Synthesis and characterization

Synthesis of DS70 (**Method A**, Scheme 1)

Fmoc-Gly-Wang preloaded resin (0.5 g, amino acid load = 0.4-0.8 mmol·g^{-1} according to the manufacturer) was placed into a syringe equipped with a frit.

Fmoc deprotection. The Fmoc protecting group was cleaved by treatment with 20% piperidine in DMF (5 mL) while bubbling nitrogen, under microwave irradiation (irradiation power = 40W, internal reaction temperature = 45°C; see above) for 2 min. The resin was filtered and washed with MeOH (5 mL), DMF (5 mL) and DCM (5 mL) in sequence. The cleavage procedure and washes were repeated twice as described above. The deprotection was qualitatively assessed by a positive Kaiser test.

Coupling reaction. The acid-partner (0.9 mmol), HOBt (0.9 mmol) and DCC (0.9 mmol) were dissolved in DMF (6 mL) at room temperature. After stirring for 5 min, the mixture was added to the resin pre-swollen in DCM (5 mL). The suspension was mechanically shaken for 10 min under microwave irradiation. Then, the resin was filtered and washed three times with the same solvents as described in the paragraph above. The coupling was assessed by the Kaiser test. The repetitive deprotection and coupling steps were carried out according to the same protocols and workup procedures (Scheme 1).

Peptide cleavage. The peptidyl-resin obtained according to the previous protocol was pre-swollen in DCM (3 mL) and treated with a 90:5:5 mixture of TFA/H$_2$O/TIS (10 mL), plus phenol (50 mg), and the mixture has mechanically shaken at room temperature for 2 h. Subsequently, the cocktail was filtered to recover the peptide, and the unloaded resin was washed with 20% TFA in Et$_2$O (5 mL), DCM (5 mL) and MeOH (5 mL) in sequence. The filtrates were collected; the volatiles were removed with a moderate nitrogen flow at room temperature. The solid residue was suspended in ice-cold Et$_2$O to favour peptide precipitation. The crude peptide was triturated and collected by centrifugation at 2000 × *g* for 10 min. The

isolated peptide was purified by semipreparative RP-HPLC (78% yield), and purity was assessed by analytical RP-HPLC (98%). The compound identity was determined by ESI-MS analysis. ^{1}H-NMR (400MHz, 3:1 CDCl$_3$/DMSOd_6,) the spectrum shows two sets of signals in 1:1 ratio, relative to conformers A and B around the amide bond which precedes β-Pro: δ 1.82-2.03 (m, 2H$_{A+B}$, β-ProH4$_{A+B}$), 2.05 (s, 3H$_{A+B}$, ArCH$_{3A+B}$), 2.78 (m, 1H$_A$, β-ProH3$_A$), 2.86 (m, 1H$_B$, β-ProH3$_B$), 3.16 (m, 1H$_B$, β-ProH5$_B$), 3.24 (m, 1H$_A$, β-ProH5$_A$), 3.33-3.39 (m, 2H$_A$, β-ProH2$_A$ + β-ProH5$_A$), 3.39-3.49 (m, 2H$_{A+B}$ + 3H$_B$, CH$_2$CO$_{A+B}$ + β-ProH5$_B$ + 2x β-ProH2$_B$), 3.54 (dd, J = 8.0, 13.6 Hz, 1H$_A$, β-ProH2$_A$), 3.70 (d, J = 4.8 Hz, 2H$_{A+B}$, GlyHα$_{A+B}$), 6.73 (t, J = 7.2 Hz, 1H$_{A+B}$, ArH4$_{A+B}$), 6.83-6.97 (m, 4H$_{A+B}$, ArH3'5'$_{A+B}$ + ArH3,5$_{A+B}$), 7.19 (d, J = 7.6 Hz, 2H$_{A+B}$, ArH2'6'$_{A+B}$), 7.22 (s, 1H$_{A+B}$, ureaNH$_{A+B}$), 7.62 (d, J = 8.0 Hz, 1H$_{A+B}$, ArH6$_{A+B}$), 8.37 (s, 1H$_{A+B}$, ureaNH$_{A+B}$). ESI-MS m/z [M+H]$^+$ calcd. for C$_{23}$H$_{26}$N$_4$O$_5$: 439.19; found: 439.30.

Synthesis of BIO1211

BIO1211 (MPUPA-LDVP) was prepared adopting the same SPPS procedure described above for DS70. Purity was evaluated by analytical RP-HPLC (98%) and chemical identity by ESI-MS m/z [M+H]$^+$ calcd. for C$_{36}$H$_{48}$N$_6$O$_6$: 709.35; found: 709.40.

Synthesis of DS23 (Method B, Scheme 1)

Boc-β-Pro (1.0 mmol), HOBt (1.1 mmol) and HBTU (1.1 mmol) were dissolved in 4:1 DCM/DMF (5 mL) and the mixture was stirred at room temperature under an inert atmosphere for 5 min. Thereafter, AMPUMP-TFA salt (1.1 mmol) was added at room temperature while stirring, followed by DIPEA (2.2 mmol). The mixture was stirred for 10 min under microwave irradiation. The mixture was diluted with DCM (40 mL) and washed with 0.5 M HCl (5 mL) and with saturated solution of NaHCO$_3$ (5 mL). The organic layer was dried over Na$_2$SO$_4$, and the solvent was removed at reduced pressure. The protected intermediate was purified (75%) by flash chromatography over silica gel (eluent: 100% ethyl acetate). Subsequently, the Boc-group was removed by treatment with mixture of 25% TFA in DCM (10 mL). The mixture was subjected to moderate nitrogen flow at room temperature until a solid residue was obtained. The resulting TFA salt was utilized without purification and coupled with 3-(benzyloxy)-3-oxopropanoic acid under the same coupling conditions described above, following the same work up and purification by flash chromatography of the intermediate. Finally, the benzyl ester was removed with H$_2$ and catalytic amount of Pd/C in EtOH for 4 h (Scheme 1) at room temperature. The mixture was filtered over Celite® and the filtrates evaporated at reduced pressure. Purification of the residue was carried out by semipreparative RP-HPLC, and purity

was determined by analytical RP-HPLC (97%). ESI-MS *m/z* [M+H]$^+$ 439.2; calcd. for C$_{23}$H$_{26}$N$_4$O$_5$: 439.19; found: 439.20.

4. DESIGN AND SYNTHESIS OF DS70-BASED HYBRID α/β-PEPTIDOMIMETICS

4.1. Introduction

On the basis of our recent and excellent results on the compound DS70,[197] and moved by our interest in the development of potent small-molecule peptidomimetics for $\alpha_4\beta_1$ integrin, we questioned whether more flexibility at the binding site could retain high affinity and inhibition activity on $\alpha_4\beta_1$ integrin. To explore this possibility, we investigated the β-amino acid scope in a small library of novel and flexible hybrid α/β-peptidomimetics, analogues of DS70 and DS23, aimed at the treatment of α_4-related inflammatory diseases. Initially, the rigid β^2-Pro central core was substituted by an (*S*)- or (*R*)-β^2-Ala and β^3-Ala, in order to confer more flexibility and high enzymatic stability toward proteases. The β^2-Pro ring-opening preserves the optimal distance of 14 C-C bonds between the two pharmacophoric groups. Similar to DS70, the straight sequence was assembled by linking the MPUPA α_4-targeting moiety at the N-terminus, and the Gly, coordinating the β_1-subunit, at the C-terminus of the β-amino acid central core. Whereas, the corresponding partially retro-inverso peptidomimetics were synthesized by connecting the central β^2-Ala and β^3-Ala to the AMPUMP diphenylurea moiety (C-terminus) and to the malonic acid (N-terminus, Figure 37). For each class of peptides (straight- and retro-) the effect of both, (*R*)- and (*S*)-stereochemistry of the β^2-Ala/β^3-Ala core on cell adhesion inhibition were also evaluated (Table 4).

Subsequently, the central β-amino acidic scaffold was modified by introducing suitable functional groups, that in perspective, can be functionalized with certain linker thus providing a useful construct with an anchoring point well-spaced from the principle integrin binding sequence. Such linkers make these constructs eligible to be conjugated on different scaffold such as polymers, nanofibers, nanoparticles, surfaces, drug delivery systems, and so on, thus opening a new way for the treatment and diagnosis of many pathologies.[198, 199] Based on this premises, we designed a small library in which the β-Ala was replaced by two different building blocks, the 2,3-diaminopropionic acid (Dap) bearing an amino group in the corresponding Ala β^2 position, while the β^3-Ala is replaced by an isoAsp carrying a carboxylic acid in the corresponding β^3 position (Figure 37). The Dap building block can be easily prepared by starting from an Asn or Asp amino acid residue via Hofmann or Curtius rearrangements.[161, 200] These methods are commonly used for the synthesis of *gem*-diamine, urea and urethane

derivatives allowing the maintenance of the configuration during the transposition (Figure 36).[200, 201]
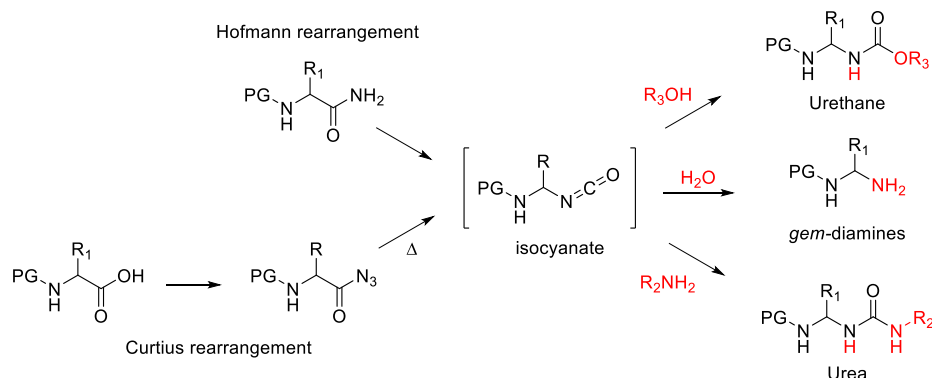

Figure 36. Hofmann and Curtius rearrangements.

The Hofmann rearrangement is a well-known reaction that provides the transformation of primary amides into amines. In the recent years, iodine(III) reagents, such as $PhI(OCOCF_3)_2$, $PhI(OAc)_2$ and $PhI(OTs)OH$, have often been used successfully with high yields of the corresponding ammonium salts to carry out the transposition under acidic conditions.[202] In our strategy, the Hofmann rearrangement was applied to the transposition of the primary amide side-chain of an N-protected (S)- and (R)-Asn residue into the corresponding β-amino-Ala using $PhI(OCOCF_3)_2$.[161]
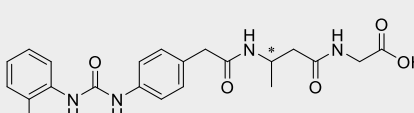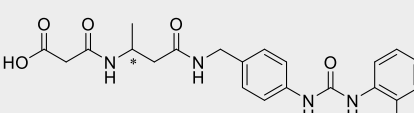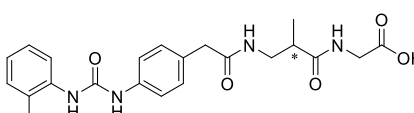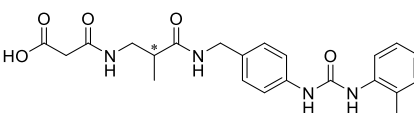
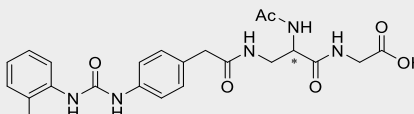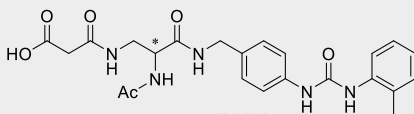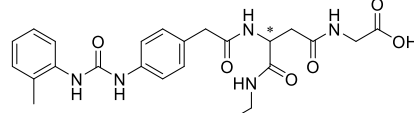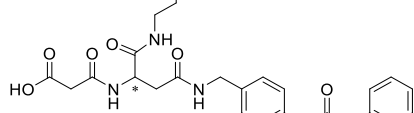The two families of compounds have been realized by flanking the respective pharmacophoric groups, MPUPA and Gly for the straight-peptides, and AMPUMP and malonic acid for the retro-peptides, to the central functionalized β-amino acid core (Figure 37). Similarly, the effect of core's (R)- and (S)-stereochemistry in cell adhesion inhibition was also evaluated (Table 4). In order to avoid unspecific or additional interactions at the integrin binding site that may cause loss of activity, in initial studies, the amino and carboxyl groups of the central β-amino acids have been blocked by acetylation or by simple coupling with a short alkyl amine (Figure 37). On the other hand, the presence of these functional groups also contributes to the spatial screening of the target and to understanding whether modifications at the central position are tolerated.
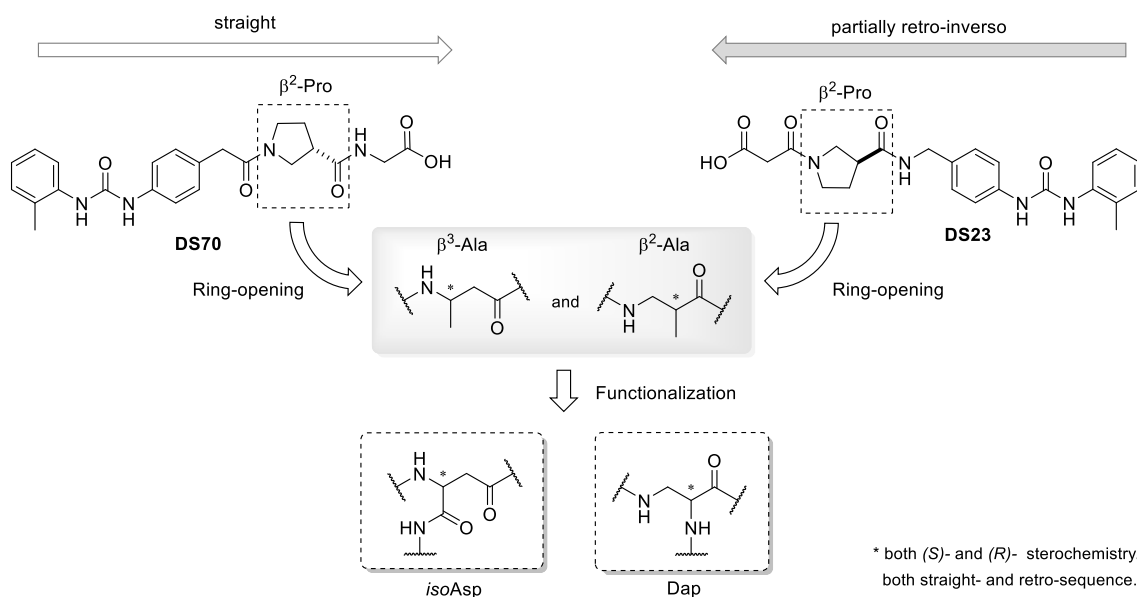
Figure 37. Design of flexible straight and partially retro-inverso hybrid α/β-peptidomimetics.

Table 4. Small libraries of novel and flexible hybrid α/β-peptides based on the structure of DS70.

In perspective, the blocking groups will be substituted by a suitable linker to allow the conjugation of the $\alpha_4\beta_1$ integrin ligands to a variety of nanomaterials or nanoparticles for theranostic applications (see Chapter 6).

4.2. Results and Discussion

4.2.1. Peptide synthesis of hybrid α/β-peptidomimetics bearing β³-homoAla as central core

The β³-amino acids, with proteinogenic or non-proteinogenic side chains, are readily obtained by direct Arndt-Eistert homologation of the *N*-Boc or *N*-Fmoc α-amino acids, although is generally less efficient and not suitable for large scale preparation.[203] Therefore, we first synthesize the enantiopure β³-amino acids core adopting a mild and scalable multi-steps procedure previously reported by Caputo *et. al.*[204] (Scheme 2). In agreement with this procedure, *N*-Boc α-Ala was reduced into *N*-protected β-aminoalcohols, (*S*)-**MA54** and (*R*)-**MA76**, via mixed anhydride under mild condition using NaBH₄. These latter were then converted into the corresponding *N*-protected β-aminoiodides, (*S*)-**MA55** and (*R*)-**MA81**, with a triphenylphosphine-iodide complex under mild conditions, without any detectable epimerization of the chiral center. Due to the poor stability under the common separation and purification procedures, the iodoamine intermediates were used directly without further purification. The subsequent replacement of the iodine by a cyano group led to (*S*)-**MA58** and (*R*)-**MA82**, while the final hydrolysis (acidic or alkaline) of the latter led to *N*-protected β³-homoAla, (*S*)-**MA60** and (*R*)-**MA84** (Scheme 2). The potential racemization was checked by HPLC on a chiral column and polarimetry. In agreement with Caputo *et. al.* no traces of racemized products have been detected.
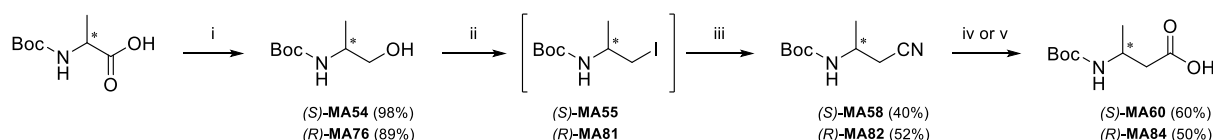
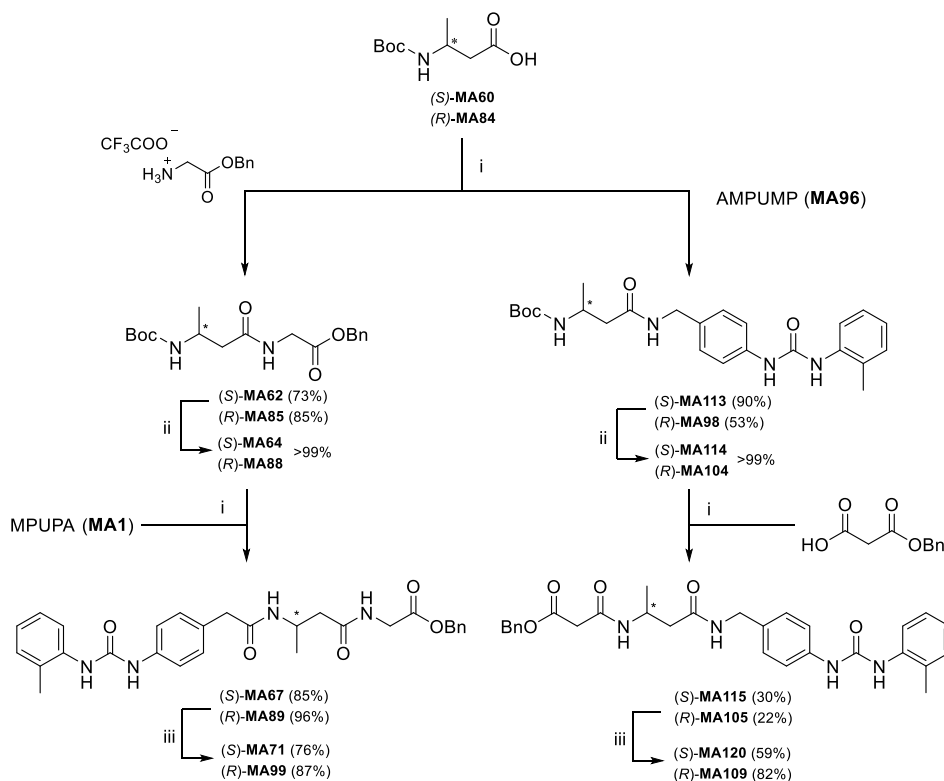
Scheme 2. Synthetic scheme for *N*-Boc β³-homoAla. *Reagents and conditions:* i) NMM, ethyl chloroformate, THF, 0 °C – RT, 15 min, then NaBH₄₍ₐq₎ 0 °C – RT, 10 min; ii) PPh₃, I₂, imidazole, DCM, reflux, 3 h; iii) KCN, DMSO, 60 °C, 4 h; iv) KOH₍ₐq₎ 1M/EtOH (1:1), 90 °C, 3 h; or v) HCl 6M, reflux, 12 h.

The diphenylurea moieties, MPUPA (**MA1**) and AMPUMP (**MA96**) were simply synthesized by a reaction between *o*-tolyl isocyanate and the appropriate aromatic amine (Scheme 3). Regarding the preparation of AMPUMP, Boc-protection of the benzylic amine is required before the urea bond formation, and afterwards, it can be easily removed by treatment with 25% of TFA in DCM giving the corresponding TFA-salt **MA96** (Scheme 3).
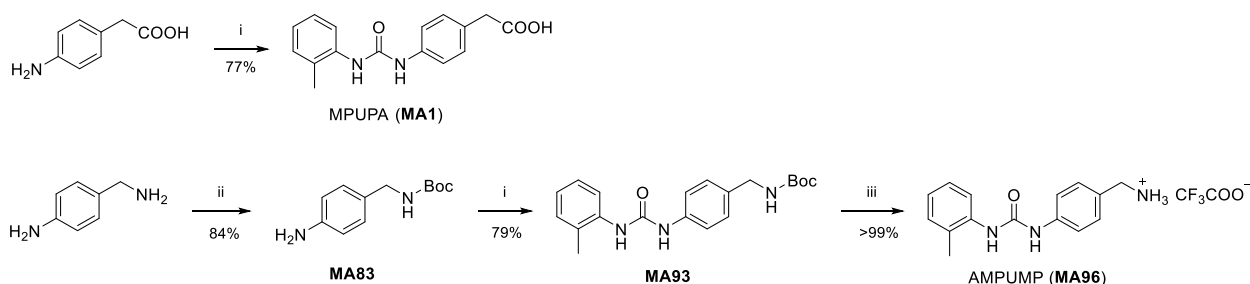
Scheme 3. Synthetic scheme for MPUPA and AMPUMP diphenylureas. *Reagents and conditions:* i) *o*-tolyl isocyanate, DMF, RT, 3 h; ii) Boc₂O, DCM, RT, 2 h; iii) 25% TFA/DCM, RT, 1 h.

Both straight and partially retro-inverso sequences were prepared in solution. In details, H-Gly-OBn·TFA salt was coupled, in turn, with *N*-Boc β³-Ala (*S*)-**MA60** and (*R*)-**MA84**, preactivated with EDC·HCl/HOBt/TEA as coupling agents in DCM/DMF (4:1). The resulting Boc-dipeptides were deprotected by treatment with 25% TFA in DCM and were followed by coupling with MPUPA (**MA1**) under the same condition described above. Final deprotection of the benzyl ester afforded (*S*)-**MA71** and (*R*)-**MA99** in good yields (76% and 88%, Scheme 4). Similarly, for retro-peptides AMPUMP (**MA96**) was coupled, in turn, with *N*-Boc β³-Ala (*S*)-**MA 60** and (*R*)-**MA84** in the presence of EDC·HCl/HOBt/TEA dissolved in DCM/DMF (4:1) as mentioned before. Boc-deprotection of the resulting dipeptides and final coupling with *mono*-benzyl malonic acid were performed under the same conditions previously described. Finally, deprotection of the benzyl ester was carried out by catalytic hydrogenation, giving (*S*)-**MA120** and (*R*)-**MA109** in good yields (60% and 82%, Scheme 4). For all peptides, the purity was assessed by RP-HPLC and the chemical identity was determined by ESI-MS, 1D and 2D NMR spectroscopy (entry 1, Table 4).

Scheme 4. Synthetic scheme for MPUPA-β³homoAla-Gly-OH and malonyl-β³homoAla-AMPUMP. *Reagent and conditions:* i) EDC·HCl, HOBt, TEA, DCM/DMF (4:1), RT, 12 h; ii) 25% TFA/DCM, RT, 1 h; iii) H₂, Pd/C, EtOH, RT, 12 h.

4.2.2. Peptide synthesis of hybrid α/β-peptidomimetics bearing β²-homoAla as central core

The enantiopure β²-amino acids core were synthesized by following a multi-step procedure previously reported by Lee *et. al.*[205] Synthesis started with tosylation of both (*S*)- and (*R*)-methyl 3-hydroxy-2-methylpropanoate, providing (*S*)-**MA162** and (*R*)-**MA184** in good yields, 87% and 91%, respectively (Scheme 5). Thus, the tosylates were treated with sodium azide in DMF to afford the corresponding (*S*)-**MA165** and (*R*)-**MA185**.

For the synthesis of the straight-peptides, the reduction of the crude azides with H₂ and catalytic amount of Pd/C gave the primary amines, (*S*)-**MA167** and (*R*)-**MA186**, that were subsequentially coupled in DCM/DMF (4:1) with MPUPA in the presence of TBTU/HOBt/DIPEA as activating agents. Ester hydrolysis of the resulting protected compounds with LiOH for 2 h gave the respective free carboxylic acids (*S*)-**MA175** and (*R*)-**MA191** that were finally coupled with H-Gly-OtBu·HCl salt, under the same coupling conditions previously described, giving (*S*)-**MA179** and (*R*)-**MA195** with acceptable yields

(50-55%). Finally, an easy deprotection of the *t*Bu group using TFA in DCM gave the final straight β²-peptidomimetics, (S)-**MA192** and (R)-**MA199** in almost quantitative yields (Scheme 5).

For the synthesis of the retro-peptides, in order to avoid a further amine protection step, we thought to use the azide group as protecting group since it is inert in the coupling reaction conditions. First, we performed the ester hydrolysis of both (S)- and (R)-methyl 3-azido-2-methylpropanoate (**MA165** and **MA185**) with LiOH for 2 h to afford the respective carboxylic acids (S)-**MA164** and (R)-**MA193**. These latter were readily coupled with AMPUMP under the same coupling conditions used for the straight sequences. Reduction of the resulting azides with H₂ and a catalytic amount of Pd/C gave the primary amines, (S)-**MA196** and (R)-**MA202**. Then, these latter were coupled with *mono-t*Bu-malonic acid under the usual conditions, yielding (S)-**MA267** and (R)-**MA203**, respectively.
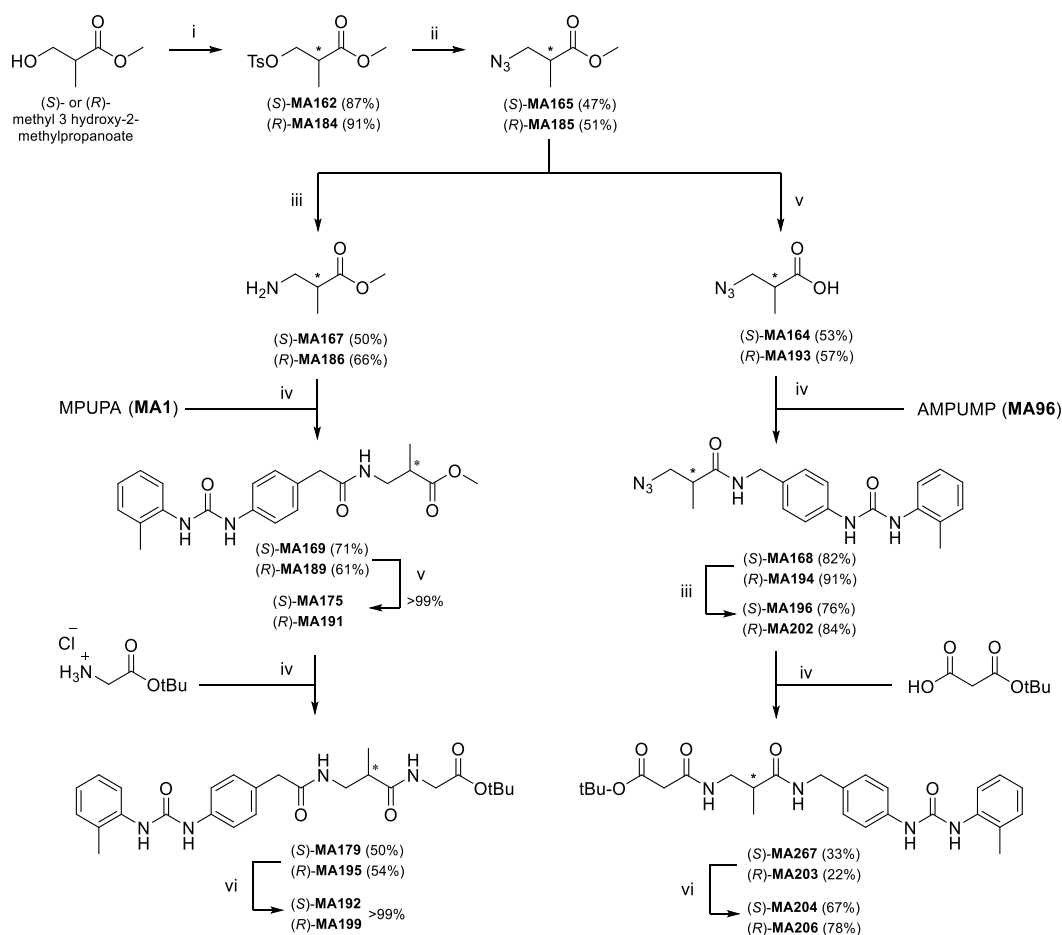
Scheme 5. Synthetic scheme for MPUPA-β²-homoAla-Gly-OH and malonyl-β²-homoAla-AMPUMP. *Reagent and conditions:* i) TsCl, TEA, DCM, 0 °C – RT, overnight; ii) NaN₃, DMF, 50 °C, 16 h; iii) H₂, Pd/C, EtOH, RT,

12 h; iv) TBTU, HOBt, DIPEA, DCM/DMF (4:1), RT, 12 h; v) LiOH, THF/H_2O (2:1), 0 °C – RT, 2 h; vi) TFA/DCM (1:1), RT, 1 h.

Finally, deprotection of the *t*Bu using TFA in DCM afforded the final retro β^2-peptidomimetics (*S*)-**MA204** and (*R*)-**MA206** in acceptable yields (67% and 78%, Scheme 5). For all peptides, the purity was assessed by RP-HPLC, and the chemical identity was determined by ESI-MS, 1D and 2D NMR spectroscopy (entry 2, Table 4).

4.2.3. Peptide synthesis of hybrid α/β-peptidomimetics bearing *iso*Asp as β^3-residue central core

In order to design hybrid α/β-peptidomimetics possessing an anchoring point for further functionalization, we selected as central core an isoAsp residue that mimics the β^3-homoAla scaffold, and in addition, carries a carboxylic acid. The latter may be properly functionalized with certain linkers by straightforward coupling reaction. Initially, this group was blocked with a short *n*-propylamine. Prior to start, we synthesized the central core building block by coupling, in turn, the (*S*)- and (*R*)-Fmoc-Asp(OtBu)-OH with the *n*-propylamine using EDC/HOBt/TEA as activating agents. Subsequent *t*Bu-deprotection with TFA in DCM afforded the respective Fmoc-Asp(OH)-*N*-propylamide building block, (*S*)-**MA59** and (*R*)-**MA156**.

The straight-peptides (*S*)-**MA63** and (*R*)-**MA158** were assembled by SPPS on a Wang resin preloaded with Fmoc-Gly, using Fmoc-protected amino acids (Method A, Scheme 6). Removal of Fmoc group was carried out twice by treatment with 20% piperidine in DMF at RT for 10 min. Coupling between each residue was carried out with the activating agents DCC and HOBt in DCM/DMF (4:1, *v/v*) at RT for 3 h. Peptide cleavage was accomplished by treatment of the peptidyl-resin with TFA in the presence of scavengers. The crude products were precipitated from ice-cold Et$_2$O and collected in acceptable yields by centrifuge (Method A, Scheme 6). On the other hand, the partially retro-inverso peptides (*S*)-**MA154** and (*R*)-**MA161** were prepared in solution (Method B, Scheme 6). AMPUMP was alternately coupled with Fmoc-Asp-*N*-propylamide, (*S*)-**MA59** and (*R*)-**MA156**, in DCM/DMF using EDC/HOBt/TEA as activating agents. Fmoc removal from (*S*)-**MA145** and (*R*)-**MA151** was carried out with 20% piperidine in DMF for 1 h at RT giving the corresponding deprotected dipeptides (*S*)-**MA146** and (*R*)-**MA152** in quantitative yields. Finally, coupling with malonic acid *mono*-benzyl ester was performed under the same conditions previously described and, was followed by catalytic hydrogenation of the benzyl ester to afford (*S*)-**MA154** and (*R*)-**MA161** in 74% and 53% yields,

respectively (Method B, Scheme 6). For all peptides, the purity was assessed by RP-HPLC, and the chemical identity was determined by ESI-MS, 1D and 2D NMR spectroscopy (entry 4, Table 4).
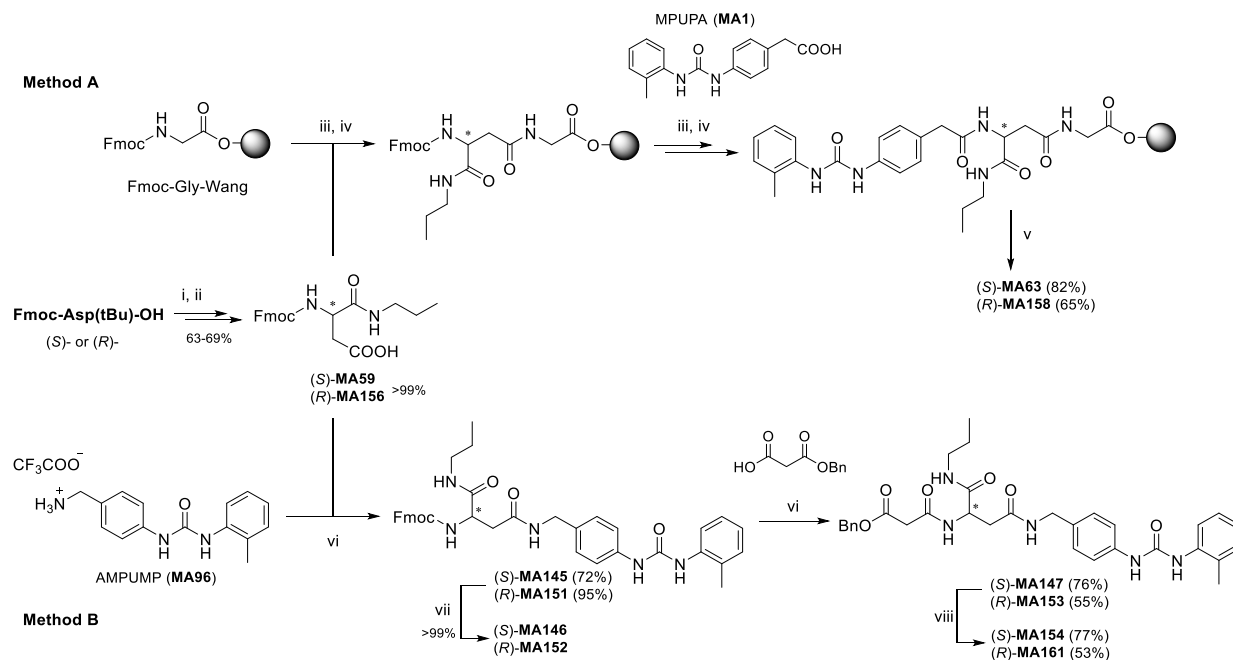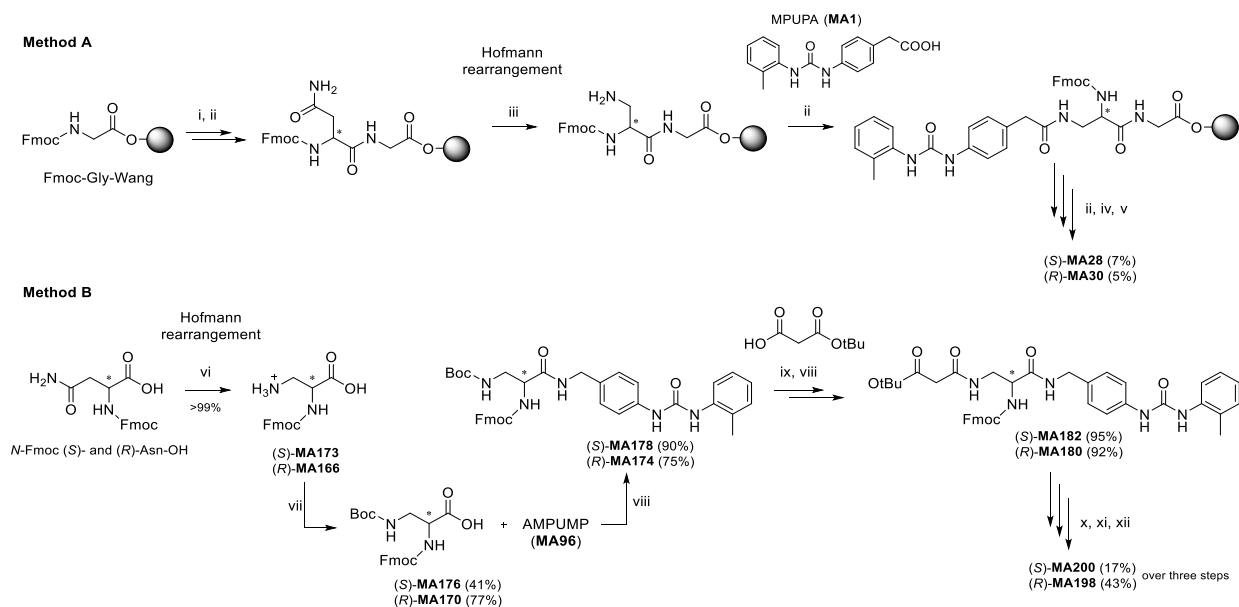

Scheme 6. Synthetic scheme for MPUPA-Asp(Gly)-*n*-propylamine and malonyl-Asp(AMPUMP)-*n*-propylamine. *Reagents and conditions.* **Method A:** i) *n*-propylamine, EDC·HCl/HOBt/TEA, DCM/DMF, RT, 3 h; ii) TFA/DCM (1:1), RT, 1 h; iii) 20% piperidine/DMF, RT, 10 min (x2); iv) Fmoc-Asp-*n*-propylamine, DCC, HOBt, DCM/DMF, RT, 3 h; same repeated for MPUPA; v) TFA/H$_2$O/TIS/PhOH (80:10:10 v/v/v), RT, 2.5 h. *Reagents and conditions.* **Method B:** vi) EDC·HCl/HOBt/TEA, DCM/DMF, RT, 12 h; same repeated for *mono*-benzyl malonic acid; vii) 20% piperidine/DMF, RT, 1 h; viii) H$_2$, Pd/C, EtOH, RT, 12 h.

4.2.4. Peptide synthesis of hybrid α/β-peptidomimetics bearing Dap β^2-residue as central core

For the design of the second family of hybrid α/β-peptidomimetics possessing the anchoring functional group at the central core of the backbone, we selected a 2,3-diaminopropionic acid (Dap) which instead mimics the β^2-homoAla scaffold and carries a functionalizable amino group. This building block can be synthesized via Hofmann rearrangement of *N*-protected Asn residue into the corresponding β-amino-Ala, using PhI(OCOCF$_3$)$_2$ (PIFA) and pyridine in DMF/H$_2$O (Scheme 7). The subsequent Boc-protection of the free amino-function provided the diprotected building block (*S*)-**MA176** and (*R*)-**MA170** that were used for the synthesis of retro-peptides. These latter were firstly coupled with AMPUMP in DCM/DMF using

TBTU/HOBt/DIPEA as activating agents yielding (*S*)-**MA178** and (*R*)-**MA174**, respectively. Boc-deprotection with TFA and the last coupling with malonic acid *mono-t*Bu ester under the same conditions previously described completed the respective retro-sequences (*S*)-**MA182** and (*R*)-**MA180**. Finally, a sequence of Fmoc-deprotection with piperidine, acetylation with acetyl chloride and DIPEA, and *t*Bu-deprotection with TFA gave the final retro-peptides (*S*)-**MA200** and (*R*)-**MA198** in quantitative yields (Method B, Scheme 7).

The straight-peptides (*S*)-**MA28** and (*R*)-**MA30** were assembled manually by SPPS on a Wang resin preloaded with Fmoc-Gly using Fmoc-protected amino acids (Method A, Scheme 7). Removal of Fmoc group was carried out twice by treatment with 20% piperidine in DMF at RT for 10 min. Coupling between each residue was done with DCC and HOBt in DCM/DMF (4:1 *v/v*) at RT for 3 h. The transposition of the primary amide of *N*-Fmoc (*S*)- and (*R*)-Asn into the corresponding amines, was performed via Hofmann rearrangement on resin using PIFA and pyridine in a mixture of THF/DMF/H_2O (2:2:1).[206] The resulting free amine was coupled with MPUPA under the same conditions described above. Finally, Fmoc-deprotection and successive acetylation with Ac_2O and pyridine completed the two linear sequences. Peptide cleavage was accomplished by treatment of the resin with TFA in the presence of scavengers.

Scheme 7. Synthetic scheme for N_α-Acetyl N_β-MPUPA Dap-Gly-OH and N_α-Acetyl N_β-malonyl Dap-AMPUMP. *Reagents and conditions.* **Method A:** i) 20% piperidine/DMF, RT, 10 min (x2); ii) Fmoc-Asn-OH, DCC/HOBt, DCM/DMF, RT, 3 h; same repeated for MPUPA; iii) PIFA, pyridine, THF/DMF/H_2O (2:2:1), RT, 3 h; iv) Ac_2O, pyridine, DCM, RT, 1 h; v) TFA/H_2O/TIS/PhOH (80:10:10 v/v/v), RT, 2.5 h. *Reagents and conditions.* **Method B:** vi) PIFA, pyridine, DMF/H_2O (2:1), RT, 12 h; vii) Boc_2O, Na_2CO_3, H_2O/dioxane (1:1), RT, 12 h; viii) AMPUMP, TBTU/HOBt/DIPEA, DCM/DMF, RT, 12 h; same repeated for *mono-t*Bu-malonic acid; ix) 25%

TFA/DCM, RT, 1 h; x) 20% piperidine/DMF, RT 1 h; xi) acetyl chloride, DIPEA, DCM, 0 °C – RT, 4 h; xii) TFA/DCM (1:1), RT, 1 h.

The crude products were precipitated from ice-cold Et₂O, collected by centrifuge and purified by semipreparative RP-HPLC (Method A, Scheme 7). For all peptides, the purity was assessed by RP-HPLC, and the chemical identity was determined by ESI-MS, 1D and 2D NMR spectroscopy (entry 3, Table 4).

4.3. Conclusion and perspectives

In summary, taking inspiration from DS70 structure, two families of flexible hybrid α/β-peptidomimetics were designed as potential $\alpha_4\beta_1$ integrin antagonist. Following the peptidomimetics approaches the constrained β^2-Pro was substituted by a more flexible central core. To this purpose β^2-, β^3-Ala and their respective functionalized residues, isoAsp and Dap, were selected as a central core for the synthesis of straight and partially retro-inverso peptidomimetics that were flanked by the diphenylurea moiety (MPUPA and AMPUMP) on one side, and the free carboxylic acid group (Gly and malonyl) on the other side. These compounds were successfully synthesized and, for each of them the influence of the diverse core's stereochemistry, (*S*)- and (*R*)-, was taken into consideration in cell adhesion assays. The potential efficacy of these compounds will be firstly assayed *in vitro* to determine their affinity toward $\alpha_4\beta_1$ integrin and their effects on the inhibition of $\alpha_4\beta_1$-mediated cell adhesion in comparison with that of the reference compound BIO1211. Unfortunately, the proposed peptidomimetics are at the early stage of their biological investigation and, no results are currently available to be discussed. In perspective, the hybrid α/β-peptidomimetic functionalized with suitable linkers may represent a useful tool for the development of peptide nanostructured biomaterials for a wide range of medical application from therapy to diagnosis.

4.4. Experimental section

General methods

All reactions requiring anhydrous conditions were performed under argon atmosphere. Standard chemicals and solvents including *N*-protected and *C*-protected amino acids, unless otherwise stated, were purchased from commercial sources and used as received without further

purification. Flash chromatography was carried out on silica gel (230–400 mesh), using mixtures of distilled solvents. Compound purities were determined by analytical RP-HPLC and elemental analysis. Analytical RP-HPLC was carried out with an Agilent 1100 series apparatus, using a reverse-phase column Phenomenex mod. Gemini 3 μm C_{18} 110 Å 100 × 3.0 mm (No 00D-4439-Y0); column description: stationary phase octadecyl-carbon-chain-bonded silica (C_{18}) with TMS (trimethylsilyl) endcap, fully porous organosilica solid support, particle size 3 μm, pore size 110 Å, length 100 mm, internal diameter 3 mm; DAD (diode-array detection) 210 nm; mobile phase: from H_2O/CH_3CN (9:1) to H_2O/CH_3CN (2:8) in 20 min at a flow rate of 1.0 mL·min^{-1}, followed by 10 min at the same composition. Semipreparative RP-HPLC was carried out with an Agilent 1100 series apparatus, using a reverse-phase column ZORBAX mod. Eclipse XDBC18 PrepHT cartridge 21.2 × 150 mm 7 μm (no. 977150-102); column description: stationary phase octadecyl-carbon-chain-bonded silica (C_{18}), double end-capped, particle size 7 μm, pore size 80 Å, length 150 mm, internal diameter 21.2 mm; DAD 210 nm; mobile phase from H_2O/CH_3CN (8:2) to CH_3CN (100 %) in 10 min at a flow rate of 12 mL·min^{-1}. ESI-MS analysis was carried out using an MS single quadrupole HP 1100 MSD detector, with a drying gas flow of 12.5 L min^{-1}, nebulizer pressure 30 psig, drying gas temp. 350 °C, capillary voltage 4500 (+) and 4000 (–), scan 50-2600 amu. Elemental analyses were carried out with a Thermo Flash 2000 CHNS/O analyser. Chiral HPLC analysis was performed with an Agilent 1200 series apparatus, using a CHIRALPAK IC column, particle size 5 mm, length 250 mm, internal diameter 4.6 mm, DAD 210/254 nm; mobile phase *n*-hexane/2-propanol (1:1) at 0.8 mL/min. NMR spectra were recorded on a Varian Gemini apparatus (^{1}H: 400 MHz, ^{13}C: 100 MHz) at 298 K in 5 mm tubes, using 0.01 M peptide. Solvent suppression was carried out by the solvent presaturation procedure implemented in Varian (PRESAT). Chemical shifts are reported in ppm (δ) and referenced to residual nondeuterated solvent signal as internal standard ($CDCl_3$ ^{1}H: 7.26 ppm, ^{13}C: 77.16 ppm; $(CD_3)_2SO$: ^{1}H: 2.50, ^{13}C: 39.52 ppm). The unambiguous assignment of ^{1}H-NMR resonances was based on 2D gCOSY experiments. Variable temperature (VT) ^{1}H-NMR experiments were carried out over the range 298-348 K; temperature calibration was done with the ethylene glycol OH-CHn chemical- shift separation method. Coupling constants (*J*) are reported in Hz with the following abbreviations used to indicate splitting: s = singlet, d = doublet, t = triplet, m = multiplet, br = broad signal.

Synthesis and characterization

A. *General procedure for N-Boc deprotection*

The *N*-Boc-protected compound (1.0 eq) was treated with 25% TFA in DCM at 0 °C. The reaction was then stirred at RT for 1 h. The solvent was evaporated at reduced pressure and the residue was re-dissolved in DCM followed by evaporation *in vacuo* again. Finally, ice-cold Et$_2$O was added to precipitate, in almost quantitative yields, the product as TFA-salt which was collected by filtration or centrifuge, and used for the next steps without further purifications.

B. *General procedure for O-tBu deprotection*

The *O*-tBu-protected compound (1.0 eq) was treated with 50% TFA in DCM at 0 °C and the reaction was stirred at RT for 1-3 h. The solvent was removed under reduced pressure and the residue was re-dissolved in DCM and Et$_2$O followed by evaporation *in vacuo* again, to afford the desired product in almost quantitative yield, which was used without further purifications.

C. *General procedure for O-Bn and N-Cbz deprotection*

Catalytic hydrogenation was performed by dissolving *O*-Bn or *N*-Cbz-protected compound (1.0 eq) in absolute EtOH or MeOH (0.1 - 0.2 M) and then Pd/C (10% w/w) was added. The mixture was stirred under H$_2$ atmosphere for 6-48 h at RT. After the catalyst was filtered off over a Celite$^®$ pad and the filtrate was evaporated *in vacuo*. The final residue was used without further purifications.

D. *General procedure for N-Fmoc deprotection*

The *N*-Fmoc-protected compound (1.0 eq) was dissolved in 20% Piperidine/DMF solution (0.1-0.2 M) and the reaction was stirred at RT for 1 h. After removal of the solvent at reduced pressure, the crude residue was triturated twice with ice-cold Et$_2$O and collected by filtration or centrifuge. The deprotected compound was used in the next step without further purification, after drying under high *vacuum.*

E. *General procedure of ester hydrolysis reaction*

To a stirred solution of ester (1.0 eq) in a mixture of THF/H$_2$O (2:1) cooled at 0 °C was added LiOH (1.5 eq). The reaction was vigorously stirred at RT and the progress was monitored by TLC (typically 2 h). The solution was then neutralized at 0 °C by adding dropwise a solution of HCl 1M and after the water was evaporated. The product was used in the next step without further purification.

   F.   *General procedure for N-Boc protection*

In a typical experimental procedure, the amine (1.0 eq) and Na_2CO_3 (2.0 eq) were suspended in a mixture of H_2O/Dioxane (1:1) cooled at 0 °C in ice-bath. Then, Boc_2O (1.2 eq) was added and the reaction was stirred at RT overnight. The mixture was concentrated under reduced pressure to remove dioxane, and the alkaline aqueous layer was adjusted to pH 3-4 with HCl 0.5 M solution and then, extracted three times with EtOAc. The combined organic phases were dried over Na_2SO_4, filtered and concentrated under reduced pressure to dryness, to afford the protected compound.

   G.   *General procedure of EDC/HOBt-mediated amide coupling reaction*

A stirred solution of *N*-protected amino acid (1.0 eq) in 4:1 DCM/DMF mixture (0.2 M) was treated with HOBt (1.3 eq), EDC·HCl (1.3 eq) and TEA (2.6 or 3.0 eq) at RT under N_2 atmosphere. After 15 min, *O*-protected amino acid (1.0 eq) was added, and the mixture was stirred under N_2 at RT overnight. Then, the mixture was concentrated at reduced pressure, and the residue was diluted with EtOAc (30 mL). The solution was washed with 0.1 M HCl solution (5 mL), and a saturated solution of $NaHCO_3$ (5 mL). The organic layer was dried over Na_2SO_4, filtered and evaporated to dryness under reduced pressure. The crude material was purified by filtration or eventually by flash chromatography over silica gel (eluent Cy/EtOAc).

   H.   *General procedure of TBTU/HOBt-mediated amide coupling reaction*

A stirred solution of *N*-protected amino acid (1.0 eq) in 4:1 DCM/DMF mixture (0.2 M) was treated with HOBt (1.3 eq), TBTU (1.3 eq) and DIPEA (2.6 eq) at RT under N_2. After 15 min, *O*-protected amino acid (1.0 eq) was added, and the mixture was stirred at RT under N_2 overnight. Then, the mixture was concentrated at reduced pressure, and the residue was diluted with EtOAc (30 mL). The solution was washed with 0.1 M HCl solution (5 mL), and a saturated solution of $NaHCO_3$ (5 mL). The organic layer was dried over Na_2SO_4 and evaporated to dryness under reduced pressure. The crude material was purified by filtration or by flash chromatography over silica gel (eluent Cy/EtOAc).

   I.   *General procedure for Hofmann rearrangement of N-protected Asn*

To a stirred solution of PIFA (1.5 eq) in DMF/H_2O (2:1) under N_2 atmosphere, Fmoc-protected Asn (1.0 eq) was added. After 15 min, pyridine (2.0 eq) was also added to the mixture and stirred overnight at RT under N_2. Then, the solvents were removed *in vacuo* and the crude

residue triturated with ice-cold Et$_2$O, collected by filtration or centrifuge, and used without further purifications.

Synthesis of MPUPA (**MA1,** Scheme 3)

To a suspension of 4-aminophenylacetic acid (1.0 g, 6.6 mmol) in DMF (6 mL) was added dropwise *o*-tolyl isocyanate (0.82 mL, 6.6 mmol). The reaction mixture was stirred at RT for 3 h under N$_2$ atmosphere. Then, the mixture was diluted with EtOAc (40 mL) giving a precipitate **MA1** (1.45 g, 77%) which was collected as a whitish solid by filtration. ESI-MS *m/z* calcd. for [C$_{16}$H$_{17}$N$_2$O$_3$]$^+$: 285.1, found: 285.2 [M+H]$^+$.

Synthesis of *t*Bu-4-aminobenzylcarbamate (**MA83**, Scheme 3)

Boc$_2$O (1.78 g, 8.18 mmol) was added portion-wise at 0 °C to a solution of 4-aminobenzylamine (1.0 g, 8.18 mmol) in DCM (27 mL). The reaction was stirred at RT for 2 h. Then, the mixture was concentrated, and the residue was dissolved in DCM (50 mL). The organic solution was washed with saturated NaHCO$_3$ solution (20 mL) and brine (20 mL), dried over Na$_2$SO$_4$ and evaporated under reduced pressure. The crude product was purified by flash column chromatography over silica gel (gradient eluent Cy/EtOAc from 80:20 to 0:100) to afford **MA83** (1.53 g, 84 %) as a yellow solid. ESI-MS *m/z* calcd. for [C$_{12}$H$_{19}$N$_2$O$_2$]$^+$: 223.1, found: 223.2 [M+H]$^+$.

Synthesis of AMPUMP (**MA96**, Scheme 3)

O-tolyl isocyanate (0.69 mL, 5.54 mmol) was added dropwise to a stirred solution of *t*Bu-4-aminobenzylcarbamate (1.23 g, 5.54 mmol) in DMF (8 mL) at RT under N$_2$ atmosphere. After 3 h the reaction was diluted with EtOAc (40 mL) to precipitate **MA93** (1.55 g, 79%) that was collected by filtration and dried under high *vacuum*. ^{1}H-NMR (400 MHz, DMSO-*d$_6$*) δ: 8.82 (s, 1H, NHb), 7.81 (d, *J* = 8.0 Hz, 1H, ArH), 7.76 (s, 1H, NHa), 7.35 (d, *J* = 8.6 Hz, 1H, ArH), 7.22-6.91 (m, 4H, ArH), 6.86 (dd, *J* = 13.2, 6.2 Hz, 2H, ArH), 4.24 (d, *J* = 5.4 Hz, 1H, NH), 4.06 (d, *J* = 5.8 Hz, 2H, PhCH$_2$), 2.22 (s, 3H, ArCH$_3$), 1.38 (s, 9H, *t*-Bu). ESI-MS *m/z* calcd. for [C$_{20}$H$_{25}$N$_3$O$_3$Na]$^+$: 378.2, found: 378.3 [M+Na]$^+$.

The resulting protected diphenylurea **MA93** (1.55 g, 4.37 mmol), was then deprotected following the general procedure (A) to give the corresponding **MA96** TFA-salt, in quantitative yield, as a yellow solid. ESI-MS *m/z* calcd. for [C$_{15}$H$_{18}$N$_3$O]$^+$: 256.1, found: 256.2 [M+H]$^+$.

Synthesis of *mono*-benzyl malonate (**MA95**)
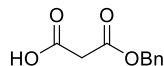
A mixture of Meldrum's acid (1.0 g, 6.94 mmol) and benzylic alcohol (0.72 mL, 6.94 mmol) was heated at 120 °C for 3 h. After cooling and evaporation of the solvent *in vacuo*, the crude residue was purified by flash chromatography over silica gel (gradient eluent Cy/EtOAc from 70:30 to 30:70) providing **MA95** (1.21 g, 90%) as an oil. Rf = 0.19 (Cy/EtOAc/AcOH drops 50:50). ESI-MS *m/z* calcd. for $[C_{10}H_{11}O_4]^+$: 195.1, found: 195.3 $[M+H]^+$.

Synthesis of *mono-t*Bu malonate (**MA155**)
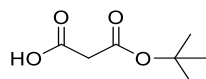
A mixture of Meldrum's acid (1.0 g, 6.94 mmol) and *tert*-butyl alcohol (0.66 mL, 6.94 mmol) was heated at reflux for 5 h. After cooling and evaporation of the solvent *in vacuo*, the crude residue was purified by flash chromatography over silica gel (gradient eluent Cy/EtOAc from 70:30 to 30:70) to afford **MA155** (1.21 g, 90%). Rf = 0.17 (Cy/EtOAc/AcOH drops 50:50). ESI-MS *m/z* calcd. for $[C_7H_{12}O_4Na]^+$: 183.1, found: 183.0 $[M+Na]^+$.

Synthesis of *t*Bu-(1-hydroxypropan-2-yl)carbamate ((*S*)-**MA54**, (*R*)-**MA76**, Scheme 2)

As previously reported by Caputo *et. al.*,[204] to a stirred solution of NMM (1.1 eq) and Boc-protected (*S*)- or (*R*)-Ala-OH (1.0 eq) in dry THF (0.4 M) at 0 °C, ethyl chloroformate (1.1 eq) was added dropwise. After 15min, the solution was filtered and NMM-HCl salt was washed with THF (3 x 5 mL). A solution of NaBH$_4$ (1.25 eq) in H$_2$O was then added dropwise to the filtrate, in ice-bath and under magnetic stirring. The ice bath was removed, and the mixture let rise to RT. After 10 min the solvent was evaporated under reduced pressure. The residue was re-dissolved in EtOAc (50 mL) and the solution washed with H$_2$O and brine, then dried Na$_2$SO$_4$. Evaporation of EtOAc *in vacuo* afforded the product (*S*)-**MA54** (500 mg, 98%) and (*R*)-**MA76** (910 mg, 89%) respectively, as a yellow oil, which were used without further purifications. ^{1}H-NMR (400 MHz, CDCl$_3$) δ 4.67 (br s, 1H, NH), 3.78-3.60 (m, 1H, CH$^\alpha$), 3.50 (dd, *J* = 13.8, 7.0

Hz, 1H, CH$^\beta$), 3.26 (dd, J = 12.4, 7.0 Hz, 1H, CH$^\beta$), 1.43 (s, 9H,C(CH$_3$)$_3$), 1.27 (d, J = 6.8 Hz, 3H, CH$_3$). ESI-MS m/z calcd. for [C$_8$H$_{18}$NO$_3$]$^+$: 176.1, found: 176.2 [M+H]$^+$.

Synthesis of *t*Bu-(1-cyanopropan-2-yl)carbamate ((*S*)-**MA58**, (*R*)-**MA82**, Scheme 2)

To a stirred solution of triphenylphosphine (1.25 eq) in dry DCM (0.1 M), I$_2$ (1.3 eq) was added at RT under N$_2$. After 15 min imidazole (2.5 eq) was also added and the mixture was stirred for additional 15 min. Crude Boc-protected aminoalcohols, (*S*)-**MA54** or (*R*)-**MA76** (1.0 eq), dissolved in dry DCM, was finally added and the reaction mixture refluxed until consumption of the starting material (3 h, TLC monitoring). The mixture was then cooled, diluted with DCM (40 mL), and washed with 10% aq Na$_2$S$_2$O$_5$ (20 mL) and brine (2 x 20 mL). The organic layer was dried over Na$_2$SO$_4$ and the solvent was evaporated *in vacuo* to give the crude iodides (*S*)-**MA55** and (*R*)-**MA81**. The crude iodide was then dissolved in dry DMSO (30 ml) and solid KCN (2.0 eq) was added in one portion. The mixture was stirred under N$_2$ at 60 °C for 4 h (TLC monitoring). The solution was then poured into water, EtOAc (40 mL) was added and finally washed with brine (2 x 20 mL). The organic layer was dried over Na$_2$SO$_4$ and then evaporated *in vacuo*. The crude residue was purified by flash chromatography over silica gel (Cy/EtOAc 80:20) to give (*S*)-**MA58** (yield 40 % over two steps) and (*R*)-**MA82** (yield 52 % over two steps) respectively, as a white solid. ^{1}H-NMR (400 MHz, CDCl$_3$) δ 4.71 (br s, 1H, NH), 4.00 – 3.88 (m, 1H, CH$^\alpha$), 2.72 (dd, J = 17.6, 5.2 Hz, 1H, CH$^\beta$), 2.52 (dd, J = 16.8, 4.0 Hz, 1H, CH$^\beta$), 1.43 (s, 9H,C(CH$_3$)$_3$), 1.31 (d, J = 6.8 Hz, 3H, CH$_3$). ESI-MS m/z calcd. for [C$_9$H$_{17}$N$_2$O$_2$]$^+$: 185.1, found: 185.2 [M+H]$^+$.

Synthesis of *N*-Boc β^{3}homoAla-OH ((*S*)-**MA60**, (*R*)-**MA84**, Scheme 2)

The amino nitriles, (*S*)-**MA58** or (*R*)-**MA82** (1.0 eq), was dissolved in a solution of EtOH/KOH(aq) 1M (1:1). The resulting mixture was stirred at 90 °C for 3 h. The mixture was cooled down to room temperature and EtOH was removed *in vacuo*. The residue was cooled to 0 °C and 1M KHSO$_4$ aqueous solution was added dropwise to reach pH 2-3. Then, the product was extracted with EtOAc (3 x 20 mL). The combined organic layers were washed with H$_2$O (2 x 10 mL) and brine (10 mL). The organic phase was dried over Na$_2$SO$_4$, filtered, and concentrated under reduced pressure to give the compounds (*S*)-**MA60** (60%) and (*R*)-**MA84** (50%) respectively. As previously reported, no racemization was observed by chiral HPLC analysis (n-hexane/2-propanol, 1:1 with a flow rate of 0.8 mL/min). (*S*)-**MA60** [α]$_D^{20}$ = -12° (c = 0.001, CHCl$_3$); (*R*)-**MA84** [α]$_D^{20}$ = 18° (c = 0.0008, CHCl$_3$). ^{1}H-NMR (400 MHz, DMSO-

d_6) δ 7.60 (br d, 1H, NH), 4.00 – 3.88 (m, 1H, CH^α), 2.42 (dd, J = 17.4, 5.6 Hz, 1H, CH^β), 2.32 (dd, J = 16.6, 4.8 Hz, 1H, CH^β), 1.43 (s, 9H,C(CH$_3$)$_3$), 1.31 (d, J = 6.8 Hz, 3H, CH$_3$). ESI-MS m/z calcd. for [C$_9$H$_{18}$NO$_4$]$^+$: 204.1, found: 204.2 [M+H]$^+$, 226.1 [M+Na]$^+$.

Synthesis of *N*-Boc β^{3}homoAla-Gly-OBn ((*S*)-MA62, (*R*)-MA85, Scheme 4)

According to general procedure (G), (*S*)-**MA60** (50 mg, 0.25 mmol) was coupled with H-Gly-OBn·TFA (90 mg, 0.25 mmol) in presence of EDC/HOBt as activating agents. Purification by flash chromatography over silica gel (gradient eluent Cy/EtOAc from 80:20 to 50:50) allow to isolate (*S*)-**MA62** (64 mg, 73%) as a white solid. Rf = 0.19 (Cy/EtOAc 60:40). ESI-MS m/z calcd. for [C$_{18}$H$_{26}$N$_2$O$_5$Na]$^+$: 373.2, found: 373.0 [M+Na]$^+$. Likewise, (*R*)-**MA84** (60 mg, 0.30 mmol) was coupled with H-Gly-OBn·TFA (100 mg, 0.30 mmol). The residue was purified by flash chromatography over silica gel (gradient eluent Cy/EtOAc from 80:20 to 60:40) affording (*R*)-**MA85** (66 mg, 63%) as a yellowish solid. Rf = 0.23 (Cy/EtOAc 50:50). ESI-MS m/z calcd. for [C$_{18}$H$_{26}$N$_2$O$_5$Na]$^+$: 373.2, found: 373.0 [M+Na]$^+$.

Synthesis of MPUPA-β^{3}homoAla-Gly-OBn ((*S*)-MA67, (*R*)-MA89, Scheme 4)

Boc-deprotection of (*S*)-**MA62** (64 mg, 0.18 mmol) and (*R*)-**MA85** (66 mg, 0.19 mmol) was performed following the general procedure (A). The resulting TFA-salts, (*S*)-**MA64** and (*R*)-**MA88** (obtained in quantitative yield), were used in the next step without further purifications. ESI-MS m/z calcd. for [C$_{13}$H$_{19}$N$_2$O$_3$]$^+$: 251.1, found: 251.2 [M+H]$^+$. According to the general procedure (G), (*S*)-**MA64** (35 mg, 0.10 mmol) and (*R*)-**MA88** (69 mg, 0.19 mmol) was coupled in turn with MPUPA (**MA1**, 1.0 eq) in presence of EDC/HOBt activating agents. During the work up a precipitate is formed which has been collected by filtration, while the resulting crude residue was purified by flash chromatography over silica gel (gradient eluent Cy/EtOAc from 80:20 to 0:100). (*S*)-**MA67** (45 mg, overall yield 85%) and (*R*)-**MA89** (95 mg, 96%) were obtained as white solids. Rf = 0.18 (EtOAc/MeOH 95:5). ESI-MS m/z calcd. for [C$_{29}$H$_{33}$N$_4$O$_5$]$^+$: 517.2, found: 517.0 [M+H]$^+$.

Synthesis of MPUPA-β^{3}homoAla-Gly-OH ((*S*)-MA97, (*R*)-MA99, Scheme 4)
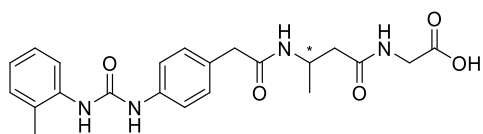
Following the general procedure (C), intermediates (*S*)-**MA67** (16 mg, 0.03 mmol) and (*R*)-**MA89** (95 mg, 0.18 mmol) were treated with H_2 and catalytic Pd/C (10%) at RT for 6 h. The mixture was filtered over Celite® and the solvent was evaporated under reduced pressure, and the residue were purified by semipreparative RP-HPLC (Eluent: H_2O/ACN/TFA 0.1% gradient from 70:30 to 0:100 in 10 min with a flow rate of 10 mL/min) yielding the final straight-peptidomimetics (*S*)-**MA71** (10 mg, 76%) and (*R*)-**MA99** (67 mg, 87%) as white solids. ^{1}H-NMR (600 MHz, DMSO-d_6) δ 8.95 (s, 1H, NHb), 8.20 (dd, *J* = 6.0, 5.4 Hz, 1H, Gly-NH), 7.90 (d, *J* = 7.8 Hz, 1H, β^{3}Ala-NH), 7.88 (s, 1H, NHa), 7.83 (d, *J* = 8.4 Hz, 1H, ArH$_6$), 7.36 (d, *J* = 8.4 Hz, 2H, ArH$_{2'6'}$), 7.20 – 7.09 (m, 4H, ArH$_{3,5}$ + ArH$_{3'5'}$), 6.93 (dd, *J* = 7.6, 7.2 Hz, 1H, ArH$_4$), 4.05 (dd, *J* = 14.4, 7.8 Hz, 1H, β^{3}Ala-CH^β), 3.72 (dd, *J* = 17.4, 6.0 Hz, 2H, Gly-CH$_2^α$), 3.30 (s, 2H, PhCH$_2$), 2.35 (dd, *J* = 13.8, 5.4 Hz, 1H, β^{3}Ala-CH^α), 2.23 (s, 3H, ArCH$_3$), 2.18 (dd, *J* = 13.8, 8.4 Hz, 1H, β^{3}Ala-CH^α), 1.05 (d, *J* = 6.6 Hz, 3H, CH$_3$). ^{13}C-NMR (150 MHz, DMSO-d_6) δ 172.0, 171.1, 170.1, 153.4, 138.8, 138.1, 130.8, 130.4, 129.9, 128.1, 126.8, 123.3, 121.6, 118.6, 43.0, 42.5, 41.2, 40.6, 20.6, 18.5. ESI-MS *m/z* calcd. for $[C_{22}H_{27}N_4O_5]^+$: 427.2, found: 427.0 $[M+H]^+$. **MA71** t_r = 4.3 min, 92% purity (λ = 254 nm); **MA99** t_r = 4.5 min, 95% purity (λ = 254 nm).

**Synthesis of *N*-Boc β^{3}homoAla-AMPUMP ((*S*)-MA113, (*R*)-MA98, Scheme 4)**

In order to obtain the analogues retro-peptides, in this case (*S*)-**MA60** (40 mg, 0.20 mmol) and (*R*)-**MA84** (30 mg, 0.15 mmol) were alternately coupled with AMPUMP (**MA96**, 1.0 eq), following the general procedure (G). The pure compounds precipitated during the workup were collected by filtration and dried under high *vacuum*. The resulting compounds (*S*)-**MA113** (80 mg, 90%) and (*R*)-**MA98** (35 mg, 53%), obtained as yellow solids, were used in the next step without further purifications. ESI-MS *m/z* calcd. for $[C_{24}H_{32}N_4O_4Na]^+$: 463.2, found: 463.0 $[M+Na]^+$.

Synthesis of BnO-Malonyl-β^{3}homoAla-AMPUMP ((*S*)-MA115, (*R*)-MA105, Scheme 4)

Boc-deprotection of intermediates (*S*)-**MA113** (50 mg, 0.11 mmol) and (*R*)-**MA98** was carried out as described in the general procedure (A), gave the corresponding TFA-salts (*S*)-**MA114** and (*R*)-**MA104**, in quantitative yields. These compounds were directly used in the next step without further purifications. ESI-MS *m/z* calcd. for $[C_{19}H_{25}N_4O_2]^+$: 341.2, found: 341.2 $[M+H]^+$. The crude **MA114** (50 mg, 0.11 mmol) and **MA104** (40 mg, 0.09 mmol) were coupled with *mono*-benzyl malonate **MA95** (2.0 eq) following the general procedure (G). Pure

(*S*)-**MA115** (20 mg, 30%) and (*R*)-**MA105** (10 mg, 22%) precipitated during the workup were collected by filtration and used without further purifications after drying under high *vacuum*. ESI-MS *m/z* calcd. for $[C_{29}H_{33}N_4O_5]^+$: 517.2, found: 517.2 $[M+H]^+$.

Synthesis of malonyl-β³homoAla-AMPUMP ((*S*)-**MA120**, (*R*)-**MA109**, Scheme 4)
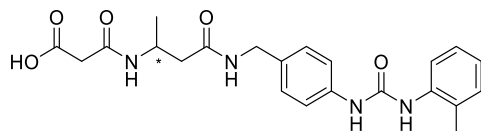
According to the general procedure (C), (*S*)-**MA115** (20 mg, 0.04 mmol) and (*R*)-**MA105** (10 mg, 0.02 mmol) were treated with H_2 and catalytic amount of Pd/C (10%) at RT for 6 h. The mixture was filtered over Celite® and the solvent evaporated under reduced pressure, and the residues were purified by semipreparative RP-HPLC (Eluent: H_2O/ACN/TFA 0.1% gradient from 70:30 to 0:100 in 10 min with a flow rate of 10 mL/min) affording the final retro-peptidomimetics (*S*)-**MA120** (10 mg, 59%) and (*R*)-**MA109** (7 mg, 82%) as white solids. ¹H-NMR (400 MHz, CDCl₃/DMSO-*d₆*, 1:1) δ 8.75 (s, 1H, NHb), 7.99 – 7.91 (m, 2H, β³Ala-NH + AMPUMP-NH), 7.78 (d, *J* = 8.4 Hz, 1H, ArH₆), 7.69 (s, 1H, NHa), 7.34 (d, *J* = 8.0 Hz, 2H, ArH₂'₆'), 7.13 – 6.99 (m, 4H, ArH₃,₅ + ArH₃'₅'), 6.86 (dd, *J* = 7.6, 7.2 Hz, 1H, ArH₄), 4.28 – 4.13 (m, 3H, β³Ala-CHᵝ + PhCH₂), 3.08 (s, 2H, -COCH₂CO-), 2.38 (dd, *J* = 14.0, 6.0 Hz, 1H, β³Ala-CHᵅ), 2.25 (dd, *J* = 14.0, 6.4 Hz, 1H, β³Ala-CHᵅ), 2.21 (s, 3H, ArCH₃), 1.11 (d, *J* = 6.4 Hz, 3H, CH₃). ¹³C-NMR (101 MHz, CDCl₃/DMSO-*d₆*, 1:1) δ 170.9, 153.6, 139.3, 137.9, 133.0, 130.6, 128.5, 128.1, 126.7, 123.3, 121.9, 118.8, 43.6, 42.8, 42.5, 20.7, 18.6. ESI-MS *m/z* calcd. for $[C_{22}H_{27}N_4O_5]^+$: 427.2, found: 427.0 $[M+H]^+$. **MA120** t_r = 4.3 min, 95% purity (λ = 254 nm); **MA109** t_r = 4.6 min, 92% purity (λ = 254 nm).

**Synthesis of methyl 2-methyl-3-(tosyloxy)propanoate** ((*S*)-**MA162**, (*R*)-**MA184**, Scheme 5)

As previously described by Lee *et. al.*,[205] to a stirred solution of (*S*)- or (*R*)-methyl 3-hydroxy-2 methylpropanoate (1.0 eq) in dry DCM, cooled at 0 °C, was sequentially added dropwise TEA (1.2 eq) and a solution of tosyl chloride (1.2 eq) in dry DCM (0.5 M). The reaction mixture was stirred overnight after warming to RT. The mixture was then diluted with DCM (20 mL) and washed with H_2O (3 x 5 mL), the organic layer was dried over Na_2SO_4, filtered and concentrated under reduced pressure. The crude material was purified by flash

chromatography over silica gel (eluent Cy/EtOAc 80:10) to yield the respective (*S*)-**MA162** (0.5 g, 87%) and (*R*)-**MA184** (1.05 g, 91%), as colourless oils. *Rf* = 0.18 (Cy/EtOAc 60:10).

Synthesis of methyl 3-amino-2-methylpropanoate ((*S*)-MA167, (*R*)-MA186, Scheme 5)

(*S*)-**MA162** (0.5 g, 1.84 mmol) or (*R*)-**MA184** (1.05 g, 3.85 mmol) was dissolved in dry DMF (1.0 M) and treated with NaN_3 (2.0 eq) at 50°C for 16 h. After cooling, the mixture was diluted with EtOAc (20 mL), and the organic layer was washed with H_2O (3 x 5 mL). The organics were dried over Na_2SO_4 and evaporated under reduced pressure to afford the crude (*S*)-**MA165** (123 mg, 47%) and (*R*)-**MA185** (280 mg, 51%) respectively, which were used without further purification in the next step. The crude azides **MA165** and **MA185** were then hydrogenated with H_2 and a catalytic amount of Pd/C 10% at RT overnight. The catalyst was removed by filtration through Celite®, and the filtrates were evaporated to afford the respective crude (*S*)-**MA167** (50 mg, 50%) and (*R*)-**MA186** (150 mg, 66%) which were triturated by adding Et_2O and collected by filtration. ESI-MS *m/z* calcd. for $[C_5H_{12}NO_2]^+$: 118.1, found: 118.3 $[M+H]^+$.

**Synthesis of MPUPA-β²homoAla-Gly-OH ((*S*)-MA192, (*R*)-MA199, Scheme 5)**
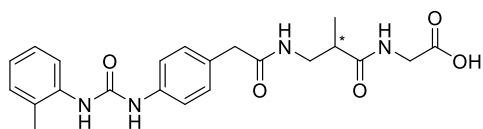
In line with the general procedure (H), coupling reaction of the primary amines **MA167** and **MA186** (1.0 eq) with MPUPA (**MA1**, 1.0 eq), afforded the respective intermediates (*S*)-**MA169** (46 mg, 71%) and (*R*)-**MA189** (40 mg, 61%), which were used in the next step without further purifications. ESI-MS *m/z* calcd. for $[C_{21}H_{26}N_3O_4]^+$: 384.2, found: 384.2 $[M+H]^+$. Ester hydrolysis of the crude (*S*)-**MA169** (46 mg, 0.12 mmol) and (*R*)-**MA189** (40 mg, 0.10 mmol) was carried out at 0 °C with LiOH (1.5 eq) in THF/H_2O (2:1) for 2.5 h at RT (see general procedure E), providing (*S*)-**MA175** and (*R*)-**MA191** in quantitative yield and immediately available for the next coupling reaction. ESI-MS *m/z* calcd. for $[C_{20}H_{24}N_3O_4]^+$: 370.2, found: 370.2 $[M+H]^+$. According to the general procedure (H), **MA175** (44 mg, 0.12 mmol) and **MA191** (40 mg, 0.11 mmol) were then coupled with H-Gly-OtBu·HCl (1.0 eq) to yield (*S*)-**MA179** (29 mg, 50%) and (*R*)-**MA195** (26 mg, 54%) respectively, after purification by semipreparative RP-HPLC (Eluent: H_2O/ACN gradient from 70:30 to 0:100 in 10 min with a flow rate of 10 mL/min). ESI-MS *m/z* calcd. for $[C_{26}H_{35}N_4O_5]^+$: 483.3, found: 483.2 $[M+H]^+$.

Finally, following the general procedure (B), *t*Bu-protecting group from **MA179** and **MA195** was removed giving the final compounds (*S*)-**MA192** and (*R*)-**MA199** in quantitative yield, as a white solid. ^{1}H-NMR (400 MHz, DMSO-d_6) δ 8.93 (s, 1H, NHb), 8.17 (dd, *J* = 6.0, 5.6 Hz, 1H, Gly-NH), 7.90 (d, *J* = 6.0 Hz, 1H, β²Ala-NH), 7.87 (s, 1H, NHa), 7.83 (d, *J* = 8.4 Hz, 1H, ArH$_6$), 7.36 (d, *J* = 8.4 Hz, 2H, ArH$_{2',6'}$), 7.20 – 7.09 (m, 4H, ArH$_{3,5}$ + ArH$_{3',5'}$), 6.93 (dd, *J* = 7.6, 7.2 Hz, 1H, ArH$_4$), 3.73 (dd, *J* = 17.6, 6.0 Hz, 2H, Gly-CH$_2$), 3.35 – 3.30 (m, 2H, PhCH$_2$ overlapped with solvent signal), 3.11 (dd, *J* = 7.2, 5.6 Hz, 2H, β²Ala-CH$_2$^{β}), 2.55 – 2.50 (m, 1H, β²Ala-CH^α overlapped with solvent signal), 2.23 (s, 3H, ArCH$_3$), 0.97 (d, *J* = 6.0 Hz, 3H, CH$_3$). ^{13}C-NMR (101 MHz, DMSO-d_6) δ 174.6, 171.4, 170.5, 152.7, 138.1, 137.4, 130.2, 129.7, 129.3, 127.4, 126.1, 122.6, 121.0, 118.0, 41.9, 41.7, 40.5, 17.9, 15.4. ESI-MS *m/z* calcd. for [C$_{22}$H$_{27}$N$_4$O$_5$]$^+$: 427.2, found: 427.2 [M+H]$^+$. **MA192** t_r = 4.2 min, 99% purity (λ = 254 nm); **MA199** t_r = 4.7 min, 99% purity (λ = 254 nm).

Synthesis of H-β²homoAla-AMPUMP ((*S*)-**MA196**, (*R*)-**MA202**, Scheme 5)

According to the general procedure (E), ester hydrolysis of the crude (*S*)-**MA165** and (*R*)-**MA185** afforded (*S*)-**MA164** (13 mg, 53%) and (*R*)-**MA193** (11 mg, 57%) respectively, which were used without further purifications in the next coupling step. Coupling reaction with AMPUMP (**MA96**, 1.0 eq) was carried out as described in the general procedure (H). The pure compounds precipitated during the workup, were collected by filtration and dried under high *vacuum* giving the respective (*S*)-**MA168** (30 mg, 82%) and (*R*)-**MA194** (28 mg, 91%) in good yields. ESI-MS *m/z* calcd. for [C$_{19}$H$_{23}$N$_6$O$_2$]$^+$: 367.2, found: 367.3 [M+H]$^+$. The resulting materials were directly treated with H$_2$ and a catalytic amount of Pd/C at RT overnight as described in general procedure (C). The resulting (*S*)-**MA196** (21 mg, 76%) and (*R*)-**MA202** (22 mg, 84%) were used in the next step without further purifications. ESI-MS *m/z* calcd. for [C$_{19}$H$_{25}$N$_4$O$_2$]$^+$: 341.2, found: 341.3 [M+H]$^+$.

Synthesis of malonyl-β²homoAla-AMPUMP ((*S*)-**MA204**, (*R*)-**MA206**, Scheme 5)
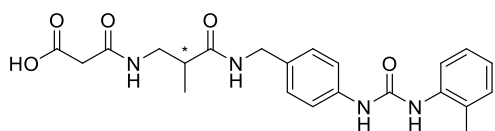
Yet, according to coupling procedure (H), crude (*S*)-**MA196** (21 mg, 0.062 mmol) and (*R*)-**MA202** (22 mg, 0.065 mmol) were alternately coupled with *mono-t*Bu malonate **MA155** (2.0 eq) to yield, after purification by semipreparative RP-HPLC (Eluent: H$_2$O/CH$_3$CN 45:55 for 6

min with a flow rate of 10 mL/min), the corresponding (*S*)-**MA267** (10 mg, 33%) and (*R*)-**MA203** (7 mg, 22%) derivatives as a white solid. ESI-MS *m/z* calcd. for $[C_{26}H_{35}N_4O_5]^+$: 483.3, found: 483.3 $[M+H]^+$. Finally, removal of *t*Bu-protecting group by following the general procedure (B), provided the final retro-peptidomimetics (*S*)-**MA204** (6 mg, 67%) and (*R*)-**MA206** (5 mg, 78%) as white solid. ^{1}H-NMR (400 MHz, DMSO-d_6) δ 8.98 (s, 1H, NHb), 8.30 (dd, *J* = 6.0, 5.6 Hz, 1H, AMPUMP-NH), 8.10 (dd, *J* = 5.6, 5.2 Hz, 1H, β^{2}Ala-NH), 7.88 (s, 1H, NHa), 7.83 (d, *J* = 8.0 Hz, 1H, ArH$_6$), 7.39 (d, *J* = 8.0 Hz, 2H, ArH$_{2'6'}$), 7.21 – 7.09 (m, 4H, ArH$_{3,5}$ + ArH$_{3',5'}$), 6.93 (dd, *J* = 7.6, 7.2 Hz, 1H, ArH$_4$), 4.20 (dd, *J* = 14.8, 6.0 Hz, 2H, PhCH$_2$), 3.23 – 3.06 (m, 4H, β^{2}Ala-CH$_2^β$ + -COCH$_2$CO-), 2.55 – 2.50 (m, 1H, β^{2}Ala-CH^α overlapped with solvent signal), 2.23 (s, 3H, ArCH$_3$), 1.02 (d, *J* = 7.2 Hz, 3H, CH$_3$). ^{13}C-NMR (101 MHz, DMSO-d_6) δ 173.9, 169.5, 166.0, 152.6, 138.5, 137.4, 132.8, 130.2, 127.7, 127.4, 126.1, 122.6, 120.9, 118.0, 42.5, 42.0, 41.5, 17.9, 15.7. ESI-MS *m/z* calcd. for $[C_{22}H_{27}N_4O_5]^+$: 427.2, found: 427.2 $[M+H]^+$. **MA204** t_r = 3.5 min, 96% purity (λ = 254 nm); **MA206** t_r = 4.4 min, 98% purity (λ = 254 nm).

Synthesis of Fmoc-Asp-*N*-propylamine ((*S*)-MA59, (*R*)-MA156, Scheme 6)

In line with the general coupling procedure (G), Fmoc-(*L*)-Asp(OtBu)-OH or Fmoc-(*D*)-Asp(OtBu)-OH (500 mg, 1.22 mmol) was activated with EDC/HOBt for 10 min, then *n*-propylamine (0.10 mL, 1.22 mmol) was added, and the mixture was stirred under N$_2$ at RT for 3 h. After the workup, the residues were purified by flash chromatography over silica gel (gradient eluent Cy/EtOAc 80:20 to 70:30) to afford (*S*)-**MA57** (350 mg, 63%) and (*R*)-**MR35** (380 mg, 69%), respectively. *Rf* = 0.36 (Cy/EtOAc 60:40). ^{1}H-NMR (400 MHz, CDCl$_3$) δ 7.78 (d, *J* = 7.5 Hz, 2H, ArH), 7.60 (d, *J* = 7.5 Hz, 2H, ArH), 7.42 (t, *J* = 7.5 Hz, 2H, ArH), 7.33 (t, *J* = 7.4 Hz, 2H, ArH), 6.47 (br s, 1H, Asp-NH), 5.97 (d, *J* = 8.0 Hz, 1H, propyl-NH), 4.45 (d, *J* = 6.8 Hz, 2H, Fmoc-CH$_2$), 4.23 (dd, *J* = 7.2, 6.8 Hz, 1H, Asp-CH^α), 3.22 (q, *J* = 5.9 Hz, 2H, propyl-CH$_2$), 2.93 (dd, *J* = 17.0, 3.8 Hz, 1H, Asp-CH^β), 2.60 (dd, *J* = 17.2, 6.8 Hz, 1H, Asp-CH^β), 1.57 – 1.48 (m, 2H, propyl-CH$_2$), 1.46 (s, 9H, *t*-Bu), 0.91 (t, *J* = 7.4 Hz, 3H, propyl-CH$_3$). ESI-MS *m/z* calcd. for $[C_{26}H_{33}N_2O_5]^+$: 453.2, found: 453.0 $[M+H]^+$.

Removal of *t*Bu-protecting group from **MA57** and **MR35** was performed as described in the general procedure (B). Pure intermediates (*S*)-**MA59** and (*R*)-**MA156** were obtained in quantitative yield and directly used in the next step without further purifications. ESI-MS *m/z* calcd. for $[C_{22}H_{25}N_2O_5]^+$: 397.2, found: 397.0 $[M+H]^+$.

Synthesis of MPUPA-Asp(Gly)-*N*-propylamine ((*S*)-**MA63**, (*R*)-**MA158**, Scheme 6)
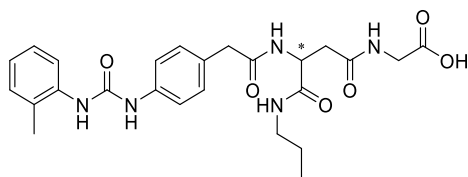

Compound (*S*)-**MA63** was synthesized manually on Wang resin preloaded with Fmoc-Gly (0.6 mmol/g, loading capacity). The resin (0.25 g, 0.15 mmol) was swollen in DMF for 30 min. Fmoc cleavage was carried out using 20 % piperidine/DMF solution (2 x 5 mL), under gentle stirring at RT for 10 min. The resin was filtered and washed with DMF (3 x 5 mL) and DCM (3 x 5 mL). The coupling reaction was performed by adding to the resin a solution of the Fmoc-amino acid (0.3 mmol, 2.0 eq), DCC (62 mg, 0.3 mmol, 2.0 eq) and HOBt (41 mg, 0.3 mmol, 2.0 eq) in DMF (4 mL) prepared in a separate vial. The mixture was gently stirred at RT for 3 h. The peptide sequence was elongated with (*S*)-**MA59** and MPUPA (**MA1**). Coupling reactions and Fmoc removals were monitored by Kaiser test. Once the linear peptide was assembled, the cleavage from the resin was carried out using a mixture of TFA/TIPS/H_2O (80:10:10 *v/v/v*) for 2.5 h at RT. The cleavage mixture was filtered in a centrifuge tube and the resin washed with Et_2O/DCM containing small portion of TFA. The collected mixture was concentrated and Et_2O was added to precipitate the crude peptide which was recovered by centrifugation. The pure compound (*S*)-**MA63** was obtained as a white solid in good yield (61 mg, 82%). The analogue (*R*)-**MA158** was synthesized on Fmoc-Gly Wang resin (0.20 g, 0.12 mmol) following the same procedure previously described. The amino acid coupling sequence was: (*R*)-**MA156** and MPUPA (**MA1**). After the cleavage from the resin, the compound was precipitated by addition of Et_2O and recovered by centrifugation (39 mg, 65% based on the estimated loading of the resin). ^{1}H-NMR (400 MHz, DMSO-d_6) δ 8.94 (s, 1H, NHb), 8.16 (t, *J* = 6.0 Hz, 1H, Gly-NH), 8.11 (d, *J* = 8.0 Hz, 1H, isoAsp-NH), 7.87 (s, 1H, NHa), 7.83 (d, *J* = 8.4 Hz, 1H, ArH$_6$), 7.67 (dd, *J* = 6.0, 5.2 Hz, 1H, propyl-NH), 7.36 (d, *J* = 8.4 Hz, 2H, ArH$_{2'6'}$), 7.20 – 7.09 (m, 4H, ArH$_{3,5}$ + ArH$_{3'5'}$), 6.93 (dd, *J* = 7.6, 7.2 Hz, 1H, ArH$_4$), 4.52 (dd, *J* = 14.4, 7.2 Hz, 1H, isoAsp-CH$^\alpha$), 3.73 (dd, *J* = 17.6, 5.6 Hz, 2H, Gly-CH$_2{}^\alpha$), 3.39 (s, 2H, PhCH$_2$), 2.98 (m, 2H, propyl-CH$_2$), 2.56 (dd, *J* = 14.8, 6.4 Hz, 1H, isoAsp-CH$^\beta$), 2.45 (dd, *J* = 15.2, 7.6 Hz, 1H, isoAsp-CH$^\beta$), 2.23 (s, 3H, ArCH$_3$), 1.42 – 1.31 (m, 2H, propyl-CH$_2$), 0.79 (t, *J* = 7.4 Hz, 3H, propyl-CH$_3$). ^{13}C-NMR (101 MHz, DMSO-d_6) δ 171.2, 170.5, 170.2, 169.6, 152.6, 138.2, 137.4, 130.1, 129.5, 129.4, 127.4, 126.1, 122.6, 120.9, 117.9, 49.8, 41.4, 40.6, 40.4, 37.5, 22.2,

17.9, 11.2. ESI-MS *m/z* calcd. for $[C_{25}H_{32}N_5O_6]^+$: 498.2, found: 498.0 [M+H]$^+$. **MA63** t_r = 4.0 min, 98% purity (λ = 254 nm); **MA158** t_r = 5.7 min, 96% purity (λ = 254 nm).

Synthesis of Fmoc-Asp(AMPUMP)-*N*-propylamine ((*S*)-MA145, (*R*)-MA151, Scheme 6)

Following the general procedure (G), (*S*)-**MA59** (45 mg, 0.11 mmol) and (*R*)-**MA156** (40 mg, 0.10 mmol) were coupled with AMPUMP (**MA96**, 1.0 eq). Pure (*S*)-**MA145** (50 mg, 72%) and (*R*)-**MA151** (60 mg, 95%) precipitated during the workup were collected by filtration and used without further purifications. ESI-MS *m/z* calcd. for $[C_{37}H_{40}N_5O_5]^+$: 634.3, found: 634.4 [M+H]$^+$.

**Synthesis of malonyl-Asp(AMPUMP)-*N*-propylamine ((*S*)-MA154, (*R*)-MA161, Scheme 6)**
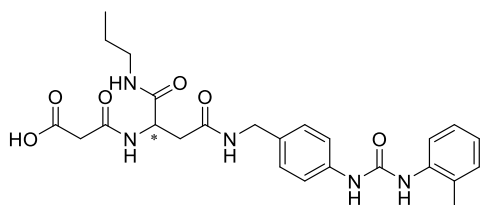
Fmoc-deprotection from the intermediates (*S*)-**MA145** and (*R*)-**MA151**, was carried out with a solution of 20% piperidine in DMF for 1 h, as described in the general procedure (D). After removal of the solvent *in vacuo*, the residue was triturated twice with ice-cold Et$_2$O affording the deprotected (*S*)-**MA146** and (*R*)-**MA152** in quantitative yield, and immediately available for the next coupling reaction. ESI-MS *m/z* calcd. for $[C_{22}H_{30}N_5O_3]^+$: 412.2, found: 412.2 [M+H]$^+$. Later, (*S*)-**MA146** (38 mg, 0.09 mmol) and (*R*)-**MA152** (59 mg, 0.14 mmol) were coupled with malonic acid *mono*-benzyl ester **MA95** (2.0 eq) using the same conditions and workup methods described in the general procedure (G). Crude compounds recovered by filtration were purified by flash chromatography over silica gel (eluent DCM/MeOH 95:5) giving (*S*)-**MA147** (40 mg, 76%) and (*R*)-**MA153** (45 mg, 55%) respectively, as white solid. ESI-MS *m/z* calcd. for $[C_{32}H_{38}N_5O_6]^+$: 588.3, found: 588.2 [M+H]$^+$.

Final deprotection of derivatives **MA147** and **MA153** following the general conditions of catalytic hydrogenation (C), provided the final compounds (*S*)-**MA154** (26 mg, 77%) and (*R*)-**MA161** (9 mg, 53%), as white solid. ^{1}H-NMR (400 MHz, DMSO-*d$_6$*) δ 9.32 (s, 1H, NHb), 8.39 (d, *J* = 7.6 Hz, 1H, Asp-NH), 8.31 (dd, *J* = 5.2, 5.6 Hz, 1H, AMPUMP-NH), 8.10 (s, 1H, NHa), 7.87 (br s, 1H, propyl-NH), 7.83 (d, *J* = 8.4 Hz, 1H, ArH$_6$), 7.40 (d, *J* = 8.4 Hz, 2H, ArH$_{2',6'}$), 7.18 – 7.09 (m, 4H, ArH$_{3,5}$ + ArH$_{3',5'}$), 6.92 (dd, *J* = 7.6, 7.2 Hz, 1H, ArH$_4$), 4.57 (dd, *J* = 14.0,

7.6 Hz, 1H, isoAsp-CH$^\alpha$), 4.19 (d, J = 5.6 Hz, 2H, PhCH$_2$), 3.27 – 3.10 (m, 2H, -COCH$_2$CO- partially overlapped with solvent signal), 3.01 – 2.96 (m, 2H, propyl-CH$_2$), 2.60 (dd, J = 15.4, 6.0 Hz, 1H, isoAsp-CH$^\beta$), 2.51 – 2.46 (m, 1H, isoAsp-CH$^\beta$), 2.25 (s, 3H, PhCH$_3$), 1.43 – 1.34 (m, 2H, propyl-CH$_2$), 0.83 (t, J = 7.6 Hz, 3H, propyl-CH$_3$). ^{13}C-NMR (101 MHz, DMSO-d_6) δ 174.5, 170.4, 169.2, 152.8, 138.8, 137.6, 132.2, 130.1, 127.7, 127.4, 126.0, 122.3, 120.8, 117.7, 50.1, 41.7, 40.5, 37.5, 22.2, 18.2, 11.3. ESI-MS m/z calcd. for $[C_{25}H_{32}N_5O_6]^+$: 498.2, found: 498.2 $[M+H]^+$. **MA154** t_r = 5.8 min, 99% purity (λ = 254 nm); **MA161** t_r = 5.7 min, 97% purity (λ = 254 nm).

Synthesis of N_α-Acetyl N_β-MPUPA-Dap-Gly-OH ((S)-MA28, (R)-MA30, Scheme 7)
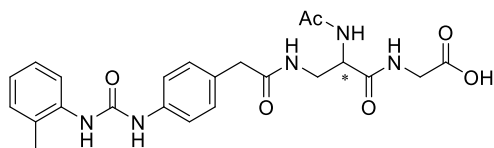
Compound (S)-**MA28** was assembled on Wang resin preloaded with Fmoc-Gly (0.20 g, 0.12 mmol, 0.6 mmol/g loading capacity). After Fmoc cleavage with 20% piperidine/DMF at RT for 2 x 10 min, coupling reaction was carried out by adding to the resin a solution of Fmoc-(S)-Asn-OH (212 mg, 0.6 mmol) preactivated with DCC (124 mg, 0.6 mmol) and HOBt (81 mg, 0.6 mmol) in DMF (4 mL). Hofmann rearrangement was performed on-resin. The resin was washed twice with a mixture of THF/DMF/H$_2$O (2:2:1 $v/v/v$) and subsequently swollen with the same mixture for 30 min. After that, a solution of PIFA (0.3 mmol, 2.5 eq) in THF/DMF/H$_2$O (2:2:1) was added to the resin followed by pyridine (0.3 mmol, 2.5 eq) and the mixture was gently stirred for 3 h. Then, the resin was washed with DMF (3 x 5 mL), DMF/DIPEA (9:1), and DMF again (3 x 5 mL). The effective rearrangement was confirmed by Positive Kaiser test. The peptide sequence was elongated with MPUPA (**MA1**) in the same coupling conditions described above. After Fmoc cleavage from central Dap residue, acetylation of the free amine was performed by adding Ac$_2$O (5.0 eq) and pyridine (5.0 eq) in DCM and the resulting suspension was shaken for 1 h. Cleavage from the resin was carried out using a mixture of TFA/TIPS/H$_2$O (80:10:10 $v/v/v$) for 2.5 h. The mixture was concentrated and ice-cold Et$_2$O was added to precipitate the crude peptide. The latter were purified by semipreparative RP-HPLC to give (S)-**MA28** (4 mg, 7% based on the estimated loading of the resin) as a white powder (Eluent H$_2$O/ACN with 0.1% TFA, 70:30 for 8 min with a flow rate of 10 mL/min). The analogue (R)-**MA30** bearing the rearranged (R)-Asn residue, was

synthesized on Fmoc-Gly Wang resin (0.20 g, 0.12 mmol) following the same protocol previously described. The crude peptide resulting from the resin cleavage was purified by semipreparative RP-HPLC and gave (*R*)-**MA30** (3 mg, 5% based on the estimated loading of the resin) as a white powder (Eluent H_2O/ACN with 0.1% TFA, 70:30 for 8 min with a flow rate of 10 mL/min). ^{1}H-NMR (400 MHz, DMSO-d_6) δ 8.97 (s, 1H, NHb), 8.19 (dd, J = 6.4, 5.2 Hz, 1H, Gly-NH), 7.97 – 7.91 (m, 2H, Dap-NH$_\alpha$ + Dap-NH$_\beta$), 7.89 (s, 1H, NHa), 7.81 (d, J = 8.0 Hz, 1H, ArH$_6$), 7.36 (d, J = 8.0 Hz, 2H, ArH$_{2'6'}$), 7.19 – 7.10 (m, 4H, ArH$_{3,5}$ + ArH$_{3'5'}$), 6.93 (dd, J = 7.6, 7.2 Hz, 1H, ArH$_4$), 4.37 (dd, J = 13.6, 8.0 Hz, 1H, Dap-CH$^\alpha$), 3.75 – 3.68 (m, 2H, Gly-CH$_2^\alpha$), 3.41 – 3.33 (m, 3H, PhCH$_2$ + Dap-CH$^\beta$ overlapped with solvent signal), 3.31 – 3.20 (m, 1H, Dap-CH$^\beta$), 2.23 (s, 3H, ArCH$_3$), 1.83 (s, 3H, Ac). ^{13}C-NMR (101 MHz, DMSO-d_6) δ 170.9, 170.3, 169.4, 152.7, 138.2, 137.5, 130.1, 129.5, 129.4, 127.4, 126.1, 122.6, 120.9, 117.9, 52.5, 41.6, 40.6, 22.6, 17.9. ESI-MS *m/z* calcd. for $[C_{23}H_{28}N_5O_6]^+$: 470.2, found: 470.2 $[M+H]^+$. **MA28** t_r = 3.4 min, 96% purity (λ = 254 nm); **MA30** t_r = 3.4 min, 95% purity (λ = 254 nm).

Synthesis of N_α-Fmoc N_β-Boc 2,3-Diaminopropionic acid ((*S*)-MA176, (*R*)-MA170, Scheme 7)

According to the general procedure (I), the Hofmann rearrangement was carried out alternately on Fmoc-(*S*)-Asn and Fmoc-(*R*)-Asn (100 mg, 0.28 mmol). Both (*S*)-**MA173** and (*R*)-**MA166** were obtained in quantitative yield as TFA-salt, and used without further purification. ESI-MS *m/z* calcd. for $[C_{18}H_{19}N_2O_4]^+$: 327.1, found: 327.2 $[M+H]^+$. Boc-protection was performed as described in the general procedure (F) yielding (*S*)-**MA176** (61 mg, 41%) and (*R*)-**MA170** (36 mg, 77%) respectively, which were directly used in the next coupling reaction without further purification. ESI-MS *m/z* calcd. for $[C_{23}H_{26}N_2O_6Na]^+$: 449.2, found: 449.2 $[M+Na]^+$.

Synthesis of N_α-Fmoc N_β-[(tBu)malonyl]-Dap-AMPUMP ((*S*)-MA182, (*R*)-MA180, scheme 7)

MA176 (61 mg, 0.14 mmol) and **MA170** (36 mg, 0.09 mmol) were coupled with AMPUMP (**MA96**, 1.0 eq) following the general procedure (H) described above. The resulting materials were purified by flash chromatography over silica gel (gradient eluent DCM/MeOH from 100:0 to 90:10) to give (*S*)-**MA178** (84 mg, 90%) and (*R*)-**MA174** (42 mg, 75%) respectively. ESI-MS *m/z* calcd. for $[C_{38}H_{42}N_5O_6]^+$: 664.3, found: 664.4 $[M+H]^+$, 686.4 $[M+Na]^+$, 564.2 [M-

Boc]$^+$. Boc deprotection according to the general procedure (A) allowed to obtain the TFA-salt intermediates (S)-**MA181** and (R)-**MA177** in quantitative yield. These compounds were directly coupled to the malonic acid *mono-t*Bu ester **MA155** (2.0 eq) following the general procedure (H). The pure material precipitated in good yield during the workup was collected by filtration and used in the next step without further purifications, (S)-**MA182** (80 mg, 95%) and (R)-**MA180** (28 mg, 92%), respectively. ESI-MS *m/z* calcd. for [C$_{40}$H$_{44}$N$_5$O$_7$]$^+$: 706.3, found: 706.4 [M+H]$^+$.

Synthesis of *N*$_\alpha$-Acetyl *N*$_\beta$-malonyl Dap-AMPUMP ((*S*)-MA200, (*R*)-MA198, Scheme 7)
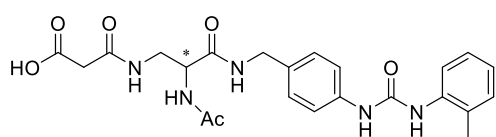
According to the procedure (D), Fmoc-deprotection gave (S)-**MA188** and (R)-**MA183** in quantitative yield, and were directly used in the next step without purifications. ESI-MS *m/z* calcd. for [C$_{25}$H$_{34}$N$_5$O$_5$]$^+$: 484.2, found: 484.2 [M+H]$^+$. Acetylation of the resulting free amine was carried out by adding to a solution of (S)-**MA188** and (R)-**MA183** (1.0 eq) in dry DCM (5 ml) cooled at 0 °C in sequence DIPEA (2.4 eq) and acetyl chloride (1.2 eq) dissolved in DCM. Then, the reaction was stirred at RT for 4 h under N$_2$ atmosphere. The mixture was diluted with DCM (20 mL) and washed twice with saturated NaHCO$_3$ solution (5 mL). The organic layer was dried over Na$_2$SO$_4$, filtered and concentrated under reduced pressure. The crude compounds were purified by semipreparative RP-HPLC (Eluent: H$_2$O/CH$_3$CN gradient from 70:30 to 0:100 in 10 min with a flow rate of 10 mL/min) to afford (S)-**MA190** (10 mg, 25%) and (R)-**MA187** (9 mg, 55%), as white solid. ESI-MS *m/z* calcd. for [C$_{27}$H$_{36}$N$_5$O$_6$]$^+$: 526.3, found: 526.2 [M+H]$^+$. According to general procedure (B), the final *t*Bu-deprotection with 50% TFA/DCM provided the retro-peptides (S)-**MA200** and (R)-**MA198** in quantitative yield. ^{1}H-NMR (400 MHz, DMSO-d_6) δ 8.97 (s, 1H, NHb), 8.35 (br t, 1H, AMPUMP-NH), 8.08 (br t, 1H, Dap-NH$^\beta$), 7.94 (d, *J* = 7.2 Hz, 1H, Dap-NH$^\alpha$), 7.88 (s, 1H, NHa), 7.83 (d, *J* = 8.0 Hz, 1H. ArH$_6$), 7.39 (d, *J* = 8.0 Hz, 2H, ArH$_{2',6'}$), 7.14 (m, 4H, ArH$_{3,5}$ +ArH$_{3',5'}$), 6.93 (dd, *J* = 7.6, 6.8 Hz, 1H, ArH$_4$), 4.39 – 4.32 (m, 1H, Dap-CH$^\alpha$), 4.24 – 4.17 (m, 2H, PhCH$_2$), 3.48 – 3.23 (m, 2H, Dap-CH$^\beta$ overlapped with solvent signal), 3.13 (s, 2H, -COCH$_2$CO-), 2.23 (s, 3H, ArCH$_3$), 1.86 (s, 3H, Ac). ^{13}C-NMR (101 MHz, DMSO-d_6) δ 169.8, 169.5, 152.7, 138.6, 137.5, 132.4, 130.1, 127.7, 127.5, 126.1, 122.6, 121.0, 117.9, 117.9, 52.8, 41.7, 40.5, 22.7, 17.9. ESI-MS *m/z*

calcd. for $[C_{23}H_{28}N_5O_6]^+$: 470.3, found: 470.2 $[M+H]^+$. **MA200** t_r = 3.4 min, 98% purity (λ = 254 nm); **MA198** t_r = 3.5 min, 98% purity (λ = 254 nm).

5. DESIGN AND SYNTHESIS OF NOVEL LDV-BASED CYCLIC PENTAPEPTIDES

5.1. Introduction

As mentioned in Chapter 2, another important, well-recognized peptidomimetic approach to improve the stability and activity is represented by the macrocyclization of peptides.[167] In nature numerous examples of cyclic peptides can be found, and they often exhibit enzymatic stability and potent biological activity. Cyclization is also an important method in peptide chemistry for generating analogues with improved bioactivity and bioavailability. Normally, native linear peptides display high flexibility, especially in aqueous solution, where the dynamic shift between the numerous conformations reduces their target affinity and selectivity. Thus, structural restrictions and more rigid peptides can be obtained by cyclization of the linear backbone which drastically reduces the conformational freedom in solution and, favours the orientation of the pharmacophoric groups in a well-defined direction. This minimizes the unfavourable loss of entropy in the peptide-receptor recognition giving enhanced binding affinity, hence, greater therapeutic potential.[85, 154, 207] Since the three-dimensional structure of the integrin $\alpha_4\beta_1$ is not yet available, cyclic peptides are optimally suited for exploring the structural requirements with respect to the three-dimensional arrangement of the pharmacophoric groups.

Inspired by the "spatial screening" approach proposed by Kessler [172] for the development of the very active Cilengitide,[85] in which the native RGD sequence found in FN was introduced within a constrained cyclic pentapeptide structure, we questioned whether the same approach might be applied with good results on the cyclization of the BIO1211 sequence. Therefore, we rationally designed a novel family of cyclic pentapeptides bearing the MPUPA-LDV structure, with the aim to develop potential $\alpha_4\beta_1$ integrin ligands for the treatment of a series of inflammatory disorders mentioned above in paragraph 1.6 (Figure 38).[128] To this purpose, suitable modifications in the parent sequence were introduced to allow the head-to-tail cyclization (C-terminus to N-terminus). In detail, to introduce an additional amine, the MPUPA (diphenylurea moiety) at the N-terminus was built on the aromatic amine (4-position) of a Phe residue producing a novel modified building block termed by us PhU (di-Phenylalanine-Urea). While at the C-terminus, different β-amino acids, including isoAsp and β³-homoAla, were introduced to promote the cyclization and carry (or not) a further carboxylic group (Figure 38).

The β-amino acids are well-known structural elements that favour defined secondary structures by acting as γ-turn inducers.[173] Indeed, β-amino acids exert a significant conformational bias on the cyclopeptide backbone conformations, because these unnatural building blocks preferably adopt a pseudo-γ-turns at the central position, and also stabilize γ-turn secondary structures at the opposite side of the macrocycle.[169, 208] In this context we synthesized a small library of cyclic LDV peptides by varying, in turn, the configuration of PhU and isoAsp residues (*S*- and *R*-; Table 5). Some of these peptides displayed interesting activity and selectivity in preliminary cell adhesion assays towards integrin $\alpha_4\beta_1$; thus, we focused our efforts on these compounds. Based on these foundings, SAR studies aimed at investigating the requirements for ligand binding were carried out. Firstly, the carboxylic acid of the isoAsp was replaced by the (*R*)-β^3-homoAla bearing a methyl group. Secondly, the Asp of the LDV sequence was substituted by the (*S*)-Ala deprived of the carboxylic acid. Removal of the carboxylic group is crucial to discriminate which one is directly involved in MIDAS coordination, hence fundamental for binding. Topologically, the (*R*)-β^3-homoAla does not affect the overall backbone conformation since assumes the same orientation of the corresponding (*S*)-configured isoAsp (Table 5).
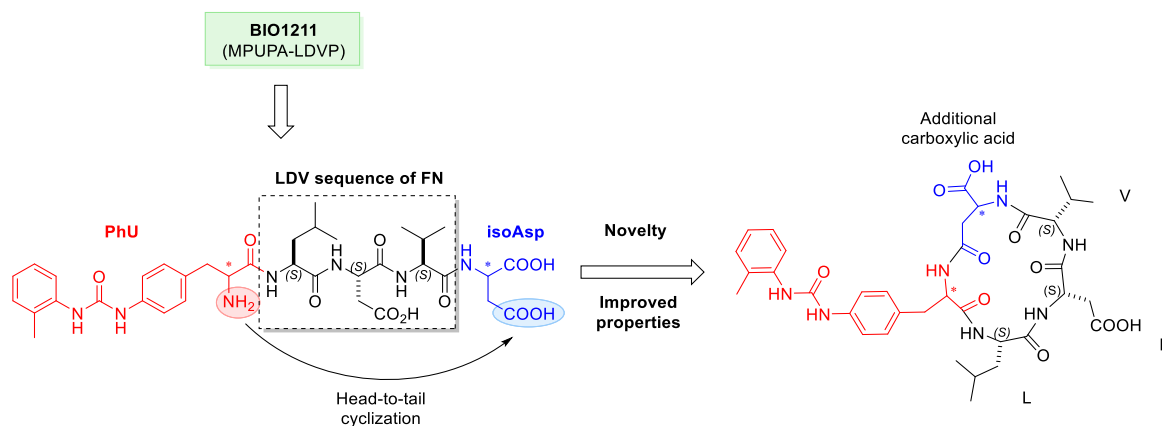
Figure 38. Design of the cyclic LDV peptides based on the structure of the reference compound BIO1211.

In addition, a combined approach of homology modelling, ligand-receptor molecular docking and molecular dynamics (MD) were applied to define the main binding modes of the LDV CPPs within the binding pocket of the $\alpha_4\beta_1$ integrin. MD simulations and molecular docking calculations were performed to identify the most prevalent ligand conformations in

solution and to establish a connection between its binding modes and the residues involved in the active site.

**Table 5.** Small libraries of LDV cyclopentapeptides (CPPs).

Type	Structure	Sequence
1		**MA144** (*S*)-PhU-LDV-(*S*)-*iso*D **MA133** (*R*)-PhU-LDV-(*S*)-*iso*D **MA86** (*S*)-PhU-LDV-(*R*)-*iso*D **MA266** (*R*)-PhU-LDV-(*R*)-*iso*D
2		**MA227** (*S*)-PhU-LDV-(*R*)-β³Ala **MA236** (*R*)-PhU-LDV-(*R*)-β³Ala
3		**MA265** (*S*)-PhU-LAV-(*S*)-*iso*D **MA264** (*R*)-PhU-LAV-(*S*)-*iso*D
4		**MA171** (*S*)-PhU-LDV-(*S*)-*iso*D-*n*-Pr

5.2. Results and discussion

5.2.1. Peptide synthesis

Each building block was synthesized prior to starting the synthesis of the linear peptides. In details, Boc-protected (*S*)- and (*R*)-PhU-OH were prepared by multi-step reactions starting from the free (*S*)- and (*R*)-Phe-OH (Scheme 8). Aromatic nitration was carried out by mixing concentrated HNO_3 and H_2SO_4 at 0 °C for 1 h. Later, Boc-protection, using Boc_2O and Na_2CO_3

in H_2O/dioxane (1:1), was followed by nitro reduction under catalytic hydrogenation on Pd/C for 3 h at RT. Finally, the urea bond was simply formed by adding *o*-tolyl isocyanate to the aromatic amine dissolved in DMF affording the Boc-PhU-OH, (*S*)-**MA254** and (*R*)-**MA255** (Scheme 8). Fmoc-(*R*)-β³Ala-OH (**MA217**) was synthesized as reported by Caputo *et. al.* (Scheme 2). After the acidic hydrolysis, the free amine was easily protected with Fmoc-chloride in the presence of Na_2CO_3 in H_2O/dioxane (1:1) at RT. Starting from Fmoc-Asp(OtBu)-OH, simple protection with benzyl bromide and successive *t*Bu-deprotection allowed to obtain the building blocks Fmoc-Asp-OBn, (*S*)-**MA45** and (*R*)-**MA246**, that were used as the first amino acid for the SPPS.
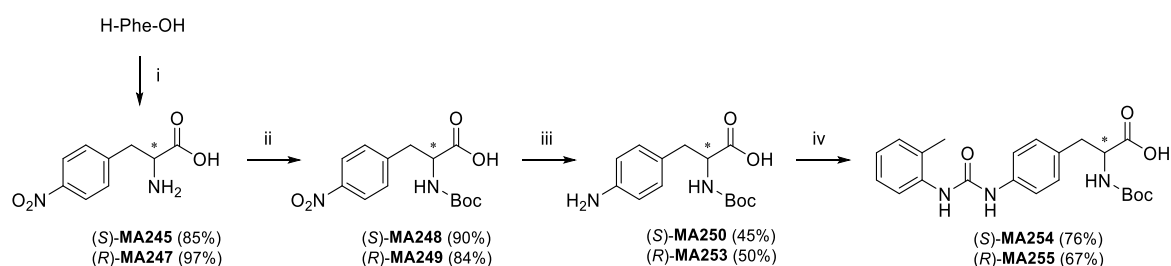

Scheme 8. Synthetic scheme for Boc-PhU-OH. *Reagents and conditions.* i) H_2SO_4, HNO_3, 0 °C, 1 h; ii) Boc_2O, Na_2CO_3, H_2O/dioxane (1:1), RT, 12 h; iii) H_2, Pd/C, MeOH, RT, 3 h; iv) *o*-tolyl isocyanate, DMF, RT, 3 h.

The linear peptides were assembled by SPPS on Wang resin using Fmoc/OBn-protected amino acids (Scheme 9). Attachment of the first amino acid, Fmoc-Asp(OtBu)-OH (**MA45**, **MA246**) or Fmoc-(*R*)-β³Ala-OH (**MA217**), was carried out by treating the pre-swollen resin with DCC, HOBt and catalytic amount of DMAP at RT for 3 h and, was followed by a treatment with Ac_2O and pyridine to endcap the unreacted 4-hydroxybenzyl alcohol linkers of the resin. Fmoc-deprotection was performed twice with a solution of 20% piperidine in DMF for 10 min. Then, the sequence was elongated alternating coupling and deprotection reactions. Fmoc-Val-OH, Fmoc-Asp(OBn)-OH/Fmoc-Ala-OH, Fmoc-Leu-OH and Boc-PhU-OH were coupled in sequence using DCC, HOBt as activating agents in DCM/DMF (4:1, *v/v*) at RT for 3 h. Each subsequent coupling and deprotection steps were carried out under the same conditions and the results were monitored by Kaiser test. Cleavage from the resin and simultaneous removal of Boc-protecting group from the last residue was performed using a mixture of TFA/TIPS/H_2O (95:2.5:2.5, *v/v/v*) for 2.5 h at RT. The crude peptides were simply precipitated from ice-cold Et_2O and collected in acceptable yield by centrifugation. The peptides, 70‑80 % pure as determined by analytical RP-HPLC, were used for the following macrolactamization step

without further purification. Cyclopentapeptides were obtained in solution by a head-to-tail cyclization (C-terminus to N-terminus) of the crude peptides using pseudo-high-dilution conditions to avoid intermolecular side reactions.[209] A solution of the linear peptide in DMF, was slowly added over 16 h using a syringe pump, to a solution of HBTU, HOBt and DIPEA in DMF (0.005 M). The reaction was stirred for an additional 2 h, and the progress was monitored by HPLC ESI-MS. The resulting crude peptide was purified by semipreparative RP-HLPC.
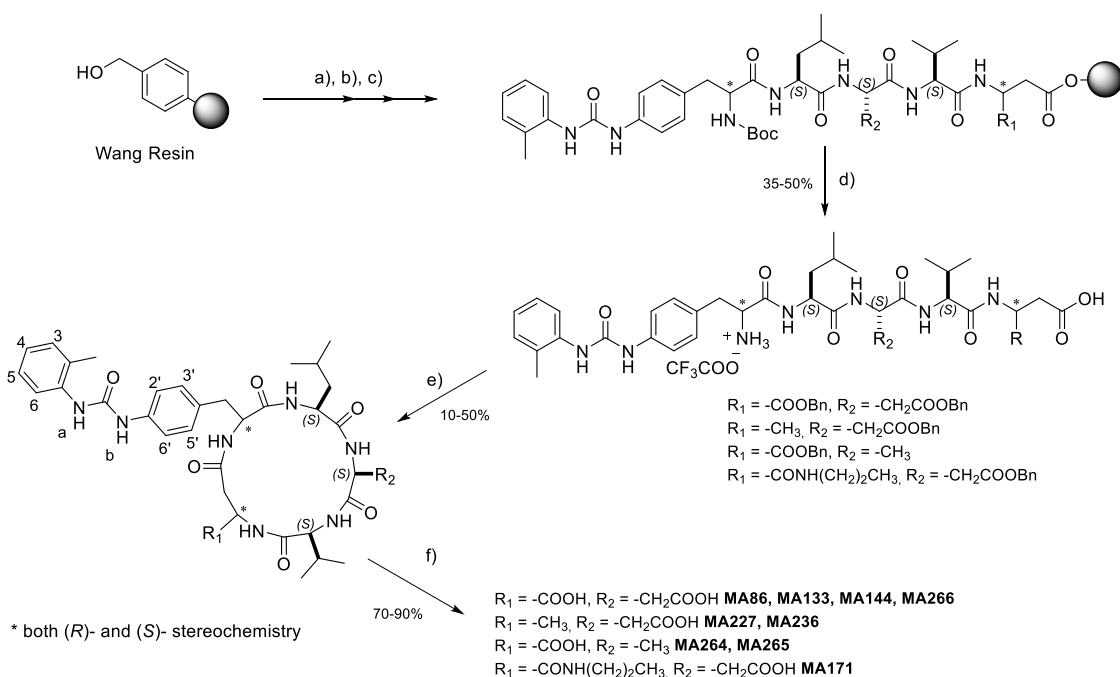
Scheme 9. Synthetic scheme for cyclic LDV peptides. *Reagents and conditions:* a) *i.* Fmoc-AA-OH (3.0 eq), DCC (3.0 eq), HOBt (3.0 eq), DMAP (0.1 eq), DMF, RT, 3 h; *ii.* Ac$_2$O (20 eq), pyridine (20 eq), RT, 30 min; b) 20% piperidine, DMF, RT, 10 min (x2); c) Fmoc-AA-OH (2.0 eq), DCC (2.0 eq), HOBt (2.0 eq), DMF, RT, 3 h. Iterative repetition of (b) and (c) using the corresponding amino acid. d) TFA/H$_2$O/TIS (95/2.5/2.5), RT, 2.5 h; e) HBTU (3.0 eq), HOBt (3.0 eq), DIPEA (6.0 eq), DMF pseudo-high dilution, RT, 18 h; f) H$_2$, Pd/C, RT, 12 h.

Finally, removal of the benzyl ester protecting group from the Asp residues afforded the pure final product with a modest yield (Table 5). This reaction was carried out under hydrogen atmosphere for 12 h at RT using a catalytic amount of Pd/C (10% *w/w*). For all cyclic peptides, the purity was assessed by RP-HPLC and the chemical identity was determined by ESI-MS, 1D and 2D (gCOSY and ROESY experiments) NMR spectroscopy at 400 MHz in DMSO*d$_6$*/H$_2$O (8:2).

Successful or failure of the ring formation relies on the ability of a linear precursor to conformationally pre-organize its reactive ends into close spatial proximity before ring closure.

A critical point for an efficient macrocyclization is the choice of the ring the disconnection. Macrocyclization is usually favoured by the introduction of turn-inducing elements and can be optimized if the site of macrocyclization is not sterically hindered by *N*-alkyl, α,α-substituted or β-branched amino acids (*i.e.,* Val or Ile) and if the macrocyclization occurs between two residues of opposite stereochemical configuration.[167] In this regard, very low yield was observed when the cyclization was attempted between the C-terminus of the Val and the N-terminus of the isoAsp residue. Therefore, we optimized the macrocyclization by identifying the new strategic retrosynthetic disconnections between the C-terminus of the isoAsp and the N-terminus of the PhU residue.

5.2.2. Biological evaluation

➢ *Integrin-mediated cell adhesion assay*

Pharmacological characterization of the new LDV cyclic pentapeptides (CPPs) was performed by the research group of Prof. Dr. M. S. Spampinato (department of Pharmacology, University of Bologna). *In vitro* experiments were carried out to measure their selectivity to the $\alpha_4\beta_1$ integrin receptor and their effects on the $\alpha_4\beta_1$-mediated cell adhesion, but also for their ability to bind other leukocytes-related integrins, including $\alpha_4\beta_7$, $\alpha_L\beta_2$, $\alpha_M\beta_2$ and $\alpha_5\beta_1$ (not expressed on leukocytes). The ability of the new compounds to inhibit the adhesion of the $\alpha_4\beta_1$ integrin-expressing Jurkat E6.1 cell to VCAM-1 or FN was compared with that of the reference compound BIO1211, known to be potent inhibitors of $\alpha_4\beta_1$-mediated cell adhesion. The adhesion of these cells to 96-well plates coated with human recombinant integrin ligands (VCAM-1, FN, MadCAM, Fg, ICAM) was concentration-dependent and no significant cell adhesion was observed for bovine serum albumin (BSA)-coated plates (negative control).[193] The results are summarized in Table 6. As expected, the reference compound BIO1211 inhibited cell adhesion to VCAM-1 and FN with an IC_{50} of 4.6 nM and 5.5 nM, respectively. Surprisingly, in contrast with our previsions, some LDV CPPs showed an opposite effect, namely increases adhesion to ligand-coated plates with a low micromolar IC_{50}. According to the configuration of the PhU/isoAsp residues, and the types of integrin-expressing cells, different agonist or antagonist behaviour was observed in cell adhesion assay. This suggests that the configuration of the cyclic backbone, hence, its conformation and pharmacophores orientation, has a strong dependent effect on integrin-mediated cell adhesion. It is currently

unclear how agonism and antagonism are correlated to the structure of these CPPs since a crystal structure of the $\alpha_4\beta_1$ integrin is still missing. Anyway, this aspect could represent an interesting starting point to the knowledge of the structural requirements needed for peptides drug design. However, analysing the complexity of the inflammatory responses, it emerges that the modulation of the integrin activity has a fundamental role in both, fast and slow, leukocytes recruitment during acute and chronic inflammation, respectively. In this complex scenario, together with the well-known role of integrin antagonist in interfering with leukocyte primary functions, the agonist activity could be exploited as a therapeutic strategy for inflammatory disorders since the induced stronger adhesion may prevent the normal cell migration processes at the site of injury.[130, 131, 210]

As reported in Table 6, in preliminary cell adhesion assays on Jurkat E6.1 cell with VCAM-1 and FN ligands, the cyclic LDV peptides (**MA144**, **MA86**, **MA133**, **MA266**) showed a low micromolar IC_{50} and, therefore, further cell adhesion assays upon different integrin-expressing cell lines have been performed. The results confirmed a similar trend in cell adhesion, showing micromolar IC_{50} values, similar to those observed in Jurkat E6.1 cells although the other cells do not express $\alpha_4\beta_1$ (Table 6). Comparable activity was observed for compounds **MA144** and **MA133** on RPMI 8866 cell adhesion which expresses integrin $\alpha_4\beta_7$, presumably due to the presence of the homologous α_4-subunit, therefore it is reasonable assumes that may be considered a dual agonist and antagonist of $\alpha_4\beta_1/\alpha_4\beta_7$ integrins, respectively. As expected, compounds **MA86** and **MA133** showed tenfolds less activity on K562 cells expressing $\alpha_5\beta_1$ while **MA144** was not active, and all of them were not active on HL60 cells expressing $\alpha_M\beta_2$. For **MA266** only preliminary cell adhesion results on Jurkat E6.1 cells with FN ligand are available and further *in vitro* investigations are currently in progress. Interestingly, although the opposite configuration of both PhU and isoAsp respect to **MA144**, a comparable low micromolar IC_{50} activity in increases cell adhesion (agonist behaviour) was observed (Table 6). Based on these premises, we focused our research efforts on the most active agonist **MA144** and antagonist **MA133**. SAR studies aimed at investigating the opposite behaviour in cell adhesion and, the importance of the pharmacophores/backbone conformation were carried out.

Table 6. Effect of cyclic LDV peptides[a] on different integrin-mediated human cell adhesion systems.

CPPs	Jurkat E6.1 cells α4β1 VCAM-1 (2 μg/mL) IC$_{50}$ (μM)[b]	Jurkat E6.1 cells α4β1 FN (10 μg/mL) IC$_{50}$ (μM)[b]	RPMI8866 cells α4β7 MAdCAM-1 IC$_{50}$ (μM)[b]	Jurkat E6.1 cells αLβ2 ICAM-1 IC$_{50}$ (μM)[b]	HL60 cells αMβ2 Fg IC$_{50}$ (μM)[b]	K562 cells α5β1 FN IC$_{50}$ (μM)[b]
BIO1211	$4.6 * 10^{-3}$ [Ant]	$5.5 * 10^{-3}$ [Ant]				
MA144 **(S)-PhU-LDV-(S)-iso**D	0.035[Ag]	0.05[Ag]	0.03[Ag]	0.098[Ag]	n a	n a
MA86 **(S)-PhU-LDV-(R)-iso**D	0.081[Ag]	0.156[Ag]	0.03[Ag]	1.11[Ant]	n a	14[Ag]
MA133 **(R)-PhU-LDV-(S)-iso**D	0.177[Ant]	0.726[Ant]	0.495[Ant]	0.71[Ant]	n a	1.95[Ag]
MA266 **(R)-PhU-LDV-(R)-iso**D		0.041[Ag]				
MA227 **(S)-PhU-LDV-(R)-β³A**	n a	n a				
MA236 **(R)-PhU-LDV-(R)-β³A**	n a	n a				
MA265 **(S)-PhU-LAV-(S)-iso**D		0.055[Ag]				
MA264 **(R)-PhU-LAV-(S)-iso**D		1.72[Ag]				
MA171 **(S)-PhU-LDV-(S)-iso**D-n-Pr	5.63[Ant]	6.97[Ant]				

[a]In a cell-based assay, the adhesion of a cell line preferentially expressing a specific integrin heterodimer to an immobilized adhesion molecule was measured. [b]Six independent experiments were run in quadruplicate. [Ag] Agonist. [Ant] Antagonist.

Replacement of the isoAsp carboxylic acid with a methyl group (β³-homoAla) in **MA227** and **MA236** was not tolerated, and the resulting compounds were not active on Jurkat E6.1 cell adhesion assay (Table 6) (see Docking analysis). On the contrary, the replacement of the carboxylic acid with a methyl group in the LDV sequence (Asp was substituted by Ala) was

tolerated as shown by compounds **MA265** and **MA264**, however, with a relevant difference in IC_{50} activity, indeed **MA264** resulted 100-folds less active than **MA265** (Table 6). Similarly, **MA265** maintained the same agonist behaviour of the parent compound **MA144,** while an opposite effect was observed for **MA264** which shifted to agonist respect to the parent integrin antagonist **MA133** (see Docking analysis).

In the absence of further results, this peculiar behaviour remains still unclear, however, further analysis is currently ongoing to clarify and correlate the different cell adhesion behaviour to a defined CPP structure. Yet, amidation of the carboxylic acid with *n*-propylamine (**MA171**) resulted in a drastic loss of activity and opposite behaviour (antagonist) on Jurkat E6.1 cell adhesion assay compared to the analogue agonist **MA144** which possesses the same backbone configuration (Table 6). These results underline the essential role of the carboxylic acid carried by the isoAsp residue in integrin binding. The conformations of cyclic LDV peptides in solution were analysed by 2D ROESY and restrained MD and, were compared to those of the 3D models determined by 3D QSAR and molecular docking (see Conformational Analysis).

➤ *FN-mediated ERK 1/2 phosphorylation signalling*

To confirm their agonist behaviour the most effective compounds, **MA86** and **MA144**, were investigated on FN-induced phosphorylation of ERK 1/2 in Jurkat E6.1 cells expressing $\alpha_4\beta_1$ integrin. Intracellular signalling generated by the interaction of ECM components with integrin $\alpha_4\beta_1$ involves an increase in the phosphorylation of cytoplasmatic second messengers such as ERK 1/2 that contribute to α_4 integrin-mediated cell functions.[190] A significant increase in ERK 1/2 phosphorylation was detected 60 min after Jurkat E6.1 cell exposure to FN-coated plates (10 µg·mL^{-1}). Pre-incubation with MA144 and MA86 (10^{-7}–10^{-9} M) for 60 min, produced a concentration-dependent increase in FN-mediated ERK 1/2 phosphorylation (Figure 39).
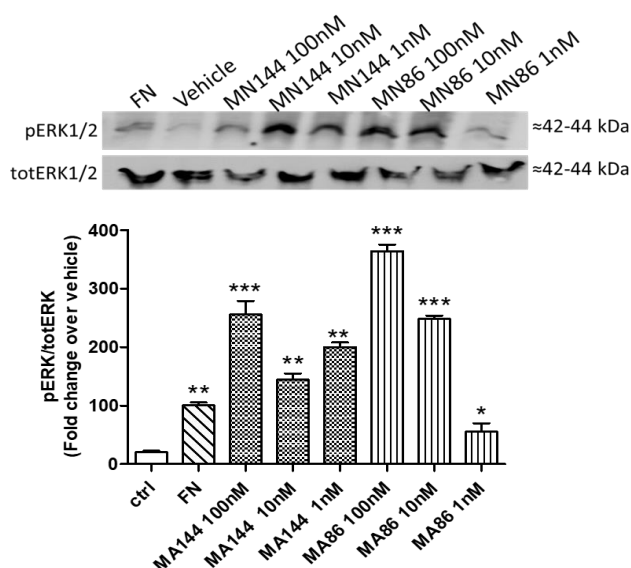
Figure 39. Effects of compounds MA144 and MA86 on ERK1/2 phosphorylation mediated by $\alpha_4\beta_1$ integrin expressed on Jurkat cells. Both compounds behaved as agonists and were able to significantly increase ERK 1/2 activation. Representative western blot shows that control cells plated on fibronectin (FN) had a stronger signal for pERK1/2 than vehicle-treated cells (vehicle). Densitometric analysis of the bands is shown (mean ± SEM; three independent experiments); the amount of pERK1/2 is normalized to that of totERK1/2. * $p<0.05$, ** $p<0.01$, *** $p<0.001$ vs vehicle (Newman-Keuls test after ANOVA).

5.2.3. Conformational analysis

The different biological activity observed in cell adhesion assays structurally correlated to the modification of the absolute configurations of PhU and isoAsp, prompted us to analyse their 3D conformations in solution by NMR spectroscopy and MD simulations,[211] in order to compare the 3D geometry of our compounds with the requirements reported in literature for $\alpha_4\beta_1$ antagonist models. The NMR analysis was carried out using standard techniques at 400 MHz in 8:2 mixtures of [D$_6$]DMSO/H$_2$O, a high viscous solvent system recommended as an excellent biomimetic vehicle [212] to favouring compact structures that are representative of the bioactive conformers. For NMR spectroscopic analysis, the main effect of cryo-mixture is to change the correlation time of the peptides, allowing the measurement of NOEs. For each peptide, ^{1}H-NMR spectroscopic data revealed a single set of resonances, indicating conformational homogeneity or a rapid interconversion between the conformers. gCOSY analysis allowed the unambiguous assignment of the resonances. Variable temperature (VT) ^{1}H-NMR experiments over the range 298‑318 K in [D$_6$]DMSO/H$_2$O (8:2) were used to elucidate the amide protons involved in intramolecular hydrogen bonding or solvent exposed (Table 7). Generally, the H-bonded amide-NH signals display moderate temperature-based

gradients that are reported in absolute value, $|\Delta\delta/\Delta T| < 2.0$ ppb $\cdot$ K^{-1}, while solvent-exposed amide-NH has higher negative values.[213] Since the viscosity of the cryo-mixture is temperature-dependent, the conformational equilibrium could change from 298 to 318 K altering the resonance pattern. However, as showed by ^{1}H-NMR spectrum, the CH resonances were perfectly maintained over the range of temperatures suggesting that the global conformations were not significantly altered.

Table 7. $\Delta\delta/\Delta T$ values [ppb K^{-1}] of amide protons for CPPs c[PhU-LDV-iAsp] by VT-NMR spectroscopy, determined in [D$_6$]DMSO/H$_2$O (8:2) at 400 MHz over the range 298‑318 K.

Group	CPPs	Sequence	NH^1	NH^2	NH^3	NH^4	NH^5	NH^6
1	MA144	c[(S)-PhU^1-Leu^2-Asp^3-Val^4-(S)-iAsp^5]	-5.0	-7.0	-4.0	-0.8	-0.5	-
	MA227	c[(S)-PhU^1-Leu^2-Asp^3-Val^4-(R)-**β^{3}Ala**^{5}]	-4.5	-4.1	-2.2	-0.6	-1.1	-
	MA265	c[(S)-PhU^1-Leu^2-**Ala**^{3}-Val^4-(S)-iAsp^5]	-5.4	+1.6	-4.4	-0.5	+0.0	-
	MA171	c[(S)-PhU^1-Leu^2-Asp^3-Val^4-(S)-iAsp(**NH^{6}nPr**)^5]	-1.7	-4.8	-4.9	-0.9	-0.2	-3.4
2	MA133	c[(R)-PhU^1-Leu^2-Asp^3-Val^4-(S)-iAsp^5]	-5.5	-5.3	-0.3	-7.9	-5.5	-
	MA236	c[(R)-PhU^1-Leu^2-Asp^3-Val^4-(R)-**β^{3}Ala**^{5}]	-6.0	-3.9	-0.7	-6.4	-2.5	-
	MA264	c[(R)-PhU^1-Leu^2-**Ala**^{3}-Val^4-(S)-iAsp^5]	-3.7	-4.2	-2.2	-6.0	-6.0	-
3	MA266	c[(R)-PhU^1-Leu^2-Asp^3-Val^4-(R)-iAsp^5]	-2.1	-2.9	+0.4	-3.0	-3.5	-
4	MA86	c[(S)-PhU^1-Leu^2-Asp^3-Val^4-(R)-iAsp^5]	-4.9	-3.5	-3.7	-1.9	-2.2	-

As shown in Table 7, the LDV cyclopentapeptides (CPPs) are grouped according to the absolute configuration of the PhU/isoAsp residues. **MA144**, **MA227**, **MA265** and **MA 171** (group 1, Table 7), the comparatively much lower $|\Delta\delta/\Delta T|$ values, in a range between 0.0 and -1.1 ppb$\cdot$K^{-1}, for Val-NH^4 and isoAspNH/β^{3}Ala-NH^5 respect to PhU-NH^1, Leu-NH^2 and Asp-NH^3 (range between -2.2 and -7.0 ppb K^{-1}) indicatively suggested that the former might be involved in a strong hydrogen bond. For **MA265**, the chemical shift of Leu-NH^2 was significantly less sensitive to increasing temperature, $|\Delta\delta/\Delta T| = +1.6$ ppb K^{-1}, which is indicative of a very strong hydrogen bond. However, the unexpectedly high chemical shift of

LeuNH (δ: 10.56 ppm) indicated the occurrence of a peculiar de-shielding effect exerted *e.g.* by the urea group, rather than a classic hydrogen-bonding effect. The VT-NMR analysis of **MA171** suggested the presence of a weak hydrogen bond involving PhU-NH[1] (-1.7 ppb K[-1]). The VT-NMR analysis of **MA133** and **MA236** (group 2, Table 7) revealed the presence of a strong hydrogen bond involving Asp-NH[3], with $|\Delta\delta/\Delta T|$ = -0.3 and -0.7 ppb·K^{-1}, respectively. As for the correlated compound **MA264**, no hydrogen bond seems to be present albeit a similar pattern involving the Asp-NH[3] (-2.2 ppb·K^{-1}) can be referable to a weak H-bond. The VT-NMR analysis of **MA266** (group 3, Table 7) revealed the presence of a very strong hydrogen bond involving Asp-NH[3] with +0.4 ppb·K^{-1} and the possibility of weaker hydrogen bonds for both PhU-NH[1] and Leu-NH[2] (-2.1 and -2.9 ppb·K^{-1}, respectively). Finally, the analysis of **MA86** (group 4, Table 7) suggested the presence of a strong hydrogen bond involving Val-NH[4] (-1.9 ppb·K^{-1}) and a possible weak hydrogen bond involving isoAsp-NH[5] (-2.2 ppb·K^{-1}).

Molecular backbone conformations of the model compounds were analysed by 2D-ROESY in [D$_6$]DMSO/H$_2$O (8:2) mixed solvent. Cross-peaks were classified, and intensities were ranked to infer plausible interproton distances as restraints (Figure 40). The NMR analysis of **MA227** and **MA171** showed a similar conformation to the parent compound **MA144** since the resonance chemical shift of H$^\alpha$ and H$^\beta$ and, the H-bonds pattern was maintained. Similarly, compounds **MA236** and **MA264** showed NMR spectra comparable to the parent compound **MA133**, clearly, the H$^\alpha$ and H$^\beta$ resonances of modified residues may vary. As already mentioned, **MA265** displayed a different chemical shift involving the Leu residue, therefore, the 2D-ROESY analysis was performed only on this derivative (Figure 40).

The amide bonds angles (ω) were set at 180° since peptides comprising only secondary amide bonds adopt all-*trans* conformations; the absence of Hα(*i*) – Hα(*i* + 1) cross-peaks reasonably excludes the occurrence of *cis*-peptide bonds.[214] Random structures were generated by simulated annealing MD in a box of explicit TIP3P[215] equilibrated with water molecules. For each random structure, the interproton distances deduced by ROESY were introduced as constraints. Each structure was subjected to restrained high-temperature MD, then the system was slowly cooled. The resulting structures were minimized with the AMBER force field,[216] and the backbones of the structures were clustered by root-mean-square deviation analysis. For all compounds, this procedure gave one major cluster comprising the large majority of the structures. The representative structures with the lowest energy and the least number of restraint violations were selected and analysed. To investigate the dynamic behaviour of the LDV CPPs,

the structures shown in Figures 40 were analysed by unrestrained MD simulations for 10 ns at 298 K in a box of explicit TIP3P equilibrated water molecules. During the simulations, the structures reported in Figure 41 were maintained, indicating that these conformations represented stable minima.
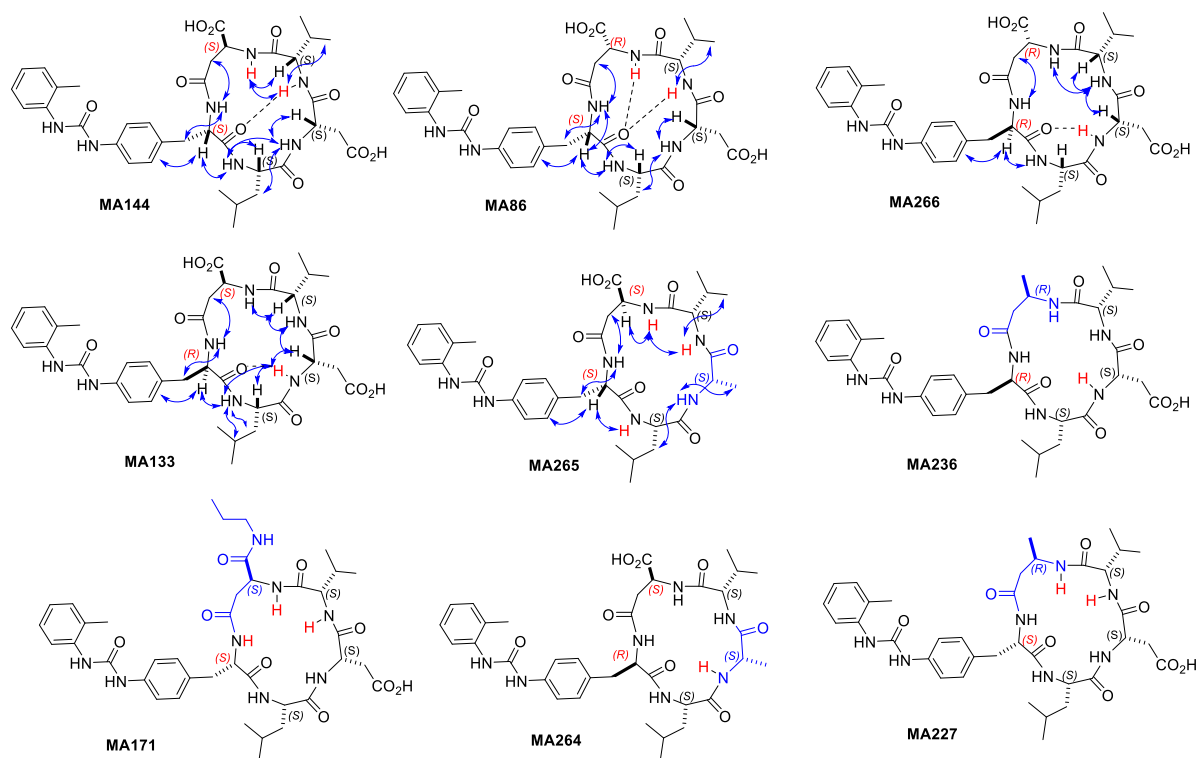
Figure 40. Sketches of LDV CPPs showing meaningful proton-proton NMR correlations indicated by arrows. Strong ROESY correlations are given in blue for MA144, MA133, MA86, MA266, MA265. The $|\Delta\delta/\Delta T|$ values (reported in Table 7) for selected amide protons involved in H-bonds are shown as red. H-bonds are shown as dashed line.

The ROESY-derived structures of **MA144** and **MA86** (Figure 41) show explicit H-bonds, as predicted by VT-NMR analysis. The representative structures of **MA144** appear characterized by a clear type II β-turn centered on Leu-Asp, stabilized by an explicit H-bond between PhU-C=O and Val-NH, and by a 9-membered turn on isoAsp stabilized by an H-bond between PhU-C=O and isoAsp-NH. In **MA86** the turn on Leu-Asp was modified into an inverse type II β-turn, plausibly due to the reversal of stereochemistry of the β-residue. The structure of **MA133** and **MA266** tend to maintain similar overall conformations, each showing an inverse γ-turn centered on Leu, stabilized by H-bonds between PhU-C=O and AspNH.
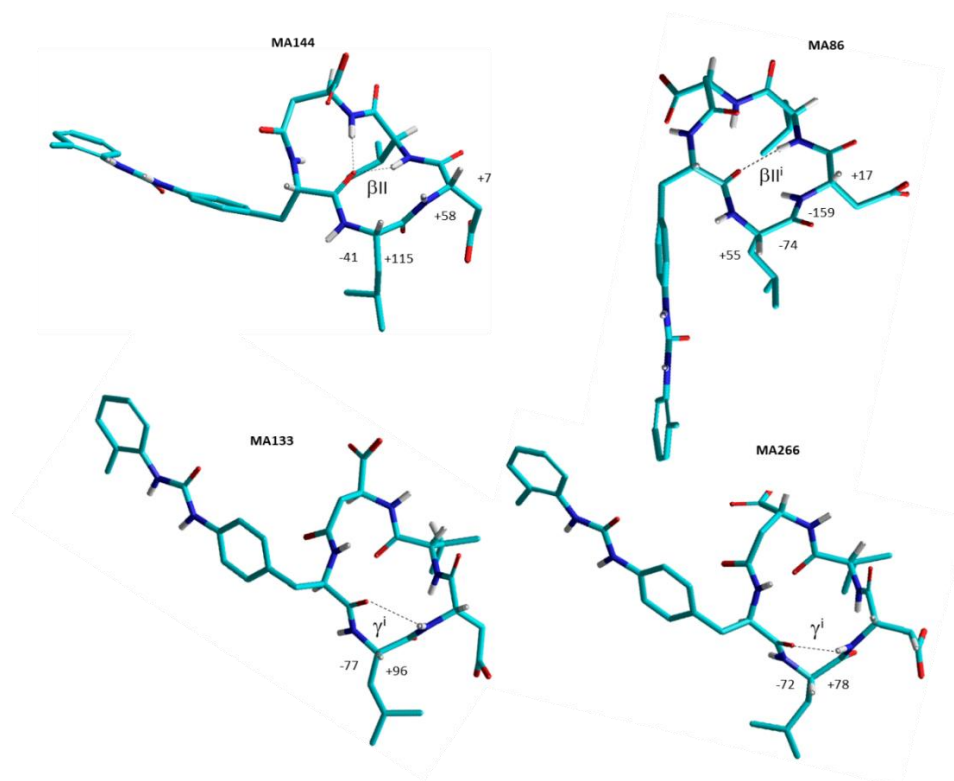
Figure 41. Representative lowest energy structures for the LDV CPPs (MA144, MA86, MA133, MA266) calculated by ROESY restrained MD in a $30 \times 30 \times 30$ Å box of standard TIP3P water molecules.

5.2.4.   Docking studies

In order to evaluate the ability to suitably fit into the receptor site and how the pharmacophores are involved, the in-solution structures of the agonist **MA144** and the antagonist **MA133**, were docked with Autodock software within an $\alpha_4\beta_1$ integrin receptor model, built by X-ray structures of the α_4-subunit (PDB: 3V4V)[125] and β_1-subunit (PDB: 3VI4).[217] Molecular docking experiments were carried out by Dr. R. Artali, at Scientia-Advice Srl, Desio (Italy). Each complex showed a tight fit of the ligand in the binding cleft (Figure 42), forming ionic, hydrogen and hydrophobic interactions with the receptor (Figure 44).
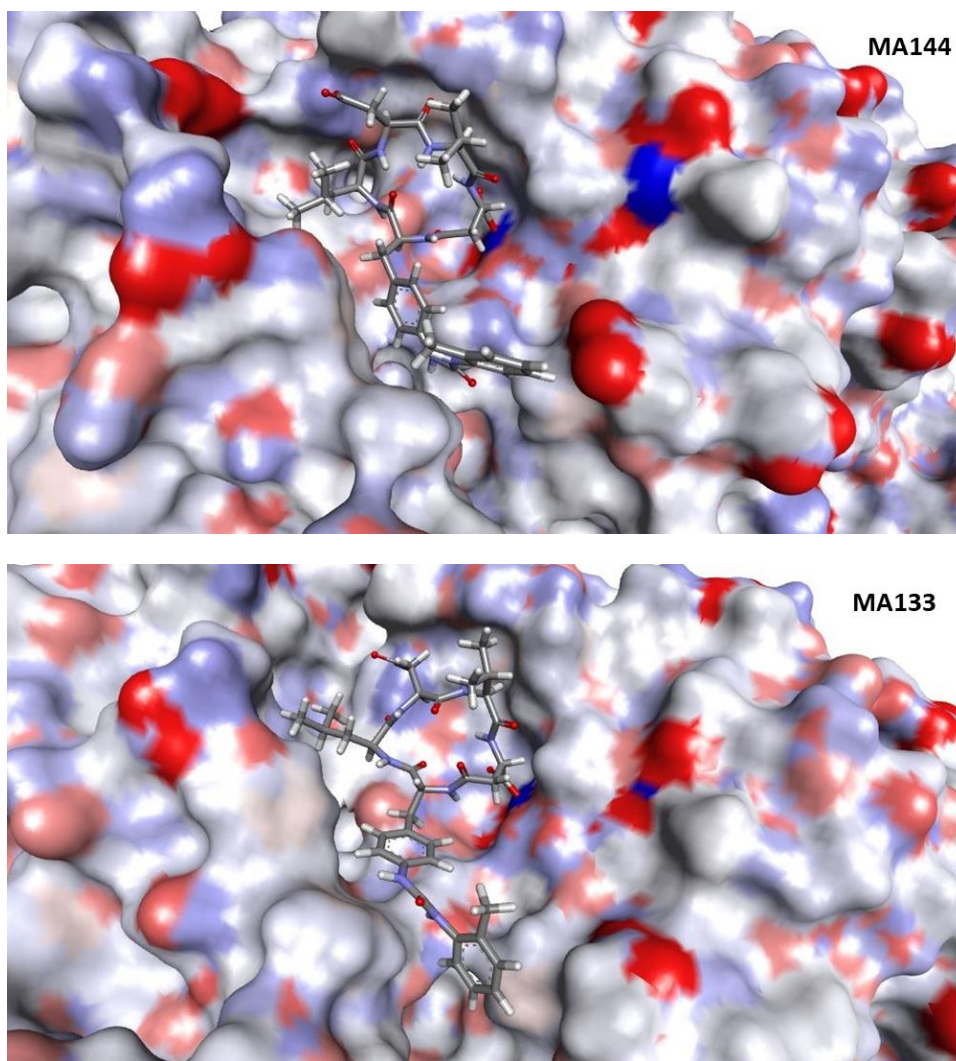
Figure 42. Binding modes of the agonist compound MA144 and the antagonist compound MA133 within the α4β1 integrin binding site.

The binding mode of our CPPs within the $\alpha_4\beta_1$ integrin receptor model (Figure 42) can be compared with that of the BIO1211 fragment diphenylurea-LDV (Figure 43) previously reported by da Silva *et. al.*[139] In this case, the $\alpha_V\beta_3$ integrin crystal structure was taken as template for the construction of the $\alpha_4\beta_1$ integrin receptor model, through homology and comparative modelling computational studies. Although the poses show differences mainly in the ligand positioning backbone within the binding pocket, a similar arrangement of the MPUPA moiety inside the crevice between α- and β-subunit can be observed in the MODE 2 pose (Figure 43).
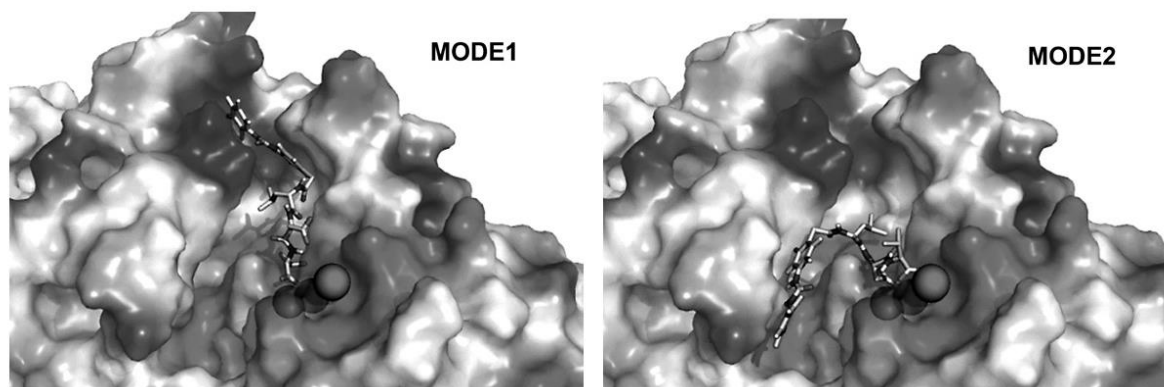
Figure 43. Binding modes of VLA-4 within the binding site represented as Connolly surface. The metal ions at the MIDAS region are represented as spheres.

Docking calculation of CPPs **MA144** and **MA133**, produced top-ranked poses conserving the key ionic interactions. For both compounds, the isoAsp carboxylate group is coordinated by ionic interaction to the metal cation in the MIDAS region of the β_1-subunit (Figure 44). **MA133** shows a further stabilizing hydrogen bond between the ligand isoAsp carboxylate group and the backbone-amide hydrogen atom of Asn224. Other stabilizing interactions occurred in docking poses of **MA144**, involved the formation of hydrogen bonds between the ligand backbone-carbonyl of Asp and the backbone-amide hydrogen atom Glu191 of the β_1-subunit, and between the ligand Asp carboxylate group side chain and the Lys182 amine side chain of the α_4-subunit. The ligand Leu backbone-oxygen forms an H-bond with Lys182 amine side chain, and CH-π interaction between its side chain and a Tyr187; while the aromatic methyl of the ligand PhU forms a downward hydrophobic CH-π interaction with a Phe214 of the α_4-subunit (Figure 44). Notably, the receptor-bound structure of **MA144** confirms the intramolecular H-bond between PhU backbone-oxygen and backbone-amide hydrogen atoms of Val deduced by VT-NMR and MD experiments, and it is also involved in a further H-bond between PhU-C=O and AspNH (compare Figure 41 and Figure 44).

Stabilizing interactions occurred in docking poses of **MA133**, involving the formation of dipole-dipole interactions at the β_1-subunit between the ligand backbone-carbonyl of Val and the backbone-hydroxyl side chain of Ser134, and an upward hydrophobic CH-π interaction of the side chain with Tyr133 (Figure 44). In contrast with **MA144**, the ligand Asp carboxylate group is involved dipole-dipole interactions with a CHα of Cys187 and Lys182 amine side chain. Similarly, the ligand Leu backbone-oxygen forms an H-bond with Lys182 amine side chain, and a further stabilizing hydrophobic CH-π interactions between its side chain and the

backbone side chain of Leu225 (β_1-subunit) and Lys157 (α_4-subunit). Finally, a π-π staking interaction at the $\beta1$-subunit between the aromatic ring of PhU and a Phe321 completed the docking pose-model (Figure 44). Compared to the NMR experimental data, **MA133** does not highlight the intramolecular H-bonds, displaying an extended cyclic backbone conformation.

Excellent agreement between SAR studies and docking results was observed. The docked poses confirmed the essential role of the isoAsp carboxylate group in integrin ligand-binding since it is fundamental to coordinate the metal cation in the MIDAS region of the β_1-subunit. Indeed, replacement of this coordinating group led to inactive compounds (**MA227** and **MA236**), while its amidation with short alkyl amines (**MA171**) led to a strong reduction in activity and opposite effect on cell adhesion. As a result of the opposite absolute configuration of the PhU stereocenter, **MA144** and **MA133**, the two poses show remarkable differences in the position of the urea group within the binding pocket. **MA144** shows a more bent arrangement inside the crevice between the propeller and the βI-domain on the integrin head as compared to the slightly planar **MA133**. Each structure shows similar orientation and interactions of the side chains at the integrin site, however, **MA133** seems to fit better in the binding pocket, resulting well-surrounded by the β_1-subunit toward which expose the side chains of Asp, Val and PhU (Figure 43). This aspect could explain the different actions of these two CPPs in cell adhesion assays, although the molecular basis related to the agonist and antagonist mechanism is still unclear.

Intriguingly, ligand **MA144** was shown to act as an agonist of $\alpha_4\beta_1$ integrin, while **MA133** displayed an antagonist behaviour. Extensive investigations on $\alpha_{IIb}\beta_3$ and $\alpha_V\beta_3$ integrins showed that the mechanism of extension and activation requires a specific reorganization of pre-existing interaction networks around Y122 of the β-subunit, in the proximity of the ligand recognition site.[26, 218] In this perspective, the receptor-bound structure of compound **MA144** shows that Tyr133 is not directly and tightly involved in the interaction with the ligand. In contrast, **MA133** appears capable to block the position of Tyr133 in the inactive conformation; antagonism would be determined by the bulky *isopropyl* group that optimally packs against Tyr133, therefore freezing hinge opening and domain translocation.[218, 219]
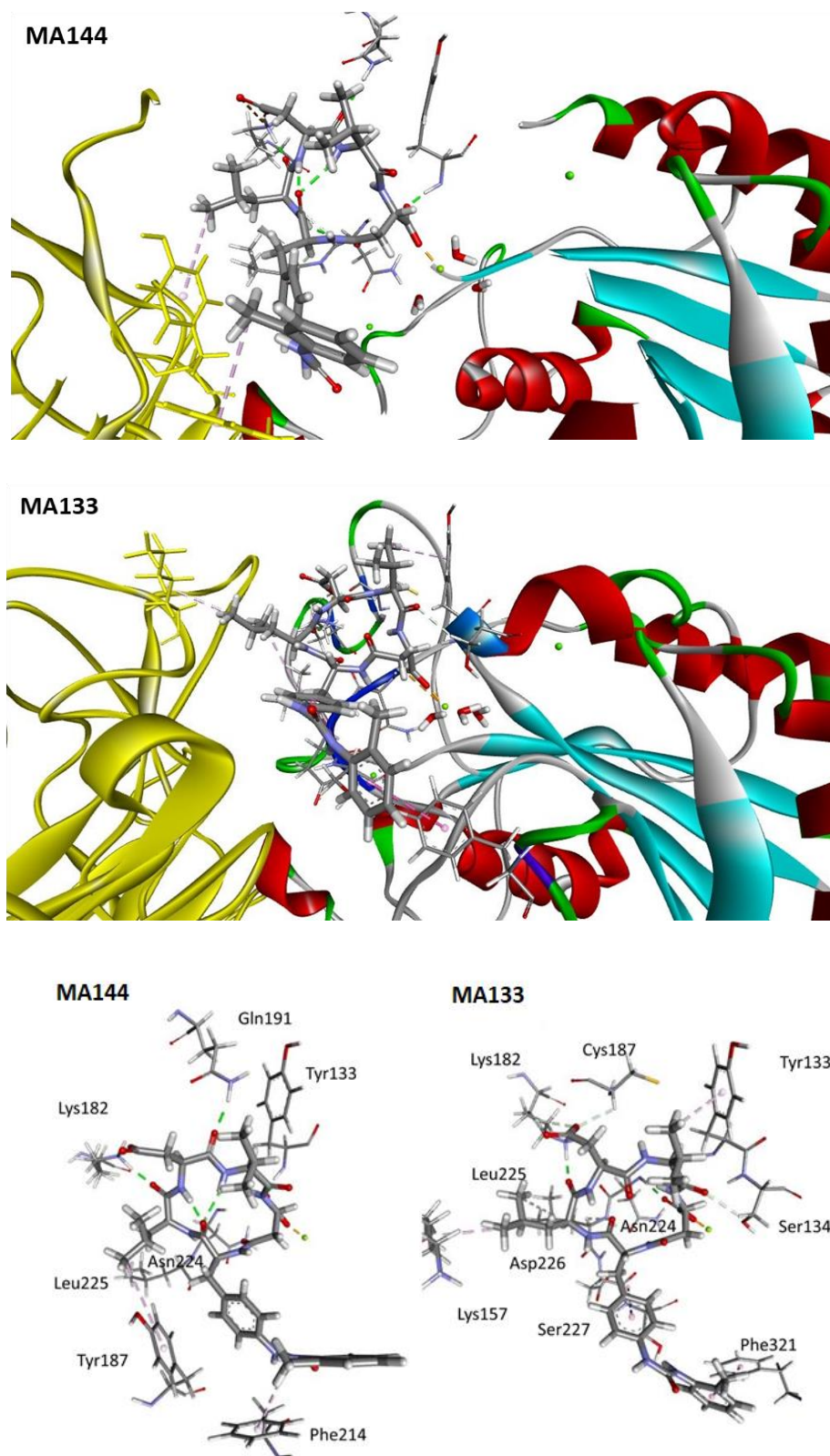
Figure 44. Ligand-receptor interactions for MA144 and MA133. The ligands are rendered in cylindersm and the residues of the receptors in thick sticks. H-bonding, ionic, π–π, and hydrophobic interactions are indicated as dashed lines. The metal ions at the MIDAS, ADMIDAS and SyMBS regions are represented as green spheres.

Based on these considerations, we hypothesized that the hydrophobic interactions of **MA133** with Tyr133, Phe321 and the direct coordination of both isoAsp carboxylate and Ser134 hydroxyl to MIDAS Mn^{2+} moved the β_1-subunit much closer to the α_4-subunit. Thus, ligand-binding would stabilize MIDAS in a high conformation, and the overall integrin binding pocket in a closed-headpiece geometry with lower affinity and poor accessibility to the natural ligand. Therefore, the transmission of the activation signal through $\alpha 7$-helix downward movement and relative hybrid domain swing out in β_1, cannot occur, resulting in an antagonist effect.

On the other hand, the docking pose of **MA144** shows less tight accommodation into the binding pocket. Lack of contacts with the β_1-subunit via Ser134 and Try133, and the presence of hydrophobic interactions toward the α_4-subunit via Tyr187 and Phe214, could stabilize the integrin binding pocket in an open-headpiece and more accessible conformation for the natural ligand. In this scenario, the presence of **MA144** at the binding site could increase the integrin affinity by favouring protein-protein interaction to its natural ligand. This would promote the transmission of the activation signal to the hybrid domain by increasing cell adhesion, thus behaving as an agonist. While the inhibition of protein-protein interaction (PPIs) by means of small-molecule drugs represents a classic approach in pharmacology for the development of basic chemical biology tools as well as drug discovery, the stabilization of protein-protein interactions with small molecules is still regarded as an "exotic" approach, being almost unexplored in the integrin field.[220]

5.3. Conclusion

Constrained cyclic peptides are optimally suited to explore the structural requirements with respect to the 3D arrangement of the pharmacophoric groups ("spatial screening"). A small library of cyclic LDV peptides was designed starting from the linear sequence of BIO1211, taken as a reference compound, to develop potent $\alpha_4\beta_1$ integrin antagonist. To this purpose, the peptidomimetic cyclization strategy has been used to improve the enzymatic stability, bioactivity and to stiffen the cyclopeptide backbone. The introduction of an extra amine and a carboxylate groups in the BIO1211 parent sequence, allowed the head-to-tail backbone cyclization of the linear peptide precursor previously assembled on Wang resin using standard SPPS. Initially, maintaining the absolute configuration of the LDV unaltered, we investigated different diastereomer combinations by changing the configuration of the PhU and isoAsp/β^3-

homoAla residues. Preliminary *in vitro* cell adhesion assays on Jurkat E6.1 $\alpha_4\beta_1$-integrin expressing cells, showed an interesting opposite effect. To parity of isoAsp (S-configured), the modification of the PhU configuration led in an increase of cell adhesion (**MA144**) or in its inhibition (**MA133**) with an IC_{50} in the nanomolar range. Therefore, in order to correlate the integrin binding mode to the opposite behaviour of the two cyclic pentapeptides in cell adhesion assays, SAR studies, NMR spectroscopy, MD and molecular docking simulations were performed. Good agreement between docking results and experimental biological data was observed. Replacement of isoAsp was not tolerated leading to inactive compound (**MA227** and **MA236**), thus, underlining the essential role in coordinating the metal cation in the MIDAS region of the $\beta1$-subunit, fundamental for effective integrin binding. The docking model suggested that CPPs agonist or antagonist can be the result of the stabilization of slightly different conformations of the receptor itself.

Despite the opposite effect observed in cell adhesion is still under investigation, our strategy may represent in perspective an optimal starting point for integrin ligand drug design. Anyway, both our CPPs could find therapeutic application in inflammatory conditions, since antagonists generally prevent leucocyte adhesion and extravasation while the $\alpha_4\beta_1$ agonist can prevent the extravasation in the inflamed tissue via an upstream strong adhesion of the circulating leukocytes.

5.4. Experimental section

General methods

Standard chemicals and solvents including *N*-protected and *C*-protected amino acids, unless otherwise stated, were purchased from commercial sources and used as received without further purification. Compound purities were determined by analytical RP-HPLC and elemental analysis. Analytical RP-HPLC was carried out with an Agilent 1100 series apparatus, using a reverse-phase column Phenomenex mod. Gemini 3 μm C_{18} 110 Å 100 × 3.0 mm (No 00D-4439-Y0); column description: stationary phase octadecyl-carbon-chain-bonded silica (C_{18}) with TMS (trimethylsilyl) endcap, fully porous organosilica solid support, particle size 3 μm, pore size 110 Å, length 100 mm, internal diameter 3 mm; DAD (diode-array detection) 210 nm; mobile phase: from H_2O/CH_3CN (9:1) to H_2O/CH_3CN (2:8) in 20 min at a flow rate of 1.0 mL $\cdot$ min^{-1}, followed by 10 min at the same composition. Semipreparative RP-HPLC was carried

out with an Agilent 1100 series apparatus, using a reverse-phase column ZORBAX mod. Eclipse XDBC18 PrepHT cartridge 21.2 × 150 mm 7 μm (no. 977150-102); column description: stationary phase octadecyl-carbon-chain-bonded silica (C_{18}), double endcapped, particle size 7 μm, pore size 80 Å, length 150 mm, internal diameter 21.2 mm; DAD 210 nm; mobile phase from H_2O/CH_3CN (8:2) to CH_3CN (100 %) in 10 min at a flow rate of 12 mL · min^{-1}. ESI-MS analysis was carried out using an MS single quadrupole HP 1100 MSD detector, with a drying gas flow of 12.5 L min^{-1}, nebulizer pressure 30 psig, drying gas temp. 350 °C, capillary voltage 4500 (+) and 4000 (–), scan 50-2600 amu. Elemental analyses were carried out with a Thermo Flash 2000 CHNS/O analyser. NMR spectra were recorded on a Varian Gemini apparatus (^{1}H: 400 MHz, ^{13}C: 100 MHz) at 298 K in 5 mm tubes, using 0.01 M peptide. Solvent suppression was carried out by the solvent presaturation procedure implemented in Varian (PRESAT). Chemical shifts are reported in ppm (δ) and referenced to residual nondeuterated solvent signal as internal standard ($CDCl_3$ ^{1}H: 7.26 ppm, ^{13}C: 77.16 ppm; $(CD_3)_2SO$: ^{1}H: 2.50, ^{13}C: 39.52 ppm). The unambiguous assignment of ^{1}H-NMR resonances was based on 2D gCOSY experiments. Variable temperature (VT) ^{1}H-NMR experiments were carried out over the range 298-348 K; temperature calibration was done with the ethylene glycol OH-CHn chemical- shift separation method. Coupling constants (J) are reported in Hz with the following abbreviations used to indicate splitting: s = singlet, d = doublet, t = triplet, m = multiplet, p = pentet, br = broad signal.

Solid-phase peptide synthesis was performed in polypropylene syringes fitted with a polyethylene porous disc. Solvents and soluble reagents were removed by suction. Washings between deprotection, coupling, and final deprotection steps were carried out with DMF (3 x 1 min) and DCM (3 x 1 min). Reactions and washes during peptide synthesis were performed at 25 °C. A dual-channel syringe pump (KD scientific Model 200) was used for slow reagent addition (cyclization in solution).

Conformational Analysis by NMR

Peptide samples were dissolved in 8:2 [D_6]DMSO/H_2O in 5 mm tubes to the final concentration of 0.01 M. At this concentration, the intramolecular aggregation in mixtures of [D_6]DMSO and H_2O is usually unimportant. Besides, self-association of the peptides was excluded based on the reproducibility of the chemical shift of non-exchangeable protons in the concentration range 0.01−0.04 M (not shown). Water suppression was achieved by the PRESAT procedure implemented in Varian. Proton resonance assignment was accomplished

through gCOSY. VT ^{1}H-NMR experiments were recorded over the range of 298-348 K; temperature calibration was done with the ethylene glycol OH-CHn chemical shift separation method. 2D ROESY experiments were done at RT, phase-sensitive mode, spin-locking field (γb2) = 2000 Hz, mixing time = 250 ms; spectra were processed in the hypercomplex approach; peaks were calibrated on the solvent. Only ROESY-derived constraints were included in the restrained molecular dynamics (MD). Cross-peak intensities were ranked and associated to the distances (Å): very strong = 2.3, strong = 2.6, medium = 3.0, weak = 5.0. The intensities of the cross-peaks arising from protons separated by known distances (e.g., geminal) were found to match with these associations but were discarded. For the absence of Hα(i), Hα (i + 1) ROESY cross-peaks, all of the ω bonds were set at 180° (f constant: 16 kcal mol^{-1} Å^{-2}).

MD Simulations

The restrained MD simulations were conducted at 300 K and 1 atm by using the AMBER force field in a $30 \times 30 \times 30$ Å^3 box of standard TIP3P models of equilibrated water, periodic boundary conditions dielectric scale factor = 1, and cutoff for the nonbonded interactions = 12 Å; all water molecules closer than 2.3 Å to a solute atom were eliminated, and 50 random structures were generated by a 100 ps simulation at 1200 K; these were subsequently subjected to restrained MD, 50 ps with a 50% scaled force field at 1200 K, then by 50 ps with full distance restraints, force constant = 7 kcal mol^{-1} Å^{-2}, after which the system was cooled in 20 ps to 50 K. H-bond interactions were not included, nor were torsion angle restraints. The resulting structures were minimized by 3000 cycles of steepest descent and 3000 cycles of conjugated gradient, and convergence = 0.01 kcal Å^{-1} mol^{-1}. The backbones of the structures were clustered by the rmsd analysis. Unrestrained MD simulations were performed starting with the conformation derived from ROESY in the box of standard TIP3P water for 10 ns at 298 K using periodic boundary conditions, at constant temperature and pressure (Berendsen scheme, bath relaxation constant of 0.2). For 1−4 scale factors, van der Waals and electrostatic interactions are scaled in AMBER to half their nominal value. The integration time step was set to 0.1 fs. The system coordinates were collected every picosecond.

Molecular docking

The ligand molecules were obtained using a systematic conformer search followed by geometry optimization of the lowest energy structure with MOPAC7 (PM3 Method, RMS gradient 0.01). The receptor model was derived from the deposited X-ray structures of the α_4-

subunit (PDB: 3V4V, Crystal structure of $\alpha_4\beta_7$ headpiece complexed with Fab ACT-1 and RO0505376) [125] and β_1-subunits (PDB: 3VI4, Crystal structure of $\alpha_5\beta_1$ integrin headpiece in complex with RGD peptide).[217] Hydrogen atoms were added with respect of hydrogen bonding network by Reduce software and the PROPKA program was employed to estimate the protonation states of the titratable residues. Molecular docking experiments were performed with Autodock 4.0.[221] We used the Lamarckian Genetic Algorithm which combines global search (Genetic Algorithm alone) to local search (Solis and Wets algorithm). Ligands and receptors were further processed using the Autodock Tool Kit (ADT). Gasteiger-Marsili charges were loaded on the ligands in ADT and solvation parameters were added to the final structure using the Addsol utility of Autodock. Each docking run consisted of an initial population of 100 randomly placed individuals, a maximum number of 200 energy evaluations, a mutation rate of 0.02, a crossover rate of 0.80, and an elitism value of 1. For the local search, the so-called pseudo-Solis and Wets algorithm was applied using a maximum of 250 iterations per local search. 250 independent docking runs were carried out for each ligand. The grid maps representing the system in the actual docking process were calculated with Autogrid. The dimensions of the grids were 100×100×100, with a spacing of 0.1 Å between the grid points and the center close to the cavity left by the ligand after its removal. The simpler inter-molecular energy function based on the Weiner force field in Autodock was used to score the docking results. Results differing by less than 1.0 Å in positional root-mean-square deviation (rmsd) were clustered together and were represented by the result with the most favorable free energy of binding. The poses thus obtained were equilibrated by a 5.0 ns of partially restrained molecular dynamics simulation using the CUDA® version of the GROMACS package [222] with a modified version of the AMBER ff03 force field, [223] a variant of the AMBER ff991 potential in which charges and main-chain torsion potentials have been derived based on QM+continuum solvent calculations and each amino acid is allowed unique main-chain charges. After the above-described MD simulations, QM/MM calculations were performed using the NWChem 6.1.1 package. The QM region contained the ligand atoms and the side chains of all major residues of the binding site. The theoretical level used for the QM region was the hybrid DFT of the B3LYP [224] exchange-correlation functional with Grimme's D3 dispersion correction (B3LYP-D3) and the 6-31G(d) basis sets while the MM atoms were subjected to an Amber ff99 force field (B3LYP- D3/6-31G(d) | Amber ff99). Hydrogen link atoms were used for the

QM/MM boundary and the non-bonded QM/MM interactions were calculated with a cut-off of 10Å. Interactions of QM atoms with all MM charges were included in calculations.

Cell adhesion assays

The assays were performed as previously described.[180, 182] SK-MEL-24, K562, D283 and HT-29 cells were seeded in 96-well plates coated by passive adsorption with FN (10 μg·mL^{-1}) overnight at 4°C. For MCF7, HEL and HL60 cells, the plates were coated with fibrinogen (10 μg·mL^{-1}). In adhesion assays carried out with Jurkat E6.1, EoL-1 and HMC 1.1 cells, plates were coated with VCAM-1 (2 μg·mL^{-1}) or FN (10 μg·mL^{-1}). Alternatively, Jurkat E6.1 cell adhesion assay was performed in plates coated with ICAM-1 (2 μg·mL^{-1}). A saturation curve for each ligand was plotted to establish the best signal-to-noise ratio. Non-specific hydrophobic binding sites were blocked, for 30 min at 37°C, by incubation with BSA (1 g·100 mL^{-1}) dissolved in HBSS. The number of adherent cells was calculated by comparison with a standard curve prepared in the same plate using known concentrations of labelled cells. The effect of antagonists was evaluated by the reduction in adherent cells in comparison to the controls. Adhesion assays were also carried out in the presence of an anti-human α_4 integrin antibody (5 μg·mL^{-1}). Experiments were carried out in quadruplicate and repeated at least five times.

Western blot analysis

Western blot analysis was performed as previously described with slight modifications.[196] Jurkat E6.1 cells were cultured for 16/18 h in RPMI medium containing a reduced amount of FBS (1 g·100·mL^{-1}). Then, 3×10^6 cells were incubated with different concentrations of compound for 60 min and then seeded for 1 h in FN (10 μg·mL^{-1}) coated plates and lysed on ice using a mammalian protein extraction reagent (M-PER; Pierce, Rockford, IL, USA) in the presence of a phosphatase inhibitor cocktail. Protein extracts were quantified using a BCA protein assay kit (Pierce, Rockford, IL, USA), heated for 5 min at 95°C, and equal amounts of the samples were separated by 12% SDS-PAGE gel, transferred onto nitrocellulose membranes and immunoblotted with the indicated antibodies. Incubations with anti-phospho-ERK1/2 (1:1000) (Cell Signaling Technology, Danvers, MA, USA) or anti-total ERK1/2 antibodies (1:2500) (Cell Signaling Technology) took place overnight at 4°C in the presence of BSA (5 g·100 mL^{-1}) in Tris buffered-saline containing Tween-20 (0.1 g·100·mL^{-1}). After washing, anti-rabbit HRP-conjugated secondary antibodies (Santa Cruz Biotechnology, Dallas, TX, USA) were added to membranes for 1.5 h at room temperature. Protocols for image acquisition and

analysis have been previously described. Experiments were replicated independently at least four times.

Synthesis and characterization

Synthesis of Fmoc-Asp(tBu)-OBn ((S)-**MA44**, (R)-**MA244**)

A mixture of Fmoc-Asp(OtBu)-OH (1.0 eq), tetra-butylammoniumbromide (1.0 eq), and anhydrous K_2CO_3 (1.1 eq) in acetonitrile (0.2 M) was stirred at RT for 20 min. Benzyl bromide (1.1 eq) in acetonitrile was then added dropwise under vigorous stirring. The mixture was stirred for 12 h at RT. Then, the precipitate was filtered off, and the filtrate was evaporated to dryness. The resulting crude material was dissolved in EtOAc, and the organic layer was washed three times with a saturated $NaHCO_3$ solution, H_2O and brine, dried over Na_2SO_4, and finally was concentrated under reduced pressure to afford the product as a white solid. This was used without further purifications: (S)-**MA44** ($> 99\%$), (R)-**MA244** (94%) respectively. ESI-MS *m/z* calcd. for $[C_{30}H_{31}NO_6Na]^+$: 524.2, found: 524.2 $[M+Na]^+$.

General procedure for OtBu deprotection: ((S)-**MA45**, (R)-**MA246**)

Both (S)-**MA44** and (R)-**MA244** compounds (1.0 eq), were treated with 50% TFA in DCM at 0 °C under stirring at RT for 3 h (TLC monitoring). The solvent was removed under reduced pressure, then ice-cold H_2O was added to the residue and the suspension was allowed to stir overnight. The resulting precipitate (quantitative yield) was collected by filtration, dried under high *vacuum* and used without further purifications: (S)-**MA45** (98%), (R)-**MA246** (99%), respectively. ESI-MS *m/z* calcd. for $[C_{26}H_{24}NO_6]^+$: 446.2, found: 446.2 $[M+H]^+$.

Synthesis of H-Phe(4-NO₂)-OH ((S)-**MA245**, (R)-**MA247**, Scheme 8)

Phenylalanine (1.0 eq) was added in small portion to conc. H_2SO_4 (6.0 eq) until complete dissolution. The reaction mixture was then cooled down to 0 °C, and conc. HNO_3 (0.65 eq) was added dropwise. The reaction was stirred for 1 h at 0 °C. Then, ice-cold H_2O was slowly added to the reaction mixture (20 mL) and stirred for additional 15 min. Later, the mixture was heated to boil and neutralized (pH 5-6) by addition of NH_4OH 28% solution after bringing down to RT. The reaction mixture was concentrated at reduced pressure and kept overnight for crystallization. The crystals formed were filtered, washed with water and dried under high

vacuum to give the pure product as white solid: (*S*)-Phe(4-NO$_2$)-OH **MA245** (85%) and (*R*)-Phe(4-NO$_2$)-OH **MA247** (97%), respectively. ESI-MS *m/z* calcd. for [C$_9$H$_{11}$N$_2$O$_4$]$^+$: 211.1, found: 211.2 [M+H]$^+$.

Synthesis of Boc-Phe(4-NO$_2$)-OH ((*S*)-MA248, (*R*)-MA249, Scheme 8)

In a typical experimental procedure, the amine (1.0 eq) and Na$_2$CO$_3$ (2.0 eq) were suspended in a mixture of H$_2$O/Dioxane (1:1) and then cooled at 0 °C in ice-bath. Boc$_2$O (1.2 eq) was added to the mixture and the reaction was stirred at RT overnight. The mixture was concentrated under reduced pressure to remove dioxane, while the alkaline aqueous layer was adjusted to pH 3-4 with HCl 0.5 M solution and then extracted three times with EtOAc. The combined organic phases were dried over Na$_2$SO$_4$, filtered and concentrated to dryness *in vacuo*, to afford the protected compound which was used without further purifications: Boc-(*S*)-Phe(4-NO$_2$)-OH **MA248** (90%) and Boc-(*R*)-Phe(4-NO$_2$)-OH **MA249** (84%), respectively. ESI-MS *m/z* calcd. for [C$_{14}$H$_{18}$N$_2$O$_6$Na]$^+$: 333.1, found: 333.2 [M+Na]$^+$.

Synthesis of Boc-Phe(4-NH$_2$)-OH ((*S*)-MA250, (*R*)-MA253, Scheme 8)

Catalytic hydrogenation of the nitro group was carried out in MeOH (0.1 M) with a catalytic amount of Pd/C (10% *w/w*) and H$_2$. The reaction mixture was stirred for 3 h at RT. After this, the catalyst was filtered off over a Celite® pad and the solvent was removed *in vacuo*. Then, Et$_2$O was added to the residue and the suspension was allowed to stir overnight. The resulting precipitate was collected by filtration, dried under high *vacuum* and used without further purifications: Boc-(*S*)-Phe(4-NH$_2$)-OH **MA250** (45%) and Boc-(*R*)-Phe(4-NH$_2$)-OH **MA253** (50%), respectively. ESI-MS *m/z* calcd. for [C$_{14}$H$_{21}$N$_2$O$_4$]$^+$: 281.1, found: 281.1 [M+H]$^+$, 181.2 [M-Boc+H]$^+$.

Synthesis of Boc-PhU-OH ((*S*)-MA254, (*R*)-MA255, Scheme 8)

To a suspension of the amine (1.0 eq) in DMF (0.2 M) was added dropwise *o*-tolyl isocyanate (1.1 eq). The reaction mixture was stirred at RT for 3 h under N$_2$ atmosphere. Then, the mixture was concentrated *in vacuo* and ice-cold Et$_2$O was added to the residue to precipitate the pure compound which was collected as a brownish solid by filtration: Boc-(*S*)-PhU-OH **MA254** (76%) and Boc-(*R*)-PhU-OH **MA255** (67%), respectively. ESI-MS *m/z* calcd. for [C$_{22}$H$_{27}$N$_3$O$_5$Na]$^+$: 436.1, found: 436.2 [M+Na]$^+$, 314.2 [M-Boc+H]$^+$.

Synthesis of Fmoc-(*R*)-β³homoAla (**MA217** Scheme 2)

The amino nitrile **MA82** (1.0 eq), prepared following the procedure described above,[204] was dissolved in 6M HCl aqueous solution (10 mL) and heated under reflux for 12 h. The reaction mixture was then cooled at 0 °C and neutralized with 2M NaOH solution (pH 7). The solution was concentrated *in vacuo* to afford the deprotected β³-homoAla **MA214** as HCl-salt (70%) which was directly used without further purifications. After, the resulting free amine (1.0 eq) and Na_2CO_3 (2.0 eq) were suspended in a mixture of H_2O/Dioxane (1:1) cooled at 0 °C in ice-bath. Then, Fmoc-Cl (1.0 eq) was added and the reaction was stirred at RT overnight. The mixture was concentrated under reduced pressure to remove dioxane and the alkaline aqueous layer was adjusted to pH 3-4 with HCl 0.5 M solution and extracted three times with EtOAc. The combined organic phases were dried over Na_2SO_4, filtered and concentrated to dryness *in vacuo*. The resulting residue was purified by flash chromatography over silica gel (eluent Cy/EtOAc/AcOH 60:40:1) to afford the protected compound **MA217** (55%) as white solid. ESI-MS *m/z* calcd. for $[C_{19}H_{20}NO_4]^+$: 326.1, found: 326.2 $[M+H]^+$.

General procedure for Solid-Phase Peptide Synthesis (SPPS)

Linear peptides were assembled manually on Wang resin (1.1 mmol/g loading capacity) using Fmoc/OBn protocol.

Attachment of the first Amino acid

Prior to use, Wang resin was swollen in DMF for 30 min. In a separate vial, Fmoc-AA-OH (3.0 eq) was activated by mixing HOBT (3.0 eq) and DCC (3.0 eq) in DMF (4 mL) for 20 min before adding to the resin. Then, a catalytic amount of DMAP (0.1 eq) was added, and the resin was gently shaken for 3 h at RT. Thereafter, a mixture of Ac_2O (20 eq) and pyridine (20 eq) was added and shaken for additional 30 min to endcap the unreacted 4-hydroxybenzyl alcohol linkers. The resin was filtered and washed sequentially with DMF (3 x 5 mL) and DCM (3 x 5 mL).

Peptide chain elongation

Fmoc cleavage was carried out using 20 % (*v/v*) piperidine in DMF (5mL), under gentle stirring at RT for 10 min. After a washing step with DMF and DCM, the deprotection was repeated once again. The resin was then washed sequentially with DMF (3 x 5 mL) and DCM (3 x 5 mL). The coupling reactions were accomplished by adding to the resin a solution of Fmoc-AA-OH (2.0 eq) activated in a separate vial with DCC (2.0 eq) and HOBt (2.0 eq) in DMF (4 mL),

and shaking the mixture for 3 h a RT. Each transformation, including coupling reactions and Fmoc removals, were monitored by Kaiser test.

Cleavage from the resin

Cleavage from the resin and simultaneous removal of Boc protecting group from the last residue was performed by using a mixture of TFA/TIPS/H$_2$O (95:2.5:2.5, *v/v/v*) for 2.5 h at RT. The mixture was filtered in a centrifuge tube and the resin washed with Et$_2$O/DCM containing a small portion of TFA. The filtrates were concentrated, and ice-cold Et$_2$O was added to precipitate the crude peptide as TFA salt, which was recovered by centrifuge.

Head-to-tail Cyclization in solution

Cyclization of the crude peptide was performed in pseudo-high dilution condition (0.005M). The linear peptide (1.0 eq) dissolved in DMF was slowly added over 16 h using a syringe pump to a solution of HBTU (3.0 eq), HOBt (3.0 eq) and DIPEA (6.0 eq) in DMF. Once the addition was complete, the reaction was stirred for additional 2 h, and the progress was monitored by HPLC ESI-MS. Then, the solvent was removed *in vacuo*, and the crude peptide was purified by semipreparative RP-HLPC to give the protected cyclopeptide.

Deprotection of OBn protecting group

Removal of benzyl esters was performed under catalytic hydrogenation conditions. To a stirred solution of the protected cyclopentapeptide (1.0 eq) in absolute EtOH (0.1-0.2 M), a catalytic amount of Pd/C (10% *w/w*) was added. The mixture was stirred under H$_2$ atmosphere for 12 h at RT. Thereafter, the catalyst was filtered off over Celite® and the solvent was removed *in vacuo* to afford the pure final product. The purity and identity of the products were determined by RP-HPLC coupled to tandem ESI-MS, and by ^{1}H-NMR at 400 MHz in DMSO-d_6/H$_2$O (8:2), gCOSY and ROESY experiments.

Synthesis of *c*[(*S*)-PhU-Leu-Asp-Val-(*R*)-isoAsp] (MA86, Scheme 9)
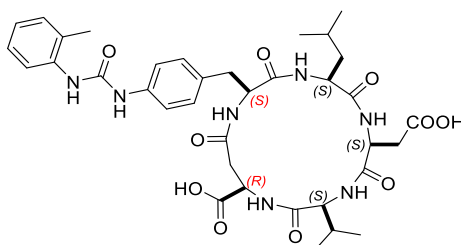
According to general procedure, the linear peptide **MA72** was assembled on Wang resin (400 mg, 0.44 mmol). The amino acid sequence was elongated in the following order: Fmoc-(*D*)-

Asp-OBn (**MA244**), Fmoc-(*L*)-Val-OH, Fmoc-(*L*)-Asp(OBn)-OH, Fmoc-(*L*)-Leu-OH and modified Boc-(*L*)-PhU-OH (**MA254**). After the cleavage from the resin the crude peptide was used without further purifications (112 mg, 24% based on the estimated loading of the resin). ESI-MS t_r = 6.1 min, m/z calcd. for $[C_{50}H_{62}N_7O_{11}]^+$: 936.4, found: 936.2 $[M+H]^+$. Cyclization was carried out following the general procedure, and the resulting crude residue was purified by semipreparative RP-HPLC (Eluent H_2O/ACN from 50:50 to 100% ACN for 13 min with a flow rate of 10 mL/min) affording **MA78** (10 mg, 10%) as a white solid. ESI-MS t_r = 11.1 min, m/z calcd. for $[C_{50}H_{60}N_7O_{10}]^+$: 918.4, found: 918.2 $[M+H]^+$. Finally, deprotection under catalytic hydrogenation condition provided the pure cyclic pentapeptide **MA86** (7 mg, 86%) as a white solid. ^{1}H-NMR (400 MHz, DMSO-d_6) δ 9.02 (s, 1H, NHb), 8.49 (br.d, 1H, Asp-NH), 8.38 (d, J = 8.4 Hz, 1H, Leu-NH), 8.32 (d, J = 8.4 Hz, 1H, PhU-NH), 8.20 (br.d, 1H, Val-NH), 8.01 (br.d, 1H, isoAsp-NH), 7.94 (s, 1H, NHa), 7.80 (d, J = 8.0 Hz, 1H, ArH$_6$), 7.36 (d, J = 8.0 Hz, 2H, ArH$_{2'6'}$), 7.18 – 7.11 (m, 4H, ArH$_{3'5'}$+ArH$_{3,5}$), 6.93 (dd, J = 7.6, 7.2 Hz, 1H, ArH$_4$), 4.40 – 4.32 (m, 2H, Asp-CH$^\alpha$ + PhU-CH$^\alpha$), 4.27 – 4.17 (m, 2H, isoAsp-CH$^\alpha$ + Leu-CH$^\alpha$), 3.96 (dd, J = 9.2, 8.8 Hz, 1H, Val-CH$^\alpha$), 3.03 (dd, J = 14.2, 3.8 Hz, 1H, PhU-CH$^\beta$), 2.80 – 2.68 (m, 4H, PhU-CH$^\beta$ + isoAsp-CH$^\beta$ + Asp-CH$_2$$^\beta$), 2.38 (dd, J = 15.2, 1.6 Hz, 1H, isoAsp-CH$^\beta$), 2.23 (s, 3H, ArCH$_3$), 2.13 – 2.05 (m, 1H, Val-CH$^\beta$), 1.72 – 1.61 (m, 1H, Leu-H$^\beta$), 1.50 – 1.48 (m, 2H, Leu-CH$^\beta$ + Leu-CH$^\gamma$), 0.87 – 0.85 (m, 12H, Val-2CH$_3$ + Leu-2CH$_3$). ^{13}C-NMR (101 MHz, DMSO-d_6) δ 171.3, 171.0, 170.5, 169.7, 169.2, 152.7, 138.3, 137.5, 130.2, 129.3, 127.5, 126.1, 122.6, 121.1, 118.5, 117.9, 58.1, 52.6, 51.6, 49.1, 48.0, 34.5, 34.3, 31.3, 28.7, 24.2, 22.9, 22.1, 21.6, 19.5, 17.9. ESI-MS m/z calcd. for $[C_{36}H_{48}N_7O_{10}]^+$: 738.3, found: 738.2 $[M+H]^+$, t_r = 7.2 min, 97% purity (λ = 254 nm).

Synthesis of *c*[(*R*)-PhU-Leu-Asp-Val-(*S*)-isoAsp] (MA133, Scheme 9)
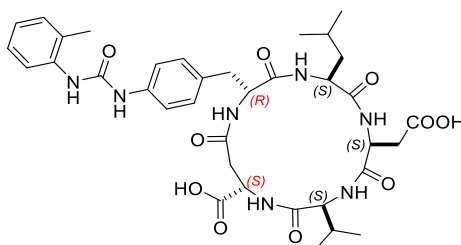
According to general procedure, the linear peptide **MA127** was assembled on Wang resin (130 mg, 0.15 mmol). The amino acid sequence was elongated starting from Fmoc-(*L*)-Asp-OBn (**MA44**), Fmoc-(*L*)-Val-OH, Fmoc-(*L*)-Asp(OBn)-OH, Fmoc-(*L*)-Leu-OH and modified Boc-(*D*)-PhU-OH (**MA255**). After the cleavage from the resin the crude peptide was used without

further purifications (50 mg, 34% based on the estimated loading of the resin). ESI-MS $t_r = 5.7$ min, *m/z* calcd. for $[C_{50}H_{62}N_7O_{11}]^+$: 936.4, found: 936.2 $[M+H]^+$. Cyclization was carried out as described in the general procedure, the resulting crude residue was purified by semipreparative RP-HPLC (Eluent H_2O/ACN from 50:50 to 100% ACN for 13 min with a flow rate of 10 mL/min) yielding **MA130** (13 mg, 29%) as a white solid. ESI-MS $t_r = 10.2$ min, *m/z* calcd. for $[C_{50}H_{60}N_7O_{10}]^+$: 918.4, found: 918.2 $[M+H]^+$. Final catalytic hydrogenation provided the pure cyclic pentapeptide **MA133** (9 mg, 87%) as a white solid. ^{1}H-NMR (400 MHz, DMSO-d_6) δ 9.04 (s, 1H, NHb), 8.30 (br.d, 1H, PhU-NH), 8.25 – 8.15 (m, 2H, isoAsp-NH + Leu-NH), 8.02 (br.d, 1H, Val-NH), 7.93 (s, 1H, NHa), 7.79 (d, $J = 8.4$ Hz, 1H, ArH$_6$), 7.70 (d, $J = 6.4$ Hz, 1H, Asp-NH), 7.34 (d, $J = 8.0$ Hz, 2H, ArH$_{2'6'}$), 7.17 – 7.11 (m, 2H, ArH$_{3,5}$), 7.06 (d, $J = 8.0$ Hz, 2H, ArH$_{3'5'}$), 6.93 (t, $J = 7.2$ Hz, 1H, ArH$_4$), 4.48 – 4.42 (m, 1H, Asp-CH^α), 4.38 – 4.35 (m, 1H, PhU-CH^α), 4.32 – 4.25 (m, 1H, isoAsp-CH^α), 4.02 – 3.92 (m, 1H, Leu-CH^α), 3.58 – 3.49 (m, 1H, Val-CH^α), 2.79 – 2.73 (m, 3H, PhU-CH$_2$^{β} + Asp-CH^β), 2.68 – 2.55 (m, 3H, isoAsp-CH$_2$^{β} + Asp-CH^β), 2.36 – 2.26 (m, 1H, Val-CH^β), 2.22 (s, 3H, ArCH$_3$), 1.38 – 1.28 (m, 2H, Leu-CH$_2$^{β}), 1.02 – 0.92 (m, 1H, Leu-CH^γ), 0.83 (d, $J = 6.4$ Hz, 3H, Leu-CH$_3$), 0.79 (d, $J = 6.4$ Hz, 3H, Leu-CH$_3$), 0.72 (d, $J = 6.0$ Hz, 3H, Val-CH$_3$), 0.64 (d, $J = 6.4$ Hz, 3H, Val-CH$_3$). ^{13}C-NMR (101 MHz, DMSO-d_6) δ 172.3, 172.0, 171.8, 171.1, 170.1, 169.8, 152.7, 138.4, 137.5, 130.1, 130.0, 129.4, 127.5, 126.1, 122.5, 121.0, 117.6, 109.5, 61.3, 54.9, 51.5, 51.2, 49.6, 36.4, 35.9, 33.6, 31.3, 23.5, 23.0, 22.1, 21.0, 19.1, 17.9. ESI-MS *m/z* calcd. for $[C_{36}H_{48}N_7O_{10}]^+$: 738.3, found: 738.2 $[M+H]^+$, $t_r = 4.2$ min, 97% purity ($λ = 254$ nm).

**Synthesis of *c*[(*S*)-PhU-Leu-Asp-Val-(*S*)-isoAsp] (MA144,** Scheme 9)**
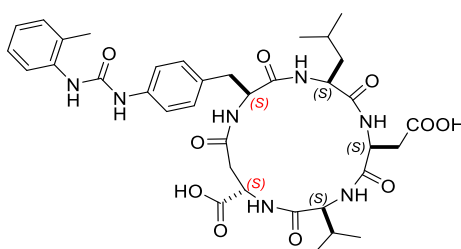
The linear peptide **MA141** was assembled on Wang resin (130 mg, 0.15 mmol) following the general procedure described above. The amino acid sequence was elongated in the following order Fmoc-(*L*)-Asp-OBn (**MA44**), Fmoc-(*L*)-Val-OH, Fmoc-(*L*)-Asp(OBn)-OH, Fmoc-(*L*)-Leu-OH and modified Boc-(*L*)-PhU-OH (**MA254**). After the cleavage from the resin the crude peptide was used without further purifications (33 mg, 22% based on the estimated loading of the resin). ESI-MS $t_r = 6.4$ min, *m/z* calcd. for $[C_{50}H_{62}N_7O_{11}]^+$: 936.4, found: 936.2 $[M+H]^+$.

Cyclization was carried out as described in the general procedure, the resulting crude residue was purified by semipreparative RP-HPLC (Eluent H_2O/ACN from 50:50 to 100% ACN for 13 min, with a flow rate of 10 mL/min) affording **MA142** (8 mg, 28%) as a white solid. ESI-MS t_r = 11.4 min, m/z calcd. for $[C_{50}H_{60}N_7O_{10}]^+$: 918.4, found: 918.2 $[M+H]^+$. Finally, a catalytic hydrogenation provided the pure cyclic pentapeptide **MA144** (6 mg, 90%) as a white solid. ^{1}H-NMR (400 MHz, DMSO-d_6) δ 8.98 (s, 1H, NHb), 8.65 (d, J = 6.0 Hz, 1H, Leu-NH), 8.22 – 8.14 (m, 2H, Asp-NH + PhU-NH), 7.90 (s, 1H, NHa), 7.80 (d, J = 7.6 Hz, 1H, ArH$_6$), 7.75 (d, J = 9.2 Hz, 1H, Val-NH), 7.37 (d, J = 7.6 Hz, 2H, ArH$_{2'6'}$), 7.22 – 7.09 (m, 5H, ArH$_{3'5'}$ + ArH$_{3,5}$ + isoAsp-NH), 6.94 (dd, J = 7.2, 6.8 Hz, 1H, ArH$_4$), 4.60 – 4.53 (m, 1H, isoAsp-CH^α), 4.38 – 4.31 (m, 1H, PhU-CH^α), 4.29 – 4.24 (m, 1H, Asp-CH^α), 4.16 (dd, J = 9.2, 4.0 Hz, 1H, Val-CH^α), 3.79 – 3.68 (m, 1H, Leu-CH^α), 2.97 – 2.89 (m, 2H, PhU-CH^β+Asp-CH^β), 2.87 (dd, J = 14.0, 7.6 Hz, 1H, Asp-CH^β), 2.74 (dd, J = 14.0, 2.0 Hz, 1H, PhU-CH^β), 2.69 (dd, J = 14.4, 2.4 Hz, 1H, isoAsp-CH^β), 2.61 (dd, J = 14.4, 4.0 Hz, 1H, isoAsp-CH^β), 2.34 – 2.25 (m, 1H, Val-CH^β), 2.23 (s, 3H, ArCH$_3$), 1.73 – 1.62 (m, 1H, Leu-CH^β), 1.55 – 1.43 (m, 1H, Leu-CH^β), 1.40 – 1.30 (m, 1H, Leu-CH^γ), 0.91 – 0.76 (m, 12H, Val-2CH$_3$ + Leu-2CH$_3$). ^{13}C-NMR (101 MHz, DMSO-d_6) δ 172.5, 172.1, 171.9, 171.2, 170.5, 170.4, 169.8, 152.7, 138.3, 137.5, 130.7, 130.2, 129.3, 127.5, 126.1, 122.6, 121.0, 117.8, 57.7, 55.5, 52.5, 51.8, 48.4, 37.9, 36.9, 36.0, 35.2, 29.3, 24.2, 23.4, 21.2, 19.8, 17.9, 17.6. ESI-MS m/z calcd. for $[C_{36}H_{48}N_7O_{10}]^+$: 738.3, found: 738.4 $[M+H]^+$, t_r = 7.5 min, 98% purity ($λ$ = 254 nm).
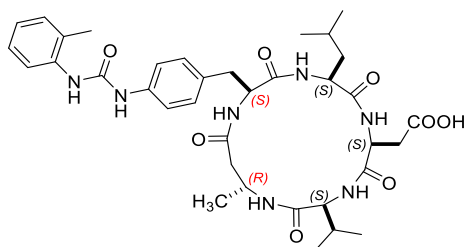
Synthesis of c[(R)-PhU-Leu-Asp-Val-(R)-isoAsp] (MA266, Scheme 9)**
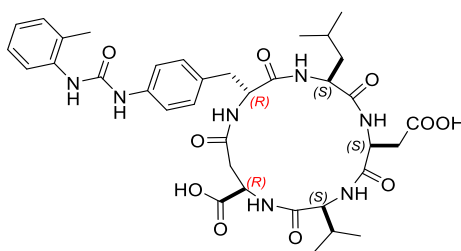
The linear peptide **MA252** was assembled on Wang resin (300 mg, 0.36 mmol) following the general procedure described above. The amino acid sequence was elongated starting from Fmoc-(D)-Asp-OBn (**MA244**), Fmoc-(L)-Val-OH, Fmoc-(L)-Asp(OBn)-OH, Fmoc-(L)-Leu-OH and modified Boc-(D)-PhU-OH (**MA255**). After the cleavage, the crude peptide was used without further purifications (168 mg, 44% based on the estimated loading of the resin). ESI-MS t_r = 6.4 min, m/z calcd. for $[C_{50}H_{62}N_7O_{11}]^+$: 936.4, found: 936.6 $[M+H]^+$. Cyclization was carried out as described in the general procedure, the resulting crude residue was purified by

semipreparative RP-HPLC (Eluent H_2O/ACN from 50:50 to 100% ACN for 13 min with a flow rate of 10 mL/min) afforded **MA261** (50 mg, 34%) as a white solid. ESI-MS t_r = 10.5 min, m/z calcd. for $[C_{50}H_{60}N_7O_{10}]^+$: 918.4, found: 918.6 $[M+H]^+$. Finally, a catalytic hydrogenation provided the pure cyclic pentapeptide **MA266** (6 mg, 90%) as a white solid. ^{1}H-NMR (400 MHz, DMSO-d_6) δ 8.99 (s, 1H, NHb), 8.55 (d, J = 6.4 Hz, 1H, Val-NH), 8.51 (d, J = 4.8 Hz, 1H, PhU-NH), 8.42 (d, J = 6.8 Hz, 1H, isoAsp-NH), 8.24 (d, J = 8.4 Hz, 1H, Leu-NH), 7.90 (s, 1H, NHa), 7.80 (d, J = 7.6 Hz, 1H, ArH$_6$), 7.35 (d, J = 7.6 Hz, 3H, Asp-NH + ArH$_{2'6'}$), 7.19 – 7.10 (m, 2H, ArH$_{3,5}$), 7.09 (d, J = 8.0 Hz, 2H, ArH$_{3'5'}$), 6.94 (dd, J = 7.6, 7.2, Hz, 1H, ArH$_4$), 4.54 (dd, J = 12.4, 4.4 Hz, 1H, Asp-CH$^\alpha$), 4.42 – 4.35 (m, 1H, isoAsp-CH$^\alpha$), 4.29 – 4.21 (m, 1H, PhU-CH$^\alpha$), 3.97 – 3.89 (m, 1H, Leu-CH$^\alpha$), 3.24 – 3.17 (m, 1H, Val-CH$^\alpha$), 2.84 – 2.69 (m, 3H, PhU-CH$_2{}^\beta$+Asp-CH$^\beta$), 2.68 – 2.54 (m, 3H, isoAsp-CH$_2{}^\beta$ + Val-CH$^\beta$), 2.46 – 2.42 (m, 1H, Asp-CH$^\beta$), 2.23 (s, 3H, ArCH$_3$), 1.40 – 1.31 (m, 1H, Leu-CH$^\beta$), 1.30 – 1.22 (m, 1H, Leu-CH$^\beta$), 0.84 (d, J = 6.4 Hz, 7H, Val-2CH$_3$ + Leu-CH$^\gamma$) 0.68 (d, J = 6.4 Hz, 3H, Leu-CH$_3$), 0.58 (d, J = 5.6 Hz, 3H, Leu-CH$_3$). ^{13}C-NMR (101 MHz, DMSO-d_6) δ 172.0, 171.9, 171.7, 171.3, 170.5, 170.3, 170.1, 152.6, 138.4, 137.4, 130.1, 129.7, 129.4, 127.5, 126.1, 122.6, 121.1, 117.6, 64.5, 55.4, 51.2, 50.3, 48.8, 36.1, 35.8, 34.9, 27.6, 23.3, 23.1, 20.8, 19.5, 19.2, 17.8. ESI-MS m/z calcd. for $[C_{36}H_{48}N_7O_{10}]^+$: 738.3, found: 738.8 $[M+H]^+$, t_r = 8.9 min, 99% purity (λ = 254 nm).
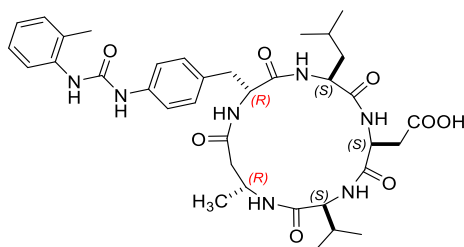
Synthesis of *c*[(*S*)-PhU-Leu-Asp-Val-(*R*)-β^{3}homoAla] (MA227, Scheme 9)**

The linear peptide **MA220** was assembled on Wang resin (250 mg, 0.28 mmol) following the general procedure described above. The amino acid sequence was Fmoc-(*D*)-β^{3}homoAla-OH (**MA217**, Scheme 2), Fmoc-(*L*)-Val-OH, Fmoc-(*L*)-Asp(OBn)-OH, Fmoc-(*L*)-Leu-OH and modified Boc-(*L*)-PhU-OH (**MA254**). After the cleavage from the resin the crude peptide was used without further purifications (70 mg, 27% based on the estimated loading of the resin). ESI-MS t_r = 3.9 min, m/z calcd. for $[C_{43}H_{58}N_7O_9]^+$: 816.4, found: 816.6 $[M+H]^+$. Cyclization was carried out as described in the general procedure, the resulting crude residue was purified by semipreparative RP-HPLC (Eluent H_2O/ACN from 50:50 to 100% ACN for 13 min with a flow rate of 10 mL/min) affording **MA224** (30 mg, 50%) as a white solid. ESI-MS t_r = 10.0

min, m/z calcd. for $[C_{43}H_{56}N_7O_8]^+$: 798.4, found: 798.2 $[M+H]^+$. Final catalytic hydrogenation gave the pure cyclic pentapeptide **MA227** (20 mg, 74%) as a white solid. ^{1}H-NMR (400 MHz, DMSO-d_6) δ 9.01 (s, 1H, NHb), 8.71 (d, J = 6.8 Hz, 1H, Leu-NH), 8.07 (d, J = 7.2 Hz, 1H, Asp-NH), 7.92 (s, 1H, NHa), 7.81 (d, J = 8.4 Hz, 2H, PhU-NH + ArH$_6$), 7.59 (d, J = 9.6 Hz, 1H, Val-NH), 7.37 (d, J = 8.8 Hz, 2H, ArH$_{2'6'}$), 7.17 (d, J = 8.8 Hz, 3H, ArH$_{3'5'}$ + ArH$_3$), 7.12 (d, J = 8.4 Hz, 1H, ArH$_5$), 7.03 (d, J = 7.6 Hz, 1H, β^{3}Ala-NH), 6.93 (dd, J = 8.0, 7.2 Hz, 1H, ArH$_4$), 4.41 (dd, J = 15.2, 7.2 Hz, 1H, PhU-CH^α), 4.24 (dd, J = 12.8, 7.2 Hz, 1H, Asp-CH^α), 4.16 – 4.14 (m, 1H, β^{3}Ala-CH^β), 4.11 (dd, J = 9.6, 5.6 Hz, 1H, Val-CH^α), 3.66 – 3.60 (m, 1H, Leu-CH^α), 2.91 – 2.84 (m, 3H, PhU-CH^β+Asp-CH$_2^β$), 2.76 (dd, J = 12.8, 8.0 Hz, 1H, PhU-CH^β), 2.53 – 4.46 (m, 1H, β^{3}Ala-CH^α overlapped with solvent signal), 2.23 – 2.20 (m, 4H, ArCH$_3$ + Val-CH^β), 2.01 (dd, J = 13.2, 6.4 Hz, 1H, β^{3}Ala-CH^α), 1.76 – 1.69 (m, 1H, Leu-CH^β), 1.50 – 1.43 (m, 1H, Leu-CH^β), 1.23 – 1.18 (m, 1H, Leu-CH^γ), 1.11 (d, J = 6.4 Hz, 3H, β^{3}Ala-CH$_3$), 0.86 (d, J = 7.2 Hz, 6H, Val-2CH$_3$), 0.82 (d, J = 6.4 Hz, 3H, Leu-CH$_3$), 0.78 (d, J = 6.0 Hz, 3H, Leu-CH$_3$). ^{13}C-NMR (101 MHz, DMSO-d_6) δ 172.5, 172.2, 171.5, 170.5, 170.4, 169.7, 152.7, 138.4, 137.5, 130.4, 130.2, 129.3, 127.5, 126.1, 122.6, 121.0, 117.8, 57.9, 54.6, 52.7, 52.3, 42.8, 41.3, 37.2, 36.3, 34.8, 24.1, 23.6, 21.1, 20.4, 19.8, 18.0, 17.8.ESI-MS m/z calcd. for $[C_{36}H_{50}N_7O_8]^+$: 708.4, found: 708.2 $[M+H]^+$. t_r = 6.6 min, 97% purity ($λ$ = 254 nm).

Synthesis of *c*[(*R*)-PhU-Leu-Asp-Val-(*R*)-β^{3}homoAla] (MA236, Scheme 9)**

The linear peptide **MA232** was assembled on Wang resin (250 mg, 0.28 mmol) following the general procedure described above. The amino acid sequence was Fmoc-(*D*)-β^{3}homoAla-OH (**MA217**, Scheme 2), Fmoc-(*L*)-Val-OH, Fmoc-(*L*)-Asp(OBn)-OH, Fmoc-(*L*)-Leu-OH and modified Boc-(*D*)-PhU-OH (**MA255**). After the cleavage from the resin the crude peptide was used without further purifications (121 mg, 47% based on the estimated loading of the resin). ESI-MS t_r = 3.9 min, m/z calcd. for $[C_{43}H_{58}N_7O_9]^+$: 816.4, found: 816.6 $[M+H]^+$. Cyclization was carried out, and the resulting crude residue was purified by semipreparative RP-HPLC (Eluent H$_2$O/ACN from 50:50 to 100% ACN for 13 min with a flow rate of 10 mL/min) affording **MA234** (17 mg, 33%) as a white solid. ESI-MS t_r = 9.8 min, m/z calcd. for

$[C_{43}H_{56}N_7O_8]^+$: 798.4, found: 798.2 $[M+H]^+$. Finally, a catalytic hydrogenation afforded the pure cyclic pentapeptide **MA236** (10 mg, 71%) as a white solid. ^{1}H-NMR (400 MHz, DMSO-d_6) δ 9.05 (s, 1H, NHb), 8.39 (d, J = 4.8 Hz, 1H, PhU-NH), 8.15 (d, J = 8.4 Hz, 1H, Leu-NH), 7.93 (s, 1H, NHa), 7.88 (d, J = 7.2 Hz, 1H, β^{3}Ala-NH), 7.85 (d, J = 8.4 Hz, 1H, Val-NH), 7.82 (d, J = 8.0 Hz, 1H, Asp-NH), 7.79 (d, J = 8.0 Hz, 1H, ArH$_6$), 7.36 (d, J = 8.4 Hz, 2H, ArH$_{2'6'}$), 7.15 (t, J = 8.2 Hz, 1H, ArH$_5$), 7.09 (d, J = 8.4 Hz, 3H, ArH$_{3'5'}$ + ArH$_3$), 6.93 (t, J = 7.2 Hz, 1H, ArH$_4$), 4.60 (dd, J = 15.2, 8.0 Hz, 1H, Asp-CH$^\alpha$), 4.28 (dd, J = 13.6, 6.4 Hz, 1H, PhU-CH$^\alpha$), 4.01 (dd, J = 11.6, 8.0 Hz, 1H, Leu-CH$^\alpha$), 3.95 – 3.92 (m, 1H, β^{3}Ala-CH$^\beta$), 3.63 (t, J = 7.2 Hz, 1H, Val-CH$^\alpha$), 2.91 (dd, J = 14.0, 8.4 Hz, 1H, Asp-CH$^\beta$), 2.87 (dd, J = 12.0, 5.6 Hz, 1H, PhU-CH$^\beta$), 2.76 (dd, J = 14.4, 8.8 Hz, 1H, PhU-CH$^\beta$), 2.55 – 2.50 (m, 1H, Asp-CH$^\beta$ partially overlapped with solvent signal), 2.39 (dd, J = 13.6 5.6 Hz, 1H, β^{3}Ala-CH$^\alpha$), 2.28 (dd, J =, 14.0, 6.8 Hz, 1H, Val-CH$^\beta$), 2.23 (s, 3H, ArCH$_3$), 2.16 (dd, J = 13.2, 3.6 Hz, 1H, β^{3}Ala-CH$^\alpha$), 1.37 (dd, J = 19.2, 6.8 Hz, 2H, Leu-CH$_2^\beta$), 1.26 – 1.10 (m, 1H, Leu-CH$^\gamma$), 1.05 (d, J = 6.8 Hz, 3H, β^{3}Ala-CH$_3$), 0.84 (d, J = 6.8 Hz, 3H, Val-CH$_3$), 0.80 (d, J = 6.4 Hz, 3H, Val-CH$_3$), 0.70 (d, J = 6.0 Hz, 3H, Leu-CH$_3$), 0.62 (d, J = 5.6 Hz, 3H, Leu-CH$_3$). ^{13}C-NMR (101 MHz, DMSO-d_6) δ 171.8, 171.7, 171.3, 171.1, 169.5, 169.2, 152.7, 138.5, 137.5, 130.1, 129.7, 129.5, 127.5, 126.1, 122.6, 121.0, 117.6, 60.4, 55.7, 51.0, 50.7, 42.7, 41.9, 36.3, 36.0, 29.0, 28.5, 23.3, 23.1, 21.0, 19.6, 19.5, 18.7, 17.9. ESI-MS m/z calcd. for $[C_{36}H_{50}N_7O_8]^+$: 708.4, found: 708.2 $[M+H]^+$. t_r = 5.2 min, 99% purity (λ = 254 nm).

Synthesis of c[(S)-PhU-Leu-Asp-Val-(S)-isoAsp-nPr] (MA171, Scheme 9)**
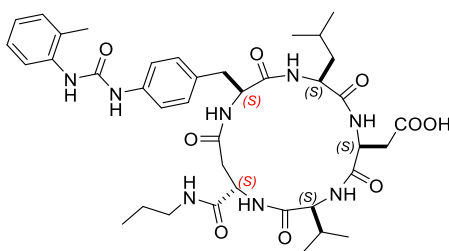
The linear peptide **MR49** was assembled on Wang resin (150 mg, 0.17 mmol) following the general procedure described above. The amino acid sequence was elongated in the following order Fmoc-(L)-Asp-NHpropylamine (**MA59**, Scheme 6) prepared as previously described above, Fmoc-(L)-Val-OH, Fmoc-(L)-Asp(OBn)-OH, Fmoc-(L)-Leu-OH and modified Boc-(L)-PhU-OH (**MA254**). After the cleavage from the resin the crude peptide was used without further purifications (76 mg, 45% based on the estimated loading of the resin). ESI-MS t_r = 6.0 min, m/z calcd. for $[C_{46}H_{63}N_8O_{10}]^+$: 887.4, found: 887.4 $[M+H]^+$. Thereafter, the cyclization

was carried out and the resulting crude residue was purified by semipreparative RP-HPLC (Eluent H_2O/ACN from 50:50 to 100% ACN for 13 min with a flow rate of 10 mL/min) affording **MA163** (18 mg, 27%) as a white solid. ESI-MS t_r = 10.1 min, m/z calcd. for $[C_{46}H_{61}N_8O_9]^+$: 869.4, found: 869.2 $[M+H]^+$. Finally, a catalytic hydrogenation provided the pure cyclic pentapeptide **MA171** (10 mg, 61%) as a white solid. ^{1}H-NMR (400 MHz, DMSO-d_6) δ 9.08 (br s, 1H, NHb), 8.73 (d, J = 7.2 Hz, 1H, Leu-NH), 8.25 (d, J = 5.2 Hz, 1H, Asp-NH), 7.99 (br s, 1H, NHa), 7.96 (br d, 1H, PhU-NH), 7.82 (d, J = 8.0 Hz, 1H, ArH$_6$), 7.71 (d, J = 8.8 Hz, 1H, Val-NH), 7.46 – 7.41 (m, 1H, propyl-NH), 7.38 (d, J = 8.4 Hz, 2H, ArH$_{2'6'}$), 7.22 – 7.10 (m, 5H, ArH$_{3'5'}$ + ArH$_{3,5}$ + isoAsp-NH), 6.93 (t, J = 7.2 Hz, 1H, ArH$_4$), 4.44 (dd, J = 12.4, 7.6 Hz, 1H, isoAsp-CH$^\alpha$), 4.32 – 4.25 (m, 2H, PhU-CH$^\alpha$ + Asp-CH$^\alpha$), 4.15 (dd, J = 8.8, 6.0 Hz, 1H, Val-CH$^\alpha$), 3.72 – 3.64 (m, 1H, Leu-CH$^\alpha$), 3.01 – 2.94 (m, 2H, propyl-CH$_2$), 2.91 – 2.80 (m, 4H, PhU-CH$_2^\beta$+Asp-CH$_2^\beta$), 2.65 (dd, J = 14.0, 4.0 Hz, 1H, isoAsp-CH$^\alpha$), 2.55 – 2.50 (m, 1H, isoAsp-CH$^\alpha$ overlapped with solvent signal), 2.34 – 2.25 (m, 1H, Val-CH$^\beta$), 2.24 (s, 3H, ArCH$_3$), 1.72 – 1.63 (m, 1H, Leu-CH$^\beta$), 1.52 – 1.43 (m, 1H, Leu-CH$^\beta$), 1.42 – 1.32 (m, 3H, propyl-CH$_2$ + Leu-CH$^\gamma$), 0.90 – 0.74 (m, 15H, Val-2CH$_3$ + Leu-2CH$_3$ + propyl-CH$_3$). ^{13}C-NMR (101 MHz, DMSO-d_6) δ 172.5, 172.2, 171.4, 170.7, 170.4, 170.2, 170.0, 152.7, 138.5, 137.5, 130.3, 130.2, 129.3, 127.5, 126.1, 122.6, 121.0, 117.8, 58.0, 55.5, 52.5, 51.9, 50.5, 40.4, 37.5, 37.2, 36.0, 34.9, 31.3, 28.7, 24.1, 23.5, 22.2, 21.0, 20.0, 18.0, 17.9, 11.2. ESI-MS m/z calcd. for $[C_{39}H_{55}N_8O_9]^+$: 779.4, found: 779.4 $[M+H]^+$. t_r = 7.6 min, 99% purity (λ = 254 nm).
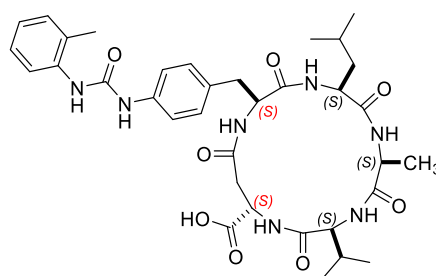
Synthesis of c[(R)-PhU-Leu-Ala-Val-(S)-isoAsp] (MA264, Scheme 9)
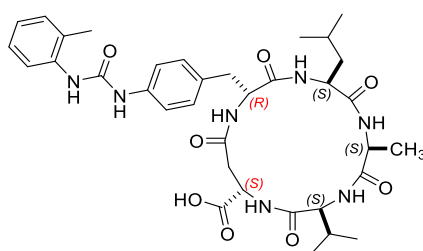
The linear peptide **MA257** was assembled on Wang resin (300 mg, 0.36 mmol) following the general procedure described above. The amino acid sequence was elongated starting from Fmoc-(L)-Asp-OBn (**MA44**), Fmoc-(L)-Val-OH, Fmoc-(L)-Ala-OH, Fmoc-(L)-Leu-OH and modified Boc-(D)-PhU-OH (**MA255**). After the cleavage from the resin the crude peptide was used without further purifications (130 mg, 40% based on the estimated loading of the resin). ESI-MS t_r = 5.2 min, m/z calcd. for $[C_{42}H_{56}N_7O_9]^+$: 802.4, found: 802.4 $[M+H]^+$. Then, cyclization and purification of the resulting crude residue by semipreparative RP-HPLC (Eluent

H_2O/ACN from 50:50 to 100% ACN for 13 min with a flow rate of 10 mL/min) gave **MA262** (17 mg, 15%) as a white solid. ESI-MS $t_r = 8.7$ min, m/z calcd. for $[C_{42}H_{54}N_7O_8]^+$: 784.4, found: 784.2 $[M+H]^+$. Finally, deprotection by catalytic hydrogenation provided the pure cyclic pentapeptide **MA264** (10 mg, 66%) as a white solid. ^{1}H-NMR (400 MHz, DMSO-d_6) δ 9.09 (s, 1H, NHb), 8.36 (br s, 1H, PhU-NH), 8.12 (d, $J = 6.8$ Hz, 1H, Leu-NH), 8.00 (s, 1H, NHa), 7.93 – 7.88 (m, 2H, Val-NH + isoAsp-NH), 7.80 (d, $J = 8.0$ Hz, 1H, ArH$_6$), 7.76 (br d, 1H, Ala-NH), 7.35 (d, $J = 7.6$ Hz, 2H, ArH$_{2'6'}$), 7.18 – 7.09 (m, 2H, ArH$_{3,5}$), 7.06 (d, $J = 7.6$ Hz, 2H, ArH$_{3'5'}$), 6.93 (dd, $J = 7.2, 6.8$ Hz, 1H, ArH$_4$), 4.41 – 4.30 (m, 2H, PhU-CH^α + isoAsp-CH^α), 4.16 (dd, $J = 7.2, 6.8$ Hz, 1H, Ala-CH^α), 4.00 – 3.92 (m, 1H, Leu-CH^α), 3.71 (dd, $J = 8.0, 6.4$ Hz, 1H, Val-CH^α), 2.78 (d, $J = 7.2$ Hz, 2H, PhU-CH$_2^β$), 2.62 – 2.52 (m, 2H, isoAsp-CH$_2^β$ partially overlapped with solvent signal), 2.33 – 2.24 (m, 1H, Val-CH^β), 2.23 (s, 3H, ArCH$_3$), 1.39 – 1.31 (m, 2H, Leu-CH$_2^β$), 1.25 (d, $J = 6.8$ Hz, 3H, Ala-CH$_3$), 1.12 – 1.03 (m, 1H, Leu-CH^γ), 0.85 (d, $J = 6.4$ Hz, 3H, Val-CH$_3$), 0.80 (d, $J = 6.4$ Hz, 3H, Val-CH$_3$), 0.76 (d, $J = 6.4$ Hz, 3H, Leu-CH$_3$), 0.68 (d, $J = 6.0$ Hz, 3H, Leu-CH$_3$). ^{13}C-NMR (101 MHz, DMSO-d_6) δ 172.6, 171.7, 171.5, 171.1, 169.9, 169.8, 152.7, 138.4, 137.5, 130.2, 130.1, 129.5, 127.6, 126.1, 122.6, 121.1, 117.6, 66.4, 59.9, 54.9, 52.0, 50.1, 36.7, 28.9, 23.7, 23.1, 21.1, 19.2, 18.6, 17.9, 17.7. ESI-MS m/z calcd. for $[C_{35}H_{48}N_7O_8]^+$: 694.3, found: 694.4 $[M+H]^+$. $t_r = 6.4$ min, 97% purity (λ = 254 nm).

Synthesis of c[(S)-PhU-Leu-Ala-Val-(S)-isoAsp] (MA265, Scheme 9)**

The linear peptide **MA251** was assembled on Wang resin (300 mg, 0.36 mmol) following the general procedure described above. The amino acid sequence was elongated in the following order Fmoc-(L)-Asp-OBn (**MA44**), Fmoc-(L)-Val-OH, Fmoc-(L)-Ala-OH, Fmoc-(L)-Leu-OH and modified Boc-(L)-PhU-OH (**MA254**). After the cleavage from the resin the crude peptide was used without further purifications (150 mg, 46% based on the estimated loading of the resin). ESI-MS $t_r = 4.6$ min, m/z calcd. for $[C_{42}H_{56}N_7O_9]^+$: 802.4, found: 802.6 $[M+H]^+$. Cyclization and purification of the resulting crude residue by semipreparative RP-HPLC

(Eluent H_2O/ACN from 50:50 to 100% ACN for 13 min with a flow rate of 10 mL/min) afforded **MA259** (48 mg, 37%) as a white solid. ESI-MS t_r = 9.2 min, *m/z* calcd. for $[C_{42}H_{54}N_7O_8]^+$: 784.4, found: 784.4 $[M+H]^+$. Final deprotection by catalytic hydrogenation provided the pure cyclic pentapeptide **MA265** (30 mg, 71%) as a white solid. ^{1}H-NMR (400 MHz, DMSO-d_6) δ 10.56 (br d, 1H, Leu-NH), 9.18 (s, 1H, NHb), 9.06 (br d, 1H, PhU-NH), 8.58 (br d, 1H, Ala-NH), 8.05 (s, 1H, NHa), 7.80 (d, *J* = 7.6 Hz, 1H, ArH$_6$), 7.51 (d, *J* = 9.6 Hz, 1H, Val-NH), 7.40 (d, *J* = 8.4 Hz, 2H, ArH$_{2'6'}$), 7.18 – 7.09 (m, 2H, ArH$_{3,5}$), 7.05 (d, *J* = 8.0 Hz, 2H, ArH$_{3'5'}$), 6.93 (dd, *J* = 7.6, 7.2, Hz, 1H, ArH$_4$), 6.86 (d, *J* = 6.0 Hz, 1H, isoAsp-NH), 4.40 (d, *J* = 8.8 Hz, 1H, Val-CH^α), 4.26 (dd, *J* = 7.2, 6.4 Hz, 1H, Ala-CH^α), 4.12 – 4.05 (m, 1H, isoAsp-CH^α), 4.04 – 3.92 (m, 2H, PhU-CH^α + Leu-CH^α), 2.94 – 2.80 (m, 2H, PhU-CH^β + isoAsp-CH^β), 2.69 – 2.56 (m, 2H, PhU-CH^β + isoAsp-CH^β), 2.56 – 2.49 (m, 1H, Val-CH^β overlapped with solvent signal), 2.24 (s, 3H, ArCH$_3$), 1.87 – 1.76 (m, 1H, Leu-CH^β), 1.40 (d, *J* = 7.6 Hz, 3H, Ala-CH$_3$), 1.15 – 1.01 (m, 4H, Leu-CH^β + Val-CH$_3$), 0.92 – 0.79 (m, 4H, Val-CH$_3$ + Leu-CH^γ), 0.73 (s, 3H, Leu-CH$_3$), 0.57 (s, 3H, Leu-CH$_3$). ^{13}C-NMR (101 MHz, DMSO-d_6) δ 176.5, 175.9, 172.2, 171.7, 171.6, 168.6, 152.7, 138.7, 137.5, 130.1, 129.3, 127.6, 126.1, 122.6, 121.1, 117.7, 56.4, 55.9, 51.8, 51.0, 50.3, 36.2, 35.8, 30.8, 28.1, 23.9, 20.0, 19.5, 18.0, 17.1, 16.6. ESI-MS *m/z* calcd. for $[C_{35}H_{48}N_7O_8]^+$: 694.3, found: 694.4 $[M+H]^+$. t_r = 7.2 min, 95% purity (λ = 254 nm).

6. PEPTIDOMIMETICS COATING OF NANOSTRUCTURED MATERIALS FOR A RAPID DETECTION OF $\alpha_4\beta_1$ INTEGRIN EXPRESSING CELLS

Part of the work described in this Chapter was published in the following article:

- De Marco R., Greco A, Calonghi N., Dattoli S. D., Baiula M., Spampinato S., Picchetti P., De Cola L., Anselmi M., Cipriani F. and Gentilucci L.* Selective detection of $\alpha_4\beta_1$ integrin (VLA-4)-expressing cells using peptide-functionalized nanostructured materials mimicking endothelial surfaces adjacent to inflammatory sites. *Biopolymers* **2018**; 110:e23081. DOI: 10.1002/bip.23081.

6.1. Introduction

As previously discussed, integrin $\alpha_4\beta_1$ is a cell-surface adhesion receptor mainly expressed on mononuclear lymphocytes (*i.e.,* eosinophils, monocytes, basophils, and T cells) that plays a key role in lymphocyte adhesion and migration across the blood-endothelial barrier during the inflammatory responses.[225] Normally, circulating leukocytes conduct the immune surveillance by "tether and rolling" mechanism involving reversible interaction, mediated by selectine and integrins, on the endothelial surface.[107] During an inflammatory reaction, the local release of pro-inflammatory cytokines and chemokines, stimulate the overexpression of VCAM-1/ICAM-1 in the immediate proximity of the vascular endothelium. Activation of the lymphocytes by chemoattractants[119] promotes a conformational change in the integrin receptors to a higher affinity state,[226] and triggers their clustering along the contact surface that rapidly strengths integrin-ligand interaction (multi-valency binding), leading to strong adhesion, and therefore, to cell arrest.[38] Once arrested, the immune cells can penetrate into the underlying tissue (extravasation/diapedesis). Persistent accumulation of immune cells in various body districts represent a clear hallmark of ongoing (acute) or chronic inflammatory responses mediated by $\alpha_4\beta_1$ integrin extravasation, and their identification represent a great challenge for the early diagnosis of autoimmune diseases such as asthma, rheumatoid arthritis, Crohn's disease, ulcerative colitis, and multiple sclerosis.[105]

Besides the identification of the clinical symptoms, frequently a combination of biochemical tests, and eventually invasive procedure are necessary to diagnose certain pathologies. Specifically, the lack of a positive countercheck towards specific biomarkers makes difficult the early diagnosis of inflammatory disorders.[227] Under these premises, a new reliable test that could be rapidly performed by using accessible body fluids (blood or urine), appears as a

promising chance to monitoring the inflammation in a non-invasive way. In this perspective, our efforts were devoted to the development of a practical test for monitoring ongoing inflammatory activity and/or treatment outcomes, by the identification and quantification of the leucocytes expressing the active $\alpha_4\beta_1$ integrins. Detection of leukocytes by integrin-based recognition, have been widely exploited for diagnostic applications.[228] Indeed, activated integrin epitopes have been directly or indirectly detected with different methods, including monoclonal antibodies,[229] soluble recombinant ECM ligands (*i.e.,* VCAM-1) [230] or a fluorescent peptide ligand, analysed by flow cytometry.[231]

In this context, given the high selectivity and specificity of peptide ligands toward the integrin receptors, we focused on the development of peptide-functionalized nanostructured devices (bioactive surface) capable to reproduce the high multi-valency integrin-mediated adhesiveness, normally present on the endothelial surfaces in the proximity of the sites of inflammation, in order to perform a rapid detection and quantification of the leucocytes. To date, nanostructured surfaces have proven to be optimal substrates for cell adhesion, therefore they represent useful tools for many biomedical and biotechnological purposes (biomaterials, implantable sensors, microdevices, cell culturing, and tissue engineering).[232] For instance, the Arg-Gly-Asp (RGD) sequence is widely exploited in the regenerative medicine field to favour the $\alpha_v\beta_3/\alpha_5\beta_1$ integrin-mediated cell adhesion and growth onto biomaterial surfaces.[233] Nowadays, bioactive surfaces composed by self-assembled monolayers (SAMs) of functionalized nanoparticles [234] have attracted special attention, mainly for their advantageous features such as small scale, unique physical properties, and multiple surfaces functionalization.[235]

In this framework, Zeolite nanoparticles have been extensively exploited thanks to their modulable shape, from long cylinders up to very flat disks.[236, 237] For instance, disk-shaped Zeolite-L crystals [238] displays a large surface area allowing a high-density superficial functionalization hence, an easy anchorage on a flat surface by covalent bonds. This generates monolayers with cavities oriented along one dimension and perpendicular to the substrate.[236, 239]

For diagnostic purposes, fluorophores with proper size can be located inside the channels.[240] Besides, the regular distance between the adjacent channels enables a spatial control of the external functionalities. RGD-functionalized SAMs have been successfully employed as peptide bioactive surface models to study cell-adhesion activity.[241, 242] Very

recently, we designed RGD-functionalized SAMs of Zeolite-L crystals, which proved to be effective for the rapid detection of cancer cells, therefore potentially useful for trapping and studying tumor cells circulating in the bloodstream.[199]

Based on these premises, we reported the design of new SAMs of Zeolite-L crystals coated with peptidomimetics (**1-3**), derived from the native ligand sequences of the $\alpha_4\beta_1$ integrin,[140] and novel hybrid α/β-peptides (**5-7**) with a suited linker, derived from peptidomimetic approaches (unpublished results).[128, 154, 156] We analysed the ability of these immobilized-peptides to capture in a significant way after very rapid incubation time, the $\alpha_4\beta_1$ integrin-expressing Jurkat E6.1 cells ($\alpha_4\beta_1+$) in comparison to HEK-293 cells not expressing the $\alpha_4\beta_1$ integrin ($\alpha_4\beta_1-$) (Figure 45).
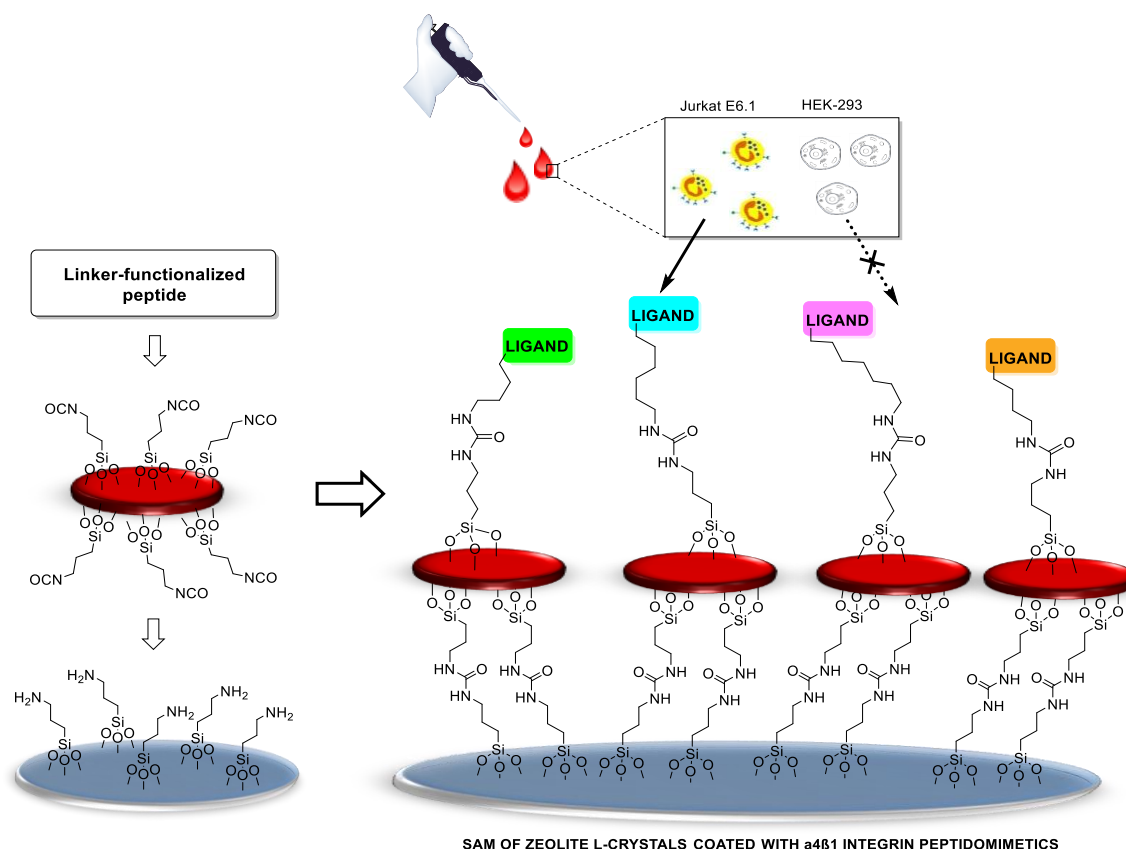

Figure 45. Design of SAMs of Zeolite-L crystals coated with peptidomimetics for rapid detection of integrin-expressing cells

6.2. Results and discussion

The general plan for the preparation of peptide-functionalized SAMs envisaged the functionalization of Zeolite-L crystals with isocyanate on their full surface. The isocyano group

was exploited to bind the crystals onto silica plate supports, which in turn was functionalized with amine group, via urea linkage. The resulting SAMs of immobilized nanocrystals presented on the outer exposed surface unreacted isocyano groups, useful for the reaction with peptidic integrin ligands supplied with suitable linkers extraneous to the integrin-binding sequence. The flat disk-shaped Zeolite-L crystals, 600-1000 nm wide x ~250 nm in height (Figure 46), were prepared as reported in the literature.[237] For visualization, the nanoparticles were labelled with the dye [*N,N'*-bis(2,6-dimethylphenyl)perylene-3,4,9,10-tetracarboxylic acid diimide] (DXP).[243] Subsequently, the surface of the DXP-zeolites was functionalized in toluene under sonication with 3-(triethoxysilyl)propyl isocyanate (ICPTES), useful for obtaining the monolayers, and for grafting the peptide ligands (Scheme 10).

The morphology of the nanoparticles was analysed by scanning electron microscopy (SEM) (Figure 46), and the successive reactions were confirmed by X-ray photoelectron spectrometry (XPS) analysis of the elemental composition. The latter showed a significant increase in the percentage of C(1s) and N(1s), from the pristine zeolite to the zeolites functionalized with organic molecules: from 6.1% C(1s) and 0.7% N(1s) for native zeolites, to 20.7% C (1s) and 2.0% N(1s) for DXP-zeolites, to 33.0% C(1s) and 5.5% N(1s) for isocyano-DXP-zeolites (see Appendix).
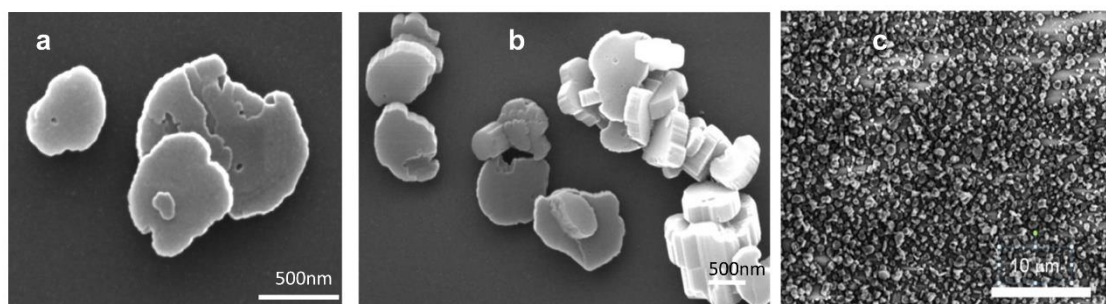
Figure 46. SEM images: (a, b) Zeolite-L crystals; (c) isocyano-DXP-Zeolite-SAM.

Thermogravimetric analyses (TGA) confirmed the increasing amount of organic molecules in the functionalized zeolites in the analysed temperature range, from a negligible weight loss for the native zeolites, to higher percentages (contribution of water excluded) for DXP-zeolites and isocyano-DXP-zeolites, 1.7% and 5.7% weight loss, respectively (see Appendix). On the other hand, attenuated total reflectance (ATR) analysis of isocyano-DXP-zeolites was scarcely useful, as it showed very weak peaks (see Appendix). The dye-loaded zeolites were immobilized via urea linkers onto silica plates (diameter 512 mm) presenting amino groups on

the surface. These were previously introduced by treatment of the clean surface of the silica plates with aminopropyltriethoxysilane (APTES) in toluene under sonication (Scheme 10). The resulting plates were immersed into a suspension of isocyano-DXP-Zeolites in toluene and sonicated, giving the isocyano-DXP-zeolite-SAMs (Scheme 10), which were characterized by SEM (Figure 46), confocal microscopy, and XPS (see Appendix). In particular, the latter showed percentages of C(1s) and N(1s) of 30.6 and 5.1, consistent with the values obtained for the unbound nanoparticles.
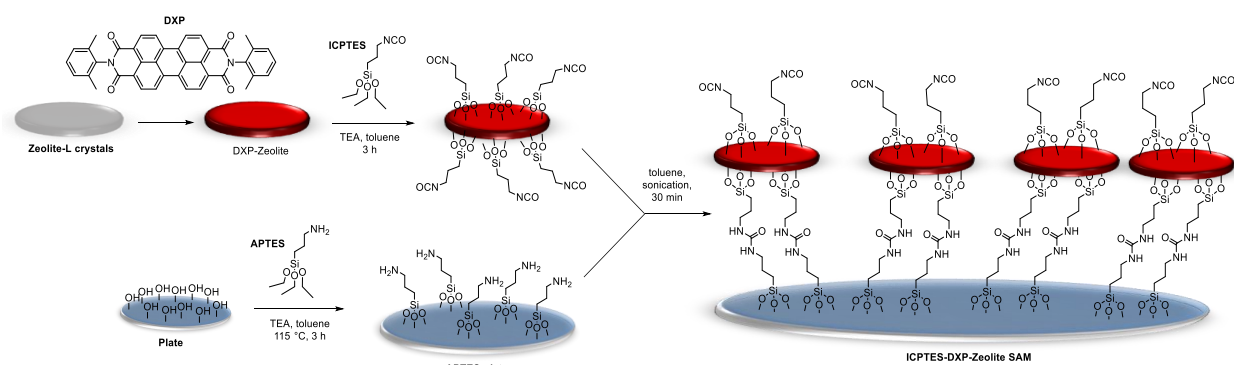
Scheme 10. Preparation of isocyano-DXP-Zeolite-SAMs onto the silica plates via urea bond.

The putative α4β1 integrin-targeting ligands **1** and **2** (Scheme 11) were designed on the basis of the minimal epitope of the natural ligand VCAM-1, namely, the sequence Gln-Ile-Asp-Ser (QIDS), that keeps a moderate micromolar affinity for α4β1 integrin. [109, 110, 112] The sequence was completed with an extra linker moiety necessary for the anchorage to the outer surface of the SAMs. Accordingly, we synthesized the QIDS peptides **1** and **2** equipped with the linker Cys or ethane-1,2-diamine, respectively. On the other hand, the peptide **3** (BIO1211, MPUPA-LDV-OH) (Scheme 11) was chosen as a reference compound to validate the proof of the concept since it is a well-known α4β1 integrin antagonist with a 6 nM IC$_{50}$ to Jurkat E6.1 cell expressing α4β1 integrin.[140] In order to perform the conjugation on the surface of the nanocrystals **3** was equipped with the same diamine linker of peptide **2** (Scheme 11),.

In the first step, putative peptides based on the natural ligand sequence were utilized. Given that these bioactive-surfaces are designed to detect biomarkers of inflammatory diseases in readily available body fluids, including blood and urine, the presence of hydrolytic enzymes in these media could leads to the hydrolysis of the enzymatically unstable "native-based" peptide

ligands, resulting in a decrease of the overall efficiency of the device over the time. Therefore, the use of peptidomimetics with enhanced enzymatic stability and high integrin affinity, may overcome this problem and increase the lifetime of the device that can be reused several times.

To this purpose in a second step, we designed DS70-derivative peptidomimetics bearing a suitable linker for their conjugation onto the surface of the nanocrystals. As mentioned in Chapter 3, these derivatives maintain the requirements for $\alpha_4\beta_1$ binding, namely MPUPA moiety spaced by a carboxylate group from 14-15 C-C bonds and a proper linker terminating with an amine group. The latter was inserted in three different positions on the "tripeptidomimetic" linear backbone (alternately on the first, second and third residue), in order to evaluate the influence of its position in integrin-mediated cells binding (**5-7,** Scheme 11).

The peptides were assembled by SPPS on a Wang resin using Fmoc-protected amino acids, under MW-assisted procedure.[169] Residues with reactive side chains were protected with acid-labile groups: Fmoc-Asp(OtBu)-OH, Fmoc-Cys(Trt)-OH, Fmoc-Ser(*t*Bu)-OH, while Gln was introduced as Ac-Gln-OH. Peptide bond formation was performed in 10 min under MW irradiation (50W, internal reaction temperature 50 °C) using HOBt and DCC as coupling agents. Fmoc deprotection was carried out twice by treatment with 20% piperidine in DMF for 3 min under MW irradiation (50W, 50 °C). For peptide **3**, the sequence H-Leu-Asp(OtBu)-Val-Wang was N-capped with MPUPA using the same reagents utilized for peptide bond formation. Cleavage of peptide **1** from the resin was performed by treatment with TFA in the presence of scavengers. Peptides **2** and **3** were conveniently cleaved from the resin via aminolysis,[244] by treatment of the peptidyl-resin with 10% *v/v* ethane-1,2-diamine in DCM for 3 h. Under these conditions, the concomitant reaction of diamine at the *t*Bu carboxylate side chain of Asp was excluded, based on the RP-HPLC ESI-MS analyses of the crude mixtures. Final removal of the *t*Bu side chain protecting group was done with TFA. The crude peptide-TFA salts were precipitated from ice-cold Et$_2$O and collected by centrifuge (Scheme 11).

Peptides **5** and **6** were assembled manually at RT by SPPS on Wang resin preloaded with Fmoc-Gly using Fmoc-protected amino acids (Scheme 11). Removal of Fmoc group was carried out twice by treatment with 20% piperidine in DMF at RT for 10 min. Coupling between each residue was done with DCC and HOBt in DCM/DMF (4:1 *v/v*) at RT for 3 h.
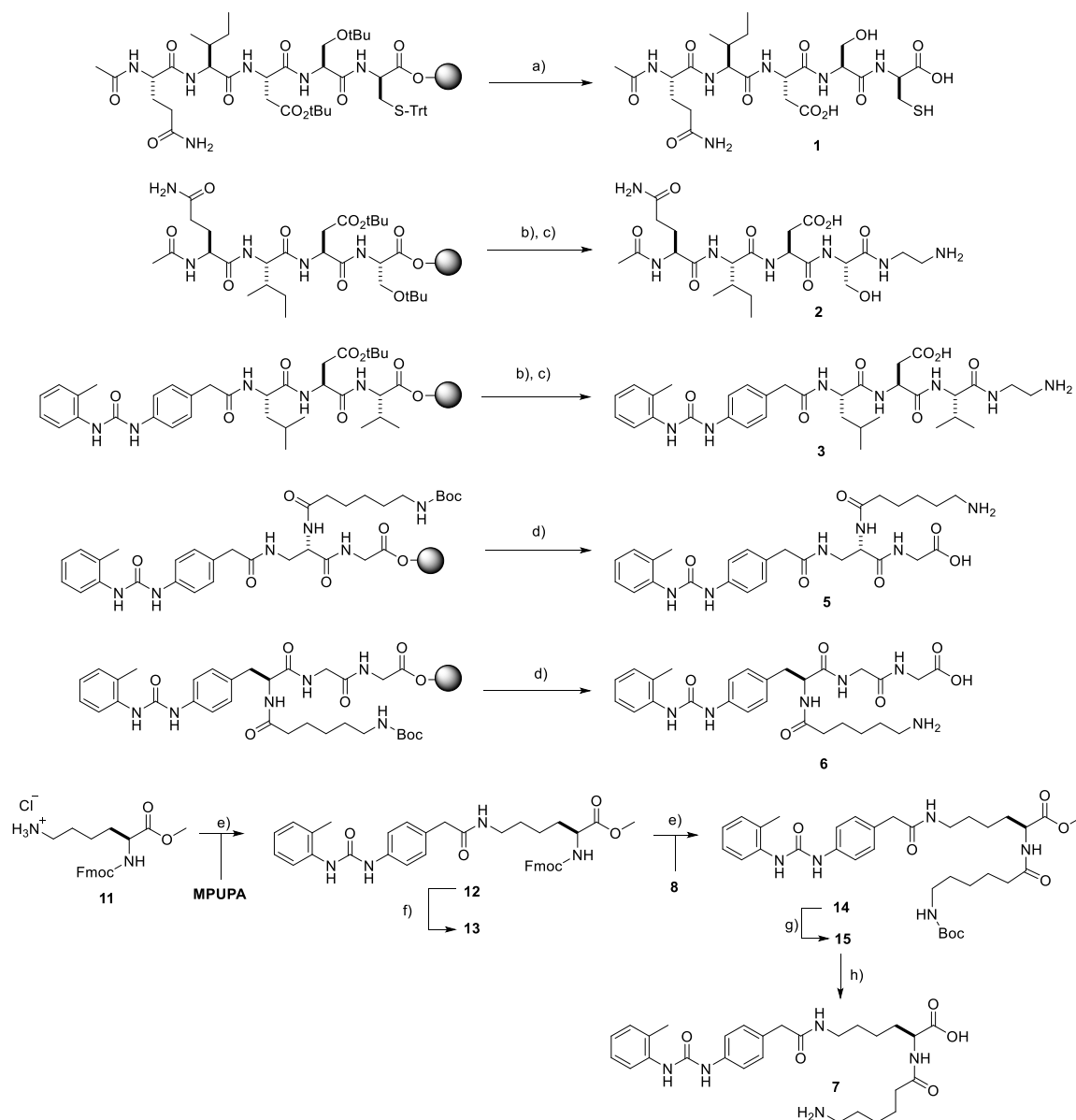
Scheme 11. SPPS of peptides and peptidomimetics. *Reagent and conditions:* a) TFA/PhOH/1,2-ethanedithiol/thiophenol (70:10:10:10, v/v), RT, 1.5 h; b) ethane-1,2-diamine in DCM (10% v/v), RT, 3 h; c) 50% TFA/DMC, RT, 1.5 h; d) TFA/TIS/H₂O (80:10:10, v/v), RT, 2.5 h; e) **MPUPA**, EDC/HOBt/TEA, RT, 12 h; same condition was repeated for *N*-Boc 6-aminocaproic acid (**8**); f) 20% piperidine/DMF, RT, 1 h; g) LiOH, THF/H₂O (2:1), 0 °C – RT, 2.5 h; h) 25% TFA/DCM, RT, 1 h.

As previously described for **MA28** and **MA30** (Chapter 4), the Hofmann rearrangement of Fmoc-(*S*)-Asn using PIFA and pyridine in a mixture of THF/DMF/H₂O generates the corresponding β-amine Alanine,[206] which was then coupled with MPUPA under the same conditions described above. Finally, Fmoc-deprotection and successive coupling with *N*-Boc 6-aminocaproic acid (**8**) completed the linear sequence **5**. Similarly, for compound **6**, the Gly

N-terminus was coupled with Fmoc-(*S*)-PhU, a PUPA-mimetic residue possessing an extra amine, that in turn it has been Fmoc-deprotected, and finally coupled with *N*-Boc 6-aminocaproic acid (**8**) in the same coupling condition. For both, the peptide cleavage and simultaneous Boc-deprotection was accomplished by treatment of the resin with TFA in the presence of scavengers. The crude products were precipitated from ice-cold Et$_2$O and collected by centrifuge (Scheme 11). Unlike, peptide **7** was easily prepared in solution starting from Fmoc-Lys(Boc)-OH, previously protected at the C-terminus with SOCl$_2$ in MeOH. Then, deprotections were alternated to coupling reactions to afford the final peptide. In details, the free $^\varepsilon$NH of Lys produced during the C-terminus protection via esterification was coupled with MPUPA in the presence of EDC/HOBt/TEA as activating agents. Thereafter, the $^\alpha$N-Fmoc deprotection with 20% of piperidine, and the last coupling with *N*-Boc 6-aminocaproic acid (**8**) was performed under the same conditions described above. Finally, saponification of the methyl ester using LiOH in a mixture of THF/H$_2$O, and Boc removal with TFA afforded the final peptide in good yield (Scheme 11). For all peptide, the purification was performed by semi-preparative RP-HPLC (for the conditions, see Materials and Methods), the purity was assessed by RP-HPLC and the chemical identity was determined by ESI-MS and ^{1}H-NMR spectroscopy.

Treatment of isocyano-DXP-zeolite-SAMs with peptides **1**-**7** in DMF in the presence of TEA gave the monolayers **1**-**7**@SAM (Scheme 12). Alternatively, functionalization with *n*-butylamine afforded **4**@SAM (Scheme 12), designed as a negative control. The peptide-monolayers were analyzed by XPS that clearly confirmed the increase of C(1s)/N(1s) compared to the non-peptide monolayer, from 30.6 and 5.1 for the isocyano-DXP-zeolite-SAMs, to 36.2-42.9 and 6.2-8.1, for **1**-**7**@SAMs, while **4**@SAM gave slightly lower values, as expected. Finally, ATR confirmed the presence of peaks compatible with the expected surface functional groups, in particular the carbonyls in the 1650-1750 cm^{-1} range (see Appendix).

As a control, flat silica plates modified with peptide **3** were also prepared. To the purpose, the silica plates were reacted with ICPTES, and the isocyano-functionalized surfaces were treated with peptide **3**, under the same conditions utilized for the preparation of **1**-**7**@SAMs. XPS analysis of the resulting **3**@plates was suggestive of a moderate functionalization, compared to the high functionalization of **3**@SAMs. Changing the experimental conditions (*e.g.* reaction temperature) for the preparation of peptide-plates did not modify the atomic percentages to a significant extent.
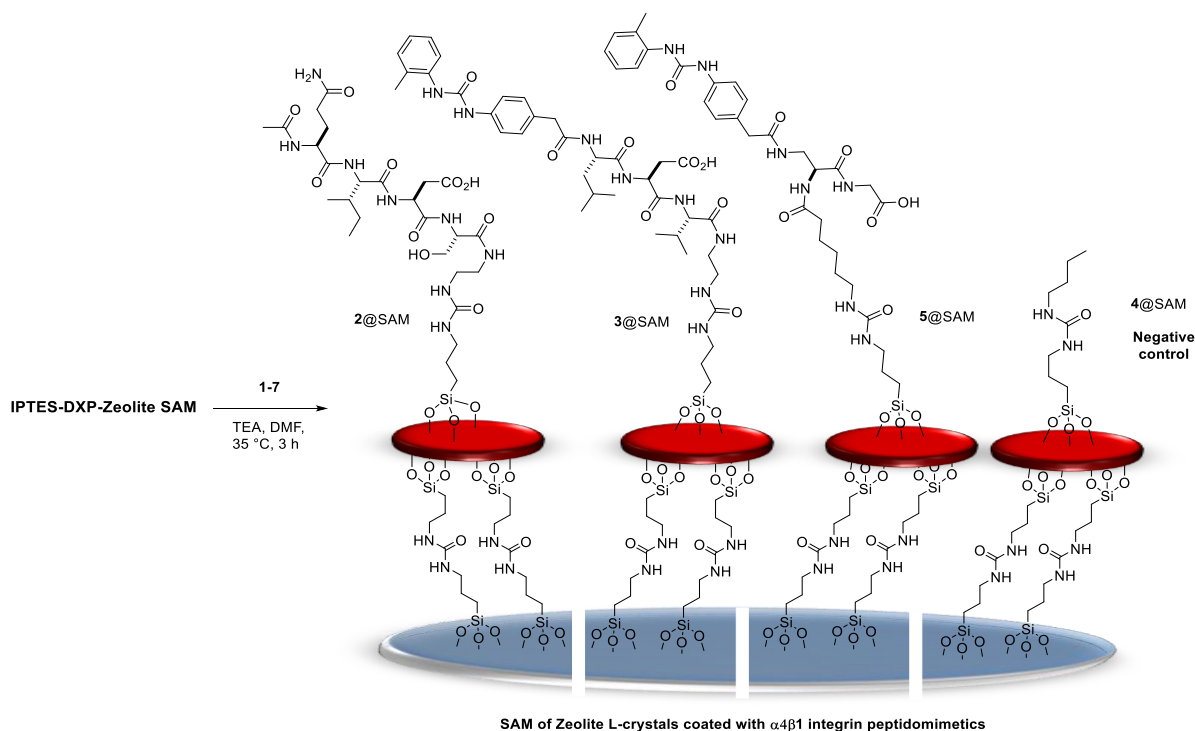
Scheme 12. Examples of peptides@SAMs of Zeolite L-cystals.

Cell adhesion experiments were performed on Jurkat E6.1 cells ($α_4β_1$+).[245] As a negative control, the experiments were repeated using HEK-293 cells not expressing $α_4β_1$ integrin ($α_4β_1$-), therefore not able to adhere onto the peptide@SAMs.[246] Specifically, $5×10^5$ Jurkat E6.1 or HEK-293 cells were stained with 5-chloromethylfluorescein diacetate (CMFDA) and seeded on the peptide@SAMs. Simple assays that may be performed rapidly and that would yield reliable information might be applicable for clinical studies.[199, 247] Since the integrin-mediated arrest of rolling cells in the bloodstream is known to be a fast process,[245] and since we were not interested in cell growth, nor in cell harvesting, the cells were incubated very shortly (15 min), then the non-adherent cells were washed away, while the attached cells were fixed with paraformaldehyde.

Confocal microscopy revealed that **1**@SAM showed moderate adhesion of both Jurkat (Figure 47 a) and control cells (Figure 47e), while both cell lines poorly bound to **2**@SAM (Figure 47 b, f). Conversely, **3**@SAM showed the highest number of adherent Jurkat cells (Figure 47 c) compared to the $α_4$ integrin not expressing HEK-293 cells (Figure 47 g), $1.4 ± 0.2 ×10^4$ vs. $1.7 ± 0.15 ×10^3$ cells/cm². Besides, confocal microscopy of the enzymatically stable

peptidomimetics **5-7** showed, in a first screening, an excellent adhesion rate of Jurkat cells only for **5**@SAM ($1.6 \pm 0.23 \times 10^4$) (Figure 47 i) respect to HEK-293 cells (Figure 47 j).
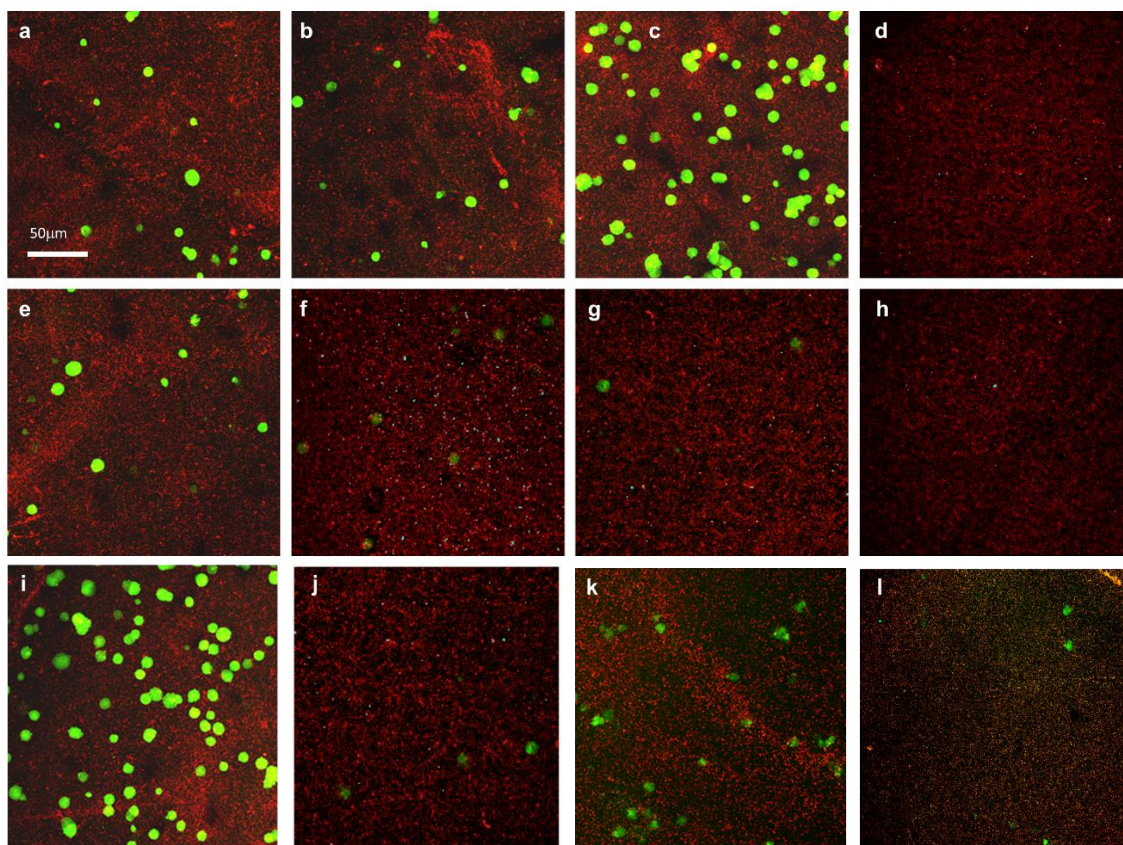

Figure 47. Confocal microscopy images of **1-7**@SAMs after 15 min incubation at 37 °C with 5 x 10^5 cells. Coated surface of DXP-zeolite nanocrystals are visualized in red while adhered cells are visualized in green; (a-d, i, k-l) cell adhesion experiments with Jurkat E6.1 cells; (e-h, j) cell adhesion experiments with HEK-293 cells; Confocal microscopy images: (a, e) **1**@SAM; (b, f) **2**@SAM; (c, g) **3**@SAM; (d, h) **4**@SAM (i, j) **5**@SAM; (k) **6**@SAM; (l) **7**@SAM. White dots correspond to red signal saturation.

Despite the surfaces of **6-7**@SAMs were not homogeneously coated with DXP-zeolite nanocrystals, as underlined by the less intensive red colour, **6**@SAM showed a moderate/poor adhesion of Jurkat cells (Figure 47 k) while **7**@SAM cannot be considered for discussion purposes since the peptide-functionalization was not optimal and the cell adhesion was not detected (Figure 47 l). For this reason, the adhesion experiment with HEK-293 was not carried out for compound **6-7**, focusing our attention only on the best **5**@SAM.

The normalized number of adherent cells, calculated as the average of 3 independent experiments for the different SAMs using the two cellular lines, is reported in Figure 48. As expected, the negative reference **4**@SAM, not presenting any integrin binding sequence,

showed negligible adhesion for both Jurkat or HEK-293 cells (Figure 47 d, h and Figure 48). In general, longer incubation times up to 12 h gave an observable but scarcely reproducible increase in the number of adherent cells.
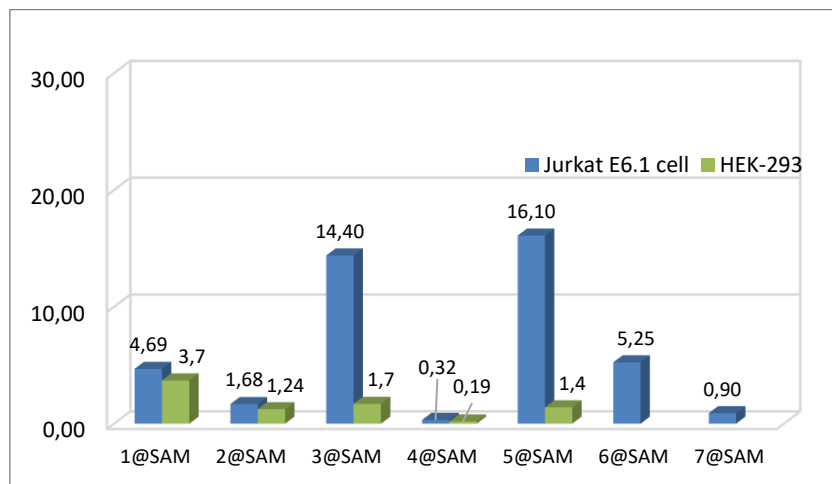
Figure 48. Number of adhered cells/cm^2 (analyzed area: 0.0025 cm^2) using the different SAMs; mean $\pm$ SE of 3 independent experiments.

3@SAM and **5@SAM** showed the highest number of adhered Jurkat cells but also an excellent selectivity toward Jurkat cells (α4β1+) rather than HEK-293 cells (α4β1-) (Figure 47 and 48). Presumably, these results are related to the higher integrin-affinity of the peptidomimetic ligands **3** and **5** given by the MPUPA unit at the N-terminus that is known to efficiently target the α4-subunit in comparison to the other peptides.[178, 181] Interestingly, the higher efficacy showed by **5@SAM** in cell adhesion can be related to the presence of the unnatural β-amino acid core (Dap) that confer higher enzymatic stability compared to the native sequences **1** and **2** that instead are probably hydrolyzed by proteases present in the body fluids.[153, 154] Therefore, the central position emerged as a suitable anchoring point for the introduction of linkers without affecting the overall ligand's ability to bind integrin receptors. This is probably due to the lower steric hindrance near the carboxylic acid, making it more accessible to the integrin approaching, during the binding process. Besides, an efficient α4β1 integrin-mediated adhesion to **3@SAM** and **5@SAM** was observed after a very rapid incubation time compared to that of the other systems that required more time (15 min *vs* > 12 h).[237, 242, 248]

Finally, to confirm if the Zeolite nanostructure fosters Jurkat adhesion compared to a flat bioactive surface deprived of the nanoparticles, compound **3** was anchored directly onto the

silica plate *via* urea linker. Therefore, **3**@plates were seeded with either Jurkat or HEK-293 cells as described above. The number of adherent cells counted at the confocal microscope was $4.0 \pm 0.2 \times 10^3$ cells/cm^2 and $3.0 \pm 0.2 \times 10^3$ cells/cm^2, for Jurkat and HEK-293 cells, respectively (see Appendix). Apparently, the monolayer of Zeolite-L crystals significantly increased the adhesive efficacy of the integrin ligand. This suggested that 3D nanostructures are possibly responsible for the enhanced cell capture yields due to higher biofunctionalization and/or the regular positioning of the biomolecules, correlated in turn to the regular distance between adjacent channels in the nanocrystals.

6.3.   Conclusion

In this study, we envisaged the opportunity to detect and quantify $\alpha_4\beta_1$ integrin-expressing cells by selective adhesion to SAMs of nanoparticles functionalized with peptide ligands. Zeolite-L crystals were readily functionalized and immobilized onto silica plates, and the resulting SAMs were biofunctionalized with peptide sequences containing the minimal integrin-binding motives QIDS (**1-2**), urea-LDV (**3**) or urea-peptidomimetics derivatives (**5-7**). To check the ability of the different ligands to selectively interact with $\alpha_4\beta_1$ integrin-expressing cells, Jurkat E6.1 and HEK-293 cells were incubated very rapidly onto different SAMs. As it turned out, SAM functionalized with sequence **3** and **5** showed high adhesion of $\alpha_4\beta_1$ integrin-expressing Jurkat cells, and excellent selectivity over HEK-293 cells, utilized as a negative reference. Peptide **5** also confirmed the fact that the insertion of appropriate linkers, fundamental to achieve the conjugation onto nanostructured materials, are well-tolerated and do not reduce the ligand binding, thus allowing the design of enzymatically stable peptides/peptidomimetics for the biofunctionalization of potential diagnostic devices. Furthermore, the slightly improved adhesion of Jurkat cells compared to **3**, it's presumably due to the presence of β-amino acid scaffold that gives high enzymatic stability. In perspective, devices based on such peptidomimetic ligands could be exploited even with body fluid samples containing hydrolytic enzymes. The enzymatic stability is reflected in an increase of the device lifetime that could be reused several times. The use of peptide-coated Zeolites instead of the simple flat glass surface peptide-coating allowed to exploit the pores of the particles, which were loaded with the fluorescent dye DXP, and hence to directly correlate the positioning of adherent cells to the underlying presence of the nanoparticles. Moreover, in Zeolite SAMs the

functional groups anchored to the NPs offered a much higher homogeneous density than the same groups just directly linked to the surfaces. In perspective, these peptide-functionalized nanostructured systems could be utilized for a rapid detection of inflammatory disease markers in patients, *i.e.* integrin $\alpha_4\beta_1$-expressed in immune cells, thus laying the basis for the development of a simple and accessible test aimed at monitoring the course of the disease and the efficacy of the therapy by using readily available biological samples.

6.4. Experimental section

General methods

The protected amino acids, DXP, and all standard chemicals were purchased from Sigma-Aldrich. Minimum Essential Media (MEM), RPMI Medium 1640, PBS solution pH = 7.2, FBS, penicillin, trypsin, were purchased from Gibco (Life Technologies). The glass plates having a diameter of 12 mm were acquired from Servoprax GmbH. Jurkat clone E6.1 was provided by the European Cell Culture Collection and cultivated as described in the provider's protocol. HEK-293 cells were obtained from ATCC, USA. SPPS was carried out on a commercially-available Wang resin, i.e. [4-(hydroxymethyl)phenoxymethyl] polystyrene cross-linked with 1% DVB, particle size 250-300 μm, ~1.7 mmol/g loading. Analytical RP HPLC apparatus: Agilent series 1100; stationary phase: octadecyl carbon chain bonded silica (C_{18}) RP (reversed-phase) column Phenomenex model Gemini 3μ 110A 100×3.0 mm (P/No 00D-4439-Y0), TMS end-capping, fully-porous organosilica solid support, particle size = 3 mm, pore size = 110 Å, length = 100 mm, internal diameter = 3 mm; mobile phase: gradient from 9:1 H_2O/CH_3CN/0.1 % TFA, to 2:8 H_2O/CH_3CN/0.1 % TFA, in 20 min, flow rate = 1.0 mL/min, then 10 min isocratic; diode array detector (DAD) λ = 210 nm. Semi-preparative RP HPLC apparatus: Agilent series 1100; stationary phase: C_{18} RP column ZORBAX mod. Eclipse XDBC18 PrepHT cartridge 21.2×150 mm 7μ (P/No 977150-102), double-end capping, particle size = 7 μm, pore size = 80 Å, length = 150 mm, internal diameter = 21.2 mm; mobile phase: gradient from 8:2 H_2O/CH_3CN/0.1 % TFA, to CH_3CN/0.1 % TFA, in 10 min, flow rate = 12 mL/min; DAD, λ = 210 nm. Electron Spray Ionization-Mass Spectroscopy (ESI-MS) apparatus: MS single quadrupole HP 1100 MSD detector; drying gas flow = 12.5 L/min, nebulizer pressure = 30 psgi, drying gas temp. = 350°C, capillary voltage = 4500 (+) and 4000 (-), scan range 50-2600 amu. Microwave (MW) oven apparatus: Micro-SYNTH Microwave Labstation for

Synthesis; temperature control: automatic built-in ATC-FO advanced fiber optic. NMR apparatus: Varian Gemini 400 MHz; ^{1}H NMR sample preparation: 0.01 M peptide in 5 mm tubes at r.t.; solvent suppression: solvent presaturation procedure PRESAT by Varian. Chemical shifts are reported as δ values, and DMSO was used as an internal standard: for ^{1}H-NMR, δ = 2.50 ppm; for ^{13}C-NMR, δ = 39.52 ppm. XPS analysis apparatus: Thermo Scientific K-Alpha™ + X-ray Photoelectron Spectrometer System; 15 keV/72 W monochromatic Al K alpha X-rays, 200 μm spot diameter, pass energy = 200 eV for survey spectra, and = 50 eV for core level spectra; sample preparation: drop-casting of a 0.1 mg/mL ethanolic dispersion of the particles onto a Emitech K575X peltier cooled Au-pre-coated glass coverslip, for 3 min at 60 mA, without further treatment. Thermogravimetric analysis apparatus: Mettler Toledo TGA 1 STAR System; sample preparation: 0.1 - 2 mg of samples were kept under 50 mL/min nitrogen flow at temp. = 50°C for 30 min for stabilization, then heated at a speed = 10°C/min from 50 to 750°C, and held at this temperature for further 30 min before cooling. SEM apparatus: FEI (Hillsboro, Oregon, USA) Quanta FEG 250; operating distance = 10 mm, acceleration voltage = 5 kV; sample preparation: drop-casting a ethanolic dispersion of the particles onto a glass cover slip, subsequently sputter coated with Emitech K575X peltier cooled Au for 60 s at 60 mA prior to fixation on an Al support, without further manipulation. Powder X-ray diffraction (PXRD) apparatus: Bruker D2 PHASER diffractometer; Cu Kα-radiation 1.54184 A, Ni Kβ-filter = 300 W, 30 kV, 10 mA, power with a LYNXEYE scintillation detector; sample preparation: samples were mounted on a zero background silicon sample holder; the measurement was performed from a 2θ value range 5 to 45° with exposure time = 1.5 second per step; all measurements were performed at room pressure and r.t. Confocal microscope apparatus: Nikon C1s confocal laser-scanning microscope, equipped with a Nikon PlanApo 60X, 1.4-NA oil immersion lens; images were quantified by ImageJ software.

Synthesis and characterization

Peptide synthesis

General procedure for coupling

Prior to use, the Wang resin (0.5 g, ~1.7 mmol/g loading) was swollen in DMF (3 mL) for 10 min into a reactor equipped with a frit. A mixture of Fmoc-protected amino acid (1.5 mmol) and HOBt (1.5 mmol) dissolved in 4:1 DCM/DMF (4 mL) was poured into the reactor containing the swollen resin, followed by the coupling reagent DCC (1.5 mmol). Attachment

of the first C-terminal amino acid residue (i.e. Cys, Ser, Val, for **1**, **2**, **3**, respectively), required also the addition of a catalytic amount of DMAP. Then the mixture was heated for 10 min under MW irradiation while gently bubbling N_2, with an initial irradiation power of 50W, monitoring the internal reaction temperature at 50°C. After the first C-terminal amino acid, the unreacted 4-(hydroxymethyl)phenoxymethyl resin linkers were capped with Ac_2O (30 mmol) and pyridine (30 mmol). The resin was washed 3 times in sequence with DMF (5 mL), MeOH (5 mL), and DCM (5 mL). For all peptides, Asp was introduced as Fmoc-Asp(O*t*Bu)-OH; for **1**, Cys was introduced as Fmoc-Cys(Trt)-OH; for **2** and **3**, Ser was introduced as Fmoc-Ser(*t*Bu)-OH, while Gln was introduced as Ac-Gln-OH; the other residues were introduced without side chains protection. Coupling efficacy was assessed by the Kaiser test. For the synthesis of peptide **3**, the sequence H-Leu-Asp(O*t*Bu)-Val-Wang was *N*-capped with MPUPA with the same reagents utilized for peptide bond formation.

General procedure of Fmoc-deprotection

Fmoc-peptidyl-resin was treated with 20% piperidine/DMF (6 mL) for 3 min under MW irradiation (50W, 50°C); this procedure was repeated twice. After that, the resin was washed 3 times in sequence with DMF (5 mL), MeOH (5 mL), and DCM (5 mL).

Peptide cleavage

To obtain peptide **1**, the peptidyl resin was treated with a 7:1:1:1 mixture of TFA, PhOH, 1,2-ethanedithiol, thiophenol (15 mL) for 90 min at r.t. Then the mixture was filtered, and the resin was washed with 10% TFA in Et_2O (10 mL), with DCM (10 mL), and finally with MeOH (10 mL). The filtrates were collected and concentrated at reduced pressure. For **2** and **3**, the peptidyl-resin was suspended in a 10% *v/v* solution of ethane-1,2-diamine in DCM (10 mL). After 3 h the mixture was filtered and the resin was washed with 10% TFA in Et_2O (10 mL), with DCM (10 mL), and finally with MeOH (10 mL). The filtrates were collected and concentrated at reduced pressure. The residue was suspended in 30% TFA in DCM (6 mL), the mixture was stirred for 30 min at r.t., after that the mixture was concentrated at reduced pressure. The treatment with TFA was repeated for additional 1h, and the mixture was concentrated at reduced pressure. The crude peptide-TFA salts were precipitated from ice-cold Et_2O (40 mL) and collected by centrifuge.

Peptide **5** was synthesized on Wang resin preloaded with Fmoc-Gly (0.25 g, 0.15 mmol, loading capacity 0.4 – 0.8 mmol/g) at room temperature into a reactor equipped with a frit. Prior to use,

the resin was swollen in DMF for 30 min. Fmoc cleavage was carried out using 20% piperidine/DMF, under gentle stirring at RT for 10 min. After washing step with DMF and DCM, the deprotection was repeated once again. The resin was then washed with DMF (3 x 5 mL) and DCM (3 x 5 mL). Next, coupling reaction was performed by adding to the resin a solution of the Fmoc-(L)-Asn (130 mg, 0.37 mmol, 2.5 eq), DCC (80 mg, 0.37 mmol, 2.5 eq) and HOBt (50 mg, 0.37 mmol, 2.5 eq) in DMF (4 mL) prepared in a separate vial, and the mixture was shaken for 3 h. The Hofmann rearrangement was then performed on-resin. The resin was washed twice with a mixture of THF/DMF/H_2O (2:2:1 $v/v/v$) and subsequently swollen with the same mixture for 30 min. After that, a solution of PIFA (159 mg, 0.37 mmol, 2.5 eq) in THF/DMF/H_2O (2:2:1) was added to the resin followed by pyridine (30 µL, 0.37 mmol, 2.5 eq), and the mixture was shaken for 3 h. Then, the resin was washed with DMF (3 x 5 mL), DMF/DIPEA (9:1), and DMF again (3 x 5 mL). Each transformation, including coupling reactions, Fmoc removals and Hofmann rearrangement were monitored by Kaiser test. The peptide sequence was elongated with MPUPA and N-Boc 6-aminocaproic acid (**8**) using the same coupling conditions. Cleavage from the resin and simultaneous Boc removal was carried out using a mixture of TFA/TIPS/H_2O (80:10:10 $v/v/v$) for 2.5 h. The cleavage mixture was filtered in a centrifuge tube and the resin washed with Et_2O containing small portions of TFA and DCM. The collected mixture was concentrated and Et_2O was added to precipitate the crude peptide which was recovered as TFA salt by centrifuge (34 mg, 42% based on the estimated loading of the resin).

Similarly, peptide **6** was assembled on Wang resin preloaded with Fmoc-Gly (0.25 g, 0.15 mmol, loading capacity 0.4 – 0.8 mmol/g) at room temperature. Swelling, Fmoc cleavage and washing procedures were performed as described above for compound **5**. The coupling reactions were carried out by adding to the resin a solution of the Fmoc-amino acid (0.37 mmol, 2.5 eq), DCC (0.37 mmol, 2.5 eq) and HOBt (0.37 mmol, 2.5 eq) in DMF (4 mL) and shaking the mixture for 3 h. The amino acid sequence was Fmoc-Gly-OH, Fmoc-(S)-PhU-OH (**10**) and N-Boc 6-aminocaproic acid (**8**). Coupling reactions and Fmoc removals were monitored by Kaiser test. Once the linear peptide was assembled, the cleavage from the resin and simultaneous Boc removal was carried out using a mixture of TFA/TIPS/H_2O (80:10:10 $v/v/v$) for 2.5 h. The cleavage mixture was collected in a centrifuge tube and the resin washed with Et_2O containing small portions of TFA and DCM. The mixture was concentrated, and the final

peptide was precipitated by adding cold Et$_2$O, recovered as TFA-salt by centrifuge (18 mg, 22% based on the estimated loading of the resin).

All peptides were purified by semi-preparative RP-HPLC (for the conditions, see Materials and Methods). The purity was determined by analytical RP HPLC, and their identity was assessed by ESI-MS and NMR spectroscopy.

(**1**) ^{1}H-NMR (400 MHz, DMSO-d_6) δ: 8.37 (d, J = 7.2 Hz, 1H), 8.33 (d, J = 8.0 Hz, 1H), 8.06 (d, J = 7.6 Hz, 1H), 7.83-7.78 (m, 2H), 7.23 (s, 1H), 6.79 (s, 1H), 4.77 (m, 1H), 4.37-4.22 (m, 2H), 4.20-4.10 (m, 2H), 3.60-3.50 (m, 4H), 2.82 (m, 1H), 2.67-2.58 (m, 2H), 2.49-2.38 (m, 2H), 2.17-2.02 (m, 2H), 1.83 (s, 3H), 1.78-1.64 (m, 2H), 1.39 (m, 1H), 1.00 (m, 1H), 0.82-0.76 (m, 6H).ESI-MS m/z calcd. for [C$_{23}$H$_{39}$N$_6$O$_{11}$S]$^+$: 607.2, found: 607.4 [M+H]$^+$. t_r = 1.9 min, 97% purity (λ = 210 nm).

(**2**) ^{1}H-NMR (400 MHz, DMSO-d_6) δ: 8.28 (d, J = 6.4 Hz, 1H), 8.06 (d, J = 8.4 Hz, 1H), 7.96 (br.d, 1H), 7.79 (d, J = 7.2 Hz, 1H), 7.72 (d, J = 6.0 Hz, 1H), 7.23 (s, 1H), 6.80 (s, 1H), 4.58 (m, 1H), 4.24 (m, 1H), 4.19-4.10 (m, 2H), 3.58 (m, 1H), 3.36-3.28 (m, 2H), 2.90-2.80 (m, 3H), 2.70 (m, 1H), 2.63-2.56 (m, 2H), 2.18-2.01 (m, 2H), 1.82 (s, 3H), 1.78-1.61 (m, 3H), 1.23-1.18 (m, 2H), 0.89-0.77 (m, 6H). ESI-MS m/z calcd. for [C$_{22}$H$_{40}$N$_7$O$_9$]$^+$: 546.3, found: 546.4 [M+H]$^+$. t_r = 1.8 min, 94% purity (λ = 210 nm).

(**3**) ^{1}H-NMR (400 MHz, DMSO-d_6) δ: 9.15 (s, 1H, NH$_{urea}$), 8.41 (d, J = 7.6 Hz, 1H, AspNH), 8.21 (d, J = 8.0 Hz, 1H, LeuNH), 8.10 (m, 2H, NH$_{urea}$+NH$_{diam}$), 7.79 (d, J = 8.4 Hz, 1H, ArH), 7.49 (d, J = 8.6 Hz, 1H, ValNH), 7.37 (d, J = 8.4 Hz, 2H, ArH), 7.17-7.10 (m, 4H, ArH), 6.93 (dd, J = 7.2, 7.6 Hz, 1H, ArH), 4.56 (ddd, J = 6.0, 7.6, 8.0 Hz, 1H, AspHα), 4.29 (m, 1H, LeuHα), 4.07 (dd, J = 6.4, 8.6, Hz, 1H, ValHα), 3.45 (d, J = 14.2 Hz, 1H, CH$_{2urea}$), 3.39 (d, J = 14.2 Hz, 1H, CH$_{2urea}$), 3.31-3.27 (m, 2H, CH$_{2diam}$), 2.86-2.81 (m, 2H, CH$_{2diam}$), 2.74 (dd, J = 6.0, 14.8 Hz, 1H, AspHβ), 2.51 (dd, J = 8.0, 14.8 Hz, 1H, AspHβ), 2.23 (s, 3H, ArCH$_3$), 1.98 (m, 1H, ValHβ), 1.57 (m, 1H LeuHγ), 1.44-1.40 (m, 2H, LeuHβ), 0.85 (d, J = 6.4 Hz, 3H, LeuCH$_3$), 0.84-0.75 (m, 9H, ValCH$_3$+LeuCH$_3$+ValCH$_3$). ^{13}C-NMR (100 MHz, DMSO-d_6) δ: 173.47, 172.92, 172.11, 171.38, 171.35, 153.69, 139.22, 138.41, 131.06, 130.39, 130.21, 128.64, 126.98, 123.54, 122.16, 119.73, 118.81, 116.74, 58.58, 55.81, 51.97, 50.49, 42.29, 42.06, 39.24, 37.35, 36.69, 31.68, 31.17, 25.07, 23.88, 22.48, 20.06, 18.75, 18.51. ESI-MS m/z calcd. for [C$_{33}$H$_{48}$N$_7$O$_7$]$^+$: 654.4, found: 654.4 [M+H]$^+$. t_r = 2.0 min, 96% purity (λ = 210 nm).

(**5**) ^{1}H-NMR (400 MHz, DMSO-d_6) δ 8.97 (s, 1H, NHb), 8.19 (dd, J = 6.4, 5.2 Hz, 1H, Gly-NH), 7.97 – 7.91 (m, 2H, Dap-NH$_\alpha$ + Dap-NH$_\beta$), 7.89 (s, 1H, NHa), 7.81 (d, J = 8.0 Hz, 1H, ArH$_6$), 7.36 (d, J = 8.0 Hz, 2H, ArH$_{2'6'}$), 7.19 – 7.10 (m, 4H, ArH$_{3,5}$ + ArH$_{3'5'}$), 6.93 (dd, J = 7.6, 7.2 Hz, 1H, ArH$_4$), 4.37 (dd, J = 13.6, 8.0 Hz, 1H, Dap-CH$^\alpha$), 3.75 – 3.68 (m, 2H, Gly-CH$_2{}^\alpha$), 3.41 – 3.33 (m, 3H, PhCH$_2$ + Dap-CH$^\beta$ overlapped with solvent signal), 3.31 – 3.20 (m, 1H, Dap-CH$^\beta$), 2.70 – 2.59 (m, 2H), 2.23 (s, 3H, ArCH$_3$), 2.05 – 1.89 (m, 2H), 1.58 – 1.47 (m, 2H), 1.40 – 1.25 (m, 4H). ESI-MS m/z calcd. for [C$_{27}$H$_{37}$N$_6$O$_6$]$^+$: 541.3, found: 541.2 [M+H]$^+$. t_r = 1.7 min, 91% purity (λ = 254 nm).

(**6**) ^{1}H-NMR (400 MHz, DMSO-d_6) δ 8.90 (s, 1H, NHb), 8.32 (br. d, 1H, PhU-NH), 8.15 (br. d, 1H, Gly-NH), 7.97 – 7.91 (m, 1H, Gly-NH), 7.89 (s, 1H, NHa), 7.81 (d, J = 8.0 Hz, 1H, ArH$_6$), 7.36 (d, J = 8.0 Hz, 2H, ArH$_{2'6'}$), 7.19 – 7.10 (m, 4H, ArH$_{3,5}$ + ArH$_{3'5'}$), 6.93 (dd, J = 7.6, 7.2 Hz, 1H, ArH$_4$), 4.41 (m, 1H, PhU-CH$^\alpha$), 3.99 – 3.68 (m, 4H, Gly-CH$_2{}^\alpha$), 3.21 – 3.03 (m, 1H, PhCH), 2.85 – 2.63 (m, 3H, PhCH + -CH$_2$NH$_2$), 2.22 (s, 3H, ArCH$_3$), 2.05 – 1.89 (m, 2H), 1.52 – 1.43 (m, 2H), 1.38 – 1.10 (m, 4H). ESI-MS m/z calcd. for [C$_{27}$H$_{37}$N$_6$O$_6$]$^+$: 541.3, found: 541.2 [M+H]$^+$. t_r = 1.9 min, 96% purity (λ = 254 nm).

A. *General procedure of EDC/HOBt-mediated amide coupling reaction*

A stirred solution of *N*-protected amino acid (1.0 eq) in 4:1 DCM/DMF mixture (0.2 M) was treated with HOBt (1.3 eq), EDC HCl (1.3 eq) and TEA (2.6 or 3.0 eq) at RT under N$_2$ atmosphere. After 15 min, *C*-protected amino acid (1.0 eq) was added, and the mixture was stirred at RT under N$_2$ overnight. Then, the mixture was concentrated at reduced pressure, and the residue was diluted with EtOAc (30 mL). The solution was washed with 0.1 M HCl solution (5 mL), and a saturated solution of NaHCO$_3$ (5 mL). The organic layer was dried over Na$_2$SO$_4$, filtered and evaporated to dryness under reduced pressure. The crude material was purified by filtration or eventually by flash chromatography over silica gel (eluent Cy/EtOAc).

B. *General procedure of N-Fmoc deprotection*

The *N*-Fmoc-protected compound (1.0 eq) was dissolved in 20% Piperidine/DMF solution (0.1-0.2 M) and the reaction was stirred at RT for 1 h. After removal of the solvent under reduced pressure, the crude residue was triturated twice with ice-cold Et$_2$O and collected by filtration or centrifuge. The deprotected compound was used in the next step without further purification, after drying under high *vacuum.*

Synthesis of *N*-Boc 6-aminohexanoic acid (**8**)
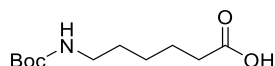
6-aminohexanoic acid (500 mg, 3.81 mmol) and Na_2CO_3 (2.0 eq) were suspended in 10 mL of a mixture of H_2O/Dioxane (1:1) and cooled at 0 °C in ice-bath. Then, Boc_2O (1.2 eq) was added and the reaction was stirred at RT overnight. The mixture was concentrated under reduced pressure to remove dioxane and the alkaline aqueous layer was adjusted to pH 3-4 with HCl 1M solution and then extracted with EtOAc (3 x 20 ml). The combined organic phases were dried over Na_2SO_4, filtered and concentrated under reduced pressure, to afford the protected compound **8** (800 mg, 91%) which was used without further purifications. ESI-MS *m/z* calcd. for $[C_{11}H_{22}NO_4]^+$: 232.1, found: 232.2 $[M+H]^+$.

Synthesis of Fmoc-(*S*)-Phe(4-NH2)-OH (**9**)
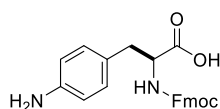
Commercially available Fmoc-(*S*)-Phe(4-NO2)-OH (500 mg, 1.16 mmol) and Zn dust (371 mg, 5.67 mmol) were suspended in absolute EtOH (12 mL). Glacial AcOH (12 mL) was added to the mixture, and the resulting suspension was stirred at 60 °C under N_2 for 4 h. The mixture was filtered over Celite® and the filtrates were evaporated at reduced pressure affording the crude **9** as a yellowish solid (450 mg, 1.12 mmol, 97%), that was used in the next step without further purifications. ESI-MS *m/z* calcd. for $[C_{24}H_{23}N_2O_4]^+$: 403.2, found: 403.2 $[M+H]^+$.

Synthesis of Fmoc-(*S*)-PhU-OH (**10**)
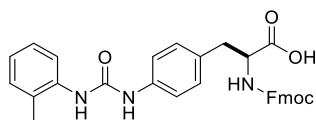
O-tolyl isocyanate (1.1 eq) was added dropwise to a stirred solution of Fmoc-Phe(4-NN2)-OH (1.0 eq) in DMF (10 mL) at RT under N_2 atmosphere. After 3 h the reaction was diluted with EtOAc (40 mL), to precipitate the pure product **10** that was collected by filtration as a whitish solid (485 mg, 81%). ESI-MS *m/z* calcd. for $[C_{32}H_{30}N_3O_5]^+$: 536.2, found: 536.3 $[M+H]^+$.

Synthesis of Fmoc-(*S*)-Lys-OCH₃ (11)
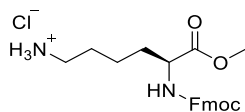
To a stirred solution of MeOH (5 mL) cooled at 0 °C in ice-bath, was added dropwise SOCl₂ (70 µL, 0.96 mmol) followed by Fmoc-(*L*)-Lys(Boc)-OH (150 mg, 0.32 mmol). The resulting mixture was stirred at RT overnight. The mixture was concentrated under reduced pressure and Et₂O was added to precipitate compound **11** as HCl salt (130 mg, 97%), that was used in the next step without further purifications. ESI-MS *m/z* calcd. for $[C_{22}H_{27}N_2O_4]^+$: 383.2, found: 383.4 $[M+H]^+$.

Synthesis of 7 (Scheme 11)
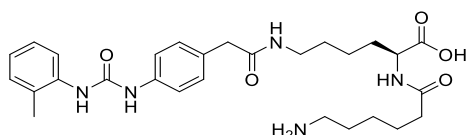
Coupling reaction between **MPUPA** (97 mg, 0.34 mmol) and **11** (130 mg, 0.34 mmol) was carried out in solution in presence of EDC/HOBt as activating agents according to general procedure (A). The resulting crude residue **12** (144 mg, 63%) was directly used in the next step. ESI-MS *m/z* calcd. for $[C_{38}H_{41}N_4O_6]^+$: 649.3, found: 649.6 $[M+H]^+$. Fmoc-deprotection was performed following the general procedure (B) to give **13** (38 mg, 41%) as a pale yellow solid that was used without purifications. ESI-MS *m/z* calcd. for $[C_{23}H_{31}N_4O_4]^+$: 427.2, found: 427.4 $[M+H]^+$. Yet, by following the general procedure (A) **13** (38 mg, 0.09 mmol) was coupled with **8** (21 mg, 0.09 mmol). The resulting crude compound was purified by flash chromatography over silica gel (gradient eluent Cy/EtOAc from 60:40 to 0:100) to yield **14** (46 mg, 80%) as a white solid. ESI-MS *m/z* calcd. for $[C_{34}H_{50}N_5O_7]^+$: 640.4, found: 640.6 $[M+H]^+$. Finally, ester hydrolysis and Boc-deprotection were performed. Firstly, **14** (46 mg, 0.07 mmol) was dissolved in a solution of THF/H₂O (2:1) then LiOH (3.0 mg, 0.11 mmol) was added at 0 °C. The mixture was stirred at RT for 2.5 h and the progress was monitored by TLC. The solution was neutralized at 0 °C by adding dropwise a solution of HCl 1M, and after the water was evaporated. The resulting product **15** (40 mg, 89%) was used in the next step without further purification. ESI-MS *m/z* calcd. for $[C_{33}H_{48}N_5O_7]^+$: 626.3, found: 626.4 $[M+H]^+$. Boc-deprotection was simply performed by adding to **15** a solution of 25% TFA/DCM and stirring the mixture at RT for 1 h. The solvent was concentrated at reduced pressure and the residue

was triturated twice with ice-cold Et_2O and collected by centrifuge and, finally purified by semi-preparative RP-HPLC to give **7** (38 mg, 93%) (for the conditions, see Materials and Methods). ^{1}H-NMR (400 MHz, DMSO-d_6) δ 8.89 (s, 1H, NHb), 8.39 (br. d, 1H, Lys-NH^α), 8.08 – 8.00 (m, 1H, Lys-NH^ε), 7.98 (s, 1H, NHa), 7.79 (d, J = 8.0 Hz, 1H, ArH$_6$), 7.38 (d, J = 8.0 Hz, 2H, ArH$_{2'6'}$), 7.21 – 7.12 (m, 4H, ArH$_{3,5}$ + ArH$_{3'5'}$), 6.93 (dd, J = 7.6, 7.2 Hz, 1H, ArH$_4$), 4.21 (m, 1H, Lys-CH^α), 3.35 – 3.13 (m, 2H, PhCH$_2$ overlapped with solvent signal), 3.10 – 2.79 (m, 4H), 2.22 (s, 3H, ArCH$_3$), 2.15 – 1.70 (m, 4H), 1.58 – 1.41 (m, 4H), 1.53 – 1.09 (m, 6H). ESI-MS m/z calcd. for $[C_{28}H_{40}N_5O_5]^+$: 526.3, found: 526.2 $[M+H]^+$. t_r = 1.8 min, 92% purity ($λ$ = 254 nm).

Preparation of the nanostructured surfaces

Zeolite loading with DXP 170 dye

The Zeolites (300 mg, width = 600-1000 nm, height ~ 250 nm, Figure 46 and Appendix) and DXP (6.23 mg) were kept overnight under high vacuum. Then, the solid mixture was heated at 300 °C in a sealed flask into a rotary furnace. Then the flask was broken and the powder was washed with butan-1-ol and centrifuged (30 min, 40 krcf), in until the supernatant ceased UV emission.

Functionalization of DXP-zeolites with isocyano group

The DXP-loaded Zeolites (50 mg) were placed into a 50 mL flask and suspended in a mixture of toluene (5 mL) and TEA (0.2 mL), and the precipitate was dissolved by sonicating for 15 min. Then ICPTES (0.8 mL) was added, and the mixture was sonicated for further 3 h. Then the suspension was cooled to RT and centrifuged for 20 min (40 krcf). The unreacted silane was removed by three cycles of dispersion of the precipitate in toluene by of sonication followed by centrifugation.

Preparation of isocyano-DXP-zeolite SAMs

Glass plates were placed into a 100 mL flask and cleaned by treatment with 3:1 H_2SO_4/H_2O_2 (10 mL) at 100 °C for 1 h. The plates were rinsed with bidistilled water (3 x 30 mL) and ethanol (3 x 20 mL) and finally dried by blowing nitrogen. The plates were then slotted onto Teflon support to avoid any contact, and the system was housed into a 100 mL round-bottom flask containing a solution of APTES (0.8 mL) and TEA (0.2 mL) in toluene (30 mL). The flask was heated overnight at 115 °C; subsequently, the plates were washed with toluene (5 mL) and

ethanol (5 mL) and dried under nitrogen flow. The supported plates were immersed into a suspension of isocyano-DXP-zeolites in toluene (1 mg/mL, 2 mL), and sonicated for 30 min, and then the plates were washed with toluene (5 mL) and air-dried.

Functionalization of isocyano-DXP-zeolite SAMs with peptides or n-butylamine (**1-7**@SAMs)

A mixture of the peptide (1 mg) or *n*-butylamine (0.2 mg) and TEA (10 μL) in DMF (1 mL) was dissolved by sonication for 5 min. The plates of the SAMs were immersed in the solution and heated at 35 °C. After 3 h, the plates were removed and washed with DMF (5 mL) and EtOH (5 mL), then air-dried.

Control plates modified with peptide **3** (3@plates)

The glass plates were cleaned with 3:1 H_2SO_4/H_2O_2 as described above, and then they were mounted onto Teflon support. The plates were placed in a round bottom flask and reacted overnight with a solution of ICPTES (0.8 mL) and TEA (0.2 mL) in toluene (30 mL) at 115 °C. Then the isocyano-plates were rinsed with toluene (5 mL) and ethanol (5 mL) and dried by nitrogen flow. The peptide **3** (1 mg) was dissolved in a solution of TEA (10 μL) in DMF (1 mL) by sonication for 5 min. The mounted isocyano-plates were immersed in the solution and heated at 35 °C for 3 h, followed by washes with DMF (5 mL) and EtOH (5 mL), and finally were air-dried.

Cell adhesion experiments

Cell culture. The $\alpha_4\beta_1$ integrin-expressing Jurkat E6.1 human T cells were cultured in RPMI-1640 and L-Gln with 10% FBS. HEK-293 cells were grown in EMEM supplemented with 10% FBS, non-essential amino acids and L-Gln. Cells were maintained at 37°C under 5% CO_2 humidified atmosphere. HEK-293 cells were detached from the culture flask by trypsination. The number of viable cells present in the cell suspension was determined by the Eosin 0,1% exclusion test.

Cell staining. 1×10^6/ml cells were suspended in serum-free buffer (PBS 1% BSA) in the presence of the dye CMFDA (6.25 μM) and incubated for 20 min at 37 °C while gently mixing. The suspension was centrifuged at 1800 rpm for 3 min, the supernatant was removed, and the cells resuspended in buffer. The washing procedure were repeated twice.

Cell adhesion and counting. The peptide@SAMs were initially washed with PBS solution, then they were placed in a 6 wells plate (growth area 8.87 cm^2) and seeded with 5×10^5 Jurkat or HEK-293 cells. Each well was filled with buffer to reach 1 mL of final volume, and the plates moved to the incubator for 15 min. After that, each well was washed twice with PBS (2 mL) and the sample fixed with 3% PFA (200 µL) for 10 min at r.t. The plates were washed twice with PBS-glycine 0,1%, and each SAM was embedded in Mowiol and analyzed by confocal laser-scanning microscope (General Methods). For visualization of the DXP-loaded zeolites in red, fluorescence was excited with a 543 nm laser and detected at 650 nm; CMFDA-stained cells were visualized in green by excitation at 488 nm and detected at 530 nm. Images were quantified by ImageJ software. The number of cells adherent to a surface of 0.0025 cm^2 was determined three times, and the average was expressed as cell/cm^2 ± S.E.

7. SYNTHESIS OF RGD-CRYPTOPHYCIN CONJUGATES BEARING β-GLUCURONIDASE-RESPONSIVE LINKER FOR TARGETED TUMOR THERAPY

The work described in this Chapter was carried out during my PhD internship at the University of Bielefeld (Germany) under the supervision of Prof. Dr. Norbert Sewald.

7.1. Introduction

Traditional chemotherapy still represents one of the most common treatments for both early and advanced stages of cancer. It is based on the administration of cytotoxic drugs, which generally interfere with highly regulated cellular functions (*e.g.,* cell division, DNA replication, apoptosis). Cytotoxic drugs can be administered as single agents or in combination with other drugs, as multi-drug therapy. To reach optimal therapeutic efficacy and minimize side effects, cytotoxic drugs need to selectively reach the targeted tumour site. This still represents a challenge as the majority of anticancer drugs do not preferentially accumulate at the tumor site, leading to systemic side effects and to suboptimal therapeutic efficacy.[249, 250] These pharmacokinetic aspects have been demonstrated using tumor-xenograft mouse models [251, 252] and, more recently, in cancer patients in positron emission tomography (PET) studies with radiolabelled cytotoxic drugs.[253] Targeted drug delivery has been proposed as a promising alternative to overcome the pharmacokinetic limitations of conventional cytotoxic agents.[254] In this context, covalent conjugation of cytotoxic agents to specific cell-membrane-receptor ligands (*e.g.,* antibodies, peptides or small molecules), capable of selective binding to tumour-overexpressed receptors, enables drug accumulation at the tumor site while reducing off-target toxicity (Figure 49).[255]

Currently, Antibody-Drug Conjugates (ADCs) represent one of the most effective strategies for achieving selective drug-delivery and consists of the conjugation of tumor specific monoclonal antibody to the anticancer drug. To date, four ADCs have reached marketing approval in cancer therapy (Kadcyla®, Adcetris®, Mylotarg® and Besponsa®) while more than 65 are currently under clinical investigation.[250, 256] Although ADCs show therapeutic benefits in clinical trials, they also display significant drawbacks, such as long circulation time, high manufacturing costs and the immunogenicity. Furthermore, the large size limits their diffusion in the tumour tissue.[257]

Recently, Small-Molecule Drug Conjugates (SMDCs) have attracted considerable interest as a valid alternative to ADCs due to their advantageous pharmacokinetic profile, simpler and more affordable synthetic routes and lack of immunogenicity.[258] Indeed, their smaller size enables rapid and homogeneous tissue diffusion, potentially resulting in high tumor/organ ratio.[259] Similarly to ADCs, SMDCs are composed of three covalently bonded building blocks: a cytotoxic agent, a self-immolative linker and a targeting ligand (Figure 49).[260] However, the targeting ligand in SMDCs is represented by a small molecule (*e.g.,* oligopeptides/peptidomimetics,[261] vitamins,[262] steroids,[263] enzyme inhibitors[264]). Furthermore, additional spacers are often inserted (Figure 49) with the aim of modifying the conjugate physicochemical properties (*e.g.,* solubility) or to improve drug release kinetics.[96]

Figure 49. General structures of antibody-drug conjugates (ADCs) and small-molecule drug conjugates (SMDCs).

Such constructs are highly specific towards the overexpressed tumor receptors and are generally designed to address the payload intracellularly in the lysosome compartment upon receptor-mediated endocytosis or to liberate the cytotoxic drug in the extracellular environment (Figure 53).[265] In fact, it has recently been demonstrated that the internalization of the payload is not strictly necessary to achieve drug-delivery efficacy, and several non-internalizing SMDCs have been reported.[266] Promising tumor-targeting results employing small peptide ligands targeting folate receptors,[267] prostate-specific membrane antigen (PSMA),[268] somatostatin receptors (SSTRs) [269, 270] and carbonic anhydrase IX (CAIX) ligands have been observed in recent times.[271, 272] Unfortunately, despite their advantages over ADCs, SMDCs are still under clinical investigation and haven't yet reached the market.

Among the tumor-associated receptors, the heterodimeric transmembrane glycoprotein integrin $\alpha_v\beta_3$ has long been considered a potential tumor target due to its overexpression in cancer cells and blood vessels of several solid tumors (*e.g.,* breast cancer, glioblastoma, pancreatic tumor, prostate carcinoma) but not on healthy tissues.[79, 83] The α_v integrin subtype plays a central role in many stages of cancer progression such as angiogenesis, tumor growth, apoptosis resistance, and metastasis.[69] Integrin $\alpha_v\beta_3$ recognizes and binds the extracellular

matrix (ECM) proteins (*e.g.,* vitronectin, fibronectin, collagen) through the minimal tripeptide sequence Arg-Gly-Asp (RGD).[84] Consequently, several linear and cyclic RGD-bearing peptides and peptidomimetics have been prepared and conjugated to different cytotoxic agents (*e. g.,* doxorubicin,[273] monomethylauristatin E,[274] camptothecin,[275] cisplatin,[276] paclitaxel [277]) in order to obtain SMDCs with high binding affinity to the integrin $\alpha_v\beta_3$.[89, 278] Many of these RGD-peptides are derivative of the well-known $\alpha_v\beta_3$ integrin antagonist Cilengitide.[86] For example, the analogue *c*[RGDfK] (Figure 50) has been widely used as targeting ligand for imaging [99] and drug delivery application due to its nanomolar binding affinity and suitable conjugation handle.[95, 101, 261]

c[RGDf(N-Me)V] or Cilengitide
$\alpha_v\beta_3$ IC$_{50}$ = 0.54 nM

R = H, n = 1, *c*[RGDfK]
R = COCH$_2$CH$_2$N$_3$, n = 1, *c*[RGDfK(**R**)] $\alpha_v\beta_3$ IC$_{50}$ = 0.71 nM (**33**)
R = COCH$_2$CH$_2$N$_3$, n = 2, *c*[RβADfK(**R**)] $\alpha_v\beta_3$ IC$_{50}$ > 1000 nM (**34**)
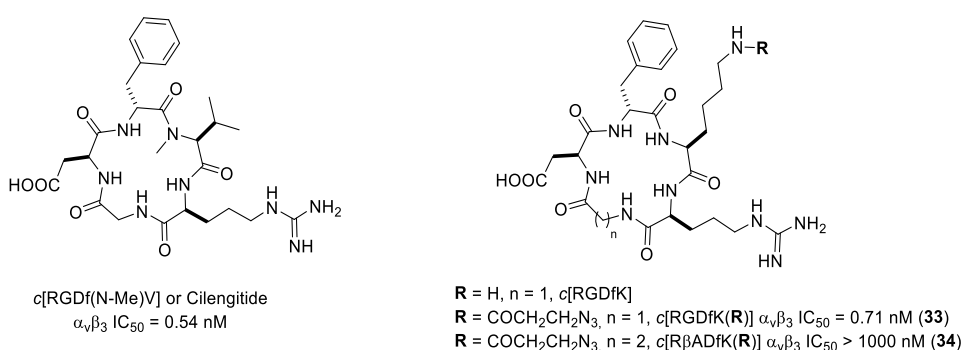
Figure 50. Structures of integrin ligands.

Beside the cytotoxic agents commonly used in chemotherapy regimens, a class of compounds called Cryptophycins, that act as a microtubule destabilizer, have shown remarkable activity despite their low selectivity. For this reason, they have been taken into consideration as promising drug candidates for targeted tumor therapy.[279]

Cryptophycins (Figure 51) are natural 16-membered macrocyclic depsipeptides that have been isolated from cyanobacteria *Nostoc sp.* ATCC 53789 in 1990.[280] This class of compounds exhibit potent cytotoxicity towards several cancer cells (typically with IC$_{50}$ in the low pM range) including multi-drug resistant (MDR) cells.[281] This is due to their low affinity for the P-gp efflux pump. Their strong antiproliferative activity is based on the irreversible inhibition of the β-tubulin polymerization during mitosis, leading to cell-cycle arrest in G$_2$/M phase and activation of apoptosis pathways.[282] Since their discovery, numerous derivatives have been designed and synthesized for Structure-Activity Relationship (SAR) studies.[283-285] The analogue Cryptophycin-52 (LY355703, Cry-52, Figure 51) has reached clinical trial phase II as a potential anticancer drug. However, its development was discontinued due to high

neurotoxicity and lack of efficacy *in vivo*.[286] In this context, the research has been focusing on the conjugation of Cryptophycins to a homing device with the aim of increasing their selectivity for cancer cells.[279, 287] However, the lack of a suitable handle in Cry-52 has motivated the design of novel and suitable modification strategies.[283, 288-290]

R$_1$ = Me R$_2$ = H, Cryptophycin-1
R$_1$ = R$_2$ = Me, Cryptophycin-52

R = H, Cryptophycin-55
R = COCH$_2$NH$_2$, Cryptophycin-55 glycinate
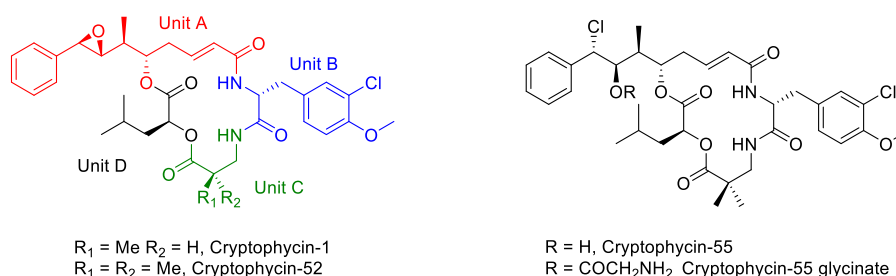
Figure 51. Structure of Cryptophycin derivatives.

Based on the previous SAR studies, each of the four units A, B, C, and D have been investigated.[279, 289] More specifically, unit A has emerged as a good site for the introduction of functional groups for its conjugation while retaining the potent cytotoxicity of its parent compound.[285, 291] Although the presence of the (*R,R*)-epoxide is essential for the high biological activity,[292] ring-opening to corresponding chlorohydrin yields Cryptophycin-55 (Cry-55, Figure 51). Cry-55 exhibits an increased *in vivo* cytotoxicity.[293, 294] However, it is characterized by lower stability, probably due to the epoxide-forming reverse reaction taking place under physiological conditions. More stable derivatives of Cry-55 can be obtained upon esterification of the secondary alcohol with Gly leading to the corresponding Cryptophycin-55 glycinate (Cry-55 gly, Figure 51).[294] Cry-55 gly displays not only higher chemical stability but also higher *in vivo* and *in vitro* activity. Further, it offers an amino functionality which makes it suitable for conjugation to tumor homing devices. Differently, modification in *para*-position on the aromatic ring had led to Cryptophycin derivatives unstable in mouse plasma.[295]

In the last decades, Sewald and coworkers have contributed to this field of research by developing novel tumor targeting ADC[296] and SMDCs bearing the potent Cry-55 gly as anticancer payload (Figure 52).[270, 272, 297, 298]
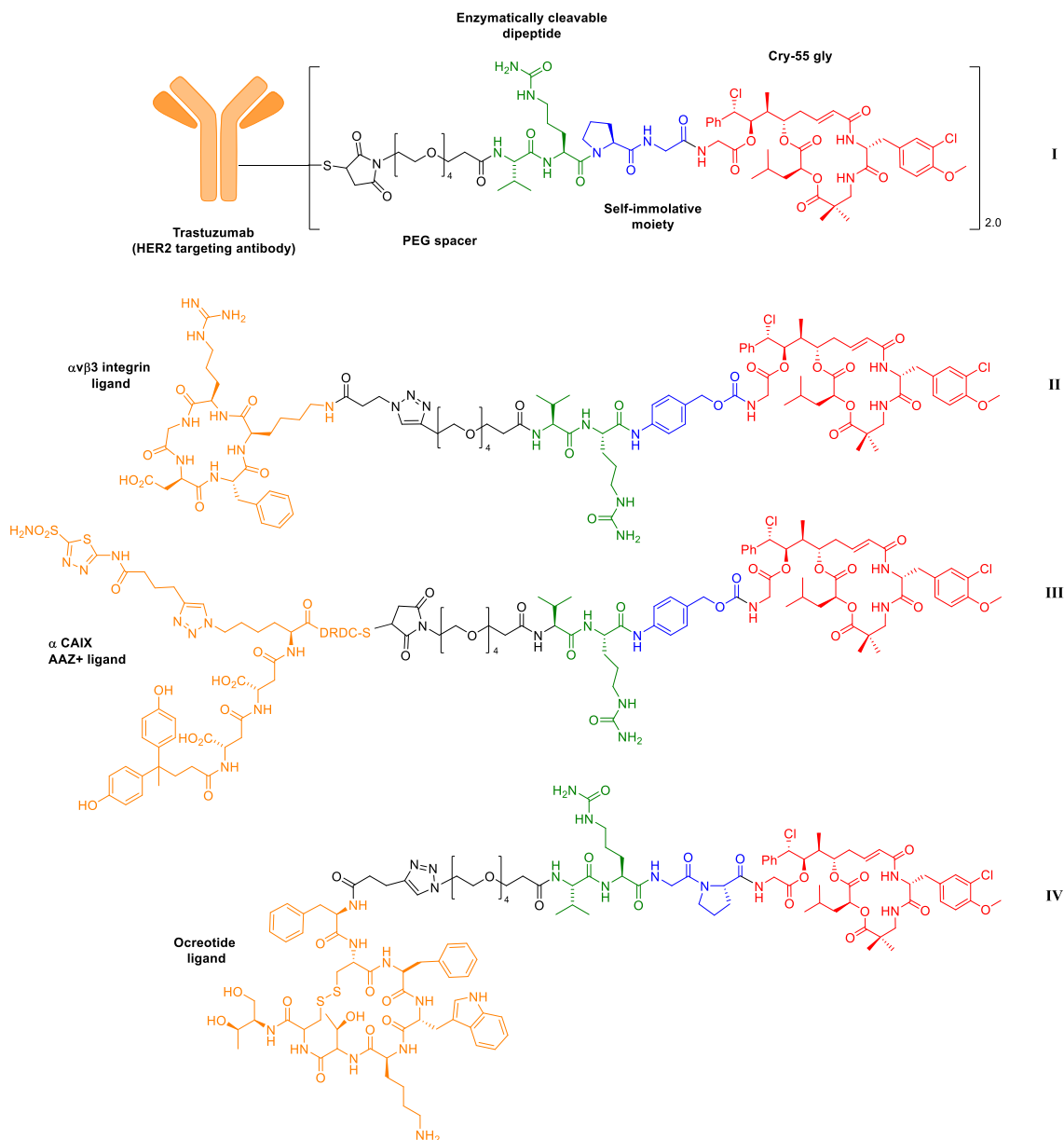
Figure 52. Molecular structures of Cryptophycin-based ADC and SMDCs.

In this drug delivery strategy, the linker plays a crucial role because it should be sufficiently stable in the bloodstream and be able to release the payload in an efficient manner selectively at the diseased site avoiding non-specific distribution in the body and off-target effects.[299] These conjugates can be ascribed to prodrugs, which are generally much less active than the free drugs due to the stability of the linkage, and have to be delivered and activated *in vivo* to generate the active drugs.[287] The discovery of the altered expression of enzymes in the microenvironment of several malignancies have been exploited for developing specific

cleavable linkers. In the presence of these proteases, the linker is cleaved and the active compound can be released inside the tumor cell (Figure 53).[300]
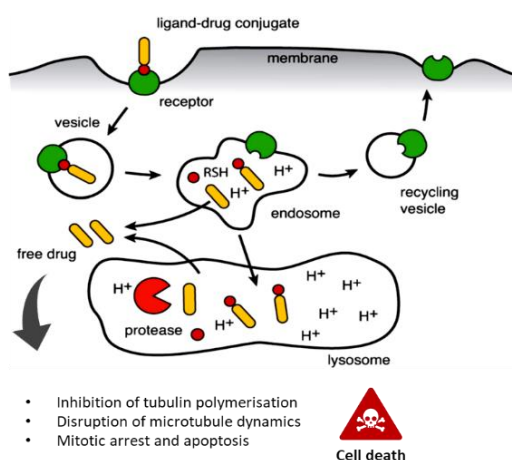
Figure 53. Mechanism of uptake and activation of ligand-targeted drug conjugates (image adapted from Krall *et. al.*)[257]

Over the years a large number of protease-sensitive linkers have been developed. β-glucuronidase is a well-known tumor-associated enzyme responsible for the hydrolysis of β-(*D*)-glucuronic acid residues from the non-reducing end of glycosaminoglycans. It has been detected in high concentrations intracellularly in lysosomes and in necrotic tumor environment of many malignancies including lung, breast, ovarian, gastrointestinal tract carcinomas and melanomas.[252, 301] For this reason, β-glucuronic acid-based linkers have been incorporated in a large number of drug-delivery systems for the release of cytotoxic drugs, both within and outside cancer cells.[302, 303]

Recently, we reported the development of first-generation RGD-cryptophycin conjugates containing the enzymatically cleavable Val-Cit linker (Figure 52, **II**) and found that conjugates displayed high *in vitro* potency but poor selectivity in cell lines with different $\alpha_v\beta_3$ integrin expression level. We proposed that the nonspecific passive cellular uptake of the conjugates could be associated with the high payload hydrophobicity.[298] Nevertheless, drug-linkers with improved hydrophilicity would provide optimal pharmacokinetic properties to the overall construct, thus preventing aggregation and/or passive permeation across the cell membrane. To this end, the protease-sensitive β-glucuronide has been incorporated as a hydrophilic alternative to the Val-Cit linker, to minimize the hydrophobicity and allow an efficient drug release.[304, 305]

Herein, we report the synthesis of first β-glucuronidase-responsive conjugates (**1-4**, Figure 54) bearing the potent Cry-55 gly and the *c*[RGDfK] integrin ligand for targeted therapy of patients with $\alpha_v\beta_3$-positive tumors. Furthermore, to evaluate drug-targeting and drug-release potential, conjugates **2-4** were developed as negative controls. The novel RGD-cryptophycin conjugates are currently under biological investigation; therefore, no data are available for the discussion. Anyway, cytotoxicity and tumor-targeting potential of **1-4** will be assayed *in vitro* by using two different isogenic human melanoma cancer cell lines: M21 overexpressing integrin $\alpha_v\beta_3$ ($\alpha_v\beta_3$+) and M21-L non-expressing $\alpha_v\beta_3$ ($\alpha_v\beta_3$-).[306]
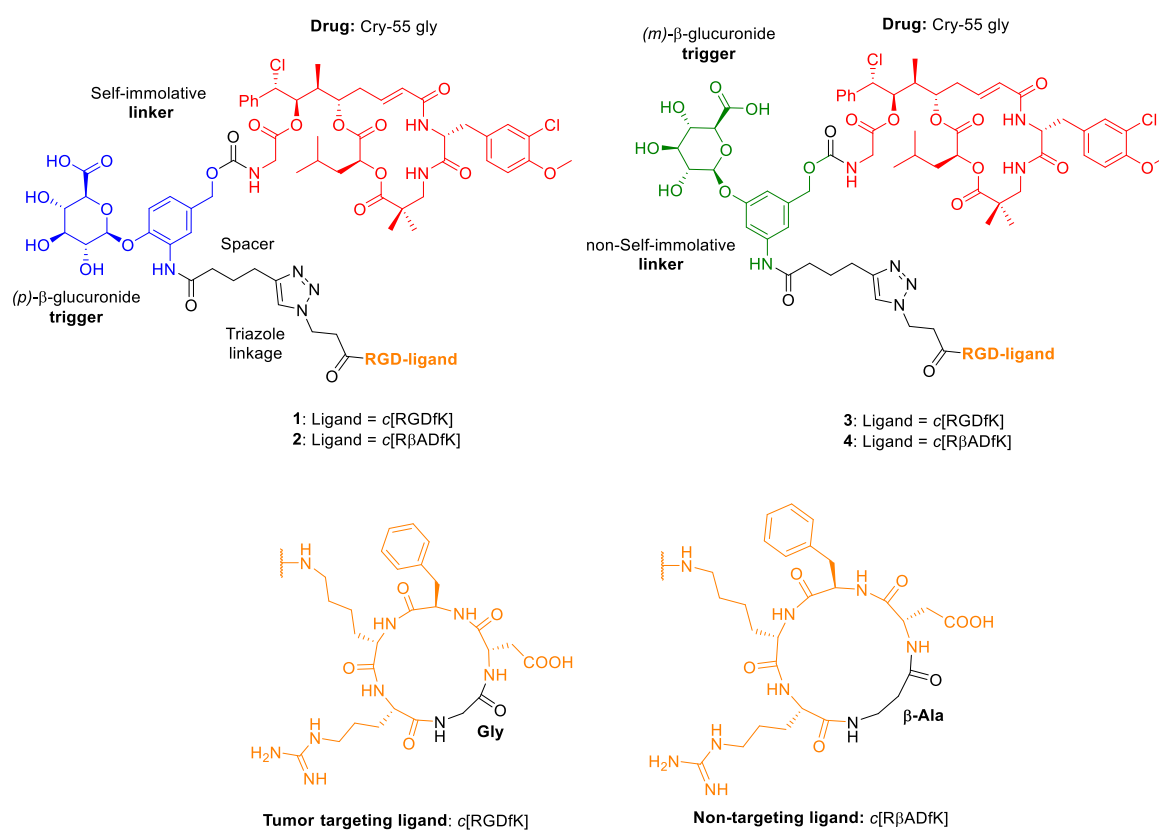
Figure 54. Molecular structures of self-immolative conjugates *c*[RGDfK]-(*p*)-gluc-linker-Cry-55gly (**1**) and *c*[RβAfK]-(*p*)-gluc-linker-Cry-55gly (**2**), and non-self-immolative conjugates *c*[RGDfK]-(*m*)-gluc-linker-Cry-55gly (**3**) and *c*[RβAfK]-(*m*)-gluc-linker-Cry-55gly (**4**) as negative control.

7.2. Results and discussion

7.2.1. Design

Over the years, the use of cryptophycin as payload for drug-delivery purposes has been exploited for the realization of several ADCs[296] and SMDCs; [270, 272, 297, 298] however, *in vivo* applications have not yet been reported. In this framework, we present the synthesis and evaluation of the first conjugates comprising of the potent antimitotic agent Cry-55 gly and the *c*[RGDfK] ligand bearing β-glucuronidase-responsive linker, suitable for the targeted therapy of solid tumors.[303] Structurally, the RGD-cryptophycin conjugates can be subdivided in three main parts covalently assembled: 1) cytotoxic Cry-55 gly, 2) β-glucuronidase-responsive self-immolative linker, and 3) *c*[RGDfK] $\alpha_v\beta_3$ tumor targeting ligand (Figure 54). The linker system incorporating the highly hydrophilic carbohydrate moiety, was designed to provide sufficient stability during circulation and to increase the overall polarity/water solubility, avoiding the tendency of SMDCs containing hydrophobic cryptophycins to undergo aggregation and/or unspecific cellular uptake by passive diffusion.[304, 307] Moreover, once the RGD-cryptophycin conjugate has reached the targeted tumor tissue, the β-glucuronidase-catalyzed hydrolysis of glicosidic bond from drug-linker triggers the release via 1,6-elimination (self-immolative process) of the cytotoxic drug in its active form (**1**, Figure 56), selectively inside the cancer cells, upon internalization via $\alpha_v\beta_3$-mediated endocytosis,[290] or in the extracellular tumor microenvironment, from where it can diffuse into surrounding cancer cells.[308]

To follow the drug-release efficiency of the targeting assembly, the synthesis of a negative control was envisaged by positioning the β-glucuronic acid (β-gluc) in *meta*-position on the aromatic ring of the linker (**3-4**, Figure 54). In the latter, enzymatic trigger is not followed by self-immolation step, thus resulting conjugate-intermediates with decreased activity (**3**, Figure 56). Whereas, to investigate the drug-targeting efficiency a modified RGD-ligand (**34**), obtained by replacing Gly from ligand **33** with β-Ala, was used to synthesize non-targeting negative control conjugates. The modified ligand *c*[RβADfK] (**34**) is unable to bind the $\alpha_v\beta_3$ integrin receptor, thereby the resulting conjugates **2** and **4** showed a dramatically lower integrin binding affinity compared to that of conjugates **1** and **3** (Figure 55).

7.2.2. Synthesis

The conjugates **1-4** were synthetized as shown in Scheme 13. Cry-55 gly was prepared as previously described (synthesis not shown).[294] Conjugates **1** and **2** were prepared in thirteen

optimized steps starting from commercially available 4-hydroxy-3-nitrobenzaldehyde (**5**). Stereoselective glycosylation of **5** to acetobromo-α-D-glucuronic acid methylester (**6**) was performed under Koenigs-Knorr conditions in the presence of silver carbonate as catalyst (**7**, 93%) which was followed by aldehyde reduction with sodium borohydride providing **8** in 95% yield without needing purification. The corresponding benzylic alcohol was treated with *tert*-butyldimethylsilyl chloride and imidazole to produce the silyl ether protected derivative **9**. At this stage as reported by Grinda *et. al.*, the protecting groups of the β-glucuronide were modified via a 3-step strategy to yield the fully allyl-protected glucuronyl derivative (**12**). Protected in this way, the glucuronide results stable and compatible during the synthesis, and furthermore the entire deprotection can be performed in a one-step procedure under mild conditions at the end of the synthesis.[309] The acetyl groups were removed from **9** using MeONa to afford the hydroxyl free derivative **10** (84%). Transesterification of the methyl ester with sodium allylate (0.126M) gave the allyl ester **11** in 83% yield. The three allyl carbonates were introduced in the presence of a large excess of allyl chloroformate using pyridine as solvent. After 3 days under these conditions, the fully allyl protected glucuronide **12** was obtained in good yield of 82%. Later, nitro reduction with Zinc powder under acidic conditions restored the free aniline (**13**) which was subsequently coupled with 5-hexynoic acid in presence of EEDQ providing **14** with a suitable alkyne-functionalized spacer for the conjugation to the peptide via triazole linkage. Cleavage of *tert*-butyldimethylsilyl ether was carried out with HF/pyridine to yield the free benzyl alcohol **15** which was subsequently treated with bis(4-nitrophenyl)carbonate and pyridine to give the activated carbonate **16** in quantitative yield. Later, Cry-55 glycinate was introduced via nucleophilic substitution in presence of DIPEA to afford the carbamate **17** in good yield after RP-HPLC purification. Full allyl deprotection of the glucuronide moiety was carried out using catalytic amount of tetrakis(triphenylphosphine)palladium(0) affording the Cry-55 gly-linker conjugate **18** in acceptable yield after RP-HPLC purification (66%). Finally, the conjugation to the targeting ligand, properly modified with 3-azidopropanoic acid on the Lys side chain, was achieved by triazole linkage. The Copper(I)-catalyzed Azide-Alkyne Cycloaddition (CuAAC "click chemistry" reaction) was carried out at 35 °C to increase the solubility of the system for 24 h in presence of the alkyne **18** and the azido-peptide derivative, *c*[RGDfK(-N₃)] **33** or *c*[RβADfK(-N₃)] **34**, using CuSO₄ and sodium ascorbate as catalysts.
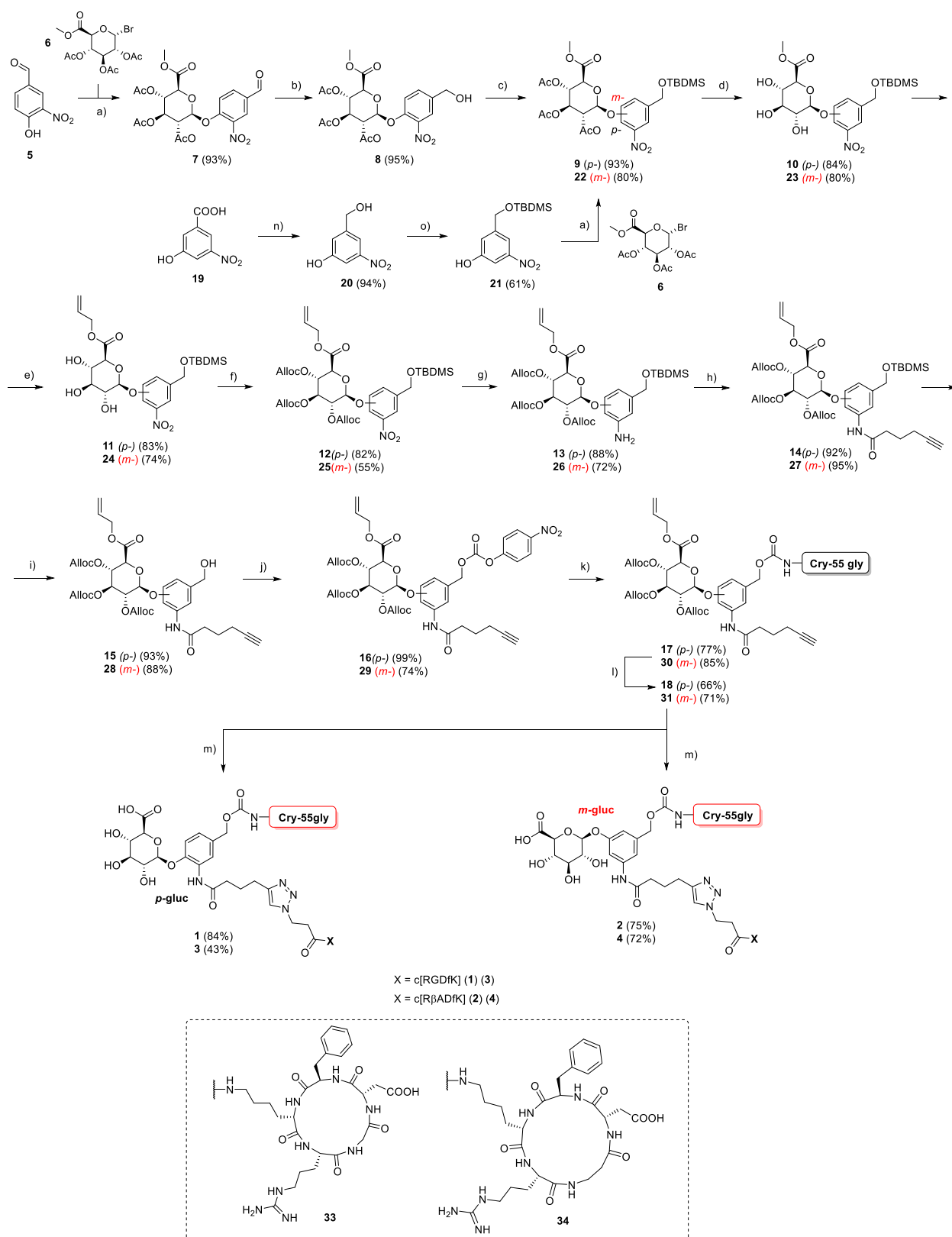
Scheme 13. Synthesis of the RGD-cryptophycin conjugates **1-4** *Reagents and conditions:* a) Acetobromo-α-D-glucuronic acid methylester, Ag₂O, CH₃CN, darkness, RT, 4 h; b) NaBH₄ CHCl₃/IPA (5:1) silica gel, 0°, 45 min; c) Imidazole, TBDMSCl, DCM, RT, 12 h; d) MeONa 30% w/v, MeOH, 0°, 1.5 h; e) Sodium allylate 0.126M,

allylic alcohol, RT, 40 min; f) Allyl chloroformate, pyridine, RT, 72 h; g) Zinc, MeOH/AcOH (10:1), RT, 30 min; h) 5-hexynoic acid, EEDQ, DCM, RT, 24 h; i) HF/Pyridine 70%, THF, RT, 1 h; j) 4-nitrophenyl chloroformate, pyridine, DCM, 0° - RT, 2 h; k) Cry-55-gly, DIPEA, DMF, RT, 4 h; l) Pd(PPh$_3$)$_4$, morpholine, DCM, RT, 1 h; m) RGD-ligand **33** (for conjugates **1** and **3**); **34** (for conjugates **2** and **4**) CuSO$_4$·5H$_2$O, sodium ascorbate, DMF/H$_2$O (1:1), 35°C, 24 h, 84% (**1**), 75% (**2**), 80% (**3**), 79% (**4**); n) BH$_3$·THF, THF, 0°- RT. overnight; o) Imidazole, TBDMSCl, THF, 0° 2 h.

After purification by preparative RP-HPLC, the final conjugates **1** and **2** were obtained in 84% and 75% yield, respectively.

Following a similar synthetic approach, the RGD-Cryptophycin conjugates **3**-**4** bearing the *meta*-β-glucuronic moiety on the linker were also prepared (negative control). First, was synthesized the precursor 3-(hydroxymethyl)-5-nitrophenol (**20**) by reduction of the commercially available 3-hydroxy 5-benzoic acid **19** using a solution of BH$_3$-THF 1.0 M at 0 °C. The resulting benzylic alcohol (**20**) was selectively protected with *tert*-butyldimethylsilyl chloride in presence of imidazole at 0 °C producing the protected silyl ether derivative **21** in acceptable yield (61%). Then, the free hydroxyl group in *meta*-position was coupled with acetobromo-α-D-glucuronic acid methylester **6** under Koenigs-Knorr conditions described above to give **22**. At this stage, by following the same synthetic scheme described above, the RGD-Cryptophycin conjugates **3** and **4** were obtained in 43% and 72% yield, after RP-HPLC purification. The resulting final conjugates **1**-**4** were characterized by analytical HPLC and HRMS.

The *c*[RGDfK(COCH$_2$CH$_2$-N$_3$)] (**33**) and *c*[RβADfK(COCH$_2$CH$_2$-N$_3$)] (**34**) were synthesized as shown in Scheme 14. Both sequences of linear ligands were assembled manually by SPPS on 2-Chlorotrityl chloride resin starting from Fmoc-Gly-OH and Fmoc-Asp-OAllyl, respectively and, using Fmoc-protected amino acids (see Experimental section). In general, after the attachment of the first amino acid, Fmoc-deprotection was performed twice by treating the peptidyl-resin with a solution of 20% piperidine in DMF for 10 min. Coupling of each amino acid was performed at RT in presence of DIC and OxymaPure as activating agents, except for the azido-modified Fmoc-Lys (**32**) in which HATU and DIPEA were used. The sequences were elongated alternating coupling and deprotection reactions. Cleavage from the resin of the protected precursor of **33** was carried out three times in 25% HFIP/DCM mixture for 5 min.

Cyclization in solution using HATU, HOAt and DIPEA was carried out in pseudo-high dilution condition to avoid intermolecular side reactions affording, after removal of the *t*Bu and Pbf protecting groups with TFA/TIS/H$_2$O (95/2.5/2.5) for 3 h, the *c*[RGDfK(-N$_3$)] (**33**) in good

yield (65%). Conversely, cyclization of **34** was performed on resin. To this purpose, once the linear sequence was completed the removal of Fmoc- and Allyl-protecting groups with tetrakis(triphenylphosphine)palladium(0) and triphenyl silane were firstly carried out. Then, head to tail cyclization was obtained on resin at RT using DIC and OxymaPure as coupling agents. Cleavage from the resin and simultaneous Pbf deprotection with TFA/TIS/H_2O (95/2.5/2.5) mixture for 3 h afforded the c[RβADfK(-N_3)] (**34**) with poor yield (16%). Both azido-functionalized cyclic peptides **33** and **34** were purified by RP-HPLC (see general methods).
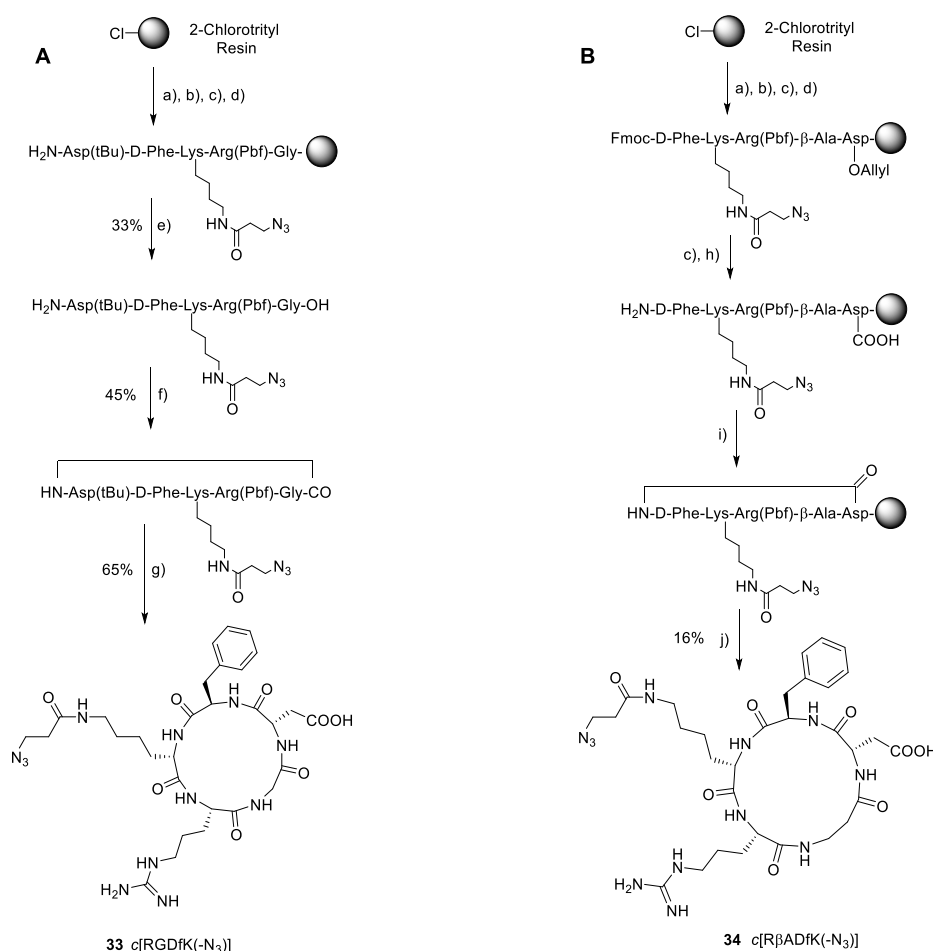
Scheme 14: Synthesis of $\alpha_V\beta_3$ integrin ligand c[RGDfK(-N_3)] (**33**) and c[RβADfK(-N_3)] (**34**). *Reagents and conditions:* a) $SOCl_2$, DCM, RT, 1 h; b) *i.* Fmoc-Gly-OH (2 eq), DIPEA (5 eq), DCM, RT, 3 h; *ii.* MeOH/DIPEA (9:1), RT, 10 min; same conditions repeated for Fmoc-Asp-OAllyl; c) 25% piperidine, DMF, RT, 15 min; d) Fmoc-AA-OH (2 eq), DIC (2 eq), OxymaPure (2 eq), DMF, RT, 3 h; Iterative repetition of (c) and (d) using the corresponding amino acid. Coupling of azido-modified Fmoc-Lys(CO-CH_2CH_2-N_3)-OH (**32**, 2 eq) was achieved using, HATU (2 eq), DIPEA (4 eq), DMF, RT, 3 h; e) HFIP/DCM (1:3), RT, 5 min (x3); f) HATU (3 eq), HOAt (3 eq), DIPEA (6 eq), DMF (pseudo-high dilution), RT, 18 h; g) TFA/H_2O/TIS (95/2.5/2.5), RT, 3 h; h) Pd(PPh$_3$)$_4$, PhSiH$_3$, DCM, RT, 10 min (x2); i) DIC (5 eq), OxymaPure (5 eq), DMF, RT, 18 h; j) TFA/H_2O/TIS (95/2.5/2.5), RT, 3 h.

7.2.3. Integrin binding affinity

Conjugates **1**-**4** were evaluated for their ability to inhibit biotinylated vitronectin binding to the isolated $\alpha_v\beta_3$ receptor. The binding affinity was evaluated using a competitive ELISA-based assay and it was compared to those of free ligands (**33** and **34**) and Cilengitide (IC$_{50}$ $\alpha_v\beta_3$ = 0.54 nM) taken as internal reference (Figure 55).[278]

entry	Compound	IC$_{50}$ (nM)
		Binding affinity to αvβ3
1	c[RGDfK(-N$_3$)] (**33**)	0.81 ± 0.28
2	c[RGDfK]-*(p)*-gluc-Cry (**1**)	21.9 ± 3.3
3	c[RGDfK]-*(m)*-gluc-Cry (**3**)	11.7 ± 2.3
4	c[RβADfK(-N$_3$)] (**34**)	> 10 000
5	c[RβADfK]-*(p)*-gluc-Cry (**2**)	> 10 000
6	c[RβADfK]-*(m)*-gluc-Cry (**4**)	> 10 000
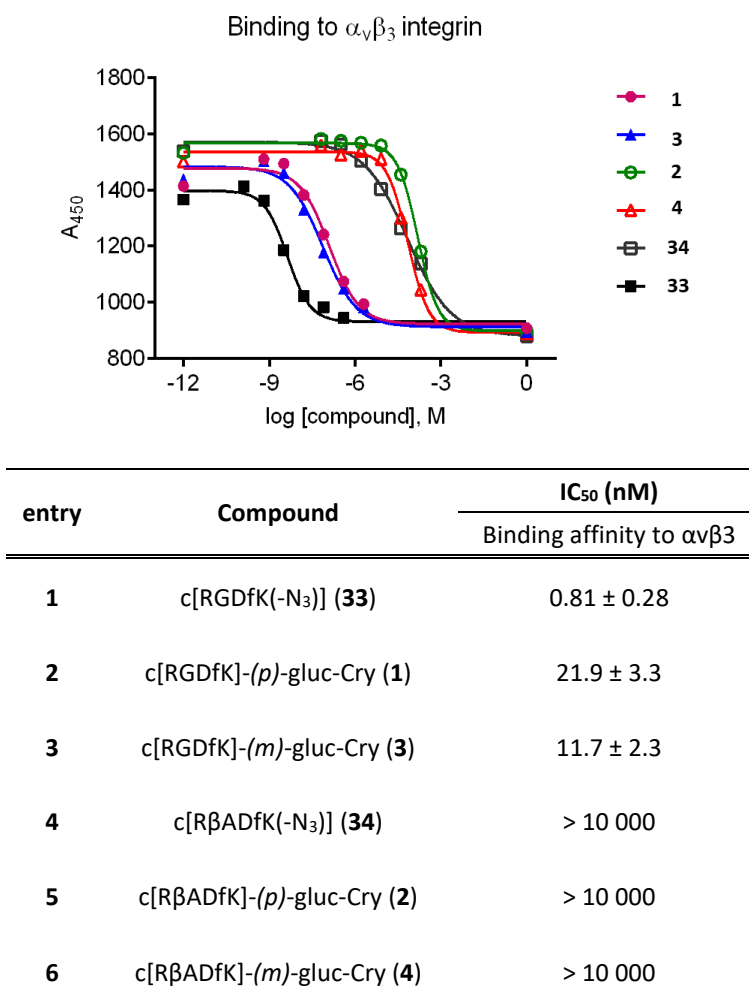
IC$_{50}$ values were determined as the compound concentration necessary for 50% inhibition of biotinylated vitronectin binding as calculated using GraphPad Prism software. All values are the average ± standard deviation of duplicate measurements.

Figure 55. Inhibition of biotinylated vitronectin binding to the isolated human integrin αvβ3.

Integrin binding assays were carried out by incubation of immobilized $\alpha_v\beta_3$ integrin with increasing concentrations of the conjugates (10^{-5}–10^{-12} M) in presence of the ECM protein vitronectin. Ligand *c*[RGDfK(-N$_3$)] (**33**) showed an IC$_{50}$ of 0.71 nM comparable to that of the reference Cilengitide (IC$_{50}$ = 0.54 nM), confirming that functionalization with 3-azido

propanoic acid did not affect the integrin receptor binding (Figure 55). In contrast, the ligand c[RβADfK(-N$_3$)] (**34**) displayed a dramatic loss of integrin binding affinity (IC$_{50}$ > 10.000 nM) compared to **33** (Figure 55). Conjugates **1** and **3** bearing ligand **33** retained good binding affinity to the receptor with IC$_{50}$ values in the nM range (21.9 nM and 11.7 nM, respectively), indicating that the increased size and the steric bulk of these conjugates have a modest effect on integrin affinity (Figure 55). As we expected, conjugates **2** and **4** bearing ligand **34** showed no affinity to the integrin receptor with IC$_{50}$ > 10.000 nM, therefore representing a valid negative control for drug-targeting studies (Figure 55).

7.2.4. β-Glucuronidase-catalysed release of Cryptophycin-55 glycinate

The general drug-release mechanism involves the enzymatic hydrolysis of the glycosidic bond from the linker that spontaneously undergoes a self-immolative process with concomitant loss of carbon dioxide and expulsion of the active drug. As proof of concept, the drug-release efficiency was tested in enzymatic cleavage assay by treating the conjugates **1-4** with *E. Coli* β-glucuronidase (200 U/mL) at 37 °C. The enzymatic hydrolysis rate and the release of Cry-55 gly were monitored by HPLC-MS over a period of 90 min. The stability was determined based on the disappearance of the test compound and appearance of the Cry-55 gly as a function of incubation time using the area. As expected, conjugates **1-4** were rapidly cleaved upon incubation with the enzyme (Figure 56). In detail, the enzymatic cleavage of the *para*-substituted β-glucuronide moiety **1-2** generated the metabolite M1 (more than 50% after 15 min) that rapidly underwent 1,6-elimination releasing the active Cry-55 gly payload within 60 min (Figure 56). As shown in the HPLC chromatogram of Figure 56, the presence of other peaks beyond that of Cry-55 is presumably related to the degradation of the metabolite M3 derived from the rearrangement of the linker-ligand system. In contrast, the β-glucuronidase mediated linker cleavage of the *meta*-substituted conjugates **3-4** led to the rapid formation of metabolite M2 (80% after 15 min) but this was not followed by 1,6-elimination (self-immolation step) and the Cry-55 gly was not released over the time (Figure 56). Control experiments indicated that both conjugates were stable in the absence of enzyme demonstrating an efficient linker self-immolative process only in the presence of β-glucuronidase.
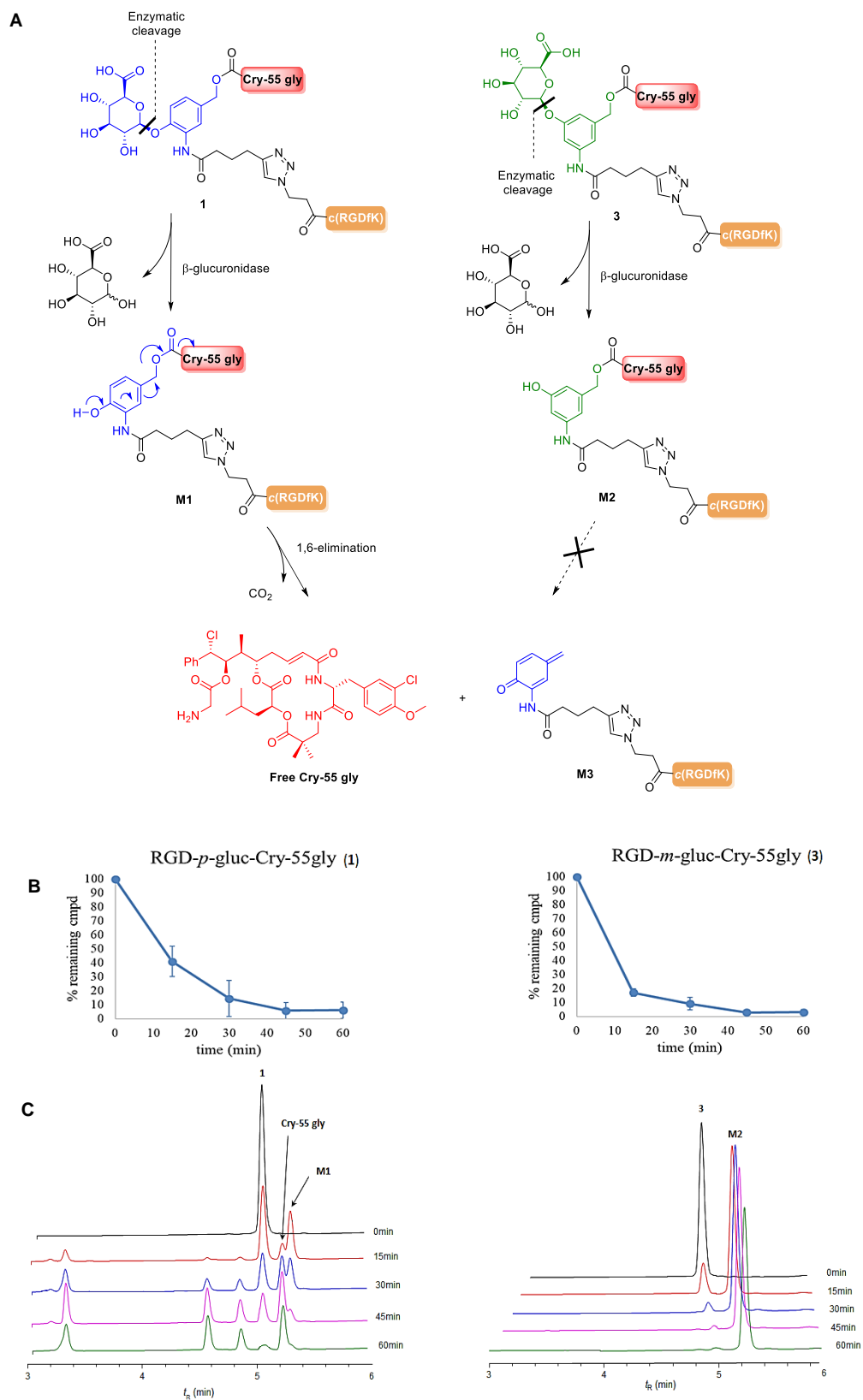
Figure 56. A) β-Glucuronidase-mediated cleavage and self-immolative mechanism of Cry-55 gly release from conjugates **1** and **3**; B) Cleavage assay and stability evaluation of conjugates **1** and **3** upon incubation with β-Glucuronidase enzyme for 90 min; C) HPLC chromatogram.

7.3. Conclusion and perspectives

In summary, we reported the synthesis of novel SMDCs to selectively deliver the highly cytotoxic Cryptophycin-55 glycinate at the tumor site while reducing off-target toxicity. The proposed SMDCs are based on the conjugation of Cry-55 gly payload to the $\alpha_v\beta_3$ integrin-targeting ligand *c*[RGDfK] through a β-glucuronidase-responsive linker. The β-glucuronide-based linker displays favourable features such as high-water solubility, serum stability, and easy drug release within antigen-positive tumor cells. In particular, the high-water solubility may be particularly useful for hydrophobic drugs such as the Cryptophycin derivatives. The generated conjugates **1** and **3** retain high binding affinity towards isolated $\alpha_v\beta_3$ integrin receptor, similarly to the free ligands, while conjugates **2** and **4** showed dramatically lower affinity as expected. The ability to release the active drug strongly depends on the linker type. β-glucuronidase-mediated cleavage studies have proved the effective cleavage of the sensitive glycosidic bond already after 15 min. However, the release of Cry-55 gly was observed only for conjugates **1** and **2** bearing the *para*-β-glucuronide linker in which the metabolite M1 spontaneously undergo 1,6-elimination. On the other hand, enzymatic cleavage of conjugates **3** and **4** with *meta*-β-glucuronide linker lacking the self-immolative step since the release of the metabolite M2 cannot undergo 1,6-elimination. All these results suggest that this new glucuronide prodrug possesses the necessary prerequisites for further *in vitro* and *in vivo* investigation in the course of a tumor targeting development. The translation of the promising biochemical properties to an *in vitro* model of human melanoma cells is currently under investigation.

7.4. Experimental section

General methods

All reactions requiring anhydrous conditions were performed under argon atmosphere. DMF was dried over 4 Å molecular sieves, CH_2Cl_2 was distilled from CaH_2, THF was distilled from sodium/benzophenone. All solvents were distilled freshly before use. All the other chemicals and solvents (HPLC-grade or reagent-grade quality), unless otherwise stated, were purchased from commercial sources and used as received without further purification. DCM, EtOAc, PE and Et_2O used for aqueous work-ups or column chromatography were purchased in technical grade and distilled prior to application. A dual-channel syringe pump (KD scientific Model 200) was used for slow reagent addition. Reactions were monitored by thin layer

chromatography (TLC) using aluminium-backed plates coated with silica gel 60 F_{254} from Merck; visualization was accomplished with UV light and/or staining with potassium permanganate or cerium molybdate solution. Flash column chromatography was performed using silica gel 40–63 μM (230-400 mesh) purchased from Macherey-Nagel. Solvents were removed on a rotational evaporator at 40 °C and appropriately reduced pressure. Solvent residues were removed at RT and 0.001 – 0.1 mbar.

Solid-phase peptide synthesis was performed in polypropylene syringes fitted with a polyethylene porous disc. Solvents and soluble reagents were removed by suction. Washings between deprotection, coupling, and final deprotection steps were carried out with DMF (3 x 1 min) and DCM (3 x 1 min). Reactions and washes during peptide synthesis were performed at 25 °C.

Liquid chromatography (β-glucuronidase cleavage assays):

β-glucuronidase cleavage assay was performed using analytical HPLC (Prominence, Shimadzu LC-20ADXR). A Phenomenex Luna® C18 100 Å (100 mm x 2 mm) 3 μm particle size was used as a column.

Eluent A: H_2O/TFA = 99.9/0.1 and eluent B: ACN/TFA = 99.9/0.1

Injection volume: 20 μL; Flow rate: 650 μL · min^{-1}

0 min	95% A	5% B
5.5 min	5% A	95% B
6 min	5% A	95% B
6.1 min	95% A	5% B
9 min	95% A	5% B

Liquid chromatography - mass spectrometry

LC-MS was conducted using an Agilent 1200 series consisting of an autosampler, degasser, binary pump, column oven, and diode array detector coupled to an Agilent 6220 accurate-mass TOF LC/MS. Column: Phenomenex Luna® C_{18} (100 mm x 2 mm, 3 μm particle size, 100 Å).

Eluent A: H_2O/CH_3CN/HCOOH = 95/5/0.1 and eluent B: H_2O/CH_3CN/HCOOH = 5/95/0.1.

Method A:

Flow rate: 300 μL min^{-1}

0 min	100% A	0% B
10 min	2% A	98% B

11 min	2% A	98% B
11.5 min	100% A	0% B
15 min	100% A	0% B

High-resolution mass spectrometry

High-resolution mass spectra were recorded in an Agilent 6220 accurate-mass TOF LC/MS. Samples were injected through an Agilent 1200 series. Hypersil Gold C_{18} (50 mm x 2.1 mm, 1.9 μm particle size) was used as a column. Same solvents than HPLC-MS were used and a linear gradient from 0 to 98% B over 4 minutes was employed. The mass spectrometer was externally calibrated using Agilent tuning mix prior to measurement.

Semi-preparative and Preparative RP-HPLC

Preparative RP-HPLC was performed on a MERCK-HITACHI unit (controller: D-7000, pump: L7150, detector: L7420, UV-absorption measured at $\lambda = 220$ nm).

Eluent A: $H_2O/CH_3CN/TFA = 95/5/0.1$ and eluent B: $H_2O/CH_3CN/TFA = 5/95/0.1$

Method M1:

Column: Macherey-Nagel Nucleosil C_{18} (250 mm x 10 mm, 7 μm particle size)

Flow rate: 4 mL min^{-1}

0 min	60% A	40% B
30 min	0% A	100% B
40 min	0% A	100% B
45 min	60% A	40% B

Method M2:

Column: Macherey-Nagel Nucleosil C_{18} (250 mm x 10 mm, 7 μm particle size)

Flow rate: 4 mL min^{-1}

0 min	100% A	0% B
2 min	100% A	0% B
35 min	0% A	100% B
40 min	0% A	100% B
45 min	100% A	0% B

Method M3:

Column: Macherey-Nagel Nucleosil C_{18} (250 mm x 21 mm, 10 μm particle size)

Flow rate: 10 mL min^{-1}

0 min	100% A	0% B
2 min	100% A	0% B
35 min	0% A	100% B
40 min	0% A	100% B
45 min	100% A	0% B

Method M4:

Column: Macherey-Nagel Nucleosil C_{18} (250 mm x 21 mm, 10 μm particle size)

Flow rate: 10 mL min^{-1}

0 min	100% A	0% B
2 min	100% A	0% B
45 min	0% A	100% B
50 min	0% A	100% B
55 min	100% A	0% B

NMR spectroscopy

NMR spectra were recorded on a Bruker Avance 500HD (^{1}H: 500 MHz, ^{13}C: 126 MHz) or Avance 600 (^{1}H: 600 MHz) at 298 K. Chemical shifts are reported in ppm (δ) and referenced to residual nondeuterated solvent signal as internal standard (CDCl$_3$: ^{1}H: 7.26 ppm, ^{13}C: 77.16 ppm; (CD$_3$)$_2$CO: ^{1}H: 2.05 ppm, ^{13}C: 29.84, 206.26 ppm; (CD$_3$)$_2$SO: ^{1}H: 2.50, ^{13}C: 39.52 ppm). Coupling constants (*J*) are reported in Hz with the following abbreviations used to indicate splitting: s = singlet, d = doublet, t = triplet, m = multiplet, p = pentet, br = broad signal.

β-glucuronidase cleavage assay

Conjugates **1-4** (stock solution 10 mM in DMSO) were diluted to 0.1 mM in 0.02 M phosphate buffer, pH = 7.0 and preincubated at 37 °C for 5 min. *Escherichia coli* β-glucuronidase (Type IX-A, # G7396-25kU, Sigma Aldrich, 200 U/mL) was added and the mixture was incubated at 37 °C for 60 min. At each sampling time (0, 15, 30, 45, 60 and 90 min) an aliquot of 50 μL was transferred into a HPLC vial and the reaction was stopped with 50 μL of ACN containing 0.1% TFA. The stability was determined based on the disappearance of the test compound as a function of incubation time using area.

Integrin binding assay

An ELISA-like assay using isolated integrins was performed to determine activity. Cilengitide (α$_v$β$_3$ 0.54 nM) was used as internal reference. All wells of flat-bottom 96-well Immuno Plates

(BRAND) were coated overnight at 4 °C with 100 µL protein 1.0 µg/mL human vitronectin (R&D) in carbonate buffer (15 mM Na_2CO_3, 35 mM $NaHCO_3$, pH 9.6). Each well was then washed with PBS-T-buffer (phosphate-buffered saline/Tween20, 137 mM NaCl, 2.7 mM KCl, 10 mM Na_2HPO_4, 2 mM KH_2PO_4, 0.01% Tween20, pH 7.4; 3 x 200 µL) and blocked for 1 h at room temperature with TS-B-buffer (Tris-saline/BSA buffer, 150 µL/well, 20 mM Tris-HCl, 150 mM NaCl, 1 mM $CaCl_2$, 1 mM $MgCl_2$, 1 mM $MnCl_2$, pH 7.5, 1% BSA). A dilution series of the compound and internal standard were prepared in TS-B-buffer. After washing the assay plate with PBS-T (3×200 µL), 50 µL of the dilution series were transferred to each well, for negative control 100 µL TS-B-buffer and for positive control 50 µL TS-B-buffer was used. 50 µL of human $\alpha_v\beta_3$ integrin (2.0 µg/mL, R&D) in TS-B-buffer were transferred to wells (except wells containing the negative control) and incubated for 1 h at RT. After washing the plates (3×200 µL) with PBS-T buffer, 100 µL primary antibody mouse anti-human CD51/61 (2.0 µg/mL BD Bioscience) was added to all wells and incubated for 1 h at RT. The plate was washed (3×200 µL) with PBS-T buffer and 100 µL of secondary antibody anti-mouse IgG-POD goat (1.0 µg/mL, Sigma Aldrich) was added to all wells and incubated for 1 h at RT. The plate was washed (3×200 µL) with PBS-T buffer and 50 µL SeramunBlau (Seramun Diagnostic GmbH, Heidesee) was added to all wells. The development was stopped with 3 M H_2SO_4 (50 µL/well) when a blue color gradient was visible (~1 min). The absorbance was measured with a plate reader at 450 nM (Tecan, Infinite M200). The resulting curves were analyzed with OriginPro 2017G with the inflection point describing the IC_{50} value. Each compound was tested in triplicates and referenced to the internal standard.

Synthesis of compound 7:
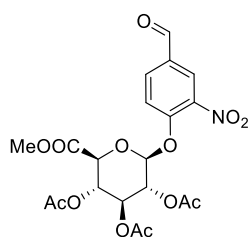
To a stirred solution of Acetobromo-α-D-glucuronic acid methylester **6** (3 g, 7.55 mmol) in anhydrous CH_3CN (75 mL) was added 4-hydroxy-3-nitrobenzaldehyde **5** (1.9 g, 11.33 mmol) followed by addition of Ag_2O (8.75 g, 37.75 mmol). The resulting mixture was stirred under darkness and argon atmosphere for 4 h at RT. The mixture was then filtered over a Celite pad to remove the solid, washed with an excess of CH_3CN and concentrated *in vacuo*. The residue

was purified by column chromatography over silica gel (gradient eluent PE/EtOAc from 70/30 to 50/50) to give **7** (3.4 g, 7.04 mmol, 93%) as a white solid. Rf = 0.28 (PE/EtOAc: 50/50). ^{1}H-NMR (500 MHz, CDCl$_3$) δ: 9.98 (s, 1H, CHO), 8.32 (d, J = 2.0 Hz, 1H, ArH), 8.09 (dd, J = 8.6, 2.1 Hz, 1H, ArH), 7.50 (d, J = 8.6 Hz, 1H, ArH), 5.45 – 5.41 (m, 2H, H-1, H-3), 5.36 – 5.26 (m, 2H, H-2, H-4), 4.32 (d, J = 8.4 Hz, 1H, H-5), 3.71 (s, 3H, COOCH$_3$), 2.13 (s, 3H, OAc), 2.09 (s, 3H, OAc), 2.08 (s, 3H, OAc).). ESI-MS: m/z calcd for $[C_{20}H_{25}N_2O_{13}]^+$: 501.10, found: 501.14 $[M + NH_4]^+$.

Synthesis of compound 8:
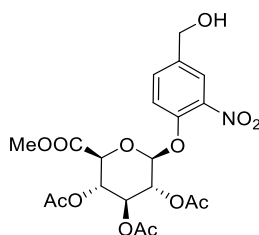
A stirred suspension of **7** (3.4 g, 7.04 mmol) with 2 g of silica gel in 100 mL of anhydrous CHCl$_3$/Isopropanol (5:1) was cooled to 0 °C and then NaBH$_4$ (399 mg, 10.55 mmol) was added. The resulting mixture was stirred at 0 °C for 45 min under argon atmosphere. The mixture was then filtered over a Celite pad to remove silica gel and washed with CHCl$_3$. The organic layer was poured into cold water (100 mL), after their separation the organic layer was then washed with brine (2 x 100 mL), dried over MgSO$_4$ and evaporated *in vacuo* to afford **8** (3.25 g, 6.69 mmol, 95%) as a white solid. Rf = 0.11 (PE/EtOAc: 50/50). ^{1}H-NMR (500 MHz, CDCl$_3$) δ: 7.81 (d, J = 2.2 Hz, 1H, ArH), 7.54 (dd, J = 8.6, 2.2 Hz, 1H, ArH), 7.37 (d, J = 8.6 Hz, 1H, ArH), 5.40 – 5.26 (m, 3H, H-2, H-3, H-4), 5.19 (d, J = 6.8 Hz, 1H, H-1), 4.73 (d, J = 5.8 Hz, 2H, CH$_2$), 4.20 (d, J = 8.7 Hz, 1H, H-5), 3.75 (s, 3H, COOCH$_3$), 2.13 (s, 3H, OAc), 2.06 (s, 3H, OAc), 2,05 (s, 3H, OAc), 1.86 (t, J = 5.8 Hz, 1H, OH). ESI-MS: m/z calcd for $[C_{20}H_{27}N_2O_{13}]^+$: 503.15, found: 503.15 $[M + NH_4]^+$.

Synthesis of compound 9:
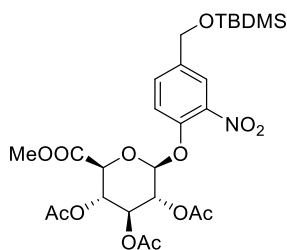
To a stirred solution of *tert*-Butyldimethylsilyl chloride (1 g, 6.64 mmol) and imidazole (452 mg, 6.64 mmol) in anhydrous CH_2Cl_2 (10 mL) cooled to 0 °C was added a solution of **8** (2.15 g, 4.43 mmol) in anhydrous CH_2Cl_2 (35 mL). The mixture was stirred overnight at RT under argon. The reaction was quenched by addition of water (40 mL) and extracted with CH_2Cl_2 (3 x 40 mL). The combined organic layers were dried over $MgSO_4$, filtered and concentrated under reduced pressure. The resulting crude compound was purified by column chromatography over silica gel (gradient eluent PE/EtOAc from 80/20 to 60/40) to afford **9** (2.46 g, 4.10 mmol, 93%) as a white powder. Rf = 0.26 (PE/EtOAc: 70/30). ^{1}H-NMR (500 MHz, $CDCl_3$) δ: 7.75 (s, 1H, ArH), 7.48 (d, J = 8.6 Hz, 1H, ArH), 7.34 (d, J = 8.6 Hz, 1H, ArH), 5.39 – 5.26 (m, 3H, H-2, H-3, H-4), 5.17 (d, J = 6.6 Hz, 1H, H-1), 4.72 (s, 2H, CH_2), 4.19 (d, J = 8.9 Hz, 1H, H-5), 3.75 (s, 3H, $COOCH_3$), 2.12 (s, 3H, OAc), 2,06 (s, 3H, OAc), 2.05 (s, 3H, OAc), 0.94 (s, 9H, -Si-C(CH$_3$)$_3$), 0.11 (s, 6H, -Si(CH$_3$)$_2$). ^{13}C NMR (126 MHz, $CDCl_3$) δ: 170.2, 169.5, 169.5, 166.9, 147.9, 141.5, 138.3, 131.2, 122.6, 120.4, 100.2, 72.8, 71.4, 70.4, 69.0, 63.5, 53.2, 26.0 (3C), 20.7, 20.7, 20.7, 18.5, -5.2 (2C). ESI-MS: *m/z* calcd for $[C_{20}H_{27}N_2O_{13}]^+$: 503.15, found: 503.14 $[M - C_6H_{14}Si + NH_4]^+$.

Synthesis of compound 10:
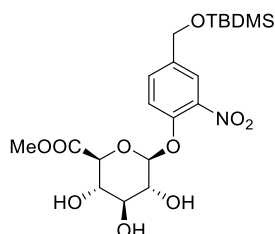
To a stirred solution of **9** (2.46 g, 4.10 mmol) in anhydrous MeOH (100 mL) cooled to 0 °C were added dropwise a solution of MeONa 30% w/v in MeOH (759 µL, 4.10 mmol). The resulting mixture was stirred at 0 °C for 100 min under argon. The reaction was quenched with glacial acetic acid (234 µL, 4.10 mmol) and the solvent was removed under reduced pressure. Crude material was purified by column chromatography over silica gel (eluent CH_2Cl_2/MeOH: 95/5) to afford **10** (1.63 g, 3.44 mmol, 84%) as a colorless oil. Rf = 0.14 (CH_2Cl_2/MeOH: 95/5). ^{1}H-NMR (500 MHz, $CDCl_3$) δ: 7.81 (d, J = 2.1 Hz, 1H, ArH), 7.52 (dd, J = 8.7, 2.1 Hz, 1H, ArH), 7.35 (d, J = 8.5 Hz, 1H, ArH), 4.95 (d, J = 7.2 Hz, 1H, H-1), 4.72 (s, 2H, CH_2), 4.06 (d, J = 9.7 Hz, 1H, H-5), 3.92 (dd, J = 9.1, 9.1 Hz, 1H, H-3), 3.85 (s, 3H, $COOCH_3$), 3.83 – 3.72 (m, 2H, H-2, H-4), 3.56 (br s, 1H, OH), 3.50 (br s, 1H, OH), 3.41 (br s, 1H, OH), 0.94 (s, 9H, -Si-C(CH$_3$)$_3$), 0.11 (s, 6H, -Si(CH$_3$)$_2$). ^{13}C NMR (126 MHz, $CDCl_3$) δ: 169.2, 149.2, 140.4,

137.7, 132.1, 123.1, 119.1, 103.2, 75.0, 74.6, 73.0, 71.1, 63.5, 53.2, 26.0 (3C), 18.5, -5.2 (2C). ESI-MS: *m/z* calcd for $[C_{14}H_{21}N_2O_{10}]^+$: 377.12 , found: 377.11 $[M - C_6H_{14}Si + NH_4]^+$.

Synthesis of compound 11:
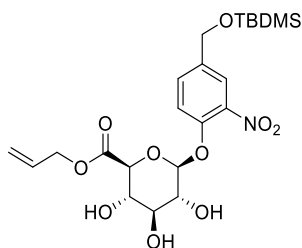
Compound **10** (1.63 g, 3.44 mmol) was dissolved in anhydrous allyl alcohol (40 mL) and the solution was cooled to 0 °C. Then, a solution of sodium allylate 0.126 M (5.5 mL, 0.69 mmol) was added dropwise and the mixture was stirred at RT for 40 min under argon atmosphere. The reaction was neutralized with glacial acetic acid (39 μL, 0.69 mmol) and after removal of solvent under reduced pressure, the crude material was purified by column chromatography over silica gel (eluent CH_2Cl_2/MeOH: 95/5) to afford **11** (1.43 g, 2.87 mmol, 83%) as a yellow oil. *Rf* = 0.35 (CH_2Cl_2/MeOH: 90/10). ^{1}H-NMR (500 MHz, $CDCl_3$) δ: 7.79 (s, 1H, ArH), 7.49 (dd, *J* = 8.8, 2.2 Hz, 1H, ArH), 7.35 (d, *J* = 8.6 Hz, 1H, ArH), 5.98 − 5.87 (m, 1H, -C$\underline{H}$=CH$_2$), 5.36 (d, *J* = 17.2 Hz, 1H, -CH=CH^{cis}$\underline{H}^{trans}$), 5.26 (d, *J* = 10.5 Hz, 1H, -CH=C$\underline{H}^{cis}$H^{trans}), 4.97 (d, *J* = 7.1 Hz, 1H, H-1), 4.75 − 4.69 (m, 4H, -OC$\underline{H}_2$-CH=CH$_2$, CH$_2$), 4.08 (d, *J* = 9.7 Hz, 1H, H-5), 3.94 (dd, *J* = 9.0, 9.0 Hz, 1H, H-3), 3.90 − 3.73 (m, 5H, H-2, H-4, OH (x3)), 0.94 (s, 9H, -Si-C(CH$_3$)$_3$), 0.10 (s, 6H, -Si(CH$_3$)$_2$). ^{13}C NMR (126 MHz, $CDCl_3$) δ: 168.4, 149.1, 140.4, 137.5, 132.0, 131.2, 123.0, 119.4, 119.2, 103.0, 75.0, 74.7, 73.0, 71.0, 66.7, 63.5, 26.0 (3C), 18.5, -5.2 (2C). ESI-MS: *m/z* calcd for $[C_{16}H_{23}N_2O_{10}]^+$: 403.13, found: 403.13 $[M − C_6H_{14}Si + NH_4]^+$.

Synthesis of compound 12:
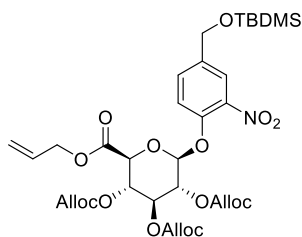
To a solution of **11** (1.43 g, 2.87 mmol) in anhydrous pyridine (14 mL) cooled at 0 °C was slowly added dropwise allyl chloroformate (9.15 mL, 86.11 mmol) (Note: strong gas release).

The mixture was stirred at RT for 72 h under argon atmosphere. The reaction was diluted with CH$_2$Cl$_2$ (20 mL) and quenched with HCl 1N (until pH 5-6). The aqueous layer was then extracted with CH$_2$Cl$_2$ (100 mL). The combined organic layers were dried over MgSO$_4$, filtered and concentrated under reduced pressure. The resulting crude material was purified by column chromatography over silica gel (eluent PE/EtOAc: 80/20) to give **12** (1.77 g, 2.35 mmol, 82%) as a colorless oil. Rf = 0.28 (PE/EtOAc: 80/20). ^{1}H-NMR (500 MHz, CDCl$_3$) δ: 7.76 (s, 1H, ArH), 7.47 (d, J = 8.5 Hz, 1H, ArH), 7.32 (d, J = 8.6 Hz, 1H, ArH), 6.01 – 5.81 (m, 4H, -CH=CH$_2$ (x4)), 5.40 – 5.23 (m, 12H, H-1, H-2, H-3, H-4, -CH=CH$_2$ (x4)), 4.77 – 4.60 (m, 10H, -OCH$_2$-CH=CH$_2$ (x4), CH$_2$), 4.30 (d, J = 8.6 Hz, 1H, H-5), 0.94 (s, 9H, -Si-C(CH$_3$)$_3$), 0.10 (s, 6H, -Si(CH$_3$)$_2$). ^{13}C NMR (126 MHz, CDCl$_3$) δ: 165.8, 154.1, 153.6, 148.0, 141.1, 138.2, 131.4, 131.3, 131.2, 131.1, 131.0, 122.8, 119.6, 119.5, 119.4, 119.4, 119.2, 100.0, 75.2, 74.1, 72.5, 72.4, 69.6, 69.4, 69.3, 67.0, 63.5, 26.0 (3C), 18.5, -5.2 (2C). ESI-MS: m/z calcd for [C$_{28}$H$_{35}$N$_2$O$_{16}$]$^+$: 655.20, found: 655.19 [M – C$_6$H$_{14}$Si + NH$_4$]$^+$.

Synthesis of compound 13:
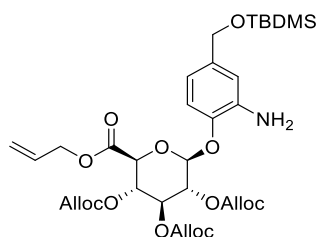
Compound **12** (1.77 g, 2.35 mmol) was dissolved in 20 mL of anhydrous MeOH/AcOH mixture (10:1, v/v). Activated zinc powder (3.08 g, 47.09 mmol), was then added and the resulting mixture was vigorously stirred for 30 min at RT under argon atmosphere. The reaction was monitored by TLC until completion (30 min to 1h). The reaction mixture was then filtered and the resulting solid washed with excess MeOH. The filtrate was azeotroped to dryness with toluene *in vacuo*. The crude material was purified by column chromatography over silica gel (gradient eluent PE/EtOAc from 90/10 to 80/20) to give **13** (1.5 g, 2.07 mmol, 88%) as a yellow oil. Rf = 0.26 (PE/EtOAc: 80/20). ^{1}H NMR (500 MHz, CDCl$_3$) δ: 6.90 (d, J = 8.2 Hz, 1H, ArH), 6.68 (s, 1H, ArH), 6.60 (d, J = 8.3 Hz, 1H, ArH), 5.96 – 5.81 (m, 4H, -CH=CH$_2$ (x4)), 5.38 – 5.13 (m, 11H, H-2, H-3, H-4, -CH=CH$_2$ (x4)), 5.05 (d, J = 7.8 Hz, 1H, H-1), 4.69 – 4.58 (m, 10H, -OCH$_2$-CH=CH$_2$ (x4), CH$_2$), 4.21 (d, J = 9.1 Hz, 1H, H-5), 0.93 (s, 9H, -Si-C(CH$_3$)$_3$), 0.08 (s, 6H, -Si(CH$_3$)$_2$). ^{13}C NMR (126 MHz, CDCl$_3$) δ: 165.8, 154.0, 153.9, 153.5, 143.0, 138.1, 137.8, 131.1, 131.1, 131.0, 131.0, 119.3, 119.2, 119.2, 119.0, 117.3, 115.8, 113.8, 100.6,

75.4, 74.6, 72.8, 72.1, 69.2, 69.2, 69.1, 66.8, 64.6, 26.0 (3C), 18.5, -5.2 (2C). ESI-MS: *m/z* calcd for $[C_{28}H_{37}N_2O_{14}]^+$ 607.19, found 607.29 $[M - C_6H_{14}Si + NH_4]^+$.

Synthesis of compound 14:
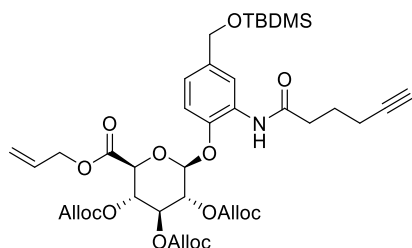
To a stirred solution of **13** (565 mg, 0.78 mmol) in anhydrous CH_2Cl_2 (10 mL) was added 5-hexynoic acid (105 μL, 0.94 mmol) followed by addition of EEDQ (387 mg, 1.57 mmol). The mixture was stirred for 24 h at RT under darkness and argon atmosphere. After removing the solvent under reduced pressure, the crude material was purified by column chromatography over silica gel (gradient eluent PE/EtOAc from 90/10 to 85/15) to give **14** (588 mg, 0.72 mmol, 92%) as a colorless oil. *Rf* = 0.44 (PE/EtOAc: 70/30). ^1H NMR (500 MHz, $CDCl_3$) δ: 8.31 (s, 1H, ArH), 8.01 (s, 1H, ArNH), 7.06 (d, *J* = 8.5 Hz, 1H, ArH), 6.95 (d, *J* = 8.4 Hz, 1H, ArH), 5.96 – 5.80 (m, 4H, -C**H**=CH$_2$ (x4)), 5.39 – 5.11 (m, 12H, H-1, H-2, H-3, H-4, -CH=C**H$_2$** (x4)), 4.70 – 4.57 (m, 10H, -OC**H$_2$**-CH=CH$_2$ (x4), CH$_2$), 4.26 (d, *J* = 9.3 Hz, 1H, H-5), 2.56 (t, *J* = 7.4 Hz, 2H, CO-C**H$_2$**-CH$_2$-CH$_2$-C≡CH), 2.33 (td, *J* = 7.0, 2.5 Hz, 2H, -C**H$_2$**-C≡CH), 1.99 (t, *J* = 2.7 Hz, 1H, -C≡CH), 1.95 (p, *J* = 7.1 Hz, 2H, -CH$_2$-C**H$_2$**-CH$_2$-C≡CH), 0.93 (s, 9H, -Si-C(CH$_3$)$_3$), 0.09 (s, 6H, -Si(CH$_3$)$_2$). ^{13}C NMR (126 MHz, $CDCl_3$) δ: 171.0, 165.8, 154.3, 154.1, 153.7, 143.8, 138.0, 131.1, 131.0, 131.0, 130.9, 121.4, 119.6, 119.5 (2C), 119.3, 118.5, 115.5, 100.0, 83.8, 75.1, 74.7, 72.8, 72.3, 69.5, 69.5, 69.4, 69.3, 67.1, 64.8, 36.2, 26.1 (3C), 24.3, 18.6, 18.1, -5.1 (2C). ESI-MS: *m/z* calcd for $[C_{34}H_{40}NO_{15}]^+$: 702.24, found: 702.25 $[M - C_6H_{14}Si + H]^+$.

Synthesis of compound 15:
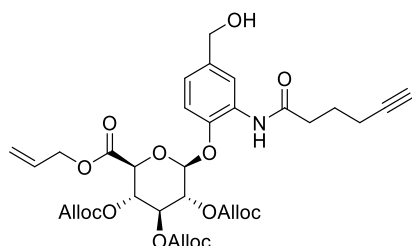
HF/Pyridine 70% (1.24 mL) was added dropwise to a solution of **14** (265 mg, 0.33 mmol) in anhydrous THF (5 mL) cooled at 0 °C. The resulting mixture was stirred for 45 min at RT under argon atmosphere. Then, the reaction was quenched with saturated solution of NaHCO₃ (6 mL) and extracted with EtOAc (3 x 20 mL). The combined organic layers were dried over MgSO₄, filtered and concentrated under reduced pressure. The resulting crude material was purified by column chromatography over silica gel (eluent PE/EtOAc: 60/40) to give **15** (214 mg, 0.32 mmol, 93%) as a colorless oil. Rf = 0.12 (PE/EtOAc: 60/40). ^{1}H NMR (500 MHz, CDCl₃) δ: 8.39 (s, 1H, ArH), 8.04 (s, 1H, ArNH), 7.06 (d, J = 8.4 Hz, 1H, ArH), 6.97 (d, J = 8.3 Hz, 1H, ArH), 5.97 – 5.79 (m, 4H, -C$\underline{H}$=CH₂ (x4)), 5.39 – 5.14 (m, 12H, H-1, H-2, H-3, H-4, -CH=C$\underline{H_2}$ (x4)), 4.72 – 4.56 (m, 10H, -OC$\underline{H_2}$-CH=CH₂ (x4), CH₂), 4.28 (d, J = 9.4 Hz, 1H, H-5), 2.57 (t, J = 7.3 Hz, 2H, CO-C$\underline{H_2}$-CH₂-CH₂-C≡CH), 2.36 – 2.29 (m, 2H, -CH₂-C$\underline{H_2}$-C≡CH), 2.00 (br s, 1H, -C≡CH), 1.95 (p, J = 7.0 Hz, 2H, -CH₂-C$\underline{H_2}$-CH₂-C≡CH). ^{13}C NMR (126 MHz, CDCl₃) δ: 171.2, 165.7, 154.3, 154.1, 153.7, 144.2, 137.5, 131.1, 131.0, 130.9, 130.9, 129.5, 122.4, 119.6, 119.6, 119.5 (2C), 119.4, 115.6, 99.8, 83.7, 75.0, 74.7, 72.7, 72.3, 69.5, 69.5, 69.4, 69.3, 67.1, 65.1, 36.1, 24.2, 18.1. ESI-MS: m/z calcd for [C₃₄H₄₀NO₁₅]⁺ 701.23, found 701.26 [M+H]⁺.

Synthesis of compound 16:
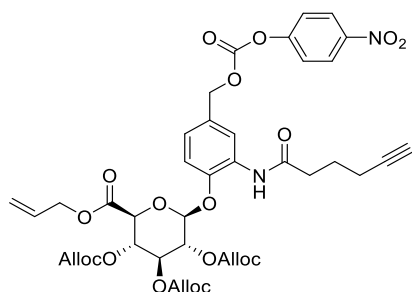
15 (188 mg, 0.27 mmol) was dissolved in anhydrous CH₂Cl₂ (2 mL) then anhydrous pyridine (54 µL, 0.67 mmol) was added at 0 °C followed by a solution of 4-nitrophenyl chloroformate (108 mg, 0.54 mmol) in anhydrous CH₂Cl₂ (3 mL). The mixture was stirred at RT under argon atmosphere for 2 h, quenched with saturated solution of NaHCO₃ (6 mL) and extracted with CH₂Cl₂ (3 x 20 mL). The combined organic layers were dried over MgSO₄, filtered and concentrated under reduced pressure. The crude oil was purified by column chromatography over silica gel (eluent PE/EtOAc: 70/30) to yield **16** (230 mg, 0.27 mmol, 99%) as a colorless oil. Rf = 0.23 (PE/EtOAc: 70/30). ^{1}H NMR (500 MHz, CDCl₃) δ: 8.56 (d, J = 1.6 Hz, 1H, ArH), 8.27 (d, J = 9.0 Hz, 2H, ArH), 8.07 (s, 1H, ArNH), 7.38 (d, J = 9.0 Hz, 2H, ArH), 7.10 (dd, J = 8.4, 2.0 Hz, 1H, ArH), 6.99 (d, J = 8.4 Hz, 1H, ArH), 5.97 – 5.79 (m, 4H, -C$\underline{H}$=CH₂ (x4)), 5.40

– 5.16 (m, 14H, H-1, H-2, H-3, H-4, -CH=C$\underline{H}_2$ (x4), CH$_2$), 4.73 – 4.58 (m, 8H, -OC$\underline{H}_2$-CH=CH$_2$ (x4)), 4.30 (d, $J = 9.3$ Hz, 1H, H-5), 2.59 (t, $J = 7.4$ Hz, 2H, CO-C$\underline{H}_2$-CH$_2$-CH$_2$-C≡CH), 2.38 – 2.29 (m, 2H, -CH$_2$-C$\underline{H}_2$-C≡CH), 2.00 (t, $J = 2.6$ Hz, 1H, -C≡CH), 1.96 (p, $J = 7.0$ Hz, 2H, -CH$_2$-C$\underline{H}_2$-CH$_2$-C≡CH). ^{13}C NMR (126 MHz, CDCl$_3$) δ: 171.3, 165.7, 155.7, 154.4, 154.1, 153.7, 152.5, 145.5, 145.0, 131.1, 131.0, 130.9, 130.8, 130.5, 129.7, 125.4 (2C), 124.1, 122.0 (2C), 121.1, 119.7, 119.6, 119.6, 119.4, 115.1, 99.4, 83.6, 74.8, 74.6, 72.7, 72.3, 70.8, 69.6, 69.5, 69.4, 69.4, 67.2, 36.1, 24.1, 18.1. ESI-MS: m/z calcd for [C$_{41}$H$_{43}$N$_2$O$_{19}$]$^+$: 867.25, found: 867.25 [M+H]$^+$.

Synthesis of compound 17:
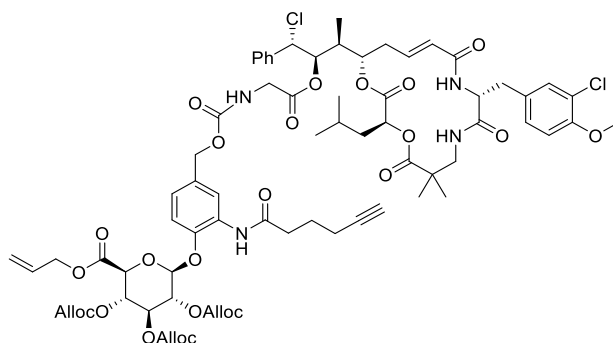
Cryptophycin-55 glycinate-trifluoroacetate salt (10 mg, 0.011 mmol), **16** (12 mg, 0.014 mmol), and DIPEA (6 μL, 0.034 mmol) were placed under argon atmosphere and dissolved in anhydrous DMF (0.5 mL). The solution was stirred for 4 h at RT and the reaction was monitored by HPLC-MS using Method A. The crude material was purified by reverse-phase (RP)-HPLC using Method M1 to afford the conjugate **17** (13 mg, 0.009 mmol, 77%) as a white powder after freeze-drying. HPLC-MS: $t_r = 12.4$ min, 83% purity ($\lambda = 220$ nm), m/z calcd for [C$_{73}$H$_{88}$Cl$_2$N$_4$O$_{25}$]$^{2+}$: 745.26, found: 745.24 [M + 2H]$^{2+}$.

Synthesis of compound 18:
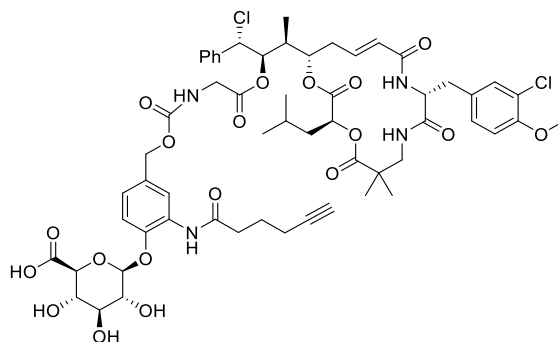
17 (13 mg, 0.009 mmol) and Pd(PPh$_3$)$_4$ 10% mol (1 mg, 0.9 μmol) were placed under argon atmosphere and dissolved in anhydrous and degassed CH$_2$Cl$_2$ (0.5 mL). Then, morpholine (4 drops) was added and the solution was stirred for 1 h at RT. The reaction was monitored by HPLC-MS using Method A. The solvent was removed under reduced pressure keeping the water bath at RT, and the crude material was purified by RP-HPLC using Method M2 to afford the deprotected conjugate **18** (6.89 mg, 0.006 mmol, 66%) as a white powder after freeze-drying. HPLC-MS: t_r = 10.4 min, > 99% purity (λ = 220 nm), *m/z* calcd for [C$_{58}$H$_{71}$Cl$_2$N$_4$O$_{19}$]$^+$: 1197.40, found: 1197.37 [M + H]$^+$.

Synthesis of compound 1:

C$_{88}$H$_{114}$Cl$_2$N$_{16}$O$_{27}$
Exact Mass: 1896,7416
MW: 1898,8650
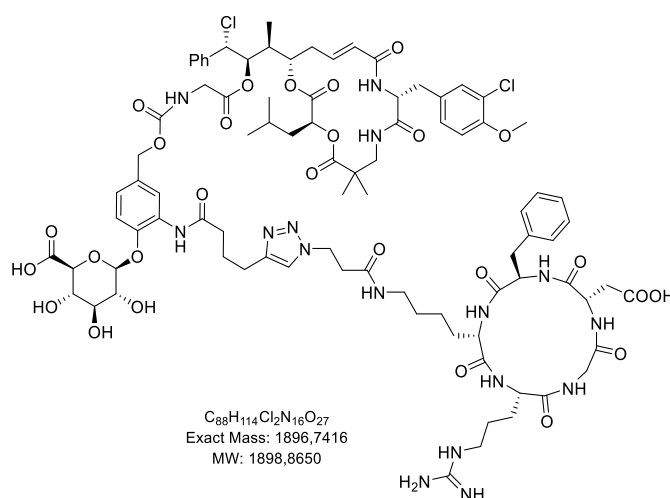
18 (3.5 mg, 2.87 μmol), **33** (2.21 mg, 3.16 μmol), CuSO$_4$ · 5H$_2$O (0.4 mg, 1.44 μmol), and sodium ascorbate (0.34 mg, 1.72 μmol) were placed under argon atmosphere and dissolved in a mixture of anhydrous DMF/H$_2$O (200 μL, 1:1) previously degassed with argon flow. The solution was stirred at 35 °C for 24 h. The reaction progress was monitored by HPLC-MS. The crude was purified by RP-HPLC using Method M2 to afford the final compound **1** (4.57 mg, 2.41 μmol, 84%) as a white powder after freeze-drying. **HPLC-MS:** t_r = 7.9 min, > 99% purity (λ = 220 nm), *m/z* calcd for [C$_{88}$H$_{115}$Cl$_2$N$_{16}$O$_{27}$]$^+$: 1897.75, found: 1897.72 [M + H]$^+$; *m/z* calcd for [C$_{88}$H$_{116}$Cl$_2$N$_{16}$O$_{27}$]$^{2+}$: 949.38, found: 949.36 [M + 2H]$^{2+}$. **HRMS (ESI-MS):** *m/z* calcd for [C$_{88}$H$_{116}$Cl$_2$N$_{16}$O$_{27}$]$^{2+}$: 949.3781, found: 949.3824 [M + 2H]$^{2+}$.

Synthesis of compound 2:

C$_{89}$H$_{116}$Cl$_2$N$_{16}$O$_{27}$
Exact Mass: 1910,7573
MW: 1912,8920
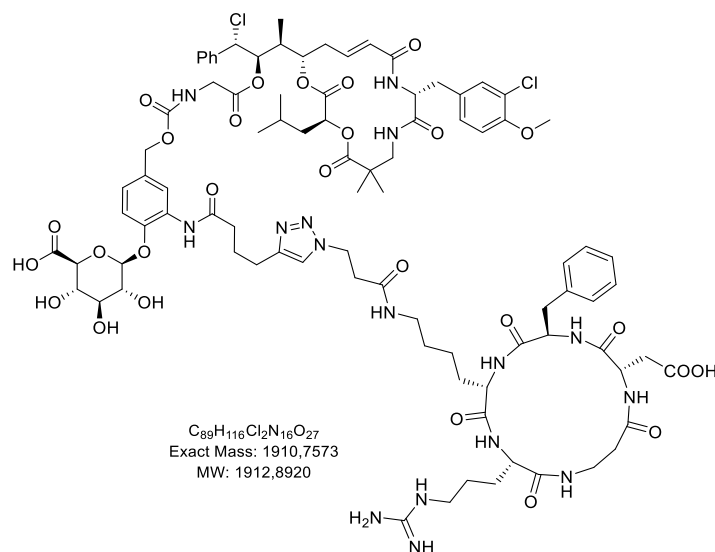
As described above, **18** (2.5 mg, 2.08 μmol), **34** (1.64 mg, 2.29 μmol), CuSO$_4$ · 5H$_2$O (0.26 mg, 1.04 μmol), and sodium ascorbate (0.25 mg, 1.25 μmol) were placed under argon atmosphere and dissolved in a mixture of anhydrous DMF/H$_2$O (200 μL, 1:1) previously degassed with argon flow. The solution was stirred at 35 °C for 24 h and monitored by HPLC-MS. The crude was purified by RP-HPLC using Method M2 to afford the final compound **2** (3 mg, 1.57 μmol, 75%) as a white powder after freeze-drying. **HPLC-MS:** t_r = 7.8 min, > 99% purity (λ = 220 nm), *m/z* calcd for [C$_{89}$H$_{117}$Cl$_2$N$_{16}$O$_{27}$]$^+$: 1911.76, found: 1911.73 [M + H]$^+$; *m/z* calcd for [C$_{89}$H$_{118}$Cl$_2$N$_{16}$O$_{27}$]$^{2+}$: 956.39, found: 956.37 [M + 2H]$^{2+}$. **HRMS (ESI-MS):** *m/z* calcd for [C$_{89}$H$_{118}$Cl$_2$N$_{16}$O$_{27}$]$^{2+}$: 956.3859, found: 956.3872 [M + 2H]$^{2+}$.

Synthesis of compound 20:
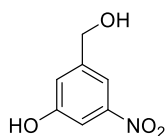
In a flame-dried round bottom flask 3-hydroxy-5-nitrobenzoic acid **19** (1.1 g, 6.01 mmol) was dissolved in anhydrous THF (20 mL) and cooled to 0 °C. Then, a solution of BH$_3$-THF 1.0 M (30 mL, 30.03 mmol) was added dropwise. The mixture was stirred under argon atmosphere at 0 °C for 30 min and at RT overnight. The mixture was cooled back to 0 °C and quenched by dropwise addition of MeOH. Solvent was concentrated under reduce pressure and the resulting residue was diluted with EtOAc (200 mL), washed with brine (100 mL), then dried over MgSO$_4$, filtered and evaporated under reduced pressure. The crude material was purified by

column chromatography over silica gel (eluent PE/EtOAc: 50/50) to give **20** (958 mg, 5.66 mmol, 94%) as a yellow solid. Rf = 0.29 (PE/EtOAc: 50/50). ^{1}H-NMR (500 MHz, (CD$_3$)$_2$CO) δ: 9.20 (br s, 1H, ArOH), 7.74 (s, 1H, ArH), 7.53 (s, 1H, ArH), 7.28 (s, 1H, ArH), 4.71 (s, 2H, CH$_2$), 4.54 (br s, 1H, BnOH). ESI-MS: m/z calcd for [C$_7$H$_8$NO$_4$]$^+$: 170.04, found: 170.21 [M + H]$^+$.

Synthesis of compound 21:
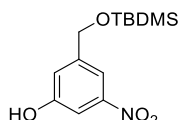
Imidazole (598 mg, 8.78 mmol) was added to a stirred solution of **20** (990 mg, 5.85 mmol) in anhydrous THF (30 mL) cooled to 0 °C. Then, a solution of *tert*-Butyldimethylsilyl chloride (1.32 g, 8.78 mmol) in anhydrous THF (20 mL) was added dropwise and the mixture stirred at 0 °C for 2 h under argon atmosphere. After 2.5 h, the reaction was quenched with H$_2$O (30 mL) and extracted with EtOAc (3 x 30 mL), dried over MgSO$_4$, filtered and evaporated under reduced pressure. The crude material was purified by column chromatography over silica gel (gradient eluent PE/EtOAc from 90/10 to 50/50) to yield **21** (1 g, 3.55 mmol, 61%) as a yellow solid. Rf = 0.32 (PE/EtOAc: 80/20). ^{1}H NMR (500 MHz, CDCl$_3$) δ: 7.75 (s, 1H, ArH), 7.55 (s, 1H, ArH), 7.17 (s, 1H, ArH), 5.48 (s, 1H, ArOH), 4.76 (s, 2H, CH$_2$), 0.96 (s, 9H, -Si-C(CH$_3$)$_3$), 0.13 (s, 6H, -Si(CH$_3$)$_2$). ^{13}C NMR (126 MHz, CDCl$_3$) δ: 156.3, 149.3, 145.3, 119.2, 113.4, 109.1, 64.0, 26.0 (3C), 18.5, -5.2 (2C). ESI-MS: m/z calcd for [C$_7$H$_8$NO$_4$]$^+$: 170.04, found: 170.04 [M – C$_6$H$_{14}$Si + H]$^+$.

Synthesis of compound 22:
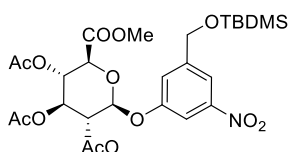
To a stirred solution of Acetobromo-α-D-glucuronic acid methylester **6** (1.15 g, 2.89 mmol) in anhydrous CH$_3$CN (15 mL) was added **21** (1.23 g, 4.34 mmol) dissolved in anhydrous CH$_3$CN (15 mL) followed by addition of Ag$_2$O (3.35 g, 14.45 mmol). The resulting mixture was stirred under darkness and argon atmosphere overnight at RT. The mixture was then filtered over a Celite pad to remove the solid, washed with an excess of CH$_3$CN and the filtrate was concentrated *in vacuo*. The brown oil residue was purified by column chromatography over

silica gel (gradient eluent PE/EtOAc from 80/20 to 60/40) to afford **22** (1.39 g, 2.31 mmol, 80%) as a white solid. Rf = 0.14 (PE/EtOAc: 80/20). ^{1}H NMR (500 MHz, CDCl$_3$) δ: 7.90 (s, 1H, ArH), 7.73 (s, 1H, ArH), 7.31 (s, 1H, ArH), 5.40-5.28 (m, 3H, H-2, H-3, H-4), 5.24 (d, J = 7.1 Hz, 1H, H-1), 4.77 (s, 2H, CH$_2$), 4.23 (dd, J = 6.6, 2.8 Hz, 1H, H-5), 3.73 (s, 3H, COOCH$_3$), 2.07 (s, 3H, OAc), 2.06 (s, 3H, OAc), 2.06 (s, , 3H, OAc), 0.95 (s, 9H, -Si-C(CH$_3$)$_3$), 0.12 (s, 6H, -Si(CH$_3$)$_2$). ^{13}C NMR (126 MHz, CDCl$_3$) δ: 170.2, 169.5, 169.3, 166.8, 157.0, 149.2, 145.4, 120.6, 115.8, 110.5, 98.9, 72.8, 71.7, 71.1, 69.0, 63.8, 53.2, 26.0 (3C), 20.7 (2C), 20.7, 18.5, -5.2, -5.2. ESI-MS: m/z calcd for [C$_{20}$H$_{27}$N$_2$O$_{13}$]$^+$: 503.15, found: 503.15 [M − C$_6$H$_{14}$Si +NH$_4$]$^+$.

Synthesis of compound 23:
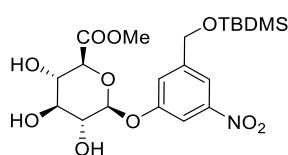
22 (1.39 g, 2.31 mmol) was dissolved in anhydrous MeOH (50 mL) cooled at 0 °C then was treated with a solution of MeONa 30% w/v in MeOH (428 μL, 2.31 mmol). The resulting mixture was stirred at 0 °C for 100 min under argon atmosphere. The reaction was quenched with acetic acid (132 μL, 2.31 mmol) and the solvent was removed under reduced pressure. Crude material was purified by column chromatography over silica gel (gradient eluent CH$_2$Cl$_2$/MeOH from 95/5 to 90/10) to afford **23** (870 mg, 1.84 mmol, 80%) as a colorless oil. Rf = 0.32 (CH$_2$Cl$_2$/MeOH: 90/10). ^{1}H NMR (500 MHz, CDCl$_3$) δ: 7.80 (s, 1H, ArH), 7.70 (s, 1H, ArH), 7.27 (s, 1H, ArH partially overlapped with solvent signal), 5.07 (d, J = 7.0 Hz, 1H, H-1), 4.83 (br s, 1H, OH), 4.70 (s, 2H, CH$_2$), 4.43 (br s, 1H, OH), 4.26 (br s, 1H, OH), 4.11 (d, J = 9.6 Hz, 1H, H-5), 3.93 (dd, J = 9.0, 9.0 Hz, 1H, H-3), 3.90 − 3.81 (m, 2H, H-2, H-4), 3.80 (s, 3H, COOCH$_3$), 0.92 (s, 9H, -Si-C(CH$_3$)$_3$), 0.09 (s, 6H, -Si(CH$_3$)$_2$). ^{13}C NMR (126 MHz, CDCl$_3$) δ: 169.6, 157.1, 149.1, 145.3, 120.3, 115.4, 110.4, 100.8, 75.5, 74.4, 72.9, 71.2, 63.8, 53.2, 26.0 (3C), 18.5, -5.3 (2C). ESI-MS: m/z calcd for [C$_{14}$H$_{21}$N$_2$O$_{10}$]$^+$: 377.12 , found: 377.11 [M − C$_6$H$_{14}$Si + NH$_4$]$^+$.

Synthesis of compound 24:
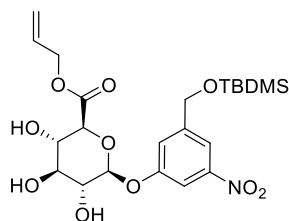
To a solution of **23** (870 mg, 1.84 mmol) in anhydrous allyl alcohol (25 mL) cooled to 0 °C was added dropwise a solution of sodium allylate 0.126 M (2.9 mL, 0.367 mmol). The mixture was stirred at RT for 40 min under argon atmosphere. The reaction was neutralized with glacial acetic acid (21 µL, 0.367 mmol) and after removal of solvent under reduced pressure, the crude material was purified by column chromatography over silica gel (eluent CH_2Cl_2/MeOH: 95/5) to yield **24** (680 mg, 1.36 mmol, 74%) as a yellowish oil. Rf = 0.30 (CH_2Cl_2/MeOH: 90/10). ^{1}HNMR (500 MHz, $CDCl_3$) δ: 7.85 (s, 1H, ArH), 7.74 (s, 1H, ArH), 7.29 (s, 1H, ArH), 5.94 – 5.83 (m, 1H, -C$\underline{H}$=CH$_2$), 5.31 (d, J = 17.1 Hz, 1H, -CH=CH$^{cis}\underline{H}^{trans}$), 5.21 (d, J = 10.4 Hz, 1H, -CH=C$\underline{H}^{cis}$H^{trans}), 5.05 (d, J = 7.1 Hz, 1H, H-1), 4.74 – 4.63 (m, 4H, -OC$\underline{H}_2$-CH=CH$_2$, CH$_2$), 4.58 (br s, 1H, OH), 4.25 (br s, 1H, OH), 4.10 (d, J = 9.7 Hz, 1H, H-5), 4.03 (br s, 1H, OH), 3.94 (dd, J = 9.1, 9.1 Hz, 1H, H-3), 3.88 – 3.77 (m, 2H, H-2, H-4), 0.93 (s, 9H, -Si-C(CH$_3$)$_3$), 0.10 (s, 6H, -Si(CH$_3$)$_2$). ^{13}CNMR (126 MHz, $CDCl_3$) δ: 168.8, 157.2, 149.1, 145.3, 131.1, 120.5, 119.4, 115.5, 110.6, 101.0, 75.5, 74.4, 72.9, 71.1, 66.8, 63.8, 26.0 (3C), 18.5, -5.2 (2C). ESI-MS: m/z calcd for [$C_{16}H_{23}N_2O_{10}$]$^+$: 403.13, found: 403.12 [M – $C_6H_{14}Si$ + NH$_4$]$^+$.

Synthesis of compound 25:
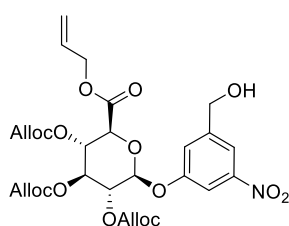
To a solution of **24** (680 mg, 1.36 mmol) in anhydrous pyridine (7 mL) cooled to 0 °C was slowly added dropwise allyl chloroformate (4.34 mL, 40.8 mmol) (Note: strong gas release). The mixture was stirred at RT for 72 h under argon atmosphere. The reaction was diluted with CH_2Cl_2 (20 mL) and quenched with HCl 1N (until pH 5-6). The aqueous layer was then extracted with CH_2Cl_2 (3 x 30 mL). The combined organic layers were dried over MgSO$_4$, filtered, and concentrated under reduced pressure. The resulting crude material was purified by

column chromatography over silica gel (gradient eluent PE/EtOAc from 90/10 to 85/15) to give **25** (565 mg, 0.75 mmol, 55%) as a colorless oil. Rf = 0.33 (PE/EtOAc: 80/20). ^{1}H NMR (500 MHz, CDCl$_3$) δ: 7.91 (s, 1H, ArH), 7.74 (s, 1H, ArH), 7.31 (s, 1H, ArH), 5.97 – 5.79 (m, 4H, -C$\underline{H}$=CH$_2$ (x4)), 5.39 – 5.14 (m, 12H, H-1, H-2, H-3, H-4, -CH=C$\underline{H_2}$ (x4)), 4.77 (s, 2H, CH$_2$), 4.70 – 4.57 (m, 8H, -OC$\underline{H_2}$-CH=CH$_2$ (x4)), 4.33 (d, J = 9.2 Hz, 1H, H-5), 0.95 (s, 9H, -Si-C(CH$_3$)$_3$), 0.12 (s, 6H, -Si(CH$_3$)$_2$). ^{13}C NMR (126 MHz, CDCl$_3$) δ: 165.8, 156.8, 154.1, 153.7, 153.6, 149.2, 145.4, 131.2, 131.1, 131.0, 120.6, 119.6, 119.5, 119.5, 119.3, 115.9, 110.9, 98.8, 75.3, 74.7, 72.5, 72.4, 69.5 (3C), 69.3, 67.1, 63.8, 26.0 (3C), 18.5, -5.2 (2C). ESI-MS: m/z calcd for [C$_{28}$H$_{35}$N$_2$O$_{16}$]$^+$: 655.20, found: 655.19 [M − C$_6$H$_{14}$Si + NH$_4$]$^+$.

Synthesis of compound 26:
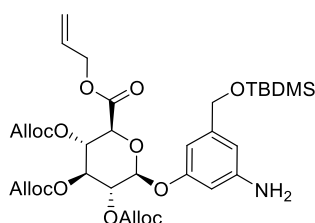
Compound **25** (565 mg, 0.75 mmol) was dissolved in 8 mL of anhydrous MeOH/AcOH mixture (10:1, *v/v*). Activated zinc powder (981 mg, 15.0 mmol), was then added and the resulting mixture was vigorously stirred for 30 min at RT under argon atmosphere. The reaction was monitored by TLC until completion (30 min to 1 h). The reaction mixture was then filtered and the resulting solid was washed with excess MeOH. The filtrate was concentrated to dryness *in vacuo*. The crude material was purified by column chromatography over silica gel (gradient eluent PE/EtOAc from 80/20 to 70/30) to give **26** (390 mg, 0.54 mmol, 72%) as a yellow oil. Rf = 0.08 (PE/EtOAc: 80/20). ^{1}H NMR (500 MHz, CDCl$_3$) δ: 6.39 (s, 1H, ArH), 6.36 (s, 1H, ArH), 6.23 (s, 1H, ArH), 5.95 – 5.80 (m, 4H, -C$\underline{H}$=CH$_2$ (x4)), 5.38 – 5.21 (m, 10H, H-1, H-3, -CH=C$\underline{H_2}$ (x4)), 5.17 – 5.07 (m, 2H, H-2, H-4), 4.68 – 4.55 (m, 10H, -OC$\underline{H_2}$-CH=CH$_2$ (x4), CH$_2$), 4.23 (d, J = 8.5 Hz, 1H, H-5), 0.93 (s, 9H, -Si-C(CH$_3$)$_3$), 0.08 (s, 6H, -Si(CH$_3$)$_2$). ^{13}C NMR (126 MHz, CDCl$_3$) δ: 166.0, 157.9, 154.2, 153.8, 153.7, 147.7, 144.5, 131.3, 131.3, 131.2, 131.1, 119.4, 119.3, 119.2, 119.1, 108.2, 104.9, 103.1, 99.3, 75.8, 74.9, 72.9, 72.4, 69.3, 69.2 (2C), 66.9, 64.8, 26.1 (3C), 18.6, -5.1 (2C). ESI-MS: m/z calcd for [C$_{28}$H$_{34}$NO$_{14}$]$^+$: 608.20, found: 608.20 [M − C$_6$H$_{14}$Si + H]$^+$.

Synthesis of compound 27:
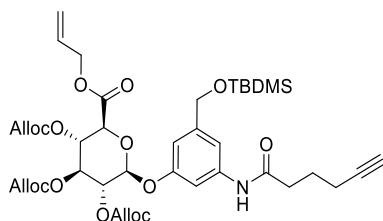
To a stirred solution of **26** (380 mg, 0.53 mmol) in anhydrous CH_2Cl_2 (5 mL) was added 5-hexynoic acid (71 μL, 0.64 mmol) followed by EEDQ (262 mg, 1.06 mmol). The mixture was stirred for 48 h at RT under darkness and argon atmosphere. After removing the solvent under reduced pressure, the crude material was purified by column chromatography over silica gel (gradient eluent PE/EtOAc from 85/15 to 80/20) to give **27** (412 mg, 0.51 mmol, 95%) as a yellow oil. Rf = 0.20 (PE/EtOAc: 80/20). ^{1}H NMR (500 MHz, CDCl$_3$) δ: 7.21 (br s, 2H, ArH, ArNH), 7.13 (s, 1H, ArH), 6.75 (s, 1H, ArH), 5.96 – 5.79 (m, 4H, -C$\underline{H}$=CH$_2$ (x4)), 5.37 – 5.19 (m, 11H, H-1, H-2, H-4, -CH=C$\underline{H_2}$ (x4)), 5.18 – 5.10 (m, 1H, H-3), 4.68 – 4.56 (m, 10H, -OC$\underline{H_2}$-CH=CH$_2$ (x4), CH$_2$), 4.26 (d, J = 8.5 Hz, 1H, H-5), 2.49 (t, J = 7.2 Hz, 2H, CO-C$\underline{H_2}$-CH$_2$-CH$_2$-C≡CH), 2.31 (td, J = 6.3, 3.2 Hz, 2H, -CH$_2$-CH$_2$-C$\underline{H_2}$-C≡CH), 2.02 (br s, 1H, -C≡CH), 1.93 (p, J = 7.0 Hz, 2H, -CH$_2$-C$\underline{H_2}$-CH$_2$-C≡CH), 0.93 (s, 9H, -Si-C(CH$_3$)$_3$), 0.09 (s, 6H, -Si(CH$_3$)$_2$). ^{13}C NMR (126 MHz, CDCl$_3$) δ: 170.5, 166.0, 157.1, 154.2, 153.8, 153.7, 144.3, 139.0, 131.3, 131.2, 131.2, 131.1, 119.4, 119.3, 119.2, 119.1, 112.3, 110.3, 107.4, 99.0, 83.6, 75.7, 74.8, 72.8, 72.4, 69.6, 69.3, 69.3, 69.2, 66.9, 64.6, 36.1, 26.1 (3C), 24.0, 18.5, 17.9, -5.1 (2C). ESI-MS: m/z calcd for [C$_{34}$H$_{40}$NO$_{15}$]$^+$: 702.24, found: 702.22 [M – C$_6$H$_{14}$Si + H]$^+$.

Synthesis of compound 28:
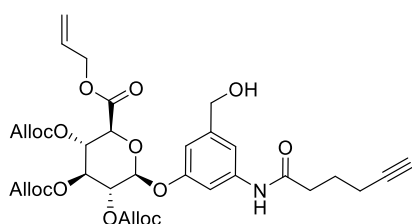
Compound **27** (400 mg, 0.49 mmol) was dissolved in anhydrous THF (8 mL) and cooled to 0 °C, then HF/Pyridine 70% (1.88 mL) was added dropwise. The mixture was stirred 1 hour at RT under argon atmosphere. The reaction was quenched with saturated solution of NaHCO$_3$ (8 mL) and extracted with CH$_2$Cl$_2$ (3 x 20 mL). The combined organic layers were dried over MgSO$_4$, filtered, and concentrated under reduced pressure. The resulting crude material was

purified by column chromatography over silica gel (gradient eluent PE/EtOAc from 70/30 to 40/60) to give **28** (302 mg, 0.43 mmol, 88%) as a colorless oil. *Rf* = 0.13 (PE/EtOAc: 60/40). ^{1}H NMR (500 MHz, CDCl$_3$) δ: 7.29 (s, 1H, ArH), , 7.11 (s, 1H, ArH), 6.76 (s, 1H, ArH), 5.97 – 5.80 (m, 4H, -C$\underline{H}$=CH$_2$ (x4)), 5.38 – 5.19 (m, 11H, H-1, H-2, H-4, -CH=C$\underline{H_2}$ (x4)), 5.12 (dd, *J* = 7.5, 7.5 Hz, 1H, H-3), 4.68 – 4.56 (m, 10H, -OC$\underline{H_2}$-CH=CH$_2$ (x4), CH$_2$), 4.27 (d, *J* = 7.5 Hz, 1H, H-5), 2.49 (t, *J* = 7.2 Hz, 2H, CO-C$\underline{H_2}$-CH$_2$-CH$_2$-C≡CH), 2.35 – 2.29 (m, 2H, -CH$_2$-CH$_2$-C$\underline{H_2}$-C≡CH), 2.03 (br s, 1H, -C≡CH), 1.93 (p, *J* = 7.2 Hz, 2H, -CH$_2$-CH$_2$-CH$_2$-C≡CH). ^{13}C NMR (126 MHz, CDCl$_3$) δ: 170.8, 166.2, 157.0, 154.2, 153.8, 153.7, 143.8, 139.3, 131.2 (2C), 131.1 (2C),119.4 (2C), 119.3, 119.2, 113.2, 111.3, 107.6, 98.8, 83.6, 75.7, 74.8, 72.7, 72.2, 69.7, 69.4, 69.3, 69.3, 67.0, 64.9, 36.1, 23.9, 17.9. ESI-MS: *m/z* calcd for [C$_{34}$H$_{40}$NO$_{15}$]$^+$: 702.24, found: 702.22 [M + H]$^+$.

Synthesis of compound 29:
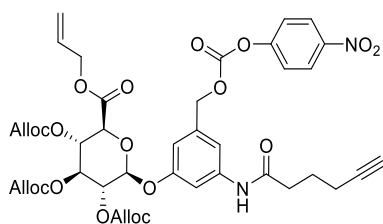
To a stirred solution of **28** (154 mg, 0.219 mmol) in anhydrous CH$_2$Cl$_2$ (2 mL) cooled to 0 °C were added dropwise anhydrous pyridine (44 μL, 0.548 mmol) followed by a solution of 4-nitrophenyl chloroformate (88 mg, 0.439 mmol) in anhydrous CH$_2$Cl$_2$ (3 mL). The mixture was stirred at RT under argon for 2 h and quenched with saturated solution of NaHCO$_3$ (6 mL) and extracted with CH$_2$Cl$_2$ (x3). The combined organic layers were dried over MgSO$_4$, filtered and concentrated under reduced pressure. The crude oil was purified by column chromatography over silica gel (gradient eluent PE/EtOAc: 70/30; 60/40) to give **29** (140 mg, 0.162 mmol, 74%) as a colourless oil. *Rf* = 0.23 (PE/EtOAc: 70/30). ^{1}H NMR (500 MHz, CDCl$_3$) δ: 8.28 (d, *J* = 9.0 Hz, 2H, ArH), 7.44 (s, 1H, ArH), 7.40 (d, *J* = 9.0 Hz, 2H, ArH), 7.27 (s, 1H, ArNH partially overlapped with solvent signal), 7.20 (s, 1H, ArH), 6.83 (s, 1H, ArH), 5.97 – 5.79 (m, 4H, -C$\underline{H}$=CH$_2$ (x4)), 5.39 – 5.19 (m, 13H, H-1, H-2, H-4, -CH=C$\underline{H_2}$ (x4), CH$_2$), 5.19 – 5.10 (m, 1H, H-3), 4.69 – 4.54 (m, 8H, -OC$\underline{H_2}$-CH=CH$_2$ (x4)), 4.35 – 4.26 (m, 1H, H-5), 2.51 (t, *J* = 7.2 Hz, 2H, CO-C$\underline{H_2}$-CH$_2$-CH$_2$-C≡CH), 2.33 (td, *J* = 6.7, 2.6 Hz, 2H, -CH$_2$-CH$_2$-C$\underline{H_2}$-C≡CH), 2.03 (t, *J* = 2.6 Hz, 1H, -C≡CH), 1.94 (p, *J* = 7.0 Hz, 2H, -CH$_2$-C$\underline{H_2}$-CH$_2$-C≡CH). ^{13}C NMR (126 MHz, CDCl$_3$) δ: 170.7, 166.0, 157.1, 155.6, 154.2, 153.8, 153.7, 152.5, 145.6, 139.6, 136.7, 131.2

(2C), 131.1 (2C), 125.5 (2C), 122.0 (2C), 119.4, 119.4 (2C), 119.2, 114.7, 113.0, 109.0, 98.9, 83.5, 75.6, 74.8, 72.6, 72.4, 70.3, 69.8, 69.4, 69.4, 69.3, 67.0, 36.1, 23.9, 17.9. ESI-MS: m/z calcd for $[C_{41}H_{43}N_2O_{19}]^+$ 867.23, found 867.26 $[M+H]^+$.

Synthesis of compound 30:
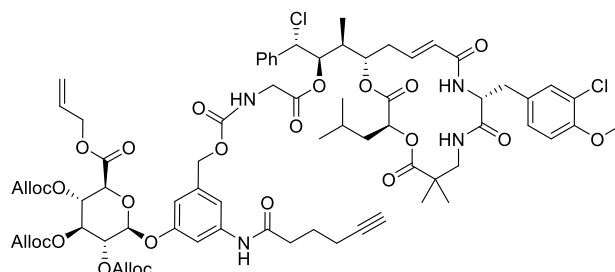
Cryptophycin-55 glycinate-trifluoroacetate salt (9 mg, 0.010 mmol), **29** (11 mg, 0.012 mmol), and DIPEA (5.4 μL, 0.031 mmol) were placed under argon atmosphere and dissolved in anhydrous DMF (0.5 mL). The solution was stirred for 4 h at RT and the reaction progress was monitored by HPLC-MS. The crude material was purified by RP-HPLC using Method M1 to afford the conjugate **30** (13 mg, 0.009 mmol, 85%) as a white powder after freeze-drying.

HPLC-MS: t_r = 12.1 min, 77% purity (λ = 220 nm), m/z calcd for $[C_{73}H_{88}Cl_2N_4O_{25}]^{2+}$: 745.26, found 745.25 $[M + 2H]^{2+}$.

Synthesis of compound 31:
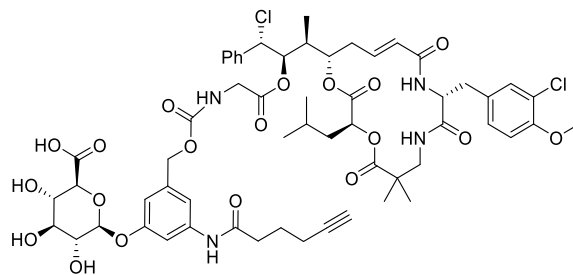
30 (11 mg, 0.007 mmol) was dissolved in degassed CH_2Cl_2 (0.5 mL), then Pd(PPh$_3$)$_4$ 10% mol (0.85 mg, 0.7 μmol) was added under argon atmosphere followed by morpholine (4 drops). The resulting mixture was stirred for 1 h at RT under argon protection. The reaction progress was monitored by HPLC-MS. After 1 h, solvent was removed under reduced pressure (bath at RT), and the crude material was purified by RP-HPLC using Method M2 to afford the deprotected conjugate **31** (6.32 mg, 0.005 mmol, 71%) as a white powder after freeze-drying.

HPLC-MS: t_r = 10.3 min, 96% purity (λ = 220 nm), m/z calcd for $[C_{58}H_{71}Cl_2N_4O_{19}]^+$: 1197.41, found: 1197.36 $[M + H]^+$.

Synthesis of compound 3:

C88H114Cl2N16O27
Exact Mass: 1896,7416
MW: 1898,8650
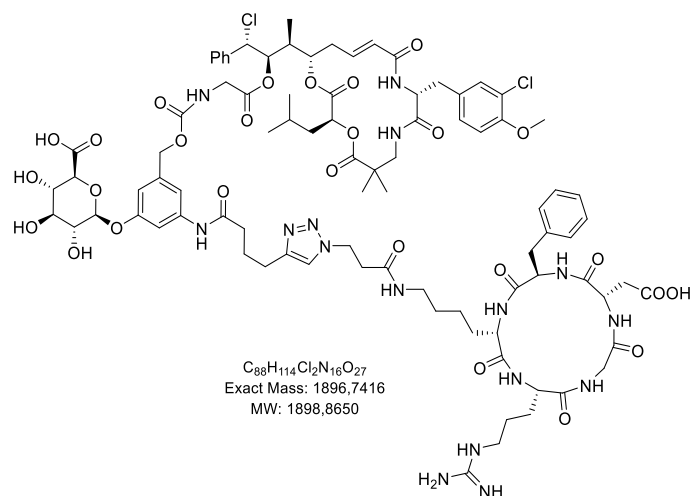
31 (2.58 mg, 2.15 μmol), **33** (1.63 mg, 2.36 μmol), CuSO₄ · 5 H₂O (0.26 mg, 1.05 μmol), and sodium ascorbate (0.25 mg, 1.26 μmol) were dissolved in a mixture of anhydrous DMF/H₂O (200 μL, 1:1) previously degassed with argon flow. The solution was stirred at 35 °C for 24 h under argon atmosphere. The reaction progress was monitored by HPLC-MS. The crude was purified by RP-HPLC using Method M2 to afford the final compound **3** (1.76 mg, 0.93 μmol, 43%) as a white powder after freeze-drying.

HPLC-MS: t_r = 7.7 min, 90% purity (λ = 220 nm), *m/z* calcd for [C₈₈H₁₁₅Cl₂N₁₆O₂₇]⁺: 1897.75, found: 1897.76 [M + H]⁺; *m/z* calcd for [C₈₈H₁₁₆Cl₂N₁₆O₂₇]²⁺: 949.38, found: 949.39 [M + 2H]²⁺. **HRMS (ESI-MS):** *m/z* calcd for [C₈₈H₁₁₆Cl₂N₁₆O₂₇]²⁺: 949.3781, found: 949.3773 [M + 2H]²⁺.

Synthesis of compound 4:

C89H116Cl2N16O27
Exact Mass: 1910,7573
MW: 1912,8920
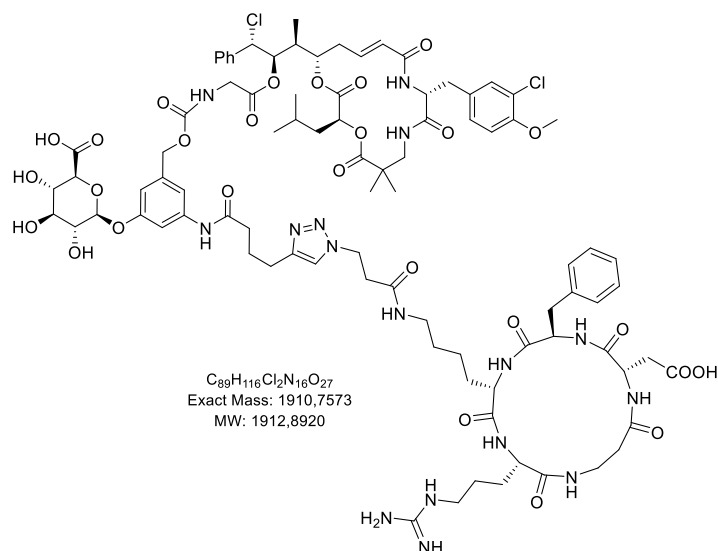
31 (2.9 mg, 2.4 μmol), **34** (2 mg, 2.9 μmol), CuSO$_4$ · 5 H$_2$O (0.30 mg, 1.2 μmol), and sodium ascorbate (0.28 mg, 1.44 μmol) were dissolved in a mixture of anhydrous DMF/H$_2$O (200 μL, 1:1) previously degassed with argon flow. Then, the solution was stirred at 35 °C for 24 h under argon atmosphere. The reaction progress was monitored by HPLC-MS. The crude was purified by RP-HPLC using Method M2 to afford the final compound **4** (3.3 mg, 1.73 μmol, 72%) as a white powder after freeze-drying.

HPLC-MS: t_r = 7.7 min, > 99% purity (λ = 220 nm), *m/z* calcd for [C$_{89}$H$_{117}$Cl$_2$N$_{16}$O$_{27}$]$^+$: 1911.76, found: 1911.78 [M + H]$^+$; *m/z* calcd for [C$_{89}$H$_{118}$Cl$_2$N$_{16}$O$_{27}$]$^{2+}$: 956.39, found: 956.40 [M + 2H]$^{2+}$. **HRMS (ESI-MS):** *m/z* calcd for [C$_{89}$H$_{118}$Cl$_2$N$_{16}$O$_{27}$]$^{2+}$: 956.3859, found: 956.3845 [M + 2H]$^{2+}$.

General procedure for Boc/tBu deprotection

To a CH$_2$Cl$_2$ solution of the N-Boc-protected compound TFA was added until 1:1 mixture was reached, and the reaction was stirred at RT for 1 h. The solvent was removed *in vacuo* and the residue was re-dissolved in CH$_2$Cl$_2$ followed by evaporation *in vacuo* again, to afford the amine TFA salt.

Synthesis of Fmoc-Lys(COCH$_2$CH$_2$N$_3$)-OH (32):
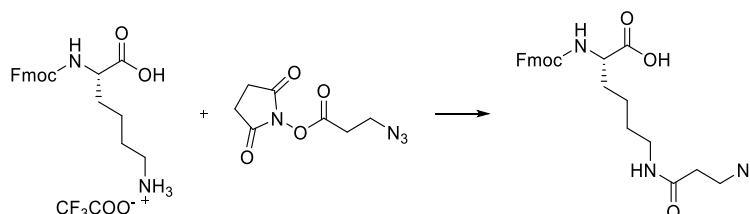
Fmoc-Lys-OH trifluoroacetate salt (1.627 g, 3.37 mmol), obtained quantitatively following the general Boc deprotection procedure, 3-azidopropanoate-NHS ester (715 mg, 3.37 mmol) and DIPEA (1.17 mL, 6.74 mmol) were placed under argon atmosphere and dissolved in DMF (14 mL). The solution was stirred for 48 h at RT. After the removal of DMF under reduced pressure, the residue was dissolved in EtOAc (100 mL) and HCl 1 M was added, the layers were separated, and the aqueous phase was further extracted with EtOAc (2 x 50 mL). The combined organic layers were dried over MgSO$_4$ and the solvent was removed under reduced pressure. The dipeptide **32** (1.52 g, 3.27 mmol, 97%) was obtained as a yellow oil and was used without further purification. **^{1}H NMR (500 MHz, CDCl$_3$) δ:** 7.76 (d, *J* = 7.6 Hz, 2H, ArH), 7.60 (dd, *J* = 6.6, 6.6 Hz, 2H, ArH), 7.39 (dd, *J* = 7.5, 7.5 Hz, 2H, ArH), 7.30 (dd, *J* = 7.5, 7.5 Hz, 2H, ArH), 5.94 (br s, 1H, $^\varepsilon$NH), 5.62 (d, *J* = 7.9 Hz, 1H, K-NH), 4.45 – 4.34 (m, 3H, Fmoc-CH-

CH$_2$-O, K-$^\alpha$H), 4.21 (t, J = 6.9 Hz, 1H, Fmoc-CH-CH$_2$-O), 3.59 (t, J = 6.4 Hz, 2H, CH$_2$-CH$_2$-N$_3$), 3.32 – 3.23 (m, 2H, $^\varepsilon$CH$_2$), 2.39 (t, J = 6.4 Hz, 2H, CH$_2$-CH$_2$-N$_3$), 1.97 – 1.90 (m, 2H), 1.77 – 1.71 (m, 2H), 1.65 – 1.53 (m, 3H), 1.37 – 1.29 (m, 2H), 1.25 – 1.16 (m, 2H). **ESI-MS:** m/z calcd for [C$_{24}$H$_{28}$N$_5$O$_5$]$^+$: 466.21, found: 466.22 [M + H]$^+$.

Solid Phase Peptide Synthesis (SPPS)

The compounds were synthesized manually on 2-chlorotrityl resin (1.5 mmol g^{-1} loading capacity) using the Fmoc protocol. The resin (1.5 g, 2.25 mmol) was previously activated by treatment with thionyl chloride (1.5 eq, 0.25 mL, 3.34 mmol) in CH$_2$Cl$_2$ for 1 hour at RT. After this, coupling of the first amino acids was carried out.

Synthesis of *c*[RGDfK(COCH$_2$CH$_2$N$_3$)] (33)
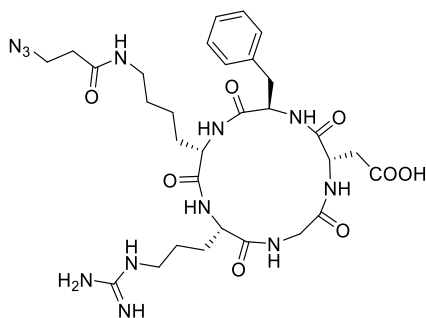
Attachment of the 1° amino acid (Fmoc-Gly-OH)

The resin (790 mg, 1.26 mmol) was placed in a flame dried round bottom flask and swollen with anhydrous CH$_2$Cl$_2$ for 15 min under argon. In another flame dried vial, Fmoc-Gly-OH (752 mg, 2.53 mmol) and DIPEA (1.10 mL, 6.32 mmol) were dissolved in anhydrous CH$_2$Cl$_2$ (6 mL) and then added to the preactivated resin. The mixture was gently stirred for 3 h at RT, then a solution of MeOH/DIPEA (9:1) was added to the resin and stirred for an additional 10 min to perform the capping of the unreacted sites. The solvents were removed by filtration and the resin was washed with DMF, CH$_2$Cl$_2$, and Et$_2$O (3 × 5 mL).

Peptide chain elongation

The resin was swollen in DMF for 15 min and the Fmoc group was removed with 25% piperidine in DMF (1 × 5 min + 1 × 10 min) then washed with DMF and CH$_2$Cl$_2$ (3 × 5 mL). The peptide sequence was elongated with Fmoc-Arg(Pbf)-OH (1.54 g, 2.37 mmol), Fmoc-D-Phe-OH (918 mg, 2.37 mmol), Fmoc-Asp(tBu)-OH (975 mg, 2.37 mmol) activated in a separate vial with DIC (367 µL, 2.37 mmol) and OxymaPure (337 mg, 2.37 mmol) in DMF (4 mL) for

10 min, then added to the resin and gently stirred for 3 h at RT. While, **32** (970 mg, 2.09 mmol) was activated with HATU (793 mg, 2.09 mmol) and DIPEA (728 µL, 4.18 mmol) in DMF (4 mL) for 10 min before adding to the resin. After each coupling, the resin was washed sequentially with DMF and CH_2Cl_2 (3 × 5 mL) Coupling reactions and Fmoc removals were monitored by Kaiser test.

Cleavage from the resin

Cleavage of the linear peptide was carried out by adding a 25% solution of HFIP in CH_2Cl_2 on the resin previously swelled with CH_2Cl_2 and stirred for 5 min at RT. The solution is filtered in a Falcon tube and the cleavage was repeated twice, in the same manner. The collected solvents were removed under air flow and the residue precipitated with Et_2O and then centrifuged. The crude peptide was purified by RP-HPLC using Method M3, to afford the linear peptide (180 mg, 0.175 mmol, 33%) as a white powder after freeze-drying. **ESI-MS:** *m/z* calcd for $[C_{47}H_{71}N_{12}O_{12}S]^+$: 1027.50, found: 1027.57 $[M + H]^+$; *m/z* calcd for $[C_{47}H_{72}N_{12}O_{12}S]^{2+}$: 514.26, found: 514.27 $[M + 2H]^{2+}$.

Cyclization in solution

The azido-functionalized linear peptide was cyclized in pseudo-high dilution condition using a syringe pump. A solution of peptide (180 mg, 0.175 mmol, 1 eq) in 10 mL DMF, was slowly added within 16 h using a syringe pump (flow rate = 0.01 mL · min^{-1}), to a solution of 20 mL DMF containing HATU (200 mg, 0.525 mmol, 3 eq), HOAt (71 mg, 0.525 mmol, 3 eq) and DIPEA (183 µL, 1.05 mmol, 6 eq). Once the addition was complete, the reaction was stirred for additional 2 h, then the solvent was removed, and the crude peptide purified by RP-HLPC (Method M3) to give the cyclic protected peptide (80 mg, 0.079 mmol, 45%) as a yellow solid after freeze-drying. **ESI-MS:** *m/z* calcd for $[C_{47}H_{69}N_{12}O_{11}S]^+$: 1009.49, found: 1009.52 $[M + H]^+$. Finally, the cyclic peptide was dissolved in 5 mL of TFA/TIS/H_2O (95/2.5/2.5) and stirred for 3 h at RT. The solvents were removed under air flow, the residue was precipitated with cold Et_2O which was then decantated. The crude solid was purified by RP-HPLC (Method M4) to yield **34** as colorless powder (36 mg, 0.0513 mmol, 65 %) after freeze-drying. **HPLC-MS:** t_R = 4.8 min, 90% purity (λ = 220 nm), *m/z* calcd for $[C_{30}H_{45}N_{12}O_8]^+$: 701.35, found: 701.38 $[M + H]^+$. **^{1}H NMR (600 MHz, DMSO-d_6) δ:** 12.27 (s, 1H, D-COOH), 8.42 (dd, *J* = 7.7, 4.4 Hz, 1H, G-NH), 8.09 (d, *J* = 8.6 Hz, 1H, D-NH), 8.04 (d, *J* = 7.4 Hz, 1H, K-NH), 8.00 (d, *J* = 7.3 Hz, 1H, f-NH), 7.97 (t, *J* = 5.6 Hz, 1H, K-$^\varepsilon$NH), 7.62 (br s, 1H, R-NH), 7.48(br s, 1H, R-$^\delta$NH),

7.25 (t, J = 7.5 Hz, 2H, f-Ph), 7.18 (d, J = 7.4 Hz, 1H, f-Ph), 7.15 (d, J = 7.0 Hz, 2H, f-Ph), 4.65 – 4.60 (m, 1H, D-$^{\alpha}$CH), 4.44 (ddd, J = 7.4 Hz, 7.3 Hz, 7.3 Hz, 1H, f-$^{\alpha}$CH), 4.16 (dd, J = 8.3, 7.8 Hz, 1H, R-$^{\alpha}$CH), 4.04 (dd, J = 15.0, 7.7 Hz, 1H, G-$^{\alpha}$CH$_2$), 3.96 – 3.90 (m, 1H, K-$^{\alpha}$CH), 3.50 (t, J = 6.4 Hz, 2H, C̲H̲$_2$-CH$_2$-N$_3$), 3.24 (dd, J = 15.0, 4.2 Hz, 1H, G-$^{\alpha}$CH$_2$), 3.15 – 3.04 (m, 2H, R-$^{\delta}$CH$_2$), 3.04 – 2.89 (m, 3H, f-$^{\beta}$CH$_2$, K-$^{\varepsilon}$CH$_2$), 2.81 (dd, J = 13.4, 6.0 Hz, 1H, f-$^{\beta}$CH$_2$), 2.72 – 2.63 (m, 1H, D-$^{\beta}$CH$_2$), 2.42 – 2.38 (m, 1H, D-$^{\beta}$CH$_2$), 2.36 (t, J = 6.4 Hz, 2H, CH$_2$-C̲H̲$_2$-N$_3$), 1.75 – 1.66 (m, 1H, R-$^{\beta}$CH$_2$), 1.57 – 1.46 (m, 2H, R-$^{\beta}$CH$_2$, K-$^{\beta}$CH$_2$), 1.43 – 1.23 (m, 5H, R-$^{\gamma}$CH$_2$, K-$^{\delta}$CH$_2$, K-$^{\beta}$CH$_2$), 1.08 – 1.00 (m, 2H, K-$^{\gamma}$CH$_2$).

Synthesis of c[RβADfK(COCH$_2$CH$_2$N$_3$)] (34)
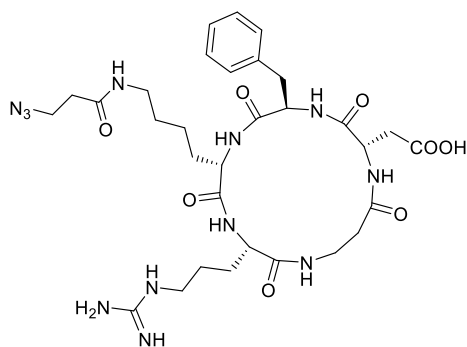
Attachment of the 1° amino acid (Fmoc-Asp-OAllyl)

As previously described, the preactivated 2-chlorotrityl resin (780 mg, 1.17 mmol) was charged with Fmoc-Asp-OAllyl (924 mg, 2.34 mmol) in anhydrous CH$_2$Cl$_2$ (6 mL) and DIPEA (1.09 mL, 6.24 mmol). After the addition of MeOH/DIPEA (9:1) for the capping of the unreacted sites, and the washing step with DMF, CH$_2$Cl$_2$, and Et$_2$O (3 × 5 mL).

Peptide chain elongation

The resin was swollen in DMF for 15 min and the Fmoc group was removed with 25% piperidine in DMF (1 × 5 min + 1 x 10 min) then washed with DMF and CH$_2$Cl$_2$ (3 × 5 mL). The peptide sequence was elongated with Fmoc-β-Ala-OH (728 mg, 2.34 mmol), Fmoc-Arg(Pbf)-OH (1.518 g, 2.34 mmol), Fmoc-D-Phe-OH (905 mg, 2.34 mmol), activated in a separate vial with DIC (362 µL, 2.34 mmol) and OxymaPure (333 mg, 2.34 mmol) in DMF (4 mL) for 10 min, then added to the resin and gentle stirred for 3 h at RT. **32** (970 mg, 2.09 mmol) was activated with HATU (793 mg, 2.09 mmol) and DIPEA (728 µL, 4.18 mmol) in DMF (4

mL) for 10 min before adding to the resin. After each coupling, the resin was washed with DMF and CH_2Cl_2 (3 x 5 mL). Coupling reactions and Fmoc removals were monitored by Kaiser test.

On resin allyl removal

The dried resin was placed under argon atmosphere and swelled with anhydrous CH_2Cl_2 (6 mL). In a flame dried flask, $PhSiH_3$ (3.37 mL, 27.36 mmol, 24 eq) was dissolved in anhydrous CH_2Cl_2 (2 mL) and was added to the resin and mixed for 5 min. Then, $Pd(PPh_3)_4$ solution (263 mg, 0.23 mmol, 0.2 eq) in anhydrous CH_2Cl_2 (2 mL) was added and the reaction was gentle stirred for 40 min at RT under argon atmosphere. After washing the resin with CH_2Cl_2 (8 x 5 mL) the removal was repeated once more. The progress of the deprotection step was confirmed by cleavage test on 1 mg of resin (1% TFA inCH_2Cl_2, 3 x 1 mL) and the resulting residue was analyzed using HPLC-MS (Method A).

On resin cyclization

The cyclization was obtained by treating the resin swelled in DMF with DIC (882 µL, 5.7 mmol, 5 eq) and OxymaPure (810 mg, 5.7 mmol, 5 eq) dissolved in DMF (6 mL) and stirred for 48 h at RT. The resin was washed with DMF, CH_2Cl_2, and Et_2O (3 × 5 mL) and the cyclization progress was monitored by Kaiser test and cleavage test on 1 mg of resin (1% TFA in CH_2Cl_2, 3 x 1 mL) using HPLC-MS (Method A).

Cleavage from the resin

Cleavage of the cyclic peptide from the resin and final deprotection was obtained by adding a mixture of $TFA/H_2O/TIS$ (95/2.5/2.5) on the resin previously washed with CH_2Cl_2 (3x) and stirred for 3 h at RT. The solution was filtered in a Falcon tube, the resin washed with CH_2Cl_2 (3 × 5 mL) and the solvent was collected in the same tube. The solvents were removed under air flow and the residue precipitated with Et_2O and then centrifugated. The crude material was purified by RP-HPLC using Method M4, to afford **34** (8 mg, 0.011 mmol, 16%) as a white powder after freeze-drying. **HPLC-MS:** t_R = 4.6 min, 95% purity (λ = 220 nm), *m/z* calcd for $[C_{31}H_{47}N_{12}O_8]^+$: 715.36, found: 715.44 $[M + H]^+$. **^{1}H NMR (600 MHz, DMSO-d_6) δ:** 12.36 (s, 1H, D-COOH), 8.60 (d, *J* = 5.2 Hz, 1H, f-NH), 8.38 (d, *J* = 6.1 Hz, 1H, K-NH), 8.11 (d, *J* = 7.7 Hz, 1H, D-NH), 7.94 (t, *J* = 5.5 Hz, 1H, K-$^\varepsilon$NH), 7.65 (d, *J* = 8.9 Hz, 1H, R-NH), 7.49 (t, *J* = 5.3 Hz, 1H, R-$^\delta$NH), 7.28 (t, *J* = 7.5 Hz, 2H, f-Ph), 7.21 (t, *J* = 7.4 Hz, 1H, f-Ph), 7.18 (d, *J* = 7.2 Hz, 2H, f-Ph), 6.72 (ddd, *J* = 7.9, 4.4 Hz, 1H, βA-NH), 4.66 (ddd, *J* = 8.1, 8.1, 8.1 Hz, 1H, D-$^\alpha$CH), 4.32 (ddd, *J* = 8.9, 5.7, 5.7 Hz, 1H, f-$^\alpha$CH), 4.08 (ddd, *J* = 10.3, 10.3, 4.3 Hz, 1H, K-

$^{\alpha}$CH), 3.70 (ddd, J = 10.2, 6.1, 3.7 Hz, 1H, R-$^{\alpha}$CH), 3.61 (ddd, J = 11.9, 3.7, 3.7 Hz, 2H, βA-CO-<u>CH$_2$</u>CH$_2$), 3.50 (t, J = 6.4 Hz, 2H, <u>CH$_2$</u>-CH$_2$-N$_3$), 3.05 (q, J = 6.8 Hz, 2H, K-$^{\varepsilon}$CH$_2$), 3.03 – 2.90 (m, 4H, βA-CO-CH$_2$<u>CH$_2$</u>, f-$^{\beta}$CH$_2$), 2.85 (dd, J = 13.3, 9.0 Hz, 1H, f-$^{\beta}$CH$_2$), 2.61 (dd, J = 16.5, 5.9 Hz, 1H, D-$^{\beta}$CH$_2$), 2.49 – 2.43 (m, 1H, D-$^{\beta}$CH$_2$), 2.36 (t, J = 6.4 Hz, 2H, CH$_2$-<u>CH$_2$</u>-N$_3$), 2.23 (td, J = 13.6, 3.5 Hz, 1H, R-$^{\delta}$CH$_2$), 2.07 (dd, J = 10.5, 3.2 Hz, 1H, R-$^{\delta}$CH$_2$), 2.02 – 1.93 (m, 1H, K-$^{\beta}$CH$_2$), 1.65 – 1.55 (m, 2H, K-$^{\beta}$CH$_2$, R-$^{\beta}$CH$_2$), 1.55 – 1.47 (m, 1H, K-$^{\delta}$CH$_2$), 1.45 – 1.35 (m, 1H, K-$^{\delta}$CH$_2$), 1.35 – 1.29 (m, 1H, R-$^{\beta}$CH$_2$), 1.29 – 1.17 (m, 2H, R-$^{\gamma}$CH$_2$, K-$^{\gamma}$CH$_2$), 0.95 – 0.82 (m, 2H, R-$^{\gamma}$CH$_2$, K-$^{\gamma}$CH$_2$).

8. GREEN SYNTHESIS OF BIOACTIVE OLIGOPEPTIDES PROMOTED BY RECYCLABLE NANOCRYSTALLINE HYDROXYAPATITE

The work described in this Chapter was recently submitted to *Future Medicinal Chemistry* journal.

8.1. Introduction

Despite their tremendous potential,[153] for long time bioactive peptide drugs have been generally considered as a specialists' niche area.[310] The reason for this reputation largely stems from their limited in vivo stability and rather low to null bioavailability. These limitations can be for the most part circumvented by the "peptidomimetic" approach, i.e. by introducing properly designed structural modifications in the active peptide.[154] Otherwise, one may consider the adoption of alternative routes of administration, e.g. subcutaneous, nasal, pulmonary, and others.[310] Consequently, in the last years there has been renewed interest in the development of more effective therapeutic peptides, in particular for the treatment of metabolic diseases (e.g. liraglutide), autoimmune diseases (e.g. glatiramer) and in oncology (e.g. octreotide).[310] Yet, the accessibility to peptidic drugs is still hampered by their expensive production and challenging purification. While sizeable peptides and proteins can be obtained by recombinant technologies, short and medium size peptides are usually prepared by chemical synthesis, being the recourse to enzymatic synthesis more limited.[311] Unfortunately, the solid-phase synthesis of peptides on insoluble polymeric supports makes use of a large excess of amino acids and of coupling agents. On the other hand, in-solution synthesis of medium size peptides requires tedious isolation steps. Furthermore, both solid-phase and solution synthetic methods require extensive protection/deprotection strategies. Finally, each coupling/deprotection cycle generally makes use of large volumes of hazardous organic solvents, such as dichloromethane (DCM), dimethylformamide (DMF), *N*-methylpyrrolidone, or methanol, producing a huge amount of wastes.[312] As a consequence, the chemical preparation of peptides is among the most problematic synthetic procedures in terms of atom economy and environmental sustainability.[312]

One opportunity for making peptide synthesis more sustainable [313] consists in the use of non-toxic reagents, for example by the replacement of standard organic solvents with green alternatives.[314, 315] In this context, some protocols have been developed to perform amino acid coupling in an aqueous environment.[316] A complementary alternative consists in a drastic reduction of the involved volumes of solvent used.[317] Coupling reactions can be performed under mechanochemical solvent-free conditions, in particular by means of high speed ball-milling.[318-320] To improve the homogeneity of the solid-state reactions, minimal amounts of solvents can be added (Liquid-Assisted Grinding, LAG), resulting in increased yields and shorter reaction times.[320-322] Finally, toxic bases as trimethylamine, iPr$_2$NEt, or lutidine, typically utilized in peptide synthesis, can be replaced by inorganic salts, e.g. NaHCO$_3$ [318, 321] or hydrotalcite.[320, 323]

Herein we present the expedient solvent-free peptide bond formation between *N*-protected amino acids and amino ester or amide counterparts, using a ball-mill and the standard *N*-ethyl-*N'*-(3-dimethylaminopropyl)carbodiimide (EDC)·HCl/hydroxybenzotriazole (HOBt) coupling agents, promoted by nanocrystalline hydroxyapatite, Ca$_{10}$(PO$_4$)$_6$(OH)$_2$, (HAp), as a bio-compatible base that can be reused without substantial loss of efficacy after easy regeneration. We also report the optimization of LAG reactions under very mild conditions, i.e. in a standard glass round bottom flask equipped with a common polytetrafluoroethylene (PTFE)-coated magnetic stirring bar.

8.2.   Results and Discussion

EDC·HCl is among the most utilized coupling agents for in-solution peptide synthesis, since the resulting urea by-product is easily removed from the reaction mixture by washing with acidic aqueous solutions. Besides, EDC·HCl has proved to be very efficient in solvent-free reactions. EDC·HCl exists exclusively in cyclic form, and easily undergoes transformation to a pseudocyclic stable intermediate in reaction with carboxylic acids forming a low-melting phase.[324] A base is necessary to activate this coupling agent. Recently, inorganic bases have been regarded as a valid alternative to the classic but toxic organic bases generally employed in peptide chemistry.[318-323]

Hydroxyapatite, a totally biocompatible inorganic base. In the present work, we turned our attention to hydroxyapatite, one of the most usual forms of calcium phosphate, as a convenient

inorganic base for potential activation of peptide synthesis. HAp is highly biocompatible, thanks to its chemical and structural similarity to the mineral phase of bone tissues. In this regard, synthetic HAp differs from natural apatites, which display much lower crystallinity and poor stoichiometry. HAp powders can be synthesized following different procedures, i.e. by means of direct synthesis in aqueous solution, under microwave or ultrasound irradiation, through mechanochemical, hydrothermal, sol-gel, as well as phase transition methods.[325, 326] The properties of HAp vary depending on the method of preparation, thus enabling their use in diverse applications, including heterogeneous catalysis (cross-couplings, condensations, oxidations, photocatalysis, etc).[327]

The structure of hexagonal HAp, space group *P*63/*m*, shows a compact assembly of tetrahedral PO_4 groups, and two crystallographically independent cation sites, Ca(I) and Ca(II). The four Ca(I) are strictly aligned in columns parallel to the crystallographic *c*-axis, whereas the six Ca(II) are positioned at the apexes of staggered equilateral triangles. These triangles form the walls of channels parallel to the *c*-axis and filled by the OH^- ions. Thus, HAp displays an "open" and flexible structure, that tolerates a large number of anionic and cationic substitutions. Stoichiometric HAp has been indicated as an efficient base-catalyst for many reactions.[327, 328] Potential Lewis basic sites, such as PO_4^3 and OH^- groups, together with Ca^{2+} Lewis acid sites and POH Brønsted acid sites, have been recognized on the surface of HAp.[328-330] The use of HAp as a base may offer numerous advantages in peptide synthesis, due to its low solubility, high thermal stability and relatively weak basic character that may prevent side reactions promoted by the support itself. Moreover, HAp displays a great affinity for amino acids, especially in the carboxylate form which interacts with the exposed Ca^{2+} ions.[331] Starting from these premises, we utilized HAp nanocrystals synthesized by a co-precipitation method to catalyze peptide bond formation in solvent free and minimal solvent-assisted conditions.

The XRD pattern of the synthesized powder (Figure 57) shows the presence of a number of diffraction peaks indicating the presence of HAp (PDF 9-432) as unique crystalline phase. The lattice constants are $a = 9.421(3)$ Å and $c = 6.885(2)$ Å.
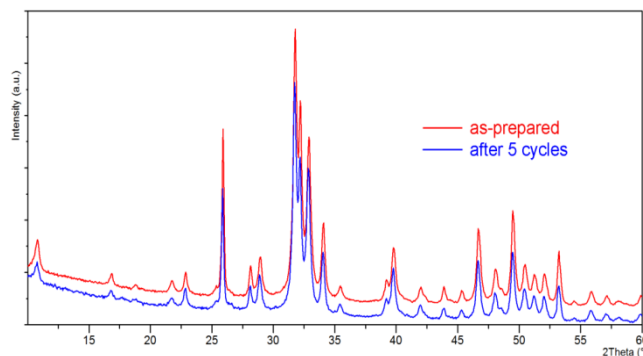
Figure 57. Powder X-ray diffraction patterns of HAp samples prior to (red) and after (blue) 5 cycles of catalyzed peptide bond formation.

The FTIR spectrum (see Appendix, Figure S1) shows the characteristic absorption bands due to phosphate groups, i.e. the anti-symmetric stretching at 1043 and 1091 cm^{-1}, the symmetric stretching at 962 cm^{-1}, and the bending modes at 601 and 570 cm^{-1}, together with the absorption bands at 3572 and 630 cm^{-1} due to OH$^-$ stretching and bending modes, respectively. The sharpness of the absorption bands confirms the good crystallinity of the powder. In agreement, HAp displays also a good stoichiometry as indicated by the value of the Ca/P ionic ratio of 1.67. The TEM micrograph (Figure 58) showed tiny plate-shaped HAp crystals with mean dimensions of about 100 nm (length) $\times$ 30 nm (width). The nanocrystals exhibit a surface area of 56 m^2/g and are negatively charged (zeta potential = -12.5 mV).
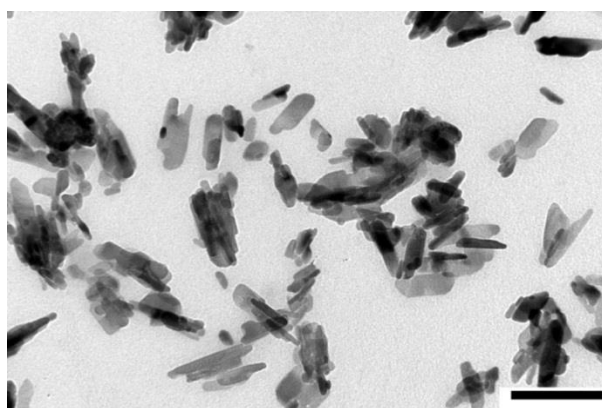
Figure 58. TEM image of HAp nanocrystals; bar = 200 nm.

Initially, this synthetic HAp was employed as a base in a model coupling reaction in solution under standard conditions. *N*-Boc-Val-OH (50 mg, 0.23 mmol) was stirred for 10 min in the presence of the coupling agent EDC·HCl and HOBt as racemization inhibitor (1.2 equiv each), in 10 mL of 4:1 DCM/DMF and a suspension of HAp (50 mg), under inert atmosphere at rt. H-

Phe-OMe·HCl (25 mg, 0.23 mmol) was then added and the resulting mixture was stirred under the same conditions for an additional four hours (Scheme 15).
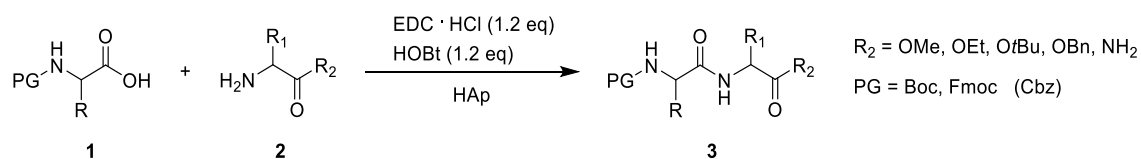
Scheme 15. Peptide bond formation, general conditions.

Following evaporation of the solvent at reduced pressure, the residue was diluted with EtOH and the resulting solution was centrifuged to recover the HAp catalyst. The supernatant was separated and concentrated at reduced pressure, and the residue was diluted with EtOAc and washed in sequence with 1M HCl, sat. Na_2CO_3, and brine. This protocol afforded 65 mg of the desired dipeptide *N*-Boc-Val-Phe-OMe (72% yield), as confirmed by the ESI MS, in a purity of 80%, as determined by RP-HPLC.

Solvent-free mechanochemistry. Next, peptide coupling reactions were performed under solvent-free conditions, in an agate jar (ø = 7.5 cm) containing 3 agate balls (ø = 2.0 cm), at the speed of 8-10 Hz. In order to determine the scope of the method, the general ball milling procedure was carried out with a variety of amino acids (Table 8). Mechanical milling was interrupted after 1 h, and the crude product was diluted with EtOH, to recover the HAp catalyst by centrifugation. The supernatant was subjected to the same work-up procedure as discussed before. Gratifyingly, most reactions gave the dipeptide in good yield (up to 86%) and high purity (up to 94%, Cf. see Appendix, Figure S3). The possibility of epimerization in the peptide forming reaction was excluded on the basis of RP-HPLC ESI-MS and ^{1}H-NMR analyses (see Appendix, Cf. Figure S4), which is in line with observations reported in the literature.[332]

In the coupling between *N*-Boc-Val-OH and H-Phe-OMe·HCl, the yield was only slightly improved when the reaction was repeated with increasing amounts of HAp (Table 8, entry 1 vs. entry 2), while the reduction of the amount of HAp to 25 mg led to a significant drop of the yield (entry 3 in Table 8).

Table 8. Mechanosynthesis of peptides **3** (see Scheme 15) from the N-protected amino acid **1** and the amino ester/amide partner HCl salts **2** (0.23 mmol each), after 1h, in the presence of EDC·HCl/HOBt (0.25 mmol each) and HAp (25-100 mg).

Entry	1	2·HCl	Hap (mg)	3 Yield (%) [a]	3 Purity (%) [a,b]
1	Boc-Val-OH	H-Phe-OMe	50	79	90
2	Boc-Val-OH	H-Phe-OMe	100	82	90
3	Boc-Val-OH	H-Phe-OMe	25	68	88
4	Boc-Val-OH	H-Phe-OEt	50	80	94
5	Boc-Val-OH	H-Phe-OEt	46[c]	78	92
6	Boc-Val-OH	H-Phe-OEt	44[c]	73	94
7	Boc-Val-OH	H-Phe-OEt	41[c]	70	93
8	Boc-Val-OH	H-Phe-OEt	38[c]	68	90
9	Boc-Phe-OH	H-Gly-OEt	50	75	91
10	Boc-Phe-OH	H-D-Val-OMe	"	85	93
11	Boc-Phe-OH	H-Gly-NH$_2$	"	76	88
12	Boc-Phe-OH	H-Leu-OtBu	"	72	93
13	Boc-Phe-OH	H-D-Ser-OMe	"	80[d]	74[d]
14	Boc-Trp-OH	H-Phe-NH$_2$	"	86	94
15	Boc-Tyr-OH	H-Phe-OEt	"	73	90
16	Boc-Tyr-OH	H-Gly-OEt	"	78	85
17	Boc-Ser(OBn)-OH	H-Pro-OBn	"	70	80
18	Fmoc-Phe-OH	H-D-Val-OMe	"	65[e]	87[e]
19	Fmoc-Asp(OtBu)-OH	H-D-Val-OMe	"	62[e]	93[e]
20	Fmoc-Lys(N-Cbz)-OH	H-D-Ser-OMe	"	55[d,e]	70[d,e]
21	Fmoc-Lys(N-Cbz)-OH	H-Ser-NH$_2$	"	60[d,e]	73[d,e]
22	Boc-Pro-OH	H-Trp-Phe-NH$_2$	"	65	77
23	Boc-Tyr-OH	H-Pro-Trp-Phe-NH$_2$	"	6[e]	85[e]

[a] *Determined after aqueous workup.* [b] *Determined by RP HPLC.* [c] *Recovered from the preceding entry.* [d] *The presence of depsi-tripeptides was also detected by RP-HPLC and ESI-MS.* [e] *After filtration through a pad of silica gel.*

Recycling of HAp for 5 cycles. Similar results were obtained for the reaction between *N*-Boc-Val-OH and H-Phe-OEt·HCl (Table 8, entry 4). Following work-up, the recovered crystalline HAp powder was dried for 12 h at 40 °C and reused in four subsequent cycles of reactions

between the same partners (see entries 5-8 in Table 8). After each cycle, the amount of recovered HAp decreased slightly, which might explain the progressive, moderate drop of peptide yields, from 80% to 68%.

The observed loss of catalyst can be attributed to its incomplete recovery after centrifugation, rather than by degradation or solubilization. Indeed, the overall morphology and dimensions of the crystals are preserved after recycling, as shown in the TEM image reported in Figure 59. Moreover, X-ray diffraction analysis of the HAp powder isolated from entry 8 showed the same X-ray diffraction patterns as the original material (see Appendix, Figure 57), indicating that the crystalline structure was preserved. This is in contrast to the behavior of HAp in a wet HCl atmosphere, where both the chemical integrity and particle morphology of HAp are modified. Carbonated domains of HAp appear to facilitate the destabilizing effect of HCl, which results in the elimination of phosphate and OH species and the generation of deep structural groves and voids in the material.[333]
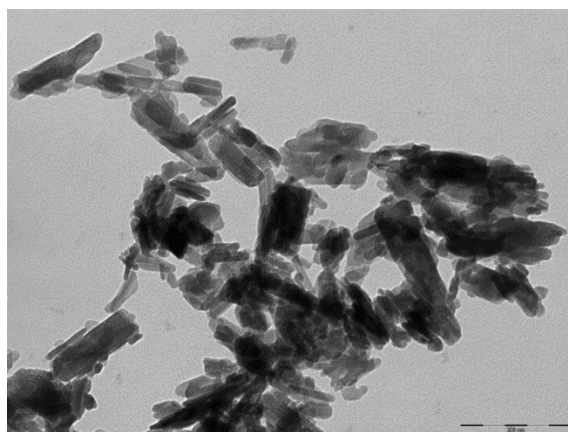
Figure 59. TEM image of HAp nanocrystals after 5 cycles; bar = 200 nm.

Amino acids scope. As mentioned above, the generality of the procedure was confirmed by coupling diverse amino acids, carrying either the *N*-Boc, *N*-Fmoc or *N*-Cbz protecting groups, with amino ester (Me, Et, *t*Bu, Bn) or primary amide partners (Scheme 15 and Table 8). In general, the *N*-Fmoc protected amino acids gave inferior results (Table 1, entries 18-21) relative to *N*-Boc protected analogs (Table 8, entries 9-17 and 22-23). Furthermore, the usual aqueous work up procedure failed to efficiently remove the unreacted *N*-Fmoc-amino acids from the crude reaction mixtures. Therefore, the mixtures were filtered through a short pad of silica gel using 1:1 cyclohexane/EtOAc as mobile phase, affording the dipeptides in moderate yield (55-65%) but acceptable purity (Table 8, entry 18, 87%; entry 19, 95%). In any case, the *N*-Fmoc

group proved to be stable during the grinding process; indeed, the analysis of the crude reaction mixture did not reveal the presence of the deprotected amino acids, nor condensation products originated by their reaction at the *N*-terminus.

Even the secondary amine in H-Pro-OBn readily reacted with *N*-Boc-Ser(OBn)-OH (entry 17 in Table 8), affording the anticipated dipeptide in good yield (70%) and purity (80%) (see Appendix, Figure S6), appearing in the ^{1}H-NMR in CDCl$_3$ as a mixture of cis/trans rotamers about the Ser-Pro peptide bond (see Appendix, Figure S7).

In addition, amino acids with functionalized side chains have been utilized: H-(D)-Ser-OMe (entries 13 and 20 in Table 8), *N*-Boc-Trp-OH (entry 14 in Table 8), *N*-Boc-Tyr-OH (entries 15 and 16 in Table 8), *N*-Boc-Ser(OBn)-OH (entry 17 in Table 8), *N*-Fmoc-Asp(O*t*Bu)-OH (entry 19 in Table 8), *N*-Fmoc-Lys(Cbz)-OH (entries 20 and 21 in Table 8), and H-Ser-NH$_2$ (entry 21 in Table 8). Notably, the reaction was tolerant to the unprotected phenol group of Tyr (entries 15 and 16 in Table 8), and analysis of the corresponding reaction mixtures did not show the formation of any depsipeptide. By contrast, the hydroxy group in H-Ser-NH$_2$ and H-(D)-Ser-OMe gave rise to the formation of significant amounts of the following depsitripeptides: entry 13 in Table 8, *N*-Boc-Phe-D-Ser(*N*-Boc-Phe)-OMe (22% yield); entry 20 in Table 8, *N*-Fmoc-Lys(*N*-Cbz)-D-Ser[*N*-Fmoc-Lys(*N*-Cbz)]-OMe (20%); entry 21 in Table 8, *N*-Fmoc-Lys(*N*-Cbz)-Ser[*N*-Fmoc-Lys(*N*-Cbz)]-NH$_2$ (20%) (see Appendix, Figure S8).

Solvent-free synthesis of H-Tyr-Pro-Trp-PheNH$_2$ (EM1). The optimized reaction conditions in the previous section are in line with the requisites of green chemistry. For example, the only organic solvents utilized for the work up procedure were the green solvents EtOH and EtOAc.[315, 334] Hence, we envisaged the opportunity to utilize the protocol described herein for the preparation of a relevant bioactive peptide. We opted for the tetrapeptide H-Tyr-Pro-Trp-Phe-NH$_2$ (EM1), the endogenous ligand of the μ-opioid receptors, currently regarded as a lead for the discovery of painkillers devoid of harmful side effects.[335] Thus, dipeptide *N*-Boc-Trp-Phe-NH$_2$ (Table 8, entry 14) was treated with gaseous HCl for the removal of the *N*-Boc protecting group,[321] to give the expected H-Trp-Phe-NH$_2$ hydrochloride salt in quantitative yield, which was coupled to Boc-Pro-OH (entry 22 in Table 8). After the usual work up, tripeptide *N*-Boc-Pro-Trp-Phe-NH$_2$ was obtained in satisfactory yield (65%) and purity (77%). The removal of *N*-Boc protecting group and subsequent coupling with *N*-Boc-Tyr-OH afforded *N*-Boc-protected EM1 (entry 23 in Table 8) in good yield and purity after rapid filtration through a short pad of silica gel (68% yield, 85% pure, see Appendix, Figure S9).

Ultra-mild grinding. The great utility of the mechanochemical approach is somewhat diminished by the need of a milling device specifically designed for mechanosynthesis.[313, 318, 320] In this respect, we decided to exploit the peculiar nanometric structure of HAp (see above) to design a mild synthetic protocol adaptable to common, inexpensive laboratory equipment. With this purpose, we performed the coupling between *N*-Boc-Phe-OH and H-Gly-OEt·HCl (0.23 mmol each) in the presence of EDC·HCl/HOBt (0.25 mmol each), and HAp (50 mg), in a 100 mL two-necked glass round bottom flask equipped with a standard olive-shaped FTFE-coated stirring bar (*l* = 3.0 cm), under inert atmosphere. The gently grinded mixture maintained a powdery appearance throughout the reaction process, and after 2 hours the expected dipeptide was obtained in modest yield (39%), albeit in fairly good purity (85%) after the usual work up. Increased reaction time had little impact on the yield (not shown), while conventional heating at 50°C led to a modest increase in yield (45%) (Table 9, entry 1).

Minimal solvent-assisted reaction. To increase the homogeneity of the mixture, the same reaction was performed in the presence of a minimal amount (80-200 µL) of a liquid additive (Table 9, entries 2-6), i.e. commonly-used DMF, and the green solvents EtOAc, *t*BuOAc, γ-valerolactone, *N*,*N*'-dimethylpropylene urea (DMPU).[314, 315, 321] After 2 h, the reaction was quenched and HAp was recovered according to the work up procedure described previously. While EtOAc, *t*BuOAc gave hardly satisfactory results (entries 2 and 3 in Table 9), the use of 80 µL of DMF (entry 4) or 100 µL DMPU (entry 5) gave the desired dipeptide in good yields (91%, 86%, respectively) and purities (94%, and 90%). Following aqueous work up, to remove the residual DMPU the mixture was filtered through a short pad of silica gel using 1:1 cyclohexane/EtOAc as mobile phase.

Table 9. Minimal solvent-assisted synthesis of peptides **3** (Scheme 15) from amino acids **1** and amino ester/amide HCl salts **2** (0.23 mmol each), after 2h at rt, in the presence of EDC·HCl/HOBt (0.25 mmol each) and HAp (50 mg), in a round bottom flask equipped with a PTFE-coated magnetic stirring bar.

Entry	1	2·HCl	Solvent	Vol (μL)	3 Yield (%) [a]	3 Purity (%) [a,b]
1	Boc-Phe-OH	H-Gly-OEt	-	-	45[c]	85
2	Boc-Phe-OH	H-Gly-OEt	EtOAc	200	48	78
3	Boc-Phe-OH	H-Gly-OEt	tBuOAc	100	52	80
4	Boc-Phe-OH	H-Gly-OEt	DMF	80	91	94
5	Boc-Phe-OH	H-Gly-OEt	DMPU	100	86[d]	90[d]
6	Boc-Phe-OH	H-Gly-OEt	γ-valerolactone	100	89	64
7	Boc-Phe-OH	H-Gly-NH$_2$	γ-valerolactone	100	88	84
8	Boc-Phe-OH	H-D-Val-OMe	DMF	80	91	96
9	Boc-Trp-OH	H-Phe-NH$_2$	DMF	80	93	95
10	Boc-Trp-OH	H-Phe-NH$_2$	DMF	80	86[e]	92[e]
11	Fmoc-Lys(Cbz)-OH	H-Ser-NH$_2$	DMF	100	70[d,f]	91[d,f]

[a] *Determined after aqueous workup.* [b] *Determined by RP-HPLC.* [c] *Conducted at 50°C.* [d] *After filtration through a pad of silica gel.* [e] *With HAp (48 mg) recovered from the preceding entry.* [f] *Traces of depsi-tripeptides (< 5% yield) were detected by RP-HPLC and ESI-MS.*

To our surprise, the reaction in γ-valerolactone (entry 6) gave the expected *N*-Boc-Phe-Gly-OEt dipeptide in low purity (64%). As it turned out, the reaction mixture presented significant amounts of various oligomers at the *N*-terminus, tripeptide *N*-Boc-Phe-Phe-Gly-OEt (18%) and tetrapeptide *N*-Boc-Phe-Phe-Phe-Gly-OEt (5%), as revealed by RP-HPLC ESI-MS analysis (see Appendix, Figure S10). Possibly, these by-products are the consequence of partial removal of the acid-labile *N*-Boc protecting group. Lewis and Brønsted acid sites coexist with basic sites on the surface of HAp.[328, 329] A recent study on the HAp-catalyzed transformation of ethanol to *n*-butanol revealed the key role played by the cooperation between the acid and basic sites, and the importance of the simultaneous presence of two weak acid-base pairs, namely Ca^{2+} - OH$^-$ and POH - OH$^-$, on the catalytic properties of HAp.[330]

On the other hand, the reaction between *N*-Boc-Phe-OH and H-Gly-NH$_2$ in γ-valerolactone (entry 7 in Table 9) gave the expected *N*-Boc-Phe-Gly-NH$_2$ protected dipeptide with better

purity (84%), being the unwanted oligomer N-Boc-Phe-Phe-Gly-NH$_2$ a side product (2% yield) (see Appendix, Figure S11).

The efficacy of using DMF as solvent was confirmed by reacting N-Boc-Phe-OH with H-(D)-Val-OMe·HCl (entry 8), and N-Boc-Trp-OH with H-Phe-NH$_2$·HCl under the same conditions (Table 9, entry 9). As it turned out, these reactions afforded better yields (91%, 93%, respectively) and purity (> 95%) when compared with solvent-free reaction conditions (compare Tables 9 and Table 8). As it was the case in the solvent-free protocol, the HAp powder recovered after the work-up from the reaction corresponding to entry 9 in Table 9 proceeded with little loss of efficiency, when reused to promote the reaction between the same, fresh reagents (compare with entry 10 in Table 9).

Finally, the reaction between N-Fmoc-Lys(N-Cbz)-OH and H-Ser-NH$_2$ (Table 9, entry 11) proceeded with slightly higher yield (70%) with respect to the solvent free variant (Cf. entry 21 in Table 8); nevertheless the desired dipeptide was obtained with much higher purity (91%). In particular, the analysis of the reaction mixture by RP-HPLC and ESI-MS showed only traces (< 5%) of the depsitripeptide N-Fmoc-Lys(N-Cbz)-D-Ser[N-Fmoc-Lys(N-Cbz)]-OMe (see Appendix, Figure S12).

8.3.   Conclusion

In conclusion, we optimized the unprecedented use of nanocrystalline HAp powder as inorganic, totally non-toxic base, to activate the reaction between N-protected amino acids and a variety of amino·HCl partners, in the presence of the coupling agents EDC·HCl/HOBt. The peculiar structure of HAp allowed smooth mechanochemical solvent-free condensation reactions under mild conditions, as well as minimal solvent-assisted reactions conducted in common laboratory glassware. Interestingly, the catalytic mineral powder could be reutilized for several cycles with little loss in efficiency. Plausibly, HAp acts as a sort of chemical sponge capable to passively absorb anhydrous HCl into its channels, leaving its crystalline structure intact, as confirmed by the comparison of the X-ray analyses of fresh and recycled powders.

8.4. Experimental Section

General methods

All purchased reagents were used without further purification. Ball milling was carried out in a Fritsch Pulverisette, using an agate jar (ø = 7.5 cm) equipped with 3 balls of the same material (ø = 2.0 cm). Purities were assessed by analytical RP-HPLC on an Agilent 1100 series apparatus, using a RP column Phenomenex mod. Gemini 3μ C18 110 Å 100 × 3.0 mm; stationary phase: octadecyl carbon chain-bonded silica (C_{18}) with TMS endcapping, fully porous organo-silica solid support, particle size 3 μm, pore size 110 Å, length 100 mm, internal diameter 3 mm; DAD 210; mobile phase: from 9:1 solvent A/solvent B to 2:8 solvent A/solvent B, in 8 min, at a flow rate of 0.5 mL min^{-1}, followed by 10 min at the same composition; for the analysis of crude reaction mixtures, the solvent system was: A = 0.5% HCOOH in H_2O, B = 0.5% HCOOH in CH_3CN; for the analyses of the mixtures after work-up, the solvent system was: A = H_2O, B = CH_3CN. Filtration of crude reaction mixture was done through a short pad of on silica gel (230-400 mesh), using a mixture of distilled solvents. ESI-MS was done on a MS single quadrupole HP 1100MSD detector, drying gas flow of 12.5 L min^{-1}, nebulizer pressure 30 psgi, drying gas temp 350 °C, capillary voltage 4500(1) and 4000(2), scan 50-2600 amu. ^{1}H-NMR was performed at 400 MHz on a Varian Gemini 400 in 5 mm tubes at rt, using the solvent $CDCl_3$; chemical shifts are reported as δ values relative to residual $CHCl_3$ ($\delta_H = 7.26$ ppm).

Hydroxyapatite nanocrystals. The procedure was performed under N_2 atmosphere and using CO_2-free distilled water as reported in the literature.[326] The synthesis of hydroxyapatite was carried out using 50 ml of 0.65 M $(NH_4)_2HPO_4$ solution at pH adjusted to 10 with NH_4OH. The solution was heated to 90 °C and 50 ml of 1.08 M $Ca(NO_3)_2 \cdot 4H_2O$ solution, pH 10 adjusted with NH_4OH was added dropwise under stirring. The resulting suspension was stirred for 5 hours at 90 °C, the precipitate that formed was isolated by centrifugation at 10000 rpm, and repeatedly washed with CO_2-free distilled water. The product was dried at 37°C overnight.

FTIR analysis was done on a Bruker Alpha FTIR spectrophotometer; 1 mg of the powdered HAp was mixed with 300 mg of KBr (infrared grade) and pelletized at the pressure of 10 tons in 2 minutes. The pellets were analyzed in the range 4000-500 cm^{-1}, 32 scans, resolution 4 cm^{-1}.

Powder X-ray diffraction patterns were recorded using a PANalytical-X'Pert PRO powder diffractometer equipped with a fast X'Celerator detector (λ = 0.154 nm, 40 mA, 40 kV). For phase identification the 2θ range was investigated from 10 to 60 $2\theta°$ with a step size of 0.1° and time/step of 100 s. For evaluation of cell parameters, X-ray powder data were collected with a fixed counting time of 400 s for each 0.033/step. The Rietveld routine of the HighScore Plus software package (PANalytical) was used to process data.

For TEM investigations, a small amount of powder was dispersed in ethanol and submitted to ultrasonication. A drop of the calcium phosphate suspension was transferred onto holey carbon foils supported on conventional copper microgrids. A Philips CM 100 transmission electron microscope operating at 80 kV was used.

Ca and P contents in HAp were measured by means of an ICP spectrometer (ICP-AES, Horiba Jobin Yvon). Sample was prepared by dissolving 20 mg of powder in 70% nitric acid solution (4 mL) and diluting to final volume of 100 mL.

Zeta potential was measured using Electrophoretic Light Scattering (ZetasizerNano; Malvern Instruments). 5 mg of HAp was suspended in 50 mL of MilliQ water after sonication for 2 min. The analysis was performed in triplicate.

The surface area was measured using a Carlo Erba Sorpty 1750 BET analyser using constant volume N_2 absorption with desorption at 80°C.

Solvent-free milling. The general procedure is as follows: A mixture of the *N*-protected-amino acid (0.23 mmol), EDC·HCl/HOBt (0.25 mmol each) and hydroxyapatite (HAp, 50 mg) was grinded in an agate jar (ø = 7.5 cm) equipped with 3 balls of the same material (ø = 2.0 cm), at the speed of 8-10 Hz, at rt for 10 min. Then the amino ester/amide counterpart (0.23 mmol) was added at rt, and the mixture was grinded for 1 h under the same conditions. The mechanical milling was interrupted, the waxy residue was diluted with EtOH (10 mL), and HAp was recovered by centrifugation (10000 rpm). The precipitated crystals were washed with EtOH and centrifuged once more and stored overnight at 40°C prior to reuse. The collected supernatant from centrifuged samples were combined and concentrated at reduced pressure, the residue was diluted with EtOAc (30 mL), and the organic layer was washed in sequence with 1M HCl, sat. Na_2CO_3, and brine (5 mL each).

N-Boc solvent free removal. *N*-Boc deprotection was accomplished under solvent free conditions as reported in the literature.[321] Briefly, the protected dipeptides were placed on a Gooch filter inside a fume hood, and HCl gas was blown through for 3 h.

Minimal solvent-assisted grinding. General procedure: A mixture of the *N*-protected-amino acid (0.23 mmol), EDC·HCl/HOBt (0.25 mmol each), HAp (50 mg), and the solvent (80-200 μL), was grinded in a two-necked glass round bottom flask equipped with an olive-shaped PTFE-coated stirring bar ($l = 3.0$ cm), under inert atmosphere at rt for 10 min. Then the amino ester/amide counterpart (0.23 mmol) was added at rt, and the mixture was grinded for 2h under the same conditions. Then the smooth amalgam was diluted with EtOH (10 mL), and HAp was recovered by centrifugation (10000 rpm). The produced crystals were washed with EtOH and centrifuged once more and stored overnight at 40 °C prior to reuse. The collected supernatants from centrifuged samples were treated as discussed for the *solvent-free* ball milling conditions.

9. APPENDIX

A. Representative NMR data for Chapter 4

MA192/199: ¹H-NMR and ¹³C-NMR (400 MHz, 101 MHz, DMSO-d_6)
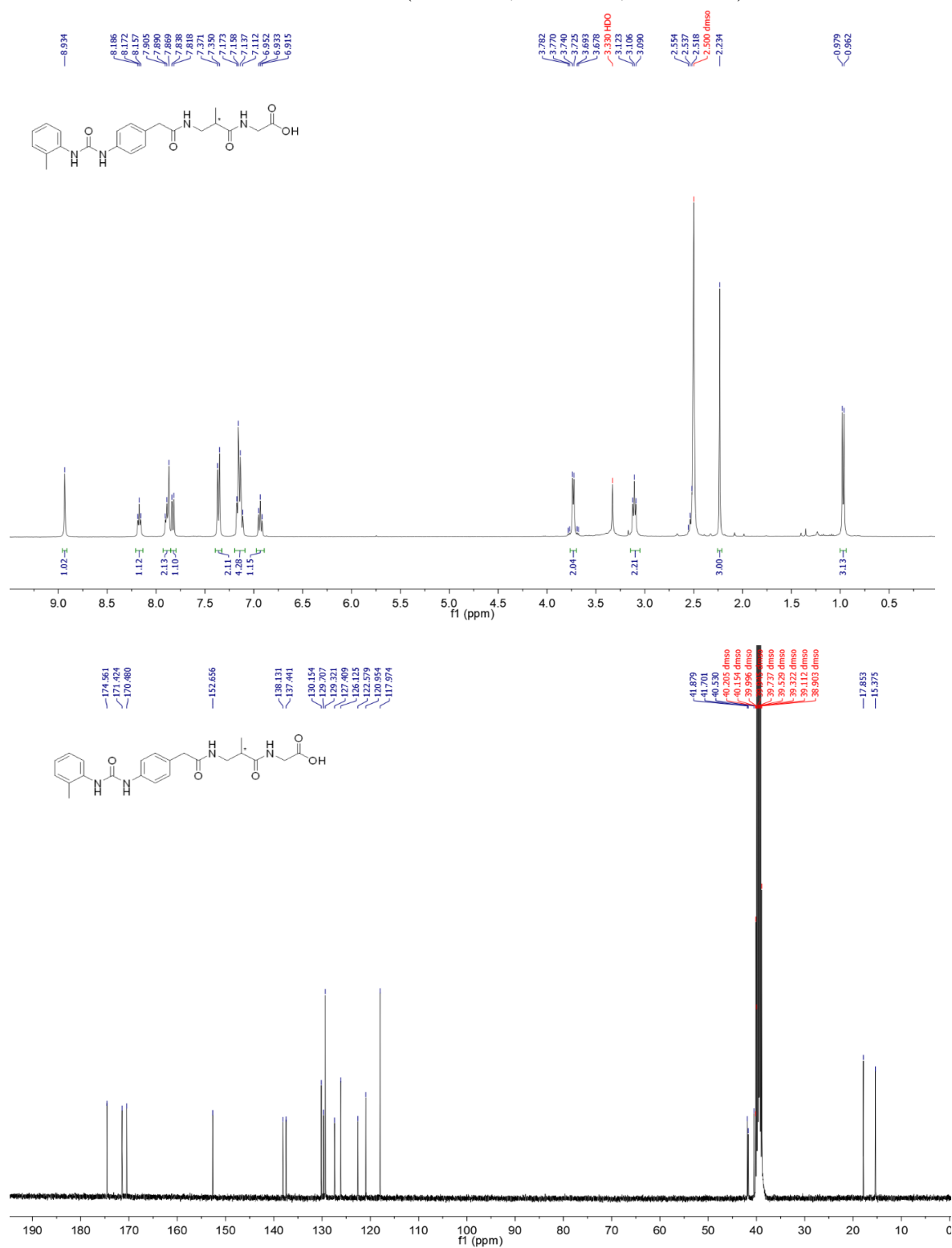
MA204/206: ^{1}H-NMR and ^{13}C-NMR (400 MHz, 101 MHz, DMSO-d_6)
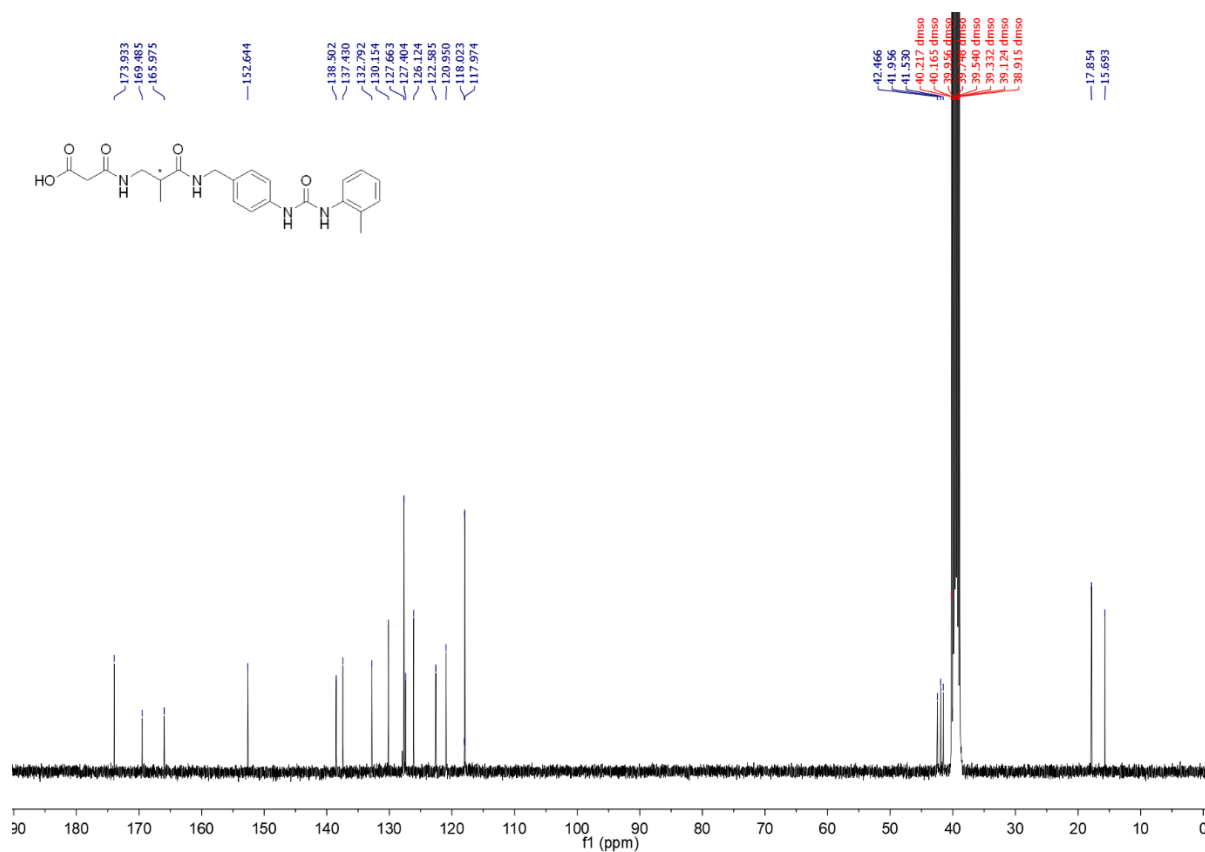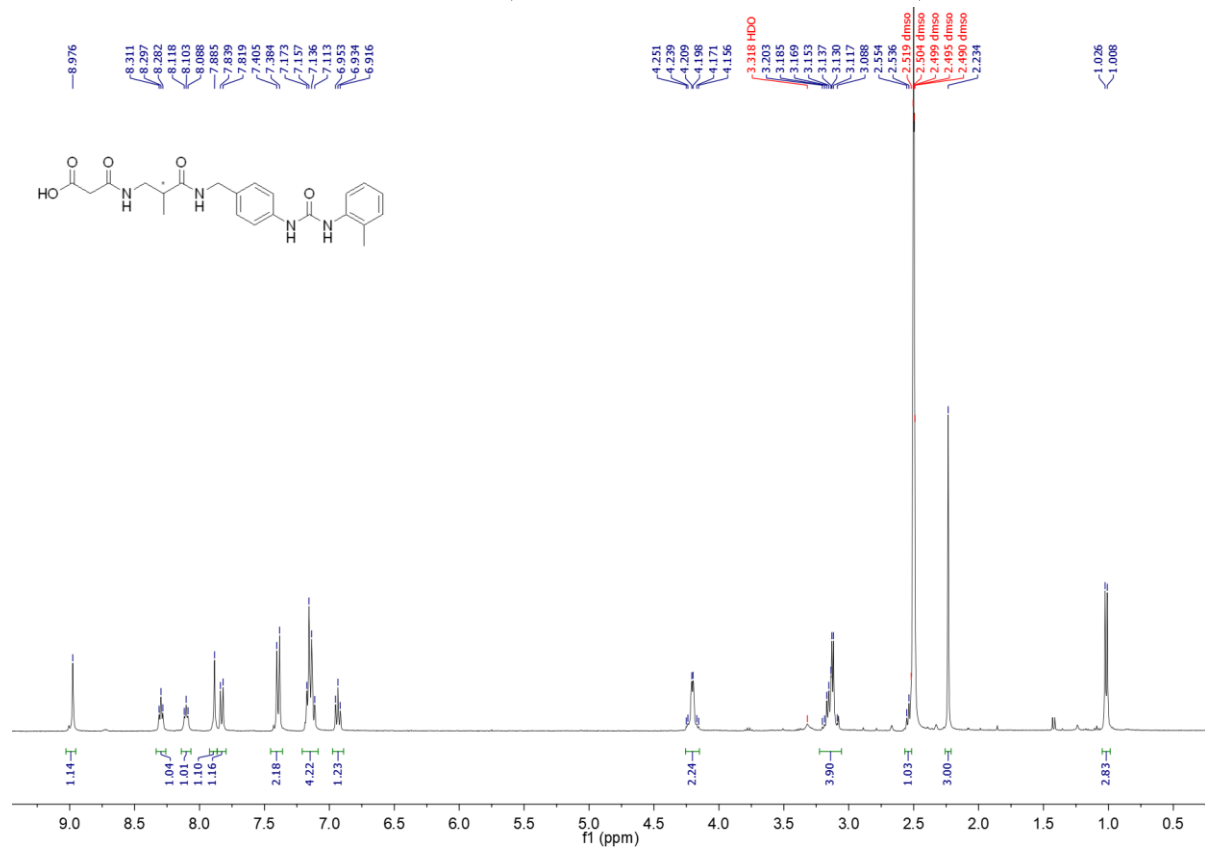
MA63/158: ^{1}H-NMR and ^{13}C-NMR (400 MHz, 101 MHz, DMSO-d_6)
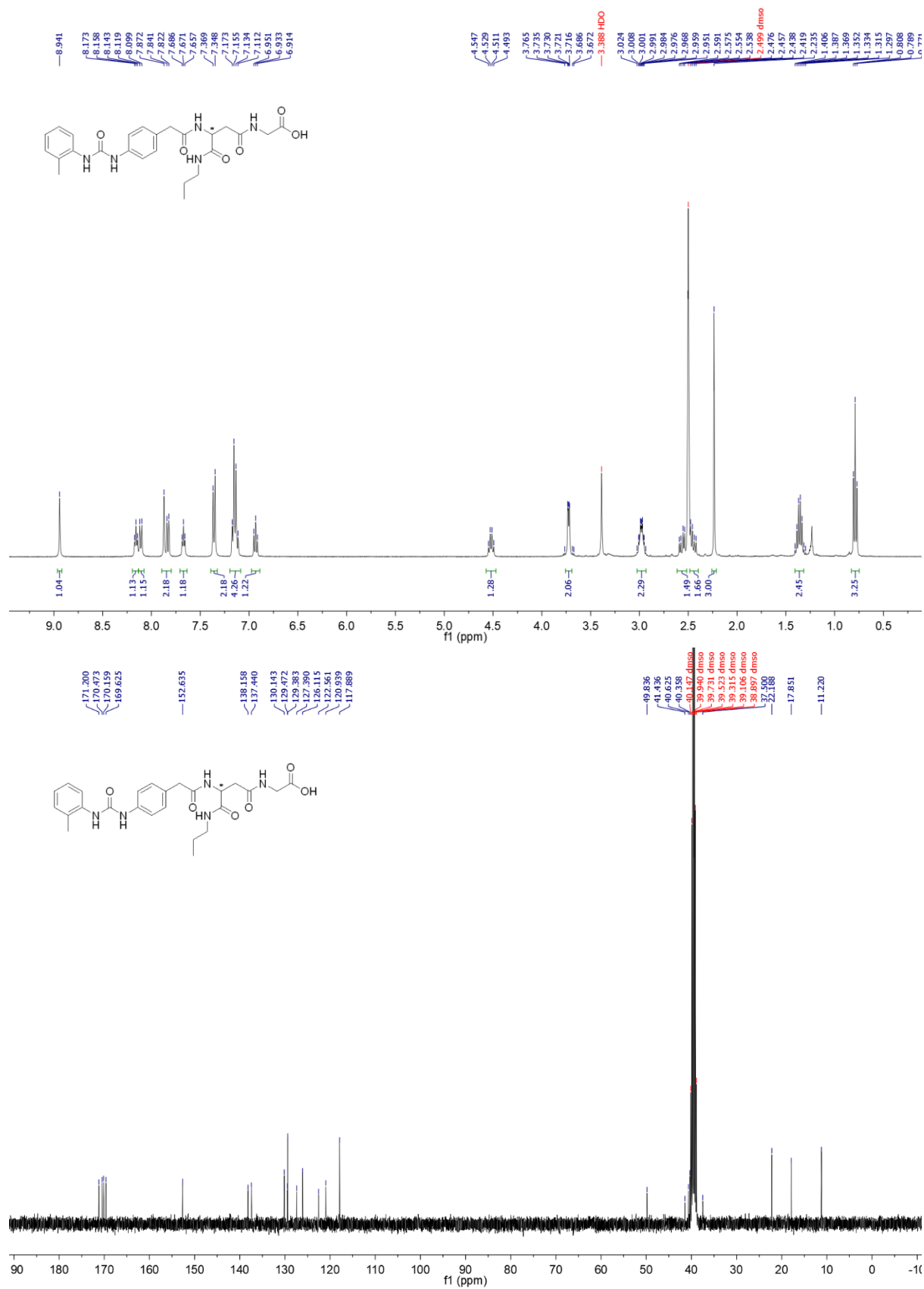
MA154/161: ^{1}H-NMR and ^{13}C-NMR (400 MHz, 101 MHz, DMSO-d_6)
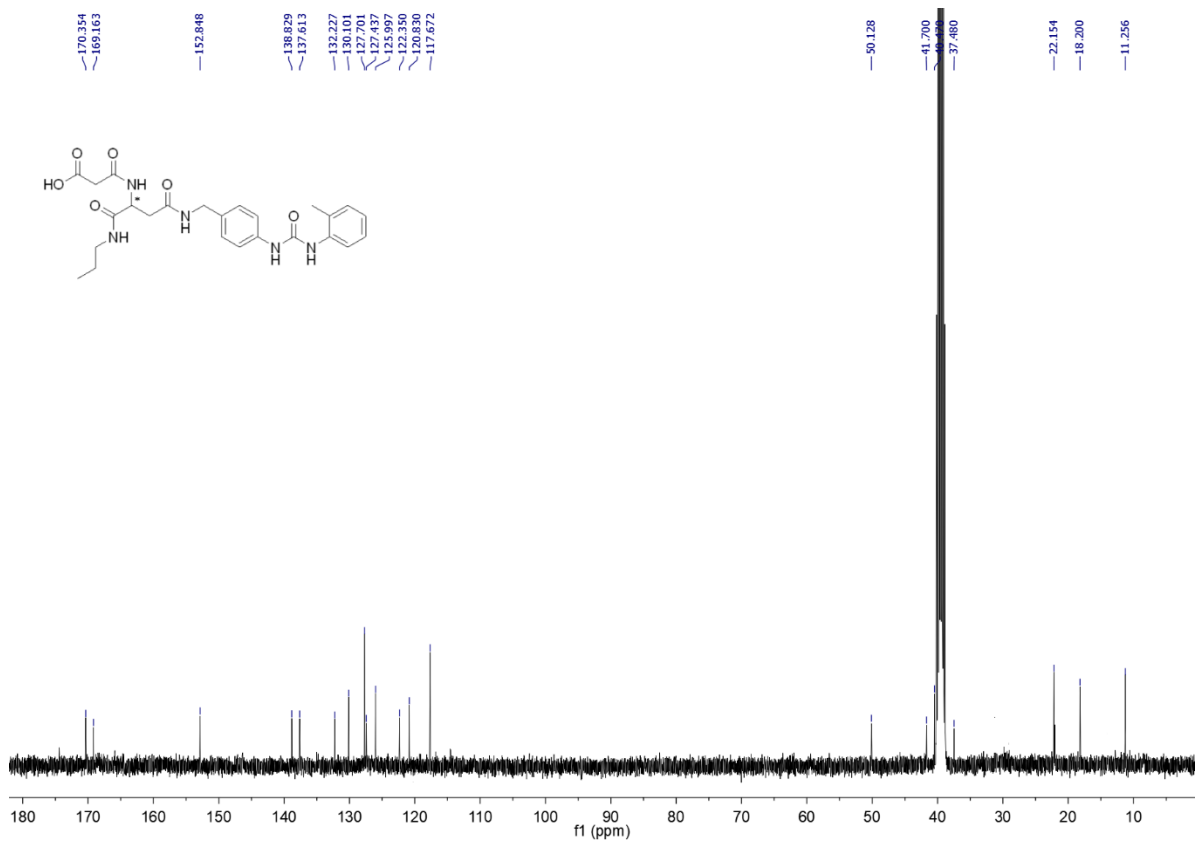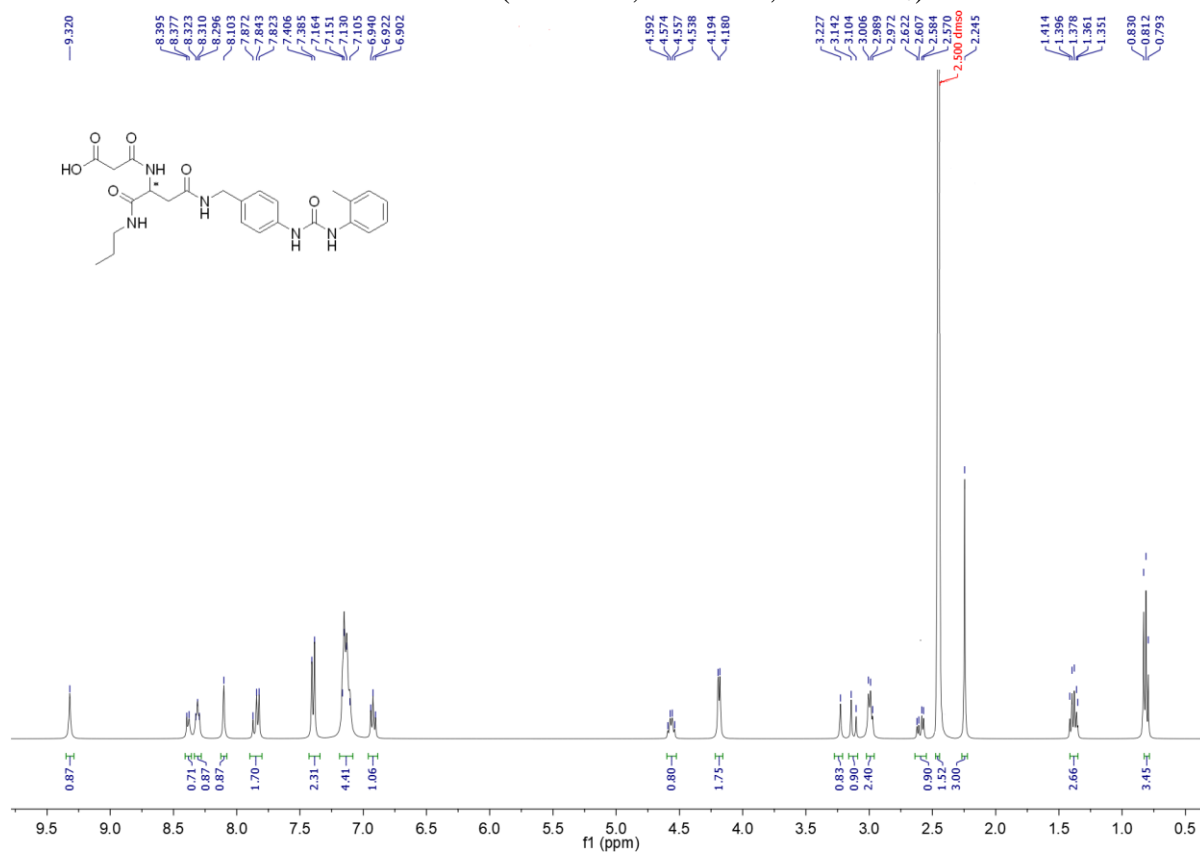
MA28/30: ^{1}H-NMR and ^{13}C-NMR (400 MHz, 101 MHz, DMSO-d_6)
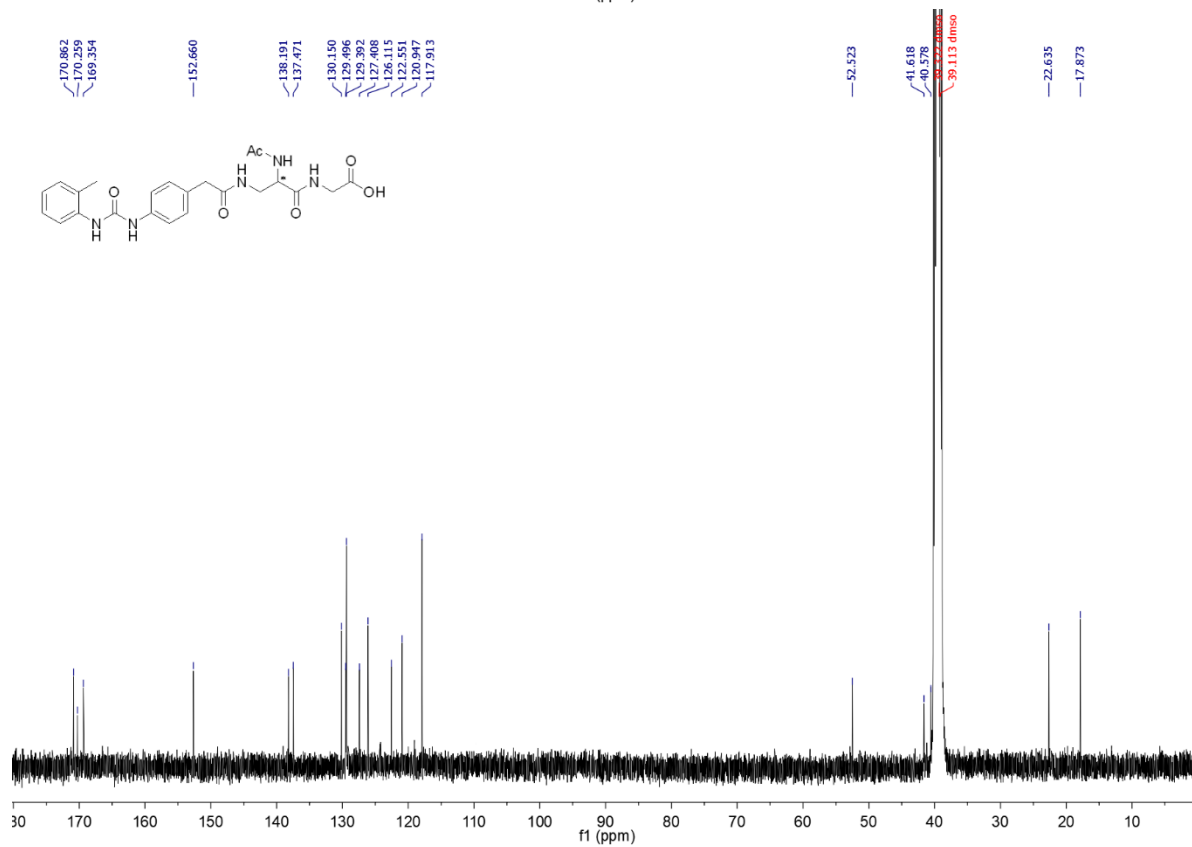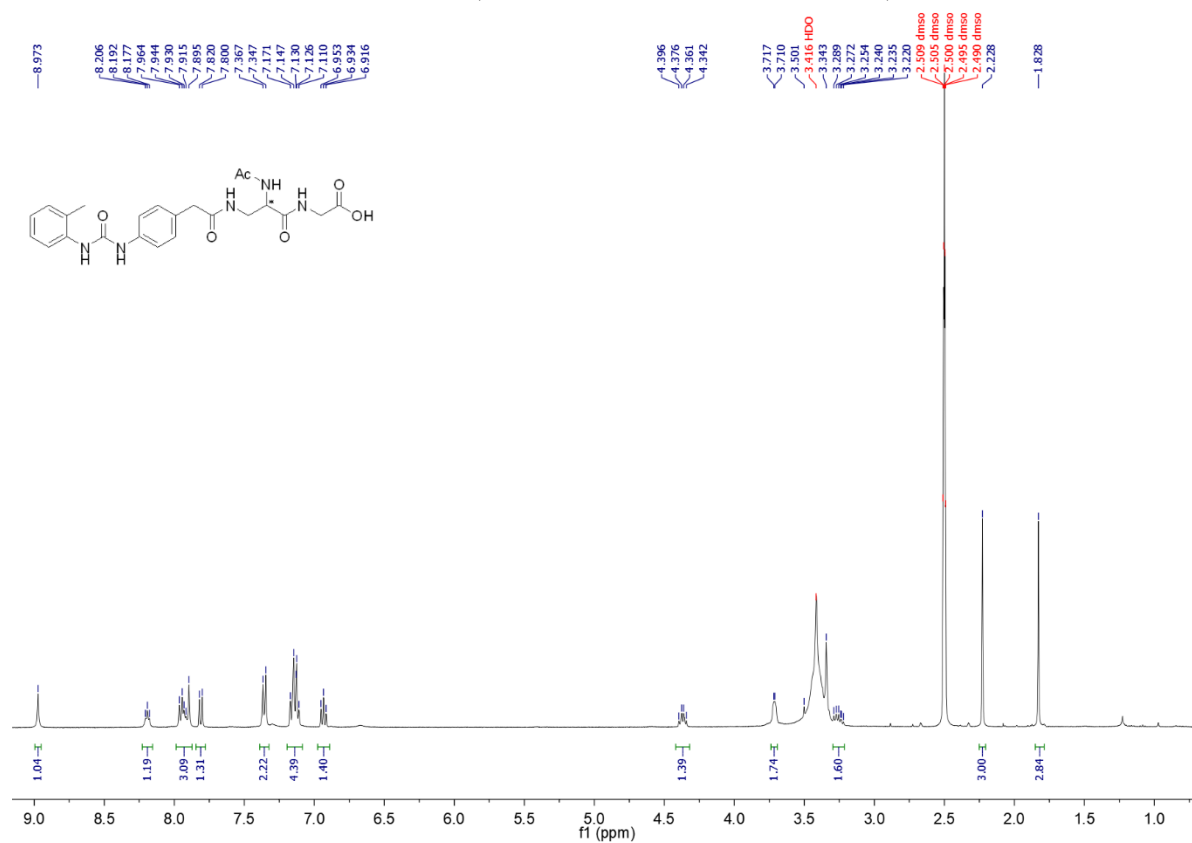
MA200/198: ^{1}H-NMR and ^{13}C-NMR (400 MHz, 101 MHz, DMSO-d_6)
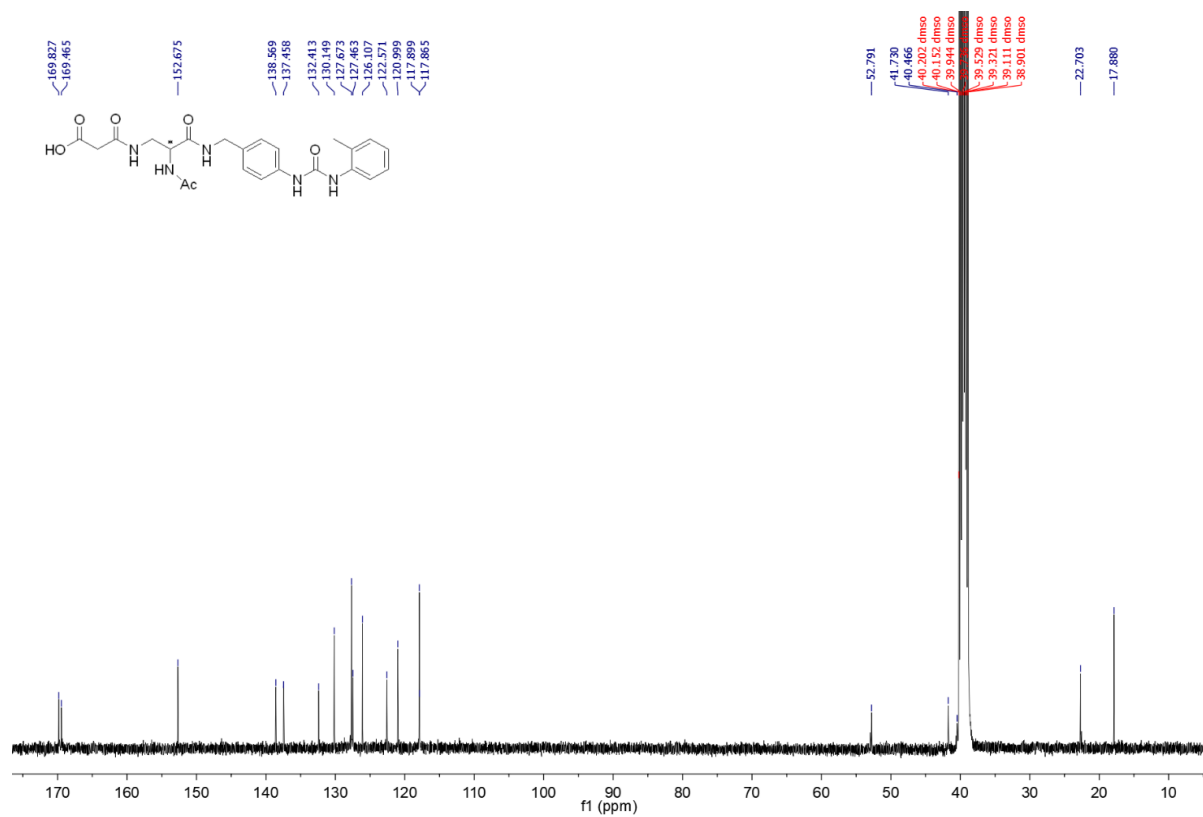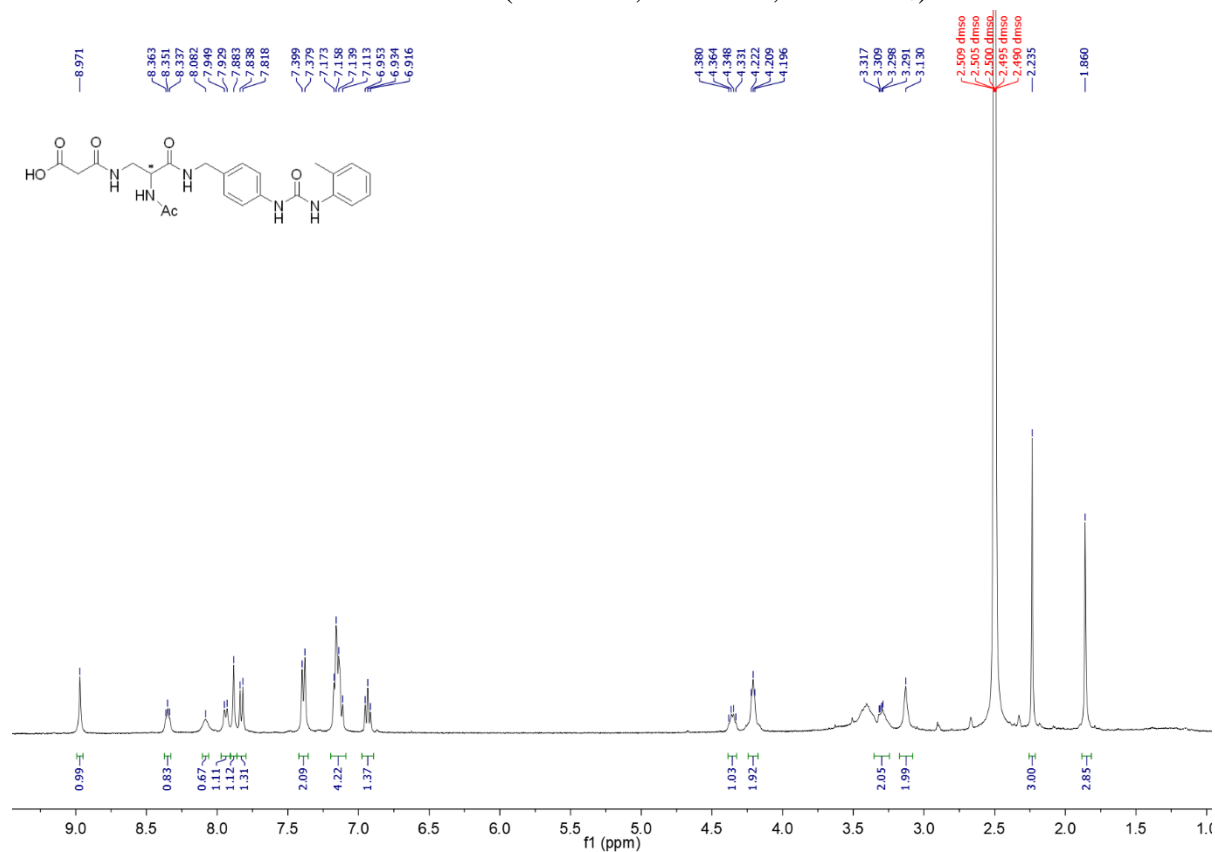
B. Representative NMR data for Chapter 5

MA86: ^{1}H-NMR and ^{13}C-NMR (400 MHz, 101 MHz, DMSO-d_6)

MA133: ^{1}H-NMR and ^{13}C-NMR (400 MHz, 101 MHz, DMSO-d_6)
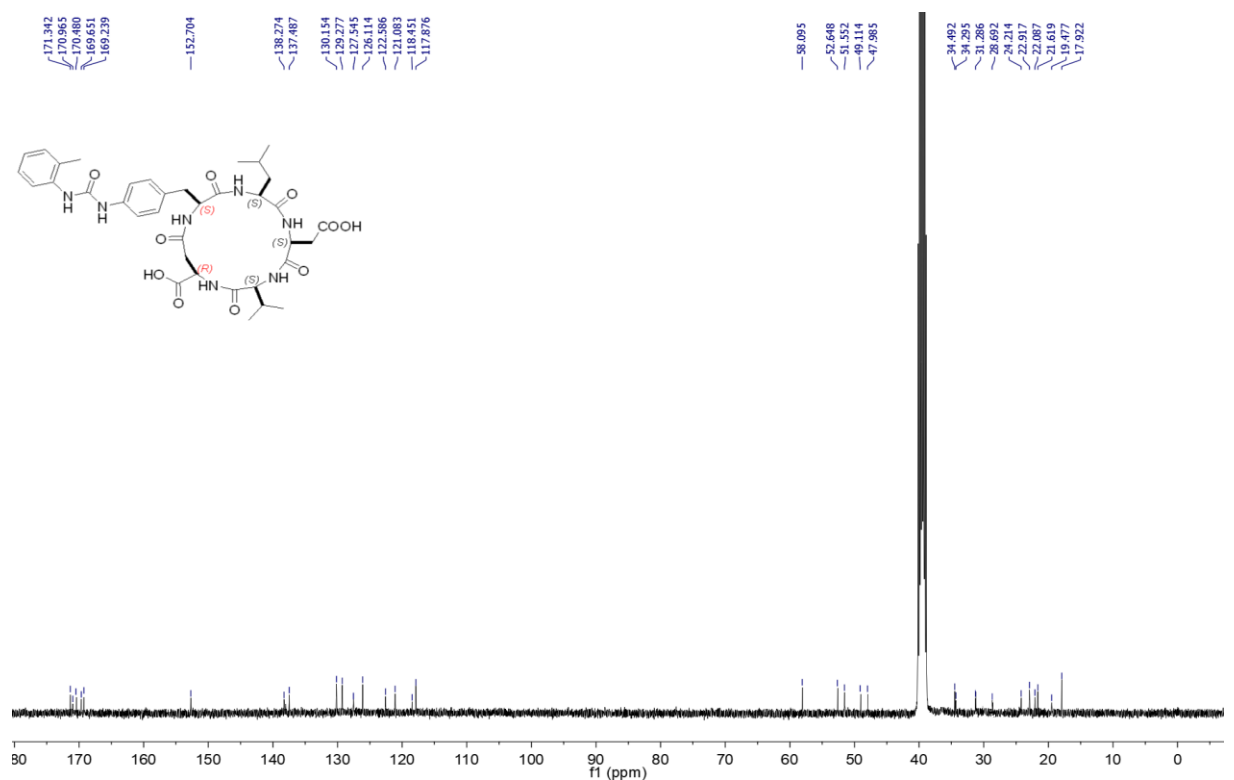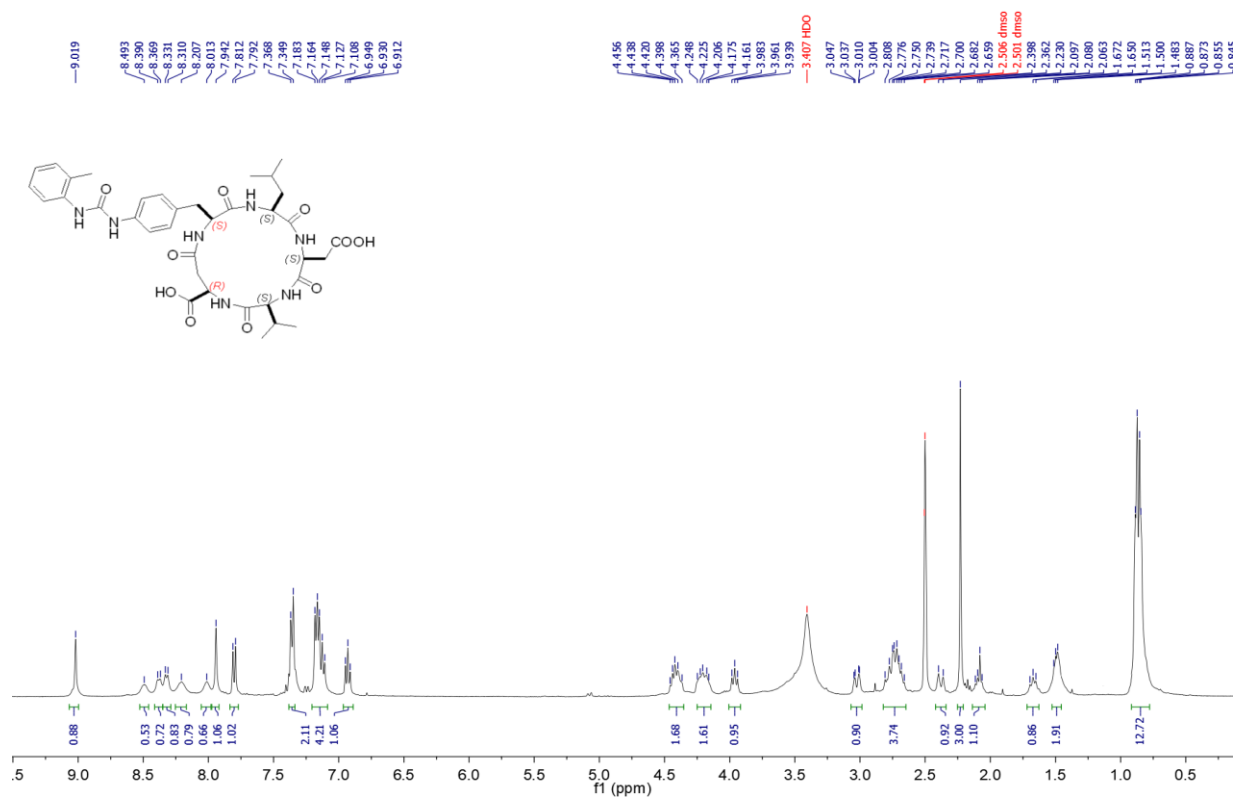
MA144: ^{1}H-NMR and ^{13}C-NMR (400 MHz, 101 MHz, DMSO-d_6)
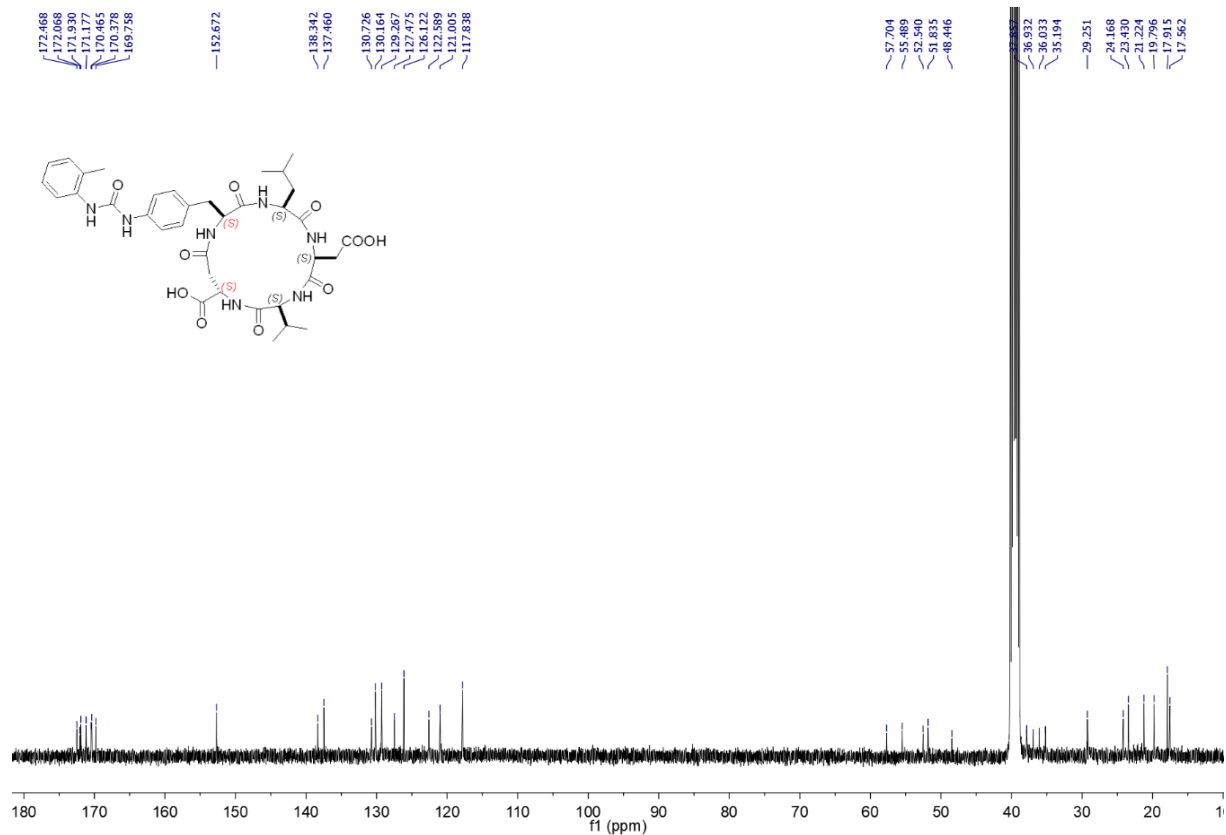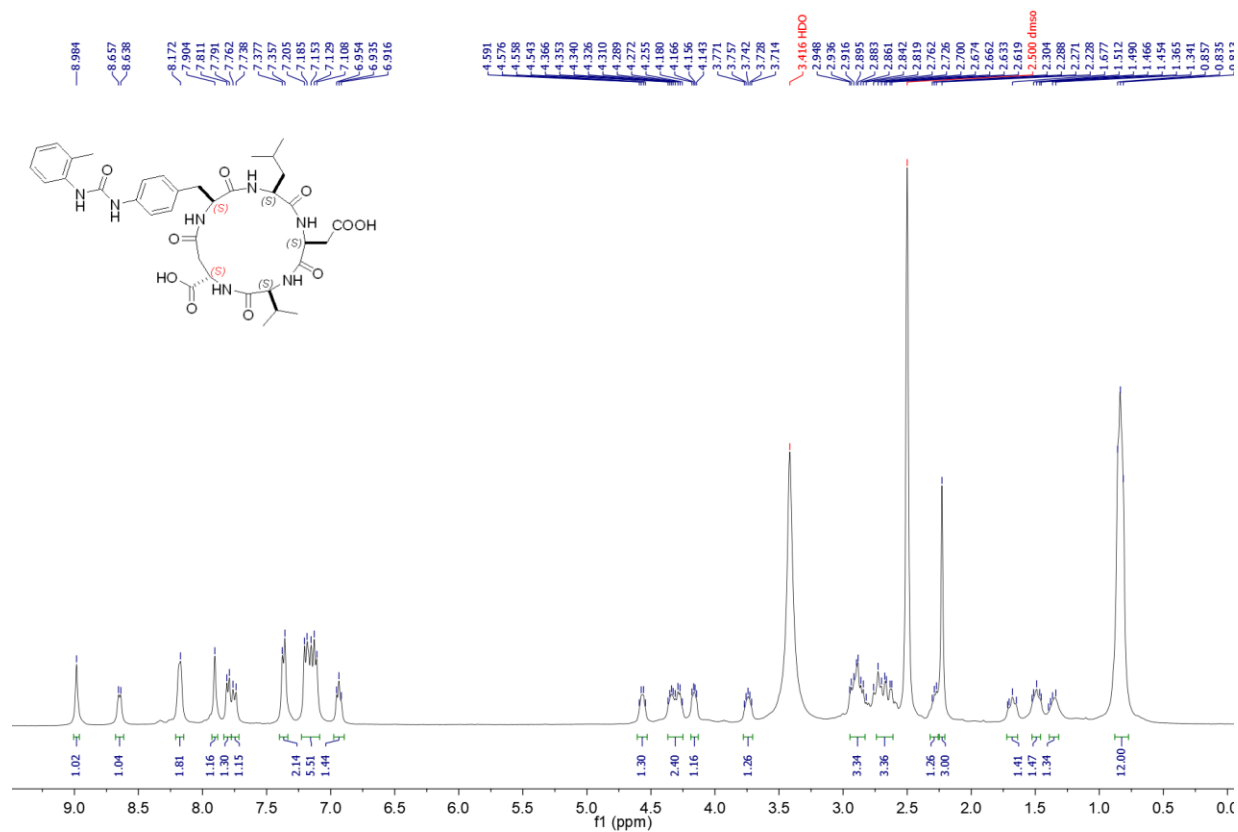
MA266: ^{1}H-NMR and ^{13}C-NMR (400 MHz, 101 MHz, DMSO-d_6)
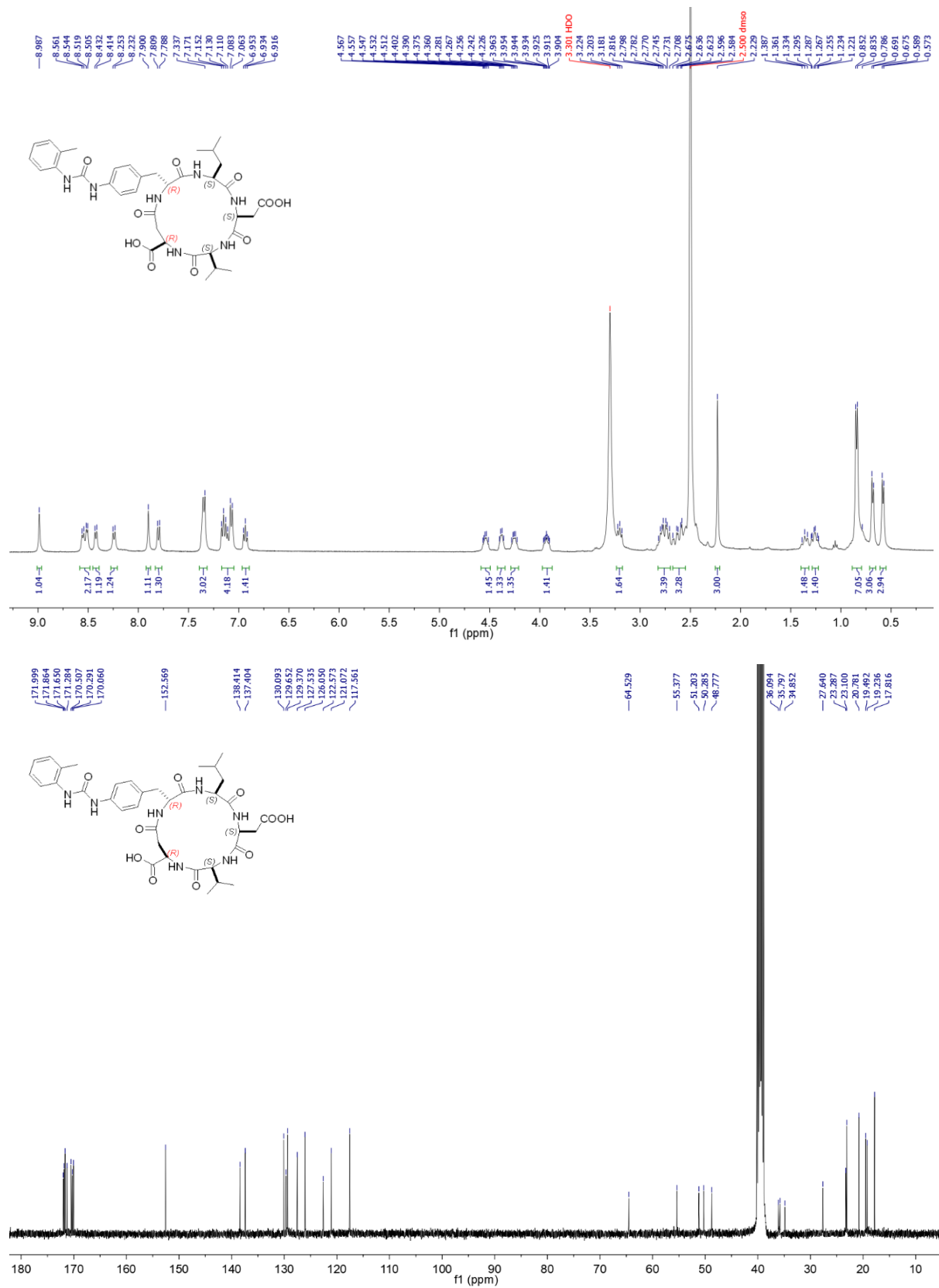
MA227: ^{1}H-NMR and ^{13}C-NMR (400 MHz, 101 MHz, DMSO-d_6)
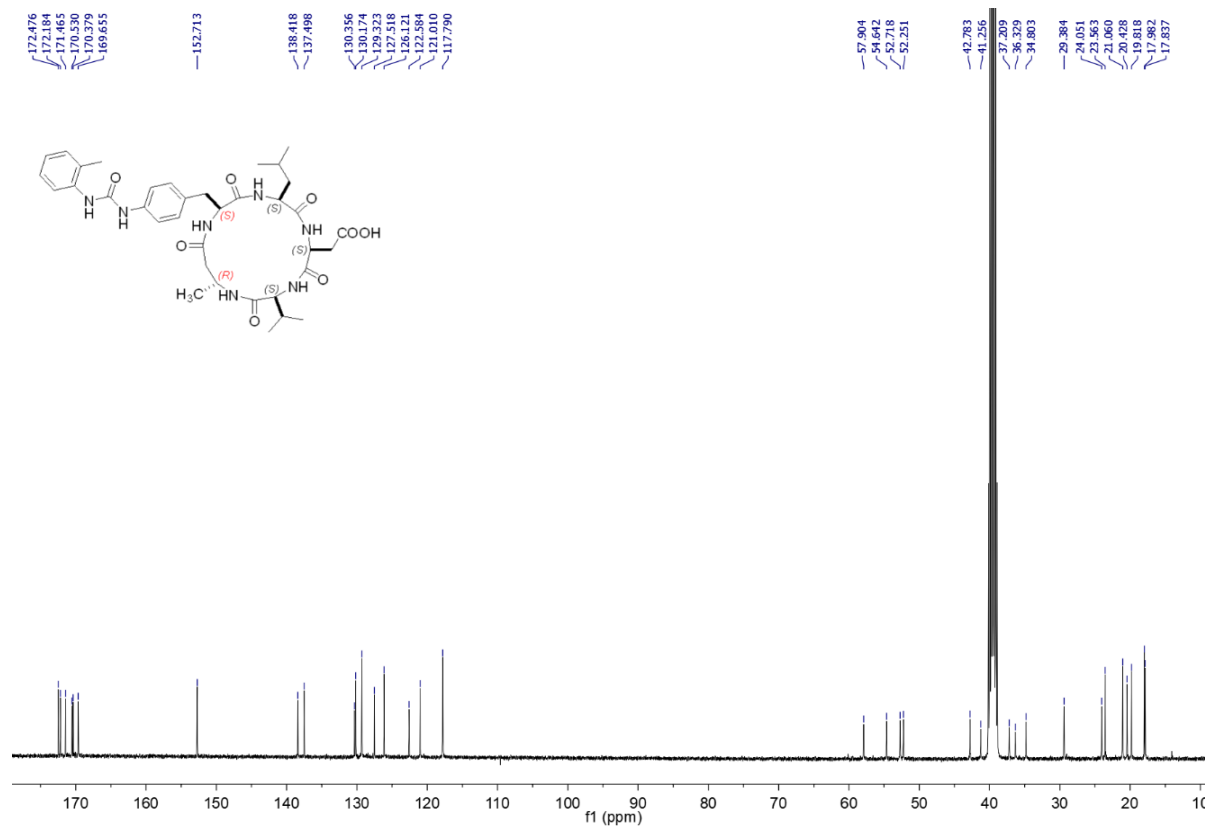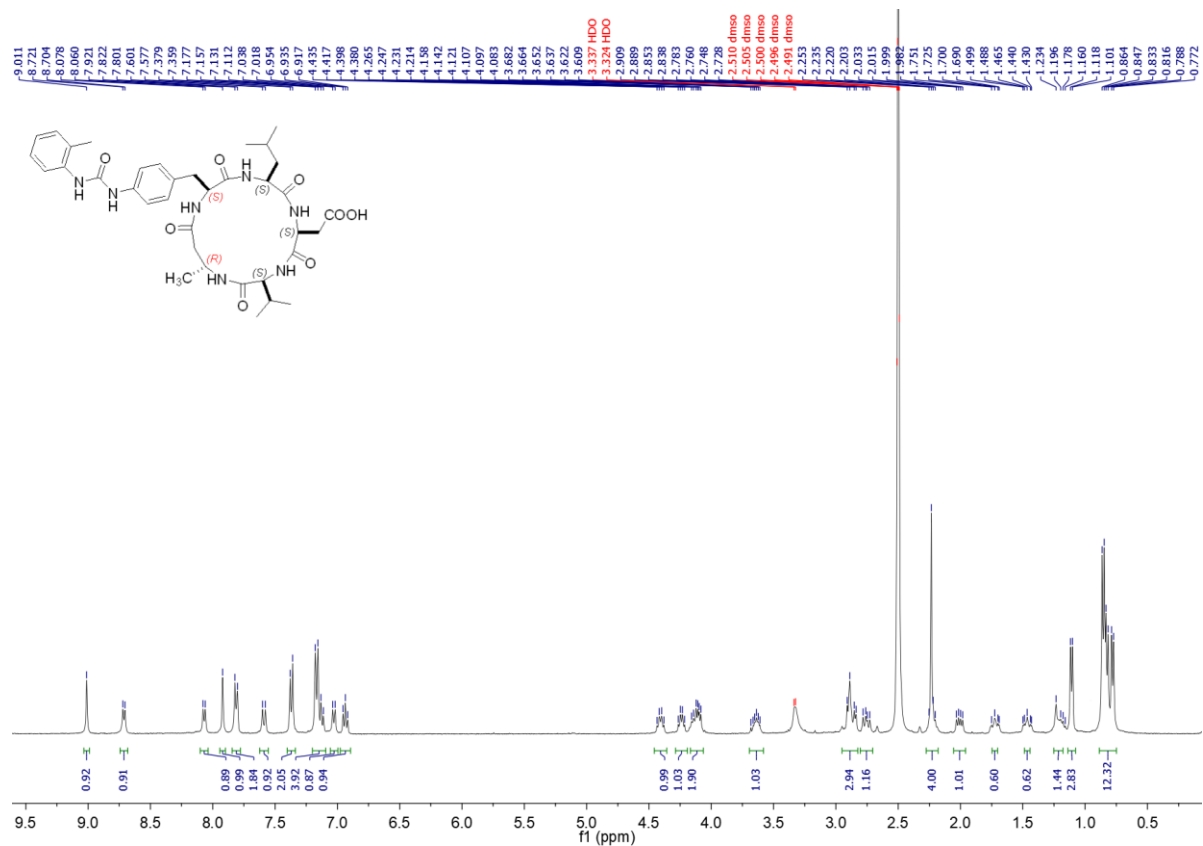
MA236: ^{1}H-NMR and ^{13}C-NMR (400 MHz, 101 MHz, DMSO-d_6)
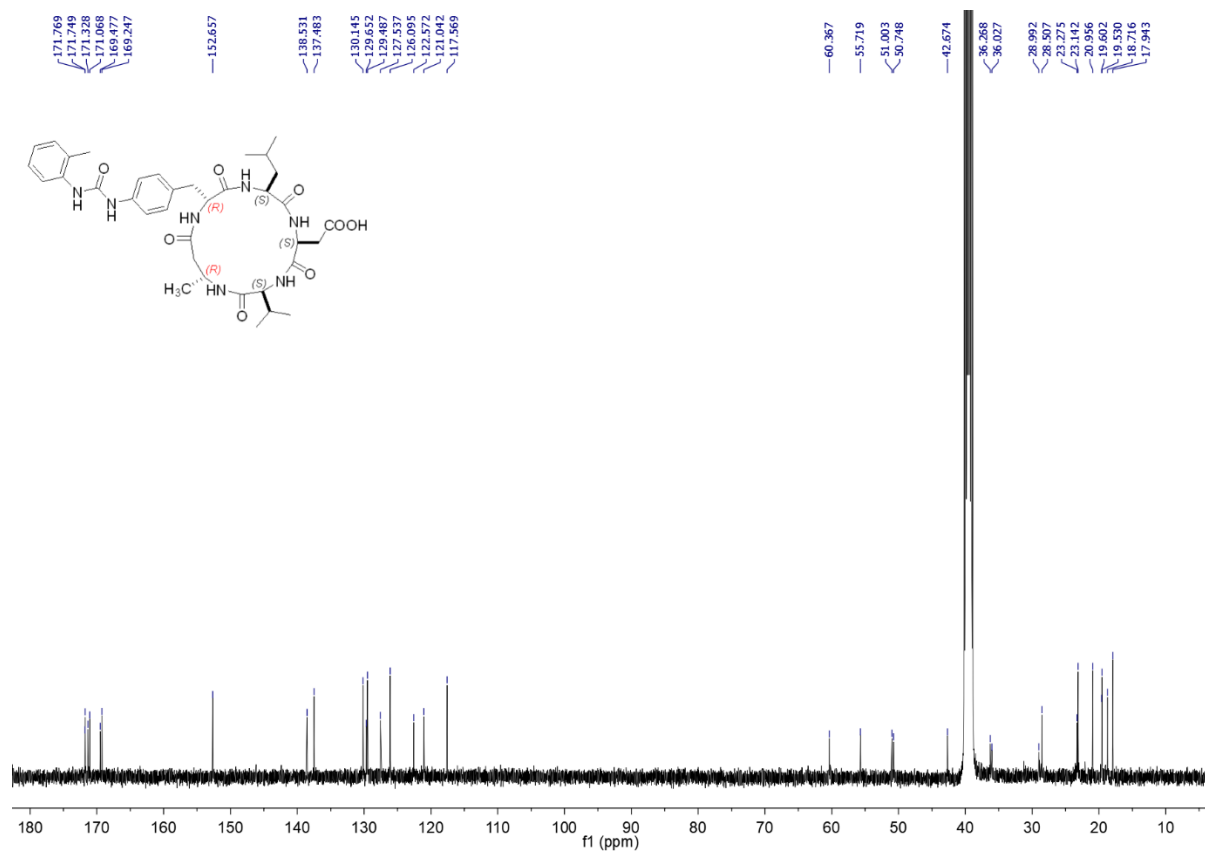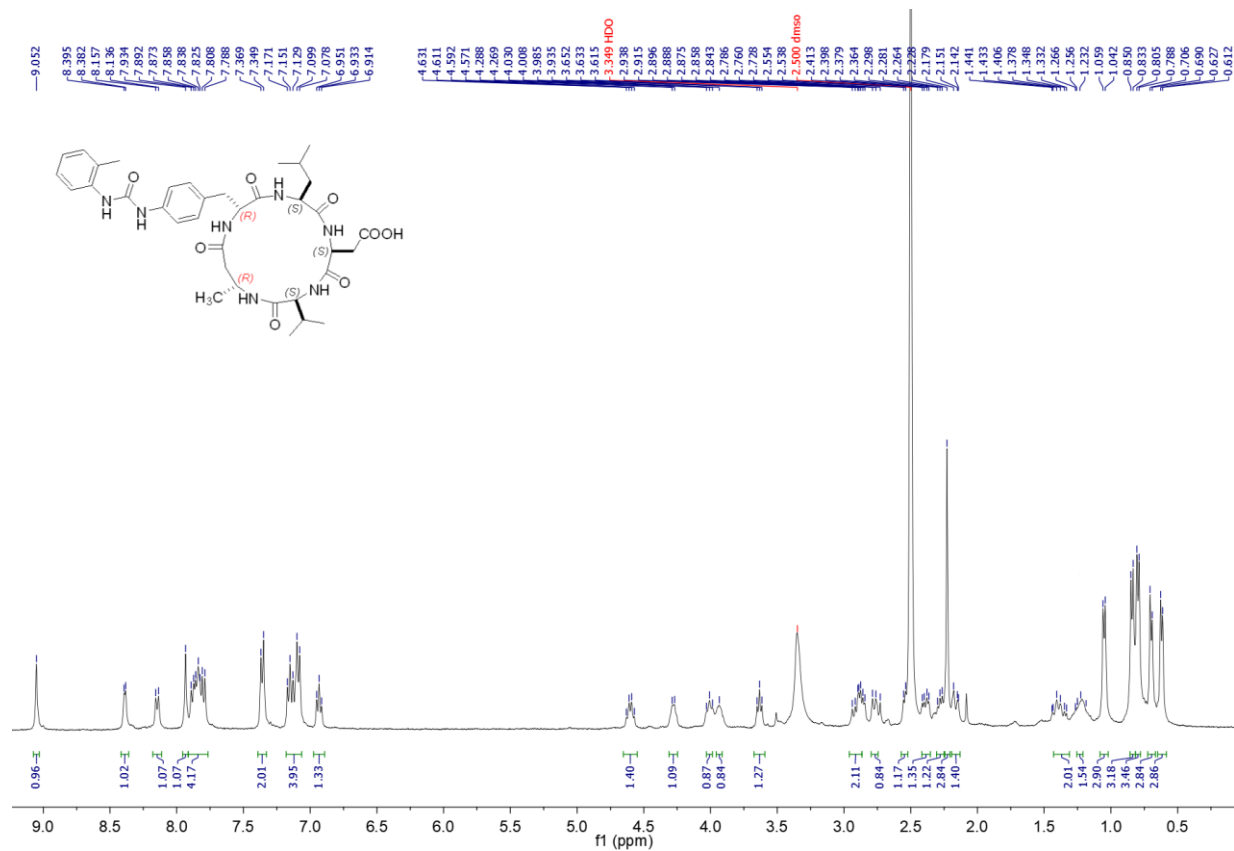
MA171: ^{1}H-NMR and ^{13}C-NMR (400 MHz, 101 MHz, DMSO-d_6)
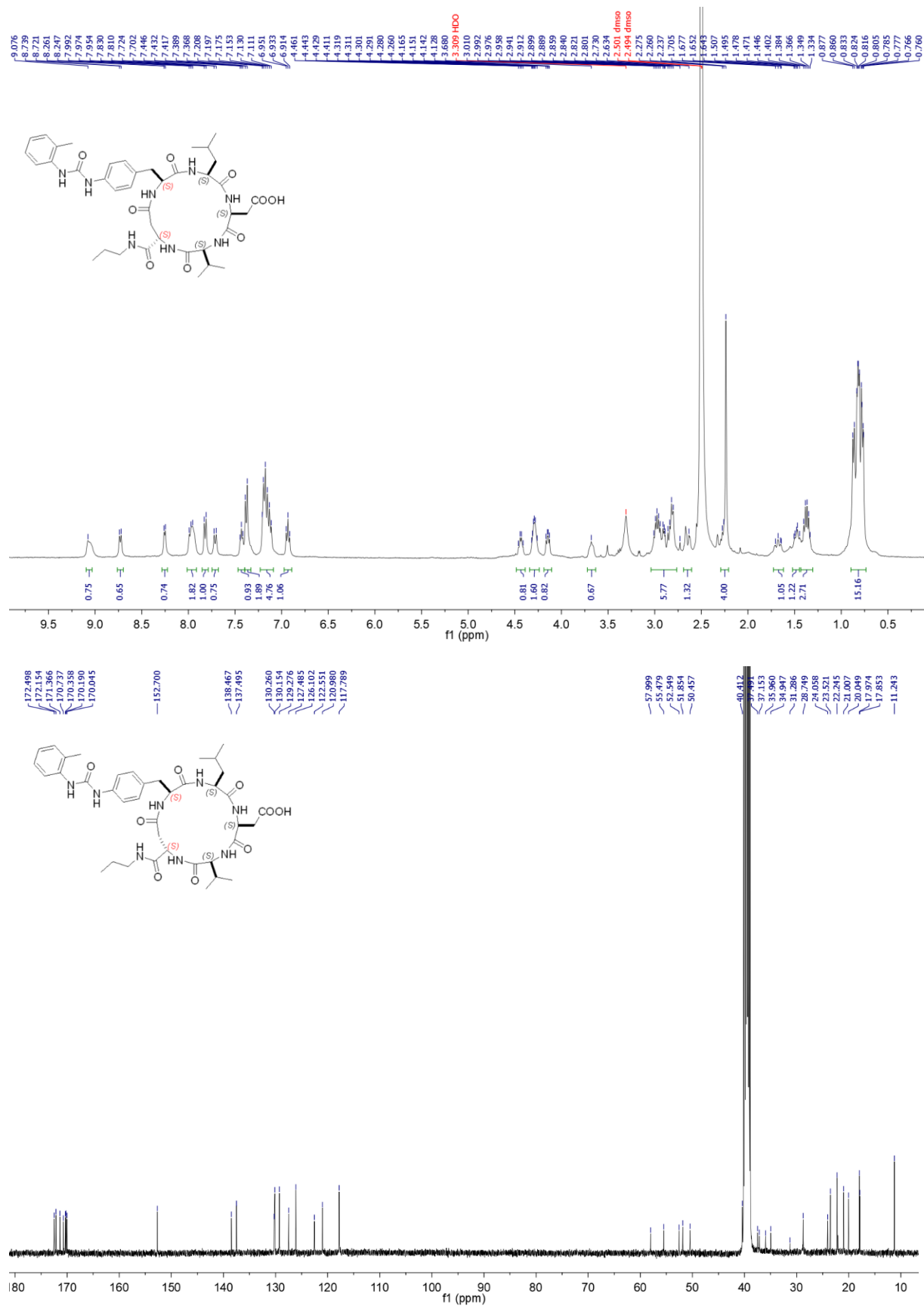
MA264: ^{1}H-NMR and ^{13}C-NMR (400 MHz, 101 MHz, DMSO-d_6)
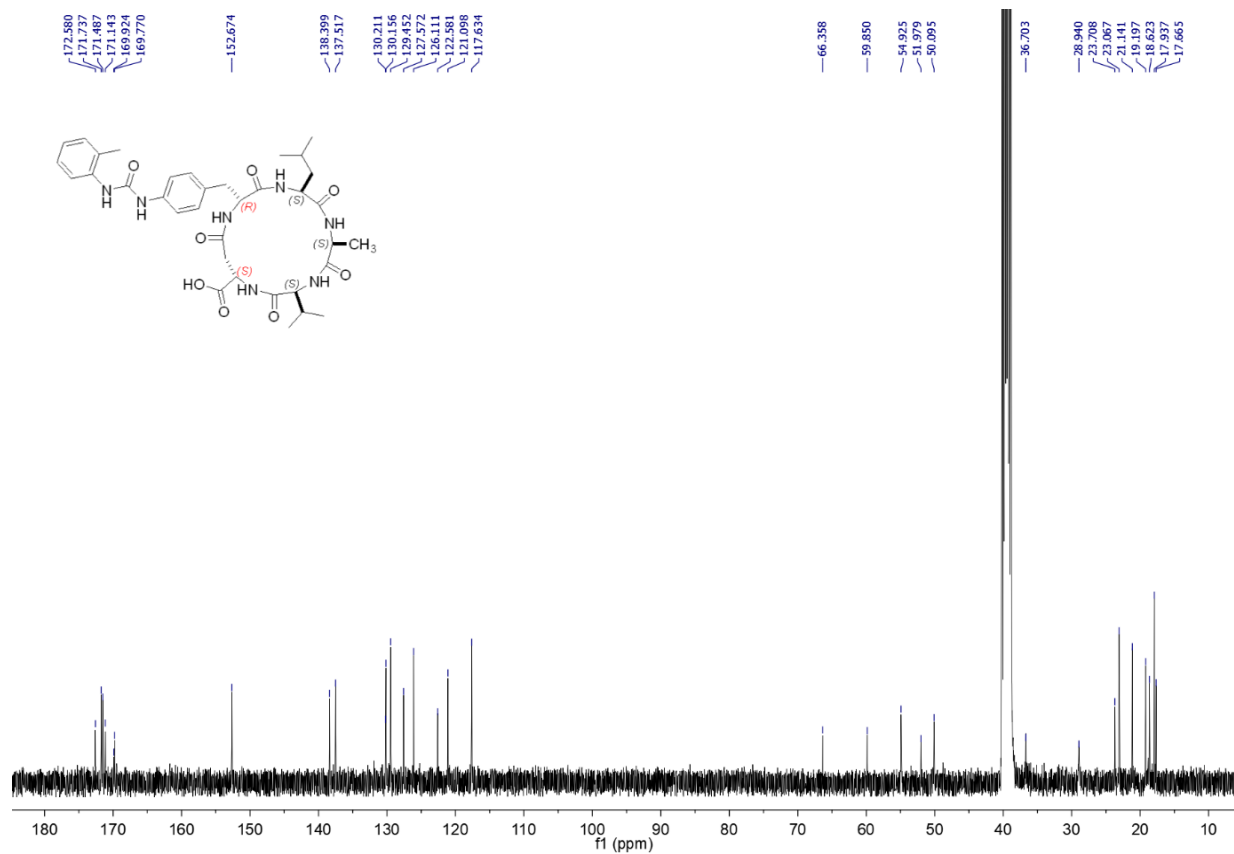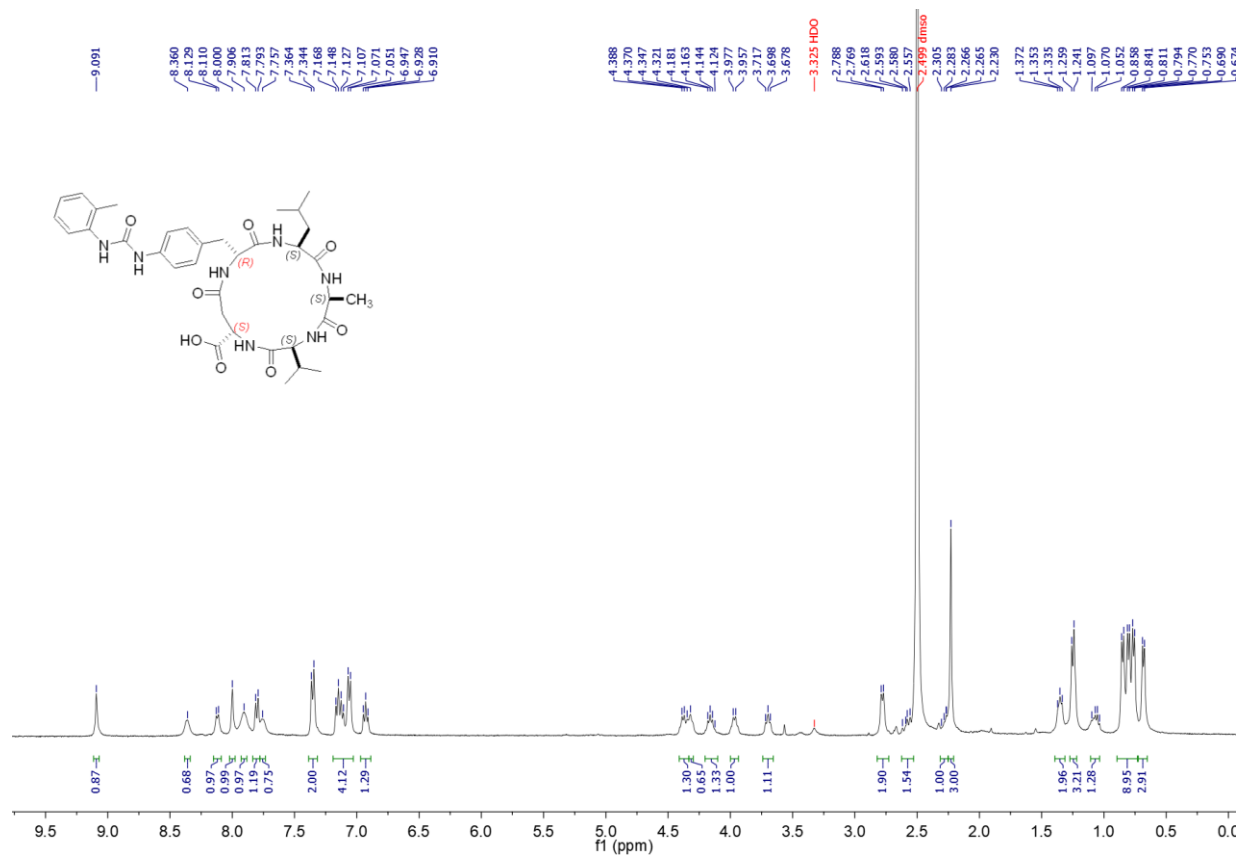
MA265: ^{1}H-NMR and ^{13}C-NMR (400 MHz, 101 MHz, DMSO-d_6)
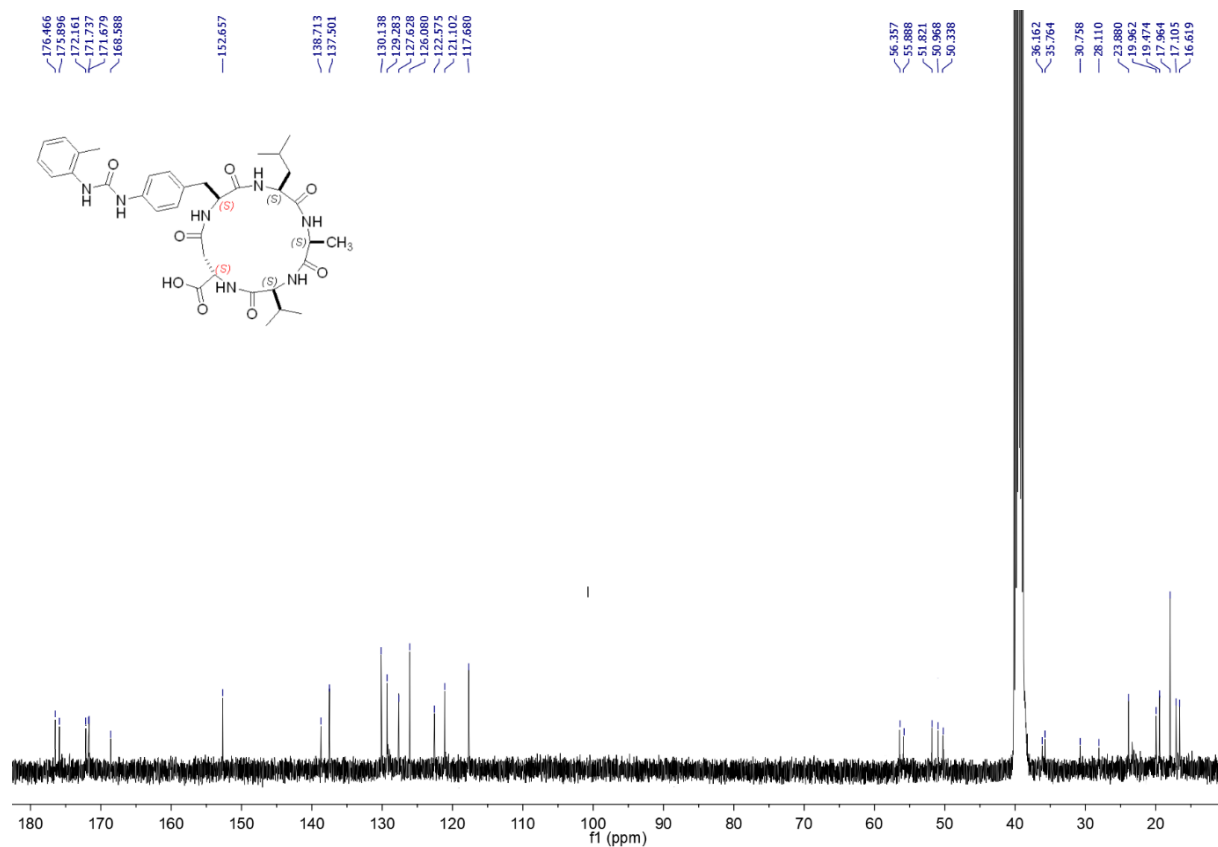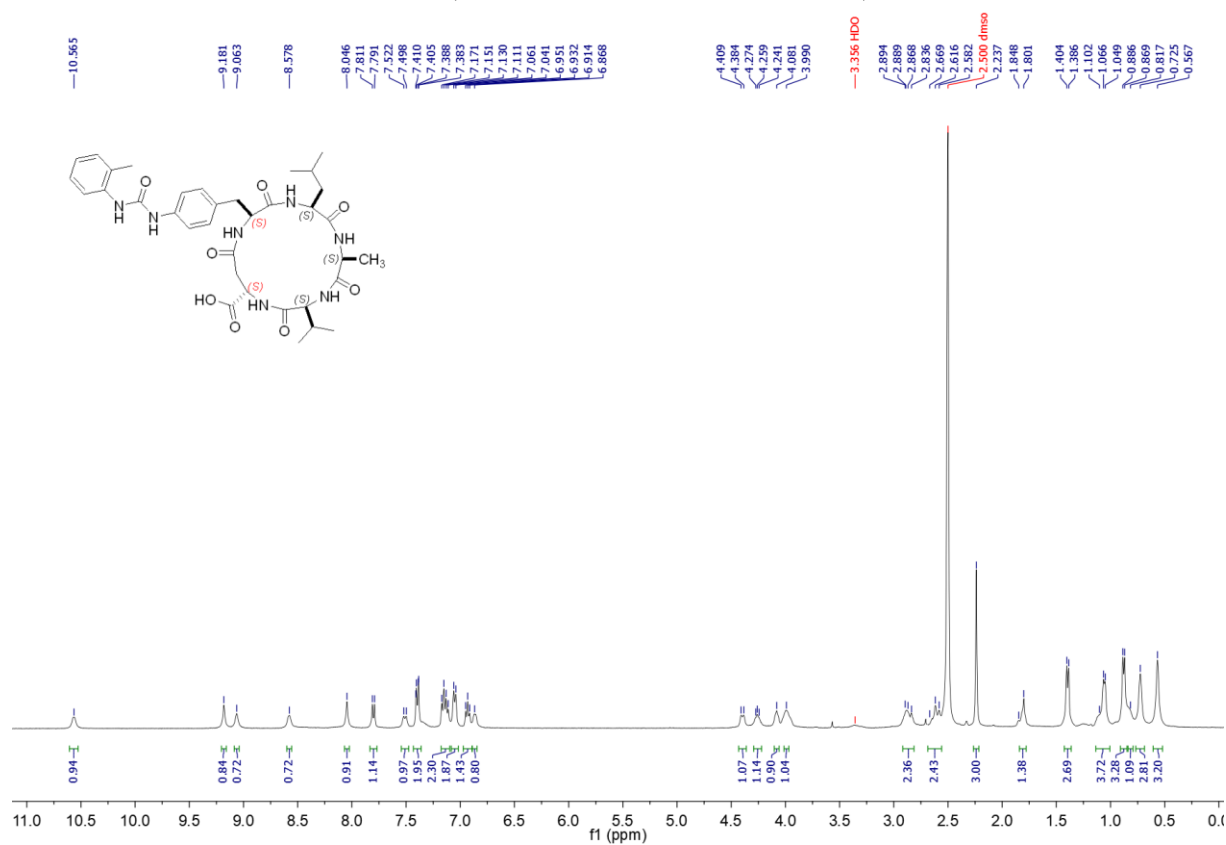
C. Supplementary images for Chapter 6
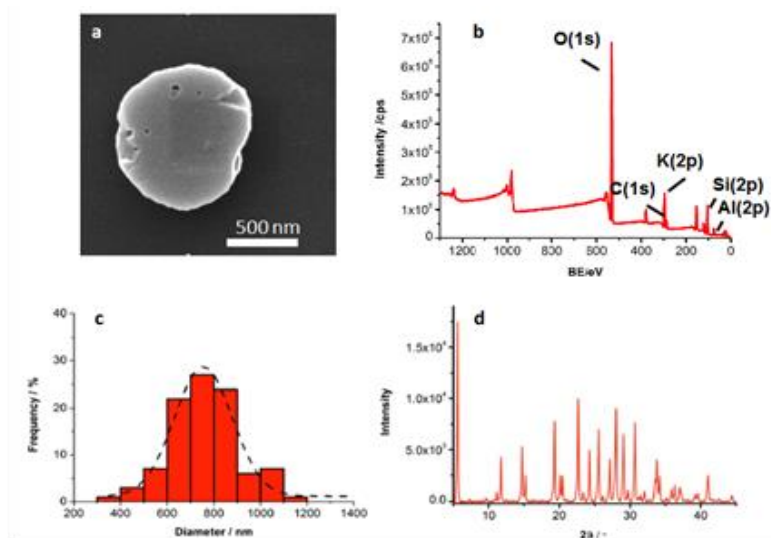
Figure S3. Characterization of disk-shaped Zeolite L crystals: (a) SEM; (b) XPS; (c) size distribution diagram derived from SEM images; (d) powder XRD diffraction pattern. The flat disk-shaped zeolite L crystals utilized for this study showed a size comprised between 600 and 1000 nm in width and about 250 nm in height.
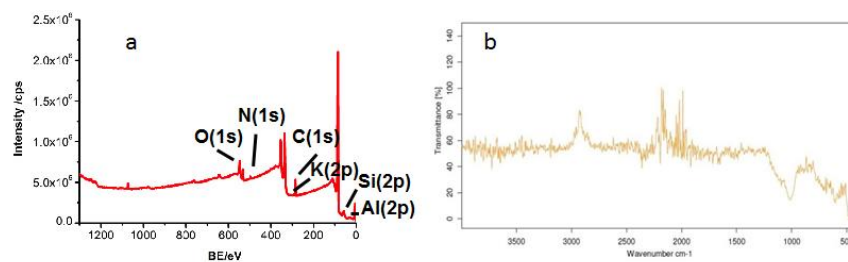
Figure S4. Characterization of DXP-zeolite L crystals; (a) XPS; (b) ATR; for TGA analysis, see Figure S5.
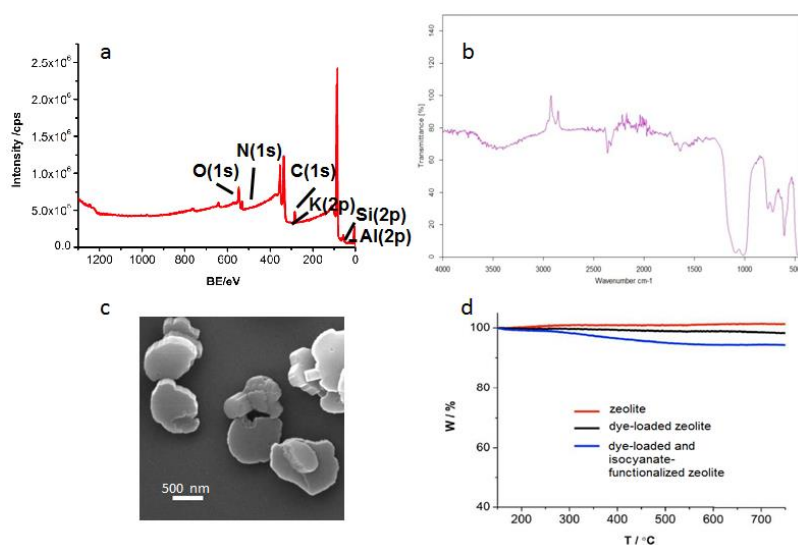
Figure S5. Characterization of isocyano-DXP-zeolite L crystals: (a) XPS; (b) ATR; (c) SEM; (d) TGA analysis of the native and the derivatized zeolites: DXP-zeolites and isocyano-DXP-zeolites showed increasing weight

loss, and hence increasing amounts of organic molecules, 1.7% and 5.7% respectively, after removing the contribution of the water present in the zeolite materials (native zeolites used as reference)
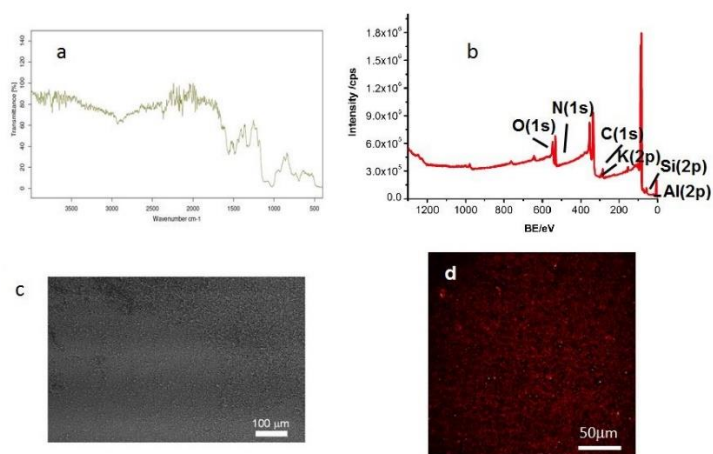
Figure S6. (a) ATR of a plate after functionalization with APTES; characterization of isocyano-DXP-zeolite SAMs: (b) XPS; (c) SEM; confocal image of **3**@SAM visualized in red.
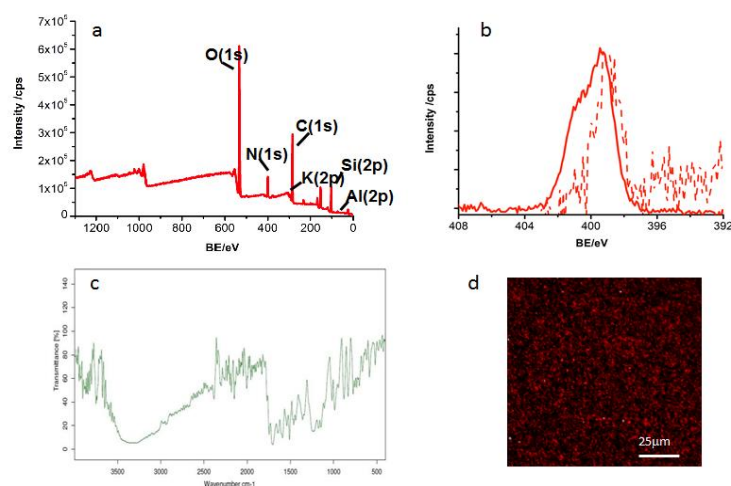
Figure S7. Characterization of **3**@SAM: (a) XPS; (b) comparison of the high resolution XPS analysis of N(1s) of the isocyano-zeolite-SAMs (dashed line) and 3@SAM (full line); (c) ATR; (d) confocal microscopy (red channel).
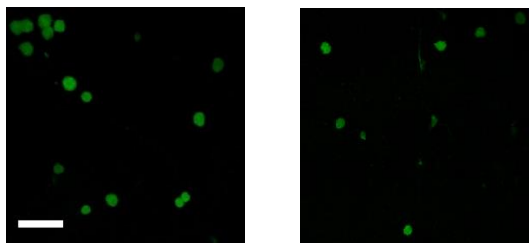
Figure S8. Confocal microscopy images of **3**@plates after 15 min incubation at 37°C with 5×10^5 Jurkat (left) or HEK-293 (right) cells visualized in green; the white bar corresponds to 50 μm.

D. Representative NMR data for Chapter 7

7: ^{1}H NMR

8: ^{1}H NMR and ^{13}C NMR

226
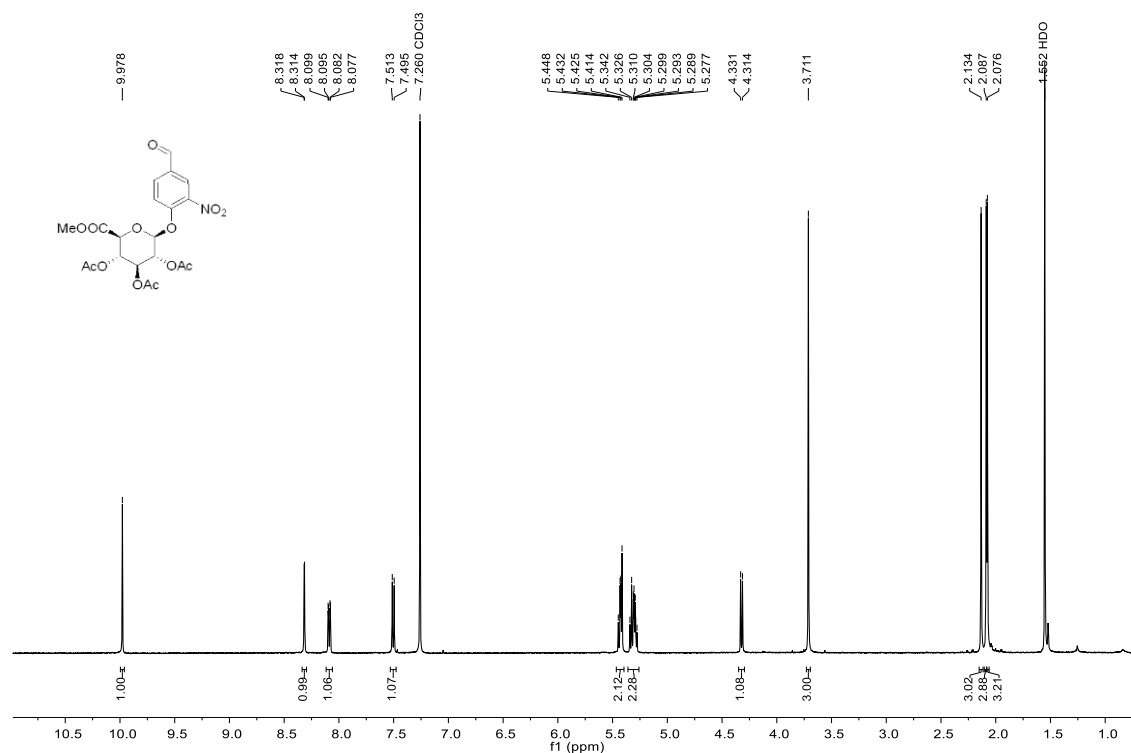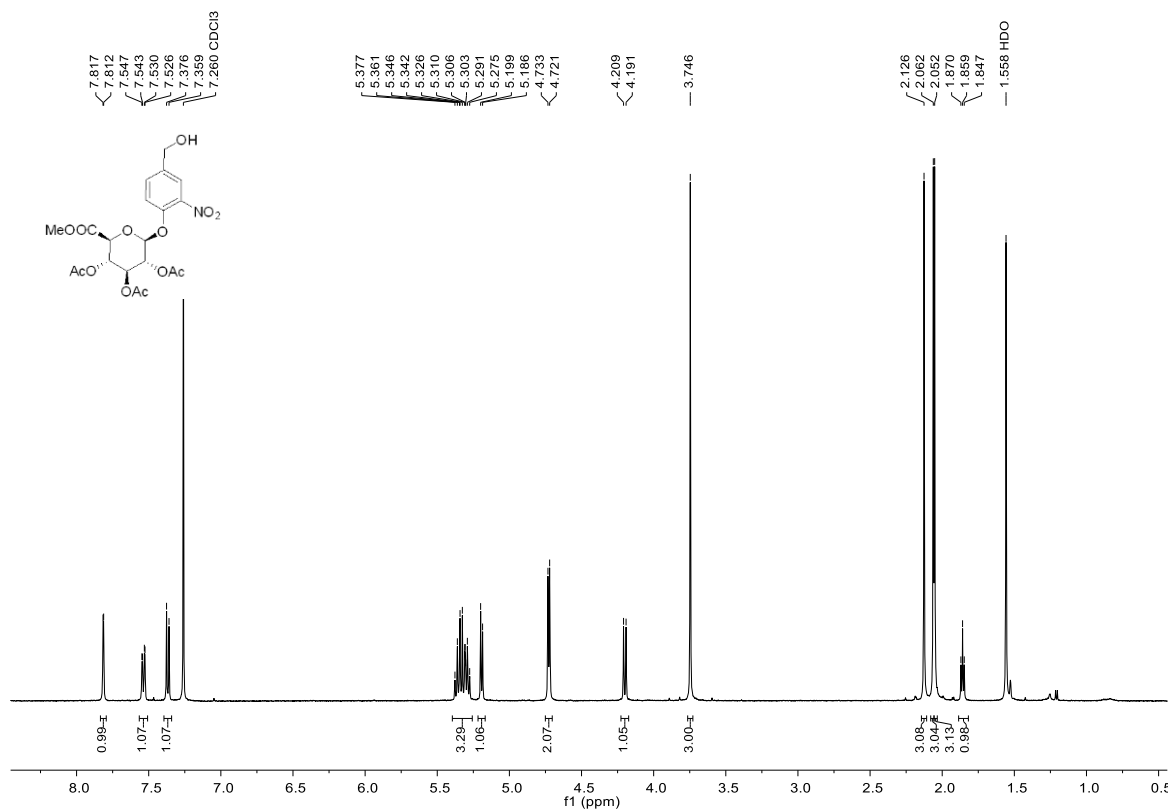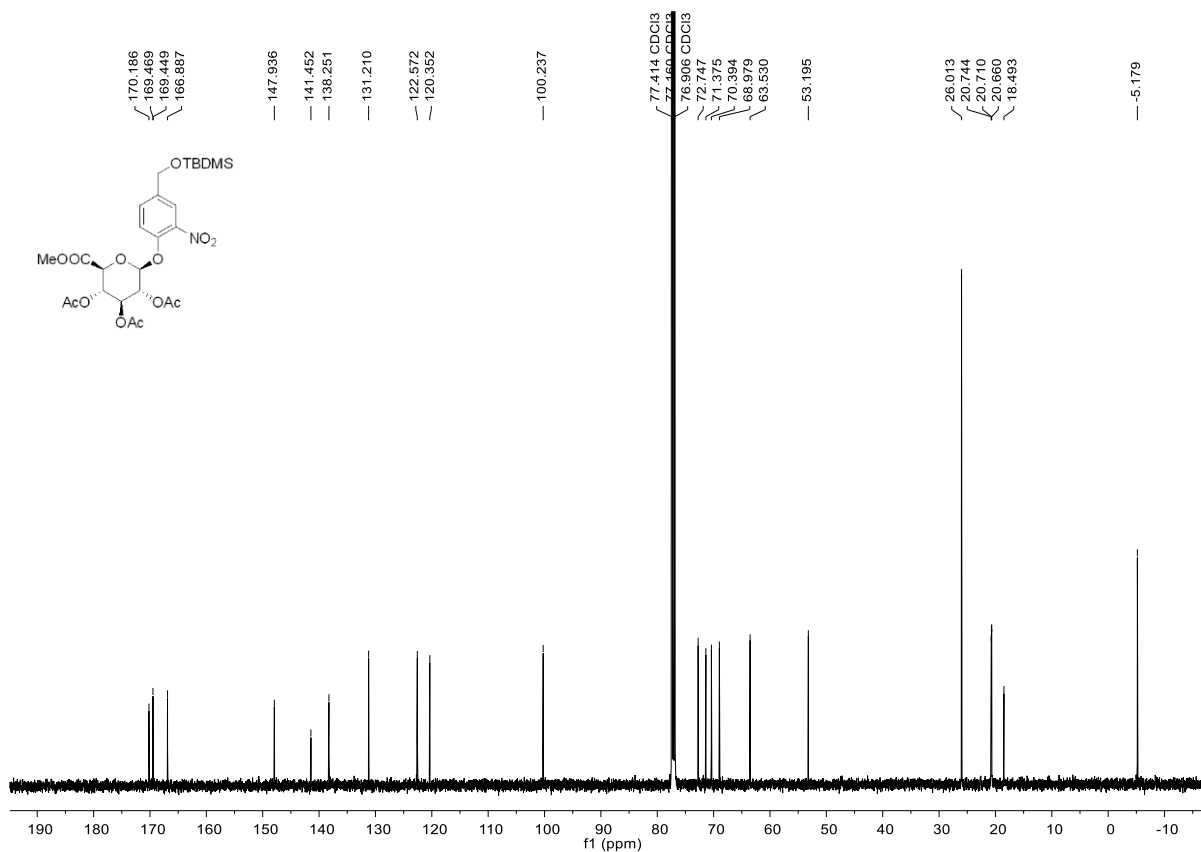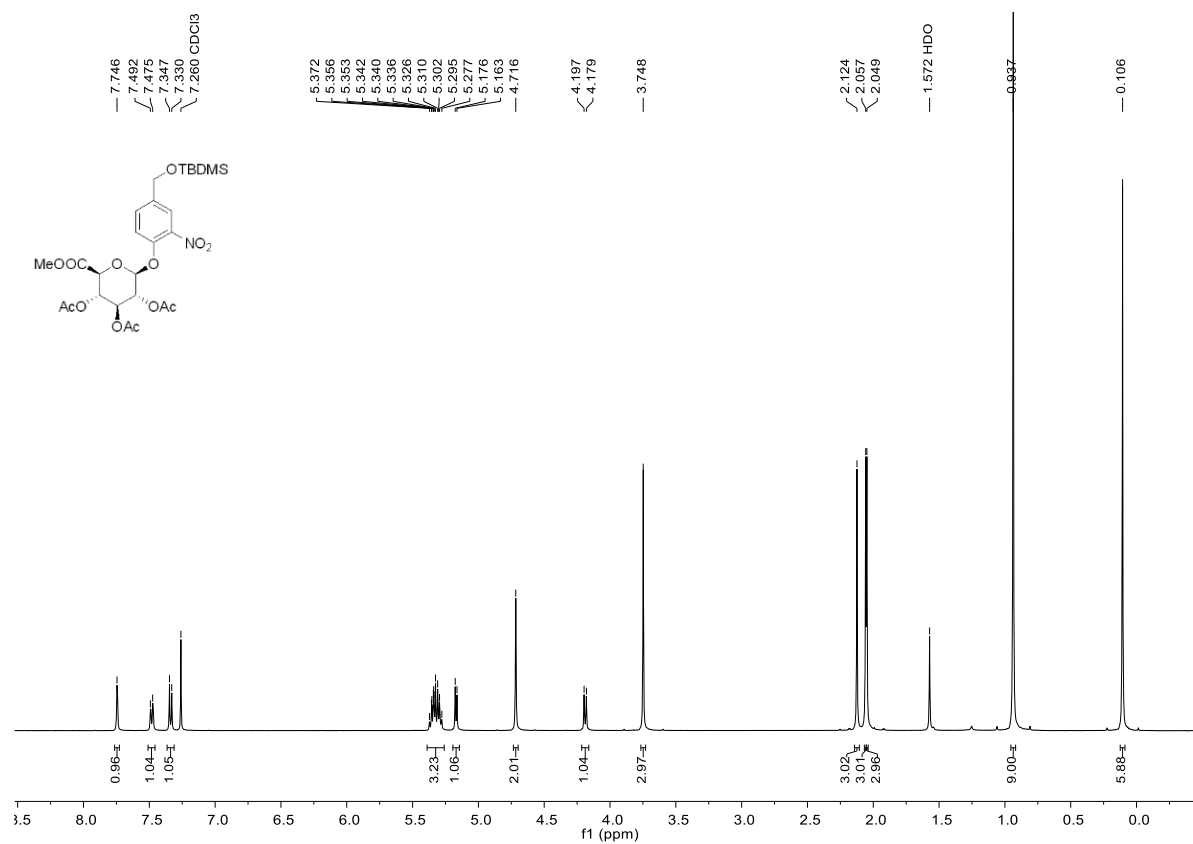
9: ^{1}H NMR and ^{13}C NMR

10: ^{1}H NMR and ^{13}C NMR
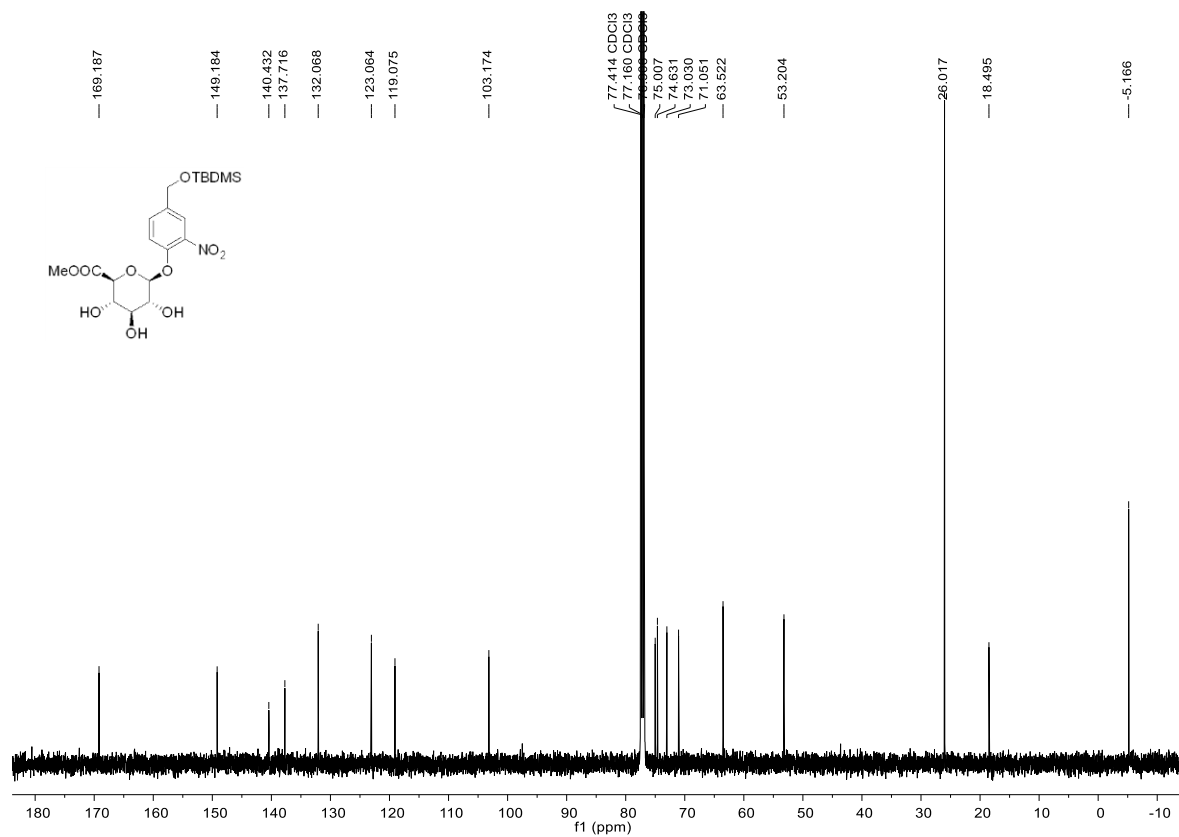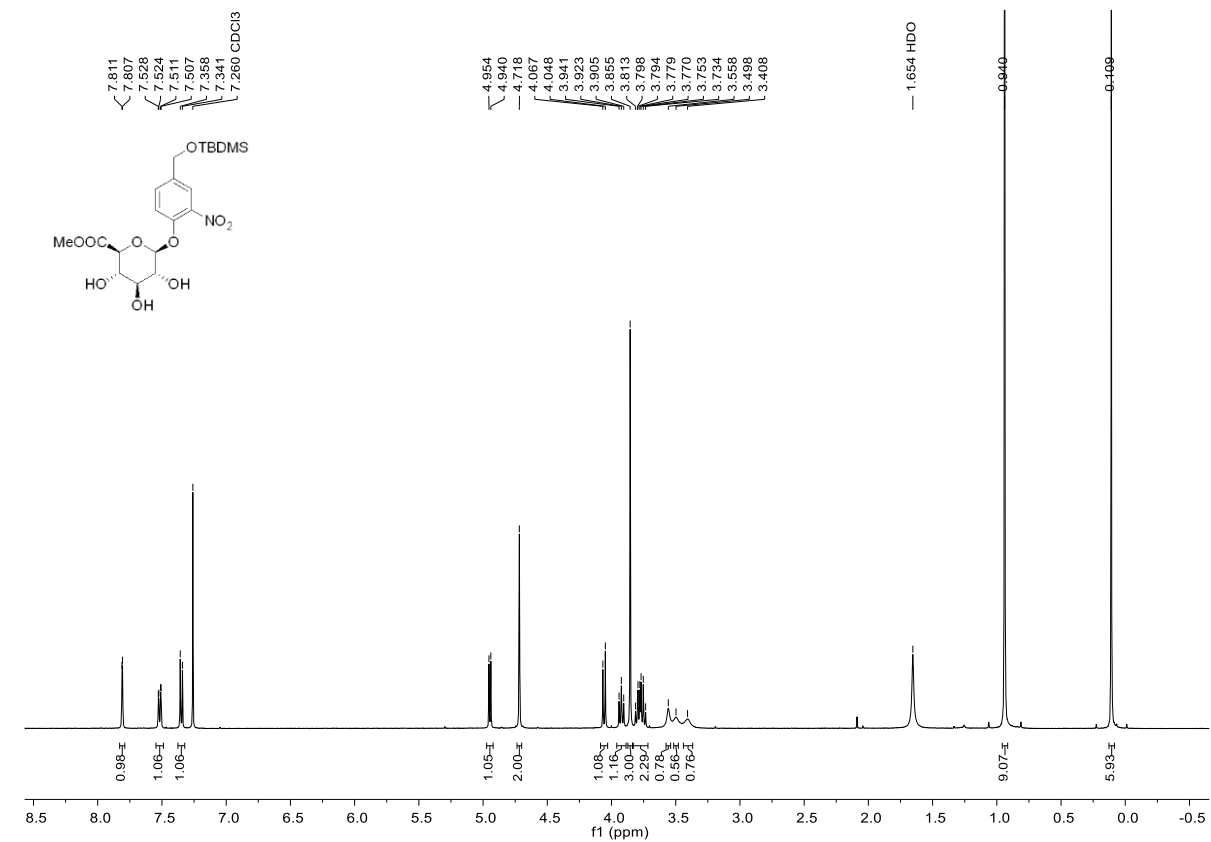
11: ^{1}H NMR and ^{13}C NMR
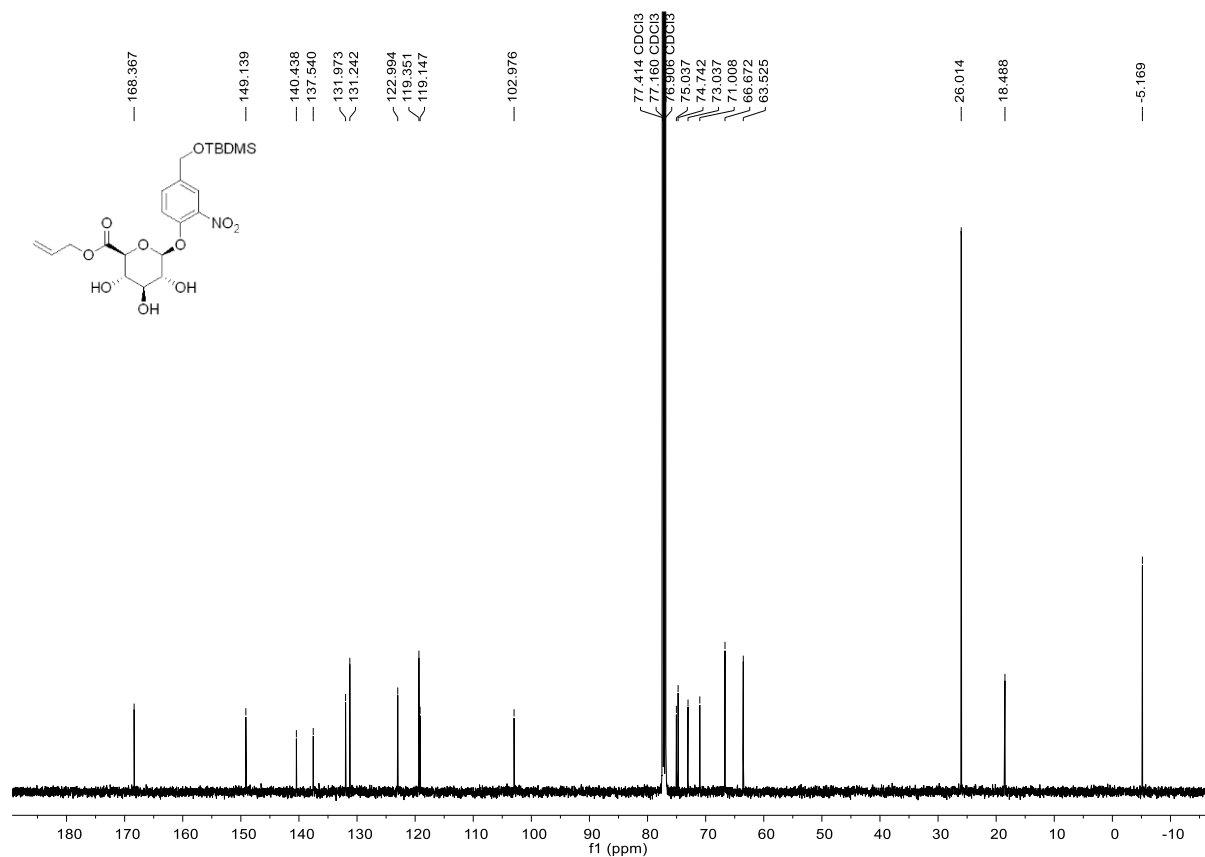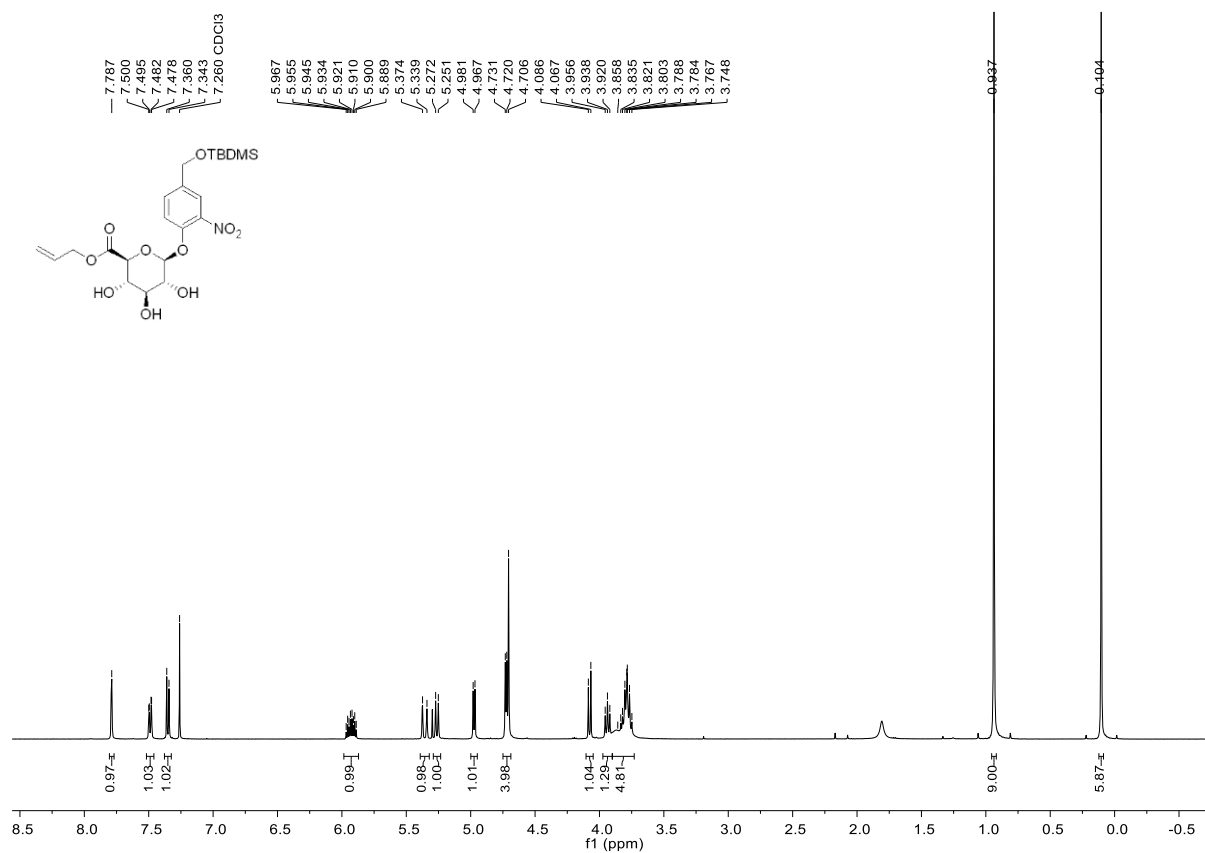
12: ¹H NMR and ¹³C NMR
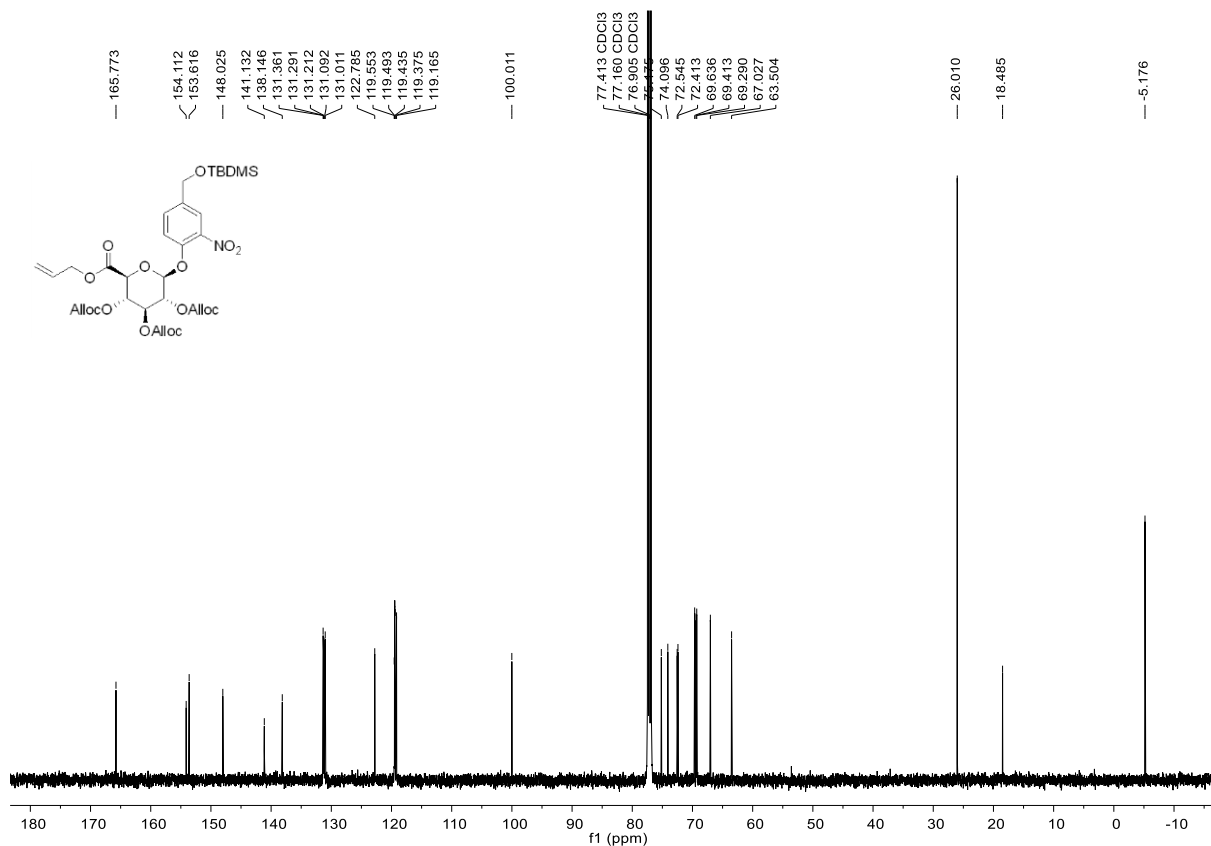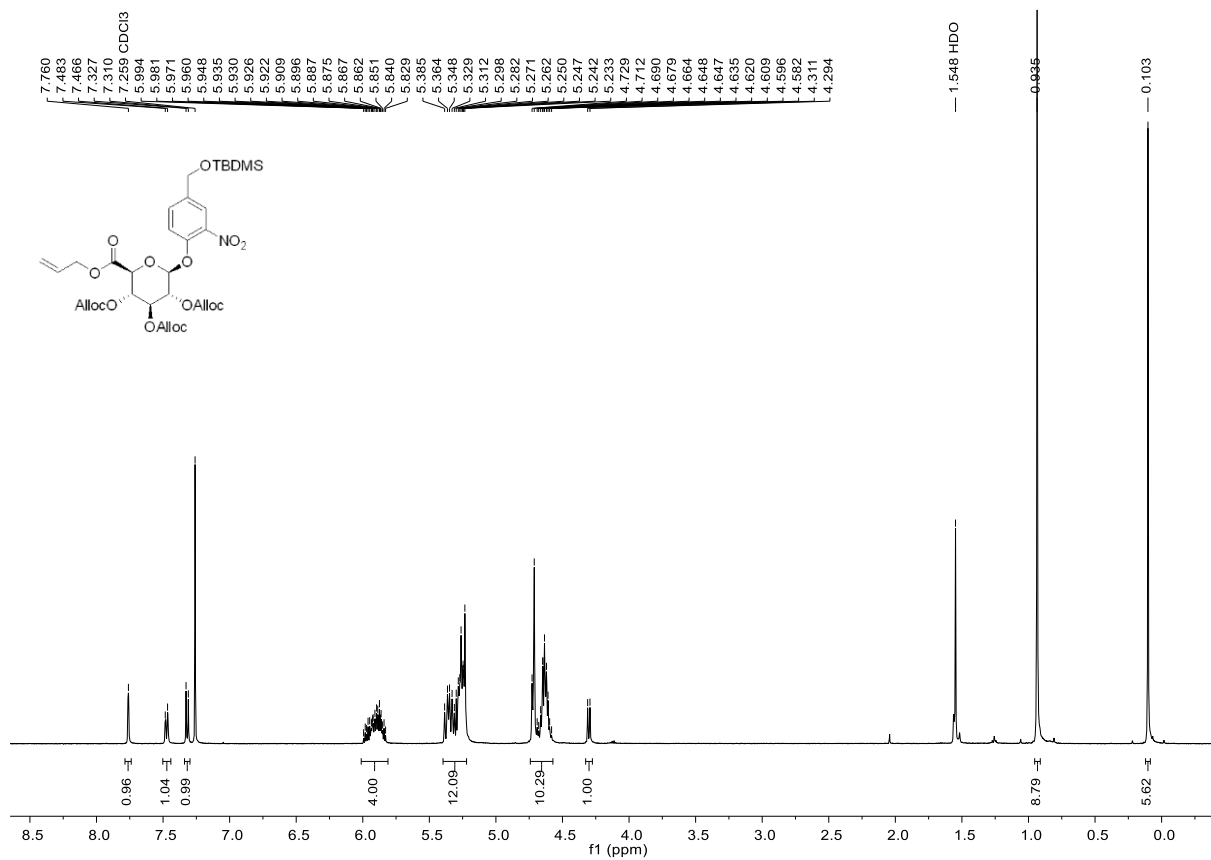
13: ^{1}H NMR and ^{13}C NMR
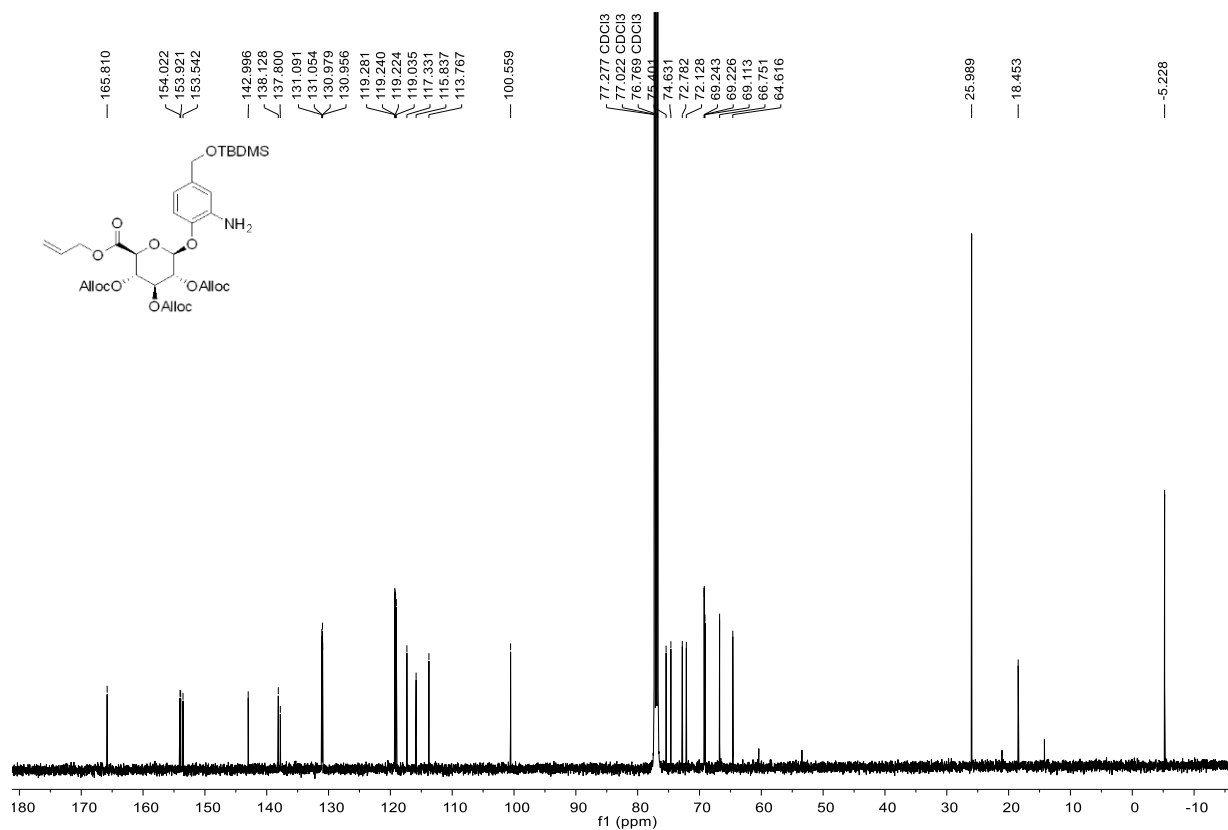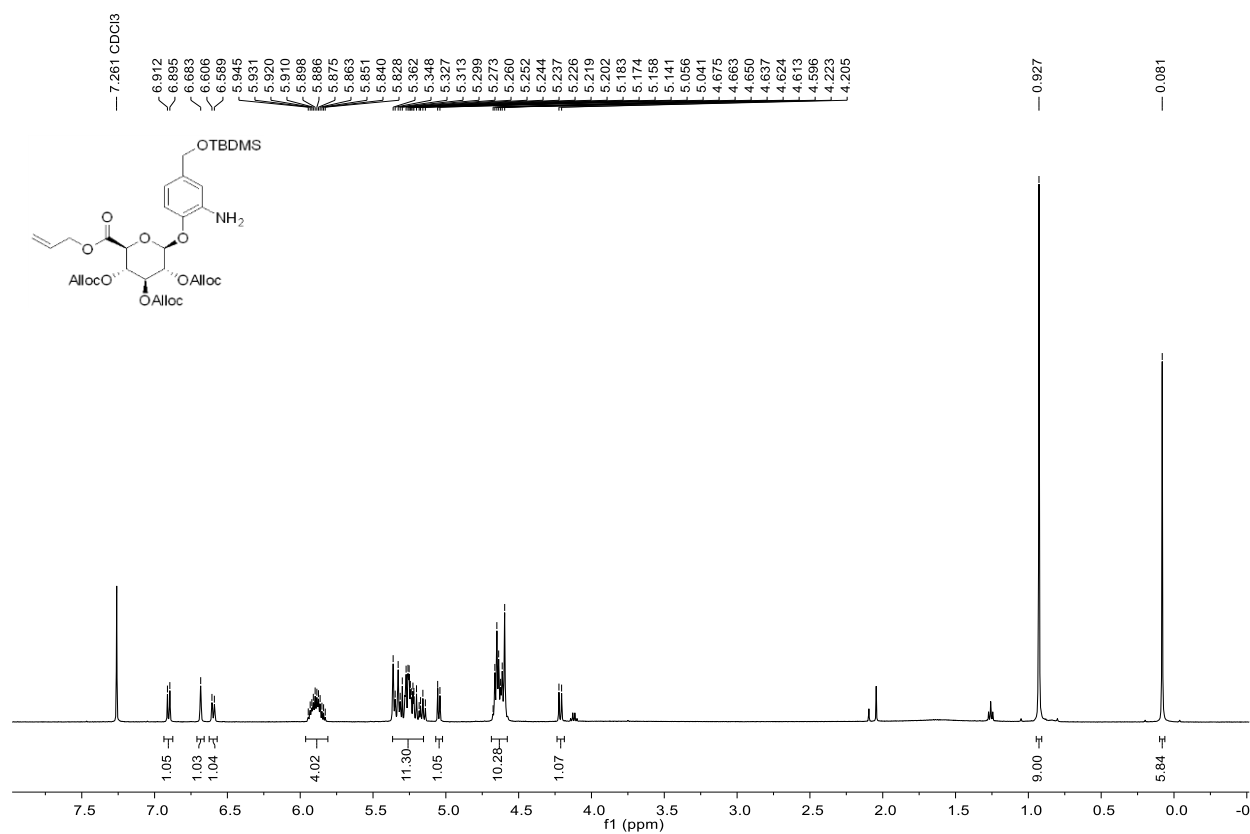
14: ^{1}H NMR and ^{13}C NMR
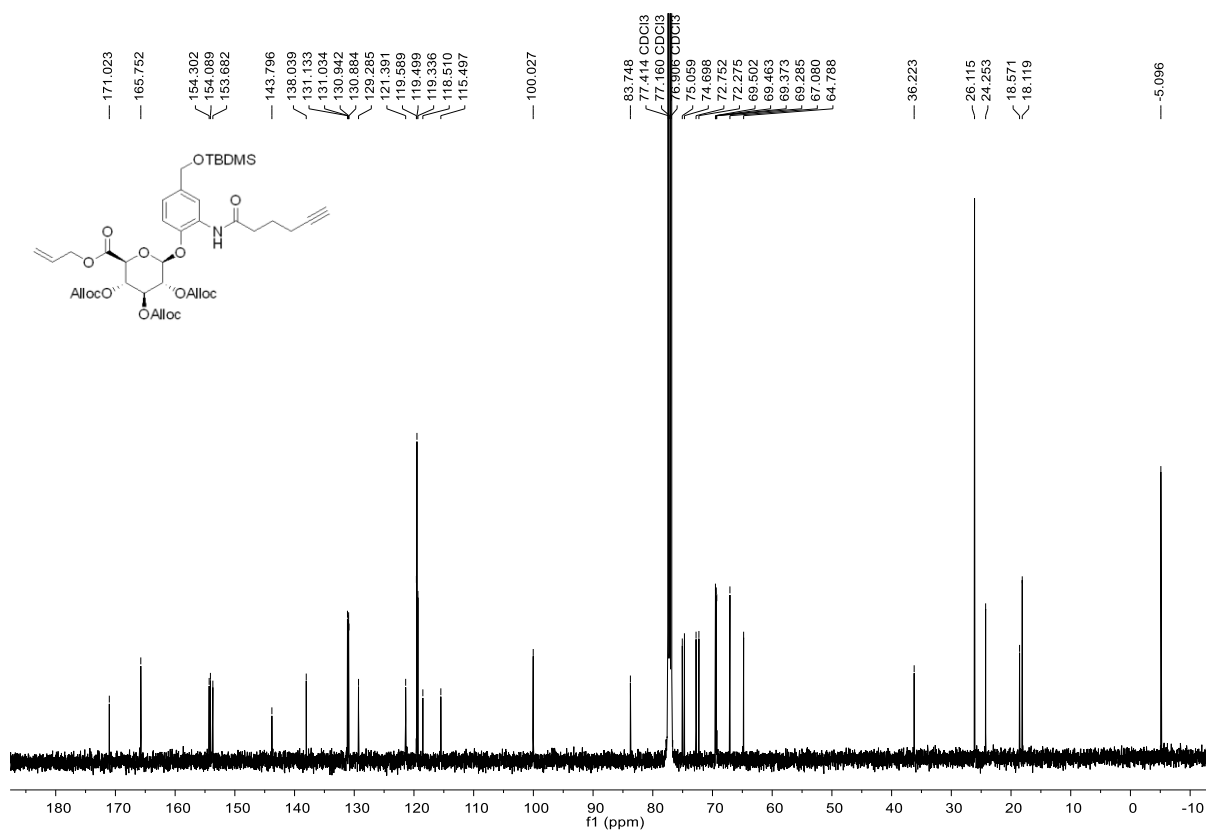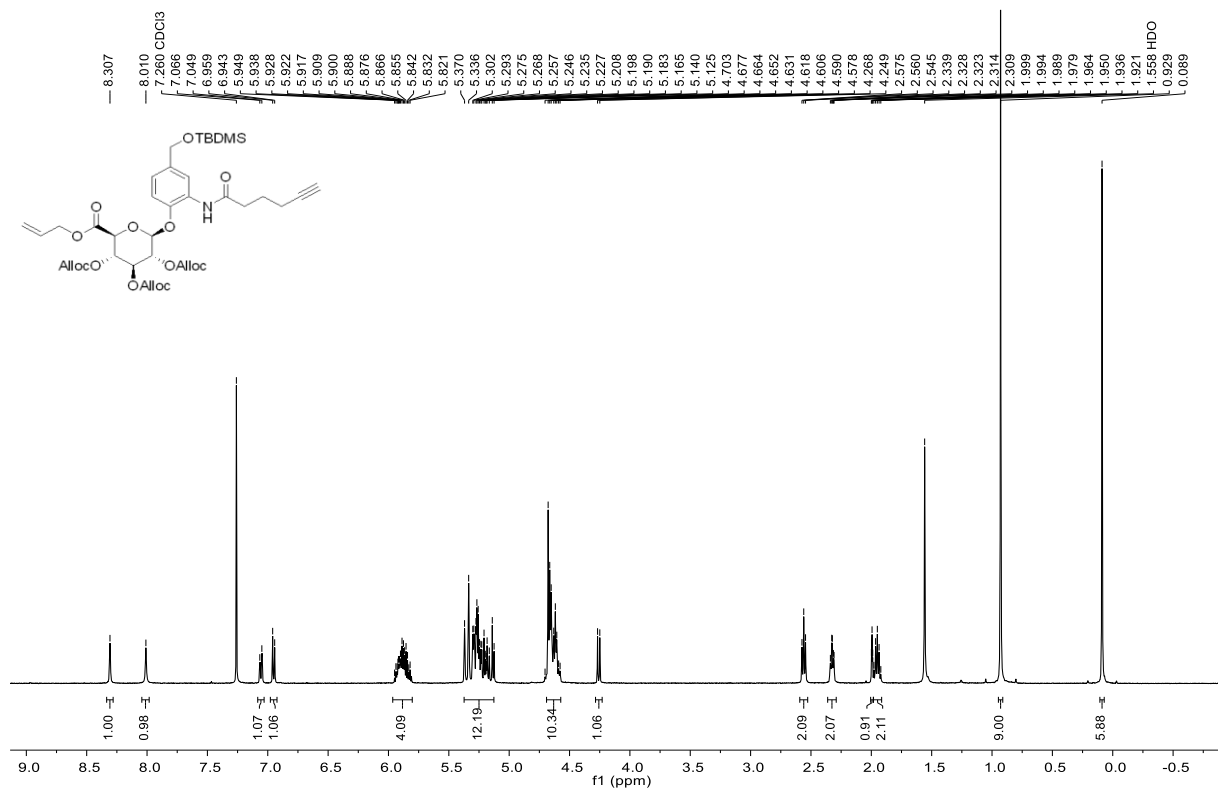
15: ^{1}H NMR and ^{13}C NMR
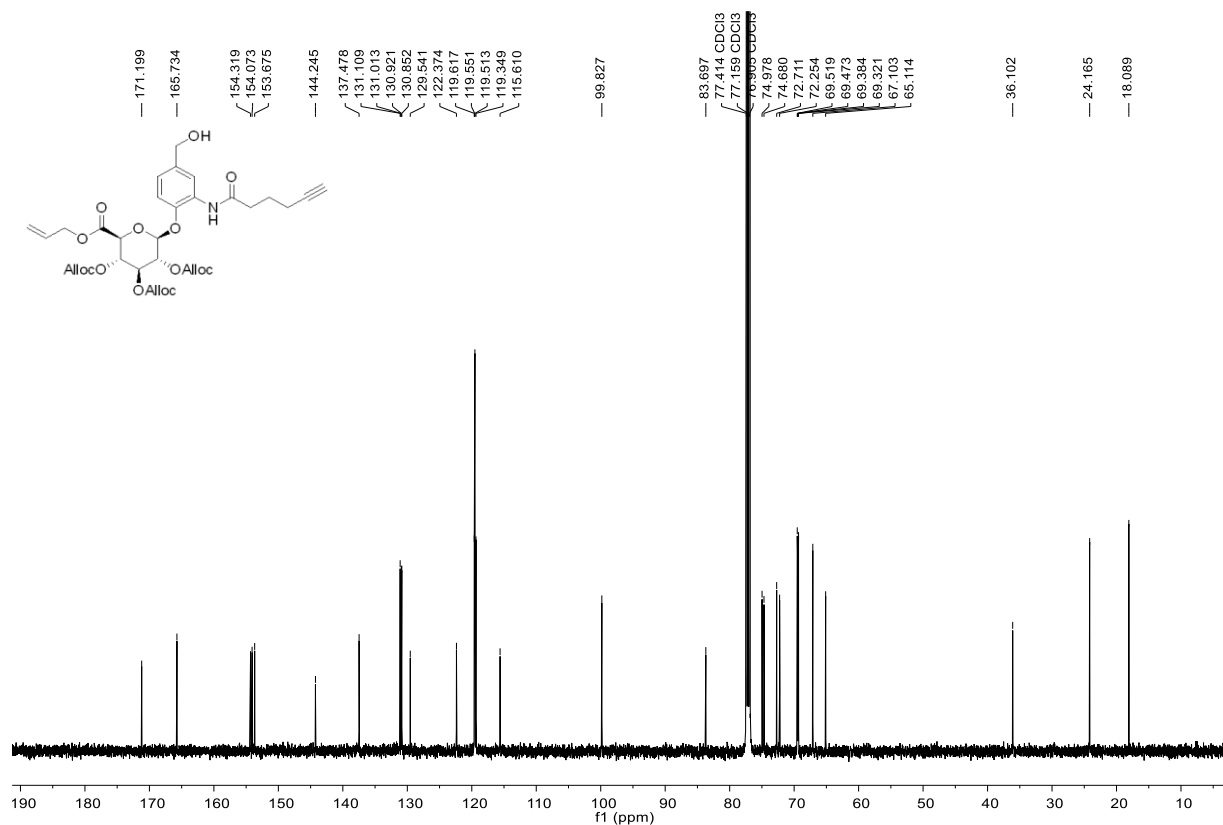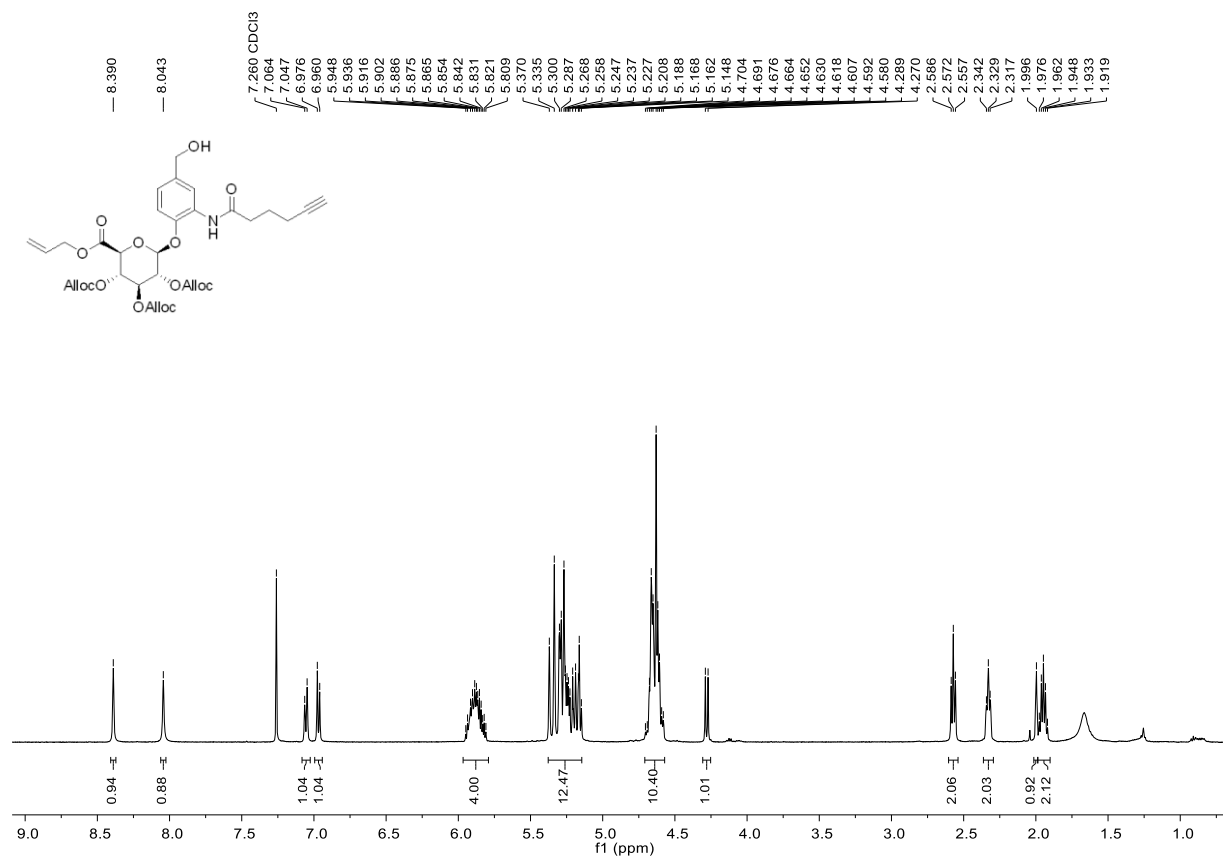
16: ^{1}H NMR and ^{13}C NMR
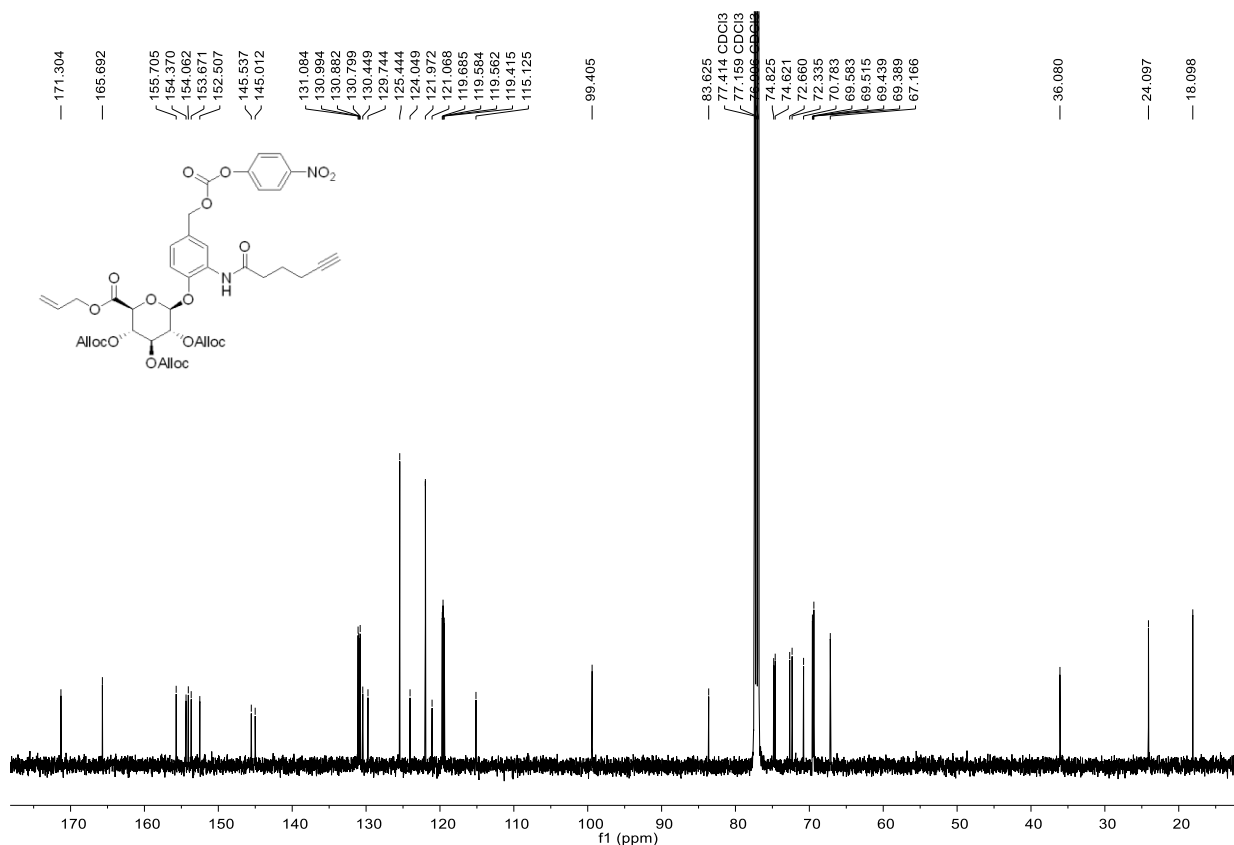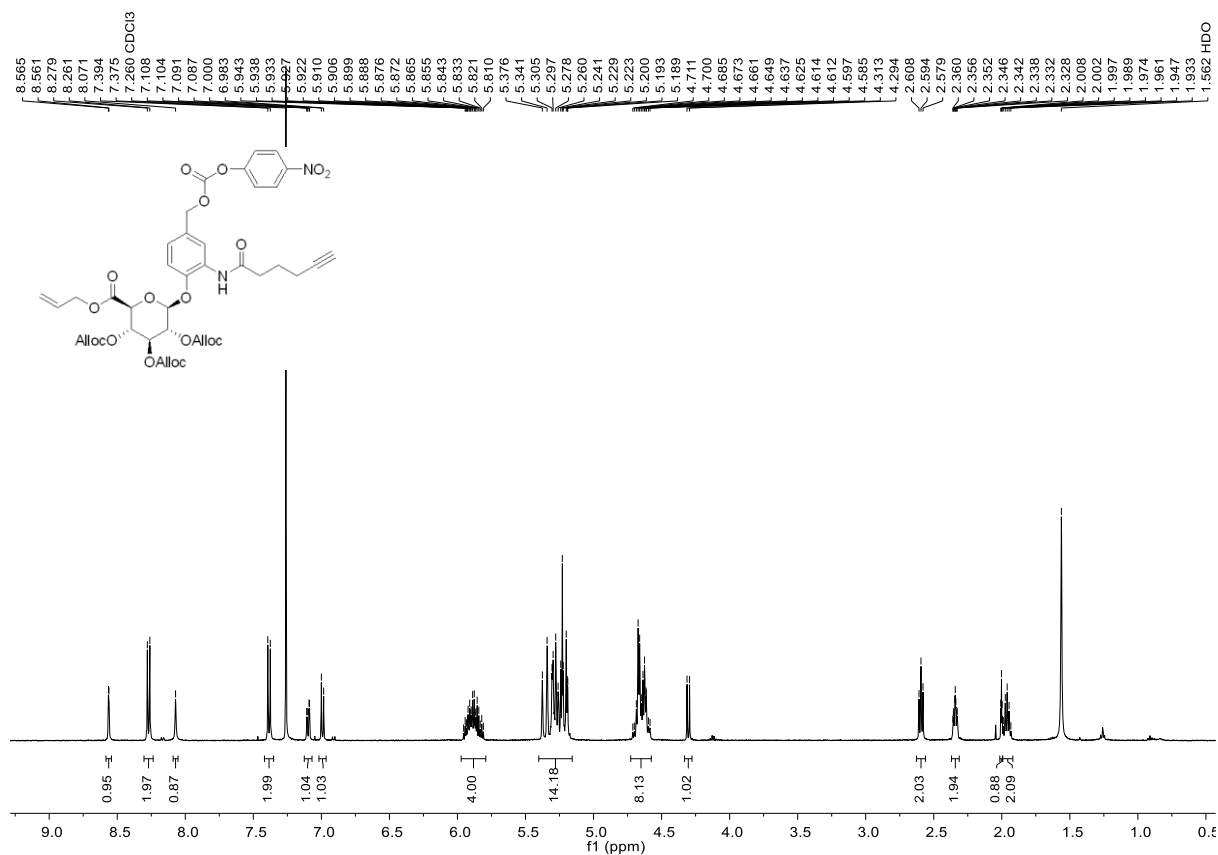
17: HPLC chromatogram (λ = 220) and MS spectra

18: HPLC chromatogram (λ = 220) and MS spectra

1: HPLC chromatogram ($\lambda = 220$) and HRMS spectra
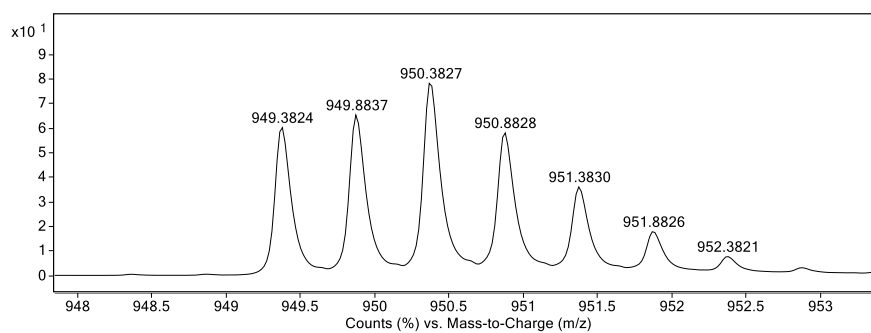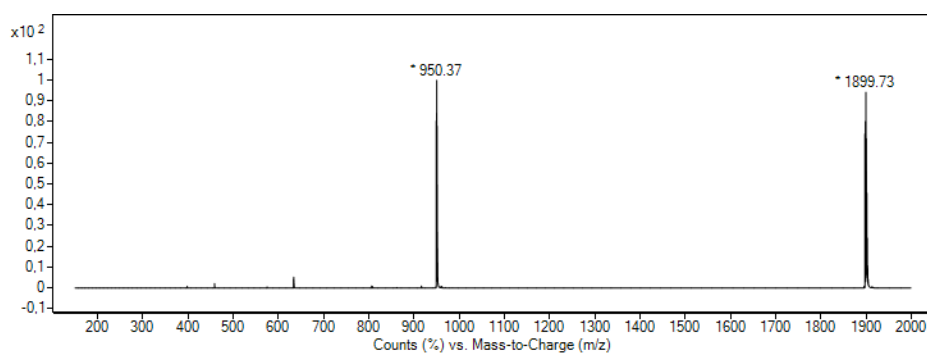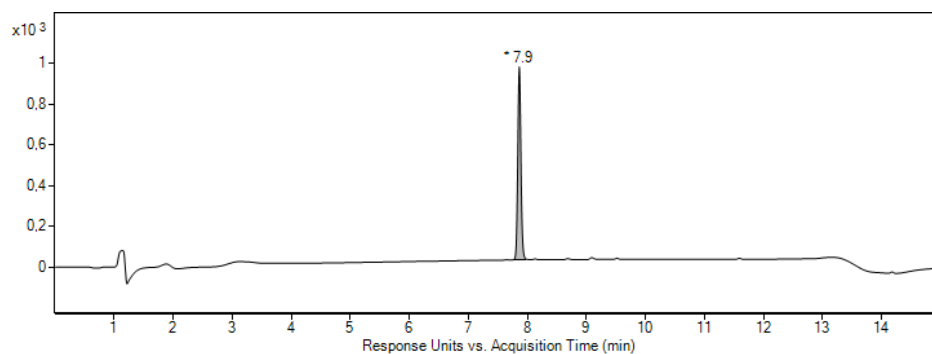
33: ¹H NMR
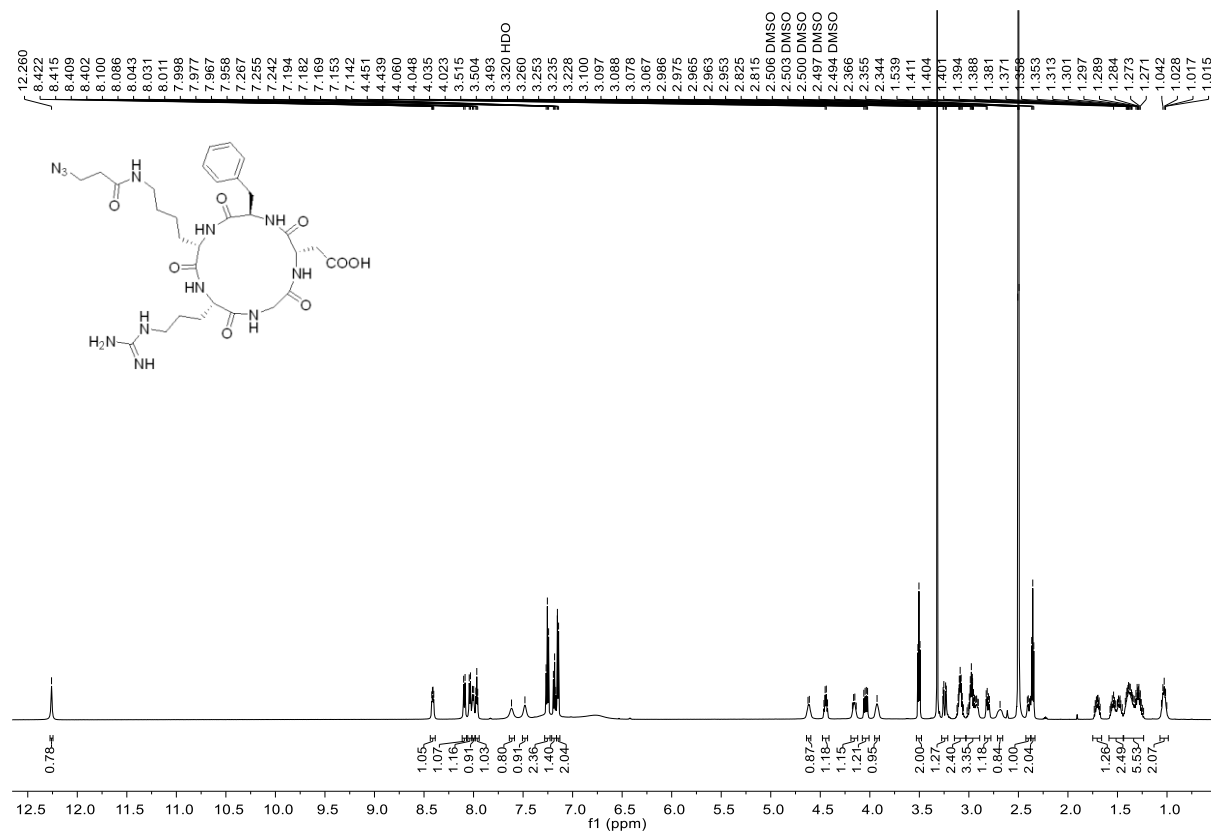
34: ¹H NMR
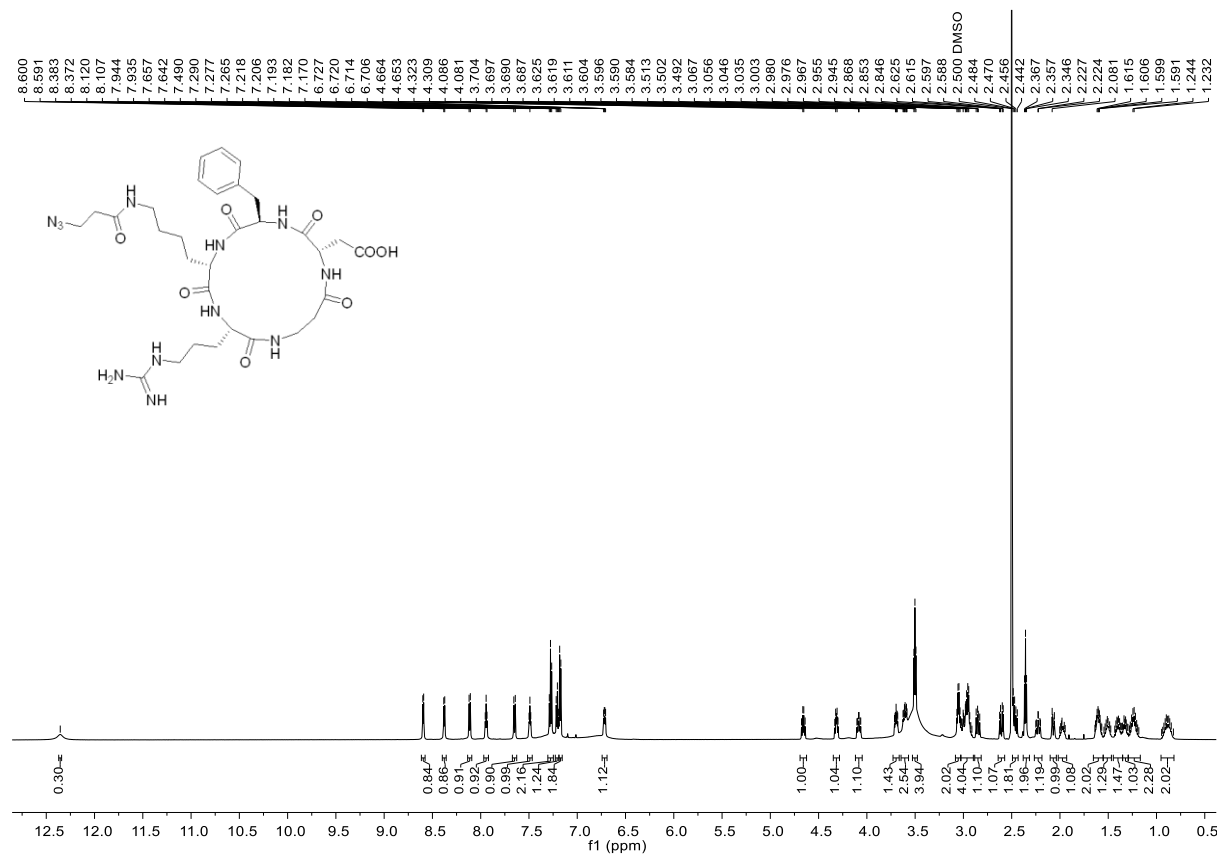
E. Representative NMR data, HPLC ESI-MS and supplementary images for Chapter 8
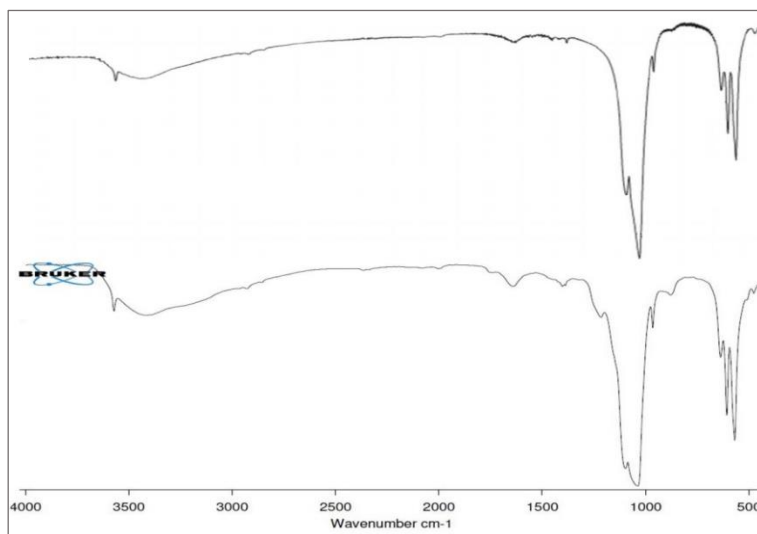
Figure S1. Infrared adsorption spectra of fresh HAp (top) and HAp after 5 cycles (bottom), pellets in KBr

Figure S2. Grinded reaction mixture in an agate jar ($\emptyset$ = 7.5 cm) containing 3 agate balls ($\emptyset$ = 2.0 cm), at the speed of 8-10 Hz.
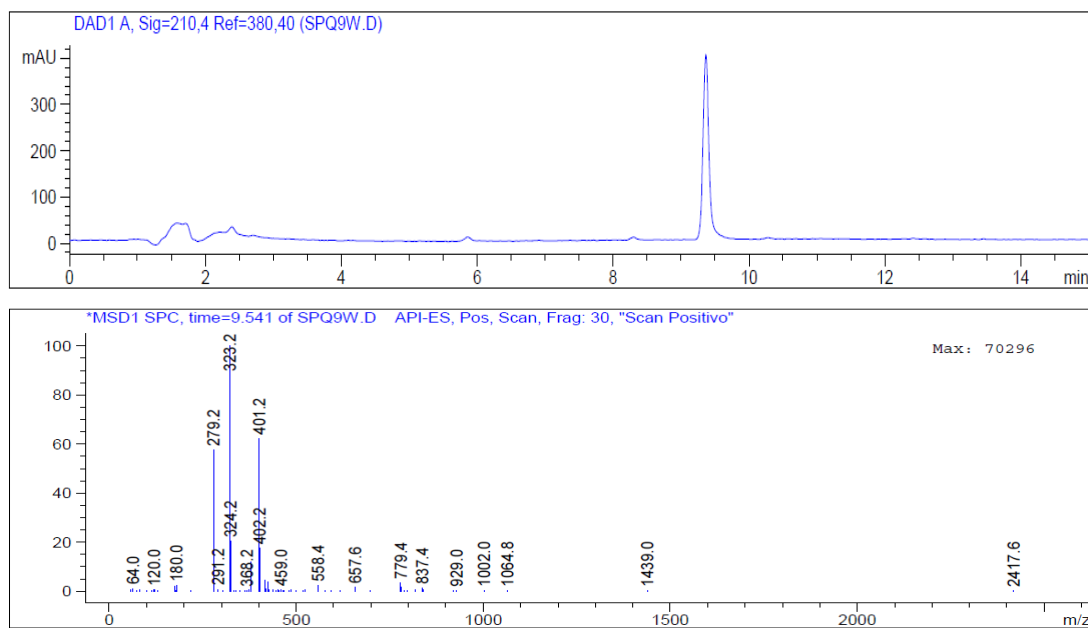
Figure S3. RP-HPLC and ESI-MS analyses of Boc-Val-Phe-OMe obtained by solvent free ball-milling.
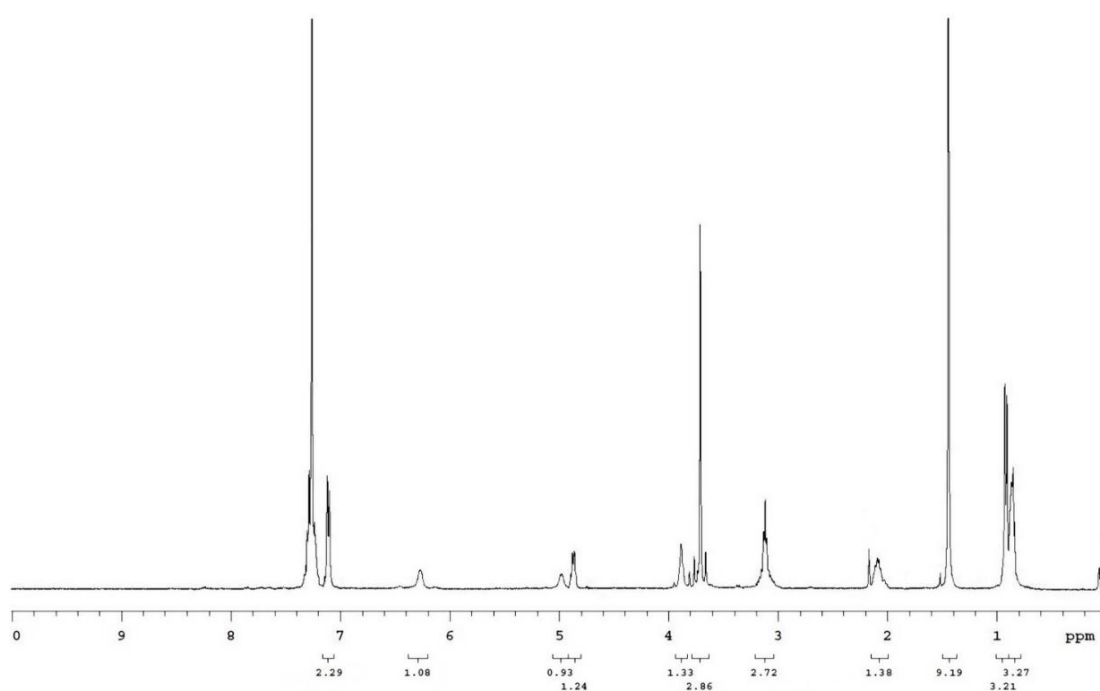
Figure S4. ^{1}H-NMR (CDCl$_3$, 400 MHz) of Boc-Val-Phe-Phe-OMe obtained by solvent free ball-milling.
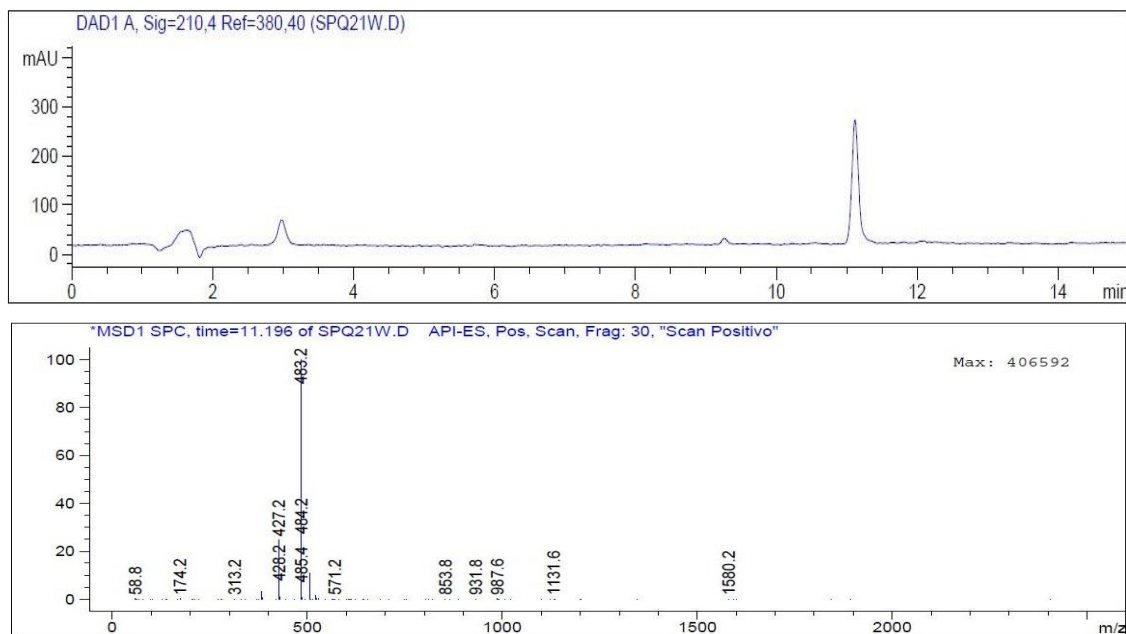
Figure S6. RP-HPLC and ESI-MS analyses of Boc-Ser(OBn)-Pro-OBn obtained by solvent free ball-milling.
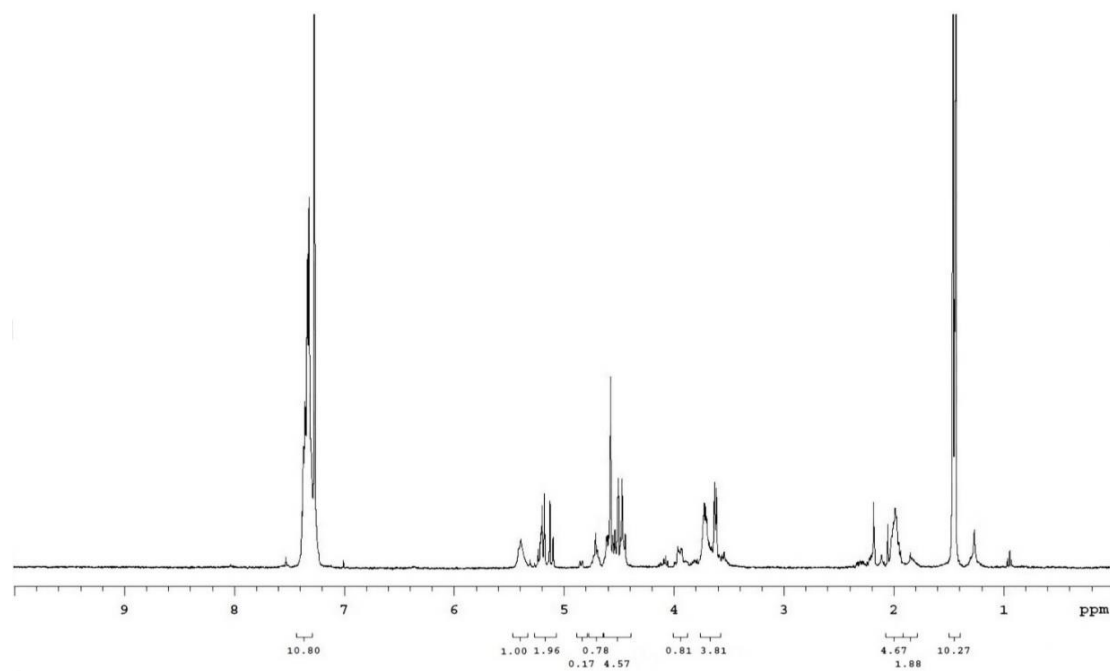
Figure S7. ^{1}H-NMR (CDCl$_3$, 400MHz) of Boc-Ser(OBn)-Pro-OBn obtained by solvent free ball-milling, showing two sets of resonances, corresponding to the cis/trans rotamers about the secondary amide bond.
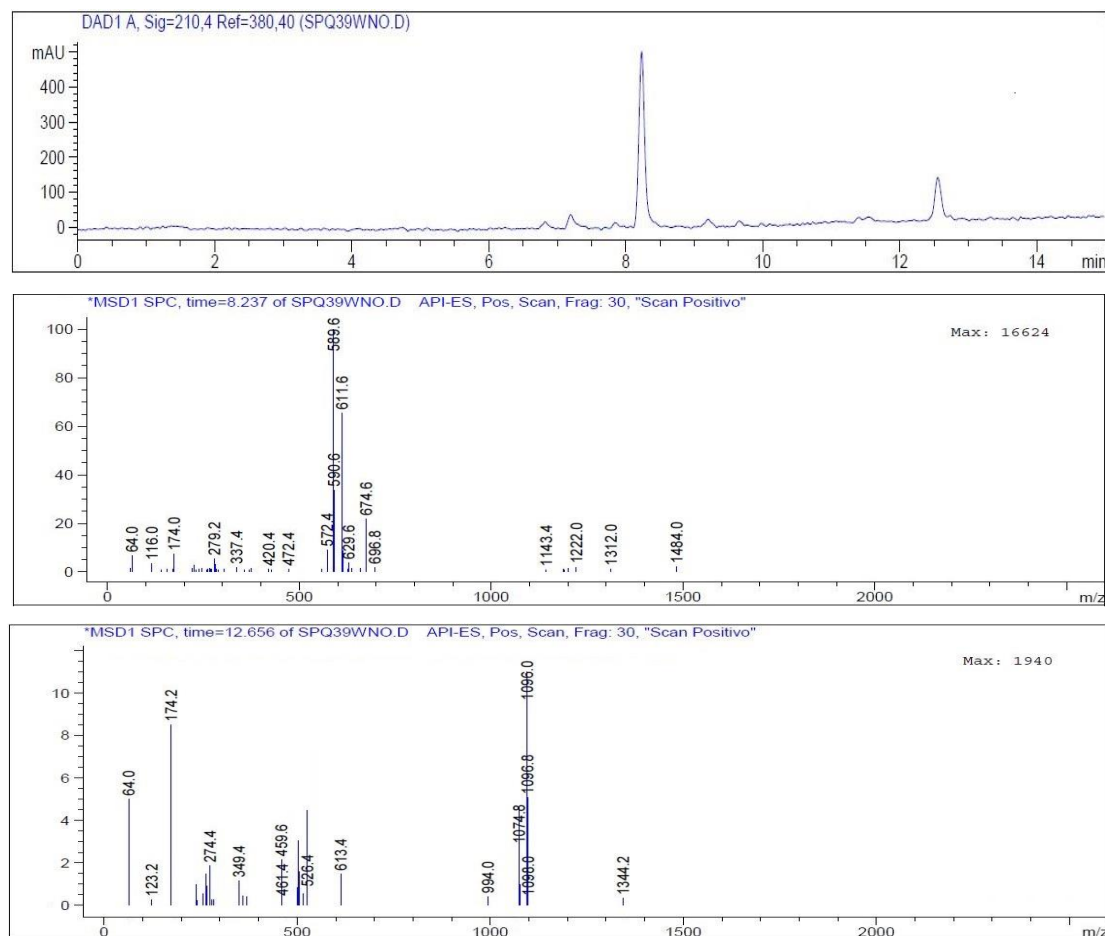
Figure S8. RP-HPLC and ESI-MS analyses of the coupling between *N*-Fmoc-Lys(N-Cbz)-OH and H-Ser-NH$_2$ obtained by solvent free ball-milling. The peak at 8.237 min accounts for dipeptide *N*-Fmoc-Lys(*N*-Cbz)-Ser-NH$_2$ (m/z): 1222.0 [2M+Na], 611.6 [M+Na], 589.6 [M+H]. 12.656 min, depsitripeptide *N*-Fmoc-Lys(*N*-Cbz)-Ser[*N*-Fmoc-Lys(*N*-Cbz)]-NH$_2$ (m/z): 1096.0 [M+Na], 1074.8 [M+H].
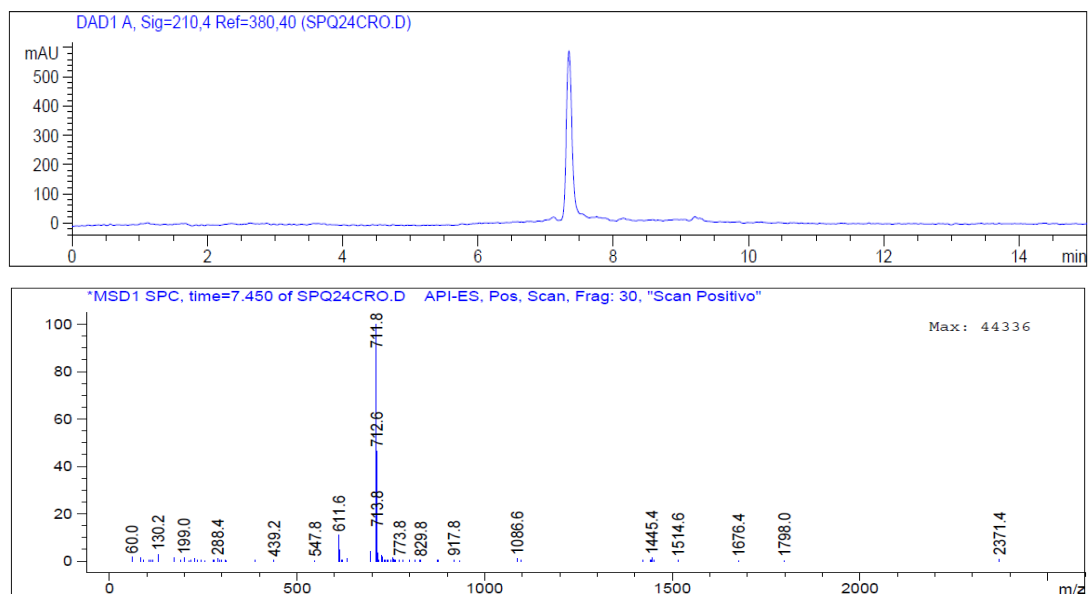
Figure S9. RP-HPLC and ESI-MS analyses of Boc-EM1 obtained by solvent free ball-milling.
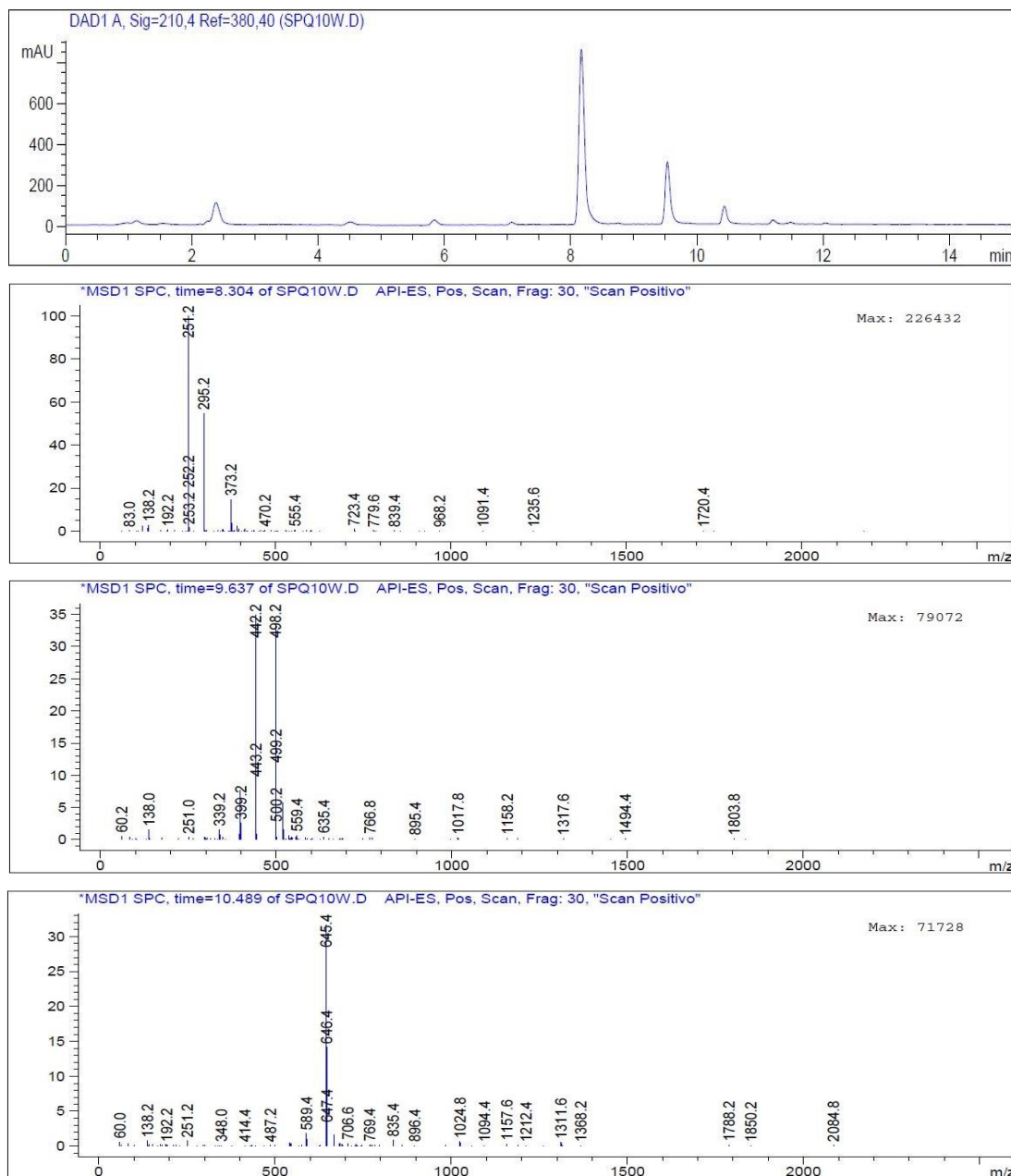
Figure S10. RP-HPLC and ESI-MS analyses of the coupling between *N*-Boc-Phe-OH and H-Gly-OEt in γ-valerolactone. The peak at 8.304 min accounts for dipeptide *N*-Boc-Phe-Gly-OEt (m/z): 723.4 [2M+Na], 373.2 [M+Na], 295.2 [M-*t*Bu], 251.2 [M-Boc]. 9.637 min, *N*-Boc-Phe-Phe-Gly-OEt (m/z): 520.2 [M+Na], 498.2 [M+H], 442.2 [M-*t*Bu], 399.2 [M-Boc]. 10.489 min, *N*-Boc-Phe-Phe-Phe-Gly-OEt (m/z): 645.4 [M+H], 589.4 [M-*t*Bu].
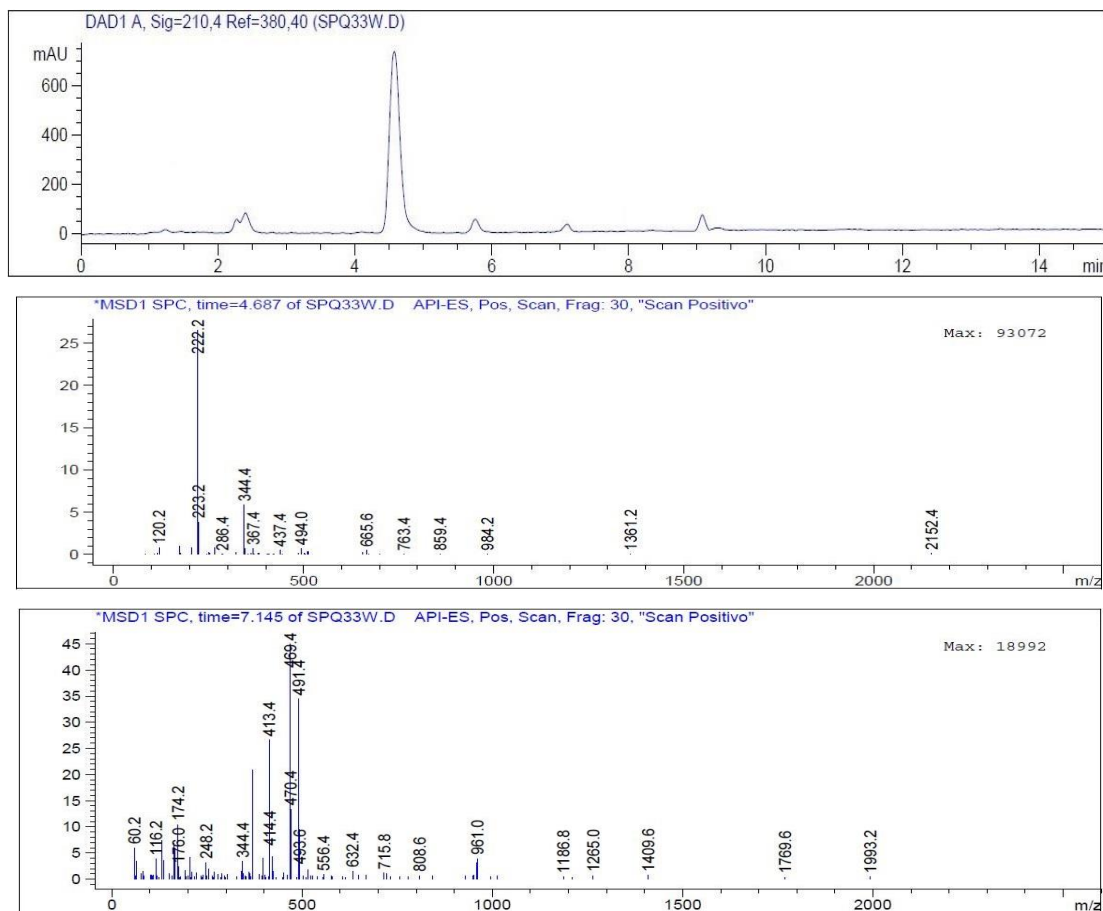
Figure S11. RP-HPLC and ESI-MS analyses of the coupling between *N*-Boc-Phe-OH and H-Gly-NH$_2$ in γ-valerolactone. The peak at 4.687 min accounts for dipeptide *N*-Boc-Phe-Gly-NH$_2$ 665.6 [2M+Na], 344.4 [M+Na], 222.2 [M-Boc]. 7.145 min, *N*-Boc-Phe-Phe-Gly-NH$_2$ (m/z): 961.0 [2M+Na], 491.4 [M+Na], 469.4 [M+H], 413.4 [M-*t*Bu].
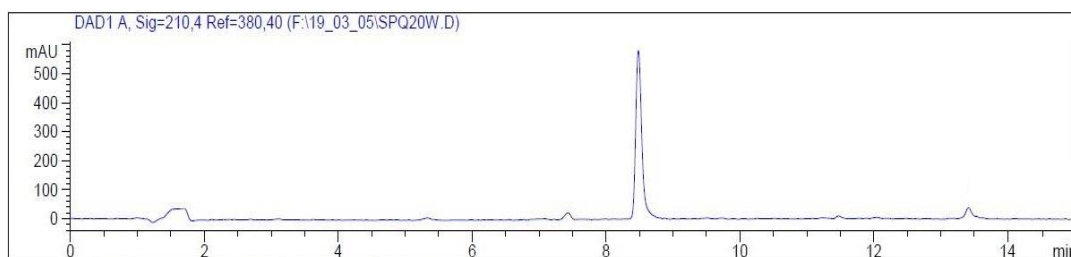
Figure S12. RP-HPLC and ESI-MS analyses of the coupling between *N*-Fmoc-Lys(N-Cbz)-OH and H-Ser-NH$_2$ obtained by minimal solvent-assisted grinding, showing the formation of traces of depsitripeptide *N*-Fmoc-Lys(*N*-Cbz)-Ser[*N*-Fmoc-Lys(*N*-Cbz)]-NH$_2$ (13.493 min).

10. References

[1]   J. W. Tamkun, D. W. DeSimone, D. Fonda, R. S. Patel, C. Buck, A. F. Horwitz, R. O. Hynes, *Cell* **1986**, *46*, 271-282.
[2]   R. O. Hynes, *Cell* **2002**, *110*, 673-687.
[3]   M. J. Humphries, *Biochem Soc Trans* **2000**, *28*, 311-339.
[4]   M. Barczyk, S. Carracedo, D. Gullberg, *Cell Tissue Res* **2010**, *339*, 269-280.
[5]   B. Garmy-Susini, J. A. Varner, *Lymphat Res Biol* **2008**, *6*, 155-163; S. E. Winograd-Katz, R. Fässler, B. Geiger, K. R. Legate, *Nat Rev Mol Cell Biol* **2014**, *15*, 273-288.
[6]   D. Arosio, C. Casagrande, L. Manzoni, *Curr Med Chem* **2012**, *19*, 3128-3151.
[7]   I. D. Campbell, M. J. Humphries, *Cold Spring Harb Perspect Biol* **2011**, *3*.
[8]   T. A. Springer, M. L. Dustin, *Curr Opin Cell Biol* **2012**, *24*, 107-115.
[9]   C. Xie, J. Zhu, X. Chen, L. Mi, N. Nishida, T. A. Springer, *EMBO J* **2010**, *29*, 666-679.
[10]   J. P. Xiong, B. Mahalingham, J. L. Alonso, L. A. Borrelli, X. Rui, S. Anand, B. T. Hyman, T. Rysiok, D. Müller-Pompalla, S. L. Goodman, M. A. Arnaout, *J Cell Biol* **2009**, *186*, 589-600.
[11]   J. P. Xiong, T. Stehle, B. Diefenbach, R. Zhang, R. Dunker, D. L. Scott, A. Joachimiak, S. L. Goodman, M. A. Arnaout, *Science* **2001**, *294*, 339-345.
[12]   J. P. Xiong, T. Stehle, R. Zhang, A. Joachimiak, M. Frech, S. L. Goodman, M. A. Arnaout, *Science* **2002**, *296*, 151-155.
[13]   J. Zhu, B. H. Luo, T. Xiao, C. Zhang, N. Nishida, T. A. Springer, *Mol Cell* **2008**, *32*, 849-861.
[14]   K. Zhang, J. Chen, *Cell Adh Migr* **2012**, *6*, 20-29.
[15]   S. J. Shattil, C. Kim, M. H. Ginsberg, *Nat Rev Mol Cell Biol* **2010**, *11*, 288-300.
[16]   M. J. Humphries, E. J. Symonds, A. P. Mould, *Curr Opin Struct Biol* **2003**, *13*, 236-243; C. Oxvig, T. A. Springer, *Proc Natl Acad Sci U S A* **1998**, *95*, 4870-4875.
[17]   A. E. Berman, N. I. Kozlova, *Membr Cell Biol* **2000**, *13*, 207-244; R. S. Larson, A. L. Corbi, L. Berman, T. Springer, *J Cell Biol* **1989**, *108*, 703-712; T. Vorup-Jensen, T. T. Waldron, N. Astrof, M. Shimaoka, T. A. Springer, *Biochim Biophys Acta* **2007**, *1774*, 1148-1155; T. A. Springer, *Proc Natl Acad Sci U S A* **1997**, *94*, 65-72.
[18]   T. Xiao, J. Takagi, B. S. Coller, J. H. Wang, T. A. Springer, *Nature* **2004**, *432*, 59-67.
[19]   M. Shimaoka, C. Lu, R. T. Palframan, U. H. von Andrian, A. McCormack, J. Takagi, T. A. Springer, *Proc Natl Acad Sci U S A* **2001**, *98*, 6009-6014.
[20]   D. Valdramidou, M. J. Humphries, A. P. Mould, *J Biol Chem* **2008**, *283*, 32704-32714.
[21]   J. O. Lee, L. A. Bankston, M. A. Arnaout, R. C. Liddington, *Structure* **1995**, *3*, 1333-1340.
[22]   B. H. Luo, C. V. Carman, T. A. Springer, *Annu Rev Immunol* **2007**, *25*, 619-647.
[23]   A. P. Mould, S. J. Barton, J. A. Askari, S. E. Craig, M. J. Humphries, *J Biol Chem* **2003**, *278*, 51622-51629.
[24]   J. Chen, A. Salas, T. A. Springer, *Nat Struct Biol* **2003**, *10*, 995-1001.
[25]   J. P. Xiong, T. Stehle, S. L. Goodman, M. A. Arnaout, *J Biol Chem* **2004**, *279*, 40252-40254.
[26]   J. Zhu, T. A. Springer, *J Cell Biol* **2013**, *201*, 1053-1068.
[27]   J. Takagi, B. M. Petre, T. Walz, T. A. Springer, *Cell* **2002**, *110*, 599-511.
[28]   N. Beglova, S. C. Blacklow, J. Takagi, T. A. Springer, *Nat Struct Biol* **2002**, *9*, 282-287.
[29]   C. Kim, F. Ye, M. H. Ginsberg, *Annu Rev Cell Dev Biol* **2011**, *27*, 321-345.
[30]   J. Zhu, B. Boylan, B. H. Luo, P. J. Newman, T. A. Springer, *J Biol Chem* **2007**, *282*, 11914-11920; J. Zhu, A. Negri, D. Provasi, M. Filizola, B. S. Coller, T. A. Springer, *Blood* **2010**, *116*, 5050-5059.
[31]   M. Arnaout, B. Mahalingam, J. Xiong, *Annual Review of Cell and Developmental Biology* **2005**, *21*, 381-410.
[32]   J. P. Xiong, T. Stehle, S. L. Goodman, M. A. Arnaout, *J Thromb Haemost* **2003**, *1*, 1642-1654.
[33]   M. H. Ginsberg, A. Lightsey, T. J. Kunicki, A. Kaufmann, G. Marguerie, E. F. Plow, *J Clin Invest* **1986**, *78*, 1103-1111; D. E. Jackson, M. Poncz, M. T. Holyst, P. J. Newman, *Eur J Biochem* **1996**, *240*, 280-287.
[34]   Y. van Kooyk, P. Weder, K. Heije, R. de Waal Malefijt, C. G. Figdor, *Cell Adhes Commun* **1993**, *1*, 21-32; I. Dransfield, C. Cabañas, A. Craig, N. Hogg, *J Cell Biol* **1992**, *116*, 219-226; D. J. Onley, C. G. Knight, D. S. Tuckwell, M. J. Barnes, R. W. Farndale, *J Biol Chem* **2000**, *275*, 24560-24564; M. J. Humphries, *Curr Opin Cell Biol* **1996**, *8*, 632-640.

[35]   M. Shimaoka, T. Xiao, J. H. Liu, Y. Yang, Y. Dong, C. D. Jun, A. McCormack, R. Zhang, A. Joachimiak, J. Takagi, J. H. Wang, T. A. Springer, *Cell* **2003**, *112*, 99-111; J. O. Lee, P. Rieu, M. A. Arnaout, R. Liddington, *Cell* **1995**, *80*, 631-638.

[36]   M. Shimaoka, J. Takagi, T. A. Springer, *Annu Rev Biophys Biomol Struct* **2002**, *31*, 485-516.

[37]   M. M. Harding *Acta Crystallogr D Biol Crystallogr* **2001**, *57*, 401-411.

[38]   R. McEver, C. Zhu, R. Schekman, L. Goldstein, R. Lehmann, *Annual Review of Cell and Developmental Biology, Vol 26* **2010**, *26*, 363-396.

[39]   J. Chen, J. Takagi, C. Xie, T. Xiao, B. H. Luo, T. A. Springer, *J Biol Chem* **2004**, *279*, 55556-55561.

[40]   J. Raborn, W. Wang, B. H. Luo, *Biochemistry* **2011**, *50*, 2084-2091.

[41]   J. Chen, W. Yang, M. Kim, C. V. Carman, T. A. Springer, *Proc Natl Acad Sci U S A* **2006**, *103*, 13062-13067; E. C. Tozer, R. C. Liddington, M. J. Sutcliffe, A. H. Smeeton, J. C. Loftus, *J Biol Chem* **1996**, *271*, 21978-21984; W. Xia, T. A. Springer, *Proc Natl Acad Sci U S A* **2014**, *111*, 17863-17868.

[42]   Y. Pan, K. Zhang, J. Qi, J. Yue, T. A. Springer, J. Chen, *Proc Natl Acad Sci U S A* **2010**, *107*, 21388-21393.

[43]   F. G. Giancotti, E. Ruoslahti, *Science* **1999**, *285*, 1028-1032.

[44]   M. A. Schwartz, M. H. Ginsberg, *Nat Cell Biol* **2002**, *4*, E65-68.

[45]   A. Tolomelli, P. Galletti, M. Baiula, D. Giacomini, *Cancers (Basel)* **2017**, *9*.

[46]   D. S. Harburger, D. A. Calderwood, *J Cell Sci* **2009**, *122*, 159-163.

[47]   F. Ye, C. Kim, M. H. Ginsberg, *J Thromb Haemost* **2011**, *9 Suppl 1*, 20-25.

[48]   D. V. Iwamoto, D. A. Calderwood, *Curr Opin Cell Biol* **2015**, *36*, 41-47.

[49]   T. L. Lau, C. Kim, M. H. Ginsberg, T. S. Ulmer, *EMBO J* **2009**, *28*, 1351-1361; J. Yang, Y. Q. Ma, R. C. Page, S. Misra, E. F. Plow, J. Qin, *Proc Natl Acad Sci U S A* **2009**, *106*, 17729-17734.

[50]   D. A. Calderwood, I. D. Campbell, D. R. Critchley, *Nat Rev Mol Cell Biol* **2013**, *14*, 503-517.

[51]   D. A. Calderwood, R. Zent, R. Grant, D. J. Rees, R. O. Hynes, M. H. Ginsberg, *J Biol Chem* **1999**, *274*, 28071-28074.

[52]   A. H. Chishti, A. C. Kim, S. M. Marfatia, M. Lutchman, M. Hanspal, H. Jindal, S. C. Liu, P. S. Low, G. A. Rouleau, N. Mohandas, J. A. Chasis, J. G. Conboy, P. Gascard, Y. Takakuwa, S. C. Huang, E. J. Benz, A. Bretscher, R. G. Fehon, J. F. Gusella, V. Ramesh, F. Solomon, V. T. Marchesi, S. Tsukita, K. B. Hoover, *Trends Biochem Sci* **1998**, *23*, 281-282.

[53]   D. A. Calderwood, B. Yan, J. M. de Pereda, B. G. Alvarez, Y. Fujioka, R. C. Liddington, M. H. Ginsberg, *J Biol Chem* **2002**, *277*, 21749-21758.

[54]   M. Moser, K. Legate, R. Zent, R. Fassler, *Science* **2009**, *324*, 895-899.

[55]   C. Oxley, N. Anthis, E. Lowe, I. Vakonakis, I. Campbell, K. Wegener, *Journal of Biological Chemistry* **2008**, *283*, 5420-5426.

[56]   C. Kim, F. Ye, X. Hu, M. H. Ginsberg, *J Cell Biol* **2012**, *197*, 605-611; K. Wegener, A. Partridge, J. Han, A. Pickford, R. Liddington, M. Ginsberg, I. Campbell, *Cell* **2007**, *128*, 171-182; N. J. Anthis, K. L. Wegener, F. Ye, C. Kim, B. T. Goult, E. D. Lowe, I. Vakonakis, N. Bate, D. R. Critchley, M. H. Ginsberg, I. D. Campbell, *EMBO J* **2009**, *28*, 3623-3632.

[57]   F. Ye, A. K. Snider, M. H. Ginsberg, *Front Med* **2014**, *8*, 6-16.

[58]   D. Calderwood, *Journal of Cell Science* **2004**, *117*, 657-666; E. Goksoy, Y. Ma, X. Wang, X. Kong, D. Perera, E. Plow, J. Qin, *Molecular Cell* **2008**, *31*, 124-133.

[59]   M. Moser, B. Nieswandt, S. Ussar, M. Pozgajova, R. Fässler, *Nat Med* **2008**, *14*, 325-330; D. S. Harburger, M. Bouaouina, D. A. Calderwood, *J Biol Chem* **2009**, *284*, 11485-11497.

[60]   C. Margadant, M. Kreft, D. J. de Groot, J. C. Norman, A. Sonnenberg, *Curr Biol* **2012**, *22*, 1554-1563.

[61]   E. Park, Y. Yuki, H. Kiyono, M. Shimaoka, *Journal of Biomedical Science* **2015**, *22*.

[62]   D. Bouvard, J. Pouwels, N. De Franceschi, J. Ivaska, *Nature Reviews Molecular Cell Biology* **2013**, *14*, 430-442.

[63]   T. Kiema, Y. Lad, P. Jiang, C. Oxley, M. Baldassarre, K. Wegener, I. Campbell, J. Ylanne, D. Calderwood, *Molecular Cell* **2006**, *21*, 337-347.

[64]   A. Millon-Fremillon, D. Bouvard, A. Grichine, S. Manet-Dupe, M. Block, C. Albiges-Rizo, *Journal of Cell Biology* **2008**, *180*, 427-441.

[65]   J. Pouwels, J. Nevo, T. Pellinen, J. Ylanne, J. Ivaska, *Journal of Cell Science* **2012**, *125*, 3271-3280.

[66]   J. Lilja, T. Zacharchenko, M. Georgiadou, G. Jacquemet, N. De Franceschi, E. Peuhu, H. Hamidi, J. Pouwels, V. Martens, F. H. Nia, M. Beifuss, T. Boeckers, H. J. Kreienkamp, I. L. Barsukov, J. Ivaska, *Nat Cell Biol* **2017**, *19*, 292-305.

[67]   M. H. Ginsberg, A. Partridge, S. J. Shattil, *Curr Opin Cell Biol* **2005**, *17*, 509-516.

[68]   B. H. Luo, T. A. Springer, *Curr Opin Cell Biol* **2006**, *18*, 579-586; W. Wang, B. H. Luo, *J Cell Biochem* **2010**, *109*, 447-452.

[69]   H. Hamidi, J. Ivaska, *Nature Reviews Cancer* **2018**, *18*, 532-547.

[70]   L. J. Kornberg, H. S. Earp, C. E. Turner, C. Prockop, R. L. Juliano, *Proc Natl Acad Sci U S A* **1991**, *88*, 8392-8396; L. Kornberg, H. S. Earp, J. T. Parsons, M. Schaller, R. L. Juliano, *J Biol Chem* **1992**, *267*, 23439-23442.

[71]   D. D. Schlaepfer, S. K. Mitra, *Curr Opin Genet Dev* **2004**, *14*, 92-101; J. T. Parsons, *J Cell Sci* **2003**, *116*, 1409-1416.

[72]   S. K. Mitra, D. A. Hanson, D. D. Schlaepfer, *Nat Rev Mol Cell Biol* **2005**, *6*, 56-68; D. D. Schlaepfer, S. K. Mitra, D. Ilic, *Biochim Biophys Acta* **2004**, *1692*, 77-102.

[73]   M. D. Schaller, J. T. Parsons, *Mol Cell Biol* **1995**, *15*, 2635-2645; J. D. Hildebrand, M. D. Schaller, J. T. Parsons, *Mol Biol Cell* **1995**, *6*, 637-647.

[74]   H. C. Chen, P. A. Appeddu, J. T. Parsons, J. D. Hildebrand, M. D. Schaller, J. L. Guan, *J Biol Chem* **1995**, *270*, 16995-16999.

[75]   D. Lietha, X. Cai, D. F. Ceccarelli, Y. Li, M. D. Schaller, M. J. Eck, *Cell* **2007**, *129*, 1177-1187; L. A. Cooper, T. L. Shen, J. L. Guan, *Mol Cell Biol* **2003**, *23*, 8030-8041.

[76]   M. D. Schaller, C. A. Otey, J. D. Hildebrand, J. T. Parsons, *J Cell Biol* **1995**, *130*, 1181-1187; J. M. Dunty, V. Gabarra-Niecko, M. L. King, D. F. Ceccarelli, M. J. Eck, M. D. Schaller, *Mol Cell Biol* **2004**, *24*, 5353-5368.

[77]   E. G. Arias-Salgado, S. Lizano, S. Sarkar, J. S. Brugge, M. H. Ginsberg, S. J. Shattil, *Proc Natl Acad Sci U S A* **2003**, *100*, 13298-13302.

[78]   G. Giannone, M. P. Sheetz, *Trends Cell Biol* **2006**, *16*, 213-223.

[79]   J. S. Desgrosellier, D. A. Cheresh, *Nat Rev Cancer* **2010**, *10*, 9-22.

[80]   C. Francavilla, L. Maddaluno, U. Cavallaro, *Semin Cancer Biol* **2009**, *19*, 298-309; F. G. Giancotti, G. Tarone, *Annu Rev Cell Dev Biol* **2003**, *19*, 173-206.

[81]   J. Folkman, *N Engl J Med* **1971**, *285*, 1182-1186; J. Folkman, *Ann Intern Med* **1975**, *82*, 96-100.

[82]   W. Guo, F. G. Giancotti, *Nat Rev Mol Cell Biol* **2004**, *5*, 816-826.

[83]   M. Nieberler, U. Reuning, F. Reichart, J. Notni, H. J. Wester, M. Schwaiger, M. Weinmüller, A. Räder, K. Steiger, H. Kessler, *Cancers (Basel)* **2017**, *9*.

[84]   M. D. Pierschbacher, E. Ruoslahti, *Nature* **1984**, *309*, 30-33; E. Ruoslahti, M. D. Pierschbacher, *Science* **1987**, *238*, 491-497.

[85]   C. Mas-Moruno, F. Rechenmacher, H. Kessler, *Anticancer Agents Med Chem* **2010**, *10*, 753-768.

[86]   M. A. Dechantsreiter, E. Planker, B. Mathä, E. Lohof, G. Hölzemann, A. Jonczyk, S. L. Goodman, H. Kessler, *J Med Chem* **1999**, *42*, 3033-3040.

[87]   D. F. Legler, G. Wiedle, F. P. Ross, B. A. Imhof, *J Cell Sci* **2001**, *114*, 1545-1553; A. R. Reynolds, I. R. Hart, A. R. Watson, J. C. Welti, R. G. Silva, S. D. Robinson, G. Da Violante, M. Gourlaouen, M. Salih, M. C. Jones, D. T. Jones, G. Saunders, V. Kostourou, F. Perron-Sierra, J. C. Norman, G. C. Tucker, K. M. Hodivala-Dilke, *Nat Med* **2009**, *15*, 392-400.

[88]   K. E. Gottschalk, H. Kessler, *Angew Chem Int Ed Engl* **2002**, *41*, 3767-3774.

[89]   L. Auzzas, F. Zanardi, L. Battistini, P. Burreddu, P. Carta, G. Rassu, C. Curti, G. Casiraghi, *Current Medicinal Chemistry* **2010**, *17*, 1255-1299.

[90]   J. S. Davies, *J Pept Sci* **2003**, *9*, 471-501.

[91]   M. Aumailley, M. Gurrath, G. Müller, J. Calvete, R. Timpl, H. Kessler, *FEBS Lett* **1991**, *291*, 50-54.

[92]   J. Chatterjee, F. Rechenmacher, H. Kessler, *Angew Chem Int Ed Engl* **2013**, *52*, 254-269.

[93]   U. K. Marelli, F. Rechenmacher, T. R. Sobahi, C. Mas-Moruno, H. Kessler, *Front Oncol* **2013**, *3*, 222.

[94]   D. Arosio, C. Casagrande, *Adv Drug Deliv Rev* **2016**, *97*, 111-143.

[95]   F. Danhier, A. Le Breton, V. Préat, *Mol Pharm* **2012**, *9*, 2961-2973; F. Araste, K. Abnous, M. Hashemi, S. M. Taghdisi, M. Ramezani, M. Alibolandi, *J Control Release* **2018**, *292*, 141-162.

[96]   A. Dal Corso, L. Pignataro, L. Belvisi, C. Gennari, *Current Topics in Medicinal Chemistry* **2016**, *16*, 314-329.

[97]   L. Battistini, P. Burreddu, A. Sartori, D. Arosio, L. Manzoni, L. Paduano, G. D'Errico, R. Sala, L. Reia, S. Bonomini, G. Rassu, F. Zanardi, *Mol Pharm* **2014**, *11*, 2280-2293; M. S. Kim, D. W. Lee, K. Park, S. J. Park, E. J. Choi, E. S. Park, H. R. Kim, *Colloids Surf B Biointerfaces* **2014**, *116*, 17-25.

[98]   D. Arosio, L. Manzoni, E. M. Araldi, C. Scolastico, *Bioconjug Chem* **2011**, *22*, 664-672; Y. Zhong, F. Meng, C. Deng, Z. Zhong, *Biomacromolecules* **2014**, *15*, 1955-1969.

[99]   H. Chen, G. Niu, H. Wu, X. Chen, *Theranostics* **2016**, *6*, 78-92; F. C. Gaertner, H. Kessler, H. J. Wester, M. Schwaiger, A. J. Beer, *Eur J Nucl Med Mol Imaging* **2012**, *39 Suppl 1*, S126-138.

[100] J. Shi, L. Wang, Y. S. Kim, S. Zhai, Z. Liu, X. Chen, S. Liu, *J Med Chem* **2008**, *51*, 7980-7990; S. Lanzardo, L. Conti, C. Brioschi, M. P. Bartolomeo, D. Arosio, L. Belvisi, L. Manzoni, A. Maiocchi, F. Maisano, G. Forni, *Contrast Media Mol Imaging* **2011**, *6*, 449-458.

[101] S. Katsamakas, T. Chatzisideri, S. Thysiadis, V. Sarli, *Future Med Chem* **2017**, *9*, 579-604.

[102] K. Temming, R. M. Schiffelers, G. Molema, R. J. Kok, *Drug Resist Updat* **2005**, *8*, 381-402.

[103] F. Zanardi, P. Burreddu, G. Rassu, L. Auzzas, L. Battistini, C. Curti, A. Sartori, G. Nicastro, G. Menchi, N. Cini, A. Bottoncetti, A. Bottonocetti, S. Raspanti, G. Casiraghi, *J Med Chem* **2008**, *51*, 1771-1782; L. Manzoni, L. Belvisi, D. Arosio, M. Civera, M. Pilkington-Miksa, D. Potenza, A. Caprini, E. M. Araldi, E. Monferini, M. Mancino, F. Podestà, C. Scolastico, *ChemMedChem* **2009**, *4*, 615-632; S. Urman, K. Gaus, Y. Yang, U. Strijowski, N. Sewald, S. De Pol, O. Reiser, *Angew Chem Int Ed Engl* **2007**, *46*, 3976-3978; M. Marchini, M. Mingozzi, R. Colombo, I. Guzzetti, L. Belvisi, F. Vasile, D. Potenza, U. Piarulli, D. Arosio, C. Gennari, *Chemistry* **2012**, *18*, 6195-6207; L. Gentilucci, G. Cardillo, S. Spampinato, A. Tolomelli, F. Squassabia, R. De Marco, A. Bedini, M. Baiula, L. Belvisi, M. Civera, *J Med Chem* **2010**, *53*, 106-118.

[104] R. Haubner, R. Gratias, B. Diefenbach, S. Goodman, A. Jonczyk, H. Kessler, *Journal of the American Chemical Society* **1996**, *118*, 7461-7472.

[105] H. Yusuf-Makagiansar, M. E. Anderson, T. V. Yakovleva, J. S. Murray, T. J. Siahaan, *Med Res Rev* **2002**, *22*, 146-167.

[106] G. X. Yang, W. K. Hagmann, *Med Res Rev* **2003**, *23*, 369-392.

[107] J. Herter, A. Zarbock, *J Immunol* **2013**, *190*, 4451-4457.

[108] M. J. Elices, L. Osborn, Y. Takada, C. Crouse, S. Luhowskyj, M. E. Hemler, R. R. Lobb, *Cell* **1990**, *60*, 577-584.

[109] J. Wang, R. Pepinsky, T. Stehle, J. Liu, M. Karpusas, B. Browning, L. Osborn, *Proc. Natl. Acad. Sci. U.S.A.* **1995**, *92*, 5714-5718.

[110] A. P. Mould, M. J. Humphries, *EMBO J* **1991**, *10*, 4089-4095.

[111] E. A. Wayner, A. Garcia-Pardo, M. J. Humphries, J. A. McDonald, W. G. Carter, *J Cell Biol* **1989**, *109*, 1321-1330.

[112] A. Komoriya, L. J. Green, M. Mervic, S. S. Yamada, K. M. Yamada, M. J. Humphries, *J Biol Chem* **1991**, *266*, 15075-15079.

[113] S. Cunningham, J. Rodriguez, M. Arrate, T. Tran, T. Brock, *J. Biol. Chem.* **2002**, *277*, 27589-27592.

[114] J. M. Clements, P. Newham, M. Shepherd, R. Gilbert, T. J. Dudgeon, L. A. Needham, R. M. Edwards, L. Berry, A. Brass, M. J. Humphries, *J Cell Sci* **1994**, *107 (Pt 8)*, 2127-2135.

[115] N. Wright, A. Hidalgo, J. M. Rodríguez-Frade, S. F. Soriano, M. Mellado, M. Parmo-Cabañas, M. J. Briskin, J. Teixidó, *J Immunol* **2002**, *168*, 5268-5277.

[116] C. Rüegg, A. A. Postigo, E. E. Sikorski, E. C. Butcher, R. Pytela, D. J. Erle, *J Cell Biol* **1992**, *117*, 179-189; C. Berlin, E. L. Berg, M. J. Briskin, D. P. Andrew, P. J. Kilshaw, B. Holzmann, I. L. Weissman, A. Hamann, E. C. Butcher, *Cell* **1993**, *74*, 185-195.

[117] M. Briskin, D. Winsor-Hines, A. Shyjan, N. Cochran, S. Bloom, J. Wilson, L. M. McEvoy, E. C. Butcher, N. Kassam, C. R. Mackay, W. Newman, D. J. Ringler, *Am J Pathol* **1997**, *151*, 97-110.

[118] J. Wang, T. A. Springer, *Immunol Rev* **1998**, *163*, 197-215.

[119] C. Laudanna, J. Kim, G. Constantin, E. Butcher, *Immunological Reviews* **2002**, *186*, 37-46.

[120] K. Ley, C. Laudanna, M. Cybulsky, S. Nourshargh, *Nature Reviews Immunology* **2007**, *7*, 678-689.

[121] Y. Kuwano, O. Spelten, H. Zhang, K. Ley, A. Zarbock, *Blood* **2010**, *116*, 617-624.

[122] J. Campbell, J. Hedrick, A. Zlotnik, M. Siani, D. Thompson, E. Butcher, *Science* **1998**, *279*, 381-384; C. Berlin, R. F. Bargatze, J. J. Campbell, U. H. von Andrian, M. C. Szabo, S. R. Hasslen, R. D. Nelson, E. L. Berg, S. L. Erlandsen, E. C. Butcher, *Cell* **1995**, *80*, 413-422.

[123] C. Carman, T. Springer, *Journal of Cell Biology* **2004**, *167*, 377-388.

[124] M. Williams, V. Azcutia, G. Newton, P. Alcaide, F. Luscinskas, *Trends in Immunology* **2011**, *32*, 461-469.

[125] Y. Yu, J. Zhu, L. Z. Mi, T. Walz, H. Sun, J. Chen, T. A. Springer, *J Cell Biol* **2012**, *196*, 131-146.

[126] B. Garmy-Susini, H. Jin, Y. Zhu, R. J. Sung, R. Hwang, J. Varner, *J Clin Invest* **2005**, *115*, 1542-1551.

[127] D. Y. Jackson, *Curr Pharm Des* **2002**, *8*, 1229-1253.

[128] R. De Marco, A. Tolomelli, E. Juaristi, L. Gentilucci, *Med Res Rev* **2016**, *36*, 389-424.

[129] D. Cox, M. Brennan, N. Moran, *Nat Rev Drug Discov* **2010**, *9*, 804-820.

[130] S. Khan, M. Faridi, L. Guo, J. George, A. Agarwal, V. Gupta, *Journal of Immunology* **2014**, *192*; D. Maiguel, M. H. Faridi, C. Wei, Y. Kuwano, K. M. Balla, D. Hernandez, C. J. Barth, G. Lugo, M. Donnelly, A. Nayer, L. F. Moita, S. Schürer, D. Traver, P. Ruiz, R. I. Vazquez-Padron, K. Ley, J. Reiser, V. Gupta, *Sci Signal* **2011**, *4*, ra57.

[131] P. Vanderslice, R. J. Biediger, D. G. Woodside, W. S. Brown, S. Khounlo, N. D. Warier, C. W. Gundlach, A. R. Caivano, W. G. Bornmann, D. S. Maxwell, B. W. McIntyre, J. T. Willerson, R. A. Dixon, *J Biol Chem* **2013**, *288*, 19414-19428.

[132] M. Clerico, C. A. Artusi, A. D. Liberto, S. Rolla, V. Bardina, P. Barbero, S. F. Mercanti, L. Durelli, *Int J Mol Sci* **2017**, *18*; S. M. Nelson, T. M. Nguyen, J. W. McDonald, J. K. MacDonald, *Cochrane Database Syst Rev* **2018**, *8*, CD006097.

[133] A. Shirani, O. Stüve, *J Immunol* **2017**, *198*, 1381-1386.

[134] B. G. Feagan, P. Rutgeerts, B. E. Sands, S. Hanauer, J. F. Colombel, W. J. Sandborn, G. Van Assche, J. Axler, H. J. Kim, S. Danese, I. Fox, C. Milch, S. Sankoh, T. Wyant, J. Xu, A. Parikh, G. S. Group, *N Engl J Med* **2013**, *369*, 699-710; W. J. Sandborn, B. G. Feagan, P. Rutgeerts, S. Hanauer, J. F. Colombel, B. E. Sands, M. Lukas, R. N. Fedorak, S. Lee, B. Bressler, I. Fox, M. Rosario, S. Sankoh, J. Xu, K. Stephens, C. Milch, A. Parikh, G. S. Group, *N Engl J Med* **2013**, *369*, 711-721.

[135] M. Baiula, S. Spampinato, L. Gentilucci, A. Tolomelli, *Front Chem* **2019**, *7*, 489.

[136] T. J. You, D. S. Maxwell, T. P. Kogan, Q. Chen, J. Li, J. Kassir, G. W. Holland, R. A. Dixon, *Biophys J* **2002**, *82*, 447-457.

[137] J. Singh, H. Van Vlijmen, Y. Liao, W. C. Lee, M. Cornebise, M. Harris, I. H. Shu, A. Gill, J. H. Cuervo, W. M. Abraham, S. P. Adams, *J Med Chem* **2002**, *45*, 2988-2993; S. A. Amin, N. Adhikari, S. Bhargava, S. Gayen, T. Jha, *Mol Divers* **2018**, *22*, 129-158.

[138] C. Carlevaro, J. Martins-Da-Silva, W. Savino, E. Caffarena, *Journal of Theoretical & Computational Chemistry* **2013**, *12*.

[139] J. da Silva, L. Dardenne, W. Savino, E. Caffarena, *Journal of the Brazilian Chemical Society* **2010**, *21*, 546-555.

[140] K. Lin, H. Ateeq, S. Hsiung, L. Chong, C. Zimmerman, A. Castro, W. Lee, C. Hammond, S. Kalkunte, L. Chen, R. Pepinsky, D. Leone, A. Sprague, W. Abraham, A. Gill, R. Lobb, S. Adams, *J. Med. Chem.* **1999**, *42*, 920-934.

[141] A. Fisher, E. DePuy, A. Jayaraj, C. Raab, M. Braun, M. Ellis-Hutchings, J. Zhang, J. Rogers, D. Musson, *Journal of Pharmaceutical and Biomedical Analysis* **2002**, *27*, 57-71; B. Karanam, A. Jayraj, M. Rabe, Z. Wang, C. Keohane, J. Strauss, S. Vincent, *Xenobiotica* **2007**, *37*, 487-502.

[142] M. Baiula, S. Spampinato, L. Gentilucci, A. Tolomelli, *Frontiers in Chemistry* **2019**, *7*.

[143] T. G. Kapp, F. Rechenmacher, T. R. Sobahi, H. Kessler, *Expert Opin Ther Pat* **2013**, *23*, 1273-1295.

[144] F. Muro, S. Iimura, Y. Sugimoto, Y. Yoneda, J. Chiba, T. Watanabe, M. Setoguchi, Y. Iigou, K. Matsumoto, A. Satoh, G. Takayama, T. Taira, M. Yokoyama, T. Takashi, A. Nakayama, N. Machinaga, *J Med Chem* **2009**, *52*, 7974-7992.

[145] M. Setoguchi, S. Iimura, Y. Sugimoto, Y. Yoneda, J. Chiba, T. Watanabe, F. Muro, Y. Iigo, G. Takayama, M. Yokoyama, T. Taira, M. Aonuma, T. Takashi, A. Nakayama, N. Machinaga, *Bioorg Med Chem* **2013**, *21*, 42-61.

[146] F. Crofts, M. Pino, B. DeLise, P. Guittin, S. Barbellion, P. Brunel, S. Potdevin, B. Bergmann, T. Hofmann, S. Lerman, R. L. Clark, *Birth Defects Res B Dev Reprod Toxicol* **2004**, *71*, 55-68.

[147] J. Gläsner, H. Blum, V. Wehner, H. U. Stilz, J. D. Humphries, G. P. Curley, A. P. Mould, M. J. Humphries, R. Hallmann, M. Röllinghoff, A. Gessner, *J Immunol* **2005**, *175*, 4724-4734.

[148] J. W. Tilley, L. Chen, A. Sidduri, N. Fotouhi, *Curr Top Med Chem* **2004**, *4*, 1509-1523.

[149] W. Hagmann, *Current Topics in Medicinal Chemistry* **2004**, *4*, 1461-1471.

[150] T. Sugiura, S. Kageyama, A. Andou, T. Miyazawa, C. Ejima, A. Nakayama, T. Dohi, H. Eda, *J Crohns Colitis* **2013**, *7*, e533-542.

[151] T. Kawaguchi, Nomura, S., Tsukimoto, M., Kume,, a. S. T., H., **2002**.

[152] R. M. Liskamp, D. T. Rijkers, J. A. Kruijtzer, J. Kemmink, *Chembiochem* **2011**, *12*, 1626-1653.

[153] L. Gentilucci, A. Tolomelli, F. Squassabia, *Curr Med Chem* **2006**, *13*, 2449-2466.

[154] L. Gentilucci, R. De Marco, L. Cerisoli, *Curr Pharm Des* **2010**, *16*, 3185-3203.

[155] J. Vagner, H. Qu, V. J. Hruby, *Curr Opin Chem Biol* **2008**, *12*, 292-296.

[156] R. De Marco, G. Mazzotti, A. Greco, L. Gentilucci, *Curr Top Med Chem* **2016**, *16*, 343-359.

[157] S. Durani, *Acc Chem Res* **2008**, *41*, 1301-1308.

[158] J. M. Ahn, N. A. Boyle, M. T. MacDonald, K. D. Janda, *Mini Rev Med Chem* **2002**, *2*, 463-473.

[159] R. Zuckermann, J. Kerr, S. Kent, W. Moos, *Journal of the American Chemical Society* **1992**, *114*, 10646-10647.

[160] C. Proulx, D. Sabatino, R. Hopewell, J. Spiegel, Y. Ramos, W. Lubell, *Future Medicinal Chemistry* **2011**, *3*, 1139-1164.

[161] M. Fletcher, M. Campbell, *Chemical Reviews* **1998**, *98*, 763-795.

[162] M. Chorev, *Biopolymers* **2005**, *80*, 67-84.

[163] D. Seebach, A. K. Beck, D. J. Bierbaum, *Chem Biodivers* **2004**, *1*, 1111-1239.

[164] D. Seebach, J. Gardiner, *Acc Chem Res* **2008**, *41*, 1366-1375.

[165]   R. Cheng, S. Gellman, W. DeGrado, *Chemical Reviews* **2001**, *101*, 3219-3232; D. Appella, L. Christianson, I. Karle, D. Powell, S. Gellman, *Journal of the American Chemical Society* **1996**, *118*, 13071-13072.

[166]   C. Goodman, S. Choi, S. Shandler, W. DeGrado, *Nature Chemical Biology* **2007**, *3*, 252-262.

[167]   C. J. White, A. K. Yudin, *Nat Chem* **2011**, *3*, 509-524.

[168]   S. Jiang, Z. Li, K. Ding, P. Roller, *Current Organic Chemistry* **2008**, *12*, 1502-1542.

[169]   L. Gentilucci, F. Gallo, F. Meloni, M. Mastandrea, B. Del Secco, R. De Marco, *European Journal of Organic Chemistry* **2016**, 3243-3251.

[170]   V. J. Hruby, *Life Sci* **1982**, *31*, 189-199.

[171]   R. Haubner, D. Finsinger, H. Kessler, *Angewandte Chemie-International Edition* **1997**, *36*, 1375-1389.

[172]   H. Kessler, R. Gratias, G. Hessler, M. Gurrath, G. Muller, *Pure and Applied Chemistry* **1996**, *68*, 1201-1205.

[173]   F. Schumann, A. Muller, M. Koksch, G. Muller, N. Sewald, *Journal of the American Chemical Society* **2000**, *122*, 12009-12010.

[174]   R. Turner, A. Oliver, R. Lokey, *Organic Letters* **2007**, *9*, 5011-5014.

[175]   J. Illesinghe, C. Guo, R. Garland, A. Ahmed, B. van Lierop, J. Elaridi, W. Jacksonb, A. Robinson, *Chemical Communications* **2009**, 295-297.

[176]   O. Vercillo, C. Andrade, L. Wessjohann, *Organic Letters* **2008**, *10*, 205-208.

[177]   N. Tsomaia, *Eur J Med Chem* **2015**, *94*, 459-470.

[178]   R. De Marco, G. Mazzotti, S. D. Dattoli, M. Baiula, S. Spampinato, A. Greco, L. Gentilucci, *Biopolymers* **2015**, *104*, 636-649.

[179]   A. Tolomelli, L. Gentilucci, E. Mosconi, A. Viola, E. Paradisi, *Amino Acids* **2011**, *41*, 575-586.

[180]   A. Tolomelli, M. Baiula, A. Viola, L. Ferrazzano, L. Gentilucci, S. D. Dattoli, S. Spampinato, E. Juaristi, M. Escudero, *ACS Med Chem Lett* **2015**, *6*, 701-706.

[181]   S. D. Dattoli, R. De Marco, M. Baiula, S. Spampinato, A. Greco, A. Tolomelli, L. Gentilucci, *Eur J Med Chem* **2014**, *73*, 225-232.

[182]   M. Baiula, P. Galletti, G. Martelli, R. Soldati, L. Belvis, M. Civera, S. Dattoli, S. Spampinato, D. Giacomini, *Journal of Medicinal Chemistry* **2016**, *59*, 9721-9742.

[183]   A. Tolomelli, L. Gentilucci, E. Mosconi, A. Viola, S. D. Dattoli, M. Baiula, S. Spampinato, L. Belvisi, M. Civera, *ChemMedChem* **2011**, *6*, 2264-2272.

[184]   M. Baiula, S. Spampinato, *Expert Opinion on Investigational Drugs* **2014**, *23*, 1671-1686.

[185]   S. H. Choi, L. Bielory, *Curr Opin Allergy Clin Immunol* **2008**, *8*, 438-444.

[186]   J. W. Oh, J. C. Shin, S. J. Jang, H. B. Lee, *Ann Allergy Asthma Immunol* **1999**, *82*, 579-585.

[187]   M. Baiula, A. Bedini, G. Carbonari, S. D. Dattoli, S. Spampinato, *Front Pharmacol* **2012**, *3*, 203.

[188]   N. Okada, K. Fukagawa, Y. Takano, M. Dogru, K. Tsubota, H. Fujishima, K. Matsumoto, T. Nakajima, H. Saito, *Invest Ophthalmol Vis Sci* **2005**, *46*, 4512-4518.

[189]   N. Ebihara, T. Yokoyama, T. Kimura, K. Nakayasu, K. Okumura, A. Kanai, C. Ra, *Curr Eye Res* **1999**, *19*, 20-25.

[190]   H. Abdala-Valencia, S. Berdnikovs, J. M. Cook-Mills, *PLoS One* **2011**, *6*, e26706.

[191]   A. Luque, M. Gomez, W. Puzon, Y. Takada, F. SanchezMadrid, C. Cabanas, *Journal of Biological Chemistry* **1996**, *271*, 11067-11075.

[192]   M. Baiula, A. Sparta, A. Bedini, G. Carbonari, C. Bucolo, K. Ward, J. Zhang, P. Govoni, S. Spampinato, *Molecular Vision* **2011**, *17*, 3208-3223.

[193]   A. R. Qasem, C. Bucolo, M. Baiula, A. Spartà, P. Govoni, A. Bedini, D. Fascì, S. Spampinato, *Biochem Pharmacol* **2008**, *76*, 751-762.

[194]   M. Hojo, K. Maghni, T. B. Issekutz, J. G. Martin, *Am J Respir Crit Care Med* **1998**, *158*, 1127-1133.

[195]   M. Nagata, J. B. Sedgwick, H. Kita, W. W. Busse, *Am J Respir Cell Mol Biol* **1998**, *19*, 158-166.

[196]   S. D. Dattoli, M. Baiula, R. De Marco, A. Bedini, M. Anselmi, L. Gentilucci, S. Spampinato, *Br J Pharmacol* **2018**, *175*, 3891-3910.

[197]   S. D. Dattoli, M. Baiula, R. De Marco, A. Bedini, M. Anselmi, L. Gentilucci, S. Spampinato, *British Journal of Pharmacology* **2018**, *175*, 3891-3910.

[198]   R. De Marco, A. Greco, N. Calonghi, S. D. Dattoli, M. Baiula, S. Spampinato, P. Picchetti, L. De Cola, M. Anselmi, F. Cipriani, L. Gentilucci, *Biopolymers* **2017**.

[199]   A. Greco, L. Maggini, L. De Cola, R. De Marco, L. Gentilucci, *Bioconjug Chem* **2015**, *26*, 1873-1878.

[200]   A. K. Ghosh, M. Brindisi, A. Sarkar, *ChemMedChem* **2018**, *13*, 2351-2373.

[201]   E. Aresu, S. Fioravanti, S. Gasbarri, L. Pellacani, F. Ramadori, *Amino Acids* **2013**, *44*, 977-982.

[202]   R. Moriarty, *Journal of Organic Chemistry* **2005**, *70*, 2893-2903.

[203]   J. Podlech, D. Seebach, *Angewandte Chemie-International Edition in English* **1995**, *34*, 471-472.

[204] R. Caputo, L. Longobardo, *Amino Acids* **2007**, *32*, 401-404.

[205] K. J. Lee, W. S. Lee, H. Yun, Y. J. Hyun, C. D. Seo, C. W. Lee, H. S. Lim, *Org Lett* **2016**, *18*, 3678-3681.

[206] C. Blettner, M. Bradley, *Tetrahedron Letters* **1994**, *35*, 467-470.

[207] V. Hruby, P. Balse, *Current Medicinal Chemistry* **2000**, *7*, 945-970.

[208] S. Urman, K. Gaus, Y. Yang, U. Strijowski, N. Sewald, S. De Pol, O. Reiser, *Angewandte Chemie-International Edition* **2007**, *46*, 3976-3978.

[209] M. Malesevic, U. Strijowski, D. Bächle, N. Sewald, *J Biotechnol* **2004**, *112*, 73-77.

[210] E. Celik, M. H. Faridi, V. Kumar, S. Deep, V. T. Moy, V. Gupta, *Biophys J* **2013**, *105*, 2517-2527.

[211] *HyperChem* , H. I. release 8.0.3, Gainesville, FL, USA, **2007**.

[212] R. Spadaccini, P. Temussi, *Cellular and Molecular Life Sciences* **2001**, *58*, 1572-1582; P. Temussi, D. Picone, G. Saviano, P. Amodeo, A. Motta, T. Tancredi, S. Salvadori, R. Tomatis, *Biopolymers* **1992**, *32*, 367-372.

[213] R. Rai, S. Raghothama, P. Balaram, *Journal of the American Chemical Society* **2006**, *128*, 2675-2681; C. Toniolo, *CRC Crit Rev Biochem* **1980**, *9*, 1-44.

[214] W. K., *NMR of Proteins and Nucleic Acids*, New York, **1986**.

[215] C. J. Jorgensen W. L., Madura J., Impey R. W., Klein M. L., *J. Chem. Phys.* **1983**, *79*, 926-935.

[216] W. Cornell, P. Cieplak, C. Bayly, I. Gould, K. Merz, D. Ferguson, D. Spellmeyer, T. Fox, J. Caldwell, P. Kollman, *Journal of the American Chemical Society* **1996**, *118*, 2309-2309.

[217] M. Nagae, S. Re, E. Mihara, T. Nogi, Y. Sugita, J. Takagi, *J Cell Biol* **2012**, *197*, 131-140.

[218] J. F. Van Agthoven, J. P. Xiong, J. L. Alonso, X. Rui, B. D. Adair, S. L. Goodman, M. A. Arnaout, *Nat Struct Mol Biol* **2014**, *21*, 383-388.

[219] A. Paladino, M. Civera, L. Belvisi, G. Colombo, *PLoS Comput Biol* **2017**, *13*, e1005334.

[220] D. Bier, P. Thiel, J. Briels, C. Ottmann, *Prog Biophys Mol Biol* **2015**, *119*, 10-19; S. A. Andrei, E. Sijbesma, M. Hann, J. Davis, G. O'Mahony, M. W. D. Perry, A. Karawajczyk, J. Eickhoff, L. Brunsveld, R. G. Doveston, L. G. Milroy, C. Ottmann, *Expert Opin Drug Discov* **2017**, *12*, 925-940.

[221] R. Huey, G. Morris, A. Olson, D. Goodsell, *Journal of Computational Chemistry* **2007**, *28*, 1145-1152.

[222] E. Lindahl, B. Hess, D. van der Spoel, *Journal of Molecular Modeling* **2001**, *7*, 306-317.

[223] Y. Duan, C. Wu, S. Chowdhury, M. Lee, G. Xiong, W. Zhang, R. Yang, P. Cieplak, R. Luo, T. Lee, J. Caldwell, J. Wang, P. Kollman, *Journal of Computational Chemistry* **2003**, *24*, 1999-2012.

[224] M. Valiev, E. Bylaska, N. Govind, K. Kowalski, T. Straatsma, H. Van Dam, D. Wang, J. Nieplocha, E. Apra, T. Windus, W. de Jong, *Computer Physics Communications* **2010**, *181*, 1477-1489.

[225] T. Kinashi, *Nat Rev Immunol* **2005**, *5*, 546-559.

[226] L. L. Chen, A. Whitty, R. R. Lobb, S. P. Adams, R. B. Pepinsky, *J Biol Chem* **1999**, *274*, 13167-13175.

[227] D. L. Koelman, F. J. Mateen, *J Neurol* **2015**, *262*, 2013-2024; A. J. Affandi, T. R. Radstake, W. Marut, *Semin Immunopathol* **2015**, *37*, 475-487; C. S. Park, T. Rhim, *Expert Rev Proteomics* **2011**, *8*, 221-230.

[228] J. R. Chan, S. J. Hyduk, M. I. Cybulsky, *J Immunol Methods* **2003**, *273*, 43-52.

[229] J. R. Chan, S. J. Hyduk, M. I. Cybulsky, *J Exp Med* **2001**, *193*, 1149-1158; M. W. Johansson, E. A. Kelly, W. W. Busse, N. N. Jarjour, D. F. Mosher, *J Immunol* **2008**, *180*, 7622-7635.

[230] T. A. Yednock, C. Cannon, C. Vandevert, E. G. Goldbach, G. Shaw, D. K. Ellis, C. Liaw, L. C. Fritz, L. I. Tanner, *J Biol Chem* **1995**, *270*, 28740-28750; A. Jakubowski, M. D. Rosa, S. Bixler, R. Lobb, L. C. Burkly, *Cell Adhes Commun* **1995**, *3*, 131-142.

[231] A. Chigaev, A. M. Blenc, J. V. Braaten, N. Kumaraswamy, C. L. Kepley, R. P. Andrews, J. M. Oliver, B. S. Edwards, E. R. Prossnitz, R. S. Larson, L. A. Sklar, *J Biol Chem* **2001**, *276*, 48670-48678.

[232] R. Langer, D. A. Tirrell, *Nature* **2004**, *428*, 487-492.

[233] M. Tirrell, E. Kokkoli, M. Biesalski, *Surface Science* **2002**, *500*, 61-83; C. Mas-Moruno, R. Fraioli, F. Abericio, J. Manero, F. Gil, *Acs Applied Materials & Interfaces* **2014**, *6*, 6525-6536; M. Kantlehner, D. Finsinger, J. Meyer, P. Schaffner, A. Jonczyk, B. Diefenbach, B. Nies, H. Kessler, *Angewandte Chemie-International Edition* **1999**, *38*, 560-562; F. Rechenmacher, S. Neubauer, C. Mas-Moruno, P. Dorfner, J. Polleux, J. Guasch, B. Conings, H. Boyen, A. Bochen, T. Sobahi, R. Burgkart, J. Spatz, R. Fassler, H. Kessler, *Chemistry-a European Journal* **2013**, *19*, 9218-9223.

[234] A. Ulman, *Chemical Reviews* **1996**, *96*, 1533-1554; M. Ekiz, G. Cinar, M. Khalily, M. Guler, *Nanotechnology* **2016**, *27*.

[235] S. Wang, H. Wang, J. Jiao, K. Chen, G. Owens, K. Kamei, J. Sun, D. Sherman, C. Behrenbruch, H. Wu, H. Tseng, *Angewandte Chemie-International Edition* **2009**, *48*, 8970-8973; J. Conde, J. Dias, V. Grazu, M. Moros, P. Baptista, J. de la Fuente, *Frontiers in Chemistry* **2014**, *2*; K. Benson, E. Prasetyanto, H. Galla, N. Kehr, *Soft Matter* **2012**, *8*, 10845-10852; N. Kehr, H. Galla, K. Riehemann, H. Fuchs, *Rsc Advances* **2015**, *5*, 5704-5710.

[236]   A. Zabala Ruiz, H. Li, G. Calzaferri, *Angew Chem Int Ed Engl* **2006**, *45*, 5282-5287.

[237]   A. Devaux, G. Calzaferri, I. Miletto, P. Cao, P. Belser, D. Bruhwiler, O. Khorev, R. Haner, A. Kunzmann, *Journal of Physical Chemistry C* **2013**, *117*, 23034-23047.

[238]   T. Ohsuna, B. Slater, F. Gao, J. Yu, Y. Sakamoto, G. Zhu, O. Terasaki, D. Vaughan, S. Qiu, C. Catlow, *Chemistry-a European Journal* **2004**, *10*, 5031-5040.

[239]   J. Lee, H. Lim, K. Ha, H. Cheong, K. Yoon, *Angewandte Chemie-International Edition* **2006**, *45*, 5288-5292.

[240]   G. Calzaferri, S. Huber, H. Maas, C. Minkowski, *Angewandte Chemie-International Edition* **2003**, *42*, 3732-3758.

[241]   N. Kehr, A. Schafer, B. Ravoo, L. De Cola, *Nanoscale* **2010**, *2*, 601-605; N. Kehr, K. Riehemann, J. El-Gindi, A. Schafer, H. Fuchs, H. Galla, L. De Cola, *Advanced Functional Materials* **2010**, *20*, 2248-2254.

[242]   J. El-Gindi, K. Benson, L. De Cola, H. Galla, N. Kehr, *Angewandte Chemie-International Edition* **2012**, *51*, 3716-3720.

[243]   M. Busby, A. Devaux, C. Blum, V. Subramaniam, G. Calzaferri, L. De Cola, *Journal of Physical Chemistry C* **2011**, *115*, 5974-5988.

[244]   L. Gentilucci, G. Cardillo, F. Squassabia, A. Tolomelli, S. Spampinato, A. Sparta, M. Baiula, *Bioorganic & Medicinal Chemistry Letters* **2007**, *17*, 2329-2333.

[245]   R. Alon, P. Kassner, M. Carr, E. Finger, M. Hemler, T. Springer, *Journal of Cell Biology* **1995**, *128*, 1243-1253.

[246]   A. Taherian, X. Li, Y. Liu, T. Haas, *Bmc Cancer* **2011**, *11*; S. Naderi Beni, S. Kouhpayeh, Z. Hejazi, N. Heidari Hafshejani, H. Khanahmad, *Adv Pharm Bull* **2015**, *5*, 429-434.

[247]   B. Crucian, M. Nelman-Gonzalez, C. Sams, *Clin Vaccine Immunol* **2006**, *13*, 403-408.

[248]   N. M. Alves, I. Pashkuleva, R. L. Reis, J. F. Mano, *Small* **2010**, *6*, 2208-2220; K. Sakakibara, J. P. Hill, K. Ariga, *Small* **2011**, *7*, 1288-1308.

[249]   R. Chari, M. Miller, W. Widdison, *Angewandte Chemie-International Edition* **2014**, *53*, 3796-3827.

[250]   A. Beck, L. Goetsch, C. Dumontet, N. Corvaïa, *Nat Rev Drug Discov* **2017**, *16*, 315-337.

[251]   Q. Cao, Z. Li, K. Chen, Z. Wu, L. He, N. Neamati, X. Chen, *European Journal of Nuclear Medicine and Molecular Imaging* **2008**, *35*, 1489-1498.

[252]   K. Bosslet, R. Straub, M. Blumrich, J. Czech, M. Gerken, B. Sperker, H. K. Kroemer, J. P. Gesson, M. Koch, C. Monneret, *Cancer Res* **1998**, *58*, 1195-1201.

[253]   A. van der Veldt, N. Hendrikse, E. Smit, M. Mooijer, A. Rijnders, W. Gerritsen, J. van der Hoeven, A. Windhorst, A. Lammertsma, M. Lubberink, *European Journal of Nuclear Medicine and Molecular Imaging* **2010**, *37*, 1950-1958; A. van der Veldt, M. Lubberink, R. Mathijssen, W. Loos, G. Herder, H. Greuter, E. Comans, H. Rutten, J. Eriksson, A. Windhorst, N. Hendrikse, P. Postmus, E. Smit, A. Lammertsma, *Clinical Cancer Research* **2013**, *19*, 4163-4173.

[254]   M. Srinivasarao, P. S. Low, *Chem Rev* **2017**, *117*, 12133-12164.

[255]   M. Srinivasarao, C. V. Galliford, P. S. Low, *Nat Rev Drug Discov* **2015**, *14*, 203-219; D. Böhme, A. G. Beck-Sickinger, *J Pept Sci* **2015**, *21*, 186-200.

[256]   B. Teicher, R. Chari, *Clinical Cancer Research* **2011**, *17*, 6389-6397; Z. R. Lu, P. Qiao, *Mol Pharm* **2018**, *15*, 3603-3616; G. Casi, D. Neri, *J Med Chem* **2015**, *58*, 8751-8761; H. P. Gerber, F. E. Koehn, R. T. Abraham, *Nat Prod Rep* **2013**, *30*, 625-639.

[257]   N. Krall, J. Scheuermann, D. Neri, *Angew Chem Int Ed Engl* **2013**, *52*, 1384-1402.

[258]   A. Kuriakose, N. Chirmule, P. Nair, *J Immunol Res* **2016**, *2016*, 1298473.

[259]   F. Yuan, M. Dellian, D. Fukumura, M. Leunig, D. A. Berk, V. P. Torchilin, R. K. Jain, *Cancer Res* **1995**, *55*, 3752-3756.

[260]   C. Zhuang, X. Guan, H. Ma, H. Cong, W. Zhang, Z. Miao, *Eur J Med Chem* **2019**, *163*, 883-895.

[261]   T. Chatzisideri, G. Leonidis, V. Sarli, *Future Med Chem* **2018**, *10*, 2201-2226.

[262]   J. G. Vineberg, T. Wang, E. S. Zuniga, I. Ojima, *J Med Chem* **2015**, *58*, 2406-2416; S. Bhuniya, S. Maiti, E. J. Kim, H. Lee, J. L. Sessler, K. S. Hong, J. S. Kim, *Angew Chem Int Ed Engl* **2014**, *53*, 4469-4474.

[263]   K. L. Dao, R. N. Hanson, *Bioconjug Chem* **2012**, *23*, 2139-2158.

[264]   S. A. Kularatne, K. Wang, H. K. Santhapuram, P. S. Low, *Mol Pharm* **2009**, *6*, 780-789; J. Roy, T. X. Nguyen, A. K. Kanduluru, C. Venkatesh, W. Lv, P. V. Reddy, P. S. Low, M. Cushman, *J Med Chem* **2015**, *58*, 3094-3103.

[265]   N. Joubert, C. Denevault-Sabourin, F. Bryden, M. C. Viaud-Massuard, *Eur J Med Chem* **2017**, *142*, 393-415; P. T. Wong, S. K. Choi, *Chem Rev* **2015**, *115*, 3388-3432.

[266]   A. Dal Corso, R. Gébleux, P. Murer, A. Soltermann, D. Neri, *J Control Release* **2017**, *264*, 211-218; S. Cazzamalli, B. Ziffels, F. Widmayer, P. Murer, G. Pellegrini, F. Pretto, S. Wulhfard, D. Neri, *Clin Cancer Res* **2018**, *24*, 3656-3667; R. Gébleux, S. Wulhfard, G. Casi, D. Neri, *Mol Cancer Ther* **2015**, *14*, 2606-

2612; R. Gébleux, M. Stringhini, R. Casanova, A. Soltermann, D. Neri, *Int J Cancer* **2017**, *140*, 1670-1679.

[267] C. P. Leamon, M. A. Parker, I. R. Vlahov, L. C. Xu, J. A. Reddy, M. Vetzel, N. Douglas, *Bioconjug Chem* **2002**, *13*, 1200-1210.

[268] S. M. Hillier, K. P. Maresca, G. Lu, R. D. Merkin, J. C. Marquis, C. N. Zimmerman, W. C. Eckelman, J. L. Joyal, J. W. Babich, *J Nucl Med* **2013**, *54*, 1369-1376.

[269] M. Ginj, H. Zhang, B. Waser, R. Cescato, D. Wild, X. Wang, J. Erchegyi, J. Rivier, H. R. Mäcke, J. C. Reubi, *Proc Natl Acad Sci U S A* **2006**, *103*, 16436-16441.

[270] E. Figueras, A. Martins, A. Borbely, V. Le Joncour, P. Cordella, R. Perego, D. Modena, P. Pagani, S. Esposito, G. Auciello, M. Frese, P. Gallinari, P. Laakkonen, C. Steinkuhler, N. Sewald, *Pharmaceutics* **2019**, *11*.

[271] S. Cazzamalli, A. Dal Corso, D. Neri, *Mol Cancer Ther* **2016**, *15*, 2926-2935; N. Krall, F. Pretto, W. Decurtins, G. J. Bernardes, C. T. Supuran, D. Neri, *Angew Chem Int Ed Engl* **2014**, *53*, 4231-4235; S. Cazzamalli, A. Dal Corso, F. Widmayer, D. Neri, *J Am Chem Soc* **2018**, *140*, 1617-1621.

[272] S. Cazzamalli, E. Figueras, L. Pethő, A. Borbély, C. Steinkühler, D. Neri, N. Sewald, *ACS Omega* **2018**, *3*, 14726-14731.

[273] F. de Groot, H. Broxterman, H. Adams, A. van Vliet, G. Tesser, Y. Elderkamp, A. Schraa, R. Kok, G. Molema, H. Pinedo, H. Scheeren, *Molecular Cancer Therapeutics* **2002**, *1*, 901-911; D. J. Burkhart, B. T. Kalet, M. P. Coleman, G. C. Post, T. H. Koch, *Mol Cancer Ther* **2004**, *3*, 1593-1604.

[274] J. L. Crisp, E. N. Savariar, H. L. Glasgow, L. G. Ellies, M. A. Whitney, R. Y. Tsien, *Mol Cancer Ther* **2014**, *13*, 1514-1525; A. Dias, L. Bodero, A. Martins, D. Arosio, S. Gazzola, L. Belvisi, L. Pignataro, C. Steinkuhler, A. Dal Corso, C. Gennari, U. Piarulli, *Chemmedchem* **2019**, *14*, 938-942.

[275] M. Lee, J. Kim, J. Han, S. Bhuniya, J. Sessler, C. Kang, J. Kim, *Journal of the American Chemical Society* **2012**, *134*, 12668-12674; A. Pina, A. Dal Corso, M. Caruso, L. Belvisi, D. Arosio, S. Zanella, F. Gasparri, C. Albanese, U. Cucchi, I. Fraietta, A. Marsiglio, L. Pignataro, D. Donati, C. Gennari, *Chemistryselect* **2017**, *2*, 4759-4766.

[276] S. Mukhopadhyay, C. Barnes, A. Haskel, S. Short, K. Barnes, S. Lippard, *Bioconjugate Chemistry* **2008**, *19*, 39-49.

[277] R. Colombo, M. Mingozzi, L. Belvisi, D. Arosio, U. Piarulli, N. Carenini, P. Perego, N. Zaffaroni, M. De Cesare, V. Castiglioni, E. Scanziani, C. Gennari, *J Med Chem* **2012**, *55*, 10460-10474; A. Dal Corso, M. Caruso, L. Belvisi, D. Arosio, U. Piarulli, C. Albanese, F. Gasparri, A. Marsiglio, F. Sola, S. Troiani, B. Valsasina, L. Pignataro, D. Donati, C. Gennari, *Chemistry-a European Journal* **2015**, *21*, 6921-6929; M. Pilkington-Miksa, D. Arosio, L. Battistini, L. Belvisi, M. De Matteo, F. Vasile, P. Burreddu, P. Carta, G. Rassu, P. Perego, N. Carenini, F. Zunino, M. De Cesare, V. Castiglioni, E. Scanziani, C. Scolastico, G. Casiraghi, F. Zanardi, L. Manzoni, *Bioconjugate Chemistry* **2012**, *23*, 1610-1622; C. Ryppa, H. Mann-Steinberg, M. L. Biniossek, R. Satchi-Fainaro, F. Kratz, *Int J Pharm* **2009**, *368*, 89-97.

[278] T. G. Kapp, F. Rechenmacher, S. Neubauer, O. V. Maltsev, E. A. Cavalcanti-Adam, R. Zarka, U. Reuning, J. Notni, H. J. Wester, C. Mas-Moruno, J. Spatz, B. Geiger, H. Kessler, *Sci Rep* **2017**, *7*, 39805.

[279] C. Weiss, E. Figueras, A. Borbely, N. Sewald, *J. Pept. Sci.* **2017**, *23*, 514-531.

[280] R. Schwartz, C. Hirsch, D. Sesin, J. Flor, M. Chartrain, R. Fromtling, G. Harris, M. Salvatore, J. Liesch, K. Yudin, *J. Ind. Microbiol* **1990**, *5*, 113-123.

[281] C. D. Smith, X. Zhang, S. L. Mooberry, G. M. Patterson, R. E. Moore, *Cancer Res* **1994**, *54*, 3779-3784; C. D. Smith, X. Zhang, *J Biol Chem* **1996**, *271*, 6192-6198.

[282] D. Panda, R. H. Himes, R. E. Moore, L. Wilson, M. A. Jordan, *Biochemistry* **1997**, *36*, 12948-12953; D. Panda, K. DeLuca, D. Williams, M. A. Jordan, L. Wilson, *Proc Natl Acad Sci U S A* **1998**, *95*, 9313-9318; P. Barbier, C. Gregoire, F. Devred, M. Sarrazin, V. Peyrot, *Biochemistry* **2001**, *40*, 13510-13519.

[283] S. Eissler, A. Stoncius, M. Nahrwold, N. Sewald, *Synthesis* **2006**, 3747-3789.

[284] N. Sewald, C. Mast, S. Eissler, M. Nahrwold, B. Sammet, T. Bogner, C. Weiss, *Journal of Peptide Science* **2010**, *16*, 34-34; B. Sammet, T. Bogner, C. Weiss, M. Nahrwold, S. Eissler, N. Sewald, *Amino Acids* **2009**, *37*, 42-42; A. Kumar, M. Kumar, S. Sharma, S. K. Guru, S. Bhushan, B. A. Shah, *Eur J Med Chem* **2015**, *93*, 55-63; C. Weiss, T. Bogner, B. Sammet, N. Sewald, *Beilstein Journal of Organic Chemistry* **2012**, *8*, 2060-2066.

[285] S. Eissler, T. Bogner, M. Nahrwold, N. Sewald, *Chem.-Eur. J.* **2009**, *15*, 11273-11287.

[286] M. Edelman, D. Gandara, P. Hausner, V. Israel, D. Thornton, J. DeSanto, L. Doyle, *Lung Cancer* **2003**, *39*, 197-199; G. D'Agostino, J. del Campo, B. Mellado, M. A. Izquierdo, T. Minarik, L. Cirri, L. Marini, J. L. Perez-Gracia, G. Scambia, *Int J Gynecol Cancer* **2006**, *16*, 71-76.

[287] F. Kratz, I. Muller, C. Ryppa, A. Warnecke, *ChemMedChem* **2008**, *3*, 20-53.

[288] B. Sammet, T. Bogner, M. Nahrwold, C. Weiss, N. Sewald, *J Org Chem* **2010**, *75*, 6953-6960.

[289] C. Weiss, B. Sammet, N. Sewald, *Natural Product Reports* **2013**, *30*, 924-940.

[290] M. Nahrwold, C. Weiß, T. Bogner, F. Mertink, J. Conradi, B. Sammet, R. Palmisano, S. Royo Gracia, T. Preuße, N. Sewald, *J Med Chem* **2013**, *56*, 1853-1864.

[291] M. Kobayashi, W. Wang, N. Ohyabu, M. Kurosu, I. Kitagawa, *Chem Pharm Bull (Tokyo)* **1995**, *43*, 1598-1600; R. S. Al-Awar, T. H. Corbett, J. E. Ray, L. Polin, J. H. Kennedy, M. M. Wagner, D. C. Williams, *Mol Cancer Ther* **2004**, *3*, 1061-1067.

[292] D. Panda, V. Ananthnarayan, G. Larson, C. Shih, M. Jordan, L. Wilson, *Biochemistry* **2000**, *39*, 14121-14127; M. Eggen, G. I. Georg, *Med Res Rev* **2002**, *22*, 85-101.

[293] G. I. Georg, S. M. Ali, V. J. Stella, W. N. Waugh, R. H. Himes, *Bioorg Med Chem Lett* **1998**, *8*, 1959-1962.

[294] J. Liang, R. E. Moore, E. D. Moher, J. E. Munroe, R. S. Al-awar, D. A. Hay, D. L. Varie, T. Y. Zhang, J. A. Aikins, M. J. Martinelli, C. Shih, J. E. Ray, L. L. Gibson, V. Vasudevan, L. Polin, K. White, J. Kushner, C. Simpson, S. Pugh, T. H. Corbett, *Invest New Drugs* **2005**, *23*, 213-224.

[295] V. A. Verma, T. H. Pillow, L. DePalatis, G. Li, G. L. Phillips, A. G. Polson, H. E. Raab, S. Spencer, B. Zheng, *Bioorg Med Chem Lett* **2015**, *25*, 864-868; B. M.-P. Bouchard H., Commercon A., Zhang J*., Vol. WO/2011/001052*, **2011**.

[296] G. P. Steinkühler C., Osswald B., Sewald N., Ritzefeld M., Frese M., Figueras E., Pethö L*., Vol. WO2016/146638 A1*, **2016**.

[297] A. Borbély, E. Figueras, A. Martins, L. Bodero, A. Raposo Moreira Dias, P. López Rivas, A. Pina, D. Arosio, P. Gallinari, M. Frese, C. Steinkühler, C. Gennari, U. Piarulli, N. Sewald, *ChemistryOpen* **2019**, *8*, 737-742.

[298] A. Borbély, E. Figueras, A. Martins, S. Esposito, G. Auciello, E. Monteagudo, A. Di Marco, V. Summa, P. Cordella, R. Perego, I. Kemker, M. Frese, P. Gallinari, C. Steinkühler, N. Sewald, *Pharmaceutics* **2019**, *11*.

[299] S. C. Alley, D. R. Benjamin, S. C. Jeffrey, N. M. Okeley, D. L. Meyer, R. J. Sanderson, P. D. Senter, *Bioconjug Chem* **2008**, *19*, 759-765.

[300] M. Rooseboom, J. N. Commandeur, N. P. Vermeulen, *Pharmacol Rev* **2004**, *56*, 53-102; S. Papot, I. Tranoy, F. Tillequin, J. C. Florent, J. P. Gesson, *Curr Med Chem Anticancer Agents* **2002**, *2*, 155-185.

[301] N. Albin, L. Massaad, C. Toussaint, M. C. Mathieu, J. Morizet, O. Parise, A. Gouyette, G. G. Chabot, *Cancer Res* **1993**, *53*, 3541-3546.

[302] M. de Graaf, E. Boven, H. W. Scheeren, H. J. Haisma, H. M. Pinedo, *Curr Pharm Des* **2002**, *8*, 1391-1403; X. Chen, B. Wu, P. G. Wang, *Curr Med Chem Anticancer Agents* **2003**, *3*, 139-150.

[303] I. Tranoy-Opalinski, T. Legigan, R. Barat, J. Clarhaut, M. Thomas, B. Renoux, S. Papot, *Eur J Med Chem* **2014**, *74*, 302-313.

[304] R. P. Lyon, T. D. Bovee, S. O. Doronina, P. J. Burke, J. H. Hunter, H. D. Neff-LaFord, M. Jonas, M. E. Anderson, J. R. Setter, P. D. Senter, *Nat Biotechnol* **2015**, *33*, 733-735.

[305] P. J. Burke, J. Z. Hamilton, S. C. Jeffrey, J. H. Hunter, S. O. Doronina, N. M. Okeley, J. B. Miyamoto, M. E. Anderson, I. J. Stone, M. L. Ulrich, J. K. Simmons, E. E. McKinney, P. D. Senter, R. P. Lyon, *Mol Cancer Ther* **2017**, *16*, 116-123.

[306] B. Felding-Habermann, B. M. Mueller, C. A. Romerdahl, D. A. Cheresh, *J Clin Invest* **1992**, *89*, 2018-2022.

[307] S. C. Jeffrey, J. B. Andreyka, S. X. Bernhardt, K. M. Kissler, T. Kline, J. S. Lenox, R. F. Moser, M. T. Nguyen, N. M. Okeley, I. J. Stone, X. Zhang, P. D. Senter, *Bioconjug Chem* **2006**, *17*, 831-840.

[308] P. López Rivas, C. Müller, C. Breunig, T. Hechler, A. Pahl, D. Arosio, L. Belvisi, L. Pignataro, A. Dal Corso, C. Gennari, *Org Biomol Chem* **2019**, *17*, 4705-4710.

[309] M. Grinda, J. Clarhaut, I. Tranoy-Opalinski, B. Renoux, A. Monvoisin, L. Cronier, S. Papot, *ChemMedChem* **2011**, *6*, 2137-2141.

[310] A. Henninot, J. C. Collins, J. M. Nuss, *J Med Chem* **2018**, *61*, 1382-1414.

[311] L. Gentilucci, P. Tosi, A. Bauer, R. De Marco, *Future Med Chem* **2016**, *8*, 2287-2304; A. A. Zompra, A. S. Galanis, O. Werbitzky, F. Albericio, *Future Med Chem* **2009**, *1*, 361-377.

[312] Y. Jad, A. Kumar, A. El-Faham, B. de la Torre, F. Albericio, *Acs Sustainable Chemistry & Engineering* **2019**, *7*, 3671-3683.

[313] K. Varnava, V. Sarojini, *Chemistry-an Asian Journal* **2019**, *14*, 1088-1097.

[314] D. Prat, J. Hayler, A. Wells, *Green Chemistry* **2014**, *16*, 4546-4551.

[315] D. Prat, A. Wells, J. Hayler, H. Sneddon, C. McElroy, S. Abou-Shehada, P. Dunn, *Green Chemistry* **2016**, *18*, 288-296.

[316] K. Hojo, N. Shinozaki, Y. Nozawa, Y. Fukumori, H. Ichikawa, *Applied Sciences-Basel* **2013**, *3*, 614-623; R. De Marco, A. Tolomelli, A. Greco, L. Gentilucci, *Acs Sustainable Chemistry & Engineering* **2013**, *1*,

566-569; A. Galanis, F. Albericio, M. Grotli, *Organic Letters* **2009**, *11*, 4488-4491; M. Cortes-Clerget, J. Berthon, I. Krolikiewicz-Renimel, L. Chaisemartin, B. Lipshutz, *Green Chemistry* **2017**, *19*, 4263-4267.

[317]   M. Castaldo, L. Barlind, F. Mauritzson, P. Wan, H. Snijder, *Scientific Reports* **2016**, *6*; R. Volkmer, *Chembiochem* **2009**, *10*, 1431-1442.

[318]   V. Declerck, P. Nun, J. Martinez, F. Lamaty, *Angewandte Chemie-International Edition* **2009**, *48*, 9318-9321.

[319]   J. Hernandez, E. Juaristi, *Journal of Organic Chemistry* **2010**, *75*, 7107-7111.

[320]   J. Landeros, E. Juaristi, *European Journal of Organic Chemistry* **2017**, 687-694.

[321]   J. Bonnamour, T. Metro, J. Martinez, F. Lamaty, *Green Chemistry* **2013**, *15*, 1116-1120.

[322]   V. Porte, M. Thioloy, T. Pigoux, T. Metro, J. Martinez, F. Lamaty, *European Journal of Organic Chemistry* **2016**, 3505-3508.

[323]   J. Morales-Serna, M. Jaime-Vasconcelos, E. Garcia-Rios, A. Cruz, D. Angeles-Beltran, L. Lomas-Romero, G. Negron-Silva, J. Cardenas, *Rsc Advances* **2013**, *3*, 23046-23050.

[324]   A. Wroblewska, P. Paluch, E. Wielgus, G. Bujacz, M. Dudek, M. Potrzebowski, *Organic Letters* **2017**, *19*, 5360-5363.

[325]   A. Bigi, E. Boanini, *J Appl Biomater Funct Mater* **2017**, *15*, e313-e325.

[326]   E. Boanini, M. Cassani, K. Rubini, C. Boga, A. Bigi, *Nanomaterials* **2018**, *8*.

[327]   A. Fihri, C. Len, R. Varma, A. Solhy, *Coordination Chemistry Reviews* **2017**, *347*, 48-76.

[328]   S. Diallo-Garcia, M. Ben Osman, J. Krafft, S. Casale, C. Thomas, J. Kubo, G. Costentin, *Journal of Physical Chemistry C* **2014**, *118*, 12744-12757.

[329]   M. Ben Osman, S. Garcia, J. Krafft, C. Methivier, J. Blanchard, T. Yoshioka, J. Kubo, G. Costentin, *Physical Chemistry Chemical Physics* **2016**, *18*, 27837-27847.

[330]   M. Ben Osman, J. Krafft, C. Thomas, T. Yoshioka, J. Kubo, G. Costentin, *Chemcatchem* **2019**, *11*, 1765-1778.

[331]   A. Bigi, E. Boanini, M. Gazzano, M. Kojdecki, K. Rubini, *Journal of Materials Chemistry* **2004**, *14*, 274-279; M. Tavafoghi, M. Cerruti, *Journal of the Royal Society Interface* **2016**, *13*.

[332]   T. V. Nguyen, D. J. Lyons, *Chem Commun (Camb)* **2015**, *51*, 3131-3134.

[333]   M. I. Zaki, H. Knözinger, B. Tesche, *Langmuir* **2006**, *22*, 749-755.

[334]   Y. Jad, G. Acosta, T. Govender, H. Kruger, A. El-Faham, B. de la Torre, F. Albericio, *Acs Sustainable Chemistry & Engineering* **2016**, *4*, 6809-6814.

[335]   L. Gentilucci, *Current Topics in Medicinal Chemistry* **2004**, *4*, 19-38.